

FORMULATION AND APPLICATION
OF A DYNAMIC MODEL
FOR ATMOSPHERIC POINT SOURCES

BY

MICHAEL MULHOLLAND B.Sc.ENG. (NATAL)

A thesis submitted in partial fulfilment of the
requirements for the degree of Doctor of Philosophy,
in the Department of Chemical Engineering,
University of Natal, South Africa.

Durban
October, 1977

PREFACE

The work described in this thesis was carried out in the Department of Chemical Engineering of the University of Natal. The work is original, except where other sources are specifically acknowledged in the text, and no part of this thesis has been submitted for a degree at any other university.

I wish to express my gratitude to Dr. M.T. Scholtz for his interest and guidance during the course of this research, and for his foresight in making the experimental programme possible. I am also grateful to Professor E.T. Woodburn, Head of the Department, for the encouragement which he gave to the project, and the stimulating discussions which I had with him.

The present study is one aspect of a cooperative programme which included the modelling of mesoscale wind-fields by Mr. C.J. Brouckaert, and a comparative study of atmospheric tracers conducted by Mr. C.E. Norden. I would like to thank these postgraduate researchers for the support and advice they have given me in their fields.

I am grateful to Mr. D. Penn and his staff in the Department of Chemical Engineering for their skilled services in constructing and maintaining the experimental equipment, and their resourceful contributions to its development over the years. Additional equipment was loaned by AECI Ltd. and the Atomic Energy Board, and this is gratefully acknowledged. Thanks are also due to Mr. J.R. Starkey for his tireless efforts in developing and commissioning the radio-telemetry system.

I am particularly indebted to Mr. B. Sharp and Mr. A. Hills for their able assistance during a demanding series of field experiments. The cooperation of the Richards Bay Town Board is also acknowledged in this respect.

My thanks also go to the staff of the University of Natal Computer Centre, in particular Mrs. M. Wright and Mr. L. Bardone, for their interest and cooperation over the years.

This thesis has been typed by Mrs. D. Denby, whom I wish to thank for work of a very high standard.

The experimental programme was funded by the National Programme for Environmental Sciences, the University of Natal Research Fund, and the Atomic Energy Board. I am especially grateful to AECI Ltd. for the extended financial assistance which has allowed me to complete this work.

M. Mulholland.

M. Mulholland.

SUMMARY

In the siting of new industries, or the establishment of pollution cause-effect relationships for existing industries, planners and industrialists frequently require accurate estimates of the distributions created by variable point sources. Current approaches to the modelling of atmospheric dispersion showed serious resolution limitations, or neglect of temporal transients and wind-shear. These problems were overcome by solving for serially-released lagrangian puffs on a "subgrid" scale.

Numerical solution for the zeroth, first and second moments of the puff distribution allowed the incorporation of time-variant diffusion, wind-shear, sedimentation, ground absorption, washout and first order reaction. The validity of the dynamic puff solution was established by comparison with analytical solutions and observations.

In a series of mesoscale tracer experiments, detailed wind-field and stability information was provided by a radio-telemetry system. Simulation of the experiments using measured wind-fields displayed the important redistribution effect of continuous temporal transients. Adequate descriptions of the wind-fields were also supplied by a wind-field model based on continuity. Use of the dynamic puff model in conjunction with this wind-field model showed that the dominant transport mechanisms could be accounted for even if minimal meteorological information were available.

Comparison of the filter dosage predictions provided by the dynamic puff model and an equivalent gaussian puff model showed that the latter model suffered systematic errors as a result of its neglect of wind-shear. Particularly where short-period distributions and peak concentrations are important, the dynamic puff model provides a class of information which is not presently available.

TABLE OF CONTENTS

	<u>Page:</u>
Title Page	(i)
Preface	(ii)
Summary	(iv)
Table of Contents	(vi)
List of Figures	(xii)
List of Tables	(xv)
List of Plates	(xvi)
 <u>Chapter:</u>	
1. INTRODUCTION	1
1.1 Realistic predictions in a complex environment	1
1.2 Micrometeorology	3
1.2.1 Heat and Momentum transfer	3
1.2.2 Roughness length and heterogeneous terrain	6
1.2.3 Flux profile relationships	9
1.3 Mesoscale wind-fields	13
1.3.1 Prediction	13
1.3.2 Interpolation	15
1.3.3 Directional shear in the surface layer	16
1.4 Atmospheric diffusion	17
1.4.1 The diffusion equation	17
1.4.2 Eddy diffusivity for mass	20
1.5 Analytical solutions for atmospheric diffusion	21
1.5.1 Continuous point sources	22
1.5.2 Instantaneous point sources	24
1.6 Applied studies in the estimation of atmospheric diffusion	30
1.6.1 Statistical methods	30
1.6.2 Random motion (particle-in-cell) methods	31

<u>Chapter:</u>	<u>Page:</u>
1.6.3 Semi-analytical methods	31
1.6.4 Numerical solution of the diffusion equation	32
1.6.4.1 Continuous emission, steady-state models	32
1.6.4.2 Time-variant, 3-dimensional grid models	34
1.6.4.3 Time-variant, vertical cell models	37
1.6.4.4 Instantaneous point source models	38
1.7 Diffusion of heavy particles	41
1.8 Macroscopic effects	44
1.9 Removal mechanisms	45
1.9.1 Sedimentation	45
1.9.2 Ground-level absorption	46
1.9.3 Washout	47
1.9.4 Chemical reaction and radioactive decay	49
1.10 Considerations in the modelling of atmospheric dispersion	50
1.10.1 Accuracy	50
1.10.2 Rationale	52
2. FORMULATION OF A GENERAL DYNAMIC MODEL FOR ATMOSPHERIC POINT-SOURCES	57
2.1 Objectives	57
2.2 Theory	60
2.2.1 Distribution in the eulerian frame	60
2.2.2 Coordinate transformations	62
2.2.3 Distribution in the lagrangian frame	67
2.2.4 Solution for the lagrangian puff	69
2.3 Numerical method	72
2.3.1 Separation of processes	72
2.3.2 Initial distribution	76
2.3.3 Solution for the diffusion step	77

<u>Chapter:</u>	<u>Page:</u>	
2.3.4	Solution for the reaction step	83
2.3.5	Reconstruction of the distribution	88
2.4	Administrative aspects	90
2.4.1	Model concepts	90
	2.4.1.1 Dosages and concentrations	90
	2.4.1.2 Region of interest	92
2.4.2	Velocity and diffusivity profiles, system properties	95
2.4.3	Release time intervals and trajectory steps	101
2.4.4	Advection in the lagrangian frame	103
	2.4.4.1 The proximate curve	103
	2.4.4.2 Relative velocity	109
2.4.5	Removal processes and ground deposition	112
3.	EVALUATION OF THE DYNAMIC PUFF MODEL	114
3.1	Comparison with analytical puff solutions	114
	3.1.1 Unbounded atmosphere	116
	3.1.2 Bounded atmosphere	118
3.2	Comparison with puff observations	120
3.3	Comparison with continuous point source models	127
	3.3.1 Gaussian plume formula	127
	3.3.2 Peters and Klinzing (1971) analytical solution	129
	3.3.3 Ito (1970) numerical solution	129
3.4	Illustrative applications of the puff model	131
4.	EXPERIMENTAL PROCEDURE	142
4.1	Atmospheric tracer system	142
	4.1.1 Zinc-Cadmium sulphide fluorescent particle tracer	142
	4.1.2 Development of a release technique	145
	4.1.3 Calibration for particle yield	151
	4.1.4 Heavy particle effects	152
	4.1.5 Air sampling and filter analysis	154
	4.1.5.1 Anisokinetic effects	154

<u>Chapter:</u>	<u>Page:</u>
4.1.5.2 Equipment	157
4.1.5.3 Statistical significance	158
4.2 Richards Bay Project	159
4.2.1 Introduction	159
4.2.2 Meteorological measurements	161
4.2.3 Experimental method	167
4.2.4 Estimation of the surface-roughness distribution	169
5. ANALYSIS OF EXPERIMENTAL RESULTS	173
5.1 Introduction	173
5.2 Simulation of tracer experiments using measured wind-fields	181
5.2.1 Run 627	181
5.2.2 Run 630	193
5.2.3 Run 705	201
5.2.4 Run 708	208
5.2.5 Run 711	215
5.2.6 Run 714	221
5.2.7 Run 722	228
5.2.8 Run 723	234
5.3 Simulation of Run 723 using predicted wind-fields	240
6. DISCUSSION	246
6.1 Motivation	246
6.2 Development of the dispersion model	248
6.3 Description of the mesoscale system	254
6.4 Simulation of tracer experiments using wind- field and stability measurements	258
6.5 Comparison with indium oxide tracer measurements	271
6.6 Simulation of Run 723 using predicted wind- fields and stability measurements	274
7. CONCLUSIONS	277

APPENDICES

<u>Chapter:</u>	<u>Page:</u>
A1 DYNAMIC PUFF MODEL	280
A1.1 Solution for the diffusion step: limiting value method	280
A1.2 Storage and interpolation of variables	284
A1.3 Release-time sequence	286
A1.3.1 Simulation of motion	286
A1.3.2 Application	293
A1.4 Computer program	295
A1.4.1 Functions of subroutines	298
A1.4.2 Input-output specifications	308
A1.4.2.1 Meteorological data	311
A1.4.2.2 Release information	313
A1.4.2.3 Specification of desired output	313
A1.4.2.4 Procedure variables	315
A1.4.3 Dynamic Puff Model: FORTRAN program listing	316
A1.4.4 Generation of a test data-set for the Dynamic Puff Model	353
A1.4.5 Dynamic Puff Model program execution for the test data-set	355
A2 GAUSSIAN PUFF MODEL	361
A2.1 Introduction	361
A2.2 Theory	361
A3 VERTICAL COLUMN PARTICLE-IN-CELL MODEL FOR DOSAGE DISTRIBUTIONS	365
A4 METEOROLOGY SUB-MODEL	368
A4.1 Objectives	368
A4.2 Input-output modes	369
A4.3 Estimation of friction velocity and stability length	372
A4.3.1 Available measurements include $S_w(z_m), T(z_2), T(z_1), z_0$	372

<u>Chapter:</u>		<u>Page:</u>
A4.3.2	Available measurements include $S_{av}, H_I, T(z_2), T(z_1), z_0$	373
A4.3.3	Some typical results	373
A4.4	Surface roughness categories for the Richards Bay area	375
NOMENCLATURE		377
BIBLIOGRAPHY		387

LIST OF FIGURES

<u>Figure:</u>		<u>Page:</u>
2.1	Transformation \tilde{T}_p	65
2.2	Ground absorption and first-order reaction with vertical diffusion	85
2.3	Region of interest	93
2.4	Locating line subject to velocity gradient	104
2.5	Horizontal locating line	105
2.6	Spatial and temporal wind-field variations	106
2.7	Lagrangian solution grid	108
2.8	Estimation of effective angle of incidence	110
3.1	Isopleth comparison - numerical and analytical solutions for an unbounded puff	117
3.2	Isopleth comparison - numerical and moment solutions for a ground-level puff	119
3.3	Comparison of predicted and measured concentration histories	123
3.4	Development of simulated puff: Nickola (1971) Run P8	125
3.5	Concentration profiles - elevated gaussian plume	128
3.6	Concentration profiles - ground-level gaussian plume	128
3.7	Concentration profiles - variable diffusivity	128
3.8	Concentration profiles - variable velocity and diffusivity	130
3.9	Concentration profiles - variable velocity and diffusivity	130
3.10	Concentration profiles - simulation of Ito (1970) result	130

<u>Figure:</u>		<u>Page:</u>
3.11	Temporal variation of wind direction (+90°)	132
3.12	Temporal variation of wind direction (+90°) with surface absorption [$\bar{w}_d = 0,0625 \text{ m s}^{-1}$]	134
3.13	Temporal variation of wind direction (+90°) with sedimentation and washout/decay	136
3.14	Temporal variation of wind direction (+90°) with uniform velocity and diffusivity profiles	138
3.15	Steady-state wind-field with spatial variation	138
3.16	Combined spatial and temporal variation of wind direction	140
4.1	Fluorescent particle tracer dissemination equipment	147
4.2	Portable filter-aspirator unit	147
4.3	Richards Bay Project - schematic organisation	166
4.4	Richards Bay Project: Locations of meteorological masts and aspirated filters	168
4.5	Estimated roughness length distribution for the Richards Bay area	171
5.1 to 5.6	Run 627 (27.6.76)	182-190
5.7 to 5.11	Run 630 (30.6.76 - 1.7.76)	194-199
5.12 to 5.16	Run 705 (5.7.76 - 6.7.76)	202-205
5.17 to 5.21	Run 708 (8.7.76)	209-213
5.22 to 5.26	Run 711 (11.7.76 - 12.7.76)	216-219
5.27 to 5.32	Run 714 (14.7.76 - 15.7.76)	222-226

<u>Figure:</u>		<u>Page:</u>
5.33 to 5.36	Run 722 (22.7.76)	229-231
5.37 to 5.41	Run 723 (23.7.76)	235-238
5.42 to 5.45	Simulation of Run 723 using predicted wind-fields	241-243
6.1	Combined results - Dynamic Puff Model and Gaussian Puff Model predictions for mean filter concentrations	265
6.2	Indium oxide tracer: Predicted versus Measured mean filter concentrations using In_2O_3 dilution factors	272
A1.1	Concentrations and diffusivities at three neighbouring points	280
A1.2	Concentration distribution for a two- dimensional puff	287
A1.3	Approximate sedimentation	291
A1.4	Dynamic Puff Model: Flow diagram	296
A1.5	Subroutine stacking	299
A1.6	Specification of time-series	308
A1.7	Data-grid and solution-grid (region- of-interest)	309
A1.8	Input-output modes	310
A2.1	Approximation of sedimentation	362
A3.1	Vertical column PIC model	366
A4.1	Origin of meteorological measurements	370
A4.2	Velocity and mass-diffusivity profiles after Dyer (1974) [Equations (2.72), (2.73)]	374

LIST OF TABLES

<u>Table:</u>		<u>Page:</u>
1.1	Observed roughness length categories	6
1.2	Continuous point source solutions	23
3.1	Interpretation of instantaneous release experiments	121
4.1	Roughness length estimates at masts	170
6.1	Analysis of DPM and GPM combined predictions	266
6.2	Analysis of DPM and GPM predictions for indium-based measurements	273
A4.1	Parameter conversions	370
A4.2	Estimated $u_{*,L}$ as a function of temperature gradient and roughness length	375
A4.3	Estimated roughness length categories for Richards Bay	376

LIST OF PLATES

<u>Plate:</u>		<u>Page:</u>
4.1	Disseminator spray-nozzle	149
4.2	Dissemination apparatus, showing pump chambers and suspension vessel (at rear)	149
4.3	25 m instrumented mast supporting tracer source	155
4.4	Membrane filter aspirator units arranged for sampling tests	155
4.5	Semi-portable telemetering mast, instrumented at 1,9 m and 11,2 m levels	162
4.6	Telemetry satellite station circuitry - calibration of platinum resistance thermometers	162
4.7	Semi-portable mast upper instrument carriage (11,2 m), showing cup anemometer, platinum resistance thermometer aspirator, and digital wind vane	164
4.8	Semi-portable mast lower instrument carriage (1,9 m), showing platinum resistance thermometer aspirator and cup anemometer	164

CHAPTER 1.

INTRODUCTION

1.1 Realistic predictions in a complex environment.

The benefits of air-quality models in pollution studies are well accepted. The only important questions remaining concern returns for refinement. The transport of heat, mass and momentum in the atmosphere occurs largely through the action of turbulent eddies, the stochastic nature of which is influenced by a wide range of surface and atmospheric properties. It will be seen that the transport processes are interdependent, and that the concentration of a pollutant in the atmosphere is necessarily a random variable.

Isolated measurements of concentration or dosage are meaningless unless they are given statistical significance. Deterministic models have the advantage that they predict mean expected quantities in terms of a fully-characterised emission and meteorology. It is also possible to vary these inputs in order to define the dominant features of the stochastic behaviour of observed concentrations.

Nevertheless, it is important to ask whether the often marginal improvements embodied in new approaches are significant in comparison with inherent statistical variability. Moreover, if diffusion and advection in the atmosphere are dependent on spatially- and temporally-variant properties,

would not a vast store of descriptive information be necessary before meaningful predictions could be made? Since the earliest proposals by Sutton (1932), growing support has been found for even simple mathematical representations of observed tracer distributions. Assuming that a new approach is mechanistically correct, it should clearly only be preferred to the accepted models if its predictions differ significantly, and if the additional information usually demanded by its sophistication can be specified.

To show that one model differs from another is easy. The task of showing that a new approach gives significantly improved estimates of real observations is hampered by the intrinsic variability of observations. The "improvement" of models usually requires additional calculation and the specification of new parameters which are often spatially, if not temporally variant. It might reasonably be argued that if these parameters cannot be properly specified, the associated effects might as well be ignored altogether.

It is contended in the present work that realistic inclusion of the underlying transport processes significantly alters predicted distributions, and that even if accurate description of the system is impossible, the important features of this effect will be accounted for by an approximate description. Before the central ideas in this approach can be developed, it will be necessary to specify the basic equations relating heat, mass and momentum transfer, and review some of the previous work in related fields.

1.2 Micrometeorology.

1.2.1 Heat and momentum transfer.

Assuming that the Coriolis acceleration does not make a significant contribution to air motion, the equations for continuity, motion and energy in a uniform gravitational field (\tilde{g}) are:

$$\frac{\partial \rho}{\partial t} + \frac{\partial}{\partial x_i} (\rho u_i) = 0 \quad (1.1)$$

$$\rho \left(\frac{\partial u_i}{\partial t} + u_j \frac{\partial u_i}{\partial x_j} \right) = \frac{\partial}{\partial x_k} \left[\mu \left(\frac{\partial u_i}{\partial x_k} + \frac{\partial u_k}{\partial x_i} \right) - \left(P + \frac{2}{3} \mu \frac{\partial u_j}{\partial x_j} \right) \delta_{ik} \right] - \rho g_i \quad (1.2)$$

$$\rho \left(\frac{\partial U_e}{\partial t} + u_j \frac{\partial U_e}{\partial x_j} \right) = k_T \frac{\partial^2 T}{\partial x_j \partial x_j} - P \frac{\partial u_j}{\partial x_j} + \psi + \Phi \quad (1.3)$$

where ρ is fluid density, μ is fluid viscosity, P is pressure, U_e is the internal energy per unit mass, k_T is the thermal conductivity, ψ is the heat generated per unit volume and time as a result of viscous dissipation, and Φ represents the heat generated by any sources in the fluid. The repetition of a subscript in a term implies summation over the three coordinate directions, x_1 , x_2 and x_3 .

Because of the interrelationship of pressure, temperature and density, equations (1.1), (1.2) and (1.3) are highly coupled. Consider motion only in a shallow layer near the ground, where $P = P_0$, $T = T_0$, $\rho = \rho_0$. If the effect of motion is to produce only small deviations \hat{P} , \hat{T} , $\hat{\rho}$ from the

equilibrium values (atmosphere at rest), it can be shown that the Boussinesq approximations [Spiegel and Veronis (1960), Calder (1968)] lead to the simplified forms

$$\frac{\partial u_i}{\partial x_i} = 0 \quad (1.4)$$

$$\frac{\partial u_i}{\partial t} + u_j \frac{\partial u_i}{\partial x_j} = \frac{1}{\rho_0} \frac{\partial \hat{P}}{\partial x_i} + \frac{\mu}{\rho_0} \frac{\partial^2 u_i}{\partial x_j \partial x_j} + g_i \frac{\hat{T}}{T_0} \quad (1.5)$$

Similarly, if it is assumed that gas behaviour is ideal, and that the contribution of viscous dissipation ψ is negligible, equation (1.3) may be expressed as

$$\rho_0 c_p \left(\frac{\partial \theta}{\partial t} + u_j \frac{\partial \theta}{\partial x_j} \right) = k_T \frac{\partial^2 \theta}{\partial x_j \partial x_j} + \Phi \quad (1.6)$$

where θ is the potential temperature, defined as the temperature which would be exhibited by a parcel of air if it were brought adiabatically to a standard pressure P_0 (ground level).

For an ideal gas

$$\theta = T \left(\frac{P}{P_0} \right)^{\frac{1-\gamma}{\gamma}} \quad \text{with } \gamma = c_p/c_v \quad (1.7)$$

If x_3 is the positive vertical direction [$\tilde{g} = (0,0,g)$], and the atmosphere is horizontally homogeneous, it follows that

$$\frac{\partial \theta}{\partial x_1} = \frac{\partial \theta}{\partial x_2} = 0, \quad \frac{\partial \theta}{\partial x_3} = \frac{\partial T}{\partial x_3} + \Gamma \quad (1.8)$$

where Γ is the adiabatic lapse rate. (ideal: $\Gamma = g/c_p$).

It is convenient to express the properties u_i , θ and \hat{P} as the sum of mean and turbulent components, $\epsilon = \bar{\epsilon} + \epsilon'$,

where

$$\bar{\epsilon} = \frac{1}{t_a} \int_{t-t_a/2}^{t+t_a/2} \epsilon(t') dt', \quad \overline{\epsilon'} = 0. \quad (1.9)$$

and the averaging time t_a is not so large as to interfere with the macroscopic features of the flow, which are treated as advective properties. Substituting in equations (1.4), (1.5) and (1.6), and averaging with respect to time, the equations for continuity, energy and motion become

$$\frac{\partial \bar{u}_i}{\partial x_i} = 0 \quad (1.10)$$

$$\begin{aligned} \frac{\partial}{\partial t}(\rho_0 \bar{u}_i) + \frac{\partial}{\partial x_j}(\rho_0 \bar{u}_i \bar{u}_j) \\ = - \frac{\partial \bar{p}}{\partial x_i} + \frac{\partial}{\partial x_j} \left(\mu \frac{\partial \bar{u}_i}{\partial x_j} - \rho_0 \overline{u'_i u'_j} \right) + g_i \frac{\bar{\theta}}{T_0} \end{aligned} \quad (1.11)$$

$$\rho_0 c_p \left(\frac{\partial \bar{\theta}}{\partial t} + \bar{u}_j \frac{\partial \bar{\theta}}{\partial x_j} \right) = \frac{\partial}{\partial x_j} \left(k_T \frac{\partial \bar{\theta}}{\partial x_j} - \rho_0 c_p \overline{u'_j \theta'} \right) \quad (1.12)$$

The new momentum flux terms $\rho_0 \overline{u'_i u'_j}$ (Reynolds stresses) and the heat flux terms $\rho_0 c_p \overline{u'_j \theta'}$ arising from turbulence represent the dominant transport mechanism in the atmosphere.

According to the mixing length hypothesis, the fluctuations ϵ' are proportional to spatial gradients in $\bar{\epsilon}$. On this basis the vertical flux terms may be approximated as

$$\left(\mu \frac{\partial \bar{u}_1}{\partial x_3} - \rho_0 \overline{u'_1 u'_3} \right) = \rho_0 K_m \frac{\partial \bar{u}_1}{\partial x_3} \quad (1.13)$$

$$\left(k_T \frac{\partial \bar{\theta}}{\partial x_3} - \rho_0 c_p \overline{u_3' \theta'} \right) = \rho_0 c_p K_T \frac{\partial \bar{\theta}}{\partial x_3} \quad (1.14)$$

where K_m and K_T are the "turbulent diffusivities" for momentum and heat respectively.

For shallow-layer horizontal flow under steady adiabatic ($\partial \bar{\theta} / \partial x_3 = 0$) conditions, equation (1.11) suggests that the shear stress in equation (1.13) will be approximately constant τ_0 . Defining a characteristic "friction velocity" $u_* = \sqrt{\tau_0 / \rho_0}$, dimensional analysis yields

$$\bar{u}_1(x_3) = \frac{u_*}{k} \ln\left(\frac{x_3}{z_0}\right) \quad (1.15)$$

for the adiabatic or "neutral" atmosphere. In this relation, k is the Kármán constant, and z_0 is the "roughness length" which is related to the aerodynamic roughness of the surface.

1.2.2 Roughness length and heterogeneous terrain.

Typical observed values of z_0 [Priestley (1959), Sutton (1953), using data published by Sheppard (1947)] are presented in table (1.1).

Table (1.1) Observed roughness length categories

SURFACE	z_0 (m)
very smooth (ice, mud flats)	1×10^{-5}
snow	5×10^{-5}
smooth sea	2×10^{-4}
level desert	3×10^{-4}
grass up to 1 cm high	1×10^{-3}
grass up to 10 cm high (thin-thick)	$1-2 \times 10^{-2}$
grass up to 50 cm high (thin-thick)	$5-9 \times 10^{-2}$
fully-grown root crops	$1,4 \times 10^{-1}$

This broad classification is supported by transient onshore wind profiles measured by Hsu (1971) and Echols and Wagner (1972). Sellers (1965) proposed that roughness length could be represented by a relationship of the form

$$z_0 = ah_*^b \quad (1.16)$$

where h_* is the average height of the roughness-producing obstacles, and a and b are constants. Experiments conducted by Hsi and Nath (1970), in which a neutral velocity profile was assumed to exist over a simulated forest canopy, support a relationship of the form (1.16) with $a = 0,29$ and $b = 1,19$ as proposed by Kung (1963).

However, Lettau (1969) maintained that the estimate cannot be effective unless it accounts for variations in the spatial distribution of the roughness elements. Instead he proposed

$$z_0 = 0,5 h_* A_i/A \quad (1.17)$$

where A_i is the projected area on which the wind is incident and A is the area of ground occupied by each element. This relationship was based on experiments conducted by Kutzbach (1961) in which hundreds of bushel baskets were laid out on a frozen lake. A similar result for equilibrium flows, based on the plan area A_p instead of the incident area, was proposed by Counihan (1971):

$$z_0 = 1,08 h_* A_p/A - 0,08 h_* \quad (1.18)$$

Leonard and Federer (1973) assumed that the velocity profile over a pine forest was log-linear in order to derive the "measured" value $z_0 = 1,0$ m. The parameters for Lettau's

equation (1.17) were obtained by representing the forest canopy as an array of close-packed paraboloids, yielding the estimate $z_0 = 0,75$ m.

Turning to less homogeneous terrain, Lettau (1969) predicts $z_0 = 12,5$ m for the mountainous state of Colorado, U.S.A. This is in contrast to the values of 0,99 m for low mountains and 1,42 m for high mountains derived by Fiedler and Panofsky (1972) by assuming that u_* is proportional to the vertical turbulent intensity.

However, the effectiveness of profile relationships relies on the attainment of equilibrium in the boundary-layer, a condition only met with an unlimited upwind fetch of homogeneous terrain. Panofsky and Townsend (1964) proposed that at a roughness change, an internal boundary-layer developed above which the flow was not influenced by the new surface. Below this layer they assumed a continuous variation of stress from the surface to the boundary-layer, where it attained the value of stress in the original flow. Their theory was supported by a number of observations, with the interface generally having a slope of order 1/10. Similar results were obtained by Taylor (1969) in numerical solutions of the two-dimensional flow equations, and by Echols and Wagner (1972) in onshore wind-profile experiments. The latter workers observed internal boundary-layer growth rates about 1/13 downwind distance.

The development of localised regions with varying stress will clearly complicate the simple picture of effective constant values over heterogeneous terrain. Peterson

(1971) points out that this spatial variation of stress may lead to significant error in diffusivity estimates based on mean properties.

1.2.3 Flux profile relationships.

It follows from equation (1.14) that the mean upwards heat flux will be given by

$$\bar{q}_3 = -\rho_0 c_p K_T \frac{\partial \bar{\theta}}{\partial x_3} \quad (1.19)$$

The development of empirical relations for a non-adiabatic ($\bar{q}_3 \neq 0$) surface-layer is facilitated by defining the Monin-Obukhov stability length

$$L = \frac{-\rho_0 c_p T_0 u_*^3}{kg \bar{q}_3} \quad (1.20)$$

By involving $\zeta = x_3/L$ as one of the dimensionless groups, Monin and Obukhov (1954) used dimensional analysis to show that

$$\frac{\partial \bar{u}_1}{\partial x_3} = \frac{u_*}{kx_3} \phi_m(\zeta) \quad (1.21)$$

$$\frac{\partial \bar{\theta}}{\partial x_3} = \frac{\theta_*}{x_3} \phi_T(\zeta) \quad \text{with} \quad \theta_* = \frac{-\bar{q}_3}{\rho c_p k u_*} \quad (1.22)$$

where ϕ_m and ϕ_T are universal functions. To satisfy the neutral velocity profile (1.15) note that $\phi_m(0) = 1$.

Assuming constant shear stress in the surface layer ($\tau_0 = \rho_0 u_*^2$), equations (1.13) and (1.21) lead to

$$K_m = u_* k x_3 / \phi_m(\zeta) \quad (1.23)$$

whilst equations (1.19) and (1.22) give

$$K_T = u_* k x_3 / \phi_T(\zeta) \quad (1.24)$$

In order to establish useful relationships for the transfer of momentum, heat and ultimately mass in the surface layer, numerous investigations have aimed to find empirical forms for the universal functions ϕ_m and ϕ_T . Monin and Obukhov (1954) originally suggested a simple expression for small $\zeta = x_3/L$ by expanding $\phi_m(\zeta)$ in a power series and retaining only the linear term

$$\phi_m(\zeta) = 1 + \alpha\zeta, \quad (1.25)$$

where α is constant. Integrating (1.21) from $x_3 = z_0$ to z , and assuming that $\bar{u}_1(z_0) \approx 0$, yields

$$\bar{u}_1(z) = \frac{u_*}{k} \left[\ln\left(\frac{z}{z_0}\right) + \alpha \frac{z}{L} \right] \quad (1.26)$$

which is the log-linear wind profile. Taylor (1960) and Takeuchi (1961) reported values of α ranging from 2 to 10 under stable conditions, whilst McVehil (1964) found $\alpha = 7$ in stable air.

Webb (1970) proposed a large range of validity for the log-linear profile (1.26) and a means for extending its use into regions of strong stability. Analysis of measurements at O'Neill, U.S.A., and Kerang and Hay, Australia, indicated that the log-linear law was valid for $-0,03 < \zeta < 1$, and that $\alpha = 4,5$ under unstable, and $\alpha = 5,2$ under stable conditions. It was found that $K_T/K_m = K_w/K_m = 1$ for the entire log-linear range. (K_w is a similar mass eddy

diffusivity for water-vapour). Webb discovered that for $\zeta \geq 1$, a second regime set in, which could be described by

$$\phi_m(\zeta) = \phi_T(\zeta) = (1+\alpha) \text{ for } 1 \leq \zeta < (1+\alpha) \quad (1.27)$$

The profiles in this region of strong stability were only quasi-determinate, though they averaged the logarithmic forms which follow from equation (1.21).

In Project Green Glow, Ito (1970) found that field measurements were best simulated using the log-linear profile with $\alpha=6$ for $\zeta < 1$. However, he proposed a proportional increase of ϕ_m ,

$$\phi_m(\zeta) = (1+\alpha)\zeta \text{ for } \zeta \geq 1, \quad (1.28)$$

leading to a linear velocity profile in this range.

If heat, mass and momentum are transported equivalently by turbulent eddies, it is reasonable to expect that $K_T/K_m = K_w/K_m = 1$. However, Businger, Wyngaard, Izumi and Bradley (1971) found that $\phi_T(0) = 0,74$ and $K_T/K_m = 1,35$ under neutral conditions, with K_T/K_m only reasonably constant for $\zeta > 0 [1, 0 < K_T/K_m < 1,35]$. In experiments at Davis, California, Pruitt, Morgan and Lourence (1973) found $K_w/K_m = 1,13$ under neutral conditions.

In a review of flux-profile relationships, Dyer (1974) considered only proposed forms of $\phi_m(\zeta)$, $\phi_T(\zeta)$ and $\phi_w(\zeta)$ which were based on measurements of "sufficient quality". After considering the results of Swinbank (1964, 1968), Webb (1970), Dyer and Hicks (1970) and Businger et al (1971), he suggested that the most convincing flux-

gradient description is given by

$$\left. \begin{aligned} \phi_m &= (1-16\zeta)^{-\frac{1}{4}} \\ \phi_T &= \phi_W = (1-16\zeta)^{-\frac{1}{2}} \end{aligned} \right\} \text{ for } \zeta < 0 \quad (1.29)$$

and

$$\phi_m = \phi_T = \phi_W = 1+5\zeta \quad \text{for } \zeta \geq 0 \quad (1.30)$$

For neutral air, $\phi_T = 1$ as opposed to $\phi_T = 0,74$ proposed by Businger et al. Dyer used a Kármán constant $k=0,41$, and suggests that Businger et al would have found $\phi_T(0)=1$ had they used $k=0,39$, a result which would have arisen had they not applied certain corrections to their measurements of wind-shear and surface stress. Further, Pruitt, Morgan and Lourence (1973) found $k=0,42$ using sensitive surface-drag lysimeters, and contend that their result will be more accurate than the $k=0,35$ proposed by Businger et al (1971) using sonic anemometer measurements of stress.

Carl, Tarbell and Panofsky (1973), in their analysis of data from towers at Cape Kennedy (150 m), Arco (61 m) and Risø (125 m), suggest that relations for $\phi_m(\zeta)$ and $\phi_T(\zeta)$ derived for the lowest 30 m or so of the surface layer, may in fact be valid for up to 10% of the planetary boundary layer. Under near-neutral conditions, no significant deviations from the logarithmic wind and temperature profiles were detected up to 150 m.

1.3 Mesoscale wind-fields.

1.3.1 Prediction.

In order to complete a reasonable representation of the wind structure on a regional scale, it is essential to account for some dominant effects on the direction of air flow in the surface layer. Surface temperature variations and topographic features cause air flow variations on the same advective scales which are of interest in the distribution of air pollutants. The possibility of continuously measuring these variations with sufficient resolution is generally remote, so that the attraction of a "best theoretical estimate" of a complex wind-field is obvious.

Anderson (1971) neglected momentum transfer, and used the equation of continuity (1.10) in order to solve for the two-dimensional (horizontal) wind-field. Integration of this equation from the surface at height h to a height H ("inversion level") above which the topographic effect is not felt ($\bar{u}_3(H)=0$) yields

$$\overline{\nabla^2 \phi} = \bar{U} \cdot \tilde{\nabla} h / H \quad (1.31)$$

In this expression, ϕ is the potential function, $\tilde{\nabla}$ is the two-dimensional gradient operator ($\partial/\partial x_1, \partial/\partial x_2$), and the overbar indicates a mean over the height $(H-h) \approx H$. It has been assumed that $\bar{u}_3(h) \approx \bar{U} \cdot \tilde{\nabla} h$, where \bar{U} is the unperturbed mean horizontal velocity vector. In their treatment of this problem, Scholtz and Brouckaert (1976) used the perturbed horizontal velocity vector, so that the potential due to

synoptic flow ϕ_1 was defined by

$$\nabla^2 \phi_1 - \frac{\tilde{\nabla} \phi_1 \cdot \tilde{\nabla} h}{(H-h)} = 0 \quad (1.32)$$

A similar treatment to that of Anderson (1971), which assumed proportional vertical velocity at height H_I , $\bar{u}_3(H_I) = A_T(T_S - \bar{T}_S)$, due to the surface temperature anomaly $(T_S - \bar{T}_S)$, led to an expression for the thermal potential

$$\nabla^2 \phi_2 - \frac{\tilde{\nabla} \phi_2 \cdot \tilde{\nabla} h}{(H-h)} = \frac{A_T(T_S - \bar{T}_S)}{(H_I-h)} \quad (1.33)$$

where H_I is generally much greater than H . Scholtz and Brouckaert (1976) showed that a significant potential ϕ_3 is contributed by katabatic flows according to

$$\nabla^2 \phi_3 - \frac{\tilde{\nabla} \phi_3 \cdot \tilde{\nabla} h}{(H-h)} = k_f \Delta \theta \nabla^2 h_f \quad (1.34)$$

where k_f is constant, $\Delta \theta$ is the potential temperature increase through the inversion layer, and h_f is a smoothed version of the topography. The assumption that synoptic, topographic, thermal and katabatic effects were uncoupled allowed separate numerical solution for the associated potentials, and direct combination to produce the flow-field. Predicted wind-fields showed reasonable agreement with measurements made at Richards Bay, Natal.

1.3.2 Interpolation.

Turning to the problem of interpreting measured wind-data, the situation often arises where data are available with acceptable spatial resolution, but where a justifiable means of interpolation is sought. Clearly, such interpolation could best be justified in terms of continuity, and thermal and topographical variations as discussed in section (1.3.1), but this would incur a prohibitive quantity of computation.

Wendell (1972) suggested a simple inverse square weighting of the separated velocity components,

$$\bar{U}_i = \left(\sum_{k=1}^N \frac{\bar{U}_{i,k}}{r_k^2} \right) / \left(\sum_{k=1}^N \frac{1}{r_k^2} \right) \quad (1.35)$$

where the r_k , $k=1, \dots, N$, are the distances from the points of measurement. This method may lead to spurious divergence.

Endlich (1967) proposed a scheme to minimise wind-field divergence,

$$\delta_w = \frac{\partial \bar{U}}{\partial x} + \frac{\partial \bar{V}}{\partial y}$$

and retain a fixed vorticity,

$$\epsilon = \frac{\partial \bar{U}}{\partial x} - \frac{\partial \bar{V}}{\partial y}$$

Starting with an initial estimate of the wind-field, the scheme involves iterative adjustment of \bar{U} , \bar{V} at grid points until all $\delta_w(i, j)$, based on finite differences, are smaller than some specified value.

Dickerson (1973) used a variational matching technique proposed by Sasaki (1970) to generate a mass-consistent

wind-field. However, Liu and Goodin (1976) found that the mean-square divergence of a test wind-field was hardly reduced using this method, and proposed instead an iterative algorithm which reduces divergence under the constraint of retaining the measured wind vectors.

Unless velocity data are readily stored as complete rationalised wind-fields, it is clear that the adjustment techniques discussed above will require considerable computation for the extraction of random point values.

1.3.3 Directional shear in the surface layer.

The wind profile in the planetary boundary-layer becomes skewed with increasing latitude, a result of the Coriolis force (Ekman effect). It can be shown that for a geostrophic wind \bar{U}_G in the x-direction, and constant momentum diffusivity, K_M , the horizontal velocity components vary as

$$\bar{U}(Z) = \bar{U}_G [1 - e^{-\alpha Z} \cos(\alpha Z)]$$

$$\bar{V}(Z) = \bar{U}_G e^{-\alpha Z} \sin(\alpha Z)$$

where $\alpha = \sqrt{f_c / 2K_M}$ and $f_c = -(\partial P / \partial y) / \rho \bar{U}_G$.

Csanady (1972) suggested that at mid-latitudes it would take a cloud of released material approximately 30 minutes to grow to a height where the effect of this shear would become appreciable. Tracer experiments conducted over 30 km indicated that the only significant deviations from expected ground-level gaussian distributions occurred

with extreme rates of cross-wind shear, accompanied by strong stability. Moreover, Csanady noted that the directional shears in these cases could not be attributed to the Coriolis effect, and probably arose through the stratification of local flows.

Of course, cross-wind shear contributions resulting from the Ekman effect may be expected to increase with height. Egan and Mahoney (1972b) solved for the distribution of a cloud under the influence of a neutral Ekman spiral following Blackadar (1962). After 30 minutes of travel, effective cross-wind diffusivities for the entire cloud were found to be about 8 times the maximum vertical diffusivity, in agreement with Csanady (1969b). This "crosswind diffusivity" includes the relative shear of cloud layers.

1.4 Atmospheric diffusion.

1.4.1 The diffusion equation.

If C is the concentration of some trace material in the air, the eulerian mass-balance over a stationary volume element yields

$$\frac{\partial C}{\partial t} + \frac{\partial}{\partial x_j} (u_j C) = D_m \frac{\partial^2 C}{\partial x_j \partial x_j} + R(C) + S(\tilde{x}, t) \quad (1.36)$$

In this relation, D_m is the molecular diffusivity of the material, R is a source term which depends on the concentration C , and represents, for example, chemical reaction, and S is an independent source term for the rate of introduction

of material at \tilde{x} and t .

Let $\langle C \rangle$ be the ensemble mean value of C which would result from an infinite number of realisations of the turbulence field, so that $C = \langle C \rangle + C'$ and $\langle C' \rangle = 0$. Substitution in equation (1.36), with $u_i = \bar{u}_i + u_i'$, and averaging over an infinite ensemble of realisations, yields

$$\begin{aligned} \frac{\partial \langle C \rangle}{\partial t} + \frac{\partial}{\partial x_j} (\bar{u}_j \langle C \rangle) + \frac{\partial}{\partial x_j} \langle u_j' C' \rangle \\ = D \frac{\partial^2 \langle C \rangle}{m \partial x_j \partial x_j} + \langle R(\langle C \rangle + C') \rangle + S(\tilde{x}, t) \end{aligned} \quad (1.37)$$

The turbulent mass fluxes $\langle u_i' C' \rangle$, $i=1,2,3$ occur as additional dependent variables, leading to an insoluble closure problem. As in the case of heat and momentum in section (1.2.1), it is attempted to relate $\langle u_i' C' \rangle$ to $\langle C \rangle$ using a mixing length model:

$$\langle u_i' C' \rangle = -K_i \frac{\partial \langle C \rangle}{\partial x_j} \quad (\text{no summation}) \quad (1.38)$$

Three further assumptions are invoked:

- (i) Molecular diffusion is negligible compared with turbulent diffusion.
- (ii) The atmosphere is incompressible $[\partial \bar{u}_i / \partial x_i = 0]$.
- (iii) The reaction rate R is not influenced by concentration fluctuations $[\langle R(C) \rangle = R(\langle C \rangle)]$.

This approximation will become cruder with increasing non-linearity of R .

Then, dropping the braces for convenience, equation (1.37) becomes

$$\frac{\partial C}{\partial t} + \bar{u}_i \frac{\partial C}{\partial x_i} = \frac{\partial}{\partial x_i} (K_i \frac{\partial C}{\partial x_i}) + R(C) + S(\tilde{x}, t) \quad (1.39)$$

It can be shown [Seinfeld (1975)] that the basic conditions to be met for the application of equation (1.39) are:

- (i) Temporal variations of $S(\tilde{x}, t)$ and R are gradual.
- (ii) Spatial variations of $S(\tilde{x}, t)$ are gradual.
- (iii) The time scale of the reaction described by R is much larger than the lagrangian time scale τ_L of the turbulence.
- (iv) The time and space scales considered are much larger than the corresponding scales of turbulence.

Since conditions (i), (ii) and (iv) are virtually never met, (e.g. near a point source), it is clear that the application of equation (1.39) will at best be approximate.

In general, the velocities \bar{u}_i , $i=1,2,3$, and the eddy diffusivities K_i , $i=1,2,3$, are functions of position and time in the atmosphere. Letting $(x,y,z) = (x_1, x_2, x_3)$, and $(\bar{u}, \bar{v}, \bar{w}) = (\bar{u}_1, \bar{u}_2, \bar{u}_3)$, consider the case $\bar{v} = \bar{w} = 0$, and \bar{u} , K_x , K_y , K_z constant (stationary homogeneous turbulence). Then for a unit instantaneous point source $\delta(x,y,z,t)$ [Dirac delta] in an unbounded atmosphere, equation (1.39) solves to:

$$C(x,y,z,t) = \frac{1}{8(\pi t)^{\frac{3}{2}} (K_x K_y K_z)^{\frac{1}{2}}} \cdot \exp \left[-\frac{1}{4t} \left\{ \frac{(x - \bar{u}t)^2}{K_x} + \frac{y^2}{K_y} + \frac{z^2}{K_z} \right\} \right] \quad (1.40)$$

Likewise, for a continuous point source of unit rate at $x=y=z=0$,

$$C(x,y,z) = \frac{1}{4\pi x (K_y K_z)^{\frac{1}{2}}} \exp \left[- \frac{\bar{u}}{4x} \left\{ \frac{y^2}{K_y} + \frac{z^2}{K_z} \right\} \right] \quad (1.41)$$

which is valid for $x \gg \sqrt{x^2 + y^2}$. Similar expressions may be obtained from the lagrangian approach by assuming that the probability of transition of a particle from \tilde{x}' to \tilde{x} during t' to t obeys a normal distribution independent of position and time [Monin and Yaglom (1971)].

1.4.2 Eddy diffusivity for mass.

Implicit in equation (1.39) is the fact that the distribution variance $\langle X_i^2(t) \rangle$ due to spatially constant "eddy diffusivity" K_i will be given by

$$\frac{d\langle X_i^2(t) \rangle}{dt} = 2K_i \quad (1.42)$$

However, Taylor (1921) showed that for particles dispersed in stationary, homogeneous turbulence

$$\langle X_i^2(t) \rangle = \begin{cases} \overline{u_i'^2} t^2, & t \rightarrow 0 \\ 2K_i^* t, & t \rightarrow \infty \end{cases} \quad (1.43)$$

where K_i^* is a constant dependent on the lagrangian time scale τ_L . It is clear that the effective diffusivity $K_i = K_i^*$ only for large travel times; in fact for times much greater than τ_L so that the perturbation velocities have become uncorrelated. Sutton (1953) effectively interpolated between the extremes in equation (1.43) by proposing that the values

$$K_i = \frac{1}{2} C_{si}^2 \bar{u}^{2-n} t^{1-n} \quad (1.44)$$

be substituted in the solved gaussian formulae (1.40) and (1.41). The constants C_{si} and n are dependent on stability and are determined by experiment [e.g. Venter, Halliday and Prinsloo (1973), and Bierly and Hewson (1963)]. The approach of other workers is to deduce the necessary gaussian variances directly from measurements of the wind fluctuations [e.g. Eimutis and Konicek (1972), and Leahey and Halitsky (1973)].

Calder (1965) used a co-ordinate transformation of the diffusion equation (1.39) to show that the diffusivity is necessarily a second-order tensor, and that the assumptions inherent in equation (1.39), with arbitrary K_i , are that this tensor is symmetric, and that $Oxyz$ are the principle axes. He showed further that such assumptions are acceptable for isotropic diffusion $K_x=K_y=K_z$, but that in general, if the vertical is chosen as a preferred axis, it is necessary that $K_x=K_y$ for equation (1.39) to be valid.

1.5 Analytical solutions for atmospheric diffusion.

In order to understand the motivation for numerical modelling of atmospheric transport, some of the analytical solutions which are currently available are reviewed. Although the application of these solutions in real situations is limited, they serve to illustrate the effect of variable velocity and diffusivity. Moreover, certain analytical solutions are used to check the accuracy of the

proposed numerical model [Chapter (3)]. It will become evident in section(1.6.4) that few of the numerical solutions suggested by earlier workers have been evaluated in terms of accuracy. If numerical solutions differ significantly from analytical solutions based on the same equations, there is little point in providing a sound mathematical basis for numerical solutions.

The gaussian solutions (1.40), (1.41) were seen to arise from the assumptions

$$\bar{u}(z) = u_1 \text{ const.}, K_y \text{ const.}, K_z \text{ const.}$$

The existence of boundaries (ground or inversion layer) is usually accounted for by assuming total reflection. Kao (1976) noted that such reflection is still valid for uneven terrain.

1.5.1. Continuous point sources.

For a continuous, infinite crosswind line source under steady conditions, equation (1.39) reduces to the two-dimensional problem:

$$\bar{u}(z) \frac{\partial C}{\partial x} + \bar{w}(z) \frac{\partial C}{\partial z} = \frac{\partial}{\partial x} \left[K_x(x, z) \frac{\partial C}{\partial x} \right] + \frac{\partial}{\partial z} \left[K_z(x, z) \frac{\partial C}{\partial z} \right] \quad (1.45)$$

Equation (1.45) has been solved with the boundary-condition $\partial C / \partial z |_{z=0} = 0$ under a variety of conditions. In the summary presented in table (1.2), z_s is the source height, H is the height of an impervious inversion surface, and u_i, w_i, K_i, m, n, p and q are constants.

table (1.2) Continuous point source solutions.

SOURCE	\bar{u}	\bar{w}	K_x	K_z	Z_s	H
Roberts (see Calder, 1949)	$u_0 z^m$	0	0	$K_0 z^n$	0	∞
Smith (1957)	$u_0 z^m$	0	0	$K_0 z^n$	h	∞
Walters (1969)	u_0	0	$K_0 z$	$K_1 z$	0	∞
Peters and Klinzing (1971)	$u_0 z^m$	0	0	$K_0 x^n$	0	∞
Dilley and Yen (1971)	$u_0 z^m + u_1 z^n x$	$w_0 z^{n+1}$	0	$K_0 z^q$	0	∞
Heines and Peters (1973)	u_0	0	0	$K_0 x^m$	h	H_I
Lebedeff and Hameed (1976) ϕ_m after Businger <u>et al</u> (1971)	$\int \frac{u_* \phi_m dz}{kz}$	0	0	$\frac{u_* kz}{\phi_m(\zeta)}$	0	∞

The dependence of K_z on downwind distance x in the conditions tackled by Peters and Klinzing (1971) is reasonable in view of equation (1.43), and the supporting experimental evidence of Gartrell et al (1964) and Singer and Smith (1966). The requirement that the ground-level concentration should be proportional to $x^{-(m+1)(n+1)/(m+2)}$ led to the following solution for unit release rate:

$$C(x, z) = \frac{(m+2) [(n+1)u_0 / (m+2)^2 K_0]^{(m+1)/(m+2)}}{u_0 \Gamma [(m+1)/(m+2)] x^{(m+1)(n+1)/(m+2)}} \cdot \exp \left\{ \frac{-(n+1)u_0 z^{(m+2)}}{(m+2)^2 K_0 x^{(n+1)}} \right\} \quad (1.46)$$

where Γ is the gamma function. The ratio of ground-level concentrations predicted without ($m=0$) and with the power-law velocity profile is seen by equation (1.46) to be

proportional to $x^{m(n+1)/2(m+2)}$. Though this effect is small under neutral and unstable conditions ($m \leq 1/7$), the effect of wind-shear, even for a steady continuous point source, is seen to be significant under stable conditions (m up to 0,83) or over rough terrain (m up to 0,5) [Davenport (1965)].

The peculiar velocity structure used by Dilley and Yen (1971) arises from an attempt to account for the convective current over an urban heat island. Heines and Peters (1973) suggest that the effect of the inversion becomes negligible for $z_s < 0,6H_I$. In their solution for realistic flux profiles, Lebedeff and Hameed (1976) had to propose an Ansatz for the form of the distribution. An integral involving ϕ_m was derived which gave the downwind position for specified surface concentrations. Values thus obtained were fitted with a power series to give an expression for $C(x, z_0)$.

The discussed continuous point source solutions clearly rely on the absence of temporal transients. Moreover, the tractable forms of spatial velocity and diffusivity variation appear to be rather limited.

1.5.2 Instantaneous point sources.

Assuming linearity, any time-variant release in the atmosphere may be considered to constitute a closely-spaced succession of instantaneous releases of variable strength. This discretization of a release suggests a means for dealing with a temporally-variant atmosphere. However, the diffusive

expansion of clouds in shear flows is necessarily transient, and the available solutions of equation (1.39) are rather limited.

Quesada (1971) provided a solution for the expansion of a cloud in unbounded shear flow with constant velocity gradient, $(\bar{u}_1, \bar{u}_2, \bar{u}_3) = (u_0 + \alpha x_3, 0, 0)$, and constant diffusivities. Substitution of the variables

$$x'_i = x_i / \sqrt{K_i} \text{ (no summation), } \epsilon = -u_0 / \sqrt{K_1}, \beta = \alpha \sqrt{K_3} / u_0 \quad (1.47)$$

converts the appropriate form of equation (1.39) to

$$\frac{\partial C}{\partial t} = \frac{\partial^2 C}{\partial x'_i \partial x'_i} + \epsilon(1 + \beta x'_3) \frac{\partial C}{\partial x'_1} \quad (1.48)$$

The transformation

$$v_0 = x'_1 + \epsilon(1 + \beta x'_3)t \quad (1.49)$$

then allows solution of equation (1.48) for a spherically-symmetric initial distribution by taking the space Fourier Transform and integrating the resultant first-order equation in t . Allowing the variance of the initial distribution to shrink to zero, Quesada obtained the solution for a unit instantaneous point source

$$C(\tilde{x}', t) = \frac{\exp\left[\frac{-x_2'^2}{4t}\right] \exp\left[-\frac{\{v_0^2 - \epsilon\beta v_0 x'_3 t + x_3'^2(1 + \frac{1}{3}\epsilon^2\beta^2 t^2)\}}{4t + \frac{1}{3}\epsilon^2\beta^2 t^3}\right]}{8(\pi t)^{\frac{3}{2}} (K_1 K_2 K_3)^{\frac{1}{2}} \sqrt{1 + \frac{1}{3}\left(\frac{\epsilon\beta t}{2}\right)^2}} \quad (1.50)$$

However, no solution has yet been found for the same problem in bounded space.

Pasquill (1962) raised the question of the combined

effect of vertical diffusion and crosswind shear in enhancing the crosswind spread in plumes. A significant shear component may operate at right-angles to a plume as a result of the decoupling of flows under conditions of strong thermal stratification. This effect had been studied by Taylor (1953, 1954) and Aris (1956) in relation to axial dispersion in pipe flows. Saffman (1962) derived some important results for the expansion of an instantaneous ground source in bounded and unbounded surface layers. Defining the moments

$$\theta_{mn}(z,t) = \int_{-\infty}^{\infty} \int_{-\infty}^{\infty} x^m y^n C(x,y,z,t) dx dy, \quad (1.51)$$

Saffman followed Aris (1956) by multiplying through equation (1.39) by $x^m y^n$ in order to obtain equations for the moments. Assuming $\bar{w}=0$, and invoking the boundary conditions:

$$\lim_{\substack{x \rightarrow \pm\infty \\ y \rightarrow \pm\infty}} x^m y^n C = 0; \quad \lim_{\substack{x \rightarrow \pm\infty \\ y \rightarrow \pm\infty}} x^m y^n \frac{\partial C}{\partial x} = 0; \quad \lim_{\substack{x \rightarrow \pm\infty \\ y \rightarrow \pm\infty}} x^m y^n \frac{\partial C}{\partial y} = 0 \quad (1.52)$$

led to the expressions

$$\frac{\partial \theta_{00}}{\partial t} = \frac{\partial}{\partial z} (K_z \frac{\partial \theta_{00}}{\partial z}) \quad (1.53)$$

$$\frac{\partial \theta_{10}}{\partial t} = \frac{\partial}{\partial z} (K_z \frac{\partial \theta_{10}}{\partial z}) + \bar{u} \theta_{00} \quad (1.54)$$

$$\frac{\partial \theta_{20}}{\partial t} = \frac{\partial}{\partial z} (K_z \frac{\partial \theta_{20}}{\partial z}) + 2\bar{u} \theta_{10} + 2K_x \theta_{00} \quad (1.55)$$

Note that $\theta_{00}(z,t)$ will describe the distribution of mass with height, at time t . It follows that the centroid of the infinitesimal layer z to $z+dz$ will lie at $(\bar{X}, \bar{Y}) = [\theta_{10}(z,t), \theta_{01}(z,t)] / \theta_{00}(z,t)$ at time t . Likewise,

the variances about this centroid will be given by

$$\sigma_x^2 = \theta_{20}/\theta_{00} - \bar{X}^2 \text{ and } \sigma_y^2 = \theta_{02}/\theta_{00} - \bar{Y}^2.$$

The last term in equation (1.55) is the normal diffusive expansion described by equation (1.42). In the case of an unbounded surface layer with K_z constant, equation (1.53) is easily solved for unit release at $t=0$, $z=0$ to give

$$\theta_{00}(z,t) = (\pi K_z t)^{-\frac{1}{2}} \exp[-z^2/4K_z t] \quad (1.56)$$

For the case $\bar{u}(z) = \alpha z$, Saffman (1962) solved equation (1.54) using Laplace transforms to obtain

$$\theta_{10}(z,t) = \frac{\alpha t}{\sqrt{2\pi}} \exp[-\rho^2/4] \{ \rho^2 D_{-1}(\rho) + \rho D_{-2}(\rho) + D_{-3}(\rho) \} \quad (1.57)$$

where $\rho = z/\sqrt{2K_z t}$ and $D_n(\rho)$ denotes the parabolic cylinder function of order n [Whittaker and Watson (1950)]. Equation (1.55) was solved for two forms of K_x : (i) $K_x = \text{constant}$; (ii) $K_x = K_x^* z$ (K_x^* constant).

$$\begin{aligned} \theta_{20}(z,t) = & \frac{\alpha^2 (2K_z t)^{\frac{5}{2}}}{8K_z^2 (2\pi)^{\frac{1}{2}}} \exp(-\rho^2/4) \{ \rho^4 D_{-2} + \frac{10}{3} \rho^3 D_{-3} + 7\rho^2 D_{-4} \\ & + 7\rho D_{-5} + 7D_{-6} \} + \begin{cases} 2K_x (\frac{t}{K_z \pi})^{\frac{1}{2}} \exp(-\rho^2/4) \{ \rho D_{-1} + D_{-2} \}, \text{for (i)} \\ (\frac{2}{\pi})^{\frac{1}{2}} K_x^* t \exp(-\rho^2/4) \{ \rho^2 D_{-1} + \rho D_{-2} + D_{-3} \}, \text{for (ii)} \end{cases} \end{aligned} \quad (1.58)$$

It follows from equations (1.56), (1.57) and (1.58) that the x centroid and variance of the ground-level distribution will be given by

$$\bar{X}(0,t) = \frac{\theta_{10}}{\theta_{00}} = \frac{1}{4} \alpha (\pi K_z t^3)^{\frac{1}{2}} \text{ (acceleration)} \quad (1.59)$$

$$\sigma_x^2(0,t) = \frac{\theta_{20}}{\theta_{00}} - \left(\frac{\theta_{10}}{\theta_{00}} \right)^2 = \left(\frac{7}{30} - \frac{\pi}{16} \right) \alpha^2 K_z t^3 + \begin{cases} 2K_x t, \text{for (i)} \\ \frac{1}{2} K_x^* (\pi K_z t^3)^{\frac{1}{2}}, \text{for (ii)} \end{cases} \quad (1.60)$$

The first term on the R.H.S. of equation (1.60) results from the interaction of shear and vertical diffusivity. It can be shown that

$$\theta_{30}(0,t) = \frac{21}{256} \alpha^3 K_z t^4 + \text{smaller terms involving } K_x \quad (1.61)$$

so that the distribution will not be asymptotically gaussian. Saffman (1962) concluded that for large times at least, horizontal diffusion in the atmosphere will be dominated by the shear/vertical diffusion interaction effect.

Gee and Davies (1963) introduced a "shearing advection" term to account for the correlation between vertical and horizontal eddies. This term makes an additional contribution to the mass flux, leading to a 16% and 20% decrease in Saffman's values for $\bar{X}(0,t)$ and $\sigma_x(0,t)$ respectively. A second additional term suggested by Matsuoka (1961) decreases the deviation for \bar{X} and increases that for σ_x slightly. [Gee and Davies (1964)]. The new terms attempt to account for the occurrence of non-zero off-diagonal terms in the diffusivity tensor K_{ij} . However, Smith (1965) followed the statistical approach of Högström (1964) to show that the omission of these terms does not seriously alter the functional form of the solution except at short distances from the source, where the K-theory approach is invalid anyway [section (1.4.1)].

Chatwin (1968) used the lagrangian similarity hypothesis proposed by Batchelor (1964) to show that for a neutral atmosphere, $K_z = ku_*z$. Note that this is equivalent to the vertical momentum diffusivity which follows from the dimensional analysis leading to equation (1.15). Using the method of moments, Chatwin shows that for a puff released at ground-level in a neutral constant-stress region,

$$\bar{X}(z,t) \approx \bar{X}(0,t) = \bar{X}_c(t) - u_*t/k \quad (1.62)$$

$$\sigma_x(z,t) \approx \sigma_x(0,t) = 0,596 u_*t/k \quad (1.63)$$

where $\bar{X}_c(t)$ is the downwind distance to the cloud centroid. Diffusion in the neutral atmosphere has resulted in $\sigma_x \sim t$ rather than $\sigma_x \sim t^{3/2}$ according to Saffman (1962) for a linear velocity profile [equation (1.60)].

In the case of an instantaneous release in the surface layer, the only available descriptions are rather limited (linear profile; neutral atmosphere), and based on the first few moments. Some linear variations of diffusivity are possible in the linear profile solution, but general temporal or spatial variations cannot be handled in these descriptions. Even if diffusivity and velocity parameters were replaced with their time-mean values for the path of the cloud, the existence of shear in a second dimension, as the result of a temporal variation in wind direction, cannot be accounted for.

1.6 Applied studies in the estimation of atmospheric dispersion.

It will be seen that in moving from the idealised situations which may be dealt with analytically, to the real atmosphere in which not only the meteorological parameters, but the pollutant sources themselves are spatially and temporally transient, it will become necessary to make additional approximations. Not the least of these is the representation of equation (1.39) in finite-difference form, and its solution as a grid of point-values. Though this practice is common, several studies use alternative routes.

1.6.1 Statistical methods.

If large quantities of simultaneous emission, meteorology and air quality measurements are available, it should be possible to construct joint probability distributions by means of a multiple regression analysis. Thus Peterson (1972) used spatially-dependent eigenvectors to relate SO_2 observations in St. Louis, Missouri, to meteorological parameters. In a different approach suggested by Fortak (1974), the diffusion equation (1.39) could be used as a mechanistic link between cause and effect. A spectral representation of the equation would allow estimation of the frequency distribution of concentration based on stochastic dynamic weather forecasting.

1.6.2 Random motion (particle-in-cell) methods.

Atmospheric dispersion is essentially a stochastic process [Taylor (1921), section (1.4.2)], so that a more realistic approach to modelling concerns the positioning of serially-released particles in space according to random turbulent velocities [Thompson (1971), Knox (1974)]. The frequency-distributions of these velocities can be made to comply with specified stability criteria. Thus Joynt and Blackman (1976) used a virtual diffusivity $K_z^* = z\sqrt{\frac{w'^2}{2}}$ in equation (1.43) to define an ellipsoidal surface of equal probability of arrival after each time-step Δt . Applied to the steady release of SO_2 in Melbourne, the model generally over-predicted. Where concentration gradients are important, such models suffer either poor cell resolution, or prohibitive computation and storage.

1.6.3 Semi-analytical methods.

A number of approaches avoid solving the diffusion equation by adapting existing analytical solutions. For example, if wind velocity is reasonably independent of height, an emission might be assumed to constitute serially-released gaussian puffs, the trajectories of which could be obtained by lagrangian tracking (integration) in the wind-field. Lamb and Neiburger (1971) proposed such a model based on an unsheared puff which included first-order ground-absorption and chemical reaction.

Ootaki (1975) used short sections of a gaussian plume instead of puffs. Sharma (1976) adapted an earlier expression for an infinite cross-wind line source in order to predict the concentrations which would arise from area sources in Bremen, Germany.

Fabrick and Sklarew (1975) proposed a continuous point-source gaussian model in which the cross-wind concentration was assumed constant in a $22\frac{1}{2}^{\circ}$ sector. This model was adapted to curvilinear streamlines by transformation of the ground surface to leave a straight trajectory. In a comparative study, Fabrick and Sklarew suggest that a 3-dimensional finite-difference solution would be more suitable for complex wind-fields.

1.6.4 Numerical solution of the diffusion equation.

1.6.4.1 Continuous emission, steady-state models.

In applied dispersion models, a common practice is to use modern digital computers for numerical solution of some form of the diffusion equation (1.39). Thus Hino (1968) used a forward-difference approximation to model a continuous release over complex topography.

Ito (1970) assumed a log-linear wind-profile with an extension according to equation (1.28) in steady-state continuous point-source simulations for Project Green Glow. Starting with a gaussian distribution near the source, equation (1.39) was integrated by moving downwind in finite

steps Δx , checking mass-conservation after each step. Ito concluded that agreement with observations would have been better had deposition and meandering been accounted for. Roffman, Rao and Grimble (1975) were able to follow a similar approach by transforming Cartesian coordinates to a new frame in which the steady wind streamline followed one axis. Whereas these solutions were performed in two dimensions (x-z), Ragland and Dennis (1975) solved for the entire cross-wind distribution at successive downwind distances, a fully-implicit finite-difference scheme dealing most effectively with the high gradients near the source.

Ragland (1973) proposed a 2-dimensional "multiple box" model for steady-state transport from continuous area sources. Material was introduced en route by stipulating the surface concentration gradient $\partial C / \partial z |_{z=0} = -Q / K_z(0)$. A further 2-dimensional area-source model was derived by Lebedeff and Hameed (1975) using the integral method [section 1.5.1]. The solution incorporated a power-law velocity profile, but ignored diffusivity variations. Summation of the solutions for area sources along the wind's route gave better agreement with observations than the time-variant models of Randerson (1970) and Hameed (1974), for SO_2 concentrations in Nashville.

Although the steady-state models may be expected to provide better spatial resolution than the time-variant

models, it will be seen in chapter (3) that their neglect of temporal transients may lead to serious under-estimation of the area affected by airborne pollutants.

1.6.4.2. Time-variant, 3-dimensional grid models.

In order to simulate the dispersion of SO_2 over Nashville, Tennessee, Randerson (1970) used the time-variant finite-difference form of equation (1.39), which was integrated explicitly over time-steps $\Delta t = 5s$ in a 1092-point 3-dimensional grid. The solution used a steady-state wind-field, extrapolated from four point-measurements in the 12 mile \times 13 mile area. These measurements were extended in the vertical using logarithmic velocity profiles (1.15). Vertical velocities induced by topography (and implied wind-field divergence) were obtained by solving a finite-difference form of the continuity equation (1.10). Representing area sources as a number of point-sources at the top boundary (60 m) of his system, Randerson obtained fair agreement with observations of SO_2 concentration. Though Δt and Δz were chosen to satisfy the von Neumann condition for stability,

$$\Delta t \leq \frac{\Delta z^2}{2K_z}, \quad (1.64)$$

the choice of $\Delta x = \Delta y = 1$ mile would have led to gross errors in horizontal diffusive fluxes, and a large "pseudo-diffusion" contribution as a result of the finite-difference solution for advection.

Inclusion of the advection terms $\bar{u}_j \partial C / \partial x_j$ in finite-difference representations generally leads to substantial additional error [Molenkamp (1968), Crowley (1968)]. This has led several workers to treat the advection process separately as a lagrangian integration [Runca and Sardei (1975), Sklarew (1970)]. However, pseudo-diffusion errors can persist in these schemes as a result of interpolation for the point-or-origin of material arriving at a grid-point.

Egan and Mahoney (1972 a) proposed a model for the transport from large area sources, in which the pseudo-diffusive errors were eliminated by locating the mass-distribution relative to a grid-point using the zeroth, first and second moments. The model neglected horizontal diffusion, but accounted for vertical diffusion using a simple forward-difference (explicit) finite-difference scheme. Egan and Mahoney (1972 b) extrapolated the Businger-Dyer profile relationships (1.29), (1.30) to describe $\bar{u}(z)$, $K_z(z)$ throughout the planetary boundary-layer. Inclusion of the Coriolis directional shear following Blackador (1962) resulted in effective horizontal diffusivities, based on the entire distribution, which were about 8 times the maximum vertical diffusivity under neutral conditions. As observed by Csanady (1972), however, the effect on the ground-level cross-wind distribution, after 30 minutes of travel, was relatively small. Egan and Mahoney found that almost any spatial or temporal change in wind direction greatly enhanced horizontal spread.

Shir and Shieh (1974) followed a similar approach to Randerson (1970), using a full 3-dimensional finite-difference solution for the modelling of SO_2 distributions in St. Louis. Wind-fields were interpolated using the method of Wendell (1972) [equation (1.35)], and extended in the vertical using power-law forms, the vertical component then being solved for by continuity. Solutions were performed in a $30 \times 40 \times 14$ -point grid, with the 30×40 horizontal positions spaced at intervals of 1 mile. Though such coarse spacing gave very poor horizontal resolution, it led to easy satisfaction of the numerical stability conditions for horizontal diffusion and advection in the central-difference Crank-Nicholson scheme [Ritchmyer and Morton (1967)]:

$$\Delta t K_h / (\Delta x^2 + \Delta y^2) \leq \frac{1}{4} \text{ and } \bar{u} \Delta t / \Delta x < 1, \bar{v} \Delta t / \Delta y < 1 \quad (1.65)$$

The large horizontal stepsizes used by Randerson (1970) and Shir and Shieh (1974) arise mainly from computation and storage limitations. The associated numerical errors will be accompanied by significant errors due to poor resolution near sources, and poor terrain and wind-field definition downwind. However, these applications dealt with large area sources, so that errors in horizontal transfer would have manifested themselves to a lesser extent than in the case of point-sources.

1.6.4.3 Time-variant, vertical cell models.

Hameed (1974b) modelled the dispersion of SO_2 in Nashville, Tennessee, during the same 2-hour period as Randerson (1970), using the same wind-field and emission data. However, the surface layer was simulated using adjacent unbounded vertical cells, in which the 1 mile \times 1 mile bases formed spatially-variant ground-level area sources. By postulating the vertical distribution, $C(z) = C_0 \exp[-z^2/2\sigma_z^2]$ with σ_z a power-law function of distance downwind, Hameed accounted for unbounded vertical diffusion. The ground-level concentration C_0 for each cell was solved for by using a mass-balance which included the advection of the vertical distribution through a logarithmic velocity profile. Though the model neglected horizontal diffusion, and only approximated the effect of differential transport with height, results compared favourably with those of Randerson (1970), probably due to Randerson's low ceiling height of 60 m.

Simple "trajectory" models, in which the transport is simulated using serially-released homogeneous vertical columns of air, have been used by Leahey (1975) for the modelling of NO_x pollution in Edmonton, and Chu and Seinfeld (1975) for the modelling of photochemical aerosols above Los Angeles. The columns have finite height determined by an inversion lid, and are transported along trajectories by lagrangian integration, in time and space, of representative mean velocities. These models clearly ignore wind-shear, horizontal diffusion, and finite vertical diffusion, but

occasionally allow consideration of important effects such as the aerosol chemistry covered by Chu and Seinfeld.

Liu and Goodin (1976) considered stationary, homogeneous vertical cells trapped beneath an inversion layer, the variable height of which was determined using a correlation due to Neiburger (1974). The wind-field was interpolated from observations using a method which reduced divergence [section (1.3.2)]. Four different numerical schemes were used to solve the diffusion equation (1.39) for the 2-dimensional eulerian grid, producing widely divergent results. These deviations probably arose from different capabilities in handling the large pseudo-diffusion effects in the 3200 m-integral grid, and highlight the necessity of providing a general accuracy check for any numerical solution.

1.6.4.4 Instantaneous point-source models.

Whereas the steady-state point-source models in section (1.6.4.1) were able to provide good spatial resolution, the time-variant grid models in section (1.6.4.2) were really only suitable for area-source applications. The combined inclusion of both vertical structure (velocity and diffusivity profiles) and temporal variations is severely hampered by present-day computation and storage limitations. Few workers have attempted to define the transient and localised distributions resulting from instantaneous releases under typical conditions.

Observations for instantaneous point sources have been given by Nickola (1970, 1971) and for instantaneous line sources by Drivas and Shair (1974). The latter workers compared observed time-history moments with the asymptotic Lagrangian moments proposed by Chatwin (1968) and Saffman (1962), claiming good agreement with Saffman [section (1.5.2)].

Tyldesley and Wallington (1965) used both analogue and numerical techniques to solve the moment equations (1.53), (1.54) and (1.55) for an instantaneous ground-level release, with arbitrary velocity and diffusivity profiles. Using a linear velocity profile and constant vertical diffusivity, good agreement was obtained with Saffman's asymptotic relations (1.59), (1.60) for an unbounded surface layer. In considering plume data assembled by Pasquill (1961), it was found that observed cross-wind spreads at distances as short as 1 km could arise entirely from relatively small cross-wind velocity gradients in the surface layer. Such gradients might occur with the stratification of the atmosphere under strongly stable conditions.

Instantaneous line-source experiments were conducted over distances of 3-5 km. Though the velocity profile was measured, Tyldesley and Wallington estimated the diffusivity profile by best fit of predicted to observed vertical distributions. The solved moments were used to reconstruct a time-history of vertical distribution which agreed reasonably with Eulerian observations, showing that the large along-wind spreads could be attributed almost entirely to the interaction of shear and vertical diffusion, even at

relatively short ranges.

Runca and Sardei (1975) presented a 2-dimensional (x-z) finite-difference model for a time-variant point source with arbitrary velocity and diffusivity profiles. In order to circumvent the advective stability criteria and pseudo-diffusion, the advection equation

$$\frac{\partial C}{\partial t} + \bar{u}(z) \frac{\partial C}{\partial x} = 0$$

was solved separately as a stratified lagrangian shift,

$$\frac{\partial C[X(z,t), z, t]}{\partial t} = 0 \text{ with } X(z,t) = X(z,t_0) + \int_{t_0}^t \bar{u}(z) dt' \quad (1.66)$$

However, numerical diffusion will persist unless material leaving a grid-point arrives exactly at a grid-point, so that Runca and Sardei approximated the wind-profile with a step-function designed for this purpose. The diffusion step was solved in the fixed (eulerian) grid, using the implicit Crank-Nicholson method. Using a gaussian distribution at the source (seed), and variable z-stepsizes, good agreement was obtained with an analytical solution of Rounds (1955) for a continuous point source with $\bar{u} = z^m$, $K_z = z$.

The instantaneous point-source studies discussed in this section, as well as the moment descriptions of Saffman (1962) and Chatwin (1968) [section (1.5.2)], all demonstrate the importance of wind-shear as a redistribution mechanism.

Although the effect of shear is significant in steady-state continuous releases [section (1.5.1)], it does not manifest itself as dramatically. A temporal variation in either emission rate or wind-direction is required to reveal the underlying form of constituent clouds.

1.7 Diffusion of heavy particles.

Ambient particles (or gas molecules) might be expected to display an identical transport behaviour to that of the air parcels themselves. Besides the obvious sedimentation characteristics of heavy particles, however, their inertia will give a slow response to turbulent eddies, whilst settling will act further to introduce them to new eddies.

If a particle size d_p is small enough to obey Stokes Law, it will accelerate from rest ($t=0$) in a stream of constant velocity u according to

$$u_p = u[1 - e^{-\beta t}] \quad \text{with } \beta = 3\mu_f \pi d_p / m_p \quad (1.67)$$

where m_p is the particle mass and μ_f the fluid viscosity. The position of a small particle starting from \tilde{x}_0 at $t=0$ may thus be approximated by

$$\tilde{y}(x_0, t) = \tilde{x}_0 + \int_0^t [1 - e^{-\beta(t-\tau)}] \tilde{u}[\tilde{y}(\tilde{x}_0, \tau), \tau] d\tau \quad (1.68)$$

For random eulerian turbulent velocities, this is a non-linear stochastic equation. Peskin (1971) showed that a "best estimate" of the acting velocity \tilde{u} could be expressed as the lagrangian velocity of a nearby reference fluid

particle modified by the eulerian velocity correlation between the solid particle position and the fluid particle position. In stationary isotropic turbulence the eulerian correlation $R_E(\tilde{y}, \tilde{x}) = R_E(|\tilde{y} - \tilde{x}|)$, and if $\Delta = |\tilde{y} - \tilde{x}|$ is small, R_E may be expanded as

$$R_E(\Delta) \approx 1 - \frac{\Delta^2}{L_E^2} + \dots \quad (1.69)$$

where L_E is the eulerian length scale. Peskin assumed that the lagrangian velocity correlation could be expressed in the exponential form

$$R_L(\tau) = \exp[-\tau/\tau_L] \quad (1.70)$$

where τ_L is the lagrangian time-scale. Squaring and averaging equation (1.68), and substitution of equations (1.69), (1.70) then yielded an expression for the variance of particle position. The ratio of particle diffusivity to fluid diffusivity was thus derived as

$$\frac{K_P}{K_F} = 1 - \frac{L_L^2}{2L_E^2} \left(\frac{3B^2}{B+2} \right) + O(\Delta^4) \quad (1.71)$$

where $B = 2/\beta\tau_L$, and the lagrangian length scale $L_L = \tau_L \sqrt{v'^2}$ with v' the lagrangian turbulent velocity.

In a gravitational field, an additional important effect operates in that a particle in free-fall is similarly forced to experience regions of differing correlation. Obtaining the zero-fall particle energy spectrum from the fluid energy spectrum by multiplying by a "particle response function" after Soo (1967), Meek and Jones (1973)

converted to the free-fall spectrum by assuming a simple frequency-shift. Integration then yielded the particle velocity autocorrelation, and a further integration [Taylor (1921)] gave the variance of particle position. In this way the particle to fluid diffusivity ratio for direction i was derived as

$$\frac{\kappa_{pi}}{\kappa_{Fi}} = \frac{\tau_{LPi}}{\tau_{LFi}} \cdot \frac{[1 - \exp(-t/\tau_{LPi}) - \epsilon_i^2 \{1 - \exp(-t/\epsilon_i \tau_{LPi})\}]}{(1 - \epsilon_i^2) [1 - \exp(-t/\tau_{LFi})]} \quad (1.72)$$

where

$$\epsilon_i = 1/\beta \tau_{LFi}, \quad \tau_{LPi} = \tau_{LFi} \left[1 + \frac{w_{si}}{u_{pi}'} \right]^{-\frac{1}{2}},$$

$$\overline{u_{pi}'^2} = \overline{u_{Fi}'^2} / (1 + \epsilon_i) \quad (1.73)$$

and w_{si} is the sedimentation velocity in direction i , τ_{LP} and τ_{LF} are the particle and fluid lagrangian time-scales according to equation (1.70), and u_{pi}' , u_{Fi}' are the particle and fluid turbulent velocity components in direction i .

For zero-fall velocity, $\tau_{LPi} = \tau_{LFi}$, and in the limit $t \rightarrow \infty$, the diffusivity ratio (1.72) reduces to unity, independent of inertia. Hence this result is fundamentally different to equation (1.71) due to Peskin (1971). In general, however, turbulence is not homogeneous, and a falling particle is likely to enter regions in which the lagrangian velocity correlations behave quite differently.

1.8 Macroscopic effects.

A number of influences may act on the concentration field as a whole, causing significant redistribution.

Fosberg, Fox, Howard and Cohen (1976) followed Roberts (1923) to show that for constant along-wind divergence $\delta_w = \nabla \cdot \tilde{u}$, the gaussian plume formula (1.41) must be corrected by a factor $\exp(-\delta_w x / \bar{u})$. Mesoscale divergences up to $\pm 10^{-3} \text{ s}^{-1}$ were estimated over complex topography, accounting for up to a factor of 2 variation in concentration.

A study of the effect of a single large obstacle on the distribution of material from a point-source was conducted by Caput, Belot, Guyot, Samie and Seguin (1973). Both the concentration and deposition of released uranine particles were observed to drop behind a flat wind-break.

Many workers have considered the effect of emission momentum and buoyancy on determining the initial rise of a plume. Briggs (1972) pointed out that several investigators [Scorer (1958), Briggs (1964, 1969), Slawson and Csanady (1967), Fay, Escudier and Hoult (1969) and Schwartz and Tulin (1971)] agree on a 2/3-power law for buoyancy-dominated plume-rise in neutral and stable surroundings:

$$\Delta H_p(x) \sim F^{1/3} x^{2/3} / \bar{u} \quad (1.74)$$

where F is the buoyancy flux. The inclusion of a strong momentum contribution in the numerical solution due to Rao, Lague, Egan and Chu (1975) gave only slight deviations from the 2/3 power-law.

1.9 Removal mechanisms.

1.9.1 Sedimentation.

The terminal velocity of a particle which obeys Stokes' law will be

$$w_s = \rho_p g d_p^2 / 18 \mu_a \quad (1.75)$$

where d_p is the effective Stokes diameter of the particle, and the buoyancy contribution of the air has been neglected ($\rho_p \gg \rho_a$). Most attempts at including this effect in descriptions of atmospheric transport have centred on modifications to the gaussian equations (1.40), (1.41). For example, Baron, Gerhard and Johnstone (1949) replaced z with $z + w_s x / \bar{u}$ in both the objective and image terms, further multiplying the image terms by a factor $\alpha < 1$ to allow for progressive depletion. The adjustment of the z -coordinate would effectively decline a plume at $\tan^{-1}(w_s / \bar{u})$.

For steady release from an infinite cross-wind line source, the diffusion equation (1.39) becomes

$$\bar{u} \frac{\partial C}{\partial x} = \frac{\partial}{\partial z} [K_z \frac{\partial C}{\partial z}] + w_s \frac{\partial C}{\partial z} \quad (1.76)$$

Rounds (1955) gave a solution for an elevated source, with $\bar{u}(z) = u_0 z^m$ and $K_z = K_0 z$. However, depending on the surface "build-up", there is the possibility of resuspension of particles (or desorption of gases) [Slinn (1976)].

1.9.2 Ground-level absorption.

For smaller particles, particularly in the sub-micron range, ground deposits are often measured which cannot be accounted for by Stokesian sedimentation. An effective deposition velocity w_d is usually expressed as the ratio of the rate of deposition per unit area to the ground-level concentration. Chamberlain (1961) suggested that particles of terminal velocity 10^{-6} ms^{-1} or less may have deposition velocities of 10^{-4} - 10^{-3} ms^{-1} . Since these particles are essentially supplied by vertical diffusion, it follows that

$$K_z \frac{\partial C}{\partial z} \Big|_{z=0} = w_d C \Big|_{z=0} \quad (1.77)$$

which is analogous to the diffusion-controlled absorption of a gas. Gifford and Pack (1962) found clear differences between the deposition rates of chemically active and inert radionuclides, whilst grass and sagebrush effected rates which were an order-of-magnitude larger than those measured on bare soil or flat plates. Clough (1975) found that particle deposition on moss and grass surfaces was dependent on particle size and wind velocity.

Using equation (1.77) as a boundary-condition, Tang (1969) provided an analytical solution for an elevated cross-wind line source with $\bar{u}(z) = \text{const}$, $K_z(z) = K_0 z^2$. However, it is commonly assumed that the rate of vertical spread of the cloud is large in comparison with w_d , in which case the shape of the vertical distribution remains unaltered by the deposition process. The source-strength term in the

gaussian distribution (1.41) may then be replaced with one which decreases downwind.

Owers and Powell (1974) used SO_2 labelled with radioactive ^{35}S to measure deposition directly, concentrations being measured at 0,2 m. Measurements over 9-13 cm grass gave $w_d=0,007 \text{ ms}^{-1}$, whilst w_d for a 1,7 m-high hedge was $0,049 \text{ ms}^{-1}$, based on its plan area. The latter case would clearly lead to a significant distribution of absorptivity with height. Over 30 mm grass, Shepherd (1974) obtained $w_d=0,008 \text{ ms}^{-1}$ (summer), $0,003 \text{ ms}^{-1}$ (winter).

In the absorption of a gas, it is possible that the surface concentration approaches the gas-phase equilibrium value, in which case the boundary condition (1.77) must be replaced by the reversible form:

$$K_z \frac{\partial C}{\partial z} \Big|_{z=0} = K_0 \left[C \Big|_{z=0} - C_E \right] \quad (1.78)$$

where K_0 is a constant (dependent on Henry's Law constant for a dilute liquid) and C_E is the gas-phase equilibrium value. Heines and Peters (1974) provided an analytical solution for an elevated cross-wind line source with the boundary-condition (1.78) and $\bar{u}(z) = \text{const}$, $K_z = K_0 x^n$.

1.9.3 Washout.

In rainfall, the absorbing medium becomes evenly distributed with height. An originally uniform layer will become asymmetric with ground absorption, whereas an originally non-uniform layer may be redistributed through reversible absorption by rain-drops.

The ability of rain to collect particulate material will depend on collision efficiencies as well as concentrations and size distributions for both drops and particles. The process is assumed irreversible, and is represented by a washout coefficient Λ , which is the fraction of particles removed per unit time [Chamberlain (1953)]. Since removal is uniform with height, the effect may be represented as an effective decrease in source strength,

$$Q(x) = Q(0) \exp[-\Lambda x/\bar{u}] \quad (1.79)$$

An effective washout coefficient may be defined for gases. Such values of Λ for sulphur dioxide and iodine lie mostly between those for particles of terminal velocity $0.0005 - 0.001 \text{ ms}^{-1}$ [Pasquill (1968)]. Again, the possibility of reversible absorption arises - and is realistic in view of the small volume of a raindrop. Defining a reversible washout coefficient Λ_r , the removal rate per unit volume becomes

$$R_w = \Lambda_r [C - C_E] \quad (1.80)$$

Hales (1972) pointed out that Λ_r will be proportional to the droplet surface area and the overall mass-transfer coefficient K_G based on the gas-phase driving force. Slinn (1974) also accounted for mass-transfer within the raindrops, in an analytical solution for the downwards redistribution of a plume by reversible absorption in rainfall.

Scriven and Fisher (1975) proposed a continuous point source box model which included an absorptive deposition

velocity w_d and irreversible washout according to Λ . A similar divergent box model was used by McMahon, Denison and Fleming (1976) in order to estimate the "wet" (Λ) and "dry" (w_d) deposition of atmospheric SO_2 and NO_x in the Great Lakes of North America.

1.9.4 Chemical reaction and radioactive decay.

The diffusion equation (1.39) will only remain linear provided the source/sink term $R(C)$ remains linear, or first-order, in C . Seinfeld (1975) discussed the general case in which the considered species may react with other airborne species, and Lamb (1973) proposed conditions of validity for equation (1.39) when R represents a second-order process. Though higher order processes are easily included in numerical solutions, the doubt really arises over the validity of the description R when the concentration is a random variable determined by turbulence.

For an irreversible first-order process the rate term may be expressed as

$$R(C) = -k_1 C \quad (1.81)$$

where k_1 is a rate-constant. Studies by Meetham (1950) and Gartrell, Thomas and Carpenter (1963) suggest a value $k_1 = 4,274 \times 10^{-5} \text{ s}^{-1}$ for industrial SO_2 . Values for radioactive decay may be calculated from quoted half-lives. A gaussian solution including first-order chemical reaction has been given by Fortak (1974).

1.10 Considerations in the modelling of atmospheric dispersion.

1.10.1 Accuracy.

In the consideration of any proposed model for atmospheric transport processes, two important questions should arise:

- (1) To what extent will the assumptions made in the formulation of the model affect its performance under the conditions to which it will be applied?
- (2) How precisely does the model compare with the theoretical solution it purports to provide? (Numerical accuracy; or non-asymptotic behaviour in the case of some analytical solutions).

With regard to the intrinsic accuracy of numerical solutions, the existence of stability criteria has been discussed [Section (1.6.4)]. Though such conditions may prevent rapid divergence of the solution, they do not guarantee accuracy. In general, the accuracy of numerical schemes is best checked by comparison with known analytical solutions in the range of application. The inclusion of advection terms in a finite-difference scheme incurs an additional accuracy burden, usually resulting in appreciable "pseudo-diffusion". Molenkamp (1968) assessed the performance of a number of finite-difference schemes by applying them to the advection equation:

$$\frac{\partial C}{\partial t} = -\bar{u} \frac{\partial C}{\partial x} - \bar{v} \frac{\partial C}{\partial y}$$

The system considered was a concentration field represented by equally-spaced concentric isopleths, which was subjected to constant angular velocity in the x-y plane. Accuracy after a fixed time-interval was determined by deviation from the original pattern. The forward-difference ("upstream", explicit) schemes commonly used in dispersion models were found to generate pseudo-diffusion of the same order as atmospheric diffusion.

Centred-difference schemes ("leap-frog", Lax-Wendroff, Arakwa-Euler, Arakwa-Adams-Bashforth) all produced displacements of the pattern, and became inaccurate and unstable for larger stepsizes. Only the Roberts-Weiss method was free of appreciable error, but required 4 times as much storage and 10-40 times as much computer time as other schemes.

Considering linear advection, if $\bar{u}\Delta t/\Delta x \ll 1$ (stability condition), the forward-difference approximation is equivalent to the expansion:

$$\frac{\partial C}{\partial t} = -\bar{u} \frac{\partial C}{\partial x} + \left\{ \frac{\bar{u}\Delta x}{2} \left(1 - \frac{\bar{u}\Delta t}{\Delta x} \right) \right\} \frac{\partial^2 C}{\partial x^2} + \text{higher order terms...}$$

in which the pseudo-diffusivity is positive. Liu and Seinfeld (1975) point out that this is the primary source of error in fixed-grid eulerian models. "Trajectory" models, in which a vertical column of air is translated in a lagrangian sense, do not suffer from horizontal numerical diffusion. However, they neglect the wind profile, horizontal eddy diffusion and vertical velocity. Liu and

Seinfeld used some of the analytical solutions discussed in section [1.5.1] to gauge the effect of omitting these three processes, obtaining deviations of up to 50%, 10% and 1000% respectively under typical conditions.

In order to assess the numerical error occurring in a grid model, a comparison was made between 1st.- and 2nd.-order forward-difference solutions, and an analytical solution for randomly-distributed area-sources. Liu and Seinfeld (1975) found that harmonic deviations of up to 50% grew with distance downwind, the error being greater for the 1st.-order model. A smooth source-distribution reduced deviations to $\pm 20\%$.

1.10.2 Rationale.

The benefits of air-quality models for the planning of industrial sites and the establishment of pollution cause-effect relationships are well-accepted. The only important questions remaining concern returns for refinement. It has been seen that atmospheric transport is a random process, the nature of which is determined by a vast number of spatially- and temporally-variant parameters. Even if one accepts that the diffusion equation (1.39) may be used as an approximate deterministic description of the process, it is impossible to provide continuous, accurate velocity and diffusivity information. Further, since the equation itself is not generally soluble, its application involves various degrees of approximation. For a particular applica-

tion, it should be possible to place these approximate forms on a scale extending from "sophisticated" solutions which account for all important phenomena, thus requiring detailed meteorological and source input, to "crude" solutions which account only for basic effects such as source-strength and wind-speed, and hence do not warrant detailed input.

Any solution may be measured in terms of computation, and there is a rough rule-of-thumb that computation increases with sophistication. Since computer-time and the acquisition of input data will involve specifiable costs, any model may be subjected to a cost-benefit analysis. Though returns may diminish with increasing sophistication, there is a strong feeling [Hameed (1974a)] that it is necessary to link the underlying physical causes to the observed effects, if a model is to be generally applicable.

The detailed input information required by sophisticated models is becoming more available - from a proliferation of air-monitoring devices in pollution-conscious cities, and occasionally from environment impact assessments for remote sources. Moreover, Fortak (1974) points out that modern methods of stochastic dynamic prediction will eventually allow statistical forecasts, one or two days in advance, of mesoscale meteorology, whilst the deterministic prediction of mesoscale wind-fields shows promise as a source of detailed advance information [e.g. Scholtz and Brouckaert (1976), section (1.3.1)].

Ruff and Fox (1974) also recognise the need for high-quality input data in advanced modelling. In a feasibility

study, they advocate the accumulation of a vast data-base for St. Louis, involving more than one million air-quality, emission and meteorological measurements daily for two years. The information would be made available for the comparison and validation of dispersion models. In a comparative study using an earlier data-base for St. Louis, three models of varying sophistication were applied to SO_2 dispersion. The grid model of Shir and Shieh (1974) [section (1.6.4.2)] produced closest predictions, accuracy decreasing for a simple box model, and the gaussian plume model. Comparison of the gaussian model with a grid model for CO dispersion in Los Angeles also led to the conclusion that model performance improved with sophistication.

The low horizontal concentration gradients associated with area sources prompted Halliday and Venter (1971) to suggest that area-source dispersion could be modelled by the simple relation

$$C \sim Q/\bar{u}$$

where Q is the area-source strength. It was claimed that this model performed as well as the 3-dimensional finite-difference solution of Randerson (1970) [section (1.6.4.2)], using the same data-base for SO_2 dispersion in Nashville. Gifford and Hanna (1973) endorsed the comments of Halliday and Venter, and suggested that since concentrations result largely from the nearest sources, a "box" approach could be used in which the concentration in a cell could be related to Q/\bar{u} for that cell by

$$C = C_A Q / \bar{u} \quad (1.82)$$

where C_A is an average proportionality constant. Analysis of data from 44 U.S. cities led to a value of $C_A = 225$ for particulate material, and 50 for SO_2 . The low value for SO_2 was attributed to the high sources supplying SO_2 , and its decay in the atmosphere.

Hameed (1974a) suggested that the large spread in C vs Q/\bar{u} data used to obtain C_A is indicative of other important phenomena, and that the data are anyway better represented by a straight-line fit with a substantial intercept, instead of the simple proportionality of equation (1.82). With regard to a comparison with the SO_2 results of Randerson (1970), in which it proved necessary to use $C_A = 50$ to obtain fair comparison, Hameed (1975) remarked that it would be necessary to assume an excessively high decay rate to justify deviations from the particulate value $C_A = 225$. Further, the multiple cell model [Hameed (1974b), section (1.6.4.3)] and the integral method [Lebedeff and Hameed (1975), section (1.6.4.1)] both produced good comparison with the Nashville observations without having to include any removal mechanisms. Hameed concluded that simple models are to be preferred if they consistently produce results which are as good as those of complex models, but that the necessity to explain the underlying physical processes cannot be avoided.

Benarie (1975) points out that since annual-average data were used by Gifford and Hanna (1973) to evaluate C_A

in equation (1.82), this is basically a statistical model best suited for predicting annual averages, and comparison with other models for the 2-hour period in Nashville is fortuitous. He suggests that such comparisons need to account for far more than just the amount of computation required in each case.

For a single point source, simplifying assumptions of this type will be far less effective. Indeed, no general model has been found for the case of a variable point-source in a spatially and temporally variable environment. Such models as have been proposed suffer from poor resolution, or involve important simplifications. Although an advanced model would require detailed meteorological input to be completely effective, it would provide the best possible estimate based on available information. The development of a general model which provides acceptable resolution and pays due regard to the fundamental transport processes would establish the significance and origin of errors associated with simpler models in real applications. Such a study would provide both a versatile tool and a means of verifying simpler results when there is cause for doubt.

CHAPTER 2

FORMULATION OF A GENERAL DYNAMIC MODEL FOR ATMOSPHERIC POINT-SOURCES

2.1 Objectives.

To avoid the inherent resolution/accuracy problems associated with eulerian finite-difference solutions, it will be necessary to provide the concentration distribution on a "sub-grid" scale. Probably the only means of doing this is by following material as it disperses, excluding regions which are in no way affected by the distribution. In the case of a linear form of the diffusion equation (1.39), the dispersing material will not interact with itself in any way. Hence a time-variant release may be considered to constitute serially-released instantaneous puffs of varying strength. An obvious conclusion is that if individual puffs could be followed as integral lagrangian parcels, it should be possible to reconstruct a detailed concentration distribution by superposition. Largely as a result of extreme shear, and the complexity of time-variant wind-fields under stable conditions, it will be found that the modelling of single puffs may reduce to consideration of a substantial part of the region of interest. Hence some important departures from the usual methods will be necessary if this approach is to be made tractable.

The field-measurements of Nickola (1970, 1971), Drivas and Shair (1974) and Tyldesley and Wallington (1965)

have shown that the ground-level concentration distribution of a single puff becomes elongated in the along-wind direction as a result of the interaction of wind-shear and vertical diffusion. This effect is associated with a considerable downwind displacement of material at greater heights. It should be noted that if a second shear component acts at right-angles to this distribution, the cloud will begin to spread in a second dimension, affecting a large area at ground-level (cross-wind shear).

It is possible that the two shear components act simultaneously, for example when a directional shear is determined by the Ekman effect. However, Csanady (1972) suggests that the Ekman effect is unlikely to influence the ground-level distribution significantly over medium ranges of travel (30 km), and that significant cross-wind shear contributions are more likely to result from the stratification of local flows under stable conditions. Since the spatial and temporal variations of such structured flows could only be established by repeated vertical sounding throughout the region, this information is generally not available. Hence the present approach ignores the possibility of simultaneous shear in two dimensions by assuming that wind direction is uniform with height. Major two-dimensional shear contributions will nevertheless result from the consecutive action of differing shear directions, as in the case of a time-variant wind-field, and the proposed model accounts for this important redistribution effect.

In order to reduce the computation requirements for the sheared puff solution, individual puffs were represented by their zeroth, first and second moments about a curvilinear vertical surface. Horizontal wind-shear was resolved into components parallel to the surface and normal to the surface. Whereas shear and diffusion effects parallel to the surface were accounted for by numerical solution for the zeroth moment, the corresponding effects at right-angles to the surface could only be expressed in terms of the numerically-solved first and second moments. The latter moments determined only the mean and variance of the displacement from any point in the surface, thus limiting the reconstructed distribution normal to the surface at this point to a gaussian form. Although such a description of the cloud will include the effects of both horizontal shear components, Saffman (1962) has pointed out that the third moment in a shear direction will be significant, with the ground-level skewness approaching unity in the case of a linear wind profile. Hence an early objective in the formulation of the present model was to define the locating surface in such a way that it lay parallel to the dominant shear component. In this way, dependence on the less accurate moment description was minimised.

2.2 Theory.

2.2.1 Distribution in the eulerian frame.

Consider the lowest layer of the atmosphere which is the predominant transport medium for pollutants. Provided that surface heat sources and topographical features do not depart too strongly from their means, a first approximation would be to assume that wind velocity is everywhere parallel to the local ground surface. This clearly neglects the vertical velocities induced by strong urban heat islands [Dilley and Yen (1971), section (1.5.1)] and those associated with convergent "cresting" over hills. However, it is expected that definition of spatial concentration gradients will play a far more important role than the minor overall variations resulting from vertical velocity. With this assumption, transformation to a coordinate system which has a fixed vertical datum ($z=0$) at ground level reduces the diffusion equation (1.39) to the form:

$$\begin{aligned} \frac{\partial C}{\partial t} + \bar{u}(x,y,z,t) \frac{\partial C}{\partial x} + \bar{v}(x,y,z,t) \frac{\partial C}{\partial y} &= \frac{\partial}{\partial x} \left[K_x(x,y,z,t) \frac{\partial C}{\partial x} \right] \\ &+ \frac{\partial}{\partial y} \left[K_y(x,y,z,t) \frac{\partial C}{\partial y} \right] + \frac{\partial}{\partial z} \left[K_z(x,y,z,t) \frac{\partial C}{\partial z} \right] + w_s \frac{\partial C}{\partial z} \\ &+ R(C,x,y,z,t) + S(x,y,z,t) \end{aligned} \quad (2.1)$$

where a sedimentation term has been included as in equation (1.76), to account for constant settling velocity w_s . Consider only the case in which there is no initial distribution, and all material in the atmosphere has been introduced

according to the source function S (zero-state response).
A necessary boundary-condition is then

$$\lim_{x,y \rightarrow \pm\infty} C(x,y,z,t) = 0 \quad (2.2)$$

The solution of equation (2.1) may be expressed in terms of the Green's function $G(x-x', y-y', z-z', t_1)$ which satisfies the equation

$$\begin{aligned} \frac{\partial G}{\partial t_1} + \bar{u} \frac{\partial G}{\partial x} + \bar{v} \frac{\partial G}{\partial y} &= \frac{\partial}{\partial x} \left[K_x \frac{\partial G}{\partial x} \right] + \frac{\partial}{\partial y} \left[K_y \frac{\partial G}{\partial y} \right] + \frac{\partial}{\partial z} \left[K_z \frac{\partial G}{\partial z} \right] \\ &+ w_s \frac{\partial G}{\partial z} + R(G, x, y, z, t_1) \end{aligned} \quad (2.3)$$

with an initial condition.

$$G(x-x', y-y', z-z', 0) = \delta(x-x')\delta(y-y')\delta(z-z') \quad (2.4)$$

where $t_1 = t-t'$ and $\delta(s)$ is the Dirac delta function defined by

$$\delta(s) = 0, \quad s \neq 0; \quad \int_{-\infty}^{\infty} \delta(s) ds = 1$$

In general, G will be dependent on more than just the deviations from initial values. If the Green's function obeys all boundary conditions imposed on $C(x,y,z,t)$, it is possible to relate $C(x,y,z,t)$ to $S(x,y,z,t)$ according to

$$C(x,y,z,t) = \int_{-\infty}^{\infty} \int_{-\infty}^{\infty} \int_0^{\infty} \int_{-\infty}^t G(x-x', y-y', z-z', t-t') S(x', y', z', t') dt' dz' dy' dx' \quad (2.5)$$

It follows that if $S(x', y', z', t') = \delta(x'-x'')\delta(y'-y'')\delta(z'-z'')\delta(t'-t'')$ then $C(x,y,z,t) = G(x-x'', y-y'', z-z'', t-t'')$ —

i.e. Green's function represents the concentration at (x,y,z,t) resulting from an instantaneous point source located at (x'',y'',z'') which emits at t'' . In particular, for a single point source at (x'',y'',z'') with strength $Q(t)$,

$$C(x,y,z,t) = \int_{-\infty}^t G(x-x'',y-y'',z-z'',t-t')Q(t')dt' \quad (2.6)$$

which is simply a mathematical statement that a continuous release may be simulated by superposition of puffs.

2.2.2 Coordinate transformations.

In the modelling of single puffs it will prove advantageous to limit the region to be considered to some "neighbourhood" of the puff. Because of the usual dominance of one linear dimension in the distribution, it is convenient to introduce a preliminary transformation. Consider the curvilinear vertical surface which projects onto the xy plane as the curve

$$P(x,y,t)=0 \quad \text{for } x_1 < x < x_2, y_1 < y < y_2 \quad (2.7)$$

at time t . Assume that there exists a unique transformation \tilde{T}_p with inverse \tilde{T}_p^{-1} which maps $[x; x \in (x_1, x_2), y; y \in (y_1, y_2), z, t]$ into the domain $[\xi; \xi \in (\xi_1, \xi_2), \eta; \eta \in (\eta_1, \eta_2), z, t]$ such that the curve $P(x,y,t)=0$ becomes a straight line in the $\xi\eta$ plane, and the parameters z and t remain unaltered. If P somehow follows the spatial distribution in (x,y,z,t) so as to "minimise" deviation from the defined vertical surface, the distribution should map into the (ξ,η,z,t)

domain such that its projection largely follows a straight line in the $\xi\eta$ plane. If this straight line were chosen to follow, say, the ξ -axis, then the η -dimensions of the cloud should be relatively small. Further, if the curvature of P is relatively small, and the transformation

$$(\xi, \eta, z, t) = \tilde{T}_P(x, y, z, t) \quad (2.8)$$

thus reasonably linear, it will be possible to make some simplifying assumptions for the continued development of the distribution in the (ξ, η, z, t) frame. The inverse transformation

$$(x, y, z, t) = \tilde{T}_P^{-1}(\xi, \eta, z, t) \quad (2.9)$$

will allow interpretation in the original frame. For convenience, the curve P on which \tilde{T}_P is based will be referred to as the "proximate curve". It is clear from the description of the proximate curve that a means must be provided for establishing the "optimum" location of $P(x, y, t) = 0$ in space, as well as its variation in time. Both these objectives may be met, and the "movement" along P minimised, by allowing $P(x, y, t)$ to evolve according to Lagrangian coordinate transformations. Let the optimum form of P at time t' be given by

$$P^{\wedge}(x, y) = \lim_{t \rightarrow t'_+} P(x, y, t) \quad (2.10)$$

By allowing the initial curve $P^{\wedge}(x, y) = 0$ to be translated in the eulerian wind-field by the velocity at some

best height, say $Z(t)$, it should be possible to make P' undergo essentially the same realignment as the concentration distribution. Define a lagrangian coordinate transformation by

$$x_{\ell}(t) = x + \int_t^{t'} \bar{u}[x_{\ell}(\tau), y_{\ell}(\tau), Z(\tau), \tau] d\tau \quad (2.11)$$

$$y_{\ell}(t) = y + \int_t^{t'} \bar{v}[x_{\ell}(\tau), y_{\ell}(\tau), Z(\tau), \tau] d\tau \quad (2.12)$$

The choice of P' must clearly satisfy the proximity requirement in the neighbourhood of the release-point (x'', y'', z'') for t close to t' . It follows that P' must allow $P'(x'', y'') = 0$. Then the tracking height may be chosen such that $Z(t') = z''$, and subsequent $Z(t)$ arranged recursively to minimise the deviation of the centroid at some representative level from the curve $P'[x_{\ell}(t), y_{\ell}(t)] = 0$, or more specifically, from $[x_{\ell}''(t), y_{\ell}''(t)]$, where this is the transform of (x'', y'') . Hence, an obvious best choice of the proximate curve P is

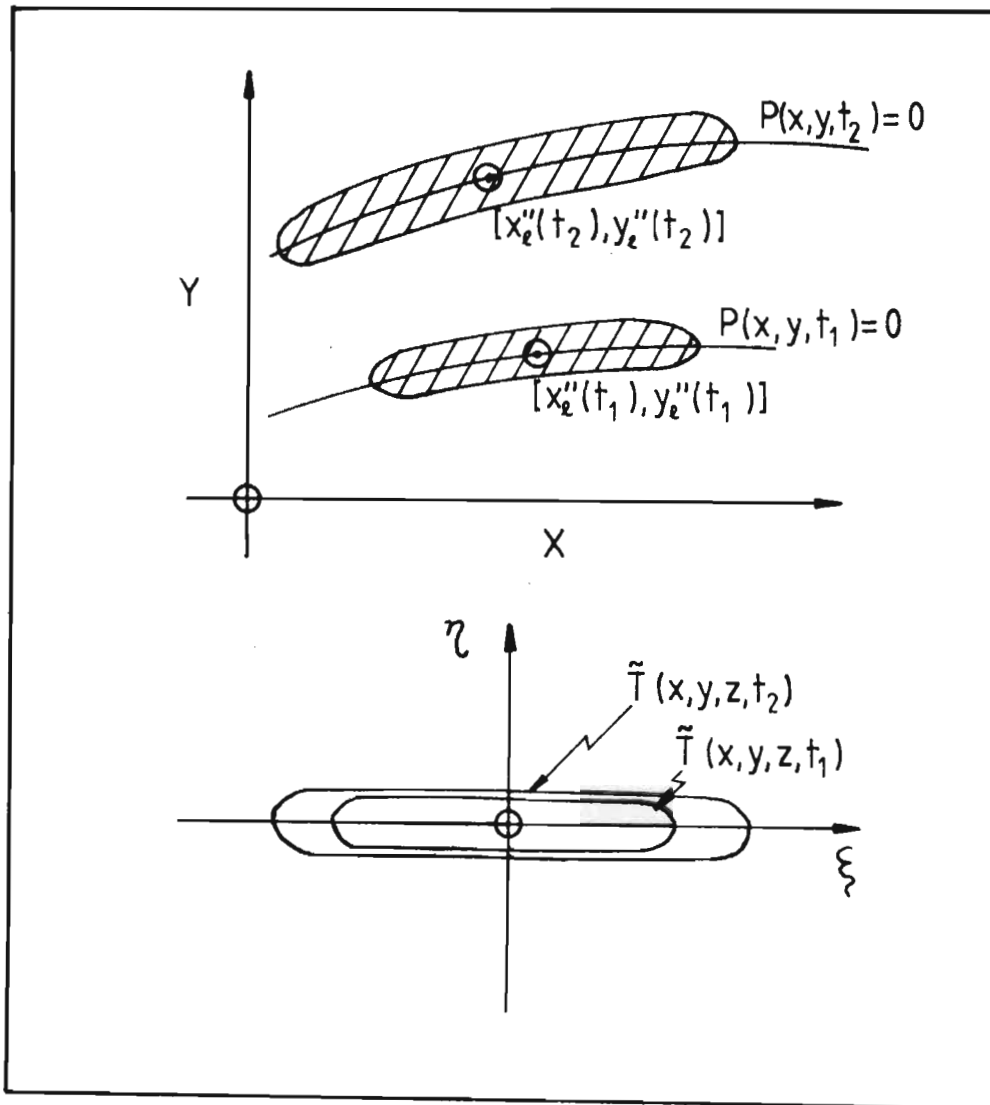
$$P(x, y, t) = P'[x_{\ell}(t), y_{\ell}(t)] \quad (2.13)$$

Of course, it is unlikely that the unique transforms $\tilde{T}_P, \tilde{T}_P^{-1}$ will exist with such an arbitrary specification of P , and an approximate form of equation (2.13) will eventually be used.

It is now possible to suggest further properties for the transformation \tilde{T}_P (2.8). Let ξ be the distance along P from the point $[x_{\ell}''(t), y_{\ell}''(t)]$ which satisfies $P(x, y, t) = 0$, and let η be the lateral distance from P to the point (x, y) ,

senses being determined according to some rule. Then \tilde{T}_p will simply "straighten out" an xy projection of the distribution at t [figure (2.1)].

fig.(2.1) Transformation \tilde{T}_p



The effect of the transformation has been to represent the distribution in a moving frame such that it is localised near the origin and distributed largely along one axis. In order to work in the new frame, however, some further assumptions are necessary. The non-linearity of the transformation \tilde{T}_P will clearly be determined by the curvature of P. If P were straight, the transformation would be linear, and a simple equivalent form of the diffusion equation (2.3) would result. Thus, if the curvature of P is small, equation (2.3) may be approximated with

$$\begin{aligned} \frac{\partial G'}{\partial t_1} + \bar{u}' \frac{\partial G'}{\partial \xi} + \bar{v}' \frac{\partial G'}{\partial \eta} &= \frac{\partial}{\partial \xi} \left[K_h \frac{\partial G'}{\partial \xi} \right] + \frac{\partial}{\partial \eta} \left[K_h \frac{\partial G'}{\partial \eta} \right] + \frac{\partial}{\partial z} \left[K_z \frac{\partial G'}{\partial z} \right] \\ &+ w_s \frac{\partial G'}{\partial z} + R(G', \xi, \eta, z, t_1) \end{aligned} \quad (2.14)$$

The diffusivities K_ξ , K_η would be directional properties, equivalent to suitable linear combinations of K_x, K_y . However, Calder (1965) [section (1.4.2)] showed that if z were chosen as a preferred axis, then necessarily $K_x = K_y$ for equation (1.39) to be valid. Hence $K_h = K_\xi = K_\eta$ may be related to $K_x = K_y$ by direct coordinate transformation, provided rotation is restricted to the horizontal. The transformed properties are thus

$$\left. \begin{aligned} G'(\xi, \eta, z, t) &= G(x, y, z, t) \\ K_h(\xi, \eta, z, t) &= K_x(x, y, z, t) = K_y(x, y, z, t) \\ \text{with } (\xi, \eta, z, t) &= \tilde{T}_P(x, y, z, t) \end{aligned} \right\} \quad (2.15)$$

Because the frame is moving, the advective properties must become relative

$$\begin{aligned}
 \bar{u}_R(x,y,z,t) &= \bar{u}(x,y,z,t) - \bar{u}(x,y,Z(t),t) \\
 \bar{v}_R(x,y,z,t) &= \bar{v}(x,y,z,t) - \bar{v}(x,y,Z(t),t) \\
 \left. \begin{aligned}
 \bar{u}'(\xi,\eta,z,t) &= \frac{\partial \xi}{\partial x} \cdot \bar{u}_R(x,y,z,t) + \frac{\partial \xi}{\partial y} \cdot \bar{v}_R(x,y,z,t) \\
 \bar{v}'(\xi,\eta,z,t) &= \frac{\partial \xi}{\partial x} \cdot \bar{u}_R(x,y,z,t) + \frac{\partial \xi}{\partial y} \cdot \bar{v}_R(x,y,z,t)
 \end{aligned} \right\} \quad (2.16)
 \end{aligned}$$

2.2.3 Distribution in the lagrangian frame.

Equation (2.6) reduced the problem of solving for a continuous point-source distribution in eulerian space to one of solving for individual unit-puffs in eulerian space. By means of the transformation \tilde{T}_p , the solution for eulerian puffs has now been reduced to an approximate solution in a lagrangian frame which exists in the neighbourhood of the developing puff. Reverting to the original eulerian symbols for convenience, let the concentration which results from a unit release be $C(x,y,z,t)$ in the lagrangian frame. Then equation (2.14) becomes

$$\begin{aligned}
 \frac{\partial C}{\partial t} + \bar{u}(x,y,z,t) \frac{\partial C}{\partial x} + \bar{v}(x,y,z,t) \frac{\partial C}{\partial y} &= \frac{\partial}{\partial x} \left[K_x(x,y,z,t) \frac{\partial C}{\partial x} \right] \\
 + \frac{\partial}{\partial y} \left[K_y(x,y,z,t) \frac{\partial C}{\partial y} \right] + \frac{\partial}{\partial z} \left[K_z(x,y,z,t) \frac{\partial C}{\partial z} \right] \\
 + w_s \frac{\partial C}{\partial z} + R(C,x,y,z,t) & \quad (2.17)
 \end{aligned}$$

Clearly, \bar{u} will be the velocity parallel to the original transformation curve $P(y=0)$, whilst \bar{v} will be the velocity normal to this curve. The functions $\bar{u}, \bar{v}, K_x, K_y, K_z, R$

may all be evaluated relative to the new frame via the transformations (2.15), (2.16).

One further approximation is made simply for ease of calculation. In a typical application, the horizontal spatial scales for variations in meteorological parameters should be somewhat larger than the horizontal dimensions of the puff. If this is the case, the values of $\bar{u}, \bar{v}, \bar{k}_x, \bar{k}_y, \bar{k}_z$ and the form of R will vary only slightly with x and y in the region occupied by the puff, again assuming that the curvature of P is small. Then $\bar{u}(x,y,z,t), \bar{v}(x,y,z,t)$ may be replaced by appropriate weighted mean values $\bar{U}(z,t), \bar{V}(z,t)$. In practice, these means are based on the movement of P in eulerian space in such a way that only relative velocities normal to P contribute to $\bar{V}(z,t)$, whilst relative velocities along P combine to give the average $\bar{U}(z,t)$. Diffusivity and removal profiles are similarly approximated by local mean values $\bar{k}_x(z,t), \bar{k}_y(z,t), \bar{k}_z(z,t)$ and $\bar{R}(C,z,t)$. However, they are based on values at the moving centroid, which will lie on $P(y=0)$ and be stationary in the lagrangian frame according to the specification of P [section (2.2.2)]. With these assumptions, equation (2.17) becomes:

$$\begin{aligned} \frac{\partial C}{\partial t} + \bar{U}(z,t) \frac{\partial C}{\partial x} + \bar{V}(z,t) \frac{\partial C}{\partial y} &= \bar{k}_x(z,t) \frac{\partial^2 C}{\partial x^2} + \bar{k}_y(z,t) \frac{\partial^2 C}{\partial y^2} \\ &+ \frac{\partial}{\partial z} \left[\bar{k}_z(z,t) \frac{\partial C}{\partial z} \right] + w_s \frac{\partial C}{\partial z} + \bar{R}(C,z,t) \end{aligned} \quad (2.18)$$

Implicit in equation (2.18) is that the wind acts on the puff as a whole, but careful choices of P, \bar{U}, \bar{V} have accounted for spatial variations in the eulerian wind-field.

It is clear from the descriptions of $\bar{U}, \bar{V}, \bar{K}_i, \bar{R}$ that their values may only be determined according to the distribution of the puff in eulerian space, using the inverse transformation \tilde{T}_p^{-1} (2.9). Hence, in general, these functions cannot be pre-evaluated, and equation (2.18) will be highly non-linear.

2.2.4 Solution for the lagrangian puff.

In section (1.5.2), consideration was given to the analytical treatment of puff expansion in the atmosphere. It was noted that though a solution exists for the case of constant velocity gradient and constant diffusivity in an unbounded atmosphere [Quesada (1971)], the more general cases involving linear [Saffman (1962)] and neutral [Chatwin (1968)] profiles in a bounded atmosphere could only be solved for in terms of their first few moments, or asymptotic values thereof. As in equation (1.51), the x-y moments of a finite puff are defined by

$$\theta_{mn}(z,t) = \int_{-\infty}^{\infty} \int_{-\infty}^{\infty} x^m y^n C(x,y,z,t) dx dy$$

By multiplying through equation (2.18) with $x^m y^n$, relations of the forms (1.53), (1.54), (1.55) could be obtained for the first few moments [Aris (1956)]. Although analytical solutions for these moments only exist in a few cases, use may be made of numerical methods - for example a finite-difference solution in z-t. Hence Tyldesley and Wallington (1965) [section (1.6.4.4)] modelled an instantaneous cross-

wind line source by solving for the zeroth, first and second moments θ_{00} , θ_{10} , θ_{20} in the direction of the wind. If one assumes that the distribution at height z is gaussian, then it may be reconstructed from these moments. In general, however, higher moments make significant contributions to the distribution. Saffman (1962) showed that in the case of a linear wind profile, the distribution will not be asymptotically gaussian [section (1.5.2)], and that the skewness factor will be about unity at ground-level, if horizontal diffusion is ignored. If higher moments are solved for, one is left with the task of formulating a joint probability distribution which observes these moments.

Returning to the description of the lagrangian frame in section (2.2.2), note that the choice of the proximate curve P must necessarily resolve the largest wind component into the direction of P . It may thus be expected that usually $|\bar{U}(z,t)| \gg |\bar{V}(z,t)|$ in equation (2.18). However, $\bar{V}(z,t)$ cannot be ignored altogether - with the present formulation of P this would be tantamount to ignoring temporal variations in the wind-field. If $\bar{V}(z,t)$ is zero, equation (2.18) must solve to give a gaussian y -distribution, assuming that the K -theory description is valid. Hence it is assumed that the y -distribution at height z will remain gaussian for reasonably small $\bar{V}(z,t)$. Then the complete distribution may be approximately represented by the moments $C_0(x,z,t)$, $C_1(x,z,t)$, $C_2(x,z,t)$, where

$$C_n(x,z,t) = \int_{-\infty}^{\infty} y^n C(x,y,z,t) dy \quad (2.19)$$

Assuming the boundary conditions

$$\lim_{y \rightarrow \pm\infty} y^n C = 0, \quad \lim_{y \rightarrow \pm\infty} y^n \frac{\partial C}{\partial y} = 0 \quad (2.20)$$

$n=0,1,2 \qquad n=0,1,2$

then multiplication through equation (2.18) by $y^n, n=0,1,2$ yields

$$\begin{aligned} \frac{\partial C_0}{\partial t} + \bar{U}(z,t) \frac{\partial C_0}{\partial x} &= \bar{K}_x(z,t) \frac{\partial^2 C_0}{\partial x^2} + \frac{\partial}{\partial z} \left[\bar{K}_z(z,t) \frac{\partial C_0}{\partial z} \right] \\ &+ w_s \frac{\partial C_0}{\partial z} + \bar{R}(C_0, z, t) \end{aligned} \quad (2.21)$$

$$\begin{aligned} \frac{\partial C_1}{\partial t} + \bar{U}(z,t) \frac{\partial C_1}{\partial x} &= \bar{K}_x(z,t) \frac{\partial^2 C_1}{\partial x^2} + \frac{\partial}{\partial z} \left[\bar{K}_z(z,t) \frac{\partial C_1}{\partial z} \right] \\ &+ w_s \frac{\partial C_1}{\partial z} + \bar{R}(C_1, z, t) + \bar{V}(z,t) C_0 \end{aligned} \quad (2.22)$$

$$\begin{aligned} \frac{\partial C_2}{\partial t} + \bar{U}(z,t) \frac{\partial C_2}{\partial x} &= \bar{K}_x(z,t) \frac{\partial^2 C_2}{\partial x^2} + \frac{\partial}{\partial z} \left[\bar{K}_z(z,t) \frac{\partial C_2}{\partial z} \right] + w_s \frac{\partial C_2}{\partial z} \\ &+ \bar{R}(C_2, z, t) + 2\bar{V}(z,t) C_1 + 2\bar{K}_y(z,t) C_0 \end{aligned} \quad (2.23)$$

Clearly, this development will only be valid if \bar{R} has the form $\bar{R}(C, z, t) = \bar{R}'(z, t)C$, i.e. if the concentration-dependent source/sink term is first-order in C . Equations (2.21) to (2.23) represent analogous advection, diffusion, reaction and sedimentation for the zeroth, first and second moments. There is a further contribution to the first moment due to bulk advective shift, and contributions to the second

moment due to advective shift of the centroid, as well as independent diffusion in the y-direction.

In applying these equations to the case of an instantaneous unit release at $(x,y,z,t)=(0,0,z'',t')$, as will be relevant in the lagrangian frame, it is reasonable to specify the boundary conditions

$$\lim_{x \rightarrow \pm\infty} C_n(x,z,t) = 0, \quad n=0,1,2 \quad (2.24)$$

and the initial conditions

$$\left. \begin{aligned} C_0(x,z,t) &= \delta(x)\delta(z-z'')\delta(t-t') \\ C_1(x,z,t) &= 0 \\ C_2(x,z,t) &= 0 \end{aligned} \right\} t \leq t' \quad (2.25)$$

It has not yet been possible to specify vertical boundary conditions because of sedimentation, the unknown form of $\bar{R}'(z,t)$, and the possible existence of an impervious inversion layer.

In order to solve equations (2.21) to (2.23) simultaneously with the boundary-conditions (2.24), (2.25) it will be necessary to make use of numerical methods.

2.3 Numerical method.

2.3.1 Separation of processes.

Define the change which occurs in $C_n(x,z,t)$ during the interval t to $t+\Delta t$ as $\Delta C_n(x,z,t,\Delta t)$. The contributions to ΔC_n which result from advection, diffusion, sedimentation and reaction may likewise be considered as $\Delta C_{na}(x,z,t,\Delta t)$,

$\Delta C_{nd}(x,z,t,\Delta t)$, $\Delta C_{ns}(x,z,t,\Delta t)$, $\Delta C_{nr}(x,z,t,\Delta t)$, though of course these values will be interdependent. Whereas equations (2.21) to (2.23) determine the unique forms of $C_n(x,z,t)$, $n=0,1,2$, they may be used to define the following integrals.

$$\Delta C_{na}(x,z,t,\Delta t) = - \int_t^{t+\Delta t} \bar{U}(z,\tau) \frac{\partial C_n(x,z,\tau)}{\partial x} d\tau \quad (2.26)$$

$$\Delta C_{nd}(x,z,t,\Delta t) = \int_t^{t+\Delta t} \bar{K}_x(z,\tau) \frac{\partial^2 C_n(x,z,\tau)}{\partial x^2} + \frac{\partial}{\partial z} \left[\bar{K}_z(z,\tau) \frac{\partial C(x,z,\tau)}{\partial z} \right] d\tau \quad (2.27)$$

$$\Delta C_{ns}(x,z,t,\Delta t) = \int_t^{t+\Delta t} w_s \frac{\partial C_n(x,z,\tau)}{\partial z} d\tau \quad (2.28)$$

$$\Delta C_{nr}(x,z,t,\Delta t) = \int_t^{t+\Delta t} \bar{R}^r(z,\tau) C_n(x,z,\tau) d\tau \quad (2.29)$$

If the additional terms in equations (2.22), (2.23) are replaced with similar integrals, the moment equations become

$$\begin{aligned} \Delta C_0(x,z,t,\Delta t) &= \Delta C_{0a}(x,z,t,\Delta t) + \Delta C_{0d}(x,z,t,\Delta t) \\ &+ \Delta C_{0s}(x,z,t,\Delta t) + \Delta C_{0r}(x,z,t,\Delta t) \end{aligned} \quad (2.30)$$

$$\begin{aligned}
\Delta C_1(x, z, t, \Delta t) &= \Delta C_{1a}(x, z, t, \Delta t) + \Delta C_{1d}(x, z, t, \Delta t) \\
&+ \Delta C_{1s}(x, z, t, \Delta t) + \Delta C_{1r}(x, z, t, \Delta t) \\
&+ \int_t^{t+\Delta t} \bar{V}(z, \tau) C_0(x, z, \tau) d\tau
\end{aligned} \tag{2.31}$$

$$\begin{aligned}
\Delta C_2(x, z, t, \Delta t) &= \Delta C_{2a}(x, z, t, \Delta t) + \Delta C_{2d}(x, z, t, \Delta t) \\
&+ \Delta C_{2s}(x, z, t, \Delta t) + \Delta C_{2r}(x, z, t, \Delta t) \\
&+ 2 \int_t^{t+\Delta t} \bar{V}(z, \tau) C_1(x, z, \tau) d\tau \\
&+ 2 \int_t^{t+\Delta t} \bar{K}_y(z, \tau) C_0(x, z, \tau) d\tau
\end{aligned} \tag{2.32}$$

If the time-step Δt is reasonably small, the integral terms resulting from the separate processes will be reasonably independent of each other, and the following approximations may be made.

$$\begin{aligned}
\text{(i)} \quad &\int_t^{t+\Delta t} \bar{U}(z, \tau) \frac{\partial C_n}{\partial x}(x, z, \tau) d\tau \approx C_n(x, z, t) \\
&- C_n \left[\left(x + \int_{t+\Delta t}^t \bar{U}(z, \tau) d\tau \right), z, \tau \right], n=0, 1, 2
\end{aligned} \tag{2.33}$$

$$\text{(ii)} \quad \int_t^{t+\Delta t} \bar{V}(z, \tau) C_n(x, z, \tau) d\tau \approx C_n(x, z, t) \int_t^{t+\Delta t} \bar{V}(z, \tau) d\tau, n=0, 1 \tag{2.34}$$

$$(iii) \int_t^{t+\Delta t} \bar{K}_y(z, \tau) C_0(x, z, \tau) d\tau \approx C_0(x, z, t) \int_t^{t+\Delta t} \bar{K}_y(z, \tau) d\tau \quad (2.35)$$

$$(iv) \int_t^{t+\Delta t} w_s \frac{\partial C_n}{\partial z}(x, z, \tau) d\tau \approx C_n(x, z + w_s \Delta t, t) - C_n(x, z, t) \quad , n=0,1,2 \quad (2.36)$$

In fact, the integrals on the right-hand sides of equations (2.33), (2.34) and (2.35), of the properties $\bar{P}_j(z, t)$ in the lagrangian frame, are evaluated by summation over smaller steps $\Delta t/n_s$ in the eulerian frame, according to equations (2.15) and (2.16).

$$\int_t^{t+\Delta t} \bar{P}_j(z, \tau) d\tau \approx \sum_{i=1}^{n_s} \bar{P}_{Ej} \left[\tilde{T}_p^{-1}(x, y, z, t + i\Delta t/n_s) \right] \Delta t/n_s \quad (2.37)$$

In the actual solution for $\Delta C_n(x, z, t, \Delta t)$ the advection, sedimentation, reaction and diffusion processes are not assumed to act independently on the initial distribution $C_n(x, z, t)$, but rather to act sequentially according to the scheme:

$$(1) \text{ Advection: } C_n^{\wedge}(x, z, t) = C_n(x, z, t) + \Delta C_{na}(x, z, t, \Delta t) \\ + [\text{contributions as in equation (2.34)} \\ \text{for } n=1,2] \quad (2.38)$$

$$(2) \text{ Sedimentation: } C_n^{\wedge}(x, z, t) = C_n^{\wedge}(x, z, t) + \Delta C_{ns}^{\wedge}(x, z, t, \Delta t) \quad (2.39)$$

$$(3) \text{ Reaction: } C_n^{\wedge}(x, z, t) = C_n^{\wedge}(x, z, t) + \Delta C_{nr}^{\wedge}(x, z, t, \Delta t) \quad (2.40)$$

$$(4) \text{ Diffusion: } C_n(x,z,t+\Delta t) = C_n^{\prime\prime}(x,z,t) + \Delta C_{nd}^{\prime\prime}(x,z,t,\Delta t) + [\text{contribution as in equation (2.35) for } n=2]. \quad (2.41)$$

Thus the final distribution is obtained after the diffusion step, which acts to "smooth" the redistributions due to advection, sedimentation and reaction.

No mention has yet been made of the methods of solution for the diffusion and reaction steps. Special procedures are adopted in these cases, and they are discussed separately.

2.3.2 Initial distribution.

The most convenient means of handling the distribution information $C_n(x,z,t), n=0,1,2$ is in the form of the discretised two-dimensional arrays, $C_{nik}(t), n=0,1,2$, where $C_{nik}(t) = C_n(x_1+i\Delta x, z_1+k\Delta z, t)$ and x_1, z_1 are fixed datum values. Interactions within these grids are then dealt with using finite-difference approximations.

However, this discretisation complicates representation of the initial distribution ex equation (2.25),

$$C_0(x,z,t) = \delta(x)\delta(z-z^{\prime\prime})\delta(t-t^{\prime}), t \leq t^{\prime}$$

In fact, it is necessary to "seed" the puff using some assumed distribution at time $t^{\prime} + \delta t$, where δt is small. Over this short time it is reasonable to neglect the effects of shear about the stationary centroid in the lagrangian

frame, as well as diffusivity variations about the release height z' . Then the equivalent zeroth moment for the gaussian distribution (1.40) becomes

$$C_0(x, z, t' + \delta t) = \frac{1}{4\pi\delta t [\bar{K}_x'(z')\bar{K}_z'(z')]^{\frac{1}{2}}} \exp\left[-\frac{1}{4\delta t}\left(\frac{x^2}{\bar{K}_x'(z')} + \frac{(z-z')^2}{\bar{K}_z'(z')}\right)\right] \quad (2.42)$$

where \bar{K}_x', \bar{K}_z' are determined according to equation (2.37) with $t=t', \Delta t=\delta t$.

2.3.3 Solution for the diffusion step.

Following equation (2.27), the rate of change of $C_n(x, z, t)$ due to diffusion may be defined as

$$\left. \frac{\partial C_n}{\partial t}(x, z, t) \right|_d = \bar{K}_x(z, t) \frac{\partial^2 C_n}{\partial x^2}(x, z, t) + \frac{\partial}{\partial z} \left[\bar{K}_z(z, t) \frac{\partial C_n}{\partial z}(x, z, t) \right] \quad (2.43)$$

Assuming that the time-scales for variations in \bar{K}_x, \bar{K}_z will be large compared with Δt , they may be replaced with mean values $\bar{K}_x'(z), \bar{K}_z'(z)$ which are determined according to equation (2.37) for the interval t to $t+\Delta t$. Further, define values $C_n'(x, z, \tau)$ with the initial conditions $C_n'(x, z, t) = C_n(x, z, t), n=0, 1, 2$, but thereafter allow $C_n', n=0, 1, 2$ to be influenced only by diffusion during t to $t+\Delta t$.

Hence,

$$\begin{aligned} \frac{\partial C'_n}{\partial t'}(x,z,t') &= \bar{K}'_x(z) \frac{\partial^2 C'_n}{\partial x^2}(x,z,t') \\ &+ \frac{\partial}{\partial z} \left[\bar{K}'_z(z) \frac{\partial C'_n}{\partial z}(x,z,t') \right], \quad t \ll t' \ll t + \Delta t \end{aligned} \quad (2.44)$$

and it is now possible to specify diffusion boundary-conditions for the ground, and an impervious inversion layer at $z=H$, if one exists.

$$\frac{\partial C'_n}{\partial z}(x,z,t') = 0, \quad z = 0, H \quad (2.45)$$

A number of solution techniques have been considered for the parabolic partial differential equation (2.44), on the basis of accuracy vs computation. Since the values of $C'_n, n=0,1,2$ are effectively stored in the three-dimensional grids C'_{nikt} , all methods have been based on finite differences. The criterion used for comparison was overall agreement with the development of an instantaneous release, for which \bar{K}'_x and \bar{K}'_z were taken constant with height. The analytical solution for this case is the gaussian puff, equation (1.40), which was considered a fair test in view of the initial high spatial and temporal gradients, and its approximation to the system under consideration. Of course, having separated out the advection terms by means of the lagrangian integration (2.33), an important source of pseudo-diffusion [section (1.10.1)] has been removed, and the necessity to satisfy advective stability conditions (1.65) has been avoided.

The explicit schemes which were considered could be solved directly in the two spatial dimensions. However, a vast amount of computation would have been required for simultaneous solution in both directions using the implicit scheme, and this scheme was adapted using the Alternating-Direction-Implicit (A.D.I.) method of Peaceman and Rachford (1955). For simplicity, consider the case of linear diffusion,

$$\frac{\partial C}{\partial t} = K_x \frac{\partial^2 C}{\partial x^2}, \quad K_x \text{ constant} \quad (2.46)$$

(i) Direct explicit (forward-difference)

stability condition : $K_x \Delta t / \Delta x^2 \leq \frac{1}{2}$ [von Neumann]

$$C_{i,t+1} = C_{i,t} + [K_x \Delta t / \Delta x^2] [C_{i+1,t} - 2C_{i,t} + C_{i-1,t}]$$

(ii) Crank-Nicholson implicit

stability condition : $K_x \Delta t / \Delta x^2 \leq \frac{1}{2}$ [Ritchmeyer and Morton (1967)].

$$C_{i,t+1} = C_{i,t} + [K_x \Delta t / 2\Delta x^2] [(C_{i+1,t} - 2C_{i,t} + C_{i-1,t}) + (C_{i+1,t+1} - 2C_{i,t+1} + C_{i-1,t+1})]$$

(iii) Gauss-Seidel iterative (row-wise explicit)

convergent for all values of $r = K_x \Delta t / \Delta x^2$ [Smith (1965)]

nth iteration

$$C_{i,t+1}^{(n+1)} = [r/2(1+r)] [C_{i-1,t+1}^{(n+1)} + C_{i,t+1}^{(n)}] + b_{it} / [1+r]$$

where

$$b_{it} = C_{i,t} + (r/2)(C_{i-1,t} - 2C_{i,t} + C_{i+1,t})$$

(iv) Gauss-Seidel with S.O.R. (Successive-Over-Relaxation).

nth iteration

$$C_{i,t+1}^{(n+1)} = w \left[\frac{r}{2(1+r)} \{ C_{i-1,t+1}^{(n+1)} + C_{i+1,t+1}^{(n)} \} + b_{i,t} / \{1+r\} \right] - (w-1) C_{i,t+1}^{(n)}$$

where w has an optimum value given by Smith (1965).

(v) Limiting value method (explicit).

unconditionally stable for all values of $r = K_x \Delta t / \Delta x^2$

$$C_{i,t+1} = C_{i,t} + \frac{1}{2} [C_{i+1,t} - 2C_{i,t} + C_{i-1,t}] [1 - e^{-2r}]$$

Whereas the explicit schemes (i), (iii), (iv) and (v) readily include the bi-directional problem (2.44), it is included in (ii) using the A.D.I. method. This scheme effectively decouples the diffusion processes in the two directions, allowing tri-diagonal solution of the resultant matrix equations.

In the instantaneous point-source tests, (ii) was more accurate than (i), but inferior to (iii) and especially (iv) in terms of computer time. In fact, a new explicit technique (v) was developed which was as accurate as (iv), but which was non-iterative, and required less computer time.

The derivation of the limiting value solution is presented in appendix (A1.1). Note that the scheme is unconditionally stable. In the general case with varying spatial stepsizes and variable diffusivity, the equations

become

$$C_{i,t+1} = C_{i,t} + b_{i,t} \left[1 - e^{-a_i \Delta t} \right] \quad (2.47)$$

with

$$b_{i,t} = \left[C_{i+1,t} - C_{i-1,t} \right] / \left[1 + \frac{K_{x_{i-1}} \cdot \Delta x_{i,i+1}}{K_{x_{i+1}} \cdot \Delta x_{i-1,i}} \right] \\ + C_{i-1,t} - C_{i,t}$$

and

$$a_i = \frac{2 [K_{x_{i+1}} \Delta x_{i-1,i} + K_{x_{i-1}} \Delta x_{i,i+1}]}{\Delta x_{i-1,i} \Delta x_{i,i+1} [\Delta x_{i-1,i} + \Delta x_{i,i+1}]}$$

In order to extend this solution to the bi-directional (xz) problem, it was assumed that the x- and z- diffusion processes acted independently during Δt , and that the resultant perturbations were directly additive.

$$C_{i,k,t+1} = C_{i,k,t} + b_{i,t} \left[1 - e^{-a_i \Delta t} \right] \Big|_k \\ + b_{k,t} \left[1 - e^{-a_k \Delta t} \right] \Big|_i \quad (2.48)$$

If the exponents $a_i \Delta t, a_k \Delta t$ are small, the exponential terms may be approximated with Taylor expansions which exclude third and higher terms. Then equation (2.48) reduces to the explicit finite-difference solution for x-z diffusion with variable diffusivity and stepsize, and it is concluded that the additivity assumption is acceptable. Further, it might be expected that optimal stepsizes will be determined by the values of $a_i \Delta t, a_k \Delta t$, and a series of comparisons

with growing gaussian puffs has shown that best agreement is obtained in the region of

$$K_x \Delta t / \Delta x^2 = 0,4 \quad , \quad K_z \Delta t / \Delta z^2 = 0,4 \quad (2.49)$$

These optimality criteria are close to the stability limits of methods (i) and (ii) above.

In applying the solution (2.47) to equation (2.44) with the boundary-conditions (2.45), it is convenient to allow x-stepsizes to expand outwards from a central point, so that the grid is cruder in regions where x-gradients are usually small. Though z-stepsizes are left constant, diffusivity varies with height. Hence, both the variable stepsize and the variable diffusivity capabilities of the scheme (2.48) are used in the solution of equation (2.44).

Because the diffusion step is solved in a finite x-z grid, it is necessary to make some assumption about the fluxes at the boundaries of the system. By setting the concentration gradients at all boundaries to zero, the diffusive fluxes become zero. In this way, the boundary conditions (2.45) are satisfied, and the effect on the distant x-boundaries is expected to be small because of the small gradients in this direction. In the absence of an inversion "lid", the optimal stepsize criterion (2.49) usually means that the upper boundary is too high to restrict the vertical spread anyway.

In the numerical model, the limiting value method is used to provide a solution to (2.44) of the form

$$\Delta C_n^{\wedge}(x,z,t,\Delta t) = C_n^{\wedge}(x,z,t + \Delta t) - C_n^{\wedge}(x,z,t)$$

The approximation is now made that the diffusion process will be effectively independent of the advection, sedimentation and reaction processes during t to $t+\Delta t$, so that

$$\Delta C_{nd}(x,z,t,\Delta t) = \Delta C_n^{\wedge}(x,z,t,\Delta t) \quad (2.50)$$

2.3.4 Solution for the reaction step.

In the discussion of removal mechanisms in section (1.9), it emerged that studies to date have chiefly concerned removal at the ground, and removal at a constant rate throughout the surface layer, though the possibility of a rate which is variable with height was not discounted. The important findings may be summarised as follows:

(i) Retention of small particles or absorption of gas tracer at the ground

Boundary condition:

$$\begin{aligned} \text{irreversible: } \bar{K}_z(z,t) \frac{\partial C}{\partial z}(x,z,t) \\ = \bar{w}_d(t) C(x,z,t), \quad z=0 \end{aligned} \quad (2.51)$$

$$\begin{aligned} \text{reversible: } \bar{K}_z(z,t) \frac{\partial C}{\partial z}(x,z,t) \\ = \bar{K}_G(t) [C(x,z,t) - C_E], \quad z=0 \end{aligned} \quad (2.52)$$

(ii) Washout of particles or absorption of tracer gas by rainfall

$$\text{irreversible: } \bar{R}(C,z,t) = -\bar{\Lambda}(t) C(x,z,t) \quad (2.53)$$

$$\text{reversible: } \bar{R}(C,z,t) = -\bar{\Lambda}_r(t) [C(x,z,t) - C_E] \quad (2.54)$$

(iii) First-order chemical reaction or radioactive decay

$$\bar{R}(C,z,t) = -\bar{k}_1(t) C(x,z,t) \quad (2.55)$$

In the taking of moments for equations (2.21), (2.22) and (2.23), it was found necessary to assume that

the region of space affected by $C_n(x,z,t)$, $n=0,1,2$ was finite. In effect, this analysis cannot consider the reversible processes (2.52) and (2.54), and $\bar{R}(C,z,t)$ must have the first-order form

$$\bar{R}(C,z,t) = \bar{R}'(z,t)C \quad (2.56)$$

The removal parameters $\bar{w}_d(t)$, $\bar{\lambda}(t)$ and $\bar{k}_1(t)$ are supplied in the lagrangian frame as mean effective values \bar{P}_j for the interval t to $t+\Delta t$, using an integral of the form (2.37). Although they are assumed spatially-constant in the lagrangian frame, spatial variations in the eulerian frame are accounted for as temporal variations via the transformation \tilde{T}_p , as in equation (2.15).

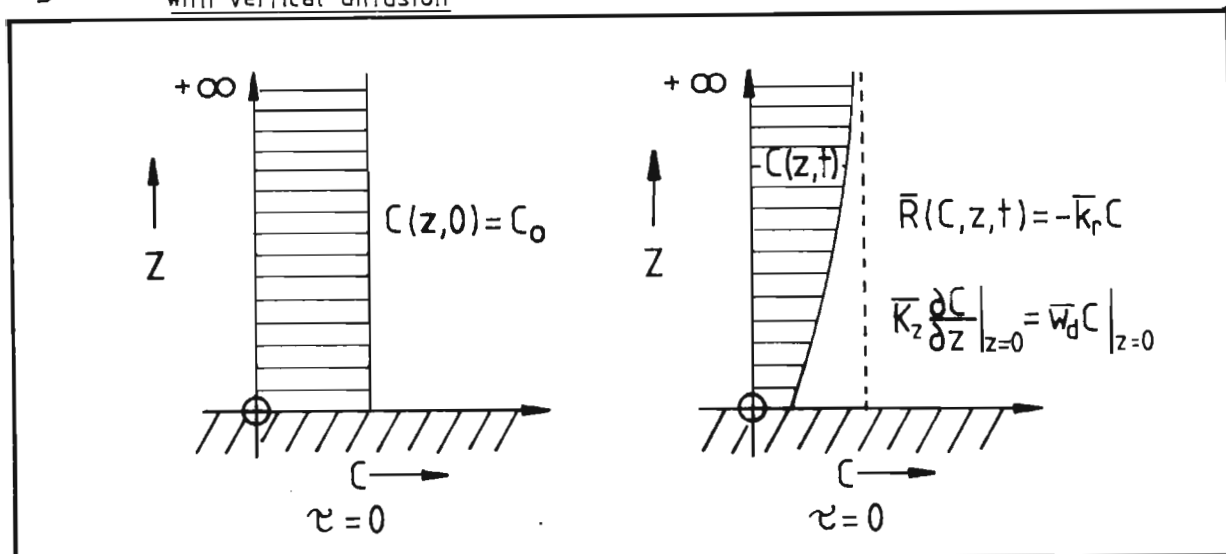
Inclusion of irreversible washout (2.53) and first-order reaction (2.55) in the numerical solution offers no problem, since the effect is uniform throughout the boundary layer, and should lead to a simple exponential growth or decay. The irreversible ground-absorption process may be considered to effect $\bar{R}'(z,t) = \bar{R}_o(t)\delta(z)$. The highly localised nature of this removal means that over any reasonable time-step, t to $t+\Delta t$, it will be necessary to consider the part played by atmospheric diffusion in supplying material to the absorbing surface. A simple approximation is derived by comparison with the system depicted in figure (2.2).

Consider a case of semi-infinite vertical diffusion with an absorbing surface at $z=0$. Allow the distribution to be subject to a first-order reaction (2.55) with rate-constant \bar{k}_r , and assume that the vertical diffusivity \bar{K}_z is

constant with height. The relevant equation is

$$\frac{\partial C}{\partial t} = \bar{K}_z \frac{\partial^2 C}{\partial z^2} - \bar{k}_r C \quad (2.57)$$

fig.(2.2) Ground absorption and first-order reaction with vertical diffusion



For simplicity, a uniform distribution is specified as the initial condition,

$$C(z,0) = C_0, \quad z \geq 0$$

and it is assumed that the deposition velocity at the absorbing surface is constant, so that the boundary condition is

$$\bar{K}_z \frac{\partial C}{\partial z} = \bar{w}_d C, \quad z=0$$

Then, solution of equation (2.57) using a Laplace transformation yields the result

$$\begin{aligned}
C(z,t) = C_0 \exp[-\bar{k}_r t] & \left[1 - \operatorname{erfc} \left(\frac{z}{2\sqrt{\bar{K}_z t}} \right) \right. \\
& \left. + \exp \left\{ \frac{\bar{w}_d}{\bar{K}_z} (z + \bar{w}_d t) \right\} \operatorname{erfc} \left\{ \frac{z + 2\bar{w}_d t}{2\sqrt{\bar{K}_z t}} \right\} \right] \quad (2.58)
\end{aligned}$$

Irreversible washout would simply add a further exponential factor, so that a combined first-order rate-constant may be defined as

$$\bar{k}_r = \bar{k}_1 + \bar{\Lambda} \quad (2.59)$$

An "adjustment factor" may be defined for the period 0 to t as

$$F_r(z,t,\bar{k}_r,\bar{w}_d,\bar{K}_z) = C(z,t)/C_0$$

In the above development, diffusive flux only occurred as a result of ground-absorption. It might be assumed, therefore that this redistribution is additive to the normal diffusion process which will occur as a result of existent spatial gradients. Since the latter process is dealt with separately [section (2.3.3)], the contribution of the removal processes is approximated by assuming independence of the initial distribution.

$$C(z,t+\Delta t) = C(z,t)F_r(z,\Delta t,\bar{k}_r,\bar{w}_d,\bar{K}_z) \quad (2.60)$$

Equation (2.29) represents the contribution of removal and reaction processes to the variation of the lagrangian moments $C_n, n=0,1,2$ during the interval t to

$t+\Delta t$, viz.

$$\Delta C_{nr}(x,z,t,\Delta t) = \int_t^{t+\Delta t} \bar{R}^{\wedge}(z,\tau) C_n(x,z,\tau) d\tau$$

If the time-step Δt is reasonably small and it is assumed that the reaction/removal processes occur independently of the advection, sedimentation and diffusion processes during Δt , this contribution might be approximated as

$$\Delta C_{nr}(x,z,t,\Delta t) = C_n(x,z,t) \int_t^{t+\Delta t} \bar{R}^{\wedge}(z,\tau) d\tau \quad (2.61)$$

It has been mentioned that $\bar{R}^{\wedge}(z,t)$ may have an arbitrary variation with height, dependent, for example, on the distribution of vegetational traps with height, and this aspect is to be considered in future work [Norden and van As (1977a)]. At present, only the absorption, washout and reaction processes outlined in equations (2.51), (2.53) and (2.55) will be accounted for. Following equations (2.60) and (2.61), the approximation is made that

$$\int_t^{t+\Delta t} \bar{R}^{\wedge}(z,\tau) d\tau = F_r [z,\Delta t, \bar{k}_r(t,\Delta t), \bar{w}_d(t,\Delta t), \bar{K}_z^{\wedge}(t,\Delta t)]^{-1} \quad (2.62)$$

where the parameters $\bar{P}_j(t,\Delta t)$ now represent mean values for the entire lagrangian frame, which have been averaged for the period t to $t+\Delta t$, and are evaluated via the inverse transformation \tilde{T}_p^{-1} using equation (2.37). In applying equation (2.62), an effective value for the constant \bar{K}_z^{\wedge} is established by averaging $\bar{K}_z(z)$ over heights which are

expected to play a part in the downwards diffusion.

Finally,

$$\Delta C_{nr}(x,z,t,\Delta t) = C_n(x,z,t) \{ F_r[z,\Delta t, \bar{k}_r(t,\Delta t), \bar{w}_d(t,\Delta t), \bar{k}'_z(t,\Delta t)] - 1 \} \quad (2.63)$$

2.3.5 Reconstruction of the distribution.

In section (2.2.4) it was proposed that provided the y-component of wind velocity in the lagrangian frame were small, the lagrangian distribution may be reconstructed from the moments $C_0(x,z,t)$, $C_1(x,z,t)$ and $C_2(x,z,t)$ with little error. The mean and variance of the y-distribution are given directly by

$$m_y(x,z,t) = C_1(x,z,t)/C_0(x,z,t) \quad (2.64)$$

$$\sigma_y^2(x,z,t) = C_2(x,z,t)/C_0(x,z,t) - m_y^2(x,z,t) \quad (2.65)$$

The assumption that higher moments are negligible is tantamount to accepting a gaussian distribution, so that finally

$$C(x,y,z,t) = \frac{C_0(x,z,t)}{\sigma_y(x,z,t)\sqrt{2\pi}} \exp \frac{-\{y-m_y(x,z,t)\}^2}{2\sigma_y^2(x,z,t)} \quad (2.66)$$

In the lagrangian frame, C_0 is the zeroth moment of the cloud distribution about the vertical xz plane passing through $y=0$. Shear and diffusion of the cloud in directions parallel to this plane have been accounted for by the numerical solution for C_0 , performed in an xz grid. Similar

numerical solutions for C_1 and C_2 included the interdependence of these moments, and their dependence on the wind component $\bar{V}(z,t)$ normal to the xz plane. Hence the mean $m_y(x,z,t)$ and variance $\sigma_y^2(x,z,t)$ for the displacement from the xz plane will include the important shear/vertical diffusion interaction effect for the expansion of the cloud in the y -direction.

The functions $C_0(x,z,t)$, $m_y(x,z,t)$ and $\sigma_y^2(x,z,t)$ exist in their discretised forms as three xz grids for time t . Expansion to form the 3-dimensional solution in the lagrangian frame follows according to equation (2.66). The lagrangian distribution is generally distorted slightly in reverting to the eulerian frame.

Allow the symbols x,y,z,t to revert to their roles as coordinates in the eulerian frame [section (2.2.2)], so that $C(\xi,\eta,z,t)$ represents the concentration distribution resulting from unit instantaneous release at (x'',y'',z'',t') . Hence equation (2.66) is effectively a solution for the Green's function.

$$G(x-x'',y-y'',z-z'',t-t') = C(\xi,\eta,z,t)$$

where it has been assumed that the transformation $(x,y,z,t) = \tilde{T}_p^{-1}(\xi,\eta,z,t)$ (2.9) is reasonably linear.

In order to obtain the distribution which results from a continuous release $Q(t)$ at (x'',y'',z'') , it is necessary to approximate the integral (2.6). Taking release-time steps Δt_R , and assuming that no release has occurred before $t=0$, the distribution in the eulerian frame

is

$$C_e(x,y,z,n\Delta t_r) = \sum_{i=1}^n G[x-x'',y-y'',z-z'',(n-i)\Delta t_R] \cdot Q[i\Delta t_R] \cdot \Delta t_R \quad (2.67)$$

Provided the release-time steps are not large, the irregularities which result from this discretised release quickly disappear with travel-time.

2.4 Administrative aspects.

2.4.1 Model concepts.

2.4.1.1 Dosages and concentrations.

Since concentration-measuring instruments generally have non-zero response times, reported values of "concentration" are in fact means based on the measured dosage during a finite time-interval, i.e.

$$\bar{C}(x,y,z,t') = D(x,y,z,t_1,t_2)/(t_2-t_1), t_1 < t' < t_2$$

$$\text{with } D(x,y,z,t_1,t_2) = \int_{t_1}^{t_2} C(x,y,z,t) dt$$

Moreover, dosage is often of more interest in pollution studies as it will reflect, for example, the total bodily accumulation of some toxic or radioactive substance. Thus Csanady (1969a) derived probabilities for the observed dosages in an eulerian frame, by assuming that dosages in the core region of a diffusing cloud were log-normally

distributed. In the modelling of atmospheric dispersion it is nevertheless necessary to solve for the fundamental behaviour $C(x,y,z,t)$ in order to predict dosages over finite intervals.

The observation of dosages $D(x,y,z,t_1,t_2)$ is likely to obscure the variation of $C(x,y,z,t)$ on time scales which are smaller than (t_2-t_1) . As opposed to area-source releases, the variable point-source release in a temporally and spatially variable environment is expected to produce concentration variations on relatively short space- and time-scales, and an effort has been made to reduce the experimental measurement intervals (t_2-t_1) in order to reveal the underlying behaviour. Further, this behaviour will be important in the case of accidental short-term release of dangerous substances.

The numerical model which has been devised to implement the lagrangian puff approach [sections (2.2), (2.3)] has two basic modes of operation:

- (i) Prediction of the ensemble-mean concentration distribution for an instant in time;
- (ii) Prediction of ensemble-mean dosages at specified points over specified time-intervals.

Whereas (ii) will be necessary in certain applications, including the field-validation of the model, (i) is likely to demonstrate some of the important differences between the dynamic puff model (DPM) and current approaches to the modelling of atmospheric dispersion.

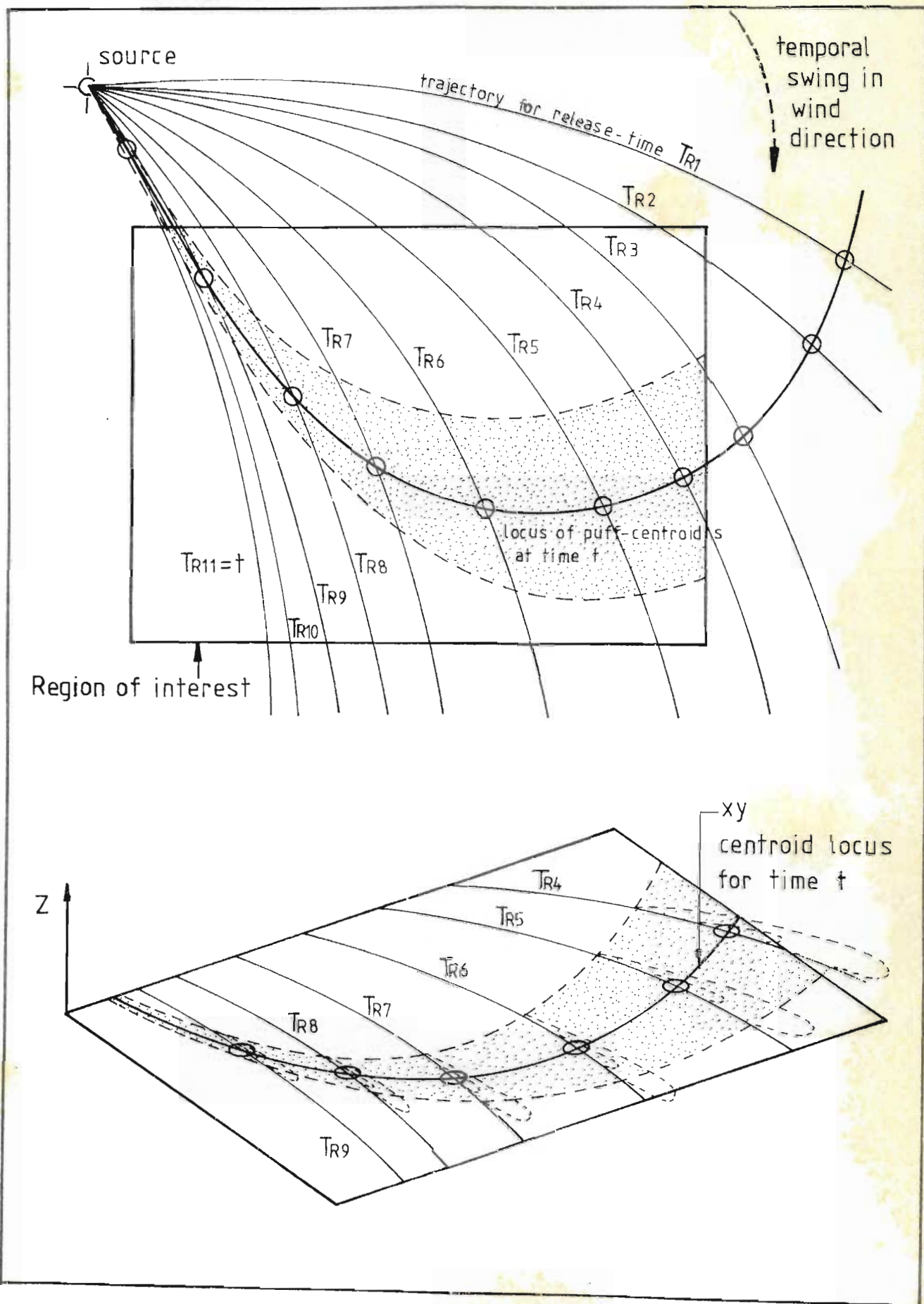
2.4.1.2 Region of interest.

The model is applied in some region for which the necessary meteorological and point-source release information is available. Some sub-region may be specified in which concentrations or dosages are of particular interest. In the case of concentration-distributions, times-of-interest are also specified, and it is necessary to solve for release-time intervals which are effective in supplying puffs which influence the region of interest at these times [appendix A1.3]. Relevant emission periods are established in terms of estimated puff-centroid loci [figure (2.3)].

The release-times which contribute to a time-of-interest locus need not be continuous, and provision is made for segmentation into up to three centroid loci. Centroids which occur outside of the region are allowed to contribute if they are within a specified release-time margin.

Turning to the case of dosage-prediction, the specified region of interest should enclose all points at which dosages are required. The earliest release-time to affect this region at the earliest dosage-interval time is then established. Thereafter, puffs are serially released until a release-time is reached which is greater than the last dosage-interval-time. Each puff-trajectory is only solved until the centroid has moved outside of a specifiable distance-margin around the region.

fig.(2.3) Region of interest



In order to minimise discretisation irregularities, release times are determined according to an optimal spacing based on prevalent wind-speeds. Typically, for gaussian puffs spaced at $\bar{u}\Delta t_R = 50\text{m}$, and an isotropic diffusivity of $0,5 \text{ m}^2 \text{ s}^{-1}$, the distribution becomes "smooth" within 400 m of the source. Generally, these time-intervals are somewhat smaller than the time-scales for meteorological variations, and the present practice is simply to interpolate puffs between solved puffs at larger release-time intervals. In this way a significant saving in computation is effected, with little loss in accuracy. The interpolations are necessarily approximate in that individual parameters, such as the concentration moments $C_n, n=0,1,2$, are interpolated separately. In the case of dosage-evaluation, a two-dimensional interpolation becomes necessary - both with respect to the real-time intervals Δt along the trajectory, and with respect to the release-time interval Δt_R "across" the trajectory. The interpolated puff then has a characteristic release-time t'_R , which determines its strength $Q(t'_R)\Delta t_R$, and a characteristic real-time t' , which determines the dosage interval to which it must contribute.

The concentration distribution is obtained by accumulation of puff-concentration contributions when the puffs $C(x,y,z,t)$ have attained their final positions at the time-of-interest. On the other hand, dosages are accumulated continuously along a puff-trajectory, thus requiring frequent location with respect to stationary

eulerian points via the inverse transformation \tilde{T}_p^{-1} (2.9). Hence, whilst it is possible to obtain concentration distributions of reasonable resolution in an eulerian grid, analogous presentation of dosage-distributions would require several orders-of-magnitude more computation. At present, dosage evaluations have been restricted to 40 arbitrary points at a fixed height, whereas concentration distributions are presented in high-resolution (e.g. 4000-point) horizontal grids covering the region of interest at one or two specified heights. A description of the computer algorithm and its use is presented in appendix (A1.4).

2.4.2 Velocity and diffusivity profiles, system properties.

Following equation (2.18), the meteorological variables required in the lagrangian frame are the mean effective velocities $\bar{U}(z,t), \bar{V}(z,t)$ and diffusivities $\bar{K}_x(z,t), \bar{K}_y(z,t)$ and $\bar{K}_z(z,t)$. Since these quantities depend on the location of the puff, they may only be evaluated as the puff evolves, from current values in the eulerian frame. Velocity information is further required in the eulerian frame for translation of the proximate curve according to equation (2.13), and for the establishment of release-time series which affect the region of interest [appendix (A1.3)]. Hence the most convenient form for storage of velocity and diffusivity data is as discretised histories for individual eulerian positions.

An enormous amount of computer-storage would be required if such data were to be stored 3-dimensionally in space. It is first assumed that the effect of directional

shear is negligible in the layer of interest [section (1.3.3)]. Velocity and diffusivity profiles may then be completely defined by 3 or 4 parameters as in section (1.2.3). The necessary parameters are thus stored 2-dimensionally (xy), and subroutines have been provided for their interpolation [appendix (A1.2)], and for evaluation of the variation of velocity and diffusivity with height.

The flux-profile relationships presently used are those suggested by Dyer (1974) with an extension due to Webb (1970) [section (1.2.3)]. If it is assumed that mass transfer is analogous to heat and momentum transfer, then equations (1.23) and (1.38) lead to

$$K_m(z) = u_* k z / \phi_m(z/L) \quad (2.68)$$

$$K_z(z) = u_* k z / \phi_w(z/L) \quad (2.69)$$

where vertical mass diffusivity will be based on published relationships for the universal function ϕ_w for water-vapour transfer. The validity of such formulae above the lowest region of the surface-layer (say >50 m) is debatable, though Carl, Tarbell and Panofsky (1973) suggest that they may in fact be valid to somewhat greater heights (10% of the planetary boundary-layer).

Webb (1970) observed that for $\zeta = z/L > 1$, velocity profiles deviated systematically from the log-linear form (1.26). On the basis of measurements at O'Neill, Kerang and Hay, he proposed that the log-linear law

$$\phi_m(\zeta) = 1 + \alpha \zeta, \quad \zeta > 0$$

could be extended into regions of strong stability by taking

$$\phi_m(\zeta) = 1 + \alpha \quad \text{for } 1 < \zeta < (\alpha + 1)$$

The present approach is to assume that the relations (1.29), (1.30) put forward by Dyer (1974) are valid in the region $-\infty < \zeta < 1$, and to extend Webb's idea by taking

$$\left. \begin{aligned} \phi_m(\zeta) &= \phi_m(1) \\ \phi_w(\zeta) &= \phi_w(1) \end{aligned} \right\} , \zeta > 1 \quad (2.70)$$

Because dispersion will be considered over relatively short ranges, often under stable conditions, the amount of material which diffuses to uncharacterised heights is expected to be negligible, and the above relations should suffice in the present application. It is usual to evaluate the velocity at height z by integration of equation (1.21) according to

$$\bar{u}(z) - \bar{u}(z_0) = \frac{u_*}{k} \int_{z_0}^z \frac{\phi_m(z'/L)}{z'} dz' \quad (2.71)$$

where z_0 is the roughness-length, and then to assume that $\bar{u}(z_0)$ is negligibly small. Equations (2.69) and (2.71) then lead to the following profile descriptions:

$$\bar{u}(z) = \begin{cases} \frac{u_*}{k} \left[2 \tan^{-1} b - 2 \tan^{-1} b_0 - \ln \left\{ \frac{b+1}{b-1} \cdot \frac{b_0-1}{b_0+1} \right\} \right], & L < 0 \\ \text{where} \\ b = \left(1 - 16 \frac{z}{L} \right)^{\frac{1}{2}}, \quad b_0 = \left(1 - 16 \frac{z_0}{L} \right)^{\frac{1}{2}} \\ \frac{u_*}{k} \left[\ln \left(\frac{z}{z_0} \right) + \frac{5}{L} (z - z_0) \right], & L > 0, z \leq L \\ \frac{u_*}{k} \left[5 - 5 \frac{z_0}{L} - \ln \left(\frac{z_0}{L} \right) + 6 \ln \left(\frac{z}{L} \right) \right], & L > 0, z \geq L \end{cases} \quad (2.72)$$

$$K_z(z) = \begin{cases} u_* k z \left[1 - 16 \frac{z}{L} \right]^{\frac{1}{2}}, & L < 0 \\ u_* k z \left[1 + 5 \frac{z}{L} \right]^{-1}, & L > 0, z \leq L \\ u_* k z / 6, & L > 0, z \geq L \end{cases} \quad (2.73)$$

The effect of dense vegetation or closely-spaced buildings has been observed to impose an upward-displacement on profiles of this form. This is accounted for by introducing a zero-plane displacement d which is characteristic of the surface, and which is incorporated in equations (2.72), (2.73) by replacing "z" with $(z-d)$ on the right-hand side. It is then usual to let $\bar{u}(z), K_z(z) = 0, z < d$.

The velocity and diffusivity profiles have thus been entirely defined in terms of the four parameters u_* , L , z_0 and d . Whereas the values of u_* , L are expected to vary with time at a point, the values of z_0 , d are effectively constant.

It remains to prescribe values for the horizontal mass diffusivities $K_x(z)$, $K_y(z)$. Calder (1965) showed

that in order to satisfy the transformation requirements of the diffusivity tensor K_{ij} , the choice of the vertical as a preferred axis necessitates $K_x = K_y = K_h$ say. Few relations have been proposed for the behaviour of K_h , and most workers just assume some constant value. In the present model, the horizontal diffusivity is related to vertical diffusivity using factors based on observed plume width.

In a series of tracer experiments conducted on the South African Highveld, Venter, Halliday and Prinsloo (1973) found that the Sutton diffusion parameters C_{sh} , C_{sz} , n [equation (1.44)] could be approximately represented by

$$\begin{aligned} n &= 0,0004 \bar{\theta}' + 0,37 \\ C_{sh} &= 0,57n + 0,106 \\ C_{sz} &= 0,38n + 0,112 \end{aligned} \quad (2.74)$$

where $\bar{\theta}'$ is a mean potential temperature gradient, $[\theta_2 - \theta_1] / [z_2 - z_1]$ ($^{\circ}\text{Cm}^{-1}$) evaluated from measurements at 97,5 m and 2,7 m according to equation (1.8). It is now assumed that the ratio C_{sz} / C_{sh} will be reasonably constant with height, so that equation (1.44) implies

$$K_h(z) = K_z(z) \left[\frac{C_{sh}}{C_{sz}} \right]^2 \quad (2.75)$$

The present approach is to evaluate the constants C_{sh} , C_{sz} using the potential temperature gradient at a specified fixed height z_G vis. $\bar{\theta}'_{z_G}$, and then to use equation (2.75) as an estimate of the horizontal diffusivity profile.

It is necessary to interpolate defining parameters such as u_* , L , $\bar{\theta}_{z_G}$, z_a and d separately in time and space in order to find their expected values at a point (x,y,t) . Since u_* and z_a are highly coupled, separate interpolation may lead to serious errors in the velocity at some representative height, say z_G . It is thus convenient to interpolate the speed at this height, $|\tilde{U}_{z_G}|$, and deduce u_* subsequently using the profile relations (2.72). The most realistic means of including wind direction is by interpolation of the separate Cartesian components U_{z_G} , V_{z_G} . The weighted combination of contributions then constitutes a vectorial addition.

It is noted that the stability length only appears as the inverse $1/L$ in the velocity and diffusivity relations (2.72), (2.73), implying a singularity at $L=0$. In fact, $L=0$ should never occur [equation (1.20)], and $1/L$ should be continuous over $L=-\infty$ (slightly unstable) to $L=+\infty$ (slightly stable). Hence it is more reasonable to interpolate the values L^{-1} for use in profile relationships at a point (x,y,t) .

The present model also allows for the specification of spatially-variant surface absorptivity [section (1.9.2)], as represented by the deposition velocity $w_d(x,y)$. These values are stored like z_a and d at discrete points in an x - y grid, and will also require interpolation.

Finally, the temporally- and spatially-variable parameters which are required to define the system may be summarised as follows:

$U_{z_G}(x,y,t)$	x velocity component at height z_G
$V_{z_G}(x,y,t)$	y velocity component at height z_G
$\bar{\theta}'_{z_G}(x,y,t)$	potential temperature gradient $\partial\theta/\partial z _{z_G}$
$L^{-1}(x,y,t)$	inverse Monin-Obukhov stability length
$z_a(x,y)$	roughness length
$d(x,y)$	zero-plane displacement
$w_d(x,y)$	deposition velocity representing ground absorption

The storage and interpolation procedures used for these parameters are discussed in appendix (A1.2).

2.4.3 Release time intervals and trajectory steps.

The release-time sequences which contribute to a particular concentration distribution or dosage interval are estimated by simulating the motion of puffs through the system [appendix (A1.3)]. Each sequence is then divided into a series of instantaneous releases spaced at release intervals of Δt_R [section (2.4.1.2)]. Having established these release-times, it is necessary to provide real-time trajectory steps Δt for individual puffs. In specifying this step-size, certain resolution/accuracy requirements must be satisfied. Too large a step Δt would provide solved puffs only at large separations, whilst too small a step-size would incur a prohibitive amount of computation. Further, as the cloud expands, spatial gradients are reduced, and sufficient accuracy is provided

by larger step-sizes than in earlier stages. The optimal spatial stepsizes for the diffusion step are given by equation (2.49).

$$\Delta x_{OPT} = (K_x \Delta t / 0.4)^{\frac{1}{2}}, \quad \Delta z_{OPT} = (K_z \Delta t / 0.4)^{\frac{1}{2}} \quad (2.76)$$

It is sufficient to keep these stepsizes within specified limits of their optimal values, but too frequent changes in Δt will require frequent changes in $\Delta x, \Delta z$, and the associated interpolation is better avoided. The compromise presently employed is to increase Δt linearly once every 5 time-steps according to

$$\begin{aligned} \Delta t_{i+5j} &= (j+1)\Delta', \quad i=1,5 \\ & \quad j=0,1,\dots,\infty \\ & \quad i+5j \neq 1 \end{aligned}$$

The exception in the case of Δt_1 arises from the use of the gaussian distribution as a seed at $(t-t') = \Delta'/2$ [section (2.3.2)] so that $\Delta t_1 = \Delta'/2$. In typical applications the choice of $\Delta' = 100s$ is usually adequate, though smaller steps may be preferable if time-resolution is important.

If there are to be n_R puff-releases at times $t_{Rj} = t'_1 + j\Delta t_R$, $j=1, n_R$, then the i th trajectory-step of the j th puff will represent a real-time step from

$$\left[t'_1 + j\Delta t_R + \sum_{k=1}^{i-1} \Delta t_k \right] \quad \text{to} \quad \left[t'_1 + j\Delta t_R + \sum_{k=1}^i \Delta t_k \right]$$

Advection of the curvilinear lagrangian frame is undertaken as a series of smaller steps $\Delta t_i/n_s$ during this time-step, with the accumulation of the spatially- and temporally-

variable parameters in section (2.4.2) as time-averages. The average values are then used to solve for the lagrangian puff development during Δt_i [section (2.3)].

2.4.4 Advection in the lagrangian frame.

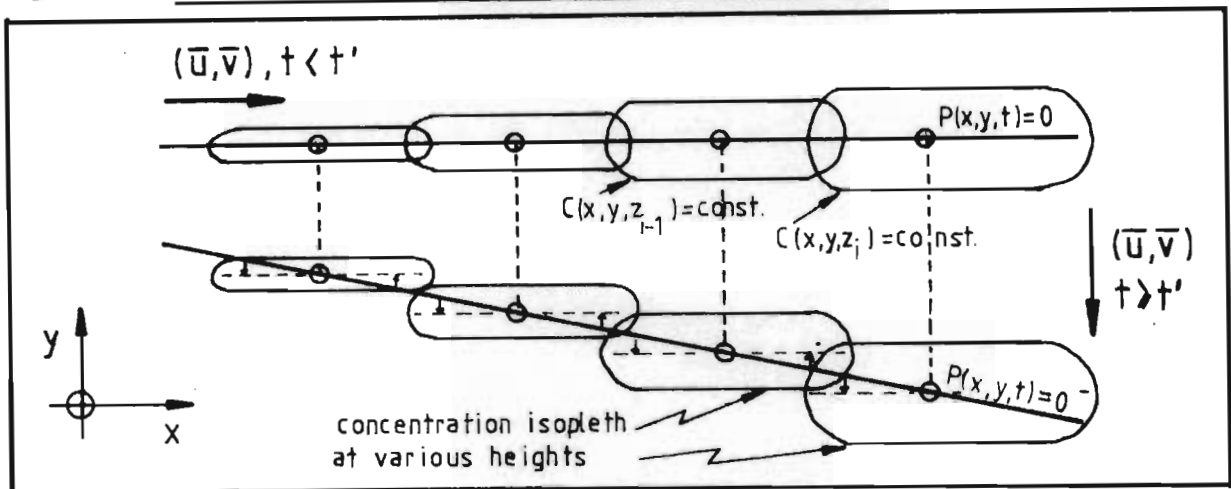
2.4.4.1 The proximate curve.

The concept of the proximate curve $P(x,y,t)=0$ was introduced in section (2.2.2) as a basis for the transformation \bar{T}_P , and it remains to specify the form of P as used in the dispersion model. The requirement of P was that it should remain "close" to the cloud distribution in eulerian space. It was pointed out that if an initial curve $P'(x,y)=0$ satisfied this requirement, then future optimum curves could be predicted by allowing the initial curve to be translated in a lagrangian sense by the wind-field velocities at some optimum height $Z(t)$ [equations (2.11) to (2.13)].

In fact, if the xy centroid at a height z is considered, this position should reflect time-integrated velocities at height z . That is, if a vertical line passing through the point of release is allowed to become deformed by the subsequent wind-field, it is likely to remain "near" the centroid at each level for subsequent times. If the curvilinear vertical surface defined by $P(x,y,t)=0$ contained this line, then it should satisfy the proximity requirement rather well. This method has been

used in previous versions of the dispersion model. However, it has the disadvantage that for a temporal variation in the wind-field, the advection step requires a directional reorientation of the distribution at each height with respect to P . Figure (2.4) represents such a variation in the case of a linear velocity profile.

fig.(2.4) Locating-line subject to velocity gradient

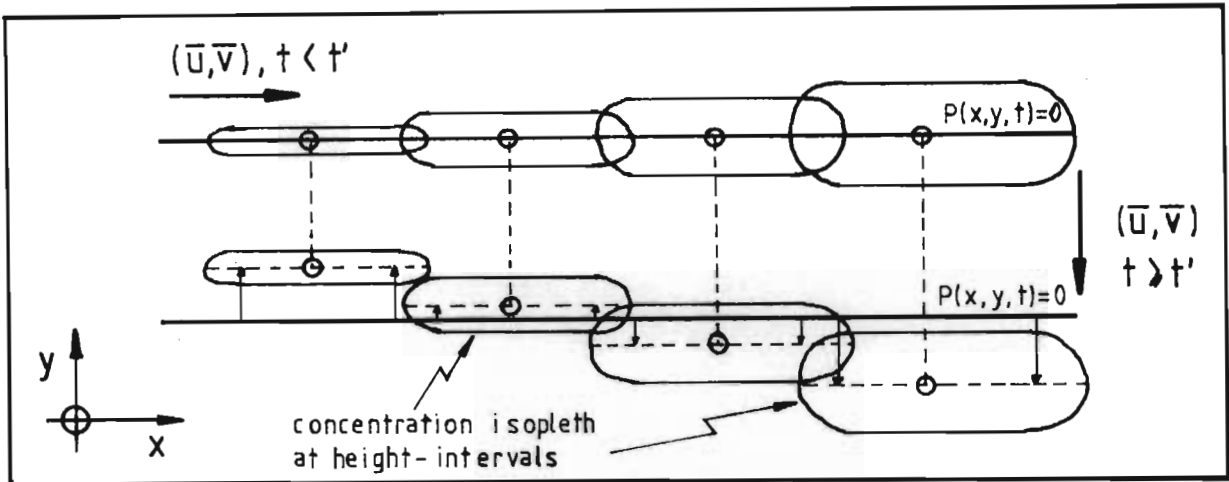


Unless the distribution at each level is correctly relocated according to the moment-representation, requiring a great deal of calculation, the obvious approach of adjusting the mean y -position $m_y(x, z, t)$ at each level (by adding the new deviations) leads to a cumulative error which may become quite significant.

Instead, the present method avoids the temporal reorientation problem by basing $P(x, y, t) = 0$ on a horizontal

line at height $Z(t)$, where the line is similarly advected by the wind-field. Figure (2.5) represents a single temporal change, when the wind-profile is linear.

fig.(2.5) Horizontal locating-line

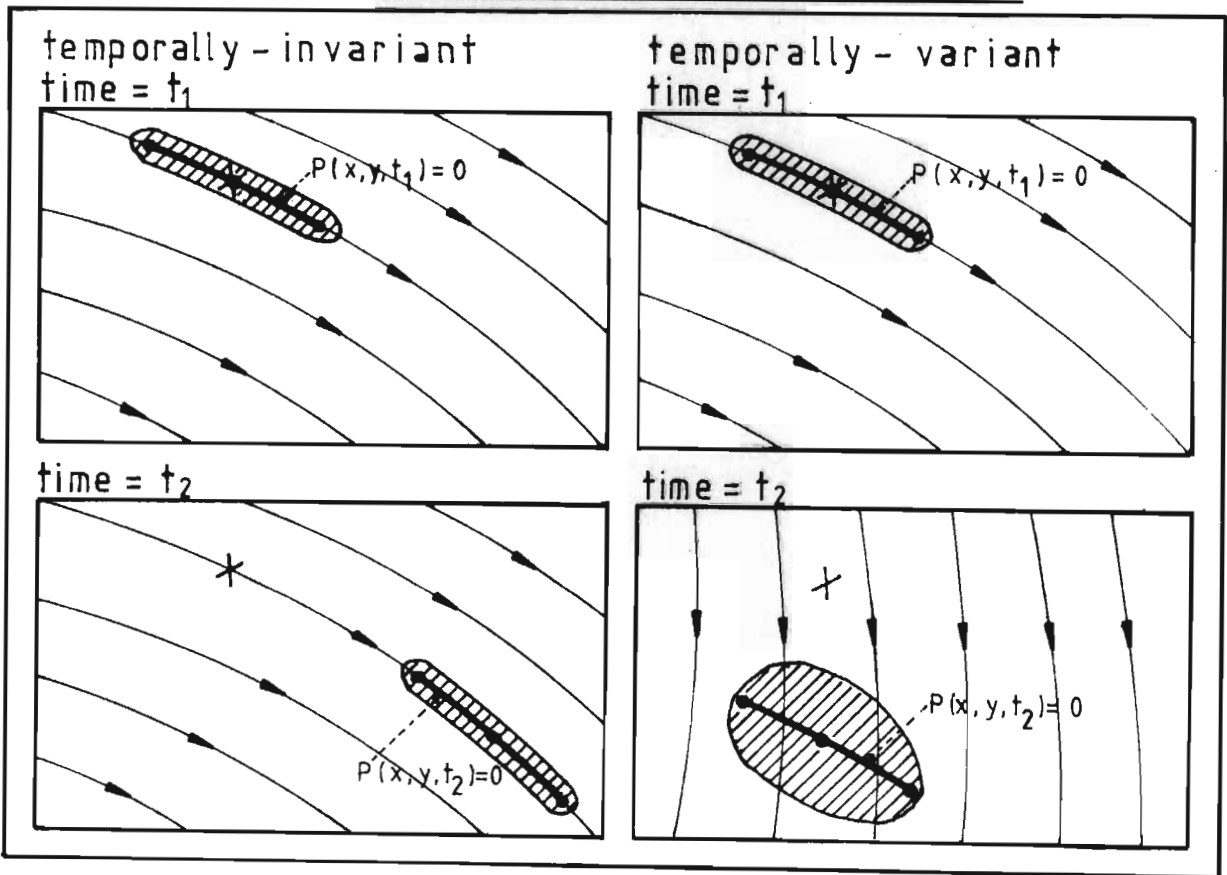


The new distribution is of course accurately represented by direct adjustment of $m_y(x, z, t)$. However, this method suffers from the disadvantage that the proximate curve does not adjust so as to minimise the cross-wise wind component, one of the criteria for accurate representation by the first three moments [section (2.2.4)]. Nevertheless, in typical applications the cross-component can usually be minimised by judicious choices of the initial curve $P'(x, y) = 0$, and the optimum tracking height $Z(t)$.

If P' is chosen to follow the streamline through the point of release at the time of release, then at least in a temporally-invariant wind-field the curve $P(x, y, t) = 0$ will

always be parallel to neighbouring streamlines. Further, if temporal variations in the wind-field are slow, it is expected that for moderate travel-times the component of wind normal to P will remain relatively small. It will be seen that even in the case of a sudden temporal change, the moment representation gives a reasonable estimate of the subsequent distribution [figure (2.6)]. However, spatial velocity variations normal to P cannot be accounted for, so that this component is best minimised.

fig. (2.6) Spatial and temporal wind-field variations



The curve P is represented by three particles at the positions $[X_i(t), Y_i(t)]$, $i=1,2,3$, which are determined

according to the lagrangian integrals

$$\begin{aligned} [X_i(t), Y_i(t)] &= [x_i^{\prime\prime}, y_i^{\prime\prime}] + \int_{t'}^t [\bar{u}(X_i(\tau), Y_i(\tau), Z(\tau), \tau), \\ &\quad \bar{v}(X_i(\tau), Y_i(\tau), Z(\tau), \tau)] d\tau, \quad i=1,2,3 \end{aligned} \quad (2.76)$$

The initial positions $[x_i^{\prime\prime}, y_i^{\prime\prime}]$ at the release-time t' are chosen along the streamline through the point of release $[x^{\prime\prime}, y^{\prime\prime}]$. The central "particle" begins at the point of release, and must thus stay close to the centroid of the cloud. The outlying particles are given initial positions at specified distances upwind and downwind of the release-point, using integrals like (2.76) in which the wind-field is held constant at $\tau=t'$.

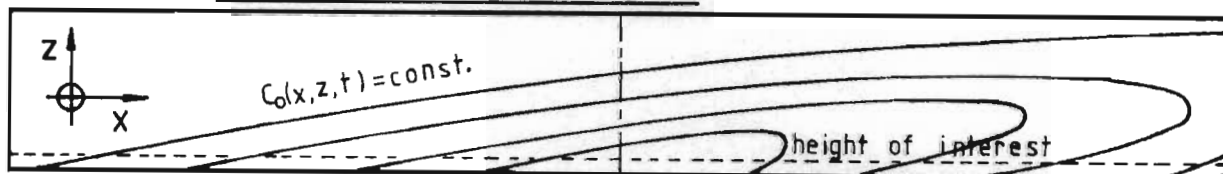
The curve chosen to be uniquely defined by these three points is the arc of a circle, because of its independence of coordinate rotations. Hence, only such simple curvatures may be accounted for, and wind-fields in which there is strong localised spatial variation must be avoided. However, the use of a circular arc allows for a unique transformation \tilde{T}_P , of which the inverse \tilde{T}_P^{-1} will exist, and it has already been concluded that the curvature of P must be reasonably small if this transformation is to be approximately linear [section (2.2.2)].

The three points $[X_i(t), Y_i(t)]$, $i=1,2,3$, will now represent stationary positions in the lagrangian frame, so that the choice of the tracking height $Z(t)$ will determine relative motion of the distribution within the lagrangian frame. Since the lagrangian frame solution grid is of

finite size, it becomes necessary to adjust $Z(t)$, and hence the effective velocity of the frame, so as to localise material within the grid. The centre of the lagrangian grid is initially fixed on the particle which began at the source at (x'', y'', t') . Hence for small travel-times, the optimum tracking height will be $Z(t) = z''$, the height of release. The criterion used for subsequent adjustment of $Z(t)$ is that the centroid at the height of interest (for dosages or concentration distributions) should remain within a specified distance of the grid-centre. This adjustment is operated as a feed-back control at each trajectory-step Δt , with the new height $Z(t + \Delta t)$ determined by the velocity gradient at the current height $Z(t)$, and the required relative movement of the grid. It will be noted that the motion of the grid-centre, as seen in the eulerian frame, thus closely parallels the simulated motion which was developed in appendix (A1.3) in order to estimate the centroid position for the height of interest.

In typical applications, the lagrangian solution grid has an "along-wind" dimension which is large enough to contain all of the original material, even in extensive shear [figure (2.7)].

fig. (2.7) Lagrangian solution grid



A provision is however made for the termination of relative advection within the grid if the fraction of material remaining within the grid drops below a specified lower limit. The frame itself will continue to move in eulerian space, with $Z(t)$ set to z'' .

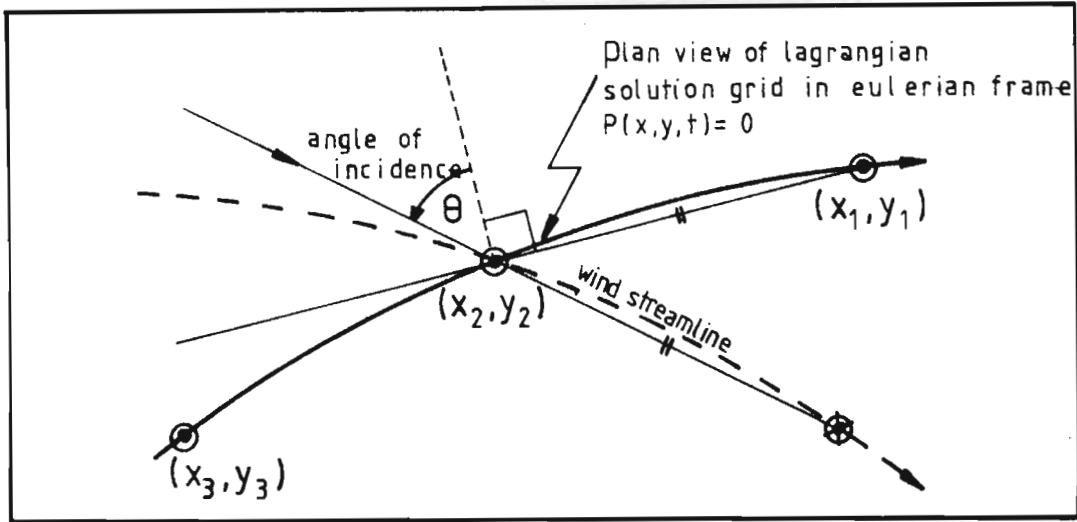
2.4.4.2 Relative velocity.

The relative velocity which acts on material at height z in the lagrangian frame will clearly be determined by the difference between the eulerian velocities at height z and at the frame tracking height $Z(t)$, according to the transformation \tilde{T}_p in equation (2.16). Moreover a simplifying assumption was made in section (2.2.3) by means of which advection in the lagrangian frame may be represented using the mean incident velocity $[\bar{U}(z,t), \bar{V}(z,t)]$ [equation (2.18)] which is only dependent on time and height.

In order to evaluate a mean effective incidence on the lagrangian frame, the streamline through the cloud centroid is followed to the same distance as the forward tracking point [fig. (2.8)].

In fact, for the effective incident velocity during the time-step t to $t+\Delta t$, the wind-field is averaged during t to $t+\Delta t$ in order to compute the streamline. Within one or two iterations, a point at the correct distance on the streamline is usually found. Note that this procedure will preserve the cross-grid component $\bar{V}(z,t)=0$ in a temporally-invariant wind-field, whilst it will provide along-grid

fig. (2.8) Estimation of effective angle of incidence



"averages" for $\bar{V}(z,t)$ if a temporal change has occurred. The relative velocity acting in the lagrangian frame is obtained by difference of the centroid velocity at (x_2, y_2) and the wind-field velocity at this point in the eulerian frame. This net velocity is resolved along P as $\bar{U}(z,t)$ and across P as $\bar{V}(z,t)$, according to the angle of incidence θ_{AZ} [figure (2.8)].

The procedure used to solve for the advection step within the lagrangian frame has been discussed in section (2.3.1). For the component $\bar{U}(z,t)$ which acts along P, the advection equation for the moments $C_n, n=0,1,2$,

$$\left. \frac{\partial C_n(x,z,t)}{\partial t} \right|_{\text{adv.}} = - \bar{U}(z,t) \frac{\partial C_n(x,z,t)}{\partial x}$$

is solved as a lagrangian transformation of the x-coordinate [equation (2.33)]. The contributions of $\bar{V}(z,t)$ to the first and second moments across P are accounted for by equations (2.31), (2.32) and (2.34). The moments C_n for material arriving at a grid-point, say $(x=i\Delta x, z=k\Delta z)$ are determined according to the point-of-origin of a "particle" arriving at this point after a time-step Δt . For particles originating outside of the solution grid, values are set to the boundary-value at the point of entry.

In general, interpolation is required to evaluate C_n at the point of origin, though Runca and Sardei (1975) approximated the velocity profile with a step function in order to avoid the associated pseudo-diffusion [section (1.6.4.4)]. In the present work, it was noted that spatial variations of $\log [C_0]$, C_1 and C_2 were reasonably linear, so that linear interpolations of these quantities are used to find $C_n, n=0,1,2$ at a particular position. Further, the large number of grid divisions along-wind (e.g. 280) should limit the contribution of pseudo-diffusion.

The sedimentation process is solved as a similar lagrangian shift [equation (2.36)], and identical linear interpolation of $\log [C_0]$, C_1 and C_2 is used in this case. It is also used in the adjustment of grid-stepsizes discussed in section (2.4.3), in order to satisfy the optimality criteria (2.76).

2.4.5 Removal processes and ground deposition.

In section (2.3.4) it was proposed that the non-settling removal processes could be modelled using a combined removal function F_r which operates during the time-step t to $t+\Delta t$ according to

$$\Delta C_{nr}(x,z,t,\Delta t) = C_n(x,z,t) \{ F_r [z,\Delta t, \bar{k}_r(t,\Delta t), \bar{w}_d(t,\Delta t), \bar{K}'_z(t,\Delta t)] - 1 \},$$

where ΔC_{nr} is the change in the n th moment at (x,z,t) due to the removal processes alone [equation (2.63)], and \bar{k}_r is the combined first-order rate constant. In the numerical model, provision is made for a constant component of \bar{k}_r , and a time-dependent component which is zero outside a specified interval, and constant within it. The latter component is designed to account for a rain-shower of fixed intensity, which only operates during one time-interval.

Ground-deposition is only evaluated in dosage applications of the numerical model, because of the analogous accumulation effect. Deposition at a point will include a sedimentation contribution, and contributions from the general removal processes represented by F_r , excluding processes such as chemical decay which do not transfer material to the ground. The changes $\Delta C'_{nr}(x,z,t,\Delta t)$ due to the deposition processes ($w_s, \bar{w}_d, \bar{\Lambda}$) alone are evaluated, and integrated with respect to height z in order to give the zeroth, first and second moments of deposition at x during the interval t to $t+\Delta t$. This deposition distribution is

transformed onto the eulerian grid via \tilde{T}_p^{-1} (2.9), and deposition-dosage points are credited according to their location, for the appropriate dosage interval.

CHAPTER 3

EVALUATION OF THE DYNAMIC PUFF MODEL

3.1 Comparison with analytical puff solutions.

Central to the modelling technique proposed in chapter (2) is the problem of solving for the development of a lagrangian puff. Peripheral procedures, such as locating the puff in eulerian space and supplying it with representative velocity and diffusivity information, can to a large extent be controlled externally, for example by improving the resolution of the available data. Though it is necessary to rely on the accuracy of the puff solution itself, an indication of the theoretical validity of the method may be obtained by comparison with certain analytical solutions.

Consider diffusion and advection of the moments $C_n(x,z,t), n=0,1,2$, in the lagrangian frame, following a unit release. The most complex case for which an analytical description is available [Quesada (1971)] includes an invariant linear wind velocity profile with constant diffusivities $\bar{K}_x, \bar{K}_y, \bar{K}_z$. For the two-dimensional x-z problem with velocity in the x-direction only, equation (1.39) may be written as

$$\frac{\partial C_n}{\partial t} + [u_\alpha + \alpha z] \frac{\partial C_n}{\partial x} = \bar{K}_x \frac{\partial^2 C_n}{\partial x^2} + \bar{K}_z \frac{\partial^2 C_n}{\partial z^2} \quad (3.1)$$

Since the velocity intercept u_0 simply transforms the x -coordinate according to $u_0 t$, equation (3.1) may be considered with $u_0=0$. Choosing time- and length-scales $\Delta t, \Delta x, \Delta z$, non-dimensionalise equation (3.1) by setting $t_1 = t/\Delta t$, $x_1 = x/\Delta x$, $z_1 = z/\Delta z$.

$$\begin{aligned} \frac{\partial C_n}{\partial t_1} + \left[\frac{\alpha \Delta t \Delta z}{\Delta x} \right] z_1 \frac{\partial C_n}{\partial x_1} &= \left[\frac{\bar{K}_x \Delta t}{(\Delta x)^2} \right] \frac{\partial^2 C_n}{\partial x_1^2} \\ &+ \left[\frac{\bar{K}_z \Delta t}{(\Delta z)^2} \right] \frac{\partial^2 C_n}{\partial z_1^2} \end{aligned} \quad (3.2)$$

In the numerical solution, the optimal values for the coefficients on the R.H.S. of equation (3.2) were found to be $\bar{K}_x \Delta t / (\Delta x)^2 = \bar{K}_z \Delta t / (\Delta z)^2 = 0,4$ [equation (2.49)].

Grid step-sizes $\Delta x, \Delta z$ are adjusted in order to approximate this condition. It follows that for constant

$$\alpha' = \alpha \Delta t \sqrt{\bar{K}_z / \bar{K}_x},$$

the numerical solutions of equation (3.2) will be similar for all t_1 . If a particular solution is accurate for $t_1 = t/\Delta t$, so will all others be at t_1 , provided α' is held constant. In order to gauge the accuracy of this solution, it suffices to compare the predicted behaviour of the zeroth moment $C_0(x, z, t)$, following a unit release at $t=0$, with solutions due to Quesada (1971) and Saffman (1962).

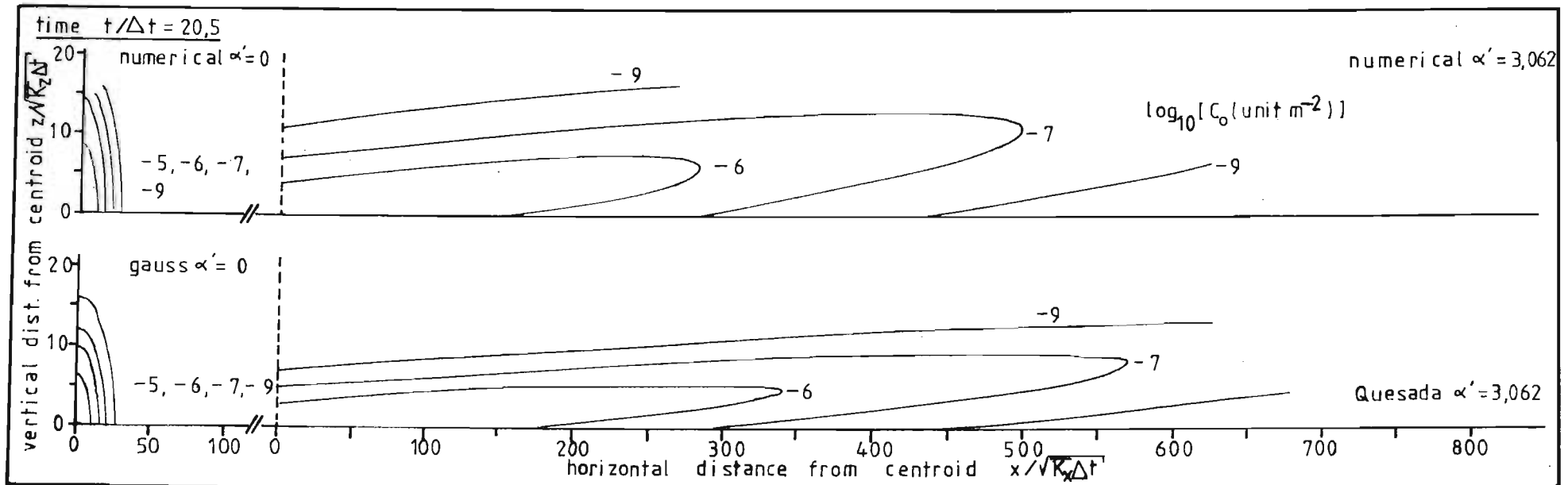
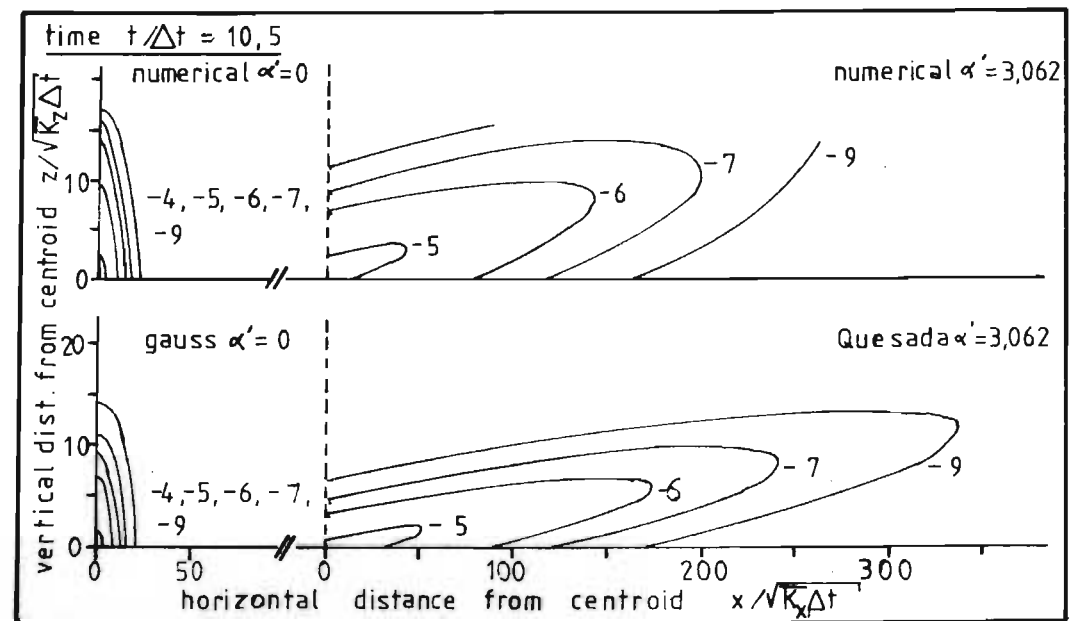
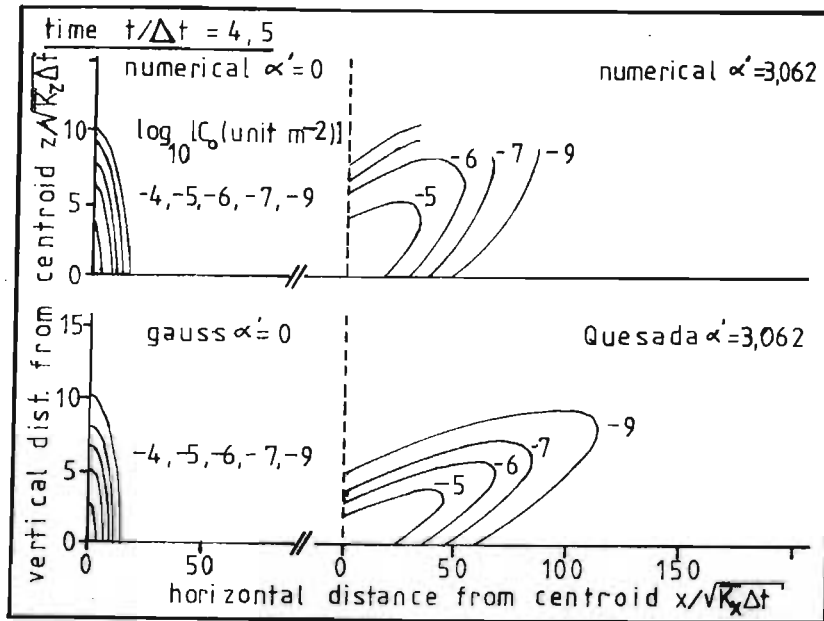
3.1.1 Unbounded atmosphere.

Quesada (1971) provided an analytical solution for the case of constant diffusivities and a linear velocity profile in an unbounded atmosphere [section (1.5.2)]. Equation (1.50) is applied to the above problem by integrating across-wind. Note that the product $\epsilon\beta = -\alpha\sqrt{\bar{K}_z/\bar{K}_x}$. Clearly, for $\alpha=0$, Quesada's solution must reduce to that for an unbounded gaussian puff.

Figure (3.1) presents a comparison of the first-quadrant isopleths predicted numerically, and analytically [Quesada], on the basis of K-theory. With regard to the gaussian puffs, it is seen that the numerical solutions do not have the perfect isotropic symmetry of the analytical solutions. Slight differences between axial and non-axial directions arise from separation of the x and z diffusion processes during Δt [section (2.3.3)].

The solutions for velocity gradient $\alpha'=3,062$ suggest that the numerical result lags slightly in its response to wind-shear, and has a falsely enhanced vertical diffusion in the presence of wind-shear. However, in view of the versatility of the numerical solution, it is felt that this accuracy is acceptable. Note especially the great differences between the sheared and unsheared solutions.

fig. (3.1) Isoleth comparison-numerical and analytical solutions for an unbounded puff

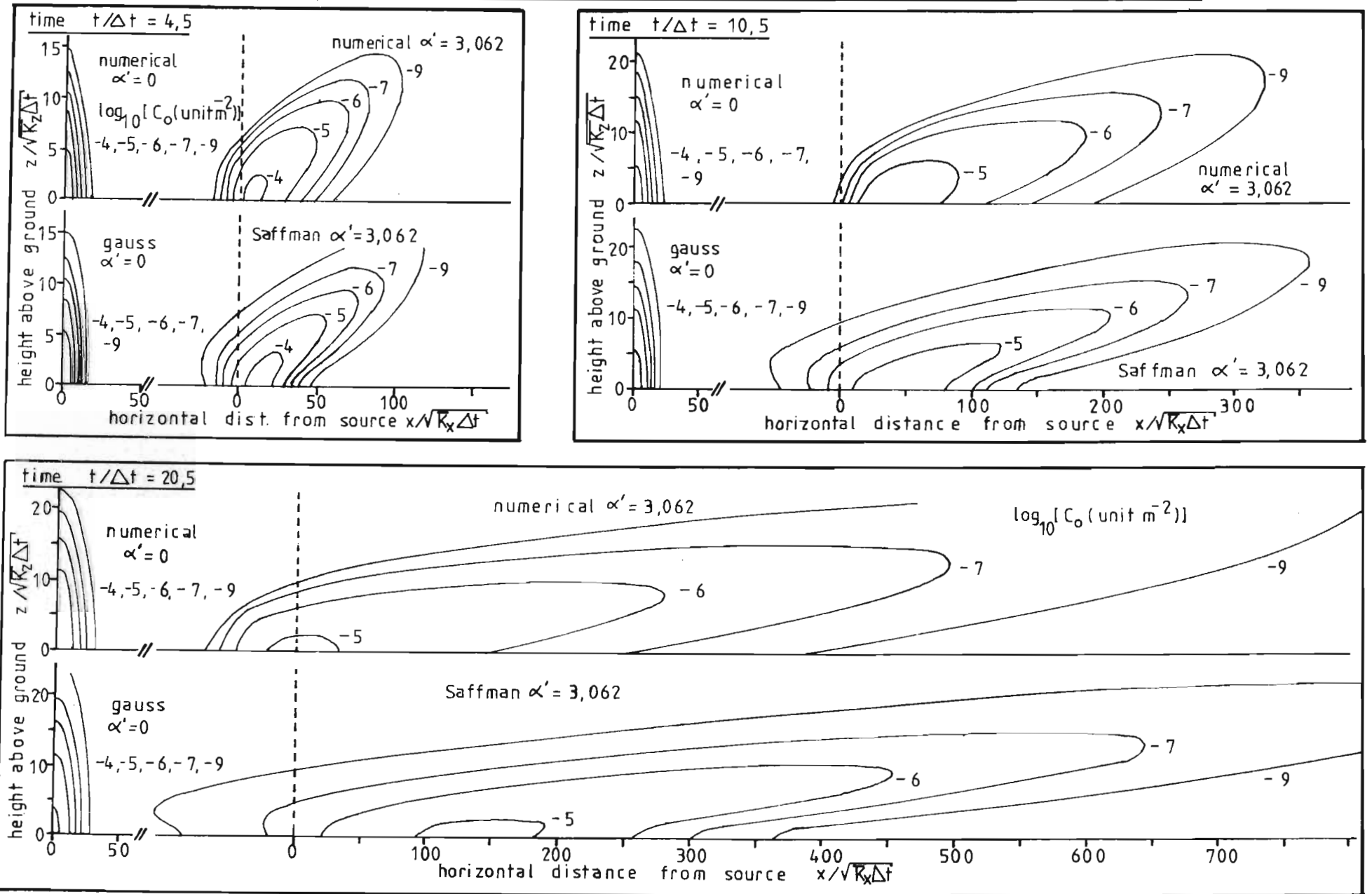


3.1.2 Bounded atmosphere.

No solution has been found for the case of a sheared puff in a bounded atmosphere, though Saffman (1962) provided analytical solutions for the first few moments following ground-level release with a linear velocity profile [section (1.5.2)]. For constant vertical diffusivity, and horizontal diffusivity which is either constant or proportional to height, Saffman shows that the along-wind distribution will not be asymptotically gaussian, and that the ground-level skewness factor will be approximately unity in the absence of horizontal diffusion. For the purpose of comparison with the equivalent numerical solution, however, the distribution at all heights will be assumed gaussian, so that only the zeroth (1.56), first (1.57) and second (1.58) [$\bar{K}_x = \text{const.}$] along-wind moments will be accounted for.

In figure (3.2), the ground-level gaussian puffs ($\alpha' = 0$) are seen to agree reasonably, though the same comments as in section (3.1.1) apply. It is apparent in the sheared puffs that the ground boundary acts to curtail the upwind spread of material, since diffusion into lower velocity strata is impossible. The rapid dissipation ($\bar{K}_z = \text{const.}$) of material drawn out on the upwind edge leads to pronounced positive skewness in the along-wind distribution, particularly at ground level. Of course, this skewness has been omitted from the moment description following Saffman, where the enhanced variance near ground-level, and the upwind "tail", would probably be absorbed if the correct skewness were present.

fig. (3.2) Isopleth comparison - numerical and moment solutions for a ground-level puff



The abscissa in figure (3.2) is the dimensionless distance downwind of the point of release, and it is notable that the numerical solution has correctly predicted this distance for a ground-level release, and velocity $\bar{u}(z)=\alpha z$.

3.2 Comparison with puff observations.

Because of spatial and temporal resolution requirements, few observations of puff behaviour have been published. However, Drivas and Shair (1974) used squeeze-bottle samplers and gas-chromatography for the analysis of SF₆ released from a quasi-instantaneous line source, whilst Nickola (1971) and Nickola, Ludwick and Ramsdell (1970) used a 3-dimensional array of 64 Geiger-counter sensors to record the passage of a cloud of radioactive ⁸⁵K_r. Unfortunately, these studies all display the same paucity of simultaneous meteorological observation, and comparisons on the basis of available meteorological measurements will be somewhat subjective.

It is important to distinguish between the existence of the cloud as a lagrangian entity, and the necessarily eulerian nature of the concentration measurements in the above studies. Measurements were made as time-histories at stationary points in the path of the cloud, and a single time-history cannot generally be used, without additional information, to reconstruct the instantaneous distribution at the height of measurement. In order to simulate these experiments, the dynamic puff numerical model was used to provide instantaneous distributions at various times along

Table (3.1) Interpretation of instantaneous release experiments.

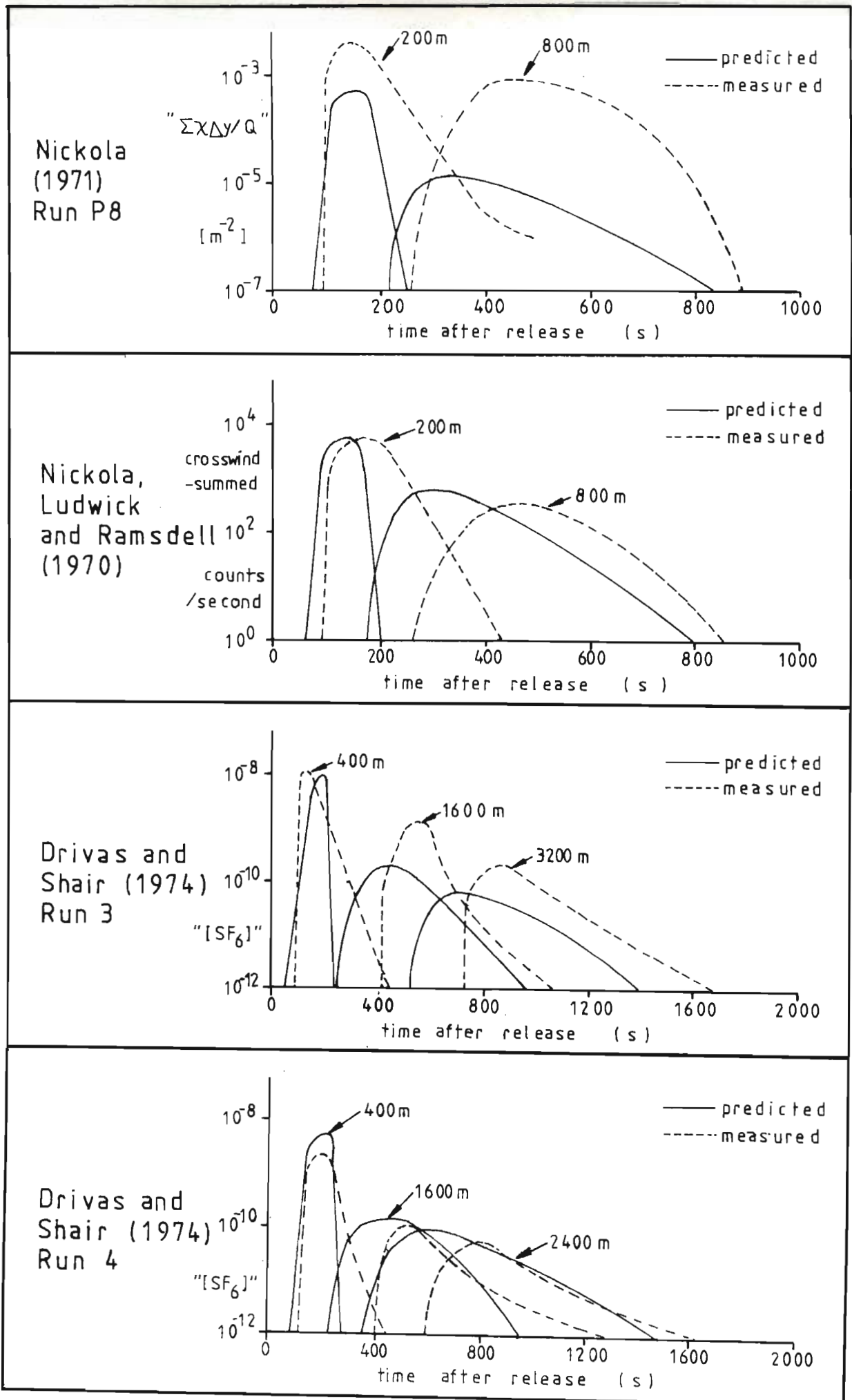
	NICKOLA (1971) RUN PB	NICKOLA, LUDWICK AND RAMSDALL (1970)	DRIVAS AND SHAIR (1974) RUN 3	DRIVAS AND SHAIR (1974) RUN 4
RELEASE	1 unit $z_s = 0$ m	10 C_i $z_s = 0$ m	crosswind line source: 44 k.SF ₄ min ⁻¹ at 88 km hr ⁻¹ = 0,1926 g m ⁻¹ $z_s = 0$ m	crosswind line source: 31 k.SF ₄ min ⁻¹ at 80 km hr ⁻¹ = 0,1493 g m ⁻¹ $z_s = 0$ m
RECEPTION	z=1,5 m x=200 m, 800 m $t_{max}=900$ s	z=1,5 m x=200 m, 800 m $t_{max}=900$ s	z=1,5 m x=400 m, 800 m, 1600 m, 2400 m, 3200 m $t_{max}=1800$ s	z=1,5 m x=400 m, 800 m, 1600 m, 2400 m $t_{max}=1800$ s
CONVERSION FROM 2-D UNIT RELEASE TO PUBLISHED RESULT	cross-wind integrated dilution factor, $\therefore F_c = 1,0$	20 detectors at 2° intervals. 9,7 (counts/ sec)/(uC _i /m ³) For count summation, F _c (200 m)=1,389 × 10 ⁷ F _c (800 m)=5,556 × 10 ⁷	"[SF ₄]"=(g m ⁻³)/(5,86 × 10 ³) $\therefore F_c = 3,267 \times 10^{-5}$	"[SF ₄]"=(g m ⁻³)/(5,86 × 10 ³) $\therefore F_c = 2,548 \times 10^{-5}$
AVAILABLE METEOROLOGICAL INFORMATION	R _Δ (2,1m-15,2m)=0,07 $\bar{u}(1,0m)=1,1$ m s ⁻¹ $\bar{u}(1,8m)=1,6$ m s ⁻¹	T(15m)-T(0,9m)=0,9 °C $\bar{u}(1,5m)=1,6$ m s ⁻¹	Partly cloudy, no inversion. $\sigma_{AZ}(2m)=8,6^\circ$ $\bar{u}(1,5m)=2,15$ m s ⁻¹ $\bar{u}=k_1 z^{0,18}$ $\bar{K}_z = k_2 z^{0,18}$	Sunny, clear, no inversion $\sigma_{AZ}(2m)=10,1^\circ$ $\bar{u}(1,5m)=1,87$ m s ⁻¹ $\bar{u}=k_1 z^{0,16}$ $\bar{K}_z = k_2 z^{0,16}$
PROPOSED VELOCITY AND DIFFUSIVITY PROFILES	$\bar{u} = \frac{u_*}{k} \left[\ln\left(\frac{z}{z_0}\right) + \frac{z}{L}(z-z_0) \right]$ $\bar{K}_z = \frac{u_* k z}{(1+5\frac{z}{L})}$ [Dyer (1974)] $\bar{K}_x = \left[\frac{C_x}{C_z} \right]^2 \bar{K}_z$	$\bar{u} = \frac{u_*}{k} \left[\ln\left(\frac{z}{z_0}\right) + \frac{z}{L}(z-z_0) \right]$ $\bar{K}_z = \frac{u_* k z}{(1+5\frac{z}{L})}$ [Dyer (1974)] $\bar{K}_x = \left[\frac{C_x}{C_z} \right]^2 \bar{K}_z$	$\bar{u} = k_1 z^p$ $\bar{K}_z = k_2 z^{(1-p)}$ (const. shear stress) $\bar{K}_x = \text{const.}$	$\bar{u} = k_1 z^p$ $\bar{K}_z = k_2 z^{(1-p)}$ (const. shear stress) $\bar{K}_x = \text{const.}$
ESTIMATED VALUES OF PARAMETERS	$z_0 = 0,2527$ m (direct fit using temp. profile ex Dyer, (1974)) $u_* = 0,2987$ m s ⁻¹ L=61,46 m $\bar{u}(10m) = 3,42$ m s ⁻¹ $\left. \frac{\partial \theta}{\partial z} \right _{z=z_0} = ,0517$ deg m ⁻¹	$z_0 = 0,2527$ m (same site; sagebrush + steppe grasses) $u_* = 0,3355$ m s ⁻¹ L=78,83 m $\bar{u}(10m) = 3,70$ m s ⁻¹ $\left. \frac{\partial \theta}{\partial z} \right _{z=z_0} = ,0458$ deg m ⁻¹	$\sigma_{AZ}(2m)$ indicates near- neutral, \therefore assume neutral diffusivity at 2m $\left[K_m = k^2 z^2 \frac{\partial \bar{u}}{\partial z} \right]_{2m}$ Then if $\bar{K}_z = \bar{K}_m$: $k_1 = 1,843$, $k_2 = 0,1804$, $p = 0,38$, $\bar{K}_x = 0,391$ m ² s ⁻¹ since (Sutton Params.) $[K_x/K_z] = 1,61$ neutral	$\sigma_{AZ}(2m)$ indicates near- neutral, \therefore assume neutral diffusivity at 2m $\left[K_m = k^2 z^2 \frac{\partial \bar{u}}{\partial z} \right]_{2m}$ Then if $\bar{K}_z = \bar{K}_m$: $k_1 = 1,552$, $k_2 = 0,2054$, $p = 0,46$, $\bar{K}_x = 0,421$ m ² s ⁻¹ since (Sutton Params.) $[K_x/K_z] = 1,61$ neutral

the puff trajectory. Distributions at intermediate times were interpolated in the usual way so as to improve the time-history resolution at stationary points on the trajectory.

The velocity and diffusivity profiles used in these simulations are detailed in table (3.1), together with the estimated profile parameters, based entirely on the available meteorological information. Conversion factors have been calculated in order to transform the numerically-solved cross-wind integrated unit release concentrations to the units employed in the various published time-histories. Figure (3.3) presents direct comparisons of the numerically-predicted, and field-measured results, in the published units.

The area under the curve represents the total dosage [section (2.4.1.1)] at the height of measurement, $z=1,5$ m. The large discrepancies in this dosage for Nickola (1971) Run P8 suggests that either vertical diffusivity has been poorly estimated, or the calculated conversion factor is incorrect. In the remaining comparisons, the earlier arrival of the numerically-solved cloud suggests over-estimation of velocity by about 50%, though the forms of the time-histories are in approximate agreement. The velocities used to simulate Runs 3 and 4 of Drivas and Shair (1974) were based on the observed mean time of arrival at the 400 m - distant receptors. Since the cloud centroid accelerates with the diffusion of material into higher velocity strata, the deduced velocity at the 1.5 m receptor-height is likely

fig. (3.3) Comparison of predicted and measured concn. histories



to be an exaggeration of the true velocity at 1.5 m. This might explain the earlier arrival of the predicted cloud, though a lower velocity would expand the time-period during which the cloud traverses a receptor. The formulation of vertical diffusivity in all four simulations is such that it will decrease if a lower velocity is specified at the "measurement" height. Although this decrease will reduce the along-wind expansion of the ground-level distribution, it is likely that predicted concentration-history shapes would only match the observed shapes if the specified wind profile were slightly flatter as well. No attempt has been made to alter the estimated profile parameters so as to fit the predicted concentration histories to the observed histories.

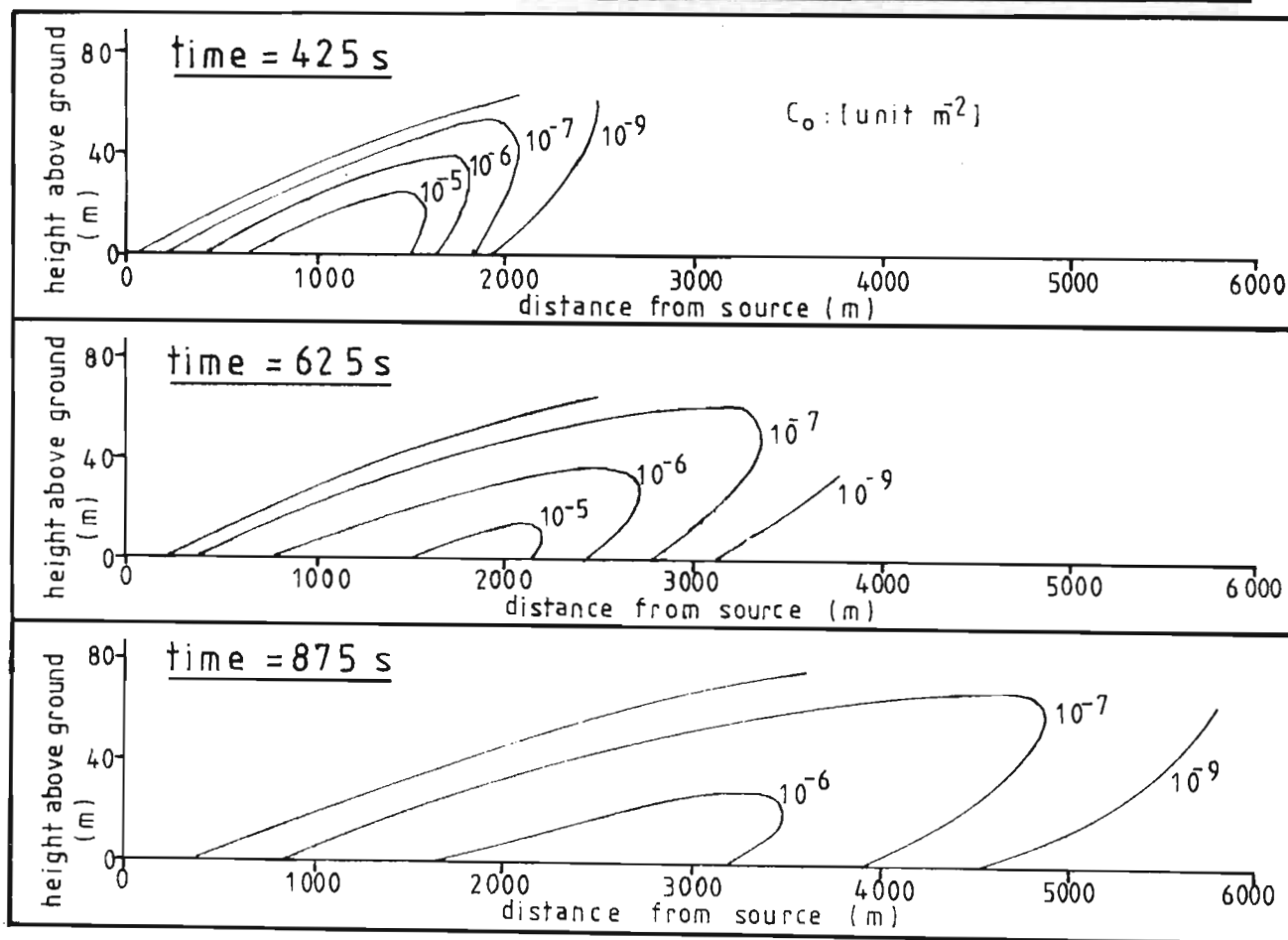
The numerical model generally under-predicts the along-wind spread near the source [200 m, 400 m]. These distances are reached soon after the puff is "seeded" [section (2.3.2)], and the discrepancy may result from initial inaccuracy in the puff solution. On the other hand, for ground-level releases, the initial along-wind spread may be artificially enhanced by retention in stagnant vegetational spaces near the source. The comparisons in fig. (3.3) should, however, be viewed with some reservations because of the speculative nature of the profile parameters.

The predicted time-histories all have the correct positive skewness, which may be defined using expectations as

$$\gamma_1 = \frac{E[(t-\bar{t})^3]}{\{E[(t-\bar{t})^2]\}^{\frac{3}{2}}}$$

Caution is necessary in relating this skewness to the instantaneous distribution in the lagrangian frame. If the puff development were "frozen" as it moved past an observation point, then positive skewness in the time-history would imply negative skewness in the lagrangian puff, if the ordinate is taken to increase downwind. The continued development of the puff as it passes a point alters this relationship, though the lagrangian ground-level distribution in the case of Nickola (1971) Run P8 is indeed seen to have slightly negative skewness [fig. (3.4)].

fig. (3.4) Development of simulated puff : Nickola(1971) Run P8



The unit release isopleths [units m^{-2}] which are plotted in figure (3.4) show substantial ground-level "tails" as a result of the low vertical diffusivity at this height [$\bar{k}_z(0)=0$ - table (3.1)]. This is in contrast to the pronounced positive skewness in the case of a linear velocity profile and constant vertical diffusivity [fig. (3.2)].

Drivas and Shair (1974) incorrectly assumed that the skewness of the observed time-histories [fig. (3.3)] represents the skewness of the lagrangian distribution. On this basis they claimed that the increasing positive skewness of the time-histories is in support of the 3rd -moment derivations of Saffman (1962). Equation (1.61) due to Saffman leads to a ground-level skewness of about +1 for a linear velocity profile with constant vertical diffusivity. Of course, this applies to the lagrangian distribution, and is supported by the present numerical solution [fig. (3.2)]. Saffman's dimensional analysis for power-law profiles will lead to a relationship between skewness and time, but the particular form of the profiles will, in general, determine the nature of such relationships. The numerically-simulated lagrangian distributions used in the comparison with Drivas and Shair (1974) Runs 3 and 4 [fig. (3.3)] did in fact display negative skewness.

3.3 Comparison with continuous point source models.

The numerical model simulates continuous releases by superposing serially-released lagrangian puffs. In a steady-state atmosphere the cross-wind integrated distribution (zeroth moment) may be considered alone, and the diffusion equation becomes

$$\bar{u}(z) \frac{\partial C}{\partial x} = \frac{\partial}{\partial z} \left[\bar{K}_z(z) \frac{\partial C}{\partial z} \right] \quad (3.3)$$

Following the result of Walters (1969), the contribution of along-wind diffusion is assumed to be negligible. The dynamic puff numerical model has been used to solve equation (3.3) for various forms of the velocity and diffusivity profiles, and some of the comparisons with analytical and numerical solutions are presented below.

3.3.1 Gaussian plume formula.

The analytical solution of equation (3.3) in the case of uniform velocity and diffusivity profiles [$\bar{u}(z)=u_0$, $\bar{K}_z(z)=K_{z0}$], is the well-known gaussian plume relation (1.41). As in section (3.1), the problem is non-dimensionalised by taking

$$x_1 = \frac{x u_0}{K_{z0}} \quad , \quad z_1 = \frac{z u_0}{K_{z0}} \quad , \quad Q_1 = \frac{Q K_{z0}}{u_0^2}$$

where Q_1 is now a dimensionless release rate. Comparisons with the lagrangian puff numerical solution are presented for an elevated source [fig. (3.5)] and for a ground-level source [fig. (3.6)]. In general, deviations increase with

fig.(3.5) Concentration profiles
—elevated gaussian plume

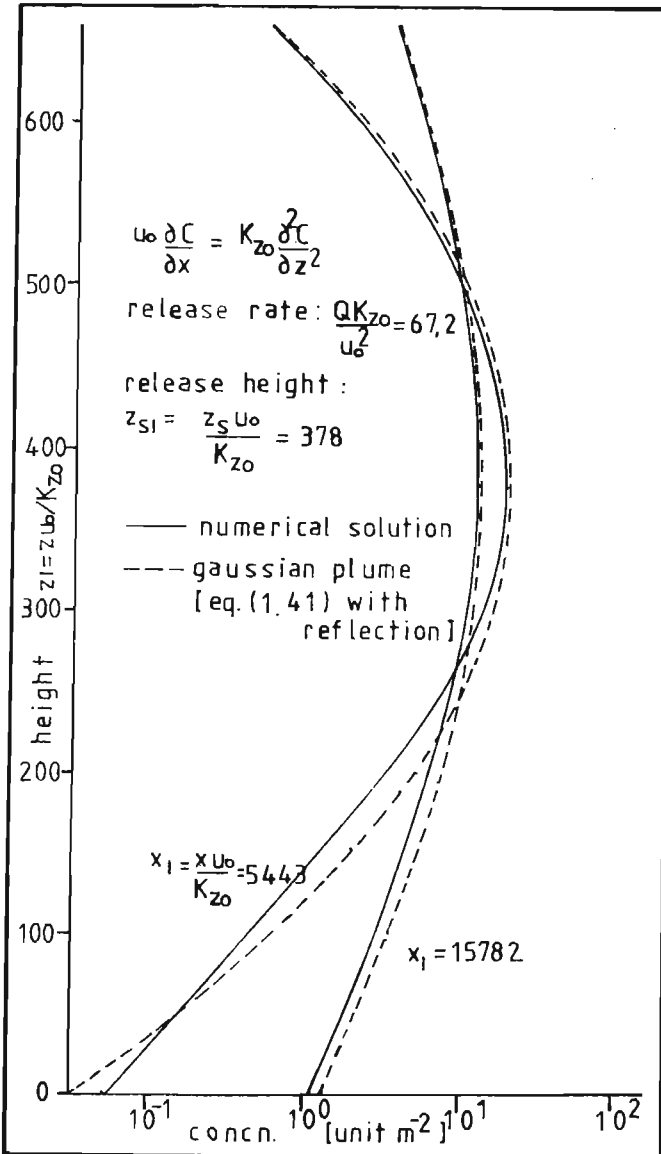


fig.(3.6) Concentration profiles
—ground-level gaussian plume

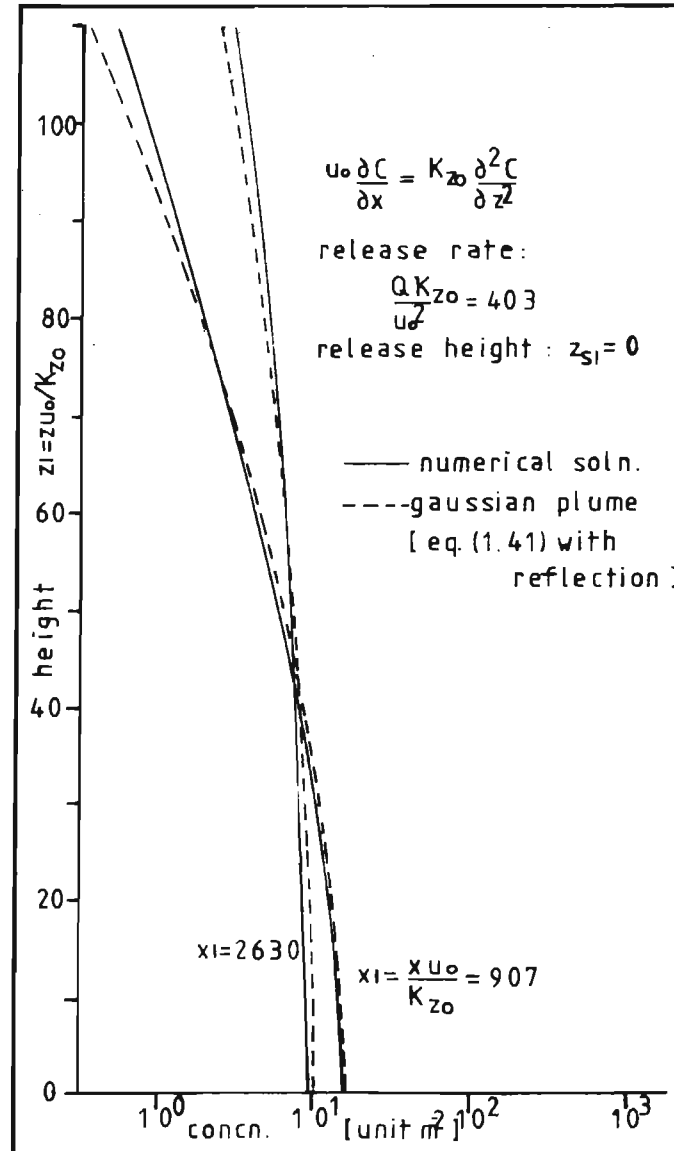
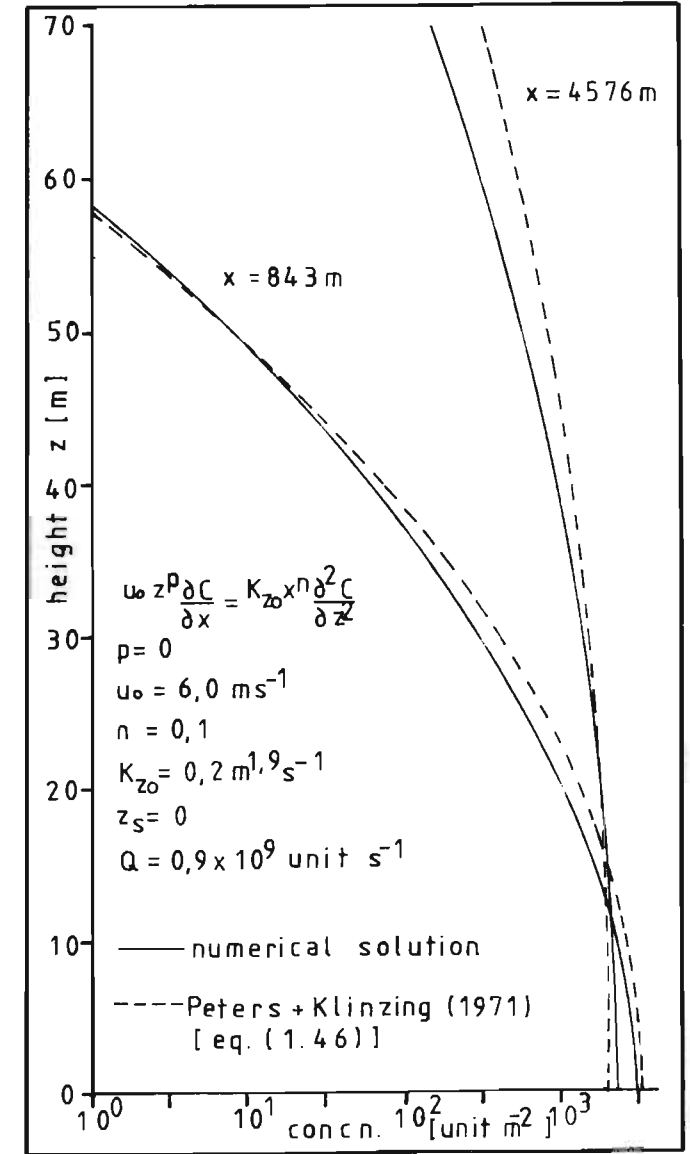


fig.(3.7) Concentration profiles
—variable diffusivity



distance from the vertical centroid, though the dominant region of the plume remains correctly modelled. Of course, the accuracy of the result is directly related to the accuracy of the gaussian puff simulations discussed in section (3.1).

3.3.2 Peters and Klinzing (1971) analytical solution.

Peters and Klinzing (1971) solved equation (3.3) for a continuous ground-level release, and velocity and diffusivity given by the power-law relations

$$\bar{u}(z) = u_0 z^P, \quad \bar{K}_z = K_{z0} x^n$$

In figures (3.7), (3.8) and (3.9), their solution [equation (1.46), section (1.5.1)] is compared with the dynamic puff numerical solution for various values of the profile parameters. Again, deviations are seen to increase with distance from the vertical centroid. Fig. (3.8) [P=0,5] and fig. (3.9) [P=0,75] have been arranged to possess the same velocity at z=100 m. The effect of the differing shear rates becomes more significant with height, where the numerical solution is usually less accurate. The correct trend is nevertheless represented, and it has been pointed out that a temporal variation is required in order to reveal the significant redistribution effect of wind-shear.

3.3.3 Ito (1970) numerical solution.

Using a log-linear velocity profile (1.26) with extensions below the vegetational canopy and above the

fig.(3.8) Concentration profiles—
variable velocity and diffusivity

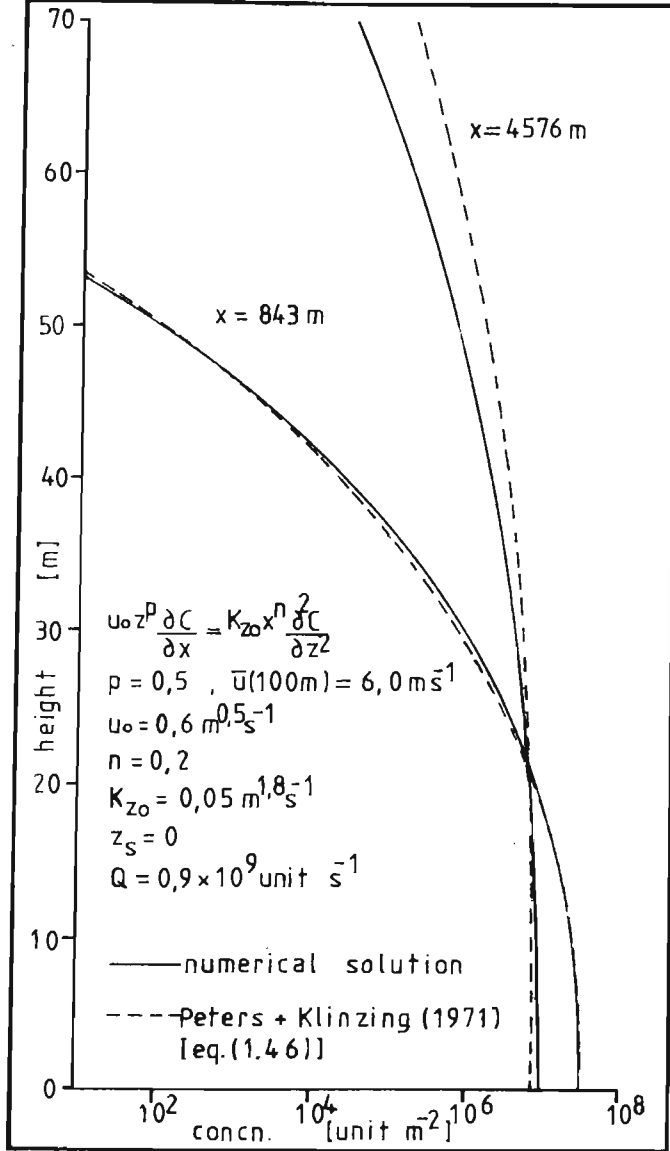


fig.(3.9) Concentration profiles—
variable velocity and diffusivity

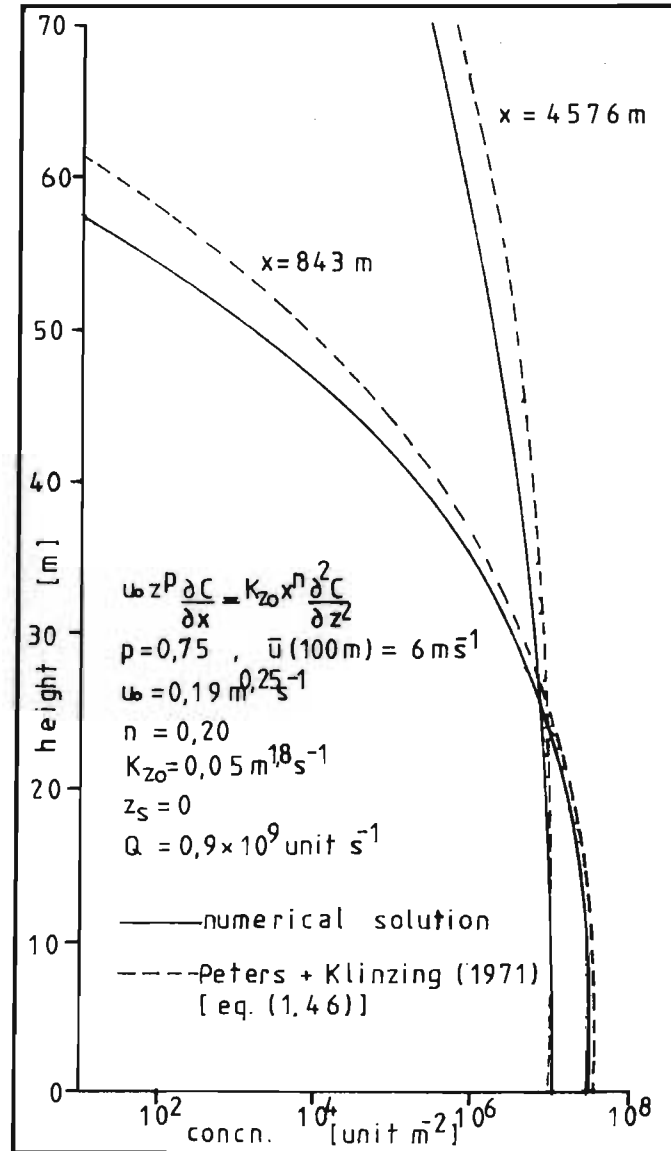
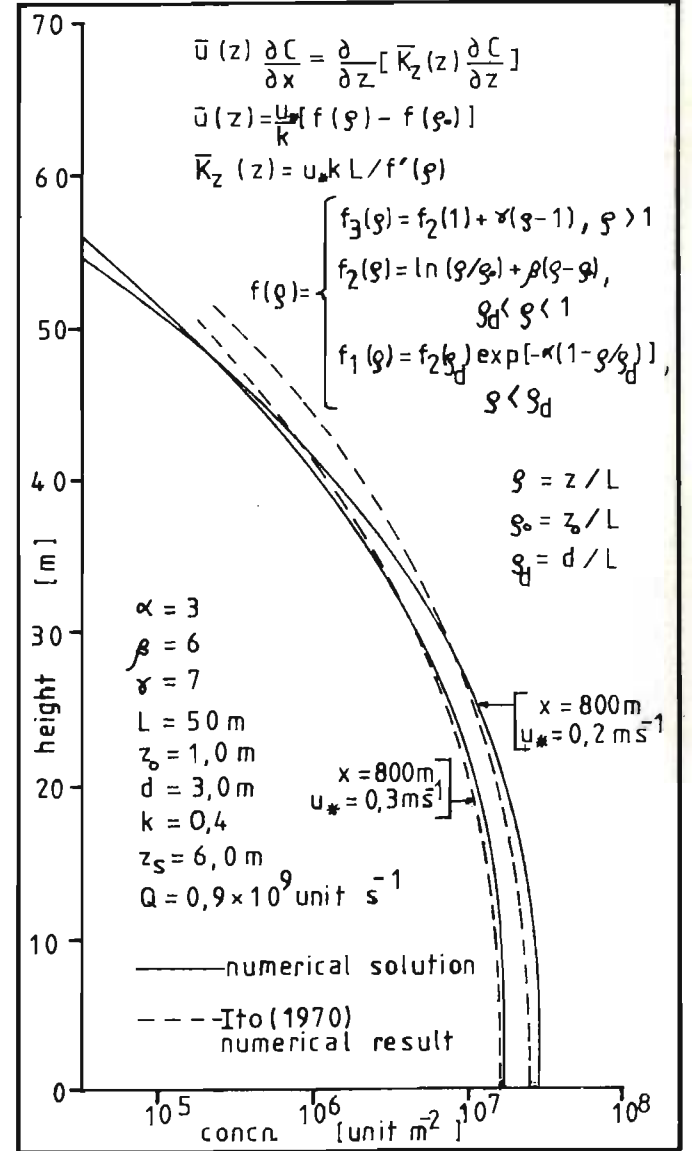


fig.(3.10) Concentration profiles—
simulation of Ito(1970) result



stability length, Ito (1970) [section (1.6.4.1)] solved equation (3.3) numerically in order to simulate field observations in Project Green Glow. The forms of the velocity and diffusivity profiles are included in fig. (3.10), together with concentration profiles due to Ito and the present dynamic puff numerical solution. Note that Ito's effective release rate was established by integrating mass flux with respect to height, giving $Q=0,1046u_*$. Appropriate shifts in the profile were then used to convert to the release rate quoted in fig. (3.10).

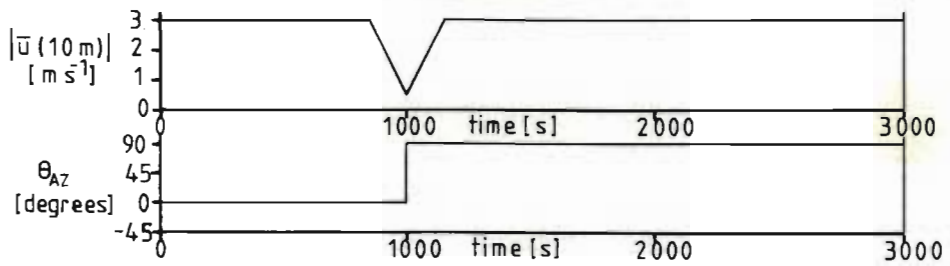
Agreement between the models is reasonable, though deviations appear to increase with height.

3.4 Illustrative applications of the puff model.

The capabilities and limitations of the full numerical model are best appreciated by considering the performance of the dynamic puff solution in various environments. Figures (3.11) to (3.16) illustrate the behaviour of the puff kernel under specified idealised conditions.

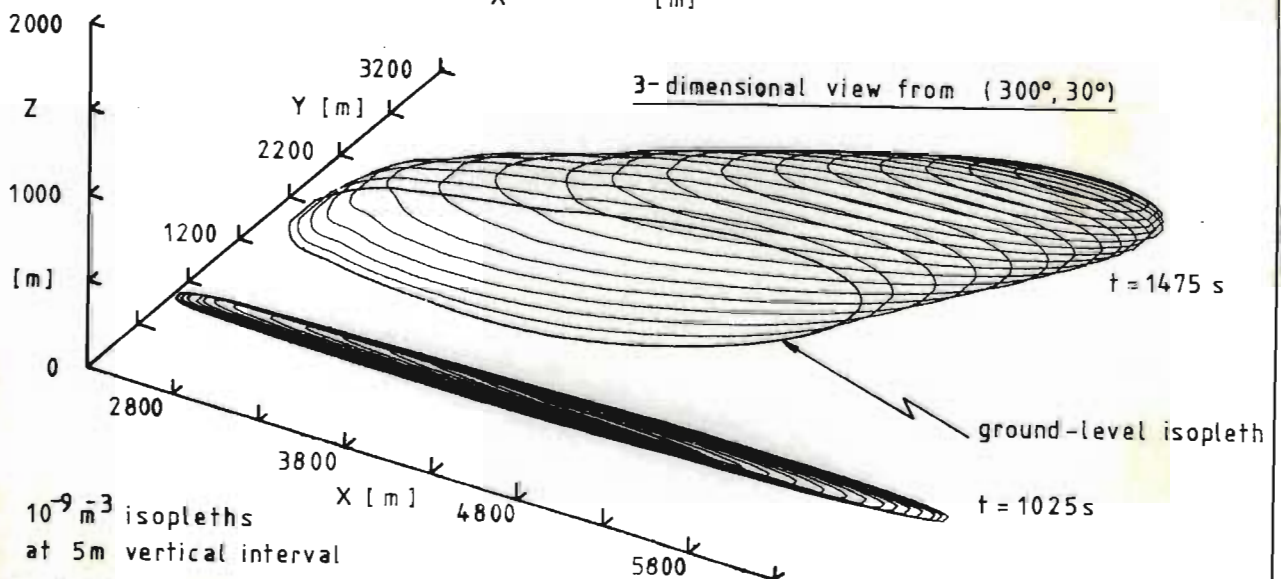
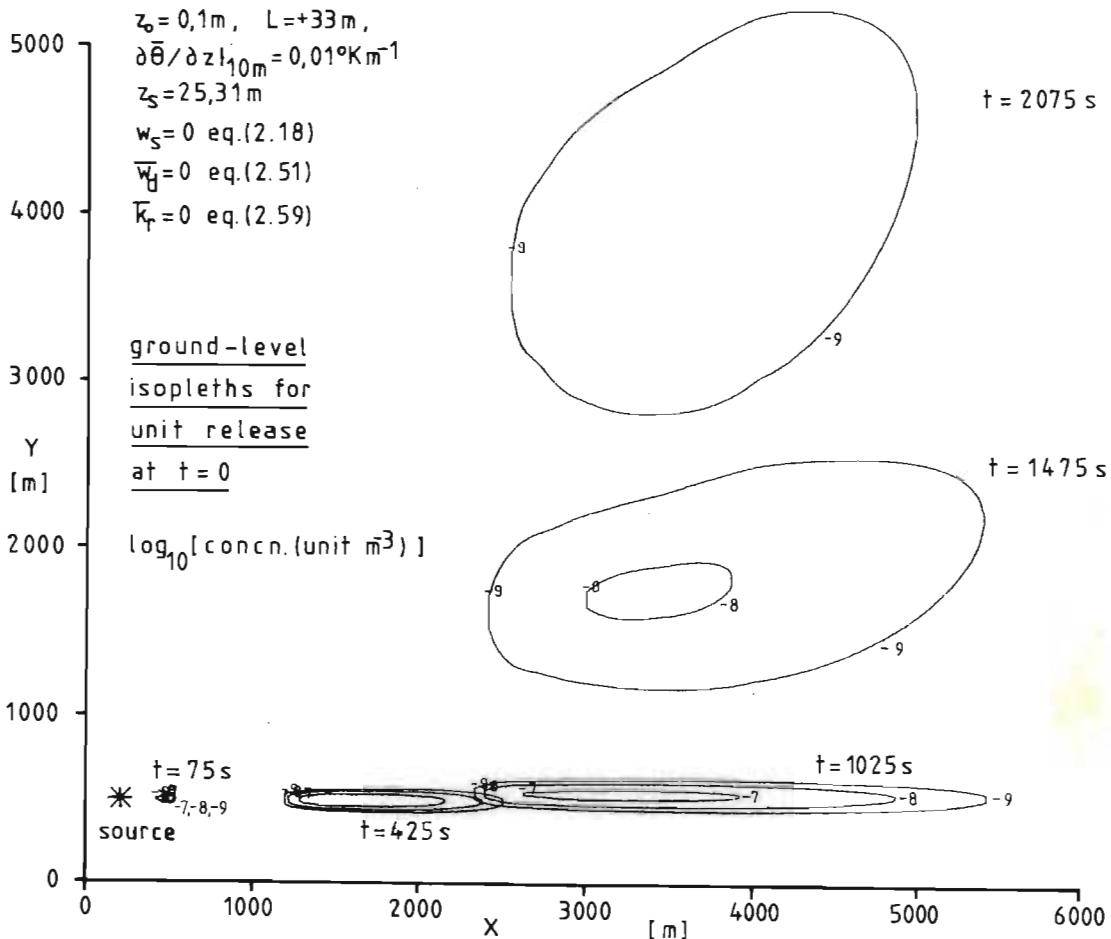
It was noted in section (2.4.4.1) that the surface of the numerical solution, represented by the proximate curve P, is chosen to coincide with the initial streamline through the point of release. Hence the solution in this direction may be considered entirely numerical, whilst that at right angles results from the moment-description [equation (2.66)]. It is thus interesting to observe the symmetry of the ground-level distribution at $t=2075s$ in fig. (3.11). This distribution represents transport for

fig. (3.11) Temporal variation of wind direction (+90°)



$\bar{u}(z)$: eq.(2.72), $\bar{K}_z(z)$: eq.(2.73), $\bar{K}_h(z)$: eq.(2.75)

$z_0 = 0,1\text{m}$, $L = +33\text{m}$,
 $\partial\bar{\theta}/\partial z|_{10\text{m}} = 0,01^\circ\text{K m}^{-1}$
 $z_s = 25,31\text{m}$
 $w_s = 0$ eq.(2.18)
 $\bar{w}_y = 0$ eq.(2.51)
 $\bar{K}_r = 0$ eq.(2.59)

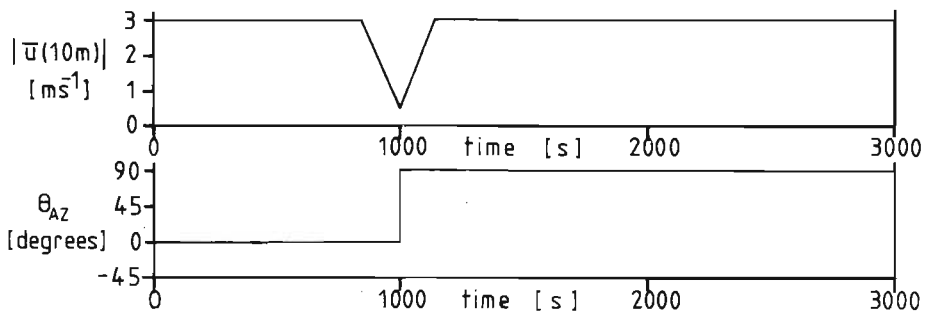


approximately equivalent periods in the x and y directions, in that order, and it is clear that the same distribution would result if the order were reversed. Thus, at least under these conditions, the gaussian moment description is equivalent to the numerical solution. [Compare section (3.1.2)].

An important effect of wind-shear is the vast difference between induced scales of variation in the vertical and horizontal directions. For example, the 3-dimensional view in fig. (3.11) shows that at $t=1475s$ the centroids at $z=85m$ and ground-level will be separated by about 2900m. This advance pollution may mix down if the cloud enters an unstable region, or with the onset of fumigation, further modifying an already extended ground-level distribution.

Perhaps the most striking effect of the inclusion of wind-shear is illustrated by comparison of figures (3.11) and (3.14), both of which exclude any removal mechanisms. The values of velocity and diffusivity used in fig. (3.14) are uniform with height, so that the distribution should be gaussian. The cross-frame (y-direction) distribution will be gaussian according to equation (2.66), and it shows good agreement with the numerical solution in the x-direction. Velocity and diffusivity were fixed on those at 10 m in the profiles used for fig. (3.11), and should represent reasonable averages between the release height ($z_s=25,31m$) and the ground. This is borne out by the relative positions of the ground-level distributions in figures (3.11) and (3.14).

fig. (3.12) Temporal variation of wind direction (+90°)
with surface absorption [$\bar{w}_d = 0,0625 \text{ m s}^{-1}$]



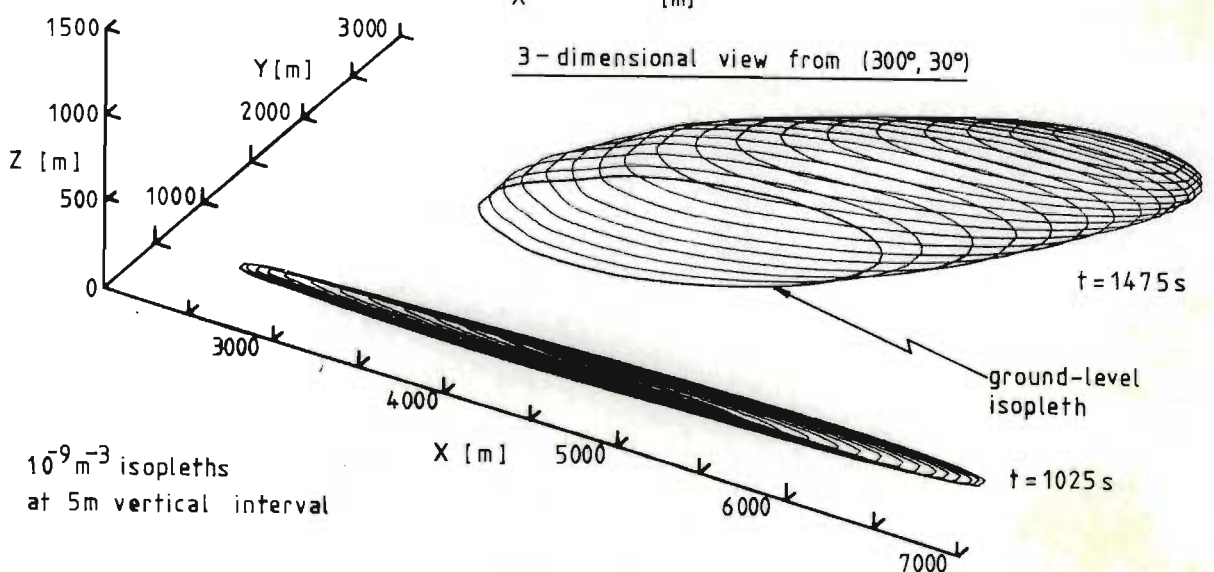
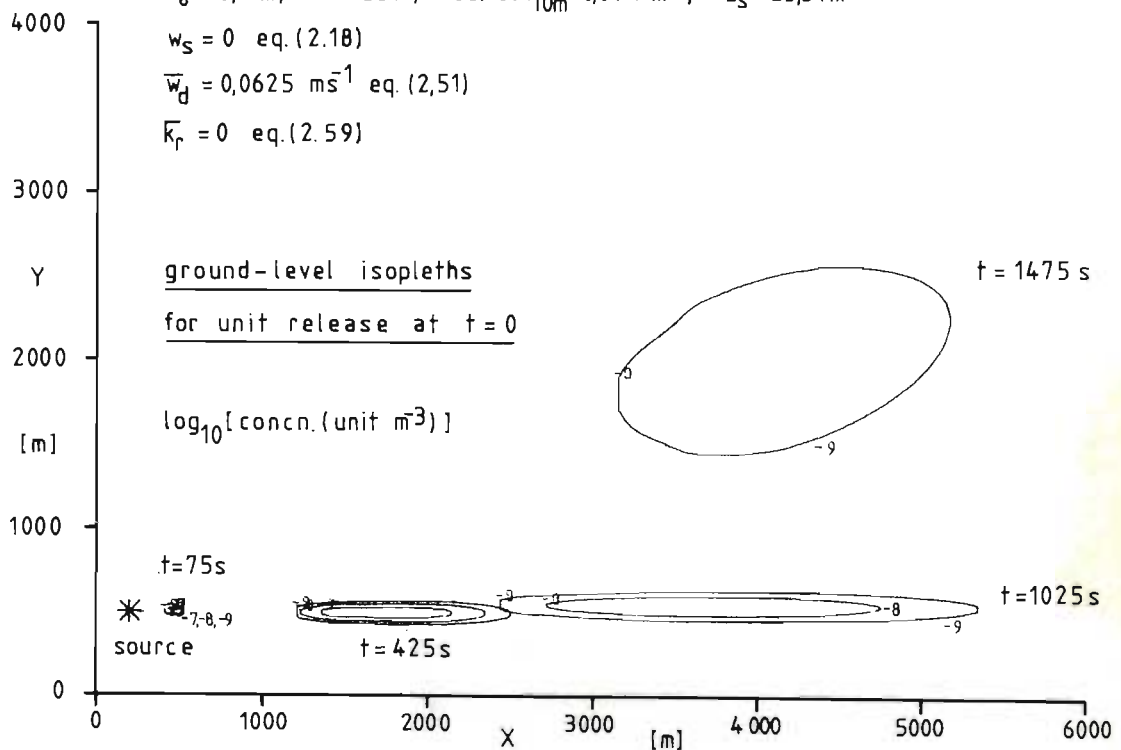
$\bar{u}(z)$: eq.(2.72), $\bar{K}_z(z)$: eq.(2.73), $\bar{K}_h(z)$: eq.(2.75)

$z_0 = 0,1 \text{ m}$, $L = +33 \text{ m}$, $\partial\bar{\theta}/\partial z|_{10\text{m}} = 0,01^\circ \text{ K m}^{-1}$, $z_s = 25,31 \text{ m}$

$w_s = 0$ eq.(2.18)

$\bar{w}_d = 0,0625 \text{ m s}^{-1}$ eq.(2.51)

$\bar{K}_r = 0$ eq.(2.59)

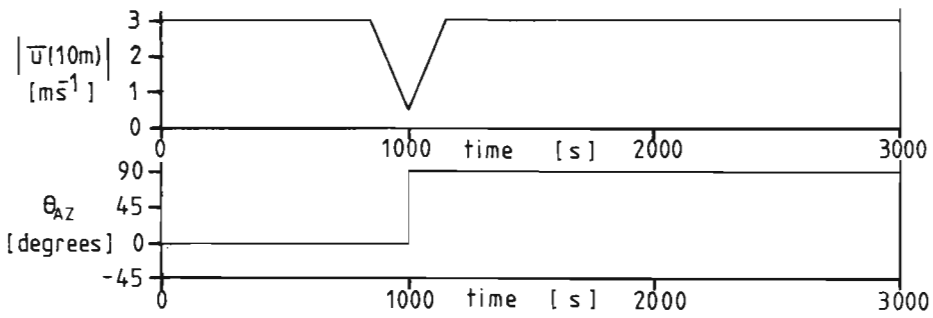


10^{-9} m^{-3} isopleths
 at 5m vertical interval

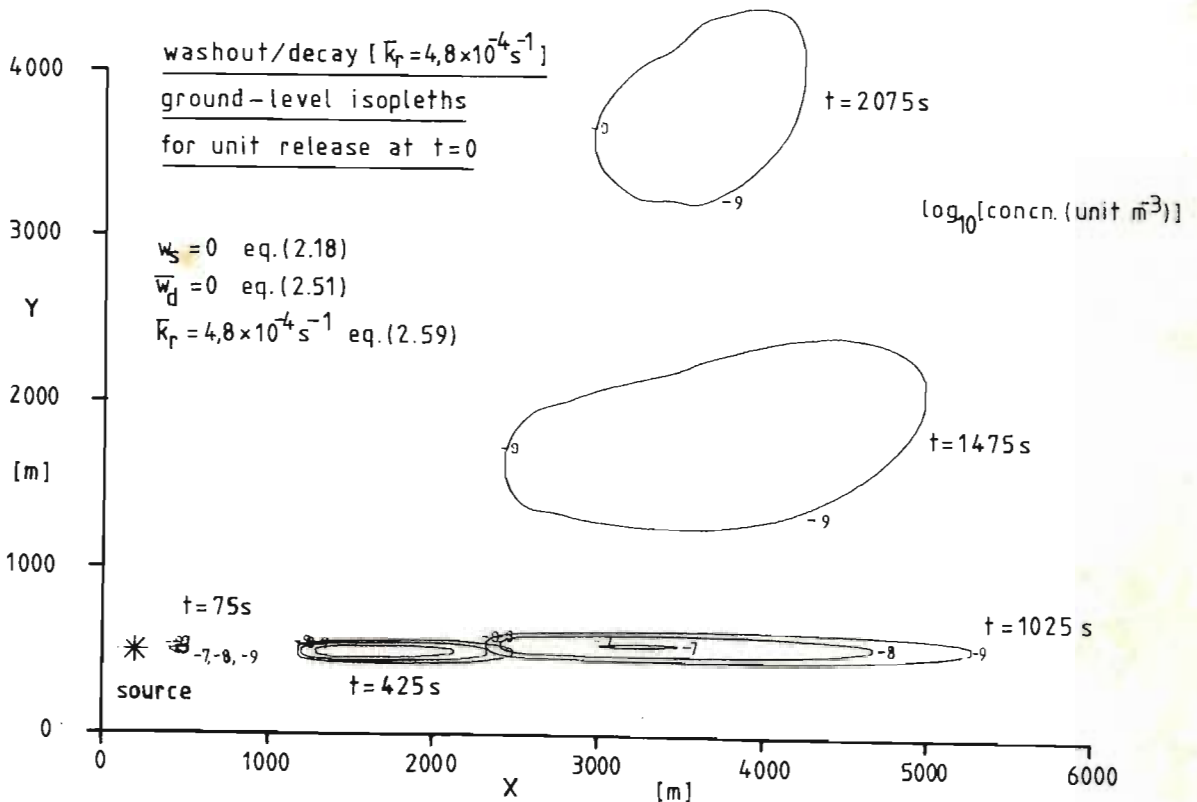
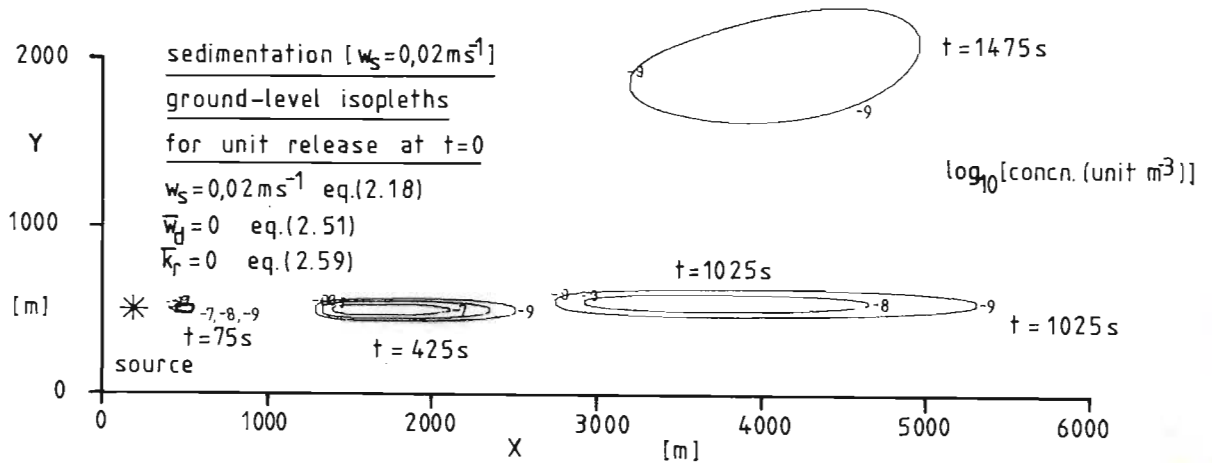
The primary effect, at $t=2075s$, is to have increased by about 70-fold the area affected down to concentrations of $10^{-9} m^{-3}$ at ground level, following a unit release. It is clear that methods neglecting wind-shear will over-predict peak concentrations, and grossly under-predict the area affected. In a steady-state wind-field the gaussian puff will under-predict the period during which a stationary point is affected by a passing puff, though for a continuous release the gaussian plume will represent steady concentrations quite reasonably because of the superposition effect. However, simulation of a continuous release in an unsteady wind-field using gaussian puffs will display the same shortcomings as in the case of the instantaneous release, owing to the neglect of cross-plume shear in this instance.

Typical mesoscale meteorology under stable conditions will usually not include the sudden development of a large orthogonal velocity component. Such occurrences are more likely during fumigation with the downward diffusion of gradient wind momentum, though the effects of synoptic weather variations are often able to transmit to ground-level without disturbing the stability of the surface layer. [section (5.2); Scholtz and Brouckaert (1976)]. Another source of temporal variation under stable conditions is the sudden arrival of a more dominant current, such as a strong katabatic flow, though the continuous temporal variations in a stable wind-field tend to be less dramatic. Real mesoscale wind-fields are seldom in effective steady state — trajectory travel-times are invariably larger than

fig. (3.13) Temporal variation of wind direction (+90°)
with sedimentation and washout/decay



$\bar{u}(z)$: eq.(2.72), $\bar{K}_z(z)$: eq.(2.73), $\bar{K}_h(z)$: eq.(2.75)
 $z_0 = 0,1m$, $L = +33m$, $\partial\bar{\theta}/\partial z|_{10m} = 0,01^\circ Km^{-1}$, $z_s = 25,31m$



the significant time-scales of meteorological variation. Thus, though the two-dimensional shear effect [fig. (3.11)] will be especially important during sudden temporal variations, it will also be responsible for significant redistribution on a more continuous basis.

The velocity and diffusivity profiles used in figures (3.11) to (3.13), (3.15) and (3.16) all reflect moderately stable conditions, ($L=+33$ m), and correspondingly high wind-shear through most of the surface layer [fig. (A4.2)]. The redistribution effect will decrease with decreasing stability.

Fig. (3.12) represents the same wind-field development, but includes surface absorption with an effective deposition velocity of $0,0625$ m s⁻¹. Such absorptivity is relatively high [section (1.9.2)] and will only be found, for example, in the case of dense vegetational structures. The expected effect of surface absorption is observed in that the lowest region of the cloud is eroded, so that the ground-level centroid moves forward due to vertical transport. Comparison of the 3-dimensional views in figures (3.11) and (3.12) shows that at $t=1475$ s the distribution above $z=60$ m remains virtually unaffected by surface absorption.

The processes of sedimentation and uniform decay are separately presented in fig. (3.13). The settling velocity $w_s=0,02$ m s⁻¹ should maximise the integrated ground-level distribution at about $t=1200$ s, and this does not appear to be the case in comparison with fig. (3.11). However, the ground-level centroid is shifted forward slightly, as

fig. (3.14) Temporal variation of wind direction (+90°)
with uniform velocity and diffusivity profiles

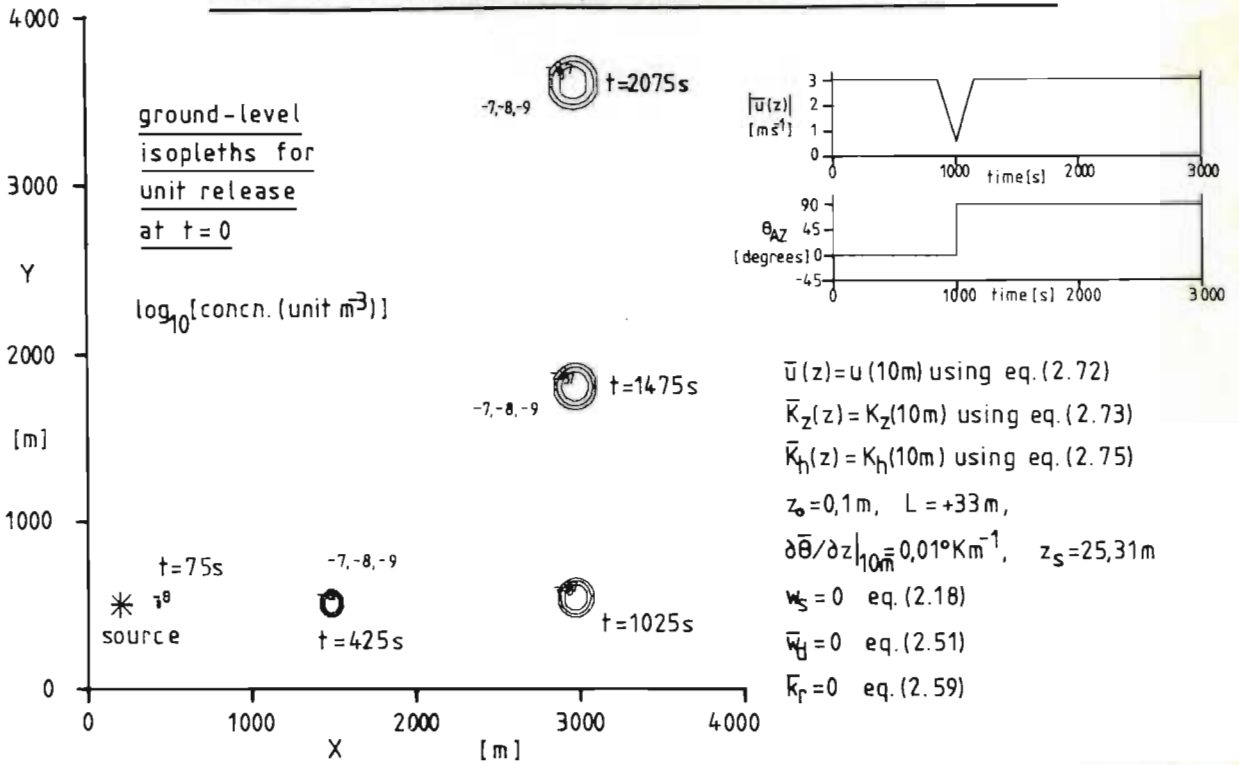
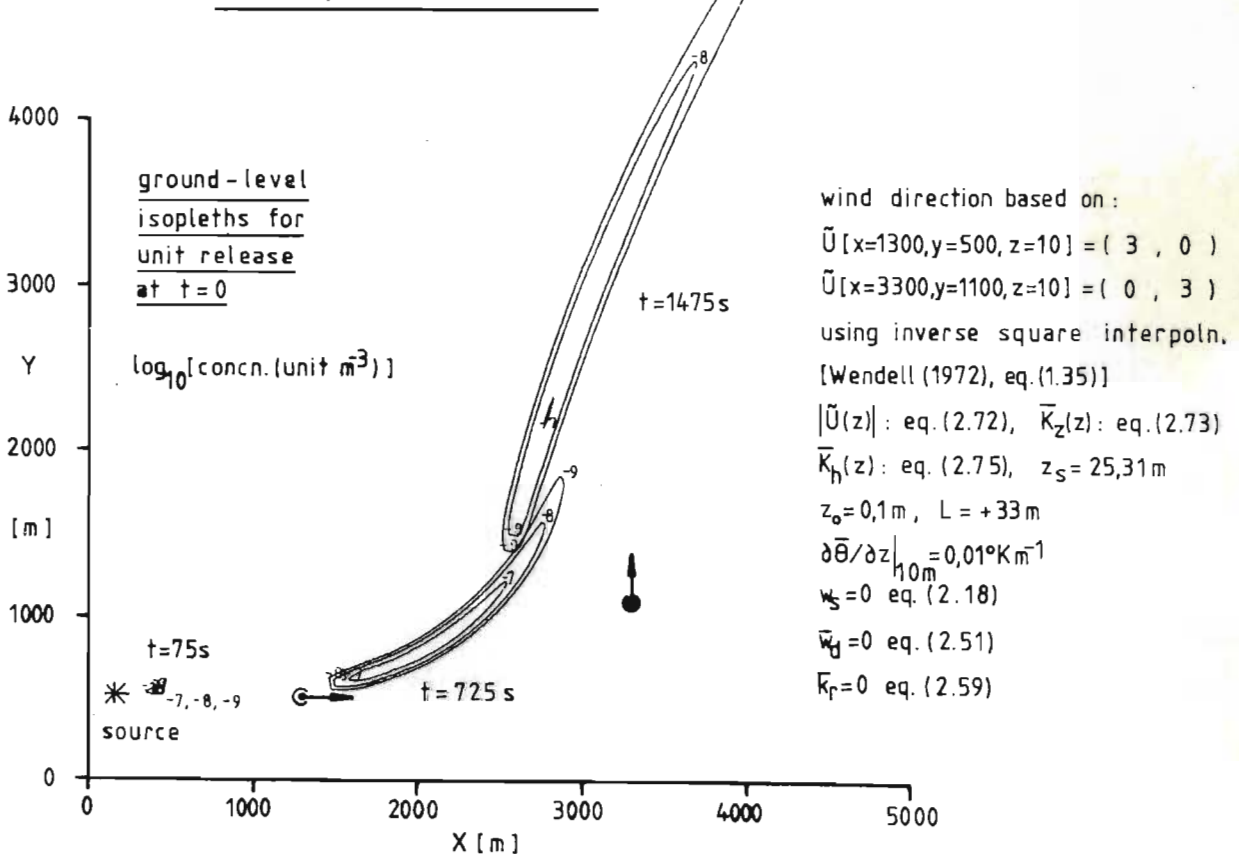


fig. (3.15) Steady-state wind-field
with spatial variation

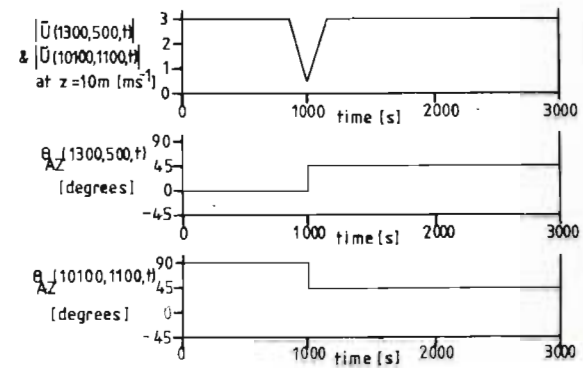
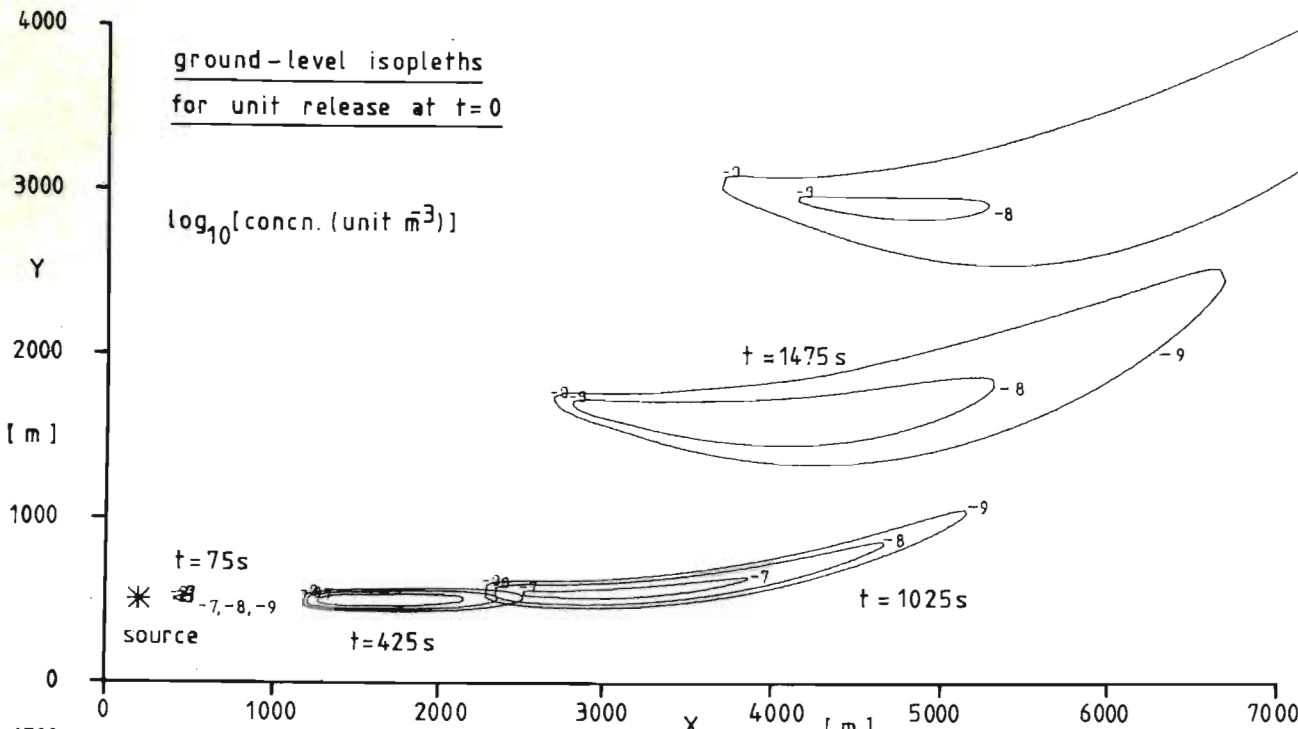


expected. In contrast, uniform decay leads to a simple shrinking of the isopleths - the shape of the cloud is identical but concentrations are uniformly reduced. The combined first-order decay rate [equation (2.59)] $\bar{k}_r = 4,8 \times 10^{-4} \text{ s}^{-1}$ is representative of that for particles with terminal velocity $0,0016 \text{ m s}^{-1}$ in rainfall at 4 mm hr^{-1} [Chamberlain (1953)].

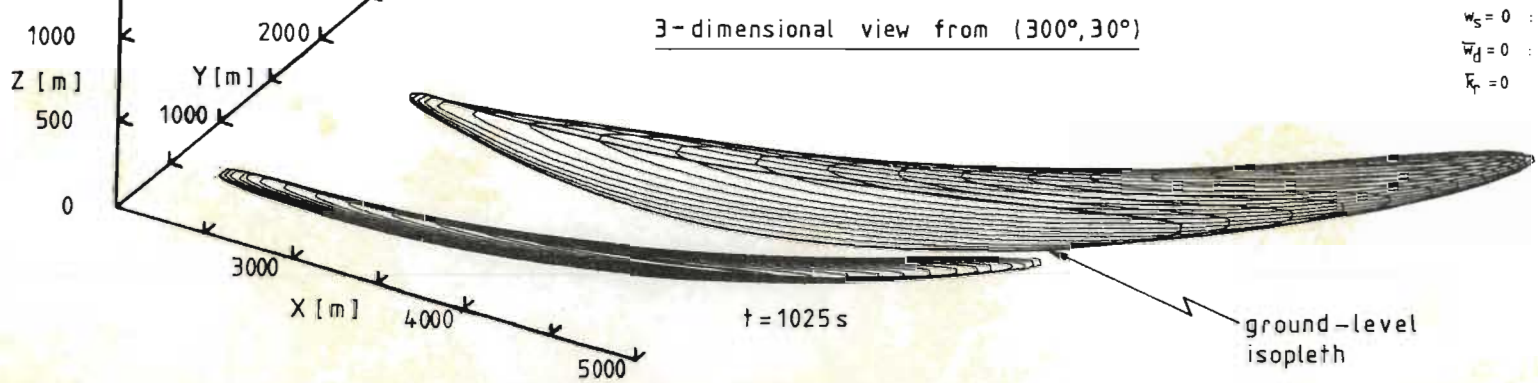
Fig. (3.15) illustrates the problem of locating the sheared puff in a steady-state wind-field with moderately strong streamline curvature. It was pointed out in section (2.4.4.1) that the proximate curve P, based on three particle positions, was best approximated using a section of circular arc. The wind-field in fig. (3.15) was interpolated from two specified point-vectors using the inverse-square method [Wendell (1972) eq. (1.35)], and the axes of the ground-level distributions may be envisaged to pass through 3 points (separated by 1500 m) which lie on the implied streamline passing through the source. There is an obvious inconsistency in that the distribution at $t=725\text{s}$ should lead directly into that at $t=1475\text{s}$, and this results directly from the approximate way in which the proximate curve follows the streamline. However, the error is not cumulative, and there are no viable alternatives for handling this problem which do not incur large computation penalties.

Fig. (3.16) illustrates combined spatial and temporal variation in a wind-field which was again interpolated from two specified point-vectors. Following from the assumption of a mean effective incident velocity for the lagrangian

fig. (3.16) Combined spatial and temporal variation of wind direction



wind-field interpolated from vectors at:
(X,Y)=(1300,500) and (10100,1100)
using inverse square method [Wendell(1972),eq.(135)]
 $|\bar{U}(z)|$: eq. (2.72), $\bar{K}_z(z)$: eq. (2.73),
 $\bar{K}_y(z)$: eq. (2.75), $z_s=25.31m$,
 $z_0=0.1m$, $L=+33m$, $\partial\bar{\theta}/\partial z|_{10m}=0.01^\circ Km^{-1}$,
 $w_s=0$: eq. (2.18)
 $\bar{w}_d=0$: eq. (2.51)
 $\bar{K}_r=0$: eq. (2.59)



frame [section (2.4.4.2)], the only additional shortcoming to manifest itself here results from a constant incident velocity in the uniform wind-field after the step-change. The angle of incidence of the relative velocity vector in the lagrangian frame is given a mean effective value for the entire frame. Since the proximate curve P is transformed to a straight line in this frame, the implication is that the relative velocity vector meets the proximate curve at a constant angle in the eulerian frame. Associated positive and negative deviations from the true incident velocities will depend largely on the curvature of P. Hence shear across the curved axes of the ground-level distributions ($t=1475s$, $t=2075s$) should be smaller at the downwind ends and greater at the upwind ends than is depicted in fig. (3.16).

CHAPTER 4

EXPERIMENTAL PROCEDURE

In order to assess the performance of the dispersion model, consideration was given to the transport of an atmospheric tracer in a mesoscale system. The meteorological input for the model was provided by wind-field and atmospheric stability measurements, whilst the simultaneous point-release of a tracer provided the source input. Though the model incorporates dosage prediction, its full potential in a dynamic system is best revealed by short-period measurements. An effort was thus made to reduce the sampling periods of aspirated filters. Comparison of predicted and measured dosages provided a basis for model evaluation.

4.1 Atmospheric tracer system.

4.1.1 Zinc-cadmium sulphide fluorescent particle tracer.

An atmospheric tracer must fulfil several requirements, among them its ability to be distinguished and detected in small quantities, and its approximation to the transport behaviour of air. Tracers which have been used include Lycopodium spores [Hay and Pasquill, (1957)], gases such as SO_2 [Cramer (1959)], SF_6 [Drivas and Shair (1974)], C_{12}FCH [Norden and van As (1977a)], radioactive gases such as Xenon 133 [Eggleton and Thompson (1961)] and Krypton 85

[Nickola (1971)], metals such as Gold, Lanthanum, Antimony and Indium [Norden and van As (1977a,b)] which respond to subsequent activation, and water-soluble dyes such as uranine [Dumbauld (1962)]. The use of inorganic fluorescent particle (FP) tracers was first reported by Perkins, Leighton, Grinnell and Webster (1952) and Braham, Seeley and Crozier (1952), and since then they have proven popular atmospheric tracers.

The present study makes use of the ZnZ-CdS particulate tracer FP2267 which is manufactured by the United States Radium Corporation (USRC). Though the particle sizes are concentrated in the region 1-5 μm , the size distribution varies somewhat from lot to lot, and it is generally necessary to characterise the particular lot in use. [Leighton et al, (1965)]. The material consists of a solid solution, about 20% CdS and 80% ZnS, which has the property of fluorescing in the visible yellow region (5000 \AA - 6500 \AA) upon excitation by near ultraviolet radiation, for which the 3660 \AA lines of the mercury arc are a convenient source.

Reported particle yields of FP tracers vary greatly, not only as a result of lot variations, but also as a result of differing dissemination and analysis techniques. Rosinski, Glaess and McCully (1956) noted the existence of numerous agglomerates, some of which were broken into single particles during experimentation. Their sedimentation analysis provided a yield some 20 times higher than a successive dilution method. Rosinski et al recorded a yield of 3.41×10^{10} particles per gram, including agglomerates, for

FP2266, suggesting a volume-mean diameter of 2,41 μm . For the same tracer Wedin, Frössling and Aurivillius (1959) conducted a more realistic yield determination, involving comparison with SO_2 , and evaluation of the total particle flux in a metered release. Values obtained were about $1,6 \times 10^{10}$ particles per gram, somewhat higher than the $0,9 \times 10^{10}$ particles per gram which they measured by dilution. For FP2267, Leighton et al (1965) recorded effective yields ranging from $1,33 \times 10^{10}$ to $1,56 \times 10^{10}$ particles per gram, where dissemination was carried out via a blower with toothed-wheel feed.

The method of air sampling may add further uncertainty to observed concentrations, though Leighton et al found that the effects of filter orientation, as well as impaction and electrostatic deposition on the filters, were negligible. Losses of particles due to surface impaction were found to be comparable with calculated sedimentation losses for 4,5 miles of travel over Palo Alto.

In a comparison with radioactive Xenon-133, Eggleton and Thompson (1961) found a 50% loss of ZnSCdS FP tracer between stations 16 km and 60 km from the source. This may have been partially due to fluorescent instability. Fluorescent pigments are known to suffer a loss of fluorescence through extended exposure to U.V. radiation, particularly under high humidity. For FP2267, Leighton et al (1965) found a maximum count reduction of 16% after 19 hours irradiation by sunlight in ambient air.

A further study conducted by Niemeyer and McCormick (1968) showed substantial losses of FP relative to SF₆ for distances over 35 km. However, the lack of systematic variation in these losses prompted their suggestion that procedural errors could amount to as much as ±50%

Another consideration in the use of FP tracer is the toxicity hazard posed by its Cadmium content [Spomer (1973)]. Human threshold limit values (TLV) have been estimated at 0,05-0,10 mg Cd m⁻³ [Prodan (1932)], typically representing about 10⁷ particles m⁻³ of FP tracer. It is usually not necessary to exceed such concentrations at ground level in mesoscale experiments. However, a body burden of over 120 mg Cd causes permanent serious kidney damage, so that safe handling and dissemination techniques are essential.

4.1.2 Development of a release technique.

The aim in the present work was to release the tracer FP2267 at controlled rates up to 10⁹ particles per second at a height of about 25 m. The release-point was to be supported on a light-weight mast, so that it was necessary to position the feed apparatus at ground-level.

The usual methods of dissemination involve feeding the dry powder through a blower [Leighton et al (1965)] or Venturi nozzle. Since the air-stream would provide a means of pneumatic transport to the top of the mast, it was first attempted to develop a reliable dry-powder feed technique. Problems were encountered in obtaining a

consistent feed-rate from screw-feeders due to arching in the feed hopper, despite agitation.

Attention then turned to the possibility of handling the FP in a liquid medium. A uniform suspension could be maintained at ground-level, and delivered through a metering pump to an atomising nozzle situated at the release-height. Such a method had several advantages:-

- (i) Accurate metering.
- (ii) Safer handling as a liquid suspension.
- (iii) A suitable liquid would wet agglomerates which had been observed in the powder, assisting their break-up in a stirred vessel.

A number of liquids, chiefly organic solvents, were considered as possible suspension media. A suitable liquid had to be generally available and inexpensive, as well as display several physical properties:

- (i) It should wet ZnSCdS particles without promoting flocculation.
- (ii) It should have low surface-tension so that droplets would break up in atomisation.
- (iii) It should be volatile so that droplets would not form pellets after atomisation.

Early consideration was given to water, which wet the particles but left many agglomerates, possibly enhancing flocculation. Ultrasonic vibration, pebble-milling and a range of surfactant tests all proved ineffective in solving this problem. One of the few liquids which had all of the

fig. (4.1) Fluorescent particle tracer dissemination equipment

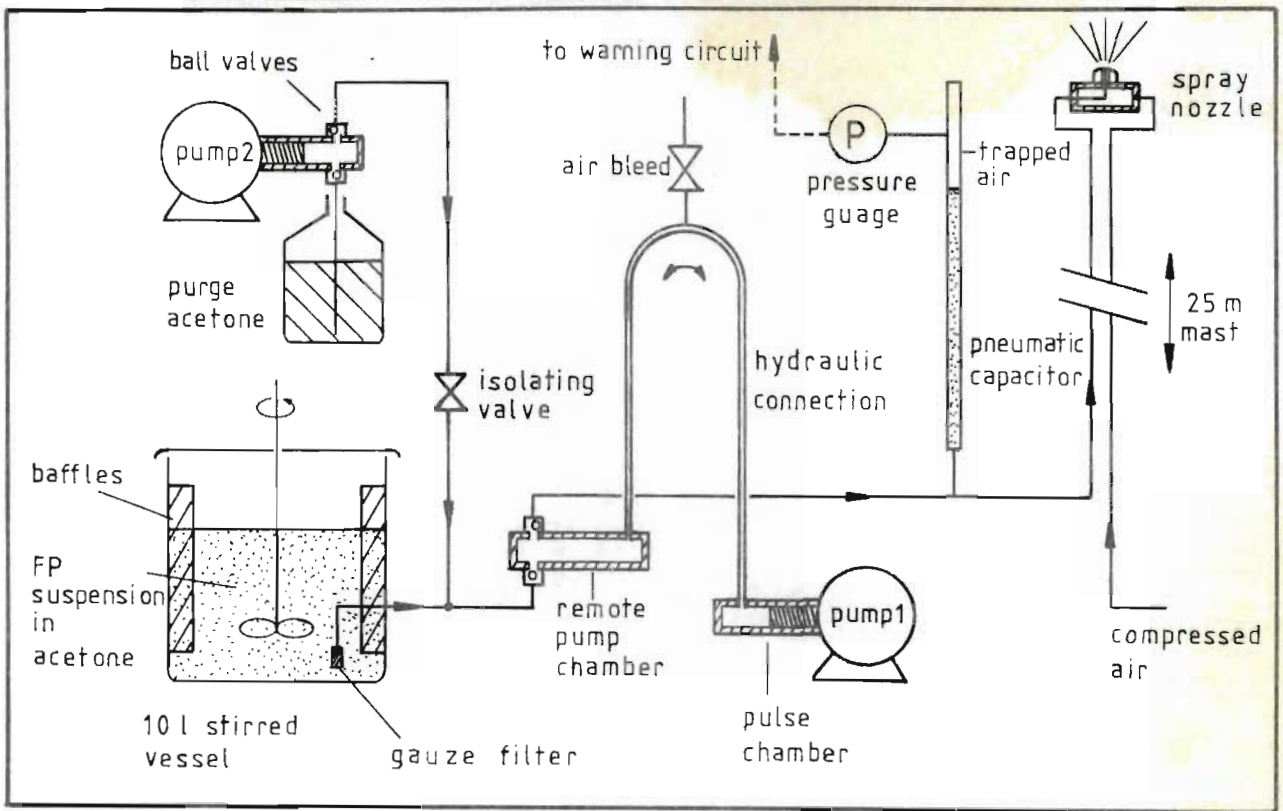
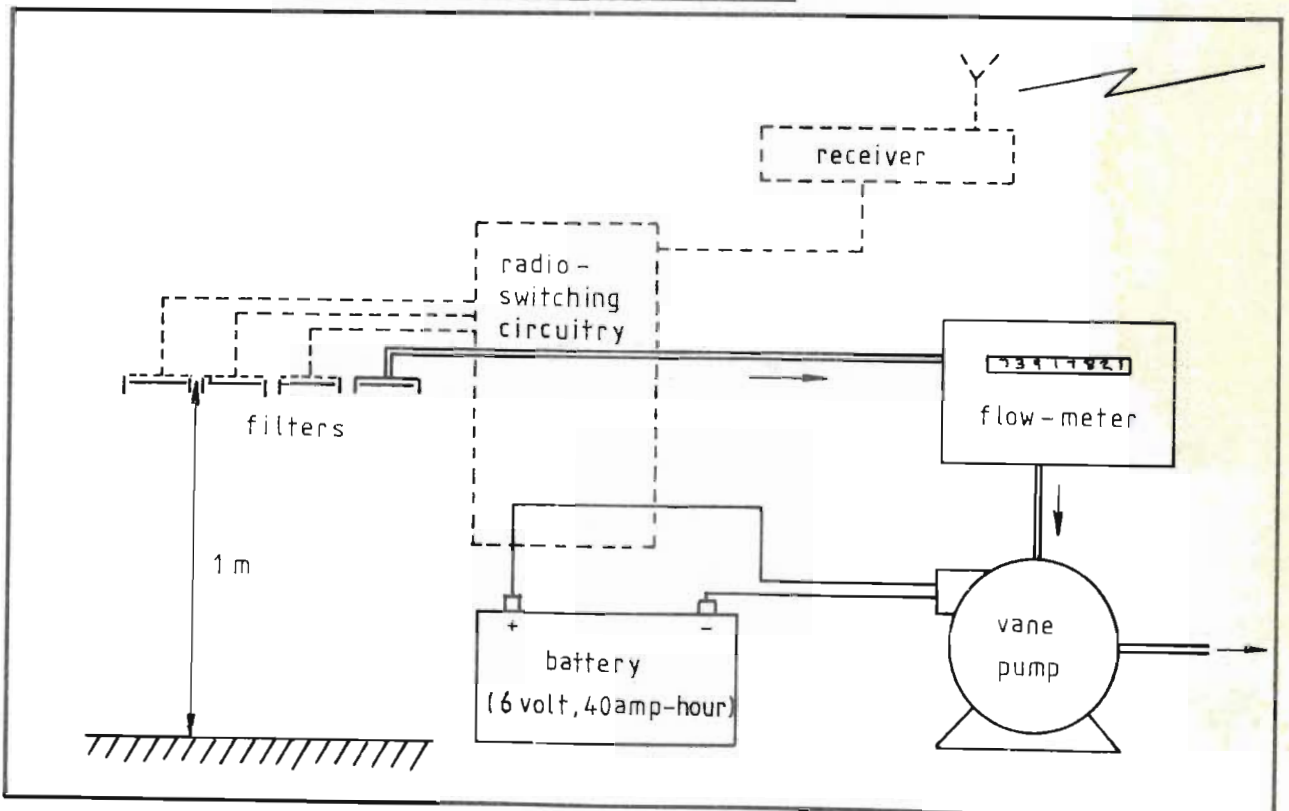


fig. (4.2) Portable filter-aspirator unit



desired physical properties was acetone, and this suspension medium has been used effectively in the present dissemination system.

In acetone suspension, FP particles form loose floccs which enhance settling. However, moderate stirring maintains uniformity in the suspension, and the floccs rapidly break up in the delivery pump and atomising nozzle [plate (4.1)]. The pump used was a reciprocating metering pump with variable stroke. Abrasion of the piston by particles trapped in the piston glands led to the use of a remote pumping chamber [fig. (4.1)]. The remote chamber may be seen in the centre of plate (4.2), with the suspension vessel behind it. For fault-free operation of the ball-valves in the remote head, it was found necessary to limit the suspension concentration to about 200 g FP l^{-1} , and prevent entry of the occasional large agglomerate by means of a mesh filter at the pump intake.

Typical release-rates were about 5×10^8 particles per second, requiring a pump rate close to $0,3 \text{ cm}^3 \text{ s}^{-1}$. In order to avoid blockage of the delivery lines through deposition, sufficient velocity was sustained by use of 1 mm I.D. nylon tubing. It was found necessary to minimise horizontal sections of tubing to prevent saltation. Further advantage was found in using a pneumatic capacitor to smooth out the reciprocal surges.

Pre-weighed pockets of dry ZnS₂Cds were stored on site. In order to recharge the stirred vessel, corresponding volumes of acetone were measured into the vessel, followed by the

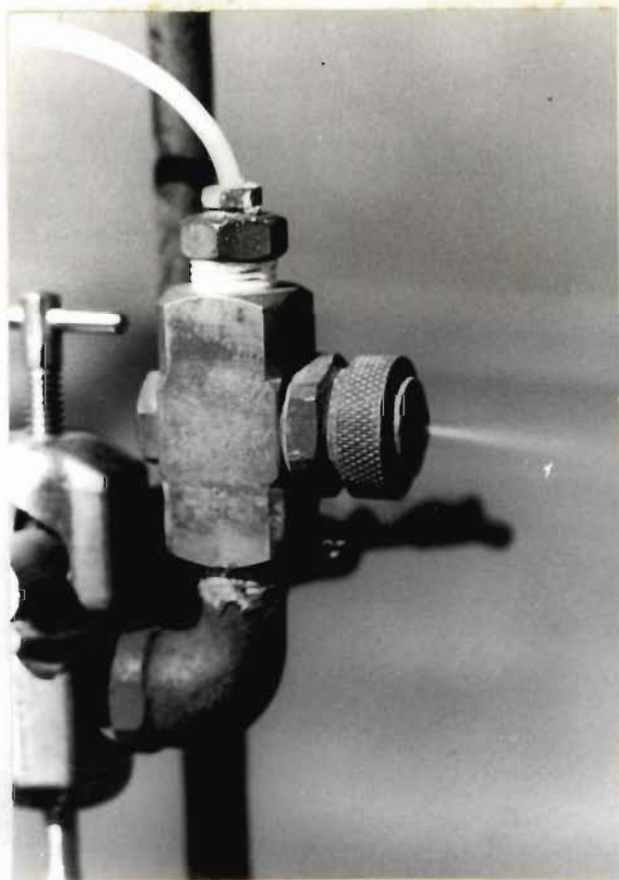


plate (4.1) Disseminator
spray-nozzle

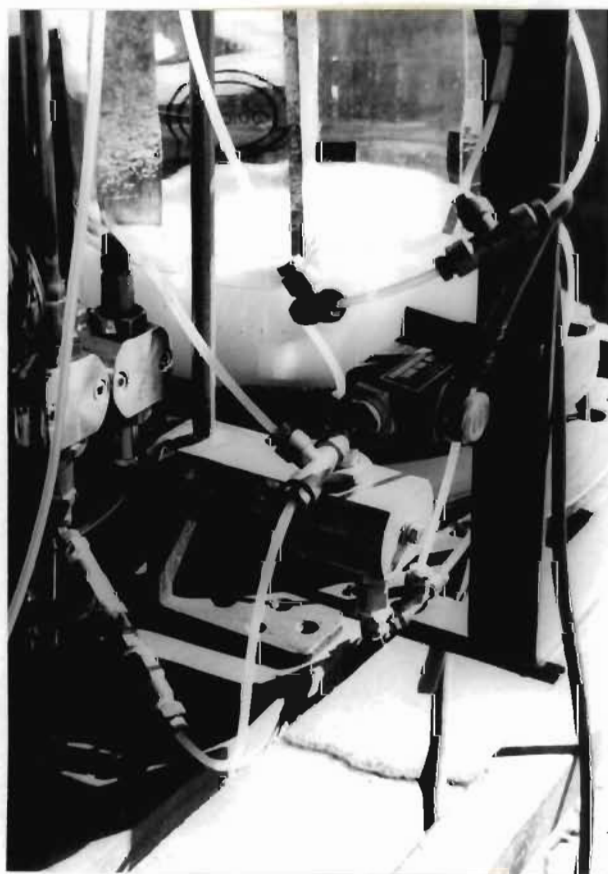


plate (4.2) Dissemination
apparatus, showing pump
chambers and suspension
vessel (at rear)

emptying of each packet below the surface. In this way, both handling of the FP and its escape into the air were minimised.

The inverted "U" hydraulic connection between the pulse chamber and the remote pump chamber was designed to prevent migration of particles into the pulse chamber. Prior to shutting down the equipment, it proved necessary to flush all lines, including the valve cages, with clean acetone. The unreliability of two-way valves led to the use of a second pump (2) in phase with the first (1) for this purpose [fig. (4.1)].

A pressure gauge and preset pressure switches were attached to the air-space in the pneumatic capacitor. The pressure switches triggered an alarm on detection of deviations outside of the normal operating range. Such deviations occurred, for example, when the level in the 10 l stirred vessel was dangerously low, and generally required immediate correction to avoid irreversible blockage of lines. Required pump delivery pressures for release at 25 m were approximately 230 kPa. The nozzle delivery line is seen to hang from the nozzle carriage in plate (4.3).

Once set, pump rates were reasonably consistent. However, the volume remaining in the stirred vessel was recorded at regular intervals, and these readings have been preferred for calculation of release rates.

4.1.3 Calibration for particle yield.

Previous workers [section (4.1.1)] have noted marked variations in measured FP yields, largely as a function of the determination procedures used. In the present work, determinations were initially based on successive dilution, and microscopic examination of measured volumes. The examinations revealed the presence of unbroken agglomerates and newly-formed floccs, and it was realised that a realistic measure had to be based on the dissemination process itself.

The release equipment was set up as in normal operation, with the spray nozzle mounted inside a 5,16 m³ rectangular tent. The tent was airtight, and stirred by a circulating blower and three ventilation fans. The FP tracer was released into the tent for a short period (10s), and a small air sample drawn through a membrane filter. The effects of settling and electrostatic attraction to the tent walls were established by taking subsequent samples. Before each re-run, the tent was purged with fresh air and a background sample taken. The effective particle yield for FP2267 was found in this way to be $0,9 \times 10^{10}$ particles per gram.

The batch nature of this evaluation could introduce several errors, and independent work was conducted by Davey (1977) with the same disseminator and acetone medium, using a continuous process. The nozzle was mounted axially in a 15 cm diameter duct. Air was drawn through

the duct and the flow-rate determined by Pitot tube traverse. Under the turbulent flow conditions, it was assumed that the concentration was uniform across the duct some 5 m downstream, and air samples were drawn off isokinetically and passed through a membrane filter. The effective yield of FP2267 was again evaluated as $0,9 \times 10^{10}$ particles per gram. This is comparable with values ranging from $1,33 \times 10^{10}$ to $1,56 \times 10^{10}$ recorded by Leighton et al (1965) for FP2267.

Using a pycnometer, the density of the ZnSCdS powder was found to be $4,07 \text{ g cm}^{-3}$, so that a yield of $0,9 \times 10^{10} \text{ p g}^{-1}$ implies a volume-mean diameter of $3,74 \text{ }\mu\text{m}$. (earlier Andreasen Pipette determinations in water had suggested only $58\% < 6 \text{ }\mu\text{m}$ Stokes diameter).

4.1.4 Heavy particle effects.

The finite size and mass of the ZnS-CdS particles will determine settling and diffusion behaviour which is not characteristic of ambient air "particles". Equation (1.75) gives the Stokes terminal velocity for particles much denser than air. For particles of Stokes diameter $3,74 \text{ }\mu\text{m}$ and density $4,07 \text{ g cm}^{-3}$ in air at 14°C ($\mu_a = 0,0175 \text{ cp}$), this relation gives a sedimentation velocity $w_s = 1,773 \times 10^{-3} \text{ m s}^{-1}$.

To assess the effects of particle inertia and drag on diffusivity, some typical turbulence observations are taken from the literature. In their analysis of the effect of incomplete data, Pasquill and Butler (1964) recorded some accurate properties for their run of 27th. April, 1962.

Under near-neutral conditions ($Ri_{2m} = -0,005$) the vertical velocity component at 2 m was found to have eulerian time-scale $\tau_E = 0,82s$ and turbulence intensity $\sqrt{w'^2}/\bar{u} = 0,084$ with $\bar{u}(2m) = 5,08 \text{ m s}^{-1}$. Hay and Pasquill (1959) suggested that the lagrangian and eulerian time-scales could be related by a proportionality constant, $\beta = \tau_L/\tau_E$. Angell, Pack, Hoecker and Delver (1971) recorded values of β (BREN and Cardington) which suggest $\beta = 4,2$ for a turbulence intensity of 0,084. An estimated value of the lagrangian time-scale would thus be 3,444s.

Peskin (1971) derived equation (1.71) to relate particle and fluid turbulent diffusivities [section (1.7)]. Substituting the turbulence measurements of Pasquill and Butler (1964) and assuming the Stokesian behaviour described above for 3,74 μm ZnSCds particles, equation (1.71) gives a particle to fluid diffusivity ratio $K_{ZP}/K_{ZF} = 0,999999855$. Turning to equation (1.72) which was derived by Meek and Jones (1973), and includes the effect of settling through uncorrelated regions, substitution of the same properties yields $K_{ZP}/K_{ZF} = 0,99999137$ for typical travel-times. On this basis, it is unlikely that the ratio will deviate significantly from unity for horizontal diffusion, or for any variation of atmospheric stability. It is thus safely assumed that the FP2267 tracer will display the same diffusion behaviour as air.

4.1.5 Air sampling and filter analysis.

Concentrations of Zinc-Cadmium sulphide particles in the air were interpreted as dosages [section (2.4.1)] by aspiration of cellulose acetate-nitrate membrane filters. The filters used had an exposed area of 14,36 cm² and a pore size of 0,65 μm. Particles about this size were probably halted near the surface due to electrostatic attraction and path tortuosity. Typical aspiration rates were about 0,2 l s⁻¹.

4.1.5.1 Anisokinetic effects.

Some early tests were carried out over ranges of about 200 m using closely-spaced arrays of 6 aspirated filters. [Maximum separation approx. 1 m; plate (4.4)]. Except for a supporting clamp-ring, filter surfaces were normally entirely open to the air, and some anisokinetic effects might be expected.

For filters facing towards the source, no systematic deviations were observed with a reduction of aspiration rate to 25% of the normal value. Typical variations in the calculated mean concentrations were about 6%, with occasional maxima of 20%. Such deviations are commensurate with 90% confidence in the observed result for a total count of 1000 particles in some sub-division of the filter. Two further filters were not aspirated at all, and registered respectively 0,2% and 1% of the particles collected by normally-aspirated filters. This compares with 0,5% obtained by

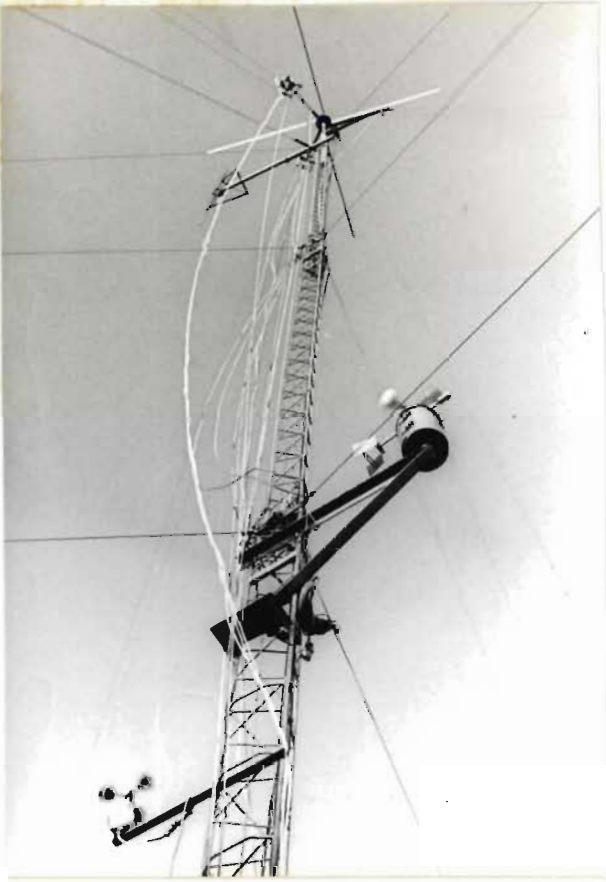


plate (4.3) 25 m
instrumented mast
supporting tracer source.



plate (4.4) Membrane
filter aspirator units
arranged for sampling
tests.

Leighton et al (1965) some 46 m from the source. Particles are probably retained electrostatically after impaction or near-impaction.

Filters with the reverse orientation were run simultaneously with the upwind-facing filters. The effect was to consistently reduce observed mean concentrations by about 50%. Further filters were run in a downwards orientation, facing the ground, thus being insensitive to the direction of approach. The calculated concentrations had an average deviation of $\pm 7\%$ from the mean concentration recorded by forward-orientated filters, with maximum deviations of $\pm 10\%$.

The insensitivity of the forward-facing filters to aspiration rate suggests that errors will not be introduced by non-isokinetic sampling in this orientation. Of course, the complexity of a mesoscale wind-field under stable conditions will make it difficult to ensure the angle of approach over typical transport ranges. A best solution is thus offered by the downward-orientated filter, and this has been the approach in the current work. With the filter plane parallel to the ground, it is also protected to some extent from passing mist. Progressive dampening of the filter by dew and mist has been observed to throttle aspiration.

4.1.5.2 Equipment.

The prime requirement of the air-sampling equipment was that it should be portable, to allow speedy and unrestricted positioning in the region of interest. The basic aspirator is represented in fig. (4.2) as a filter holder, flow meter and vane pump, with a 6 volt battery power supply. The assembly was mounted in a suitcase-like container [plate (4.4)]. Of the 10 units which were available, 5 had been converted to allow remote switching by radio to any one of 4 filters. This prototype facility was used only in one experiment, and was subsequently scrapped due to unreliability.

Filter-holders were positioned so as to be unobstructed, with the filter 1 m above ground level in an open space. In a normal experimental run, filters were changed sequentially by a mobile team. The entire filter holder was detached and replaced by a previously-loaded holder. Filter-holders were stored separately in new plastic packets, and only loaded or unloaded in an uncontaminated laboratory.

At each filter-change the integrated meter-reading was recorded. Unless there was evidence to the contrary, it was assumed that the aspiration-rate remained constant during these intervals. Flow-calibration tests showed that a small rate-dependent correction had to be applied to apparent flow rates, probably due to the pressure drop across the filter.

Exposed filters were transferred directly into enclosed microscope slides, which were stored for subsequent examination. For examination, the area of filter below the microscope objective was irradiated with intense U.V. light by passing the parallel rays from a mercury lamp through a 50 mm convergent lens. An arrangement of optical filters restricted the incident light to a narrow band about 3650 Å. A further yellow filter in the microscope optical train limited observed light to a band in the fluorescence region, also preventing eye damage by reflected U.V. light.

4.1.5.3 Statistical significance.

In the program of field experiments, tracer release rates were close to 5×10^8 particles per second. Membrane filter dosage measurements were made 1 m above ground-level, and at distances extending to 8 km. During a typical dosage interval, 1 m³ air would be drawn through the filter, resulting in an accumulation which ranged from 0 to 10⁴ particles. Due to the variability of wind direction, however, counts were more often at the lower end of this range. In order to make use of the low counts, it will be necessary to attach some sort of statistical significance to them.

Volume samples drawn from a large volume of air, which has a random particle distribution, should contain numbers of particles which follow a Poisson distribution. The Poisson distribution parameters are directly additive for combined samples, so that slow temporal variations in

concentration will not affect the nature of the distribution. (Over long periods, observed concentrations in the atmosphere typically follow a log-normal distribution [Bencala and Seinfeld (1976), Hale (1972)]). The objective is to define confidence limits based on actual particle counts.

Assume that the sampled volume consists of N smaller volumes with an observed mean count $\bar{p} = p_T/N$. If N is large, \bar{p} will be asymptotically normal ($m, \sigma/\sqrt{N}$), where m and σ^2 are the true mean and variance of the sampled volumes. For a Poisson distribution $\sigma^2 = m$, and the approximation $\sigma^2 = \bar{p}$ is made. It follows that the true total count has a probability of $(100-P)\%$ of being contained in the interval $p_T \pm \lambda_p \sqrt{p_T}$ where p_T is the observed total count and $\lambda_p = \sqrt{2} \operatorname{erf}^{-1}\{1-P/100\}$.

Particle counts for the membrane filters, including the FP yield determination filters, were all performed in the same way ($100\times$ magnification) by the same worker. Subjective errors should thus be minimal.

4.2 Richards Bay Project.

4.2.1 Introduction.

The development of a large new harbour at Richards Bay, some 150 km north of Durban on the Natal North Coast, has encouraged the growth of several new industries, and the planning of many more. The absence of earlier development has allowed some flexibility in the location of residential, business and industrial areas, and considerable interest has

been shown in the likely distribution of air pollutants from the proposed industrial sites.

Climatic variations on the Natal Coast result from the passage of a succession of coastal low pressure systems [Preston-Whyte (1975)]. During winter, these lows are preceded by intense anticyclonic subsidence and weak pressure gradients. The clear, dry weather accompanying subsidence results in strong nocturnal cooling, and the consequent formation of a radiation inversion which may combine with the subsidence inversion above. Low gradient winds, weak sea breezes and reduced surface heating all act to reduce daytime mixing depths. As a result, the poor dilution of air pollutants during a stable winter night may be followed by appreciable fumigation the following day.

The sharp diurnal anomaly which occurs in surface temperature at the land-sea interface, and significant topographic effects, combine to produce a complex wind-field under stable conditions [section (1.3.1)]. Whereas pollutant concentrations are highest when the atmosphere is stable, the problem of predicting pollutant levels in the region is made extremely difficult by the complexity of the wind field. For this reason, a predictive model for meso-scale wind-fields has been developed by Scholtz and Brouckaert (1976) [section (1.3.1)]. Though the wind-field model, and the point-source dispersion model [chapter (2)], have been designed to operate under arbitrary conditions, the transport behaviour of the atmosphere over Richards Bay specifically has been investigated to assess the performance

of these models. The Richards Bay Project was thus conceived with three purposes:-

- (1) Assessment of pollution potential from direct measurements of the wind-field and the distribution of a tracer.
- (2) Verification of the wind-field model from measurements of the wind-field.
- (3) Verification of the dispersion model by comparison with tracer dosages, using both wind-field measurements and predictions as input information.

4.2.2 Meteorological measurements.

The measurements required by the meteorological sub-model are discussed in appendix (A4). To provide adequate spatial resolution in these measurements, use has been made of 8 semi-portable instrumented masts and two permanent masts. The semi-portable masts were instrumented for wind-direction, speed and temperature at the 11,2 m level, and for wind-speed and temperature at the 1,9 m level [fig. (4.3), plates (4.5), (4.7) and (4.8)]. To facilitate data-handling and provide sufficient temporal resolution, a radio-telemetry system has been developed to handle these measurements [Starkey (1976)]. This system provides an on-line description of the wind-field, and thus allows some optimisation in the planning of tracer experiments.



plate (4.5) Semi-portable
telemetering mast, instrumented
at 1,9 m and 11,2 m levels.



plate (4.6) Telemetry satellite
station circuitry - calibration
of platinum resistance
thermometers.

Satellite stations at each of the semi-portable masts are interrogated sequentially once every 3 minutes on the transmission of identifying tones by the main station. Each station replies by transmitting accumulated anemometer counts and averaged wind-direction for the 3-minute cycle, as well as instantaneous measurements of the lower temperature and the temperature difference. These measurements are digitally-encoded and transmitted as a series of five frequency-shift-keyed pulse trains. On receipt of the signal via VHF radio link, the main station decodes and displays the five data-quantities. Identifying time-marks and the satellite station number are combined with the signal, and it is passed directly to a magnetic tape-recorder. The system allows for the interrogation of 10 stations at 15-second intervals. An eleventh auxiliary tone may be transmitted for the purpose of remote filter-changing. The selection of one of four frequencies will switch an aspirator on (if it was off) and direct aspiration to one of four corresponding filters.

During the experiments, sensitive Casella anemometers and an especially-designed wind-vane supplied digital signals to the satellite station directly. In order to represent accurately the temperature difference over a vertical distance of 9,3 m, platinum resistance thermometers, normally housed in shielded aspirators, were carefully matched and calibrated [plate (4.6)]. The transmitted pulse-count for temperature difference had a sensitivity of about 25 counts/ $^{\circ}$ C. One revolution of the digital wind-vane was divided into 64



plate (4.7) Semi-portable mast upper instrument carriage (11,2 m), showing cup anemometer, platinum resistance thermometer aspirator, and digital wind vane.

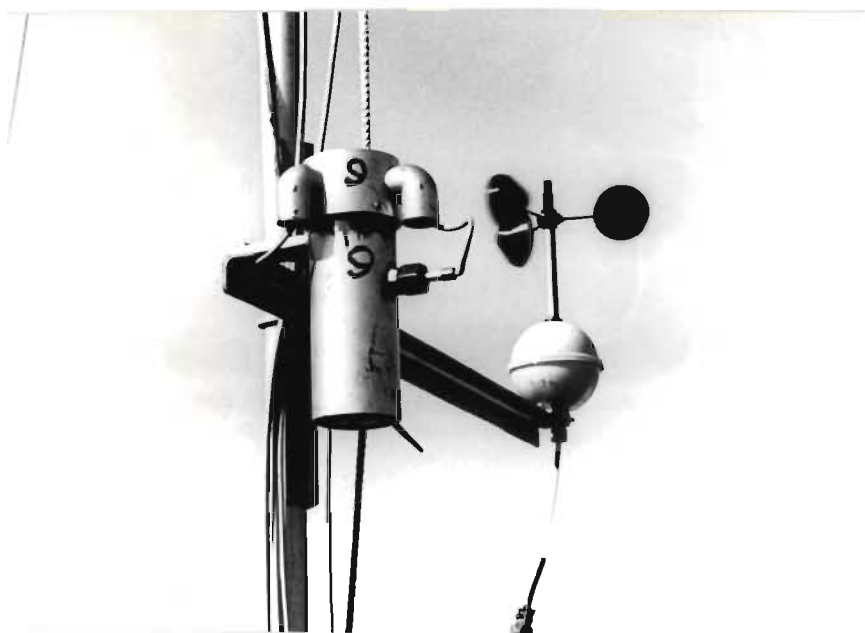


plate (4.8) Semi-portable mast lower instrument carriage (1,9 m), showing platinum resistance thermometer aspirator and cup anemometer.

sectors, so that directions were correct to the nearest $5,625^{\circ}$. Further errors up to $\pm 2^{\circ}$ may have resulted from mis-alignment. The vane could undergo up to 10 complete revolutions during the 3-minute cycle without affecting the averaging process.

The semi-portable masts comprised 3 sections of 30 mm steel tubing, and satellite stations were powered by 6 v and 12 v lead-acid batteries. This allowed some flexibility in the positioning of the masts, which were located at mast sites 1 to 8 in the Richards Bay area [fig. (4.4)]. The permanent installations consisted of clockwork chart-recording Lamprecht anemometers mounted at 8.0 m on the main-station mast (site 9) and at 10 m on a permanent mast at site 10. The 25 m main-station mast [plate (4.3)] also had aspirated thermistors mounted at 3,0 m and 23,6 m, providing a continuous chart record of temperature and temperature-difference [fig. (4.3)]. Permanent installations at greater distances from the region of interest were not included in this investigation.

During the first tracer experiment [section (5.2.1)], remote filter-changing units [fig. (4.2)] were coupled to the transceivers at masts 3,4,5,6 and 7. These were subsequently scrapped due to the unreliability of the solenoid valves. Masts 1 and 7 were equipped with Casella anemometers only at the 11,2 m level. The availability of speed measurements at both 11,2 m and 1,9 m allowed estimation of roughness length z_0 at masts 2,3,4,5,6,8 [section (4.2.4)].

fig.(4.3) Richards Bay Project : Schematic organisation

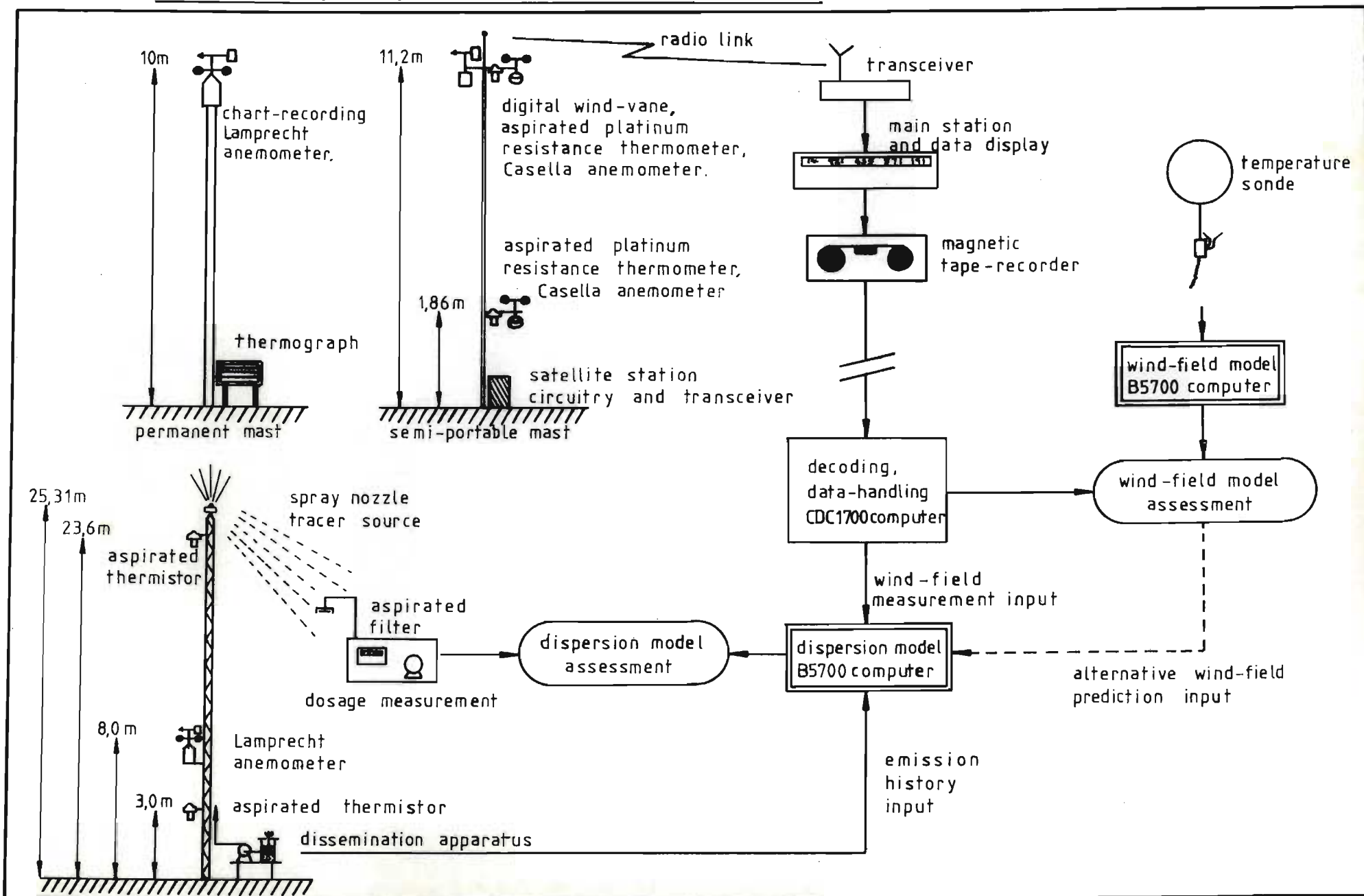
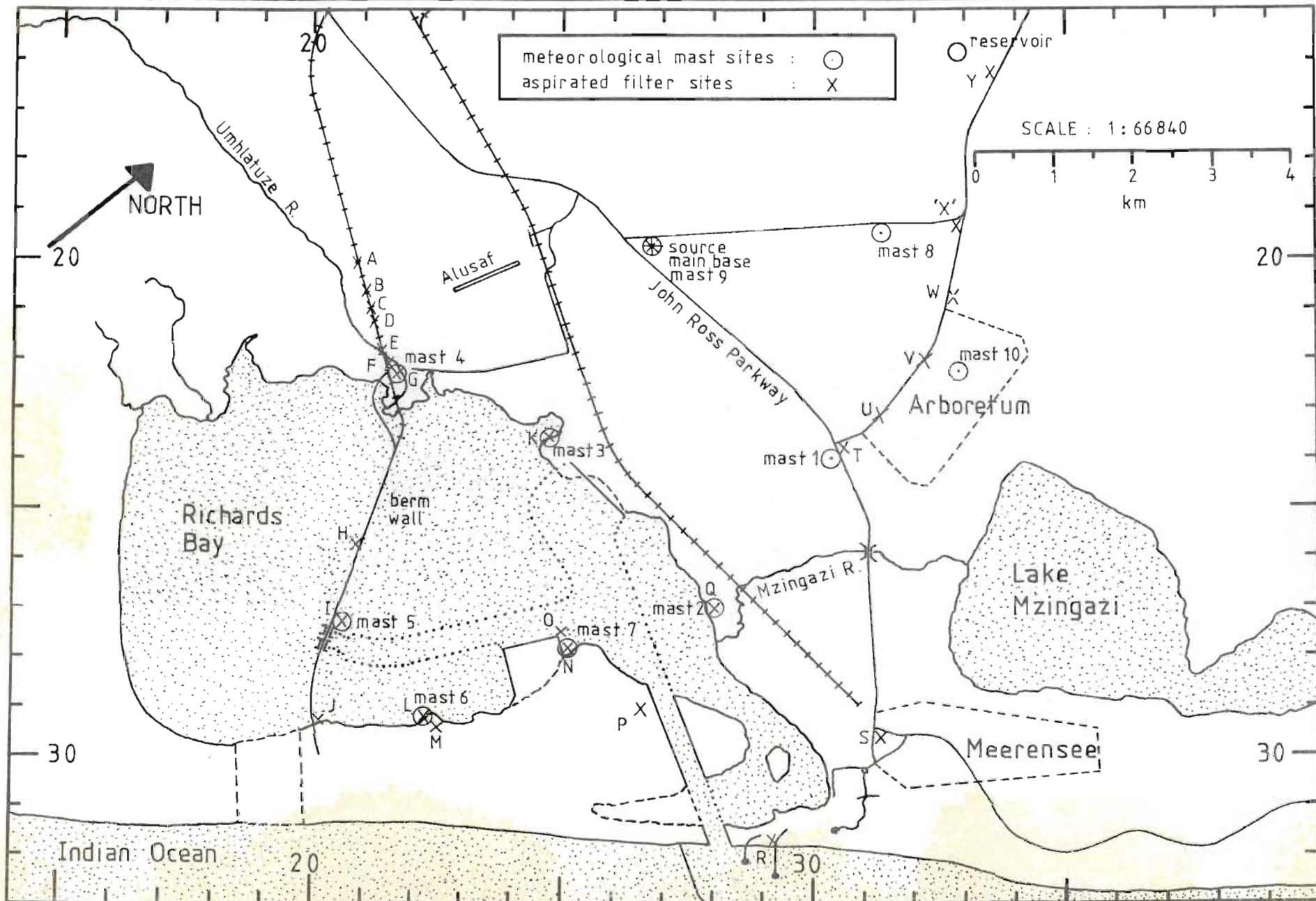


Figure (4.3) is a schematic representation of the various data-routes. Magnetic tapes containing the digitised telemetry information were input to a CDC 1700 computer via the event-counters available on this machine. Decoding and the application of calibrations were followed by exclusion of any faulty data. The information was then transferred to a B 5700 computer where it was used as input to the meteorology sub-model [appendix (A4)] and finally the dispersion model [appendix (A1.4.3)]. Information available on charts was input to the CDC 1700 using a manually-operated analogue reader. The entire meteorology data-set, together with all pertinent source and receptor information, is presented in a separate publication [Mulholland, Scholtz and Brouckaert (1977)].

4.2.3 Experimental method.

The ZnSCdS particulate tracer, FP2267, was released at a height of 25,31 m from mast 9 [fig. (4.4), plate (4.3)]. Also located at mast 9 was the radio-telemetry system main station. Wind-field observations were begun before emission in order to assess the suitability of the weather, and to plan locations for the filter receptors. Typical experimental runs lasted about 14 hours, beginning before midnight and ending about midday. This period usually included stratified stable flow until the onset of fumigation or the mixing of a strong gradient wind to ground-level. During a run, filters on any one of the 10 aspirator units [section

fig.(4.4) Richards Bay Project: Locations of meteorological masts and aspirated filters



(4.1.5.2)] would be changed up to 6 times, depending on the estimated tracer distribution and the rapidity of temporal transients. Once all 45 preloaded filter-holders had been used, exposed filters were transferred to enclosed microscope slides in a laboratory near mast 10. Filter-handling personnel were kept clear of the tracer dissemination apparatus to avoid contamination.

A simultaneous release of smaller particles ($\sim 0,1 \mu\text{m}$) of In_2O_3 was conducted at the same height as the ZnSCdS tracer by combustion of an $\text{In}_2\text{O}_3/\text{Et.OH}$ solution at a spray nozzle [Norden and van As (1977a)]. Few of these particles pass right through the $0,65 \mu\text{m}$ pore membrane filters which were used, and they were determined by neutron-activation after the FP counts.

4.2.4 Estimation of the surface roughness distribution.

The possibility of estimating surface roughness z_0 from velocity and temperature measurements at two heights is discussed in appendix (A4.2). The availability of these measurements at masts 2,3,4,5,6 and 8 during June and July, 1976, provided a basis for the distribution of z_0 in the Richards Bay area.

Estimations of z_0 were made by interactive processing of entire telemetry records. A first guess of z_0 allowed calculation of the profile parameters according to procedure (1), table (A4.1). This allowed calculation of the

theoretical lower velocity using equation (2.72). The roughness length z_0 was adjusted iteratively so as to minimise the standard deviation between observed and theoretical lower velocity for the whole record. Table (4.1) lists the resultant estimates, and some comparable values estimated from data presented by Sutton (1953) [section (1.2.2)].

Table (4.1) ROUGHNESS LENGTH ESTIMATES AT MASTS.

MAST	UPWIND TERRAIN	Z_0 [m] from measure- ments.	Z_0 [m] following Sutton (1953)
2	Sparse sugar-cane $\sim 1,5$ m high	0,2	>0,09
3	Flat sand and water	0,00001	0,00001
4	Short grass ~ 15 cm high, no obstacles	0,02	0,007
5	Short, sparse grass ~ 15 cm high	0,01	0,007
6	Flat sand and water	0,00007	0,00001
8	Thick grass ~ 40 cm high, some small bushes	0,2	0,09

In order to estimate surface roughness more generally, the various types of surface coverage in the Richards Bay area were divided into seventeen categories [appendix (A4.4)]. Each of these categories was allocated a roughness length based on the estimates in table (4.1), equation (1.17) due to Lettau (1969), and the tabulated

results of Priestley (1959), Sutton (1953) and Sheppard (1947) [section (1.2.2)]. Thus, for example, the region between masts 8 and 9, consisting of isolated stands of trees with 50% open grassland, was given a roughness $z_0 = 0,2$ m according to equation (1.17).

Choosing points in such a way as to define the major surface-roughness variations, z_0 was specified at 152 locations in the region of interest. This data-set constituted a basic input to the meteorology sub-model, which performed an inverse square interpolation of $\log(z_0)$ in order to store z_0 more readily in a grid consisting of about 2000 points. Figure (4.5) shows a computer-generated contour plot of this grid.

CHAPTER 5

ANALYSIS OF EXPERIMENTAL RESULTS

5.1 Introduction.

Typical pollution episodes on the Natal Coast include the development of a complex, stratified wind-field during stable winter nights, followed by an extended, calm fumigation period after sunrise. In the series of experiments conducted at Richards Bay during June and July, 1976, an attempt was made to record such episodes, so that the results are presented as a series of experimental runs varying from 6 to 16 hours in length. No single run could be considered to represent a typical development - in each case a unique behaviour was determined largely as a function of overlying synoptic weather patterns. Only in two of the eight experiments were long fumigation periods observed, a more frequent development being the early mixing of gradient-wind momentum to ground-level. The influence of synoptic weather variations is likely to be less significant during early winter (May, June) when conditions are more settled.

The transport of ZnSCdS tracer (FP2267) during each experiment was simulated using both the dynamic puff model (DPM) [chapter (2)] and the gaussian puff model (GPM) [appendix (A2)]. Except in the simulation of Run 723 using predicted wind-fields [section (5.3)], the meteorological

input for these models was provided by the radio-telemetry system [section (4.2.2)] and chart records at mast 9 [fig. (4.4)]. Because of the relatively poor temporal resolution of the charts, the latter data were provided only at $\frac{1}{2}$ -hour intervals. To account for the coarseness of these measurements, the inverse-square interpolation scheme (1.17) has been weighted such that contributions from mast 9 are reduced to 5% of their normal value. (In fact, effective distances from the mast are increased by the ratio $1/\sqrt{0,05}$). In the same way, contributions from masts 6 and 7 have been reduced to 60% and 50% respectively of their normal values in order to account for the non-representativeness of their locations, positioned as they were about 300 m from a large coastal dune. These weighting factors are based on a subjective impression of the distance within which local velocities should be distorted by the obstacle. The isolated locations of masts 6 and 7 meant that the unweighted interpolation scheme would have carried the distortion further into the predicted wind-field than the expected real distance.

The spray nozzle used for release of the FP tracer [section (4.1.2)] was mounted at a height of 24,31 m on mast 9, which was located in the planned industrial area. The nozzle sprayed upwards, giving an effective release height which appeared to be 1 m higher (25,31 m) for typical wind-speeds, and this was the release-height used in the model simulation. Release-rates were determined by recording volumes retained in the suspension vessel at

intervals in time. For the purpose of modelling, it was assumed that an average release-rate applied during each interval. The resultant release histories, presented as particles per second, were occasionally interrupted by blank periods of about 5 minutes during which the suspension vessel was recharged.

The effect of Stokesian settling was accounted for by assuming a mean sedimentation velocity $w_s = 1,64 \times 10^{-3} \text{ ms}^{-1}$, which corresponds to 3,6 μm spherical particles in air at 14°C [section (4.1.4)]. Although the dynamic puff model allows for the specification of an absorptive deposition velocity w_d and first order removal mechanisms (washout, decay) [section (2.3.4)], these effects were assumed to be negligible due to the absence of general information. In fact, it is likely that particles of this size will deposit significantly through impaction at ground level. In experiments with dry moss surfaces, Clough (1975) observed deposition velocities for ZnSCds particles which were two or three times larger than the above sedimentation velocity. Leighton et al (1965) found that impaction losses were comparable with deposition losses for 4,5 miles of travel over Palo Alto. The present experiments were conducted in clear, stable weather, so that no losses were sustained through washout, though nucleation of the occasional ground-mist may have been significant. The only other decay process which may have been active is the loss of fluorescence due to exposure to U.V. radiation after sunrise. Leighton et al (1965) suggested that this effect should be small [section (4.1.1)].

The results for each experiment are presented as a comparison of the dynamic puff model and gaussian puff model predictions. For comparison with the dosages (or mean concentrations) recorded by aspirated membrane filters at a height of 1 m, these models have been employed in their dosage modes, though predicted instantaneous concentration distributions are provided in some cases. In the DPM, puffs were solved for at release-intervals of 900 seconds, with further releases interpolated at 90-second intervals. Along the trajectory, solutions were provided at a maximum interval of 90 seconds by means of interpolation. The lagrangian puff was solved in a 12(vertical) \times 280 (horizontal) grid until the puff centroid had moved outside a 2500 m margin surrounding the region of interest.

In the GPM, puff solutions were provided at release intervals of 360 s and trajectory-steps of 360 s, with further solutions interpolated at intervals of 36 s and 12 s respectively. The gaussian puff model included the sedimentation velocity $w_s = 1,64 \times 10^{-3} \text{ ms}^{-1}$ by means of the vertical shift discussed in appendix (A2.2). Both the dosage solutions and the concentration distribution solutions were based on the velocity and diffusivity at a height of 10 m. For a release at 25,31 m, it was found that parameters evaluated at 10 m provided acceptable effective values from the point of view of ground-level concentration [section (3.4)].

In order to store the dosage contribution at each filter-site, the entire dosage period was divided into the

minimum number of time intervals required to define the start and finish of every filter. A particular filter dosage could then be represented by combining the relevant dosage intervals for that filter site. This procedure was designed to streamline the dosage allocations during execution of the model, but has the disadvantage that the concentration at a point may only be presented as a mean concentration histogram, the temporal resolution of which depends on the current frequency of filter changes. Comparisons with filter measurements are made on the basis of time-mean concentrations, which are evaluated from the dosages predicted at the uniform filter height of 1 m. The assumption of a typical sampled volume of 1 m^3 allowed a delineation of the statistical significance of measured concentrations [section (4.1.5.3)]. The 95% confidence limits which are presented illustrate the diminishing agreement which may be expected for low particle counts. Predicted and measured filter concentrations are plotted on logarithmic scales which intersect at 1 pm^{-3} . Where greater concentrations are predicted but not measured, or vice versa, the comparison point is marked on the appropriate axis. If both predicted and measured concentrations are below 1 pm^{-3} , the point is listed separately.

A limited description of the atmospheric behaviour for each run is provided by the temperature-gradient history at each mast, and a series of interpolated wind-fields at half-hour intervals. All diffusivity and velocity profile parameters are based on equations (2.72), (2.73), (2.75),

and are evaluated by the meteorology sub-model [appendix (A4)]. These parameters are stored as time-histories for each mast [appendix (A1.2)], and the potential-temperature gradients have been calculated from them according to equations (1.20), (1.22), (1.29), (1.30) and (2.70). In order to make the overall trends clear, the gradient histories, evaluated at a height of 10 m, have been subjected to a smoothing process with an averaging time of 1800s. They provide a useful indication of thermal stratification and hence of atmospheric stability. Sub-adiabatic temperature gradients ($\partial\bar{\theta}/\partial z > 0$) result in stable conditions whilst superadiabatic gradients ($\partial\bar{\theta}/\partial z < 0$) result in unstable conditions. Significant variations occur with differences in location and upwind terrain.

An indication of the degree of spatial variation in stability is provided by contour plots of the inverse stability length L^{-1} at selected times. The contours are established by inverse square interpolation (weighted) amongst the meteorological masts, in the same way that values are acquired by the dispersion models. For the purpose of the presented plots, L^{-1} values were averaged during centred half-hours.

The series of wind-fields presented with each run in section (5.2) has been constructed by inverse square interpolation (weighted) of the separate Cartesian components [Wendell (1972)]. The masts which have contributed information for this interpolation are marked in with additional wind vectors, and serve to indicate the

sense of the vector field, since the vector trails on the downwind side of the mast. The usual direction of flow at night, representing a land breeze, is towards the coast. Note that all wind directions referred to in the text represent the conventional direction-of-origin, except where the direction is suffixed with "-ward", in which case a wind heading is implied. The distance separating vector origins represents 4 m s^{-1} in vector length. Velocities at 10 m are interpolated in the same way in the dispersion models DPM and GPM, and are used in conjunction with L and z_0 to evaluate the friction velocity u_* at a point. However, the presented wind-fields have been subjected to a centred 15-minute smoothing period.

Since the radio-telemetry system provided 5 measurements at each of 8 masts every 3 minutes, much additional meteorological information is available, and the entire database has been tabulated in a separate publication [Mulholland, Scholtz and Brouckaert (1977)].

Accompanying the experimental runs in section (5.2) are estimates of the dosage distributions, which are expressed as mean concentration distributions for specified periods. These rather crude estimates have been established using the vertical column particle-in-cell model which is discussed in appendix (A3). As in the GPM, velocity and vertical diffusivity were based on values calculated at 10 m above ground level.

In the case of Run 723, section (5.3), an additional simulation is performed using wind-fields predicted using the continuity model of Scholtz and Brouckaert (1976) [section (1.3.1)]. The predictions were based on velocity measurements at mast 9 and temperature measurements at mast 8. Velocities at a height of 10 m were provided for the entire region in the form of two-dimensional grids with a horizontal interval of 635 m. The time-interval between available solved wind-fields was 30 minutes. Specific point values of the Cartesian components were obtained from these grids by linear interpolation in time and space. The stability parameters were stored in similar grids, using an inverse-square interpolation of measurements made at the available masts in order to set up the grids.

5.2 Simulation of tracer experiments using measured wind-fields.

5.2.1 Run 627 (27.6.76).

The passage of a coastal low-pressure system along the Natal Coast is usually preceded by a period of fine weather accompanied by light North-Easterly winds. As stability increases during the night, the surface flow becomes dominated by a land-breeze. Run 627 depicts a typical development in which a light land-breeze competes with the fluctuating influence of the N.E. gradient wind during the night, the latter wind mixing to ground-level with inversion break-up after 11h00 [fig. (5.2)]. An additional effect is the channelling of the land-breeze southwards over Lake Mzingazi by the high coastal dune to the ^{EAST} West of this lake. The tendency for this channelling to occur is indicated by the southwards deviation of the wind direction at mast 2, near Lake Mzingazi [e.g. 01h30, 05h30]. Although the overall variation of wind-direction during this run is less than 90° , it is seen that the wind-field is subject to continuous temporal variation.

Figure (5.1a) shows relatively small fluctuations in the subadiabatic temperature gradients recorded until 07h00, after sun-rise ($\partial\bar{\theta}/\partial z > 0$, stable atmosphere). Whereas masts 1, 2, 4 and 9 register superadiabatic gradients shortly thereafter ($\partial\bar{\theta}/\partial z < 0$, unstable atmosphere), masts 3, 6 and 7 which are near the water surface, or downwind of the water

RUN 627 (27/6/76)

fig. (5.1a)

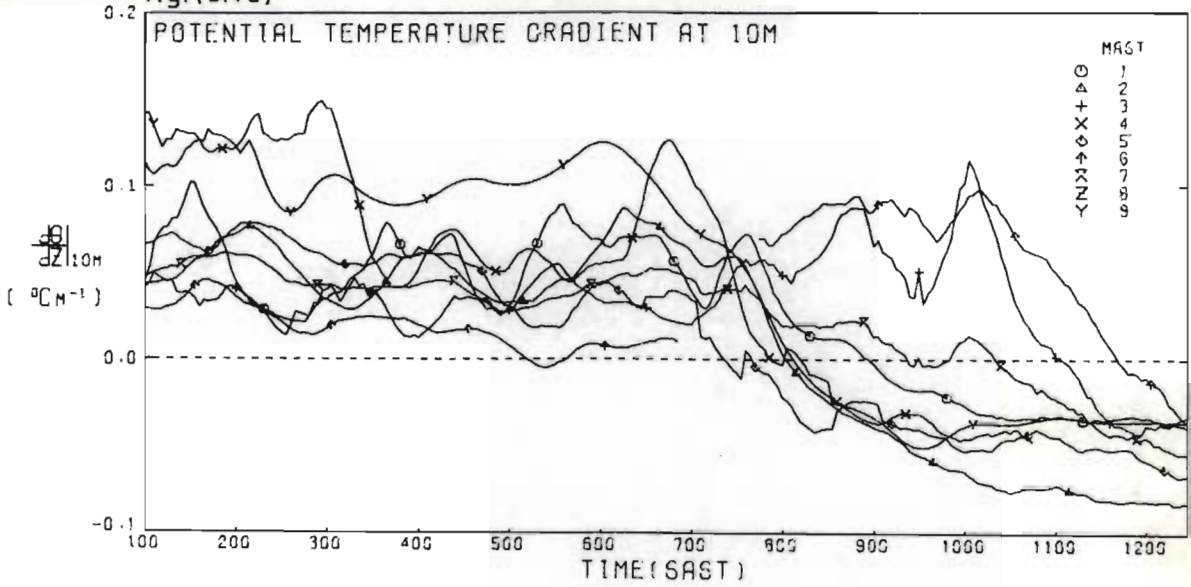


fig. (5.1b)

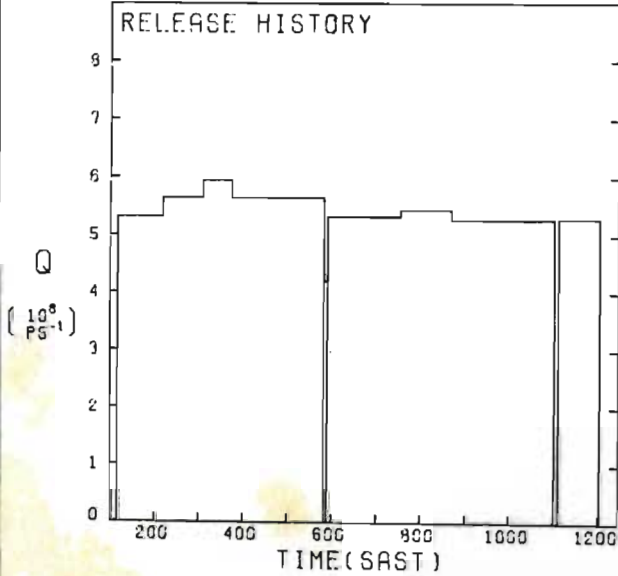


fig. (5.1c)

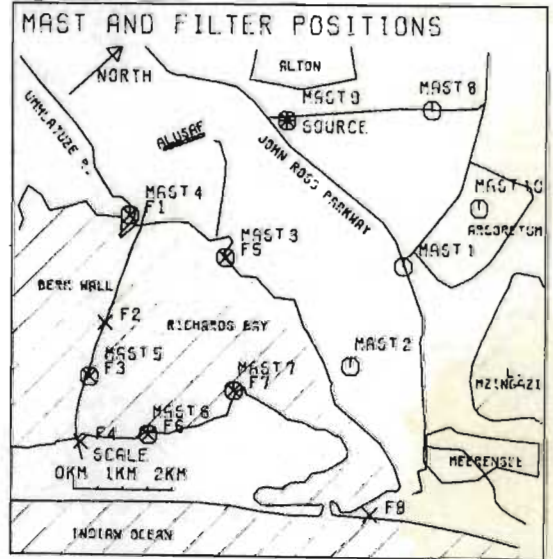


fig. (5.1d)

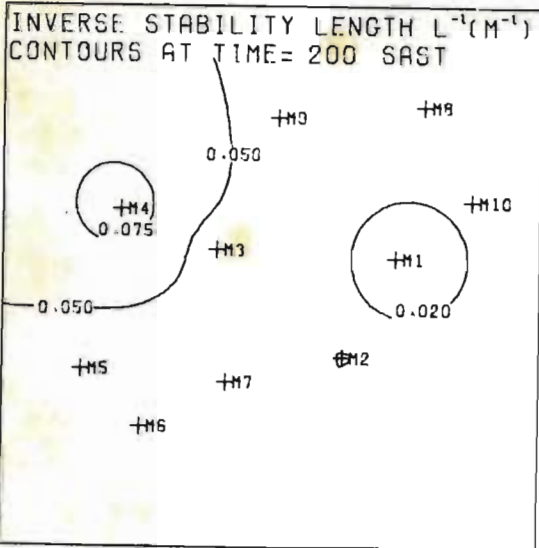
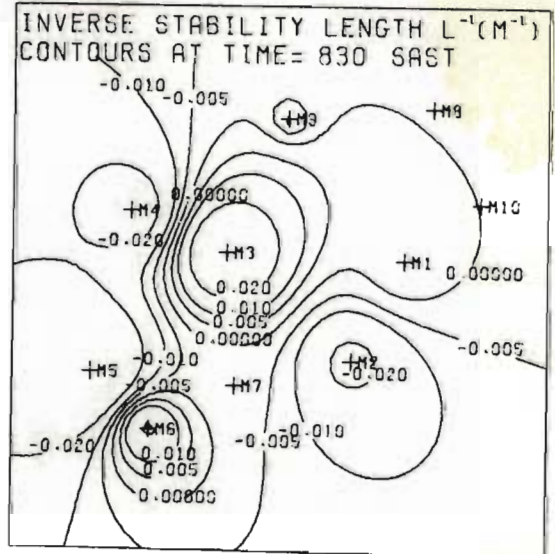


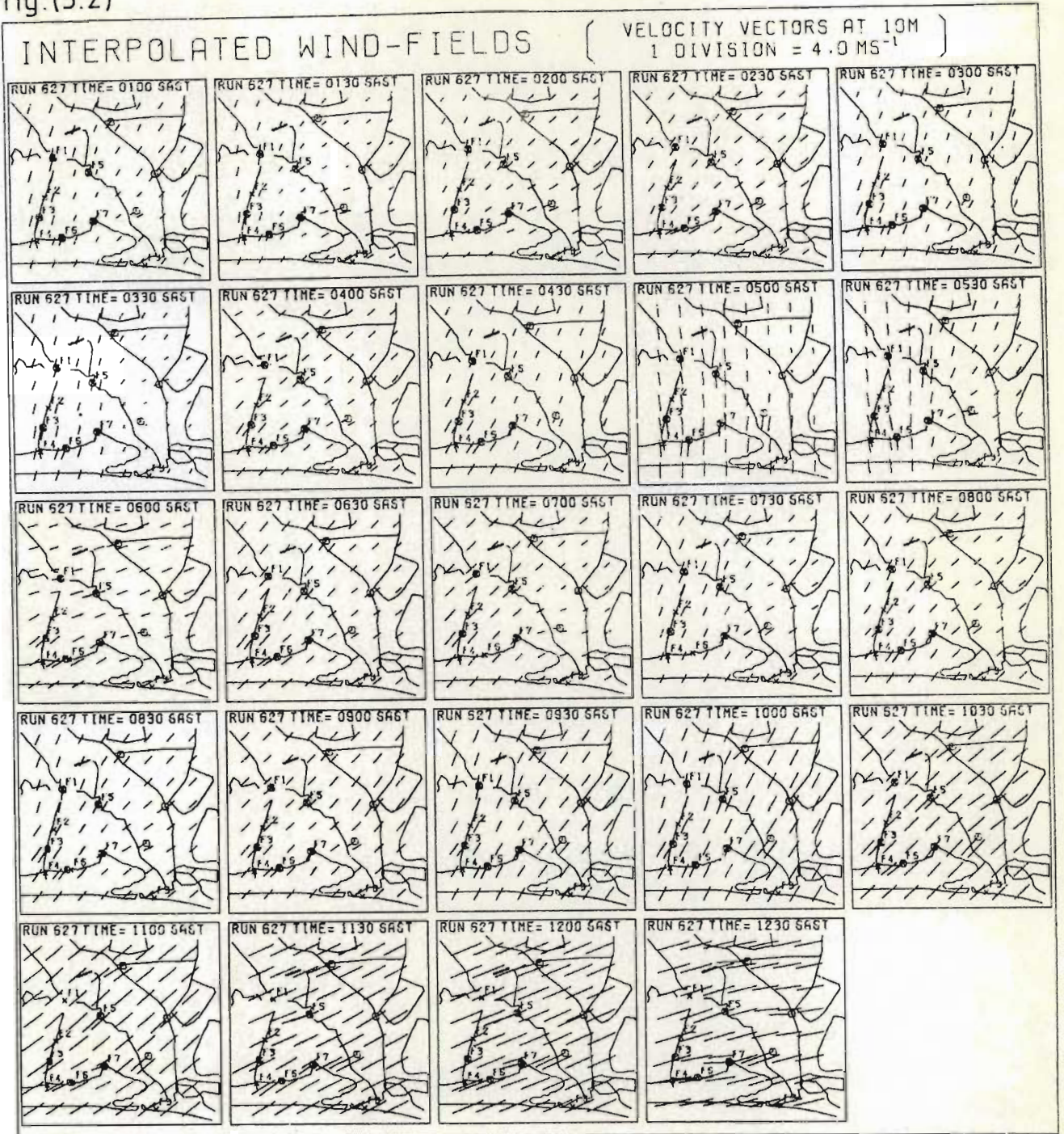
fig. (5.1e)



surface, show persistent stability until after 10h00. The low gradients at the latter masts before sunrise arise from the maintenance of a higher temperature at the water surface than at the land surface, due to the convective distribution of heat throughout the water bulk. This capacitive "dampening" of diurnal temperature oscillations leads to a similar lag behind the land surface temperature after sunrise. As warm air from the adjacent land surface begins to move over the cool water surface, a subadiabatic temperature gradient is created which is usually greater than that experienced before sunrise [fig. (5.1a)]. Analogous effects resulting from the water-temperature lag have been recorded by Munn and Richards (1963). The gradient recorded at mast 5 is somewhat anomalous, behaving much like the land stations. In subsequent runs it will be seen to behave more like the water stations, though the early dissipation of the subadiabatic gradient at this point may be due to the fact that the mast was sited on an eastward-facing slope.

The effect of the measured temperature-gradient anomalies in creating a spatially-variant interpolated stability field for the dispersion models is illustrated in figs. (5.1d), (5.1e). At 02h00 the region appears to be almost uniformly stable, with stability lengths L as low as +10 m. After sunrise, at 08h30, measurements at masts 3 and 6 lead to a stable nucleus over the bay, whilst surrounding areas experience unstable stability lengths with magnitudes as small as 50 m. Though the interpolated stability field is somewhat crude in terms of the underlying causes,

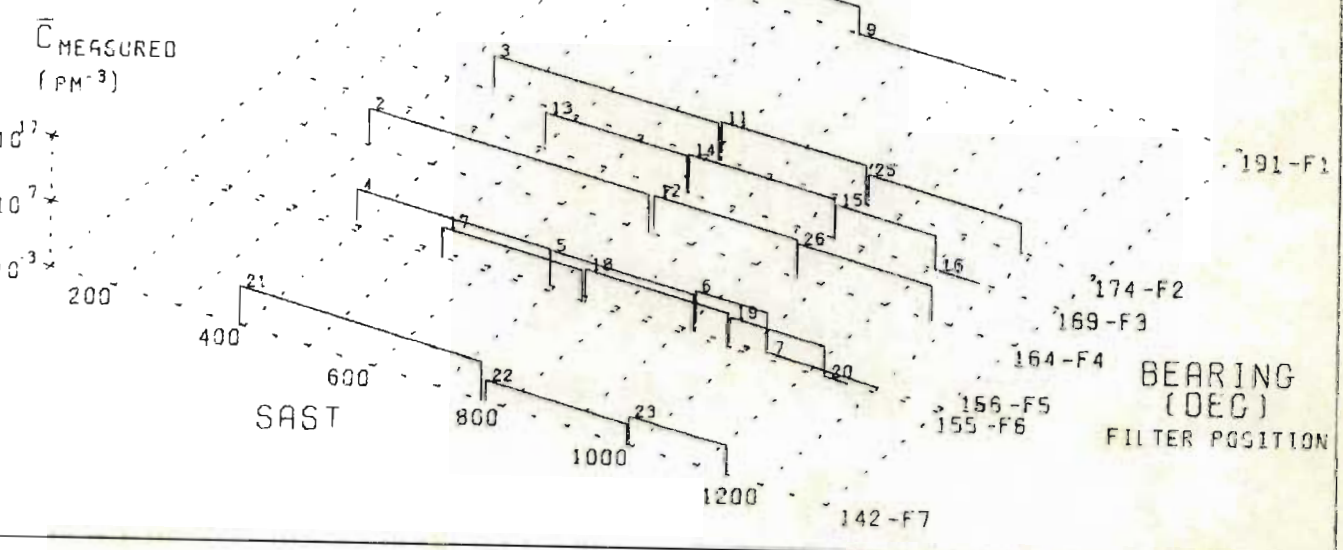
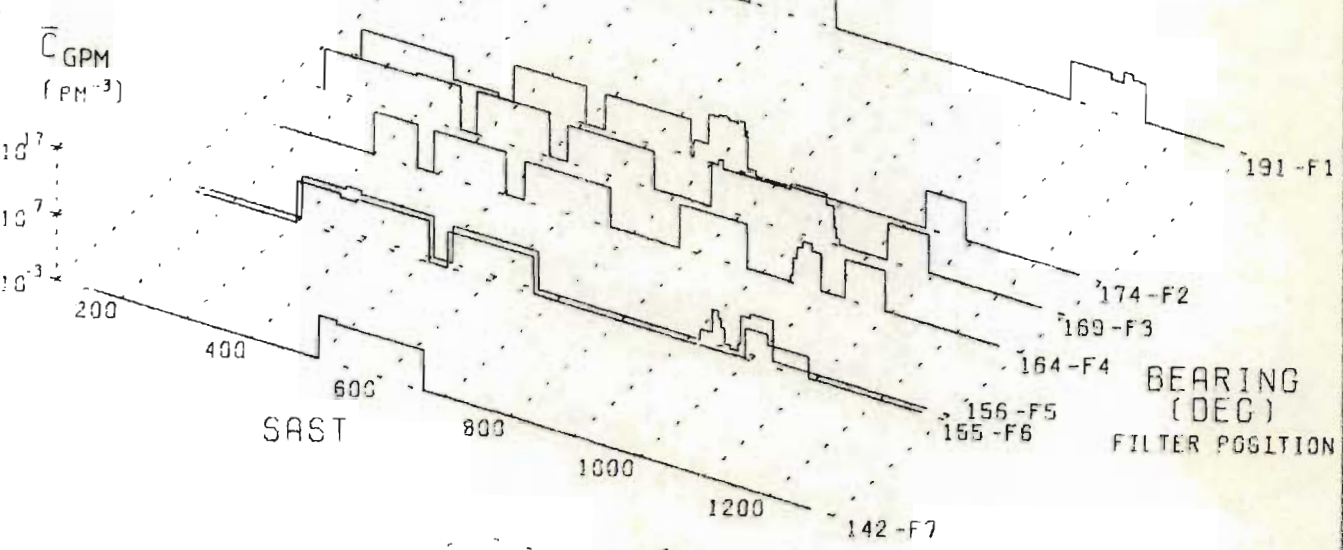
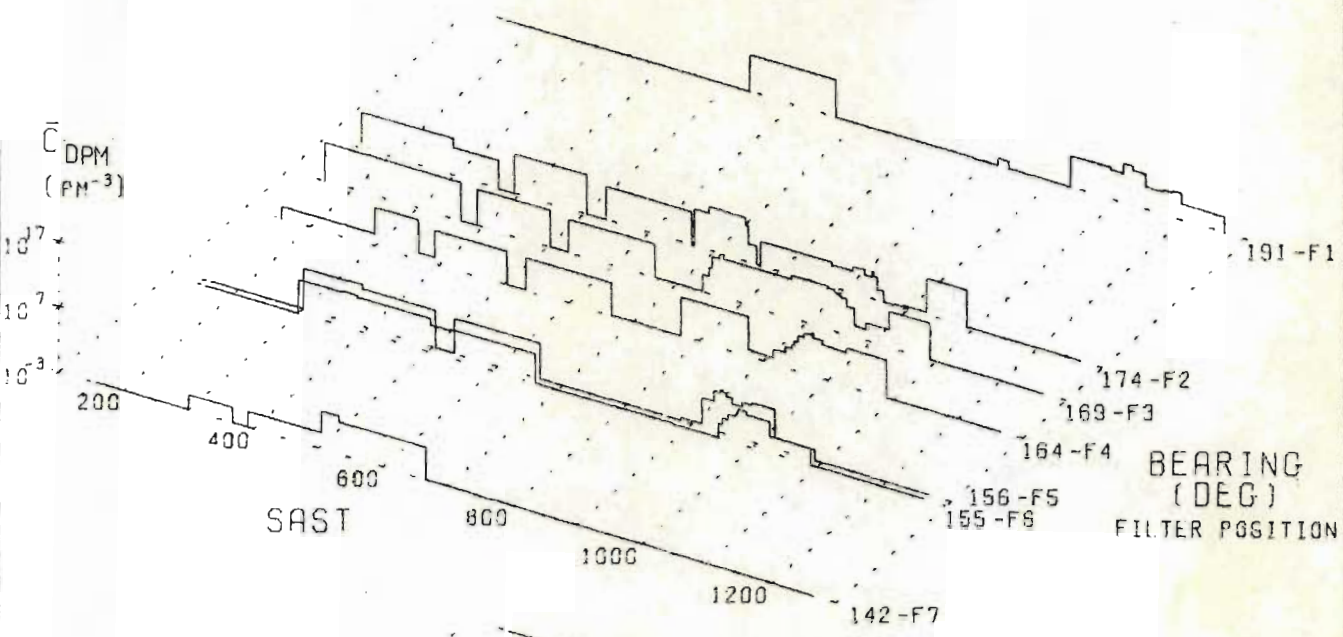
fig. (5.2)



it will provide some basis for the varying stability regimes through which the dispersing material must move.

The predicted and measured concentration histograms in fig. (5.3) provide the most convenient means of viewing the overall development of the system, and of relating

RUN 627 : PREDICTED AND MEASURED MEAN CONCENTRATION HISTOGRAMS



suggested by the relative crudeness of the filter measurements. The prime difference between gaussian puff model (GPM) and dynamic puff model (DPM) predictions lies in the degree of spread. Gaussian plume traverses lead to sharply peaked concentration histories with very large peak values. Since the traverse itself results from a temporal variation, dynamic puffs undergo significant lateral shear, so that peaks are flatter and the influence of the cloud is felt for a longer period. An example of this effect lies in the DPM and GPM predicted histograms between 03h00 and 07h00 at site F7. (Note that filter sites are coded in this way for clarity, and that the site codes in fig. (5.3) are preceded by the angular bearing of the site as observed from the release-point. The corresponding map positions are indicated in fig. (5.1c). The "filter numbers" indicated on the measured histograms are not prefixed, and refer to the individual membrane filters used in the experiment). Occasionally the influence of the sheared DPM plume persists for long periods during which the gaussian model gives no indication of the presence of the plume (e.g. 08h00 to 09h30 at site F2, though the preceding peak contributes dominantly to filter 11 at this point).

Filter integration periods appear to have been too long to detect major differences between DPM and GPM predictions, though fig. (5.4) shows that the GPM over-predicts in most cases. The predicted vs measured comparison points in fig. (5.4) are marked with the

fig.(5.5a) DPM : Ground-level concentration distribution at 0530 SAST

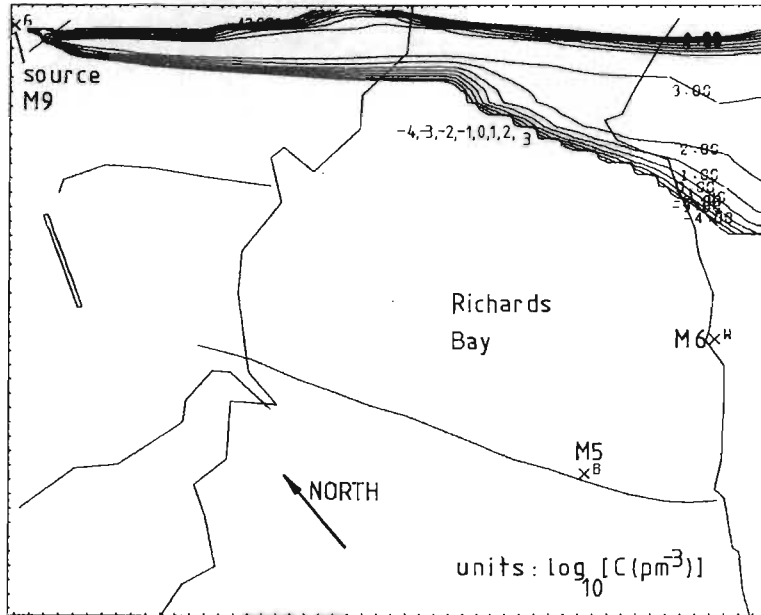


fig.(5.5b) DPM : Ground-level concentration distribution at 0600 SAST

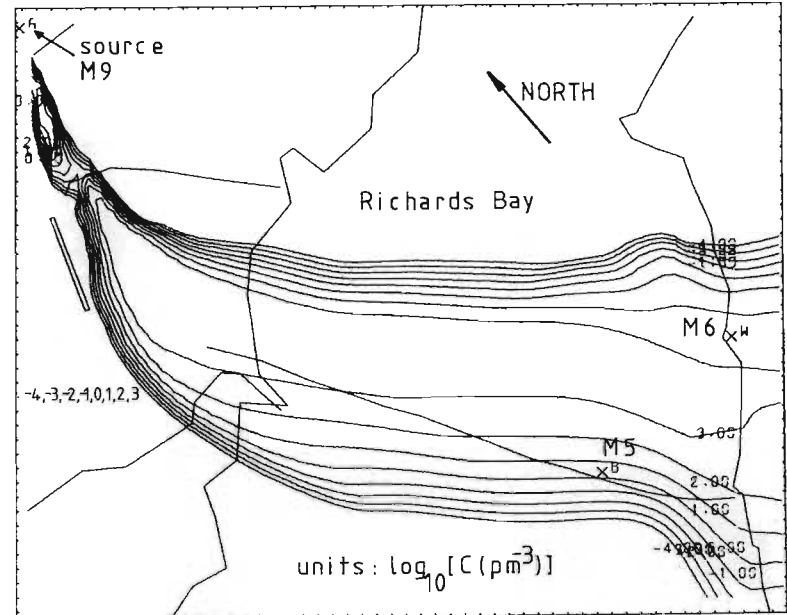


fig.(5.5c) GPM : Ground-level concentration distribution at 0530 SAST

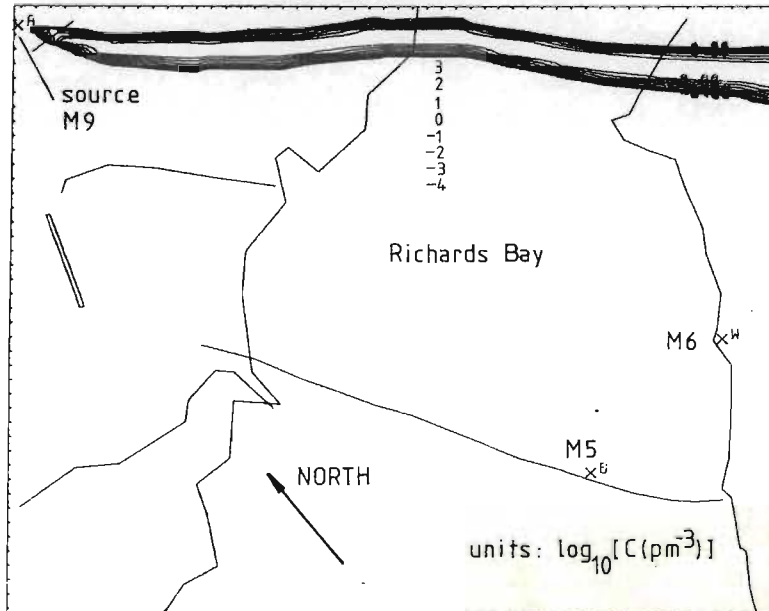
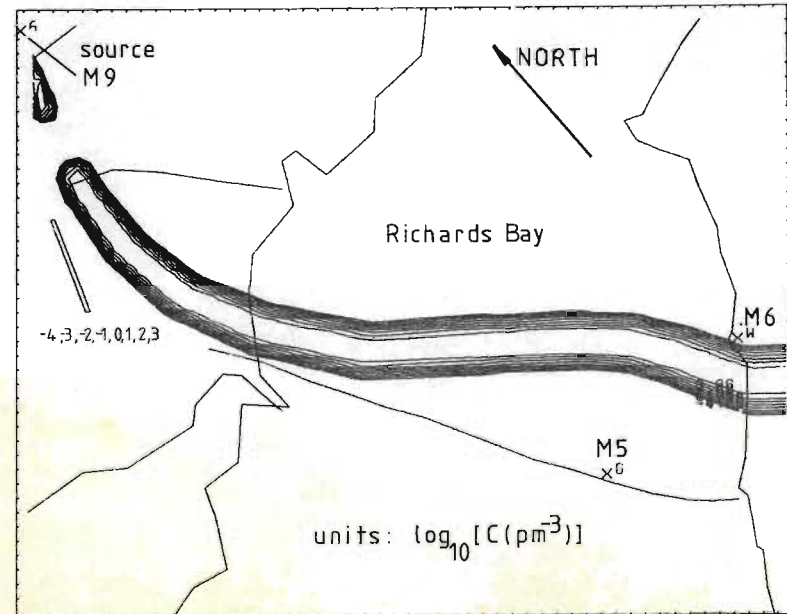


fig.(5.5d) GPM : Ground-level concentration distribution at 0600 SAST



corresponding filter numbers for both DPM and GPM predictions. Both models were unable to predict the concentrations recorded by filters 5 and 18. Since these filters (sites F5, F6, 07h00-09h30) would have registered particles at the extremes of the eastward oscillations of the wind-field, only slight inaccuracies in the interpolated wind-field would have been required to produce the discrepancy.

Figure (5.5) shows the theoretical concentration fields at the onset of, and at the end of the southwards temporal swing which occurred between 05h30 and 06h00 [fig. (5.2)]. The incipient southward flow near mast 2 at 05h30 produces significant cross-wind shear in the plume in this region. By 06h00 the entire wind-field has swung southwards, and the shear effect has progressed to the rest of the plume. Differences between GPM and DPM predictions clearly illustrate the origin of the more diffuse traverse peaks observed in the DPM concentration histograms, though the long histogram interval at this time conceals all detail.

The break in the plume which is obvious in the GPM prediction for 06h00 [fig. (5.5d)] results from an interruption of tracer release from 05h49 to 05h54 [fig. (5.1b)] during which time the suspension vessel was recharged. This break is seen to be more diffuse in the DPM prediction as a result of the merging effect of along-wind shear. The slight waviness which occurs in some contours results from the calculation of contours from grid-stored data.

During run 627, the vertical concentration profile was measured at mast 3 (site F5) by means of membrane

filters positioned 1 m, 2 m and 9 m above ground-level, and running from 03h56 to 10h17. The measured mean concentrations for this period were 417,555 and 1365 p m⁻³ (particles per cubic metre) respectively, indicating a significant vertical variation at this distance of 3 km from the source. If a mean wind-speed of 2 m s⁻¹ is assumed [fig. (5.2)] and the gaussian plume formula (1.41) is employed with a reflection term, it would be necessary to assume an effective vertical diffusivity of about 0,04 m² s⁻¹ in order to account for this vertical structure. Such low diffusivities are more likely to occur during the night, so that it is surprising to observe that the bulk of the material collected at site F5 [filters 4, 5 and 6, fig. (5.3)] was registered after sunrise. Concentration variations of this magnitude over relatively small vertical distances indicate the spatial sensitivity of the predictive problem. Note that all dosage predictions have been calculated at the normal filter height of 1 m.

Long-period mean concentration distributions based on dosage distributions predicted by the PIC column model [appendix (A3)] are shown in fig. (5.6). The concentration of trajectories about filter sites F2 to F6 has restricted the affected region largely to this sector. Fig. (5.6b) suggests a reasonable estimate for filter 21 (513 p m⁻³ measured) at site F7, and likewise fig. (5.6d) for filters 25 (33,5 p m⁻³ measured, site F2) and 26 (122 p m⁻³ measured, site F4) [See figs. (5.3) and (5.4)]. The abrupt and irregular

boundaries surrounding the affected regions result from the lack of horizontal diffusion in the P.I.C. model.

5.2.2 Run 630 (30.6.76 to 1.7.76).

Immediately preceding the south-westerly gradient wind which follows the passage of a coastal low along the Natal Coast, it is usual to experience a period of exceptionally calm, fine weather. During the reversal of synoptic pressure gradients, local breezes and katabatic flows are able to assert themselves. Run 630 depicts a development in which the land-breeze appears to compete with the remnant of a N.E. gradient wind during the night, finally giving way to a S.W. wind with the break-up of the inversion after 08h30 [fig. (5.8)]. The fluctuating influence of the N.E. gradient wind, and the existence of a southwards-channelled flow over Lake Mzingazi lead to a complex and variable wind-field [e.g. 03h00-04h00]. The calm period about 08h00 leads to strong fumigation conditions which are aggravated by the cross-wind shear of existing tracer concentrations by the incipient S.W. wind.

Figure (5.7a) shows that the highest subadiabatic temperature gradients were experienced at the "inland" masts 9, 8 and 1 before sunrise. After 08h00 these gradients become superadiabatic, whereas the gradients at masts near the water surface, which have been low during the night, tend to lag, or even increase at first. This is again due to the capacitive effect that water has on surface temperature. Fig. (5.7d) shows that the measurements at masts 9, 8 and 1 lead to the interpolation of a relatively stable region at 03h00, with stability lengths down to +10 m. By 10h00

RUN 630 (30/6/76- 1/7/76)

fig.(5.7a)

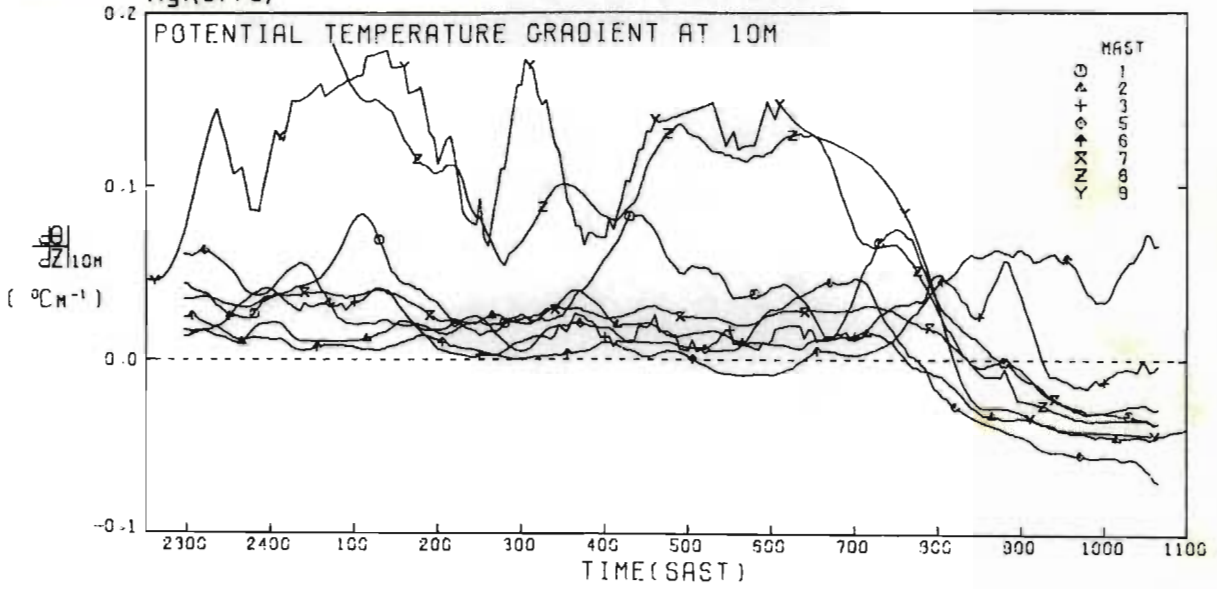


fig. (5.7b)

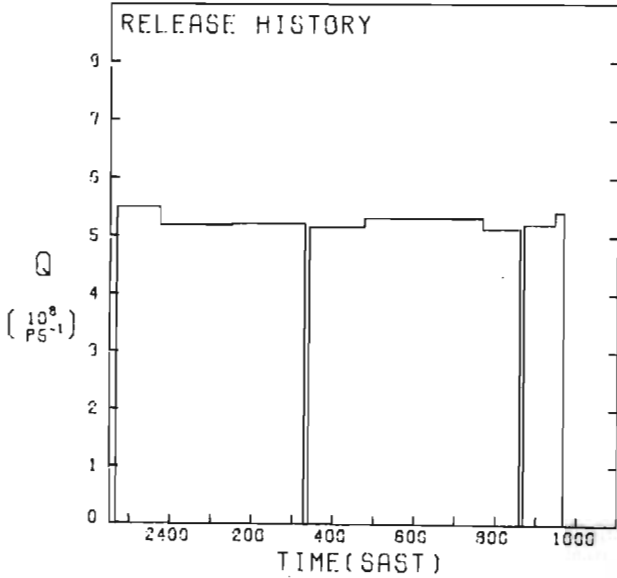


fig.(5.7c)

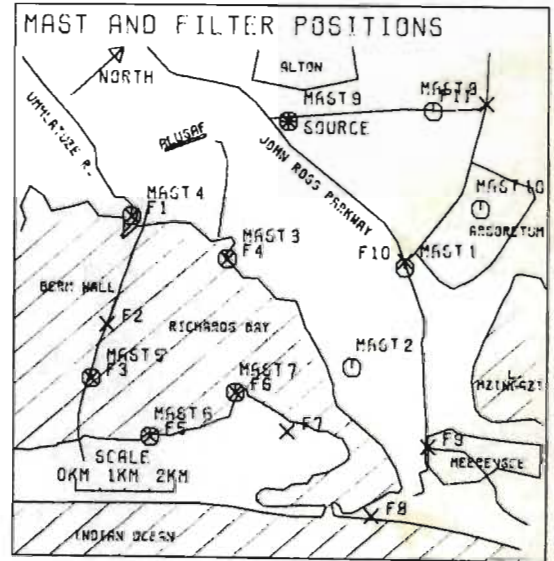


fig.(5.7d)

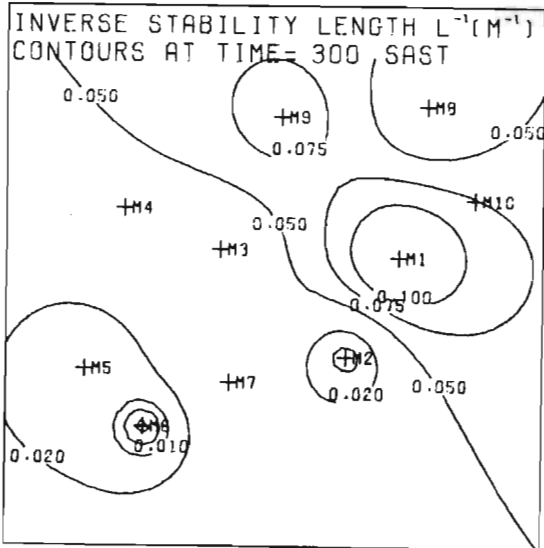


fig.(5.7e)

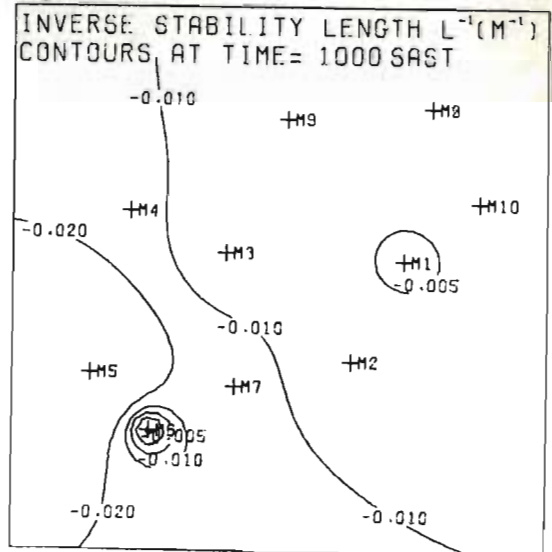


fig. (5.8)

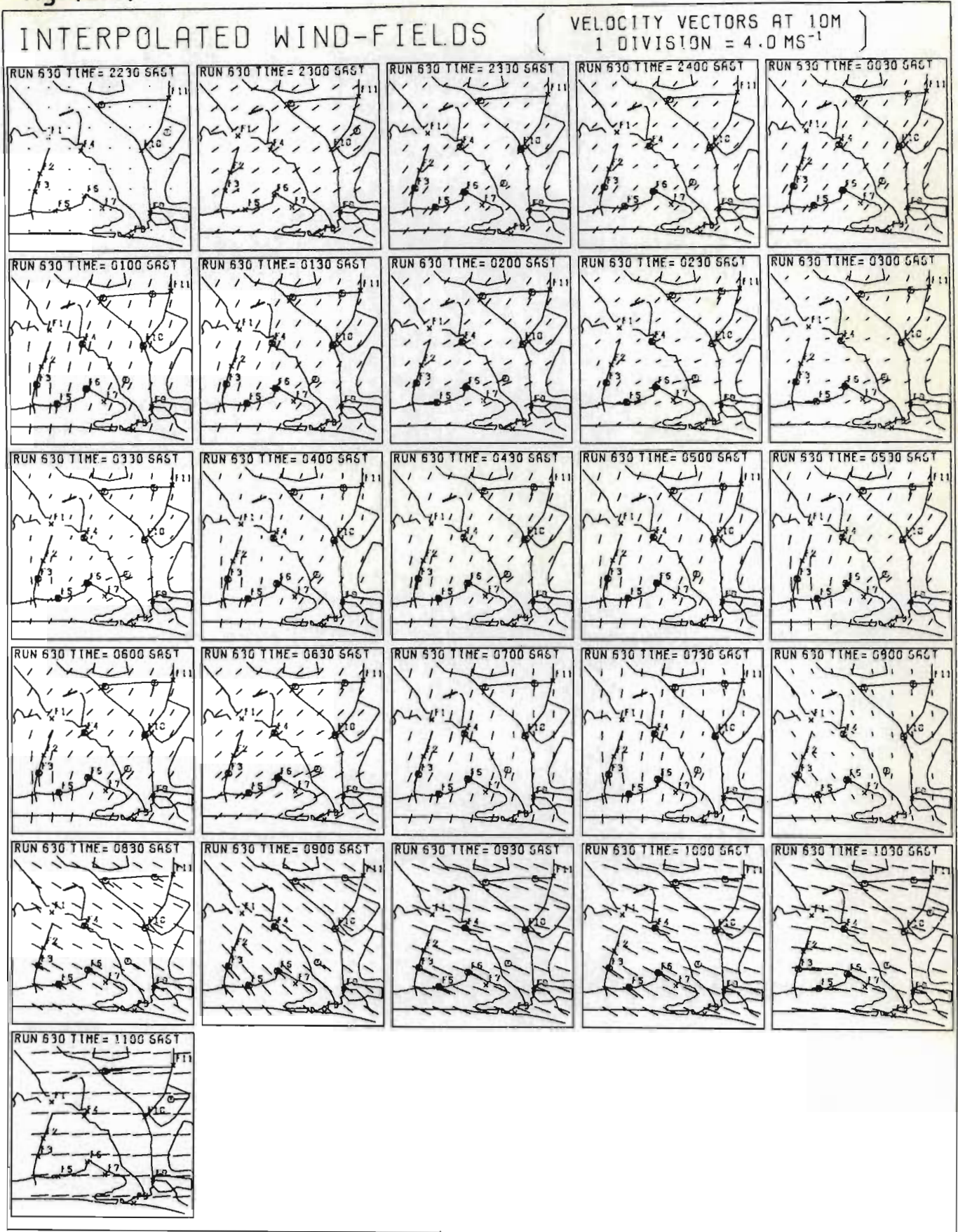


fig. (5.9)

RUN 630 : PREDICTED AND MEASURED MEAN CONCENTRATION HISTOGRAMS

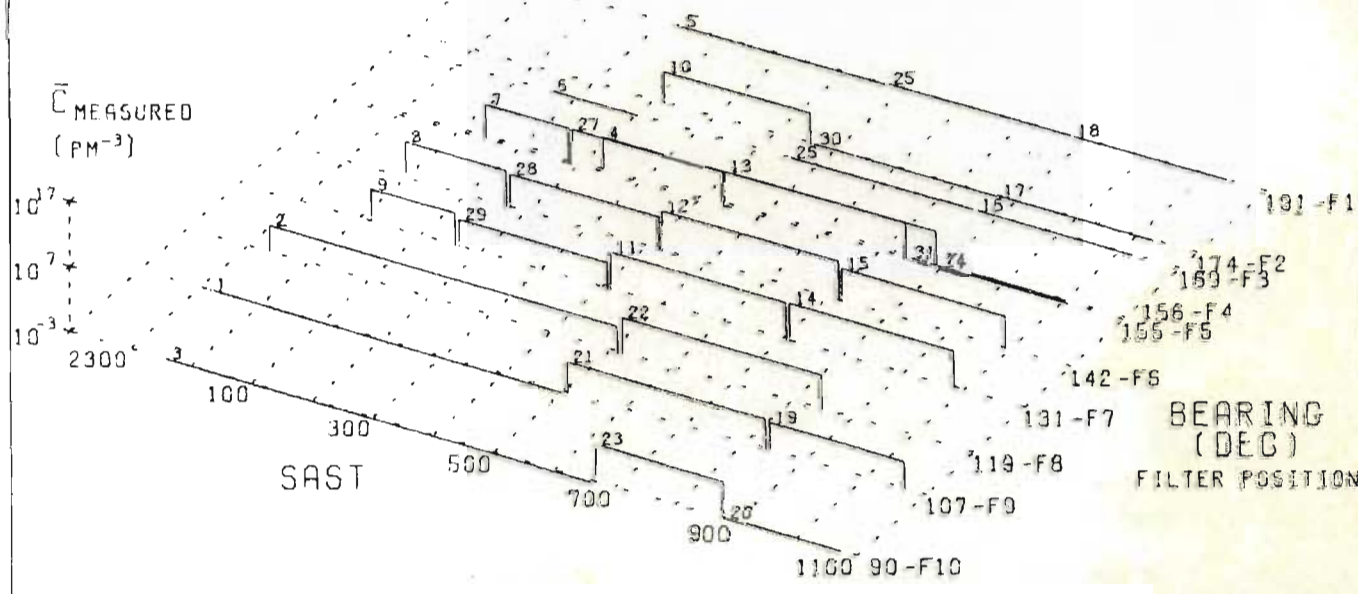
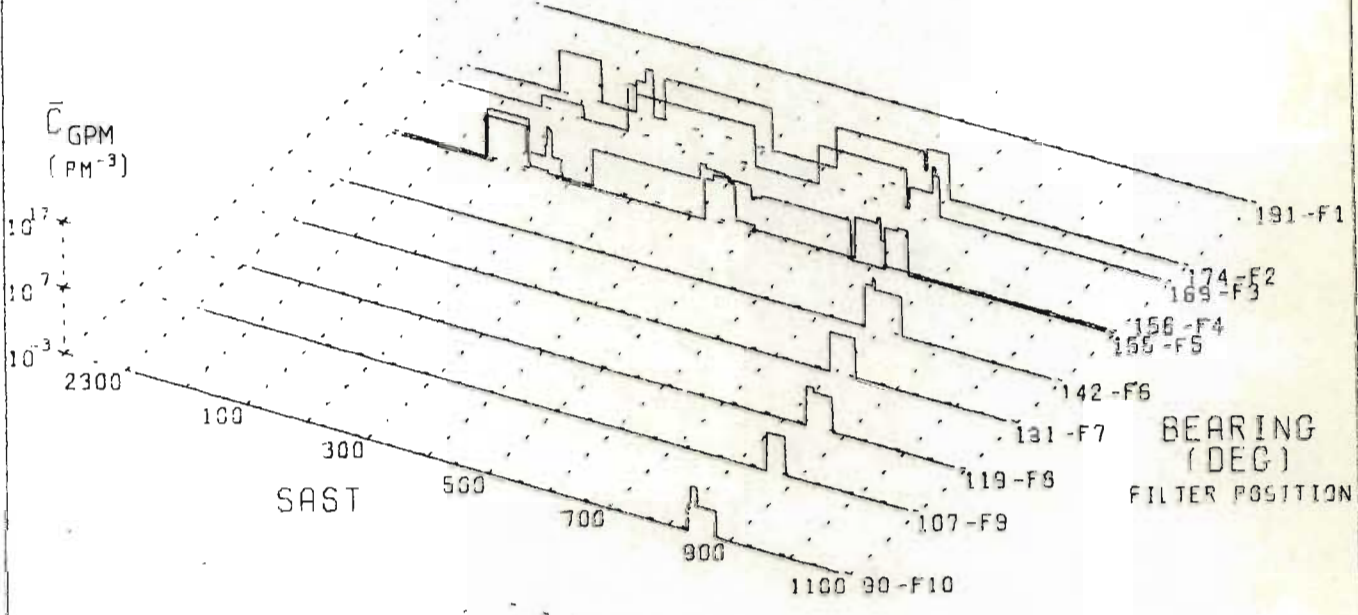
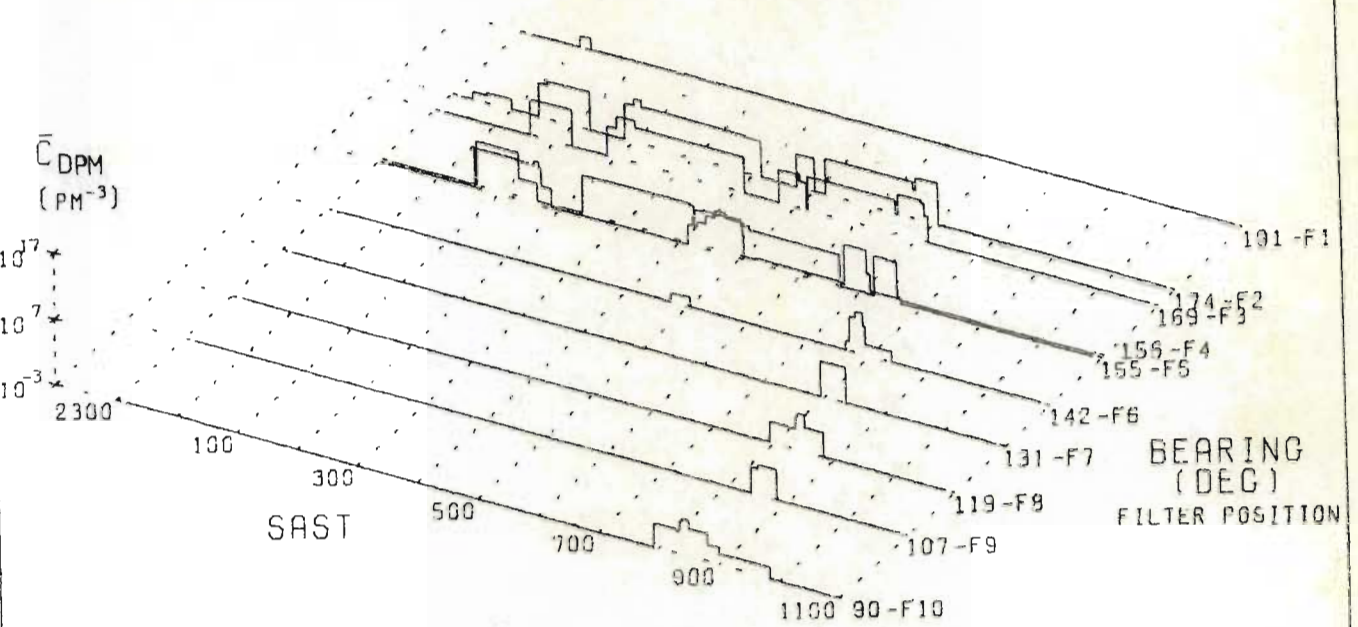
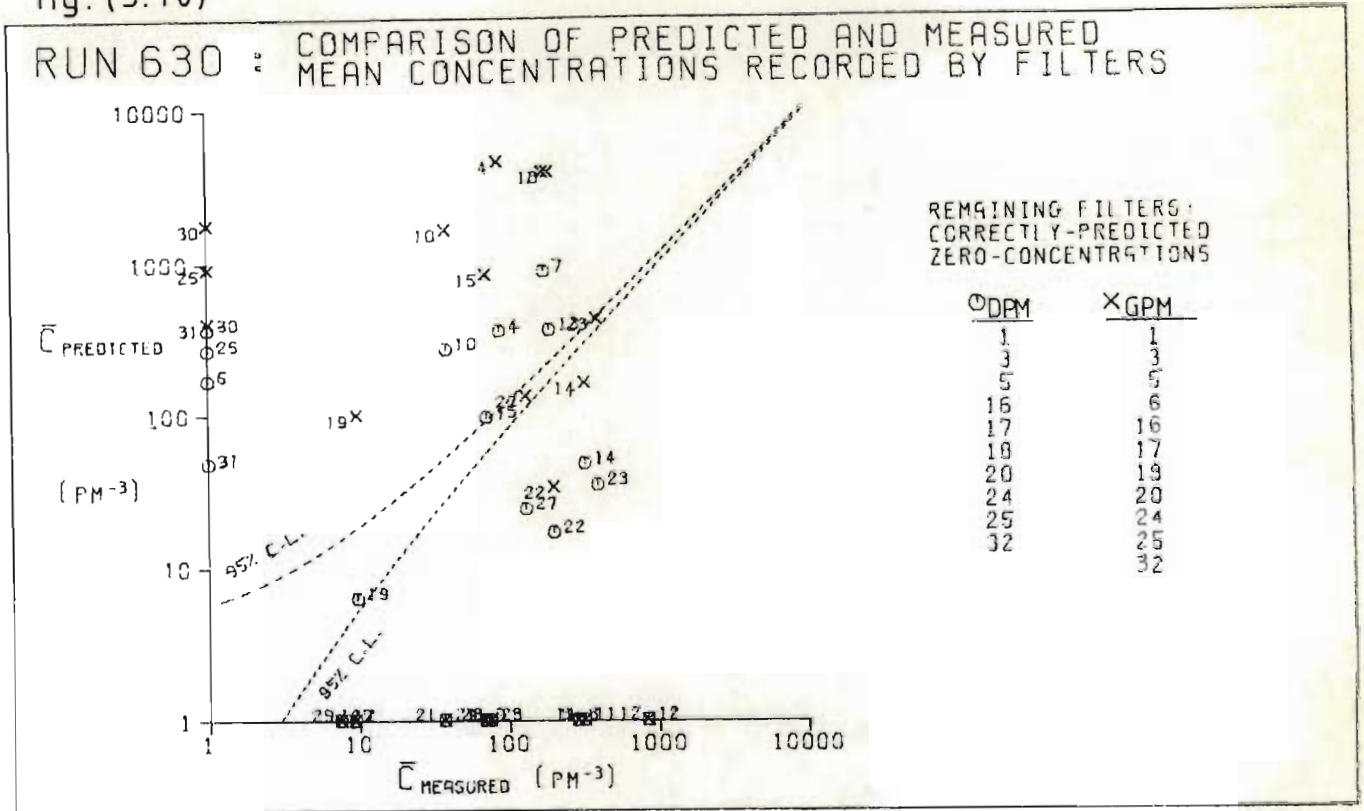


fig. (5.10)



[fig. (5.7e)] the only stable region remaining is highly localised around mast 6, as is evident from the temperature gradients at this time.

Reference to figures (5.9) and (5.10) shows that both the DPM and the GPM have produced generally poor estimates of the mean concentrations recorded by filters. Some eight of these filters were positioned and timed at the extremes of the eastward oscillations of the wind-field at 01h30 and 05h30 [sites F6, F7 and F8], and recorded particle concentrations which were not predicted by either model. The fact that predictions to the west of westward oscillations were too high, and those to the east of eastward oscillations too low suggested the possibility of some

form of uniform directional shear with height. However, inclusion of a linear directional shear in the DPM, from the measured wind-field at ground level to a S.W. wind at $z = 1000$ m, produced no significant differences in the predictions.

Temporal transients in the wind-field are again seen to spread the traverse concentration histograms predicted by the DPM [fig. (5.9)]. Extension of the cloud by wind-shear increases the traverse time at site F10, 08h00-09h00, about three-fold relative to the GPM. However, the cloud has still not arrived early enough to contribute to the concentration measured by filter 21.

Predicted ground-level concentration distributions at 08h25, during the temporal transient induced by the S.W. wind, are presented for the DPM in fig. (5.11a) and for the GPM in fig. (5.11b). The high diffusivities at this time lead to a wide gaussian plume, though it still under-predicts the extent of the affected region. The gaussian plume apparently expands as it passes over the bay. This is because it has for some time passed close to mast 2, which has recorded a superadiabatic temperature gradient since 07h30, indicating atmospheric instability. In the same way, this instability has led to the prediction of more uniform wind-profiles near mast 2, resulting in reduced lateral expansion in the region of the DPM plume which has traversed this area, due to the lower lateral shear experienced by the plume. The "fanning" of the

fig.(5.11a) DPM : Ground-level concentration distribution at 0825 SAST

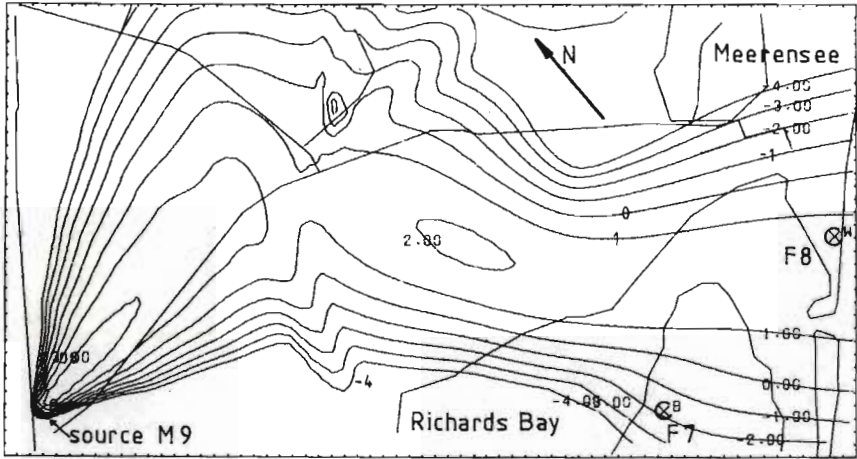


fig.(5.11b) GPM : Ground-level concentration distribution at 0825 SAST

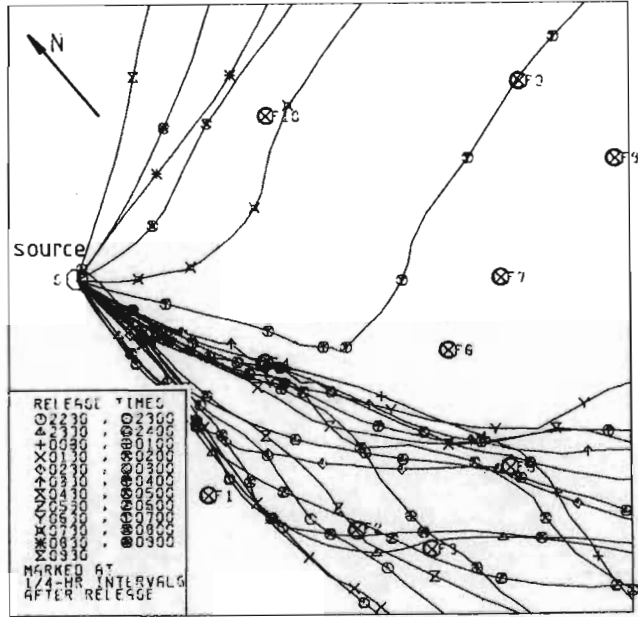
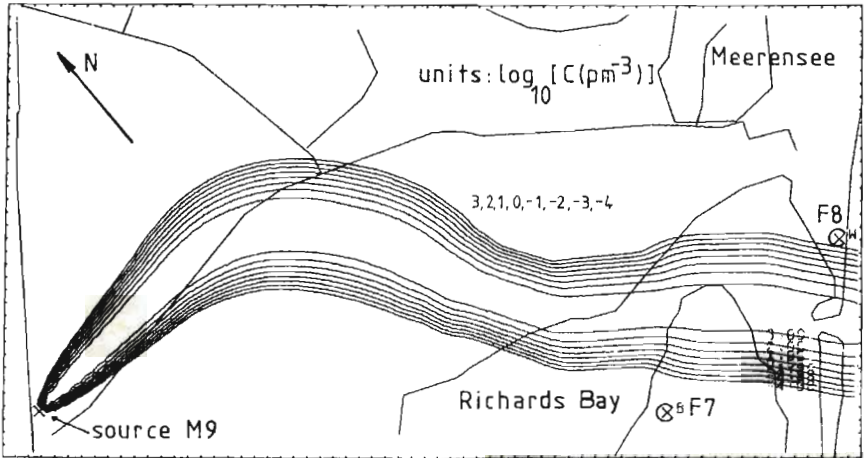


fig.(5.11c) Mean trajectories at z=10m

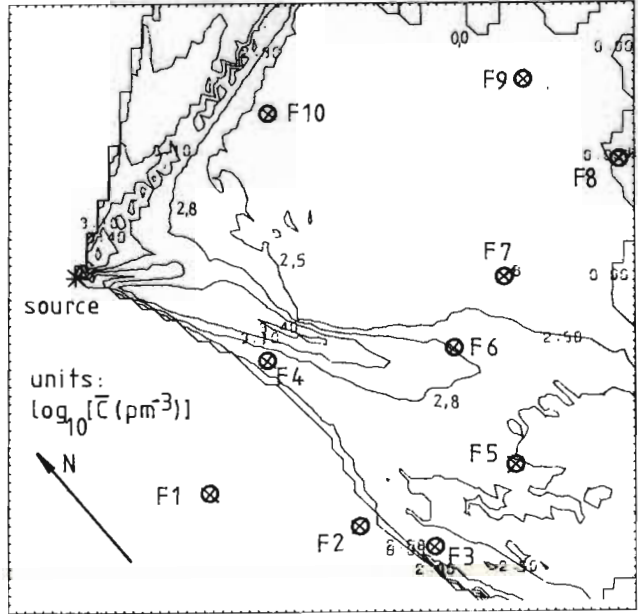


fig.(5.11d) PIC model: Mean ground-level concentration distribution from 0700 to 1100 SAST

plume beyond this point may arise from the earlier arrival of the transient wind component in that region.

The abrupt arrival of the S.W. wind is clearly demonstrated at 08h00 on the 07h00 trajectory in fig. (5.11c). In the sweep across filter sites F7 to F10 the P.I.C. model [fig. (5.11d)] has created a large region with mean concentrations between $316 (10^{2,5})$ and 1 p m^{-3} . These limits embrace the concentrations recorded by filters 19 ($9,6 \text{ p m}^{-3}$) and 23 (395 p m^{-3}) in this area.

5.2.3 Run 705 (5.7.76 to 6.7.76).

Run 705 appears to follow the classical fine-weather development in which a persistent light land-breeze gives way to a long, calm fumigation period before the onset of the N.E. wind about 12h30 [fig. (5.13)]. However, stratified layers of smoke, injected to high altitudes by sugar-cane fires, were observed to be moving towards the north-east at about 07h00. This suggests that the extended absence of gradient winds, despite the break-up of the inversion, arose as a result of a transition in the synoptic weather. The resultant calm weather has encouraged a katabatic flow down the Umhlatuze river valley, and a channelled flow southwards over Lake Mzingazi. These two currents converge over Richards Bay [fig. (5.13), e.g. 03h00, 03h30], their interaction with the land-breeze resulting in a complex and variable wind-field.

Figure (5.12a) shows that high subadiabatic temperature gradients were recorded until 08h00 by masts remote from the water surface indicating extreme stability in these areas. Masts associated with the water again show increased stability after 09h00. Persistence of subadiabatic gradients at the latter masts until 13h00 may result from the relatively low temperatures of the preceding night. [7,8°C at 06h08 at mast 9]. The subadiabatic gradient at mast 8 at 11h00 is somewhat anomalous. Figure (5.12d) shows that the measurements at masts 4, 5 and 6 lead to the interpolation of a less stable region over the bay at 02h30. By 08h30,

RUN 705 (5/7/76- 6/7/76)

fig.(5.12a)

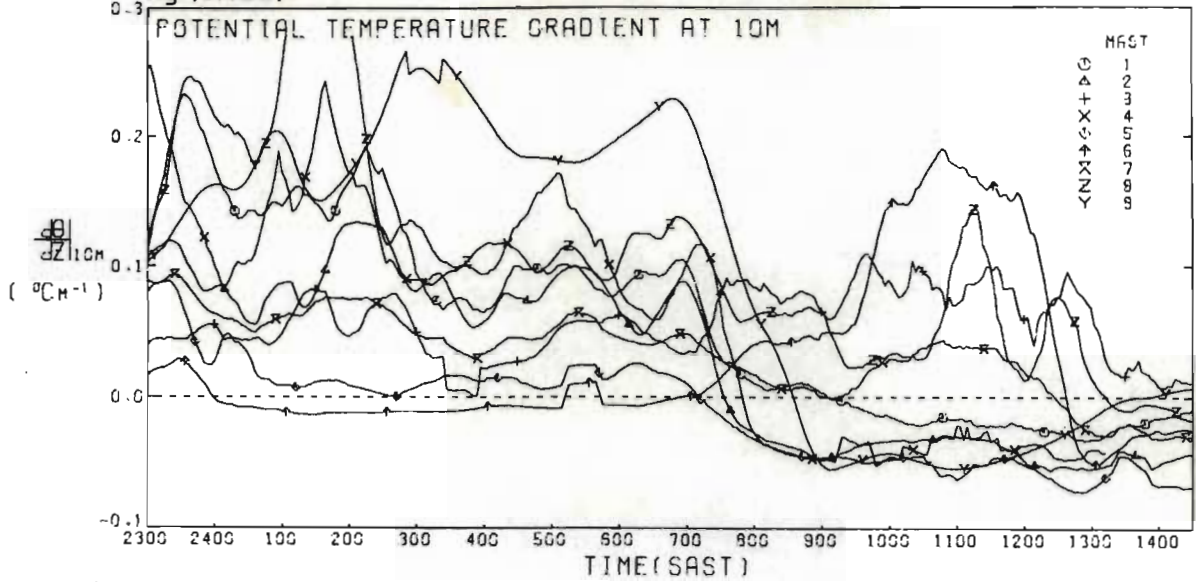


fig.(5.12b)

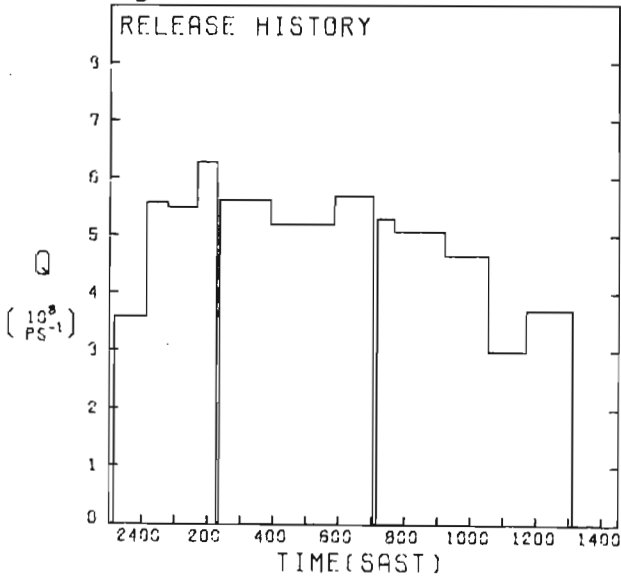


fig.(5.12c)

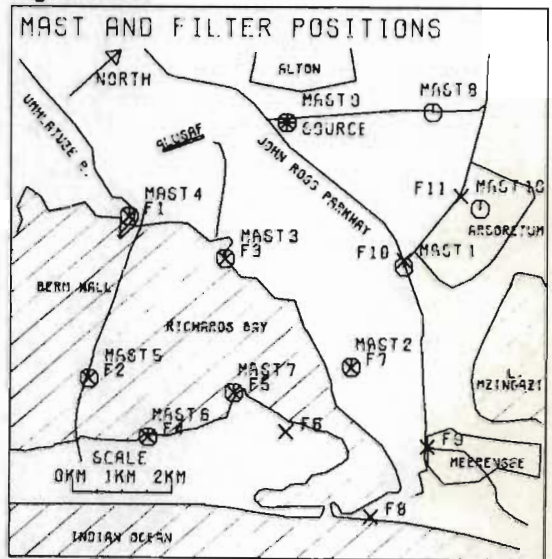


fig.(5.12d)

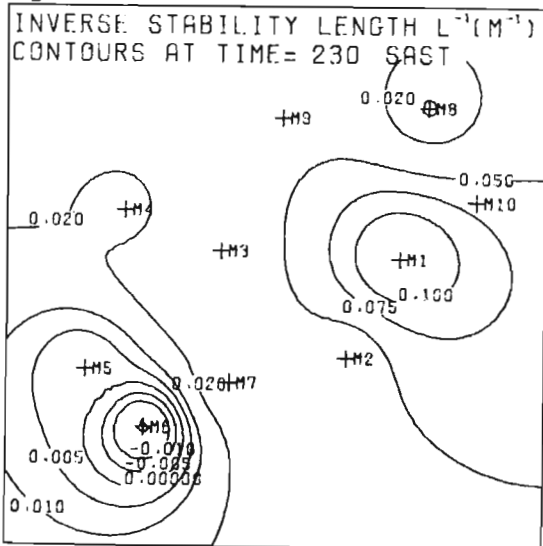


fig.(5.12e)

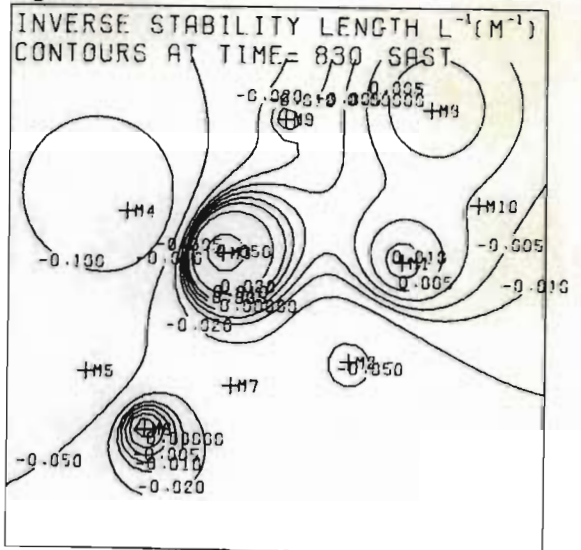


fig. (5.13)

INTERPOLATED WIND-FIELDS

{ VELOCITY VECTORS AT 10M
1 DIVISION = 4.0 MS⁻¹ }



RUN 705 : PREDICTED AND MEASURED MEAN CONCENTRATION HISTOGRAMS

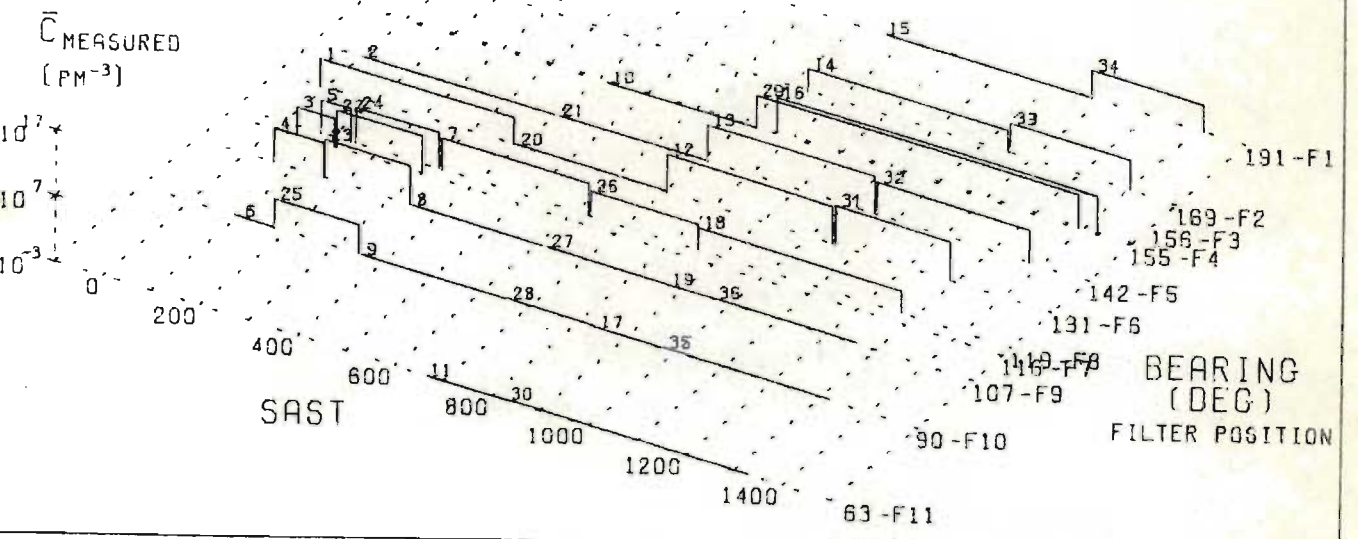
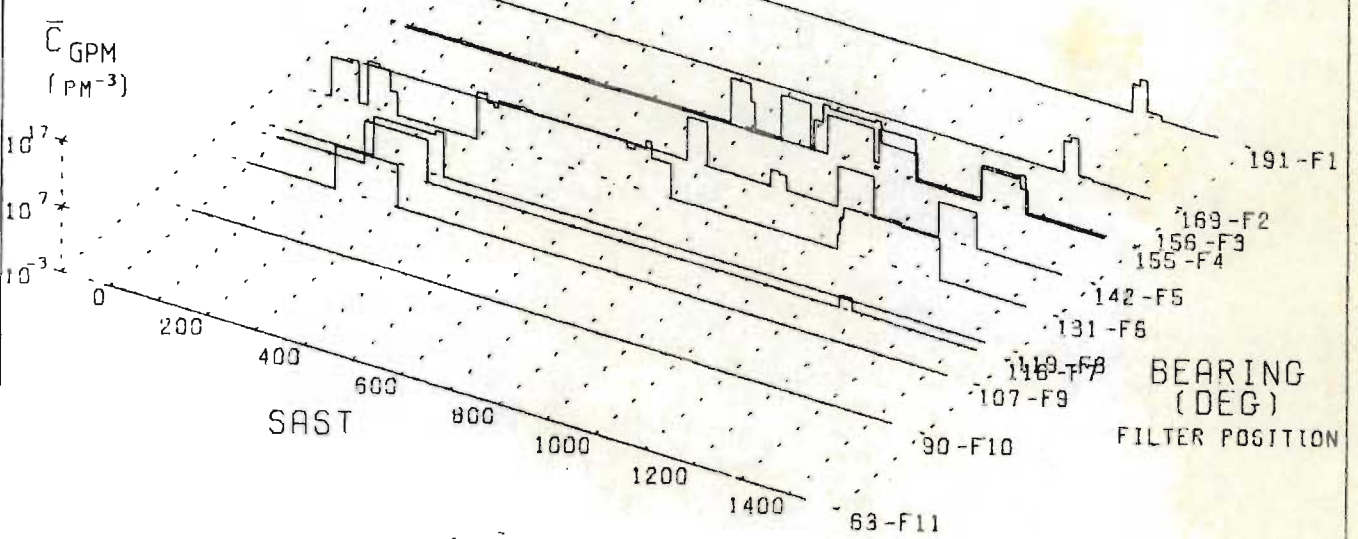
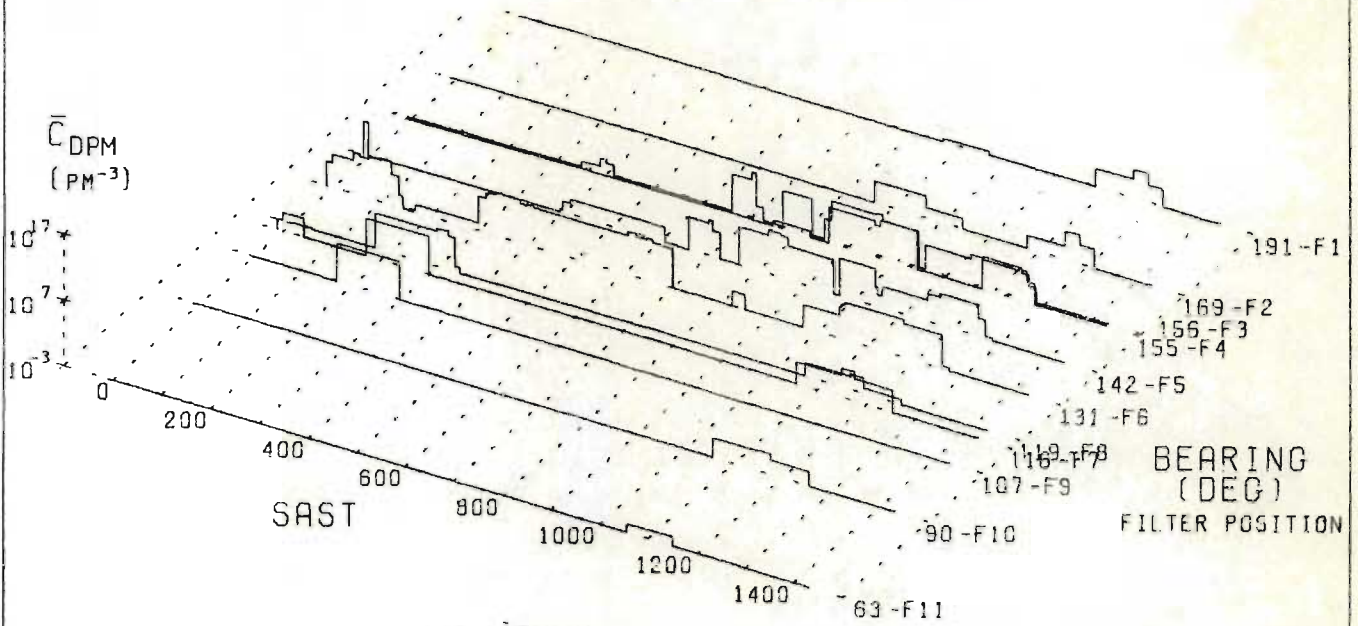


fig. (5.15)

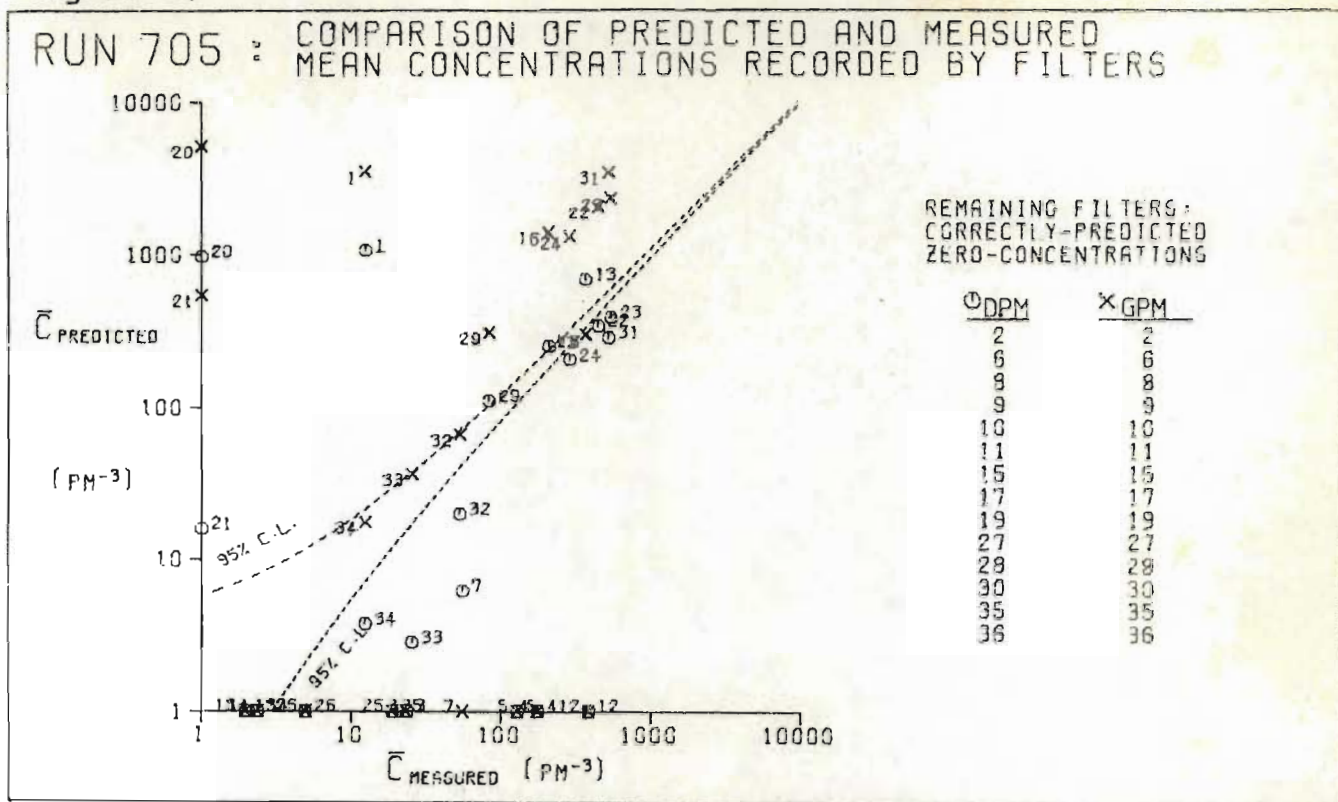


fig.(5.16a) Mean trajectories at z=10m

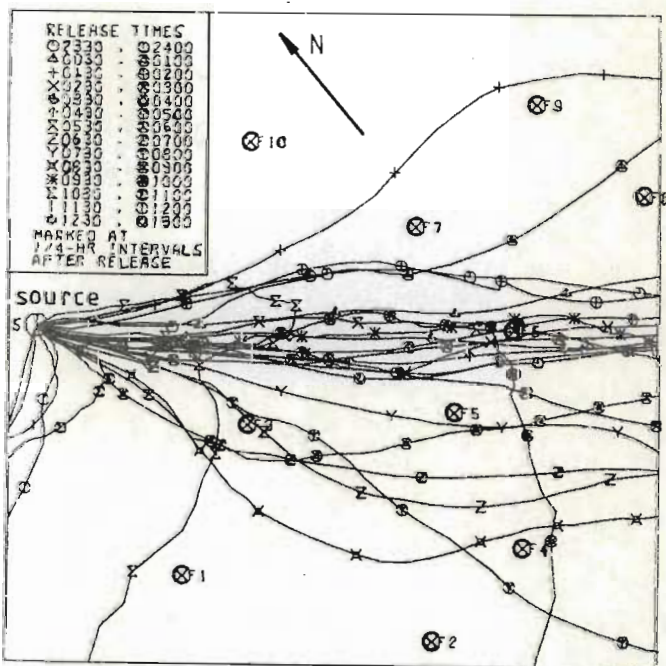
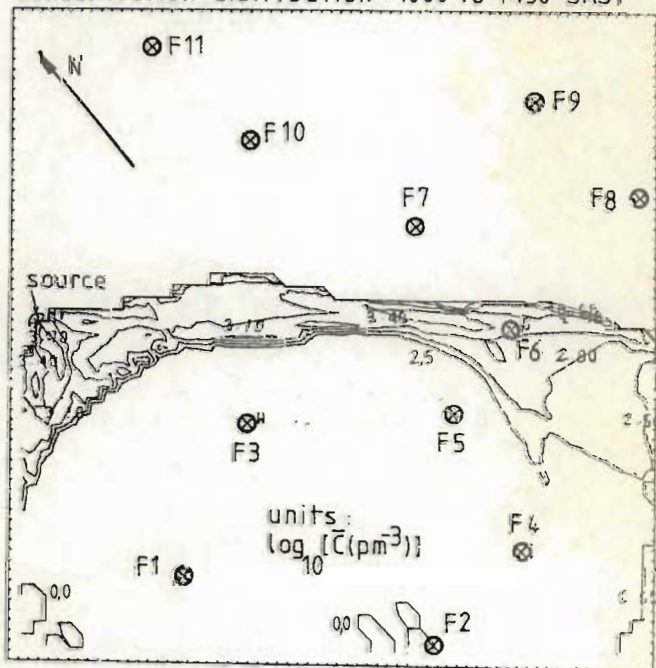


fig. (5.16b) PIC model : Mean ground-level concentration distribution- 1000 to 1430 SAST



measurements at masts 3 and 6 have set up a stable axis across the bay [fig. (5.12e)].

Neglecting some of the smaller developments, the wind-field is seen to undergo two major oscillations, reaching eastward maxima at 02h30 and 11h00; and a westward maximum at 09h00, before becoming a predominantly N.E. wind at 12h30 [fig. (5.13)]. These oscillations are quite apparent in fig. (5.14), the DPM concentration histograms providing clear evidence of a significant wind-shear contribution. DPM predictions show that the cloud should reach site F2 during the westward transient at 09h00, and site F8 during the eastward transient at 11h00. Low concentrations were in fact recorded by filters 14 and 18 at these positions, whereas the gaussian plume did not manifest itself at all.

Filter concentration predictions provided by the DPM were generally good, when the lower statistical significance of filters 7, 32, 33 and 34 is taken into account [fig. (5.15)]. Note that the prediction for filter 7 has benefited from the increased spread present in the DPM plume during the eastward transient of 02h30. The DPM histogram at site F8 shows significant concentrations for 10 minutes longer than the GPM. This extension is just sufficient to overlap with the aspiration period of filter 7 at this site, giving a mean concentration prediction of $6,1 \text{ p m}^{-3}$ in comparison with the GPM prediction of 0 p m^{-3} ($\bar{C}_{\text{measured}} = 55,1 \text{ p m}^{-3}$). However, predictions by the GPM are too high in most cases.

The mean concentration distribution predicted by the P.I.C. model for the period 10h30 to 14h00 [fig. (5.16b)] shows that the uncertain trajectories from 10h00 to 12h00 [fig. (5.16a)] lead to an effective "fumigation" covering a large area, despite the neglect of horizontal diffusion. Concentrations at sites F1 and F2 have magnitudes which are similar to those recorded by filters 34 (12,3 μm^{-3}) and 33 (25,4 μm^{-3}) during this period.

5.2.4 Run 708 (8.7.76).

During late winter, gradient wind transitions usually become more rapid. Run 708 covers a relatively short stable period hemmed in between N.E. and S.W. gradient wind conditions. Indecisive synoptic pressure gradients gave a calm period from 02h30 to 04h00 [fig. (5.18)]. It is unlikely that local breezes became established during this period, and the complexity of the wind-field may be attributed to interplay between the two pressure gradients.

Although tracer-release was begun at 01h06, the apparent deterioration of stability [fig. (5.17a)] and reappearance of a N.E. wind component led to a decision to terminate the release at 01h54 [fig. (5.17b)]. By 03h00, wind-speeds had dropped, and release was recommenced at 03h06. It is interesting to note that relatively high subadiabatic temperature gradients persisted despite the higher wind-speeds from 01h00 to 02h00. The calm period from 03h00 to 04h30 is seen to encourage an increase in atmospheric stability again, though gradients at masts 5 and 6 remain low due to their positions downwind of the water surface. Calculated values of the stability length are seen to vary only gradually, both spatially and temporally [figs. (5.17a), (5.17b)]. The establishment of an almost neutral region over the bay is indicated by masts 5 and 6 at 06h00.

RUN 708 (8/7/76)

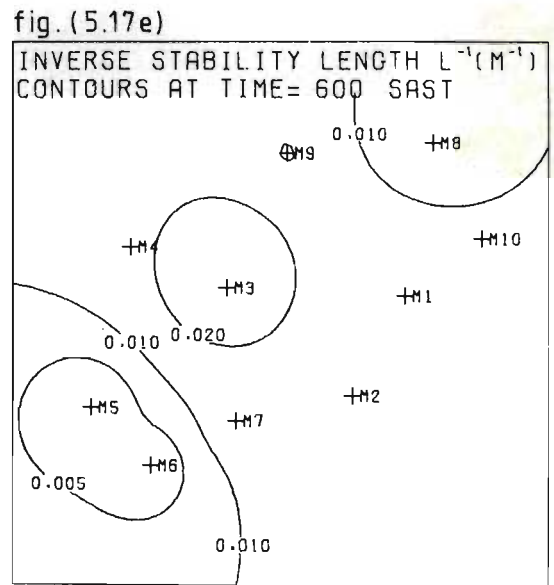
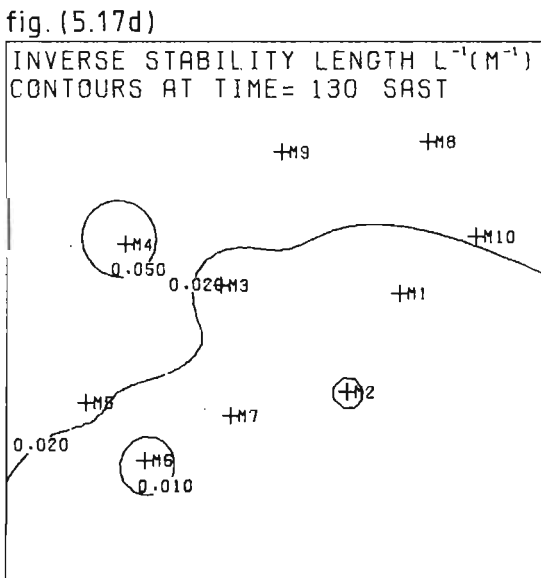
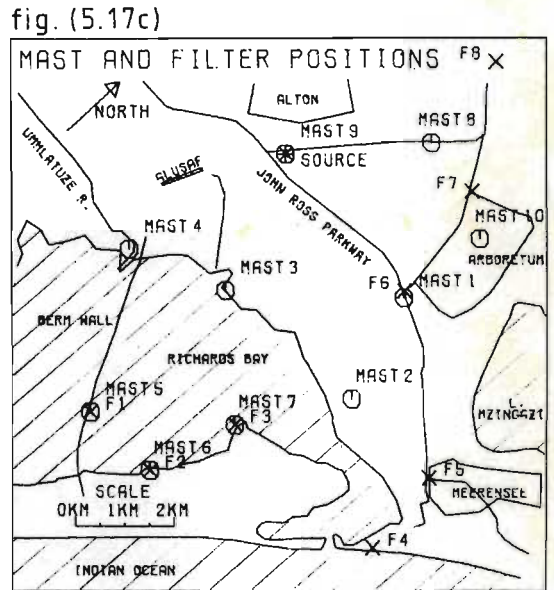
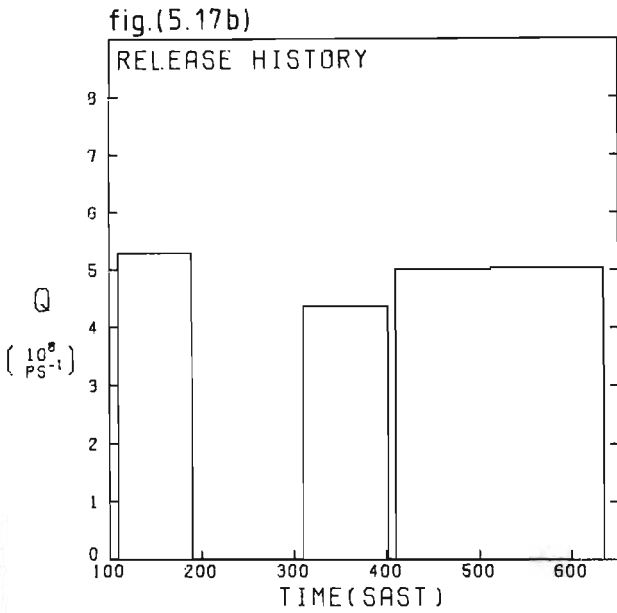
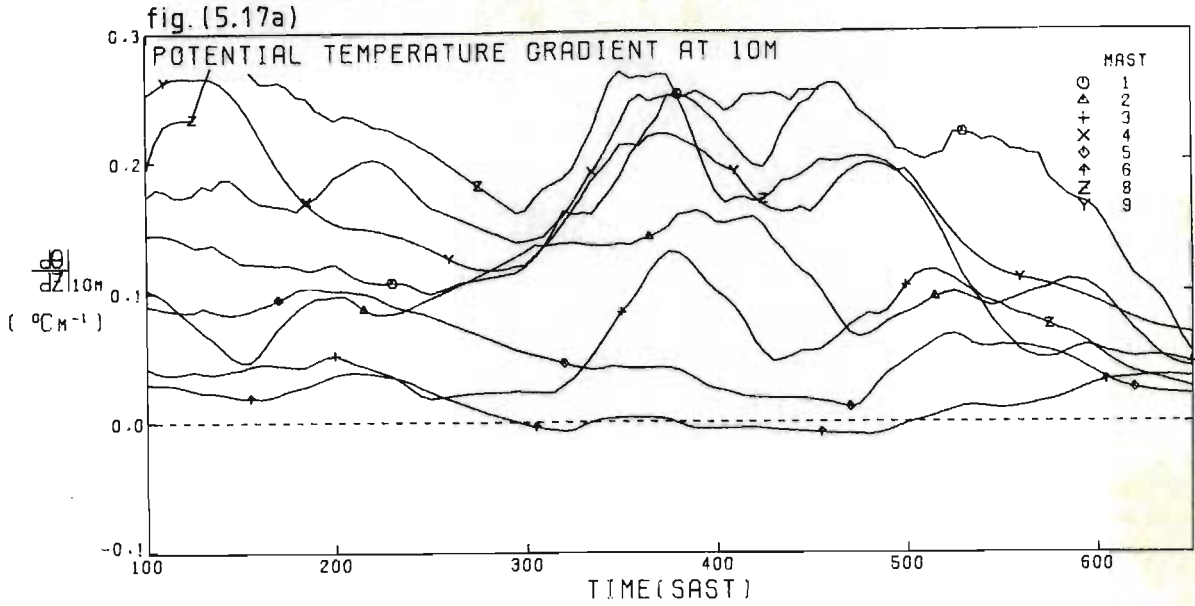


fig. (5.18)

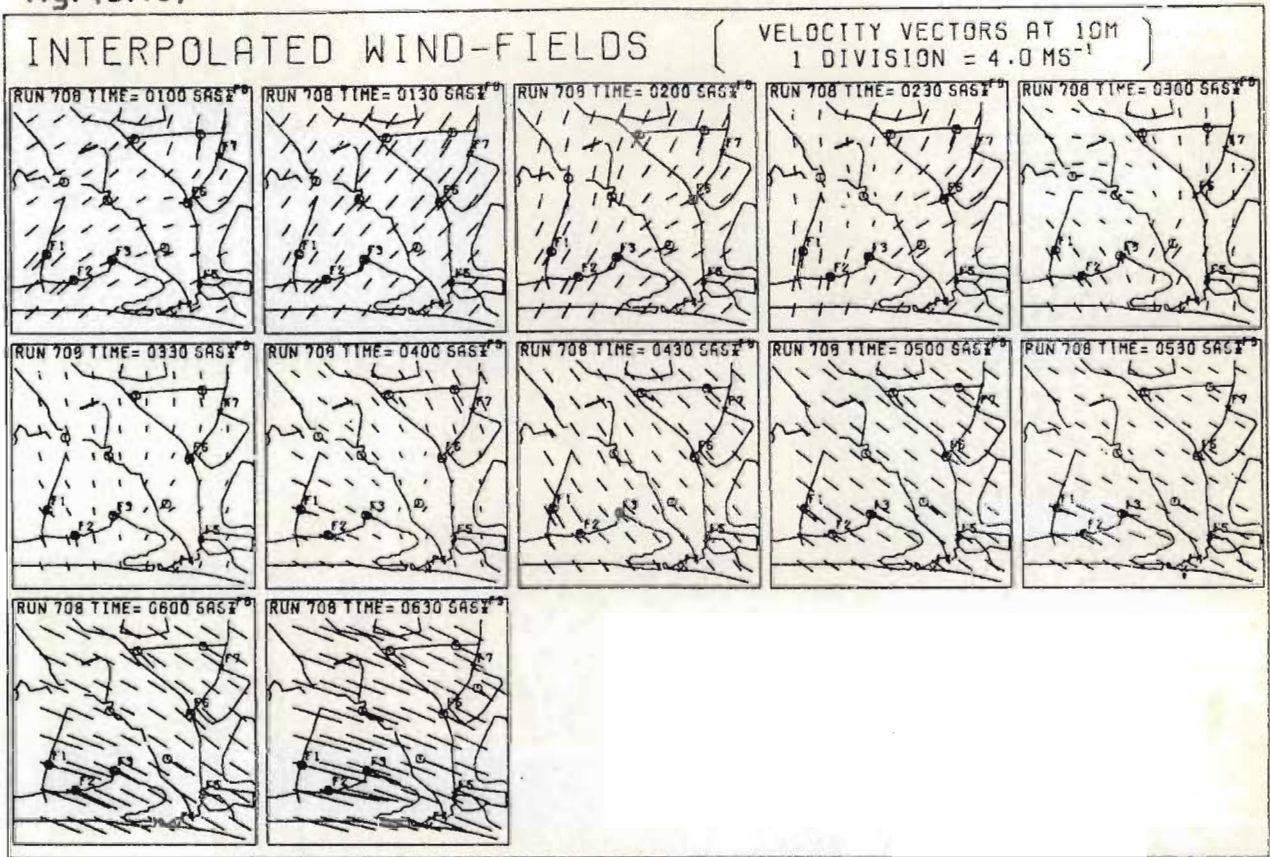
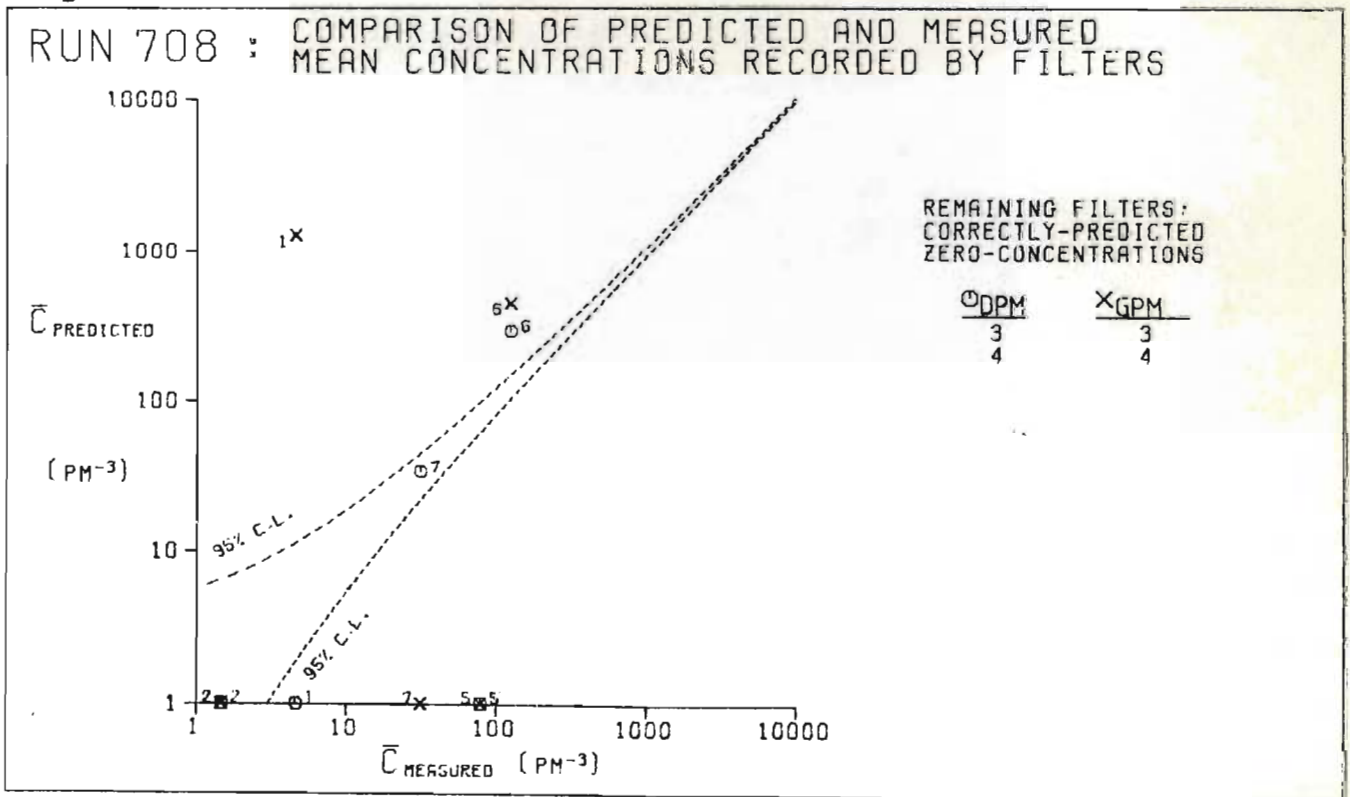
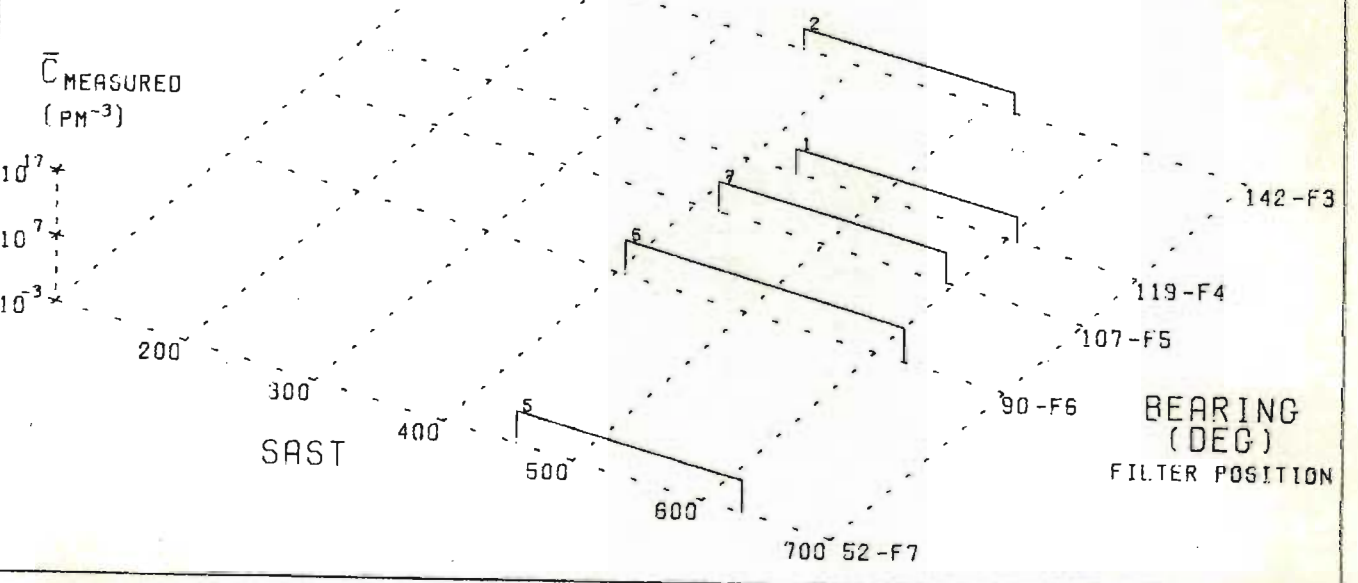
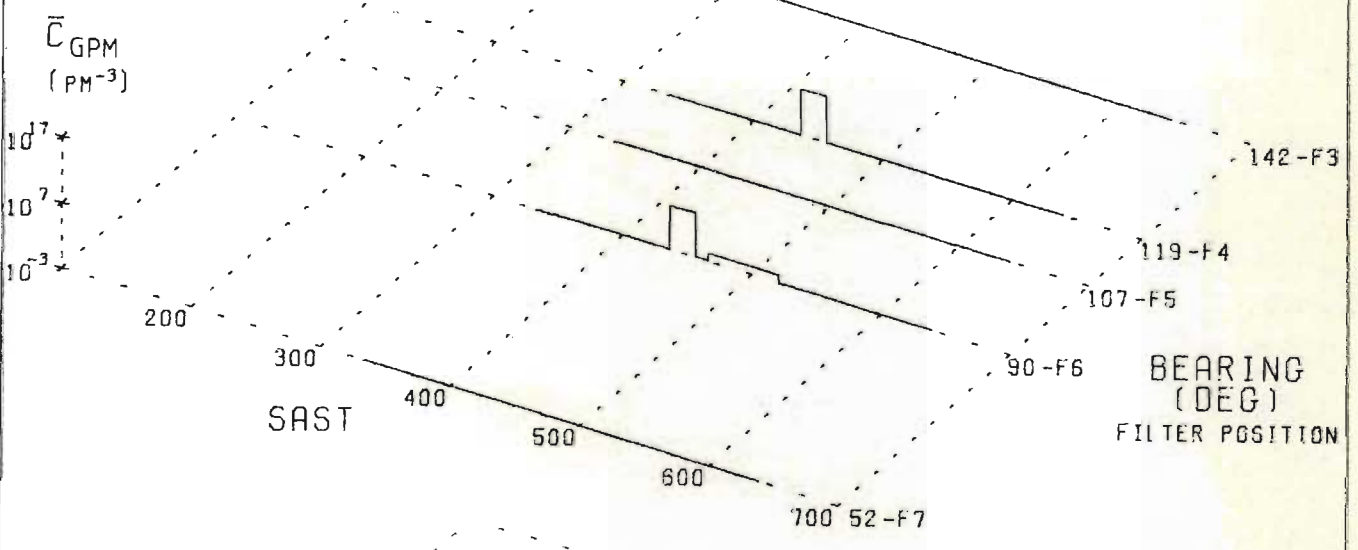
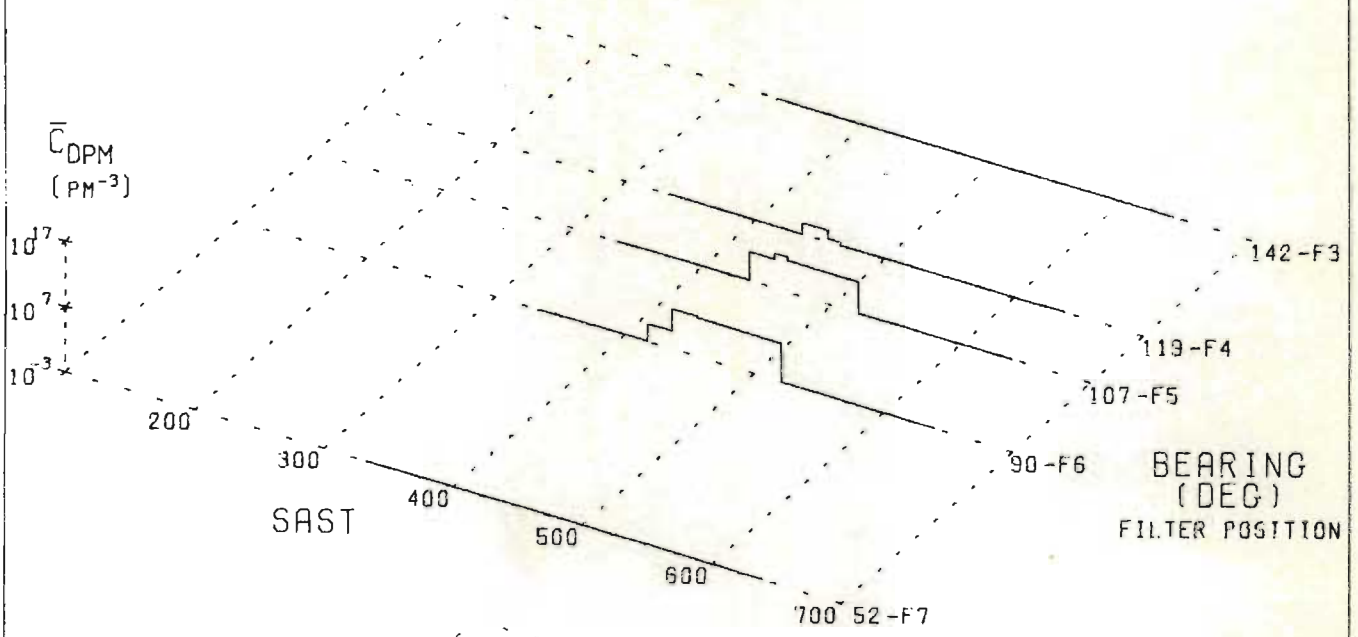


fig. (5.19)



RUN 708 : PREDICTED AND MEASURED
MEAN CONCENTRATION HISTOGRAMS



Filter concentrations predicted by the DPM are in good agreement with measurements [fig. (5.19)], whereas GPM predictions are rather poor. Filters 1, 7, 6 and 5 are all associated with the sweeping of the sheared plume across sites F4 to F7. The gaussian prediction does not register at F5 [fig. (5.20)] due to the break in the plume created by the interruption of release [figs. (5.21b)], (5.21d). However, lateral and longitudinal shear act to extend the DPM distribution, providing an accurate prediction for filter 7.

This incident serves to illustrate the important part played by wind-shear in the distribution of airborne material during short or variable releases.

Figure (5.20) shows that DPM concentration histograms become significantly spread during the temporal transient which began at 04h00. The reason for this is evident in the concentration distribution at 04h00 [fig. (5.21a)], where the S.W. wind component has begun to act slightly earlier on the older portion of the plume. The irregularity in the lower concentration contours near the source probable arises from misalignment of the curvilinear lagrangian puff frame due to rapid spatial variations in the wind-field near the source [section (2.4.4.1)], though implied wind-field divergence might lead to a similar intersection. Wind-shear has acted to virtually close the gap created by release-interruption, whilst the GPM predicts very localised distributions [fig. (5.21b)].

fig.(5.21a) DPM : Ground-level concentration distribution at 0400 SAST

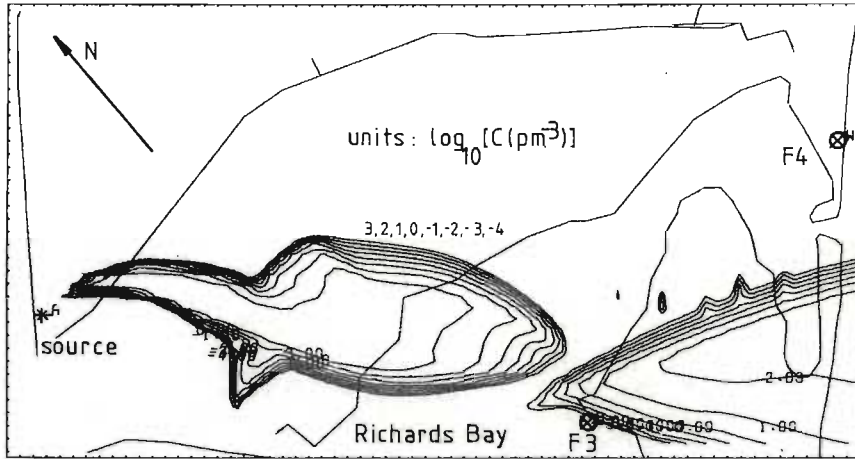


fig.(5.21b) GPM : Ground-level concentration distribution at 0400 SAST

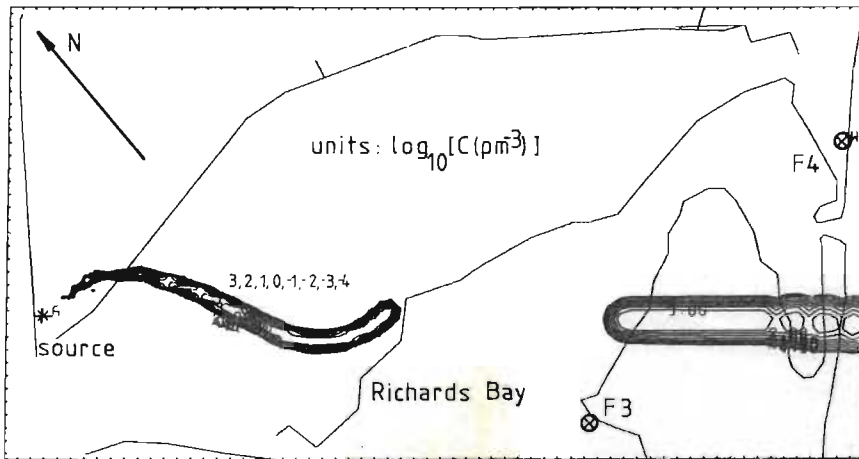


fig.(5.21c) Mean trajectories at z=10m

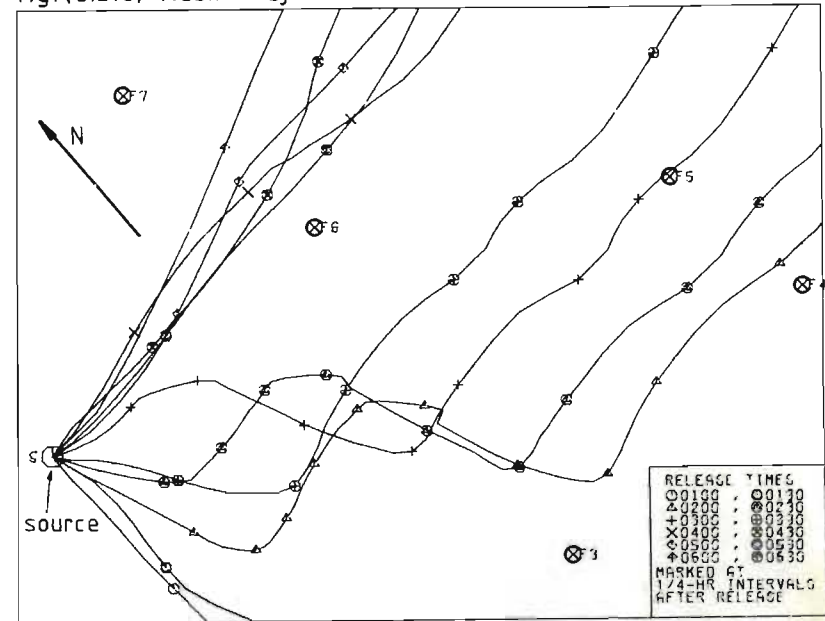
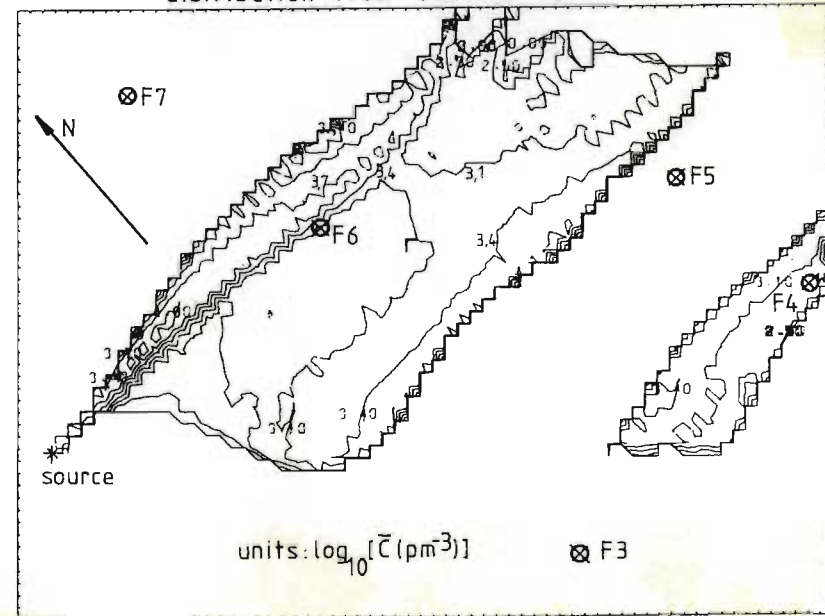


fig.(5.21d) PIC model : Mean ground-level concentration distribution from 0400 to 0500 SAST



The P.I.C. mean concentration distribution between 04h00 and 05h00 [fig. (5.21d)] behaves in the same way as the GPM prediction, and shows clearly why no dosage was predicted at site F5. The decisive reversals in the trajectories for releases at 02h00, 02h30, 03h00 and 03h30 [fig. (5.21c)] illustrate the purely temporal nature of the competing gradient-wind influences.

5.2.5 Run 711 (11.7.76 to 12.7.76)

Run 711 covers a period of only moderate stability during which an initial land-breeze is supplanted by a light westerly wind. From 21h00 to 08h30 this westerly wind shows relatively small variation, and it finally becomes the usual gradient-induced south-westerly wind after 09h30 [fig. (5.23)]. An interesting aspect of this run is the high dosage which occurs in the Meerensee residential area as a result of the invariability of wind-direction.

Temperature gradients at masts 3,5 and 6 near the bay show low stability from 20h00 to 07h00, when gradients become higher at masts 3 and 6 due to the temperature lag of the water surface [fig. (5.22a)]. The almost uniformly neutral stability of the region at 07h00 [fig. (5.22d)] is upset by 07h30 [fig. (5.22e)] as masts 2 and 5 begin to record superadiabatic temperature gradients ($\partial\bar{\theta}/\partial z < 0$).

The absence of major temporal transients in the wind-field is demonstrated by the concentration of mean trajectories in fig. (5.26). As a result, relatively few filters registered particles [fig. (5.25)]. The prediction of significant concentrations for filters 13 and 19 (site F8) by both DPM and GPM solutions may result from a clockwise directional shear with height. The direction at the elevated position of mast 9, which receives a low weighting, is perhaps an indication of this [24h00-06h00, fig. (5.23)]. The DPM provides fair estimates for the remaining filter

RUN 711 (11/7/76-12/7/76)

fig. (5.22a)

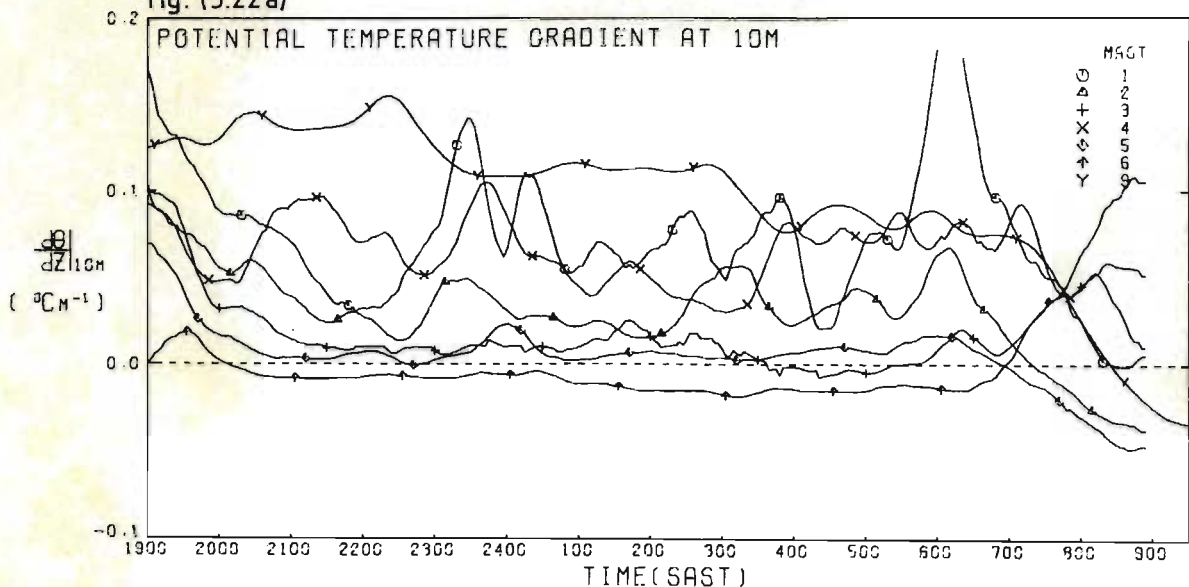


fig. (5.22b)

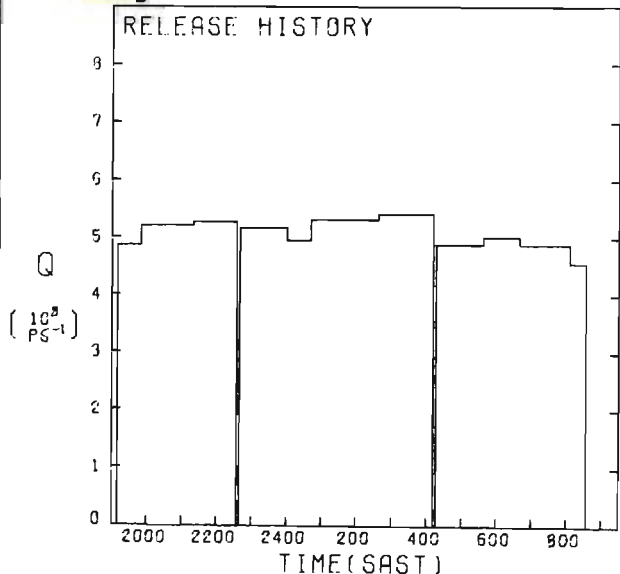


fig. (5.22c)

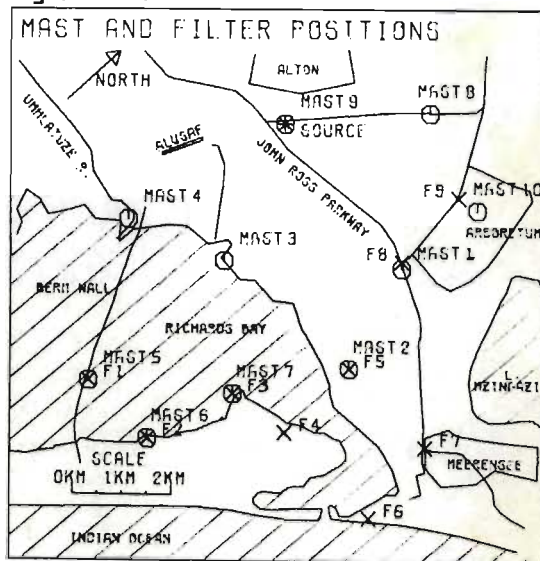


fig. (5.22d)

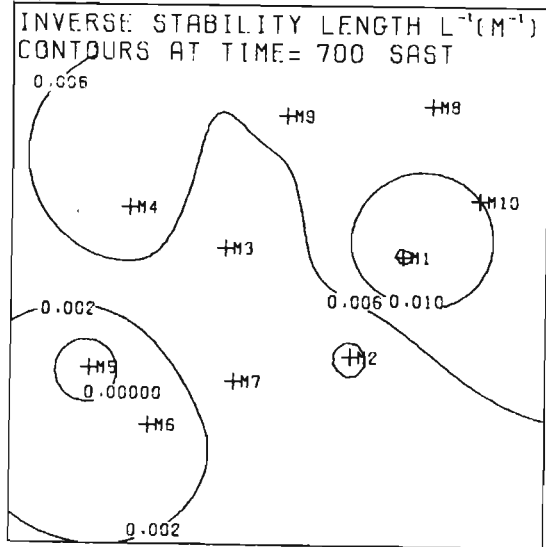


fig. (5.22e)

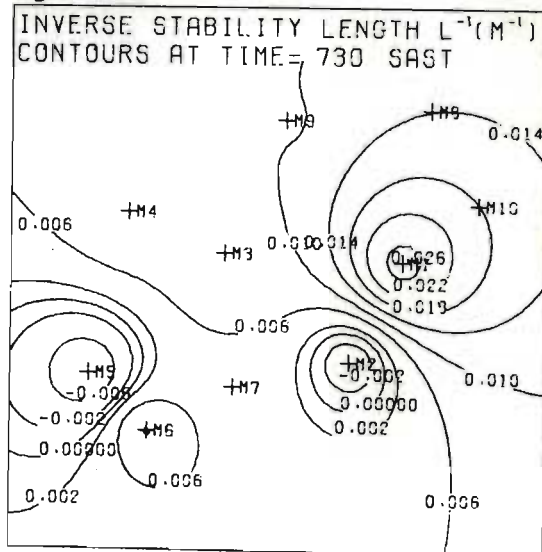


fig. (5.23)



RUN 711 : PREDICTED AND MEASURED MEAN CONCENTRATION HISTOGRAMS

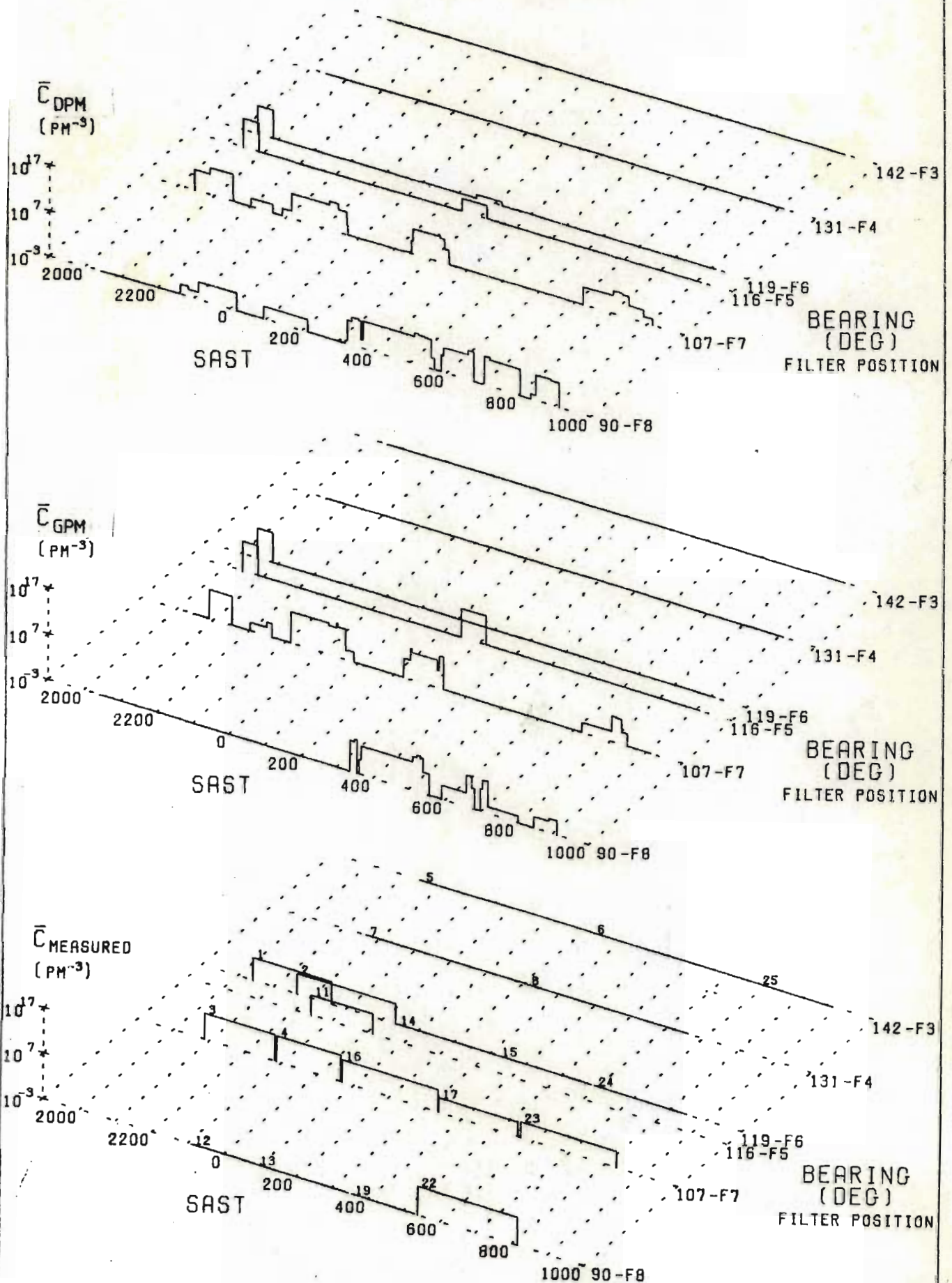


fig. (5.25)

RUN 711 : COMPARISON OF PREDICTED AND MEASURED MEAN CONCENTRATIONS RECORDED BY FILTERS

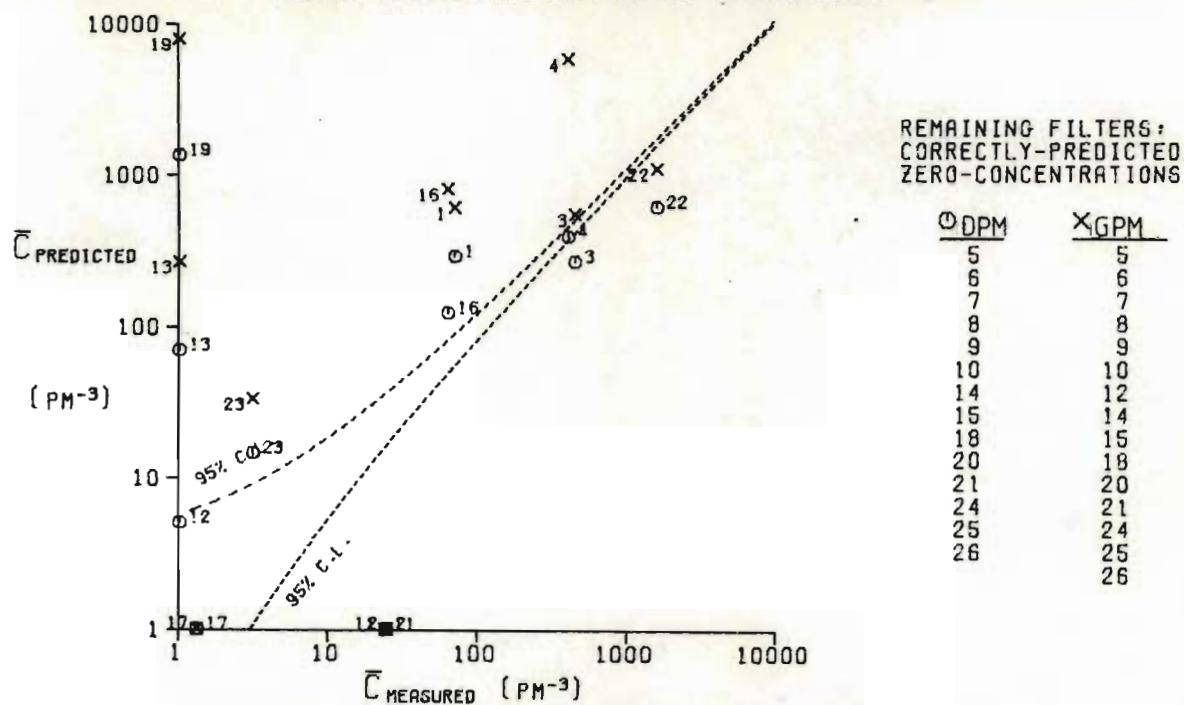
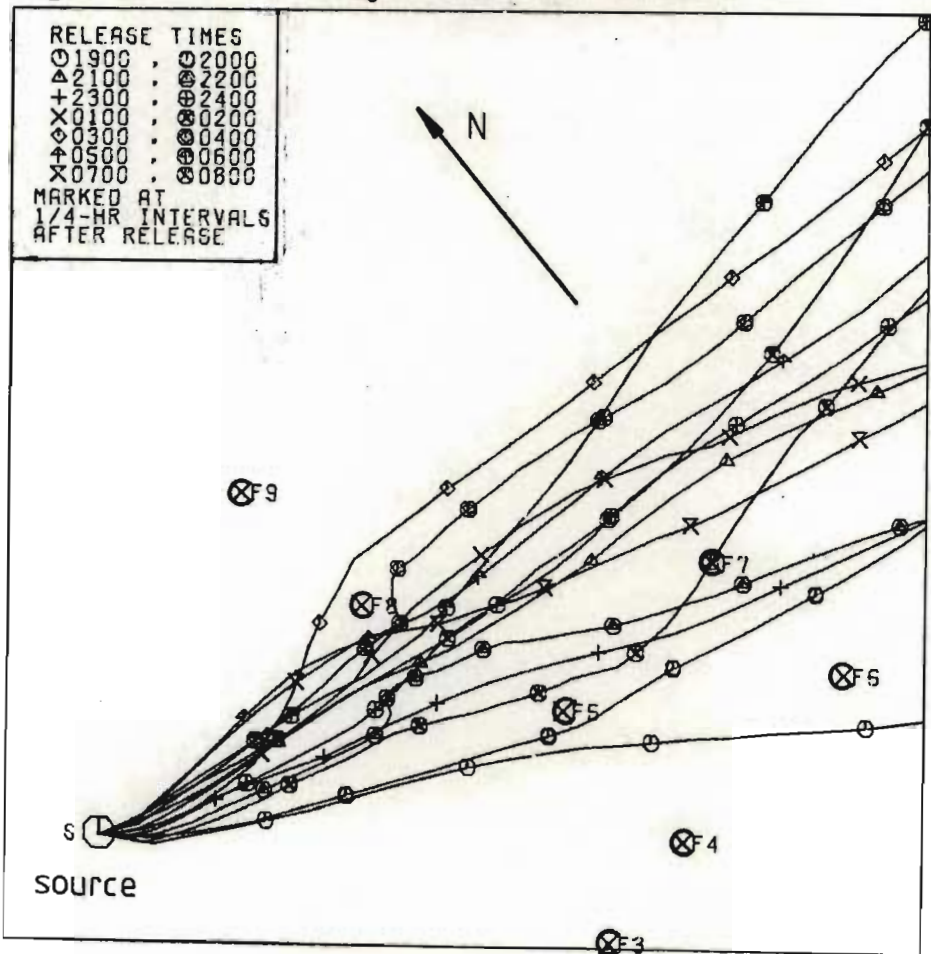


fig.(5.26) Mean trajectories at z=10 m



concentrations, though predictions by the GPM are in better agreement for filters 3 and 22 [fig. (5.25)].

Filters at site F7 in Meerensee record a mean concentration of 157,5 particles per cubic metre between 20h52 and 08h20. Based on a release rate of $5 \times 10^8 \text{ p s}^{-1}$ this represents a dilution of $3,15 \times 10^{-7} \text{ s m}^{-3}$, and a total dosage of $0,013 \text{ s}^2 \text{ m}^{-3} \times Q$.

5.2.6 Run 714 (14.7.76 to 15.7.76).

It is quite likely that the development of a stable surface layer during the night acts to insulate the surface from moderate synoptic weather variations. This appears to be the case in Run 714 where the calm conditions after sunset allow the establishment of a light land-breeze [fig. (5.28), 20h30 to 24h00]. The influence of a south-westerly gradient wind finally dominates the wind-field after 01h00. Between 22h00 and 24h00 there is a slight convergence over Richards Bay, probably due to a katabatic flow down the Umhlatuze river valley, and a current channelled southwards over Lake Mzingazi by the coastal dune.

An interesting feature of figure (5.27a) is that the subadiabatic temperature gradients remain unaffected by the higher wind-speeds associated with the S.W. wind after 02h00. Gradients are consistently near-adiabatic close to the bay, remote masts showing an inexplicable minimum at 23h00. Figure (5.27d) shows that the entire region is stable at 20h00, a small area over the bay becoming more neutral by 04h00 [fig. (5.27e)].

Between 19h00 and 21h00 the wind direction moves eastward, reaching a maximum after 21h00. Figure (5.29) shows that this temporal variation has induced sufficient lateral shear in the DPM distribution to account for the concentration measured at filter 3 ($15,8 \text{ p m}^{-3}$, site F7) whereas the GPM distribution does not extend this far. A further westward maximum is evident at 22h00 before the

RUN 714 (14/7/76-15/7/76)

fig. (5.27a)

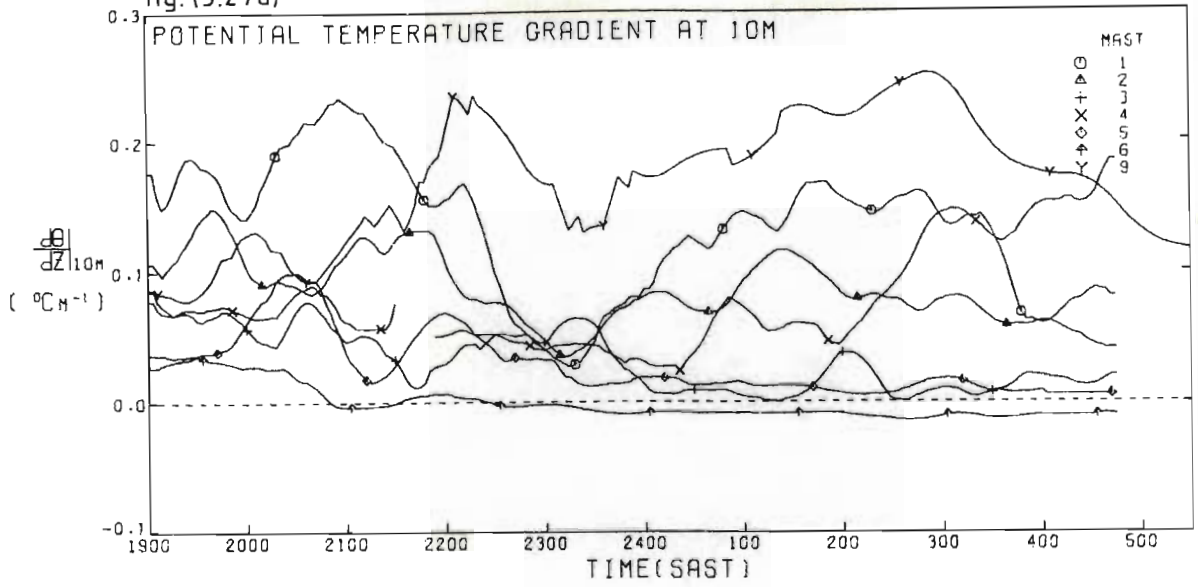


fig. (5.27b)

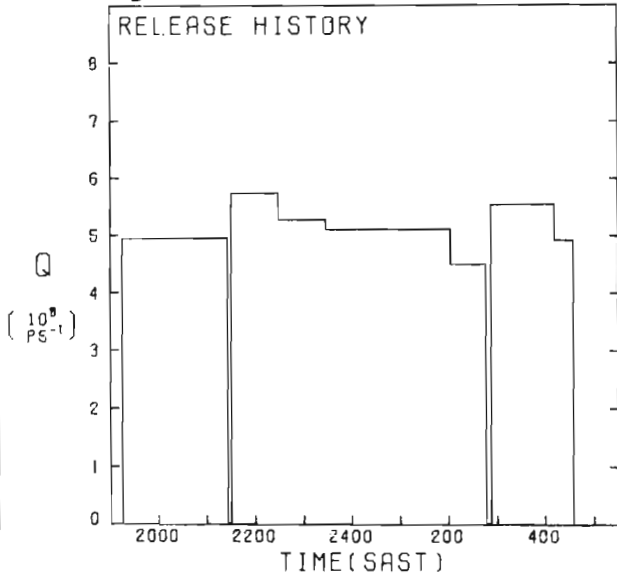


fig. (5.27c)

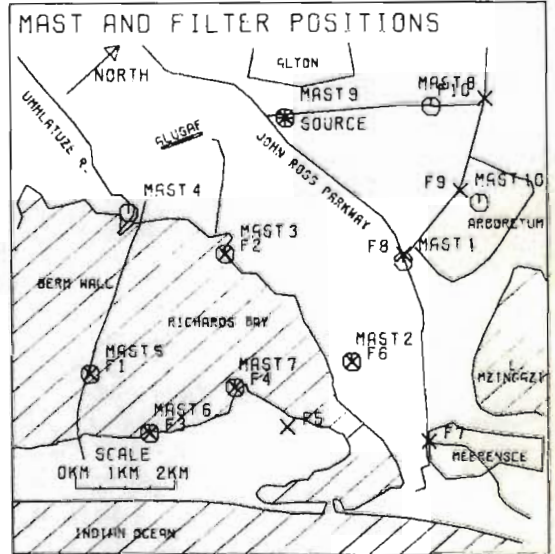


fig. (5.27d)

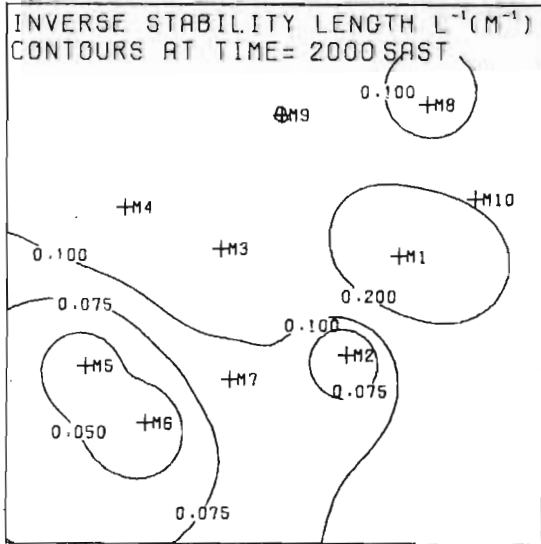


fig. (5.27e)

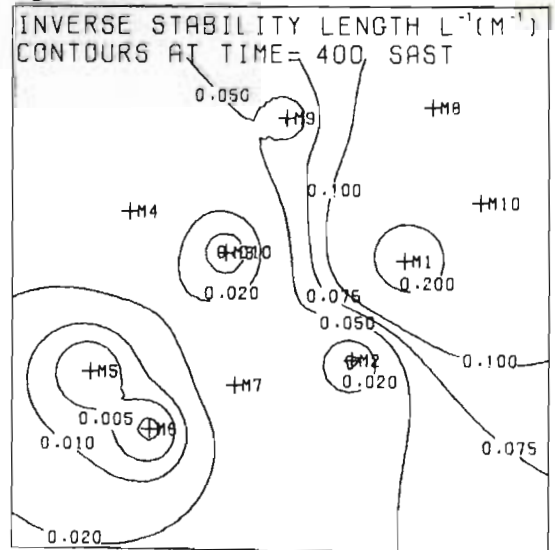


fig. (5.28)

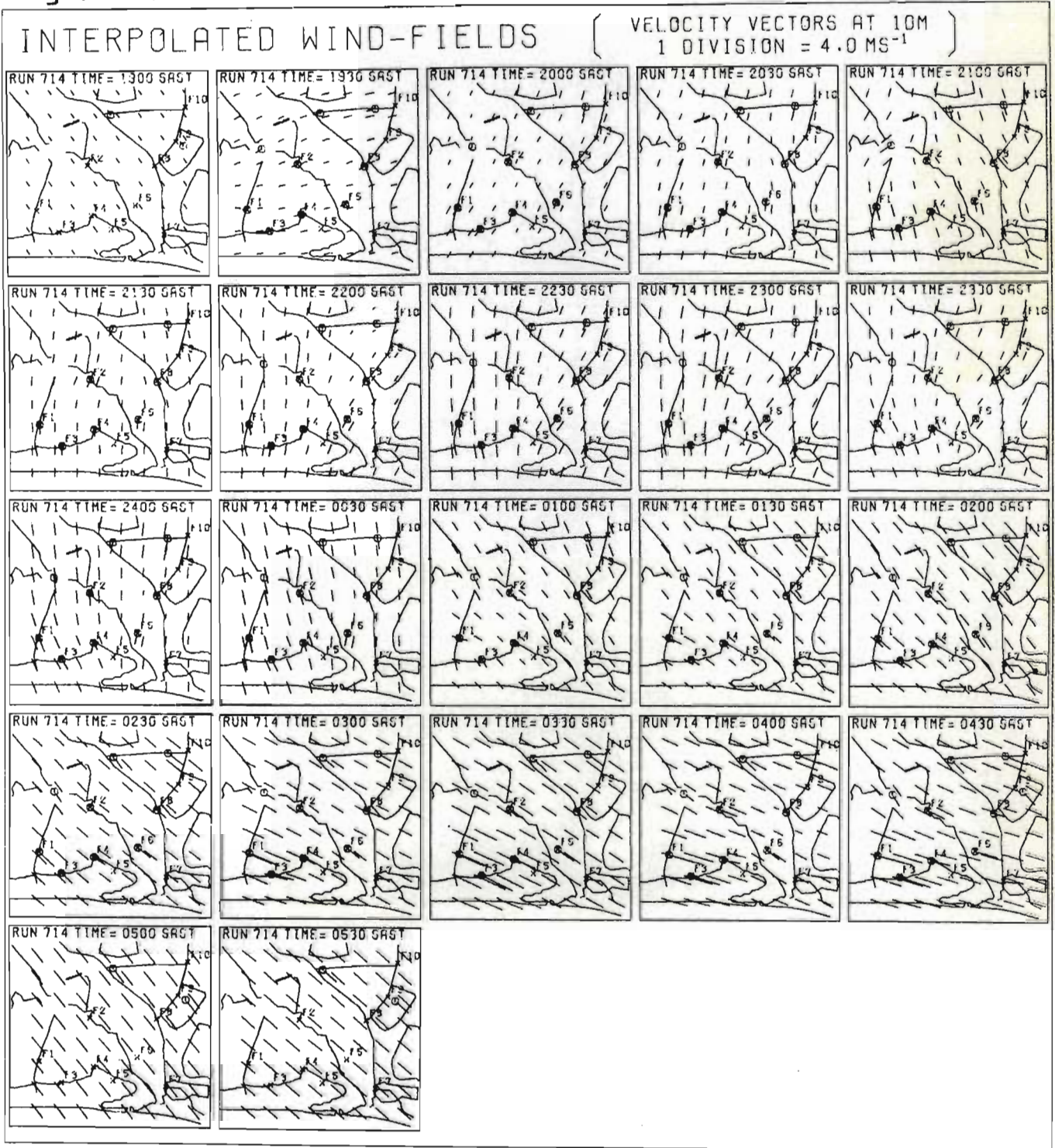
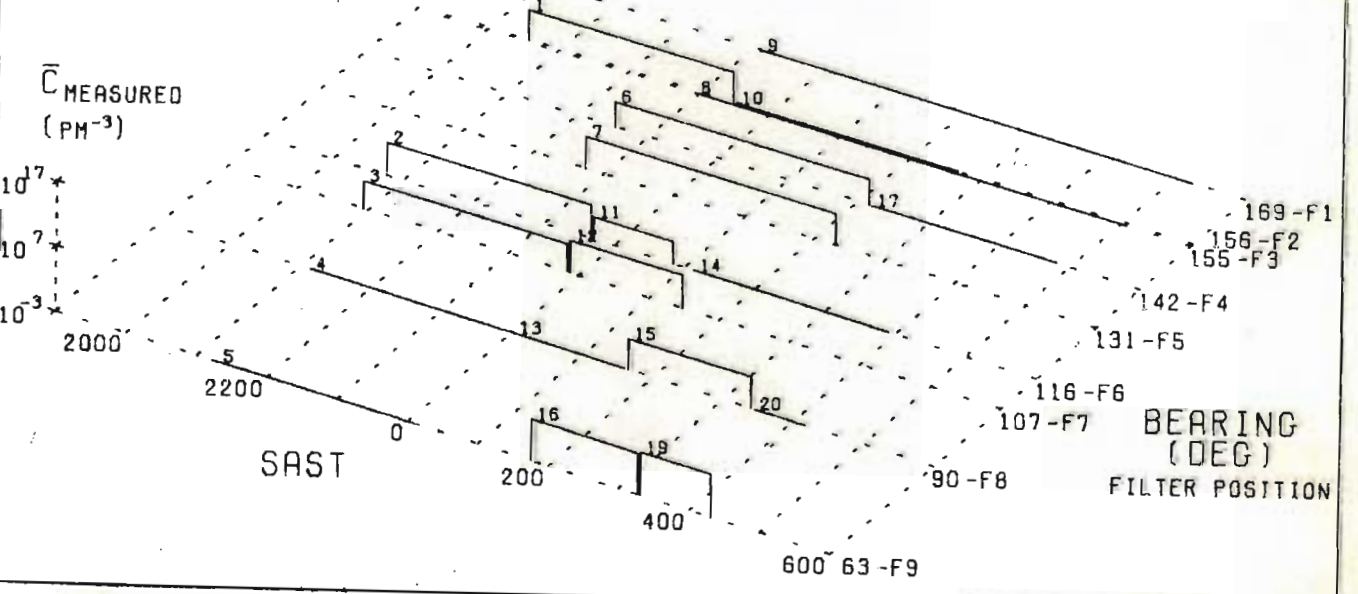
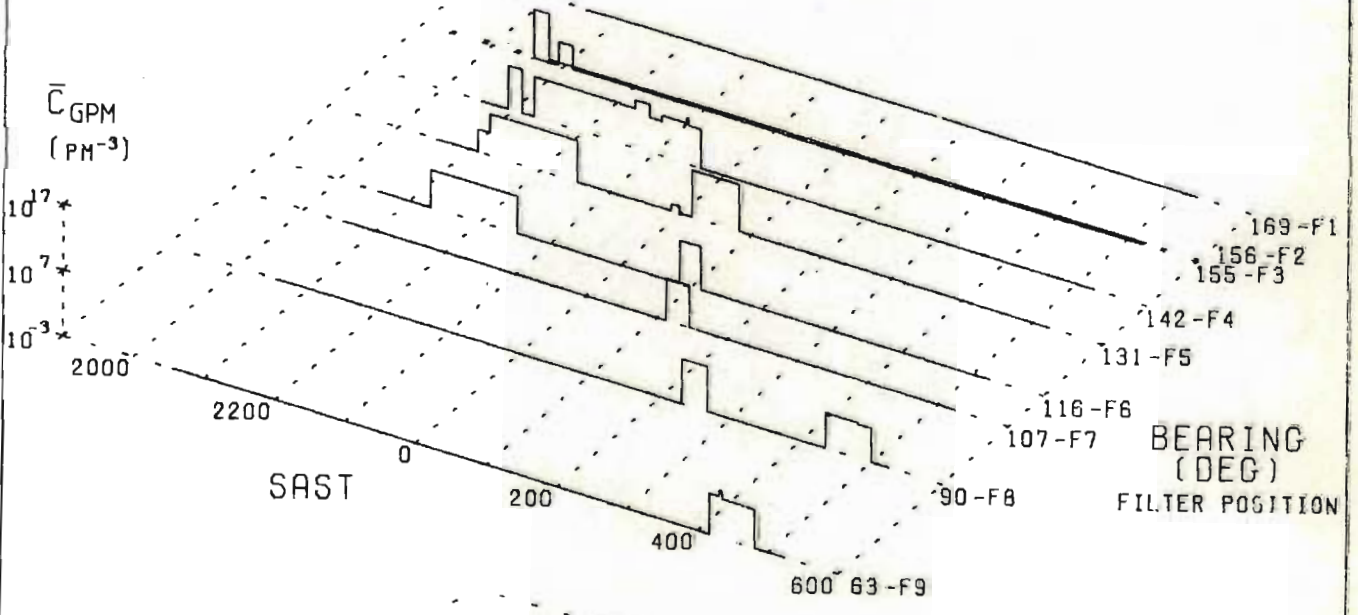
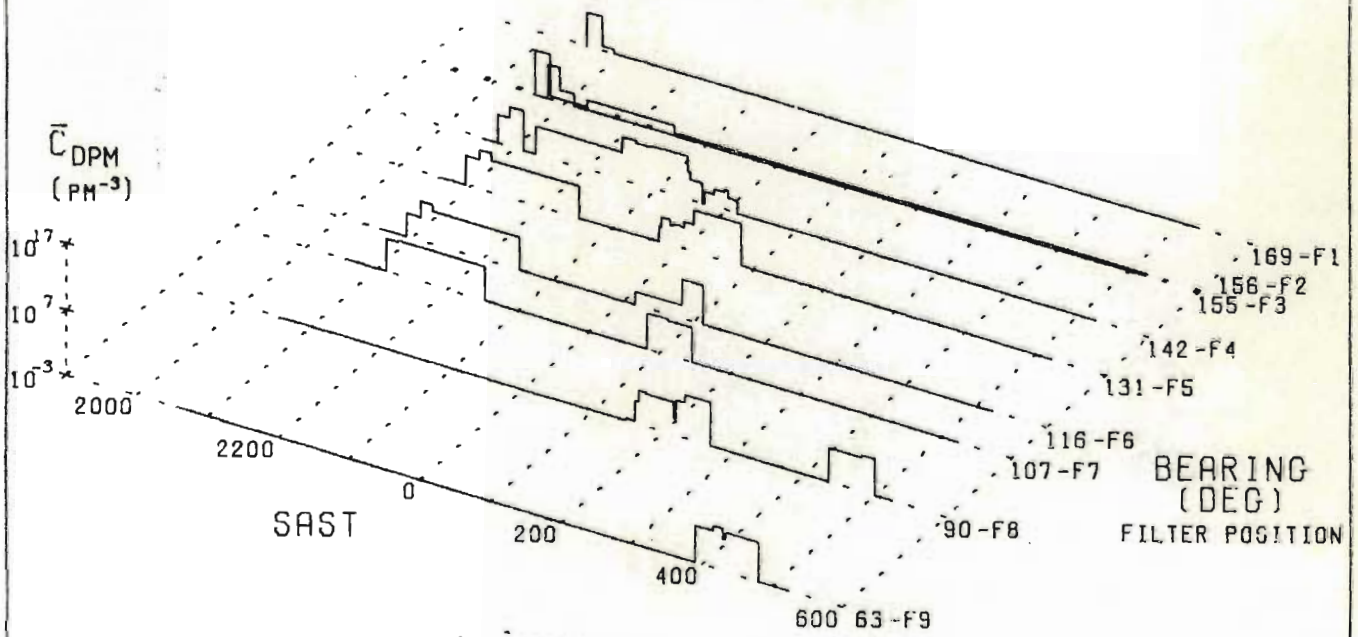


fig.(5.29)

RUN 714 : PREDICTED AND MEASURED MEAN CONCENTRATION HISTOGRAMS



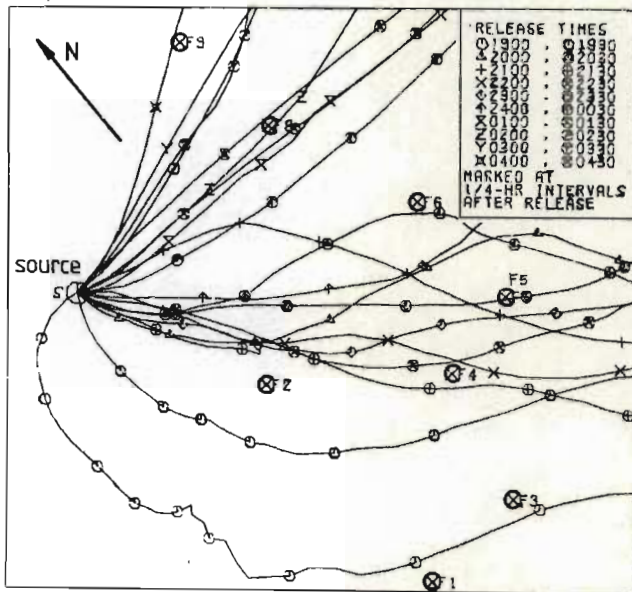
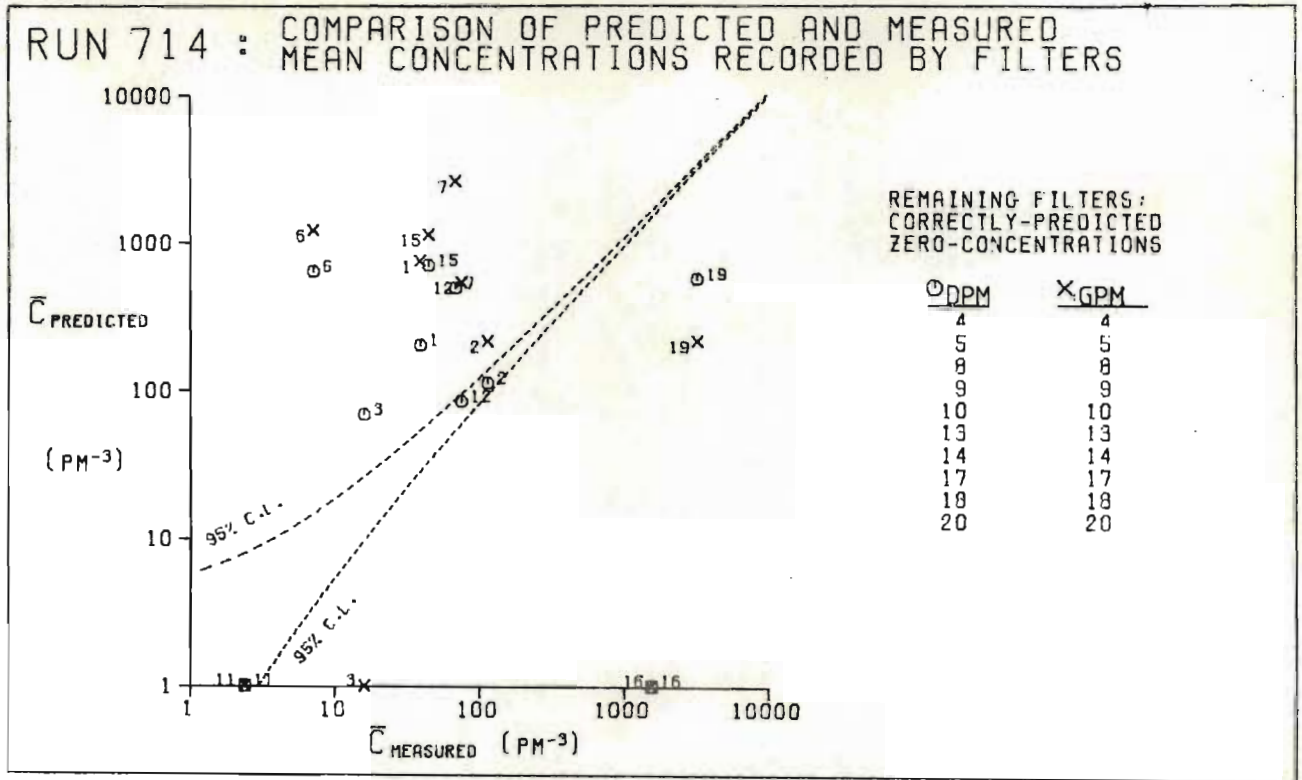


fig. (5.31a)
Mean trajectories at z=10m

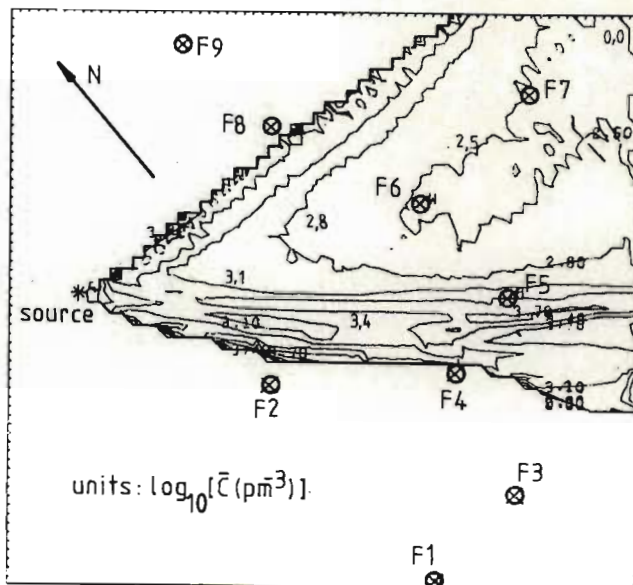


fig. (5.31b)
PIC model: Mean ground-level
concentration distribution
from 2300 to 0200 SAST

fig.(5.32a) DPM : Ground-level concentration distribution at 2340 SAST

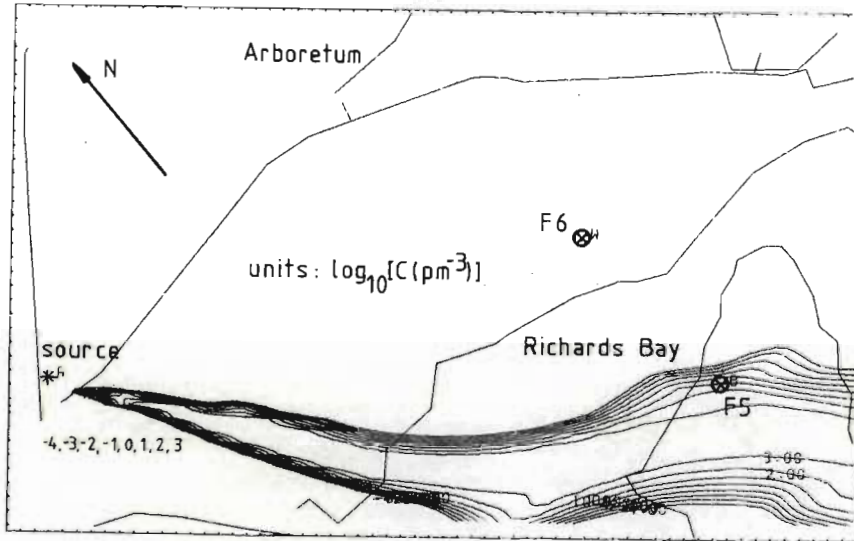


fig.(5.32b) DPM : Ground-level concentration distribution at 0055 SAST

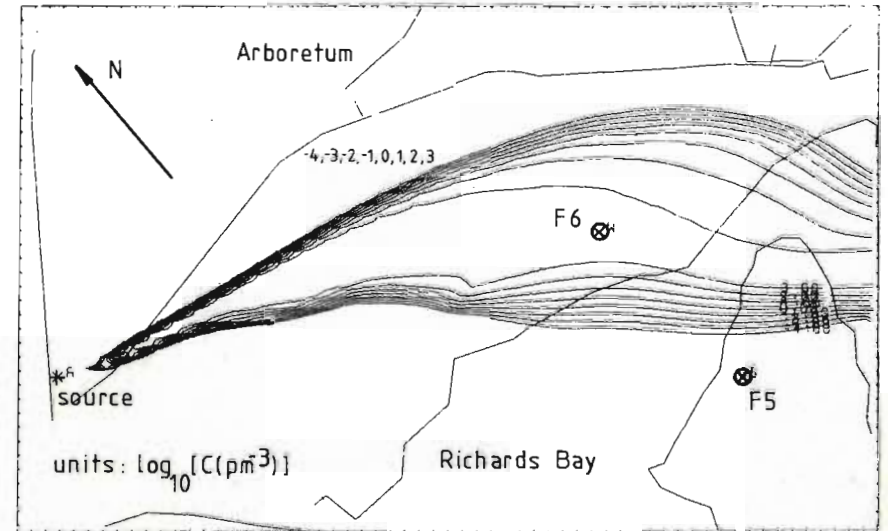


fig.(5.32c) GPM : Ground-level concentration distribution at 2340 SAST

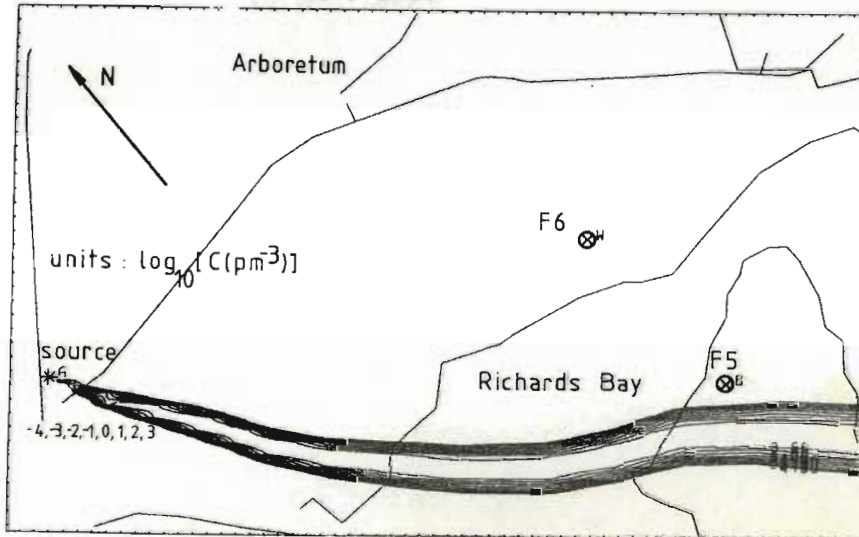
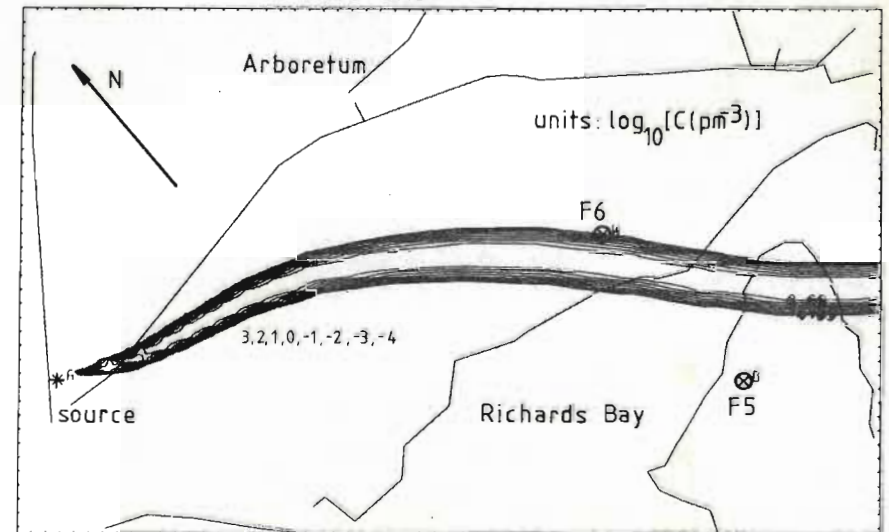


fig.(5.32d) GPM : Ground-level concentration distribution at 0055 SAST



final, slow sweep towards the east between 23h30 and 04h30. Figure (5.32) shows predicted concentration distributions at 23h40 and 00h55 during this eastward transient, clearly demonstrating the origin of the more diffuse concentration histograms predicted by the DPM. In figs. (5.32a) and (5.32b) the older portions of the plume show more lateral spread because of the earlier action of the new wind component in this region. Filter concentrations predicted by the DPM are generally in poor agreement with measurements, though GPM predictions are somewhat worse [fig. (5.30)].

The final eastward transient creates a large region of low dosage between filter sites F5 and F8. Mean concentrations predicted by the P.I.C. model between 23h00 and 02h00 [fig. (5.31b)] seem to embrace most filter measurements in this region [filters 7 ($68,5 \text{ p m}^{-3}$), 11 ($2,4 \text{ p m}^{-3}$) and 12 ($75,1 \text{ p m}^{-3}$)], though any improvement on GPM predictions should be purely fortuitous. This is because the P.I.C. model only differs from the GPM by its neglect of horizontal diffusion. The Meerensee residential area is seen to experience mean concentrations between 1 and 316 p m^{-3} during this period, whilst the southern end of Arboretum experiences about 1000 p m^{-3} . This is comparable with 3200 p m^{-3} recorded later by filter 19 in central Arboretum.

5.2.7 Run 722 (22.7.76).

Temporal transients and wind-shear are of particular importance in determining the distribution of dangerous pollutants following a short accidental release. An attempt was made in run 722 to simulate an instantaneous release. A total of 574 g FP2267 was released between 12h39½ and 12h40½ from a height of 21 m on mast 9. In order to achieve this high release-rate, it was necessary to release the powder in dry form from a canister with perforations in one end. Although the particle yield of $0,9 \times 10^{10} \text{ p g}^{-1}$ [section (4.1.3)] applies specifically to the acetone-medium dissemination system [section (4.1.2)], it was used in this case to obtain an estimate of the total release. Hence a release-rate of $8,61 \times 10^{10} \text{ p s}^{-1}$ is assumed between 12h39½ and 12h40½ [fig. (5.33b)]. During release, it was noted that a number of large agglomerates fell to the ground within a short distance of the mast. The assumed yield should thus lead to over-estimates of the recorded filter-concentrations.

Potential temperature gradients [fig. (5.33a)] during the run led to near-neutral conditions throughout the region [figs. (5.33d), (5.33e)], with only mast 9 displaying a subadiabatic gradient. This anomaly may arise from an inaccuracy in the manual digitisation of the thermistor chart record at mast 9. The effect extends some distance from the mast, since mast 9, with its key position in the run, did not receive its usual low weighting [see section (5.1)].

RUN 722 (22/7/76)

fig. (5.33a)

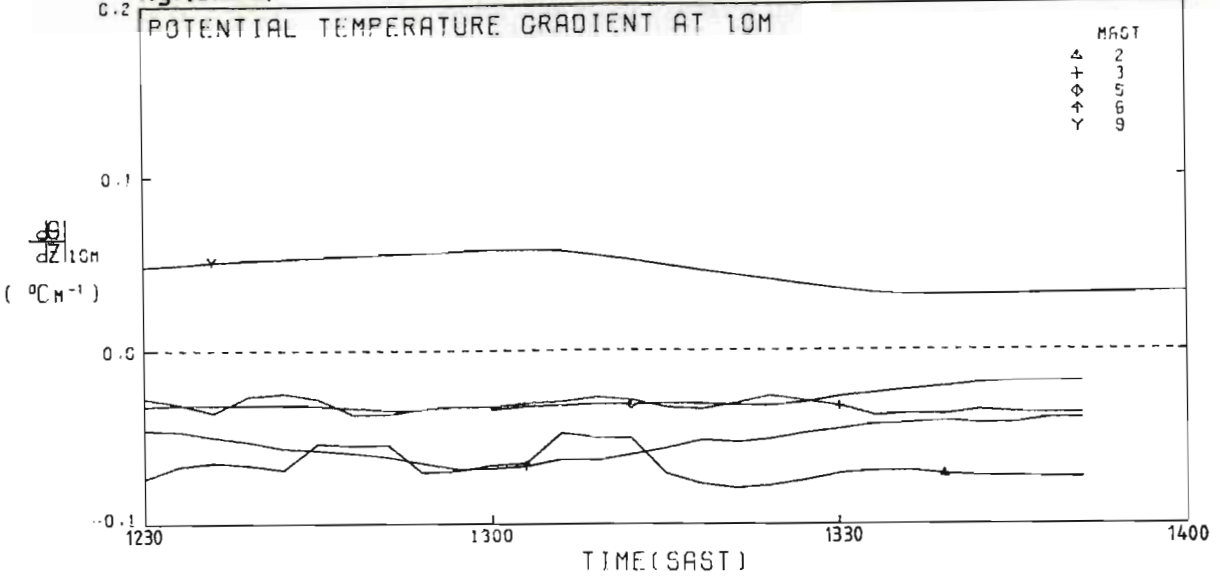


fig. (5.33b)

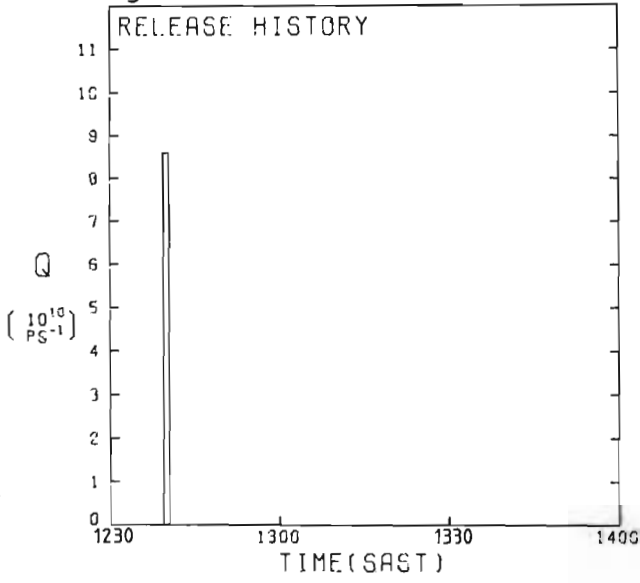


fig. (5.33c)

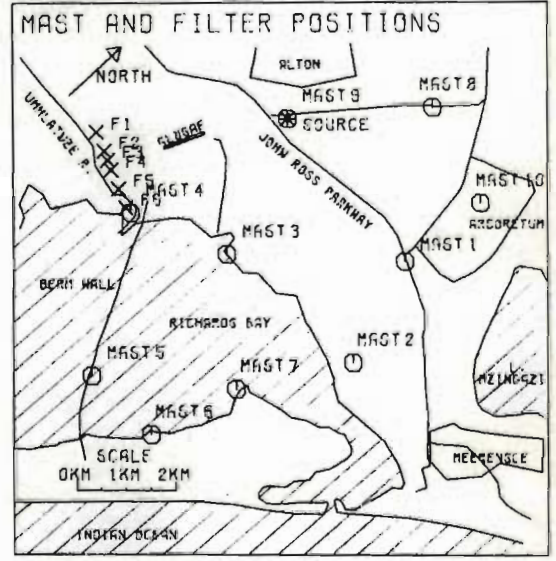


fig. (5.33d)

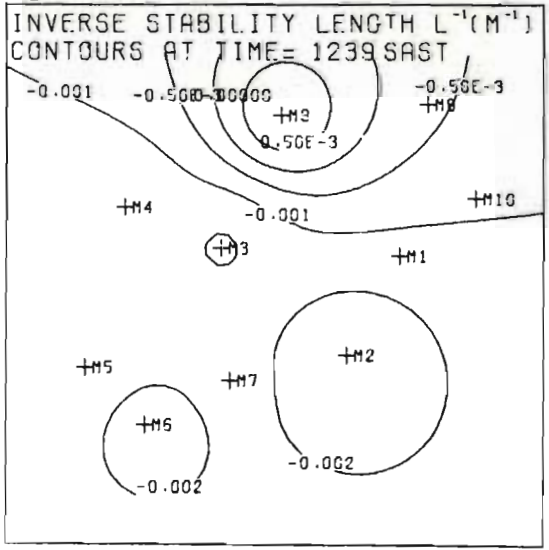


fig. (5.33e)

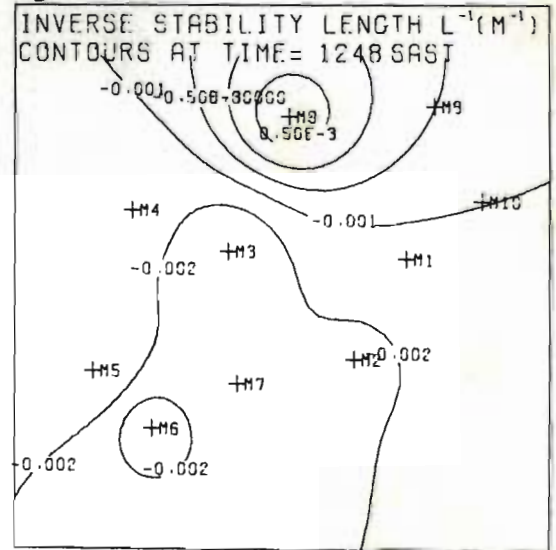


fig. (5.34)

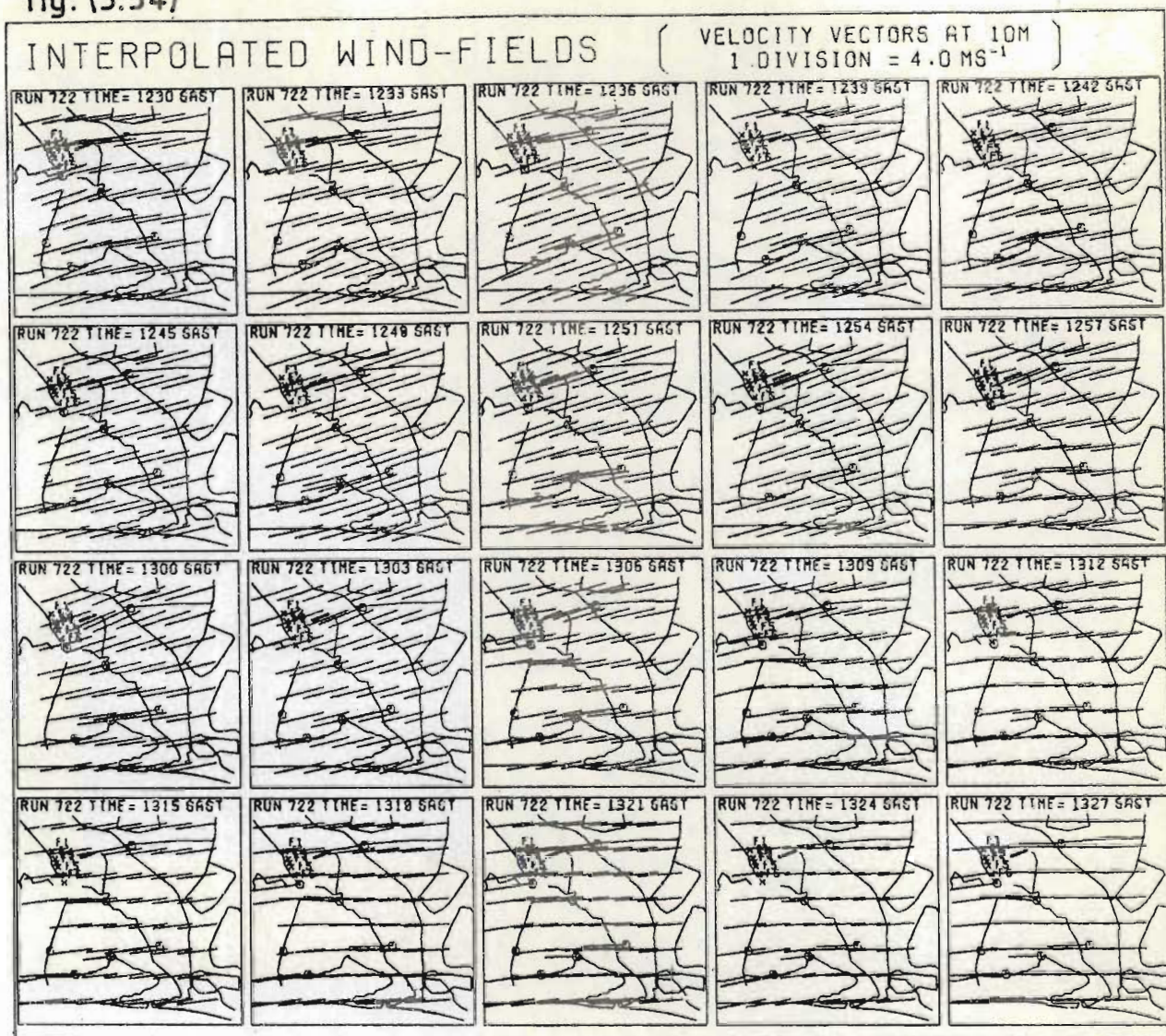
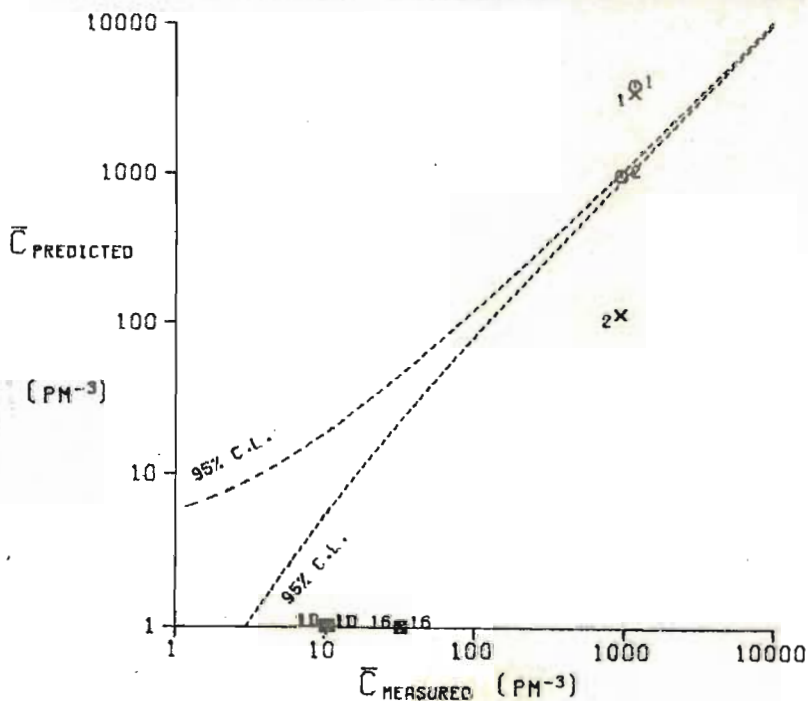


fig. (5.35)

RUN 722 : COMPARISON OF PREDICTED AND MEASURED MEAN CONCENTRATIONS RECORDED BY FILTERS



REMAINING FILTERS:
 CORRECTLY-PREDICTED
 ZERO-CONCENTRATIONS

○DPM	×GPM
3	3
4	4
5	5
7	7
8	8
9	9
12	12
13	13
14	14
15	15

fig.(5.36)

RUN 722 : PREDICTED AND MEASURED MEAN CONCENTRATION HISTOGRAMS

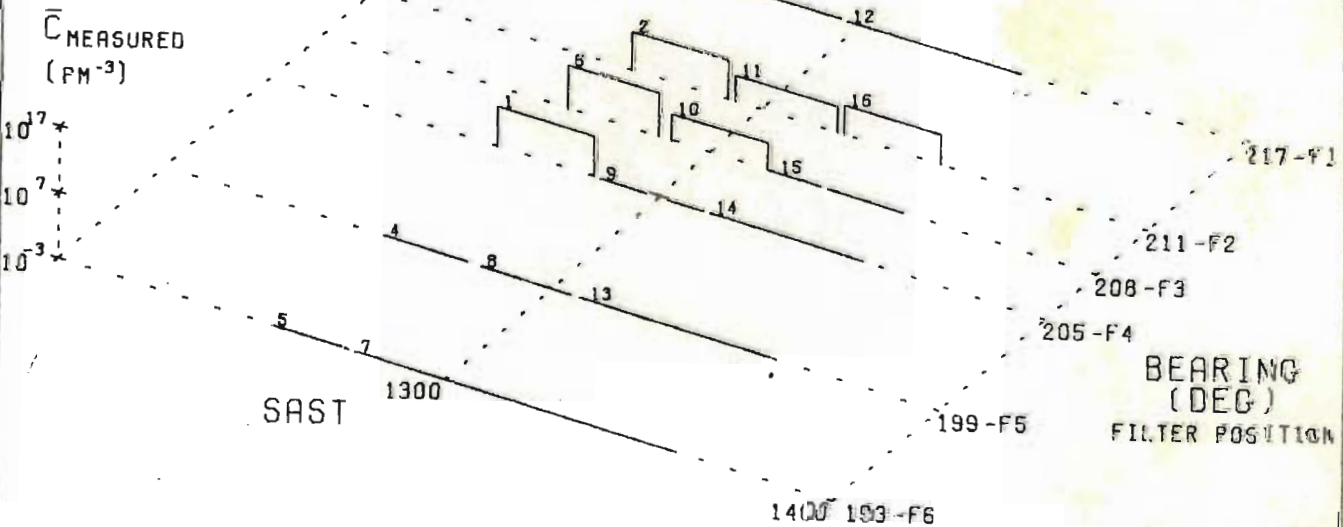
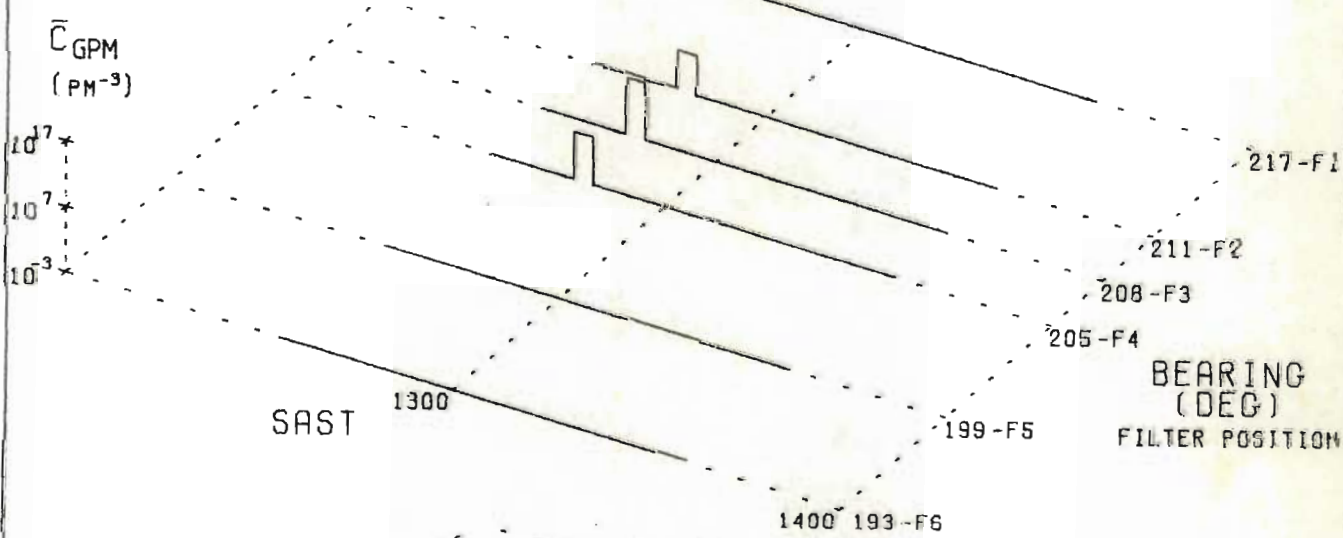
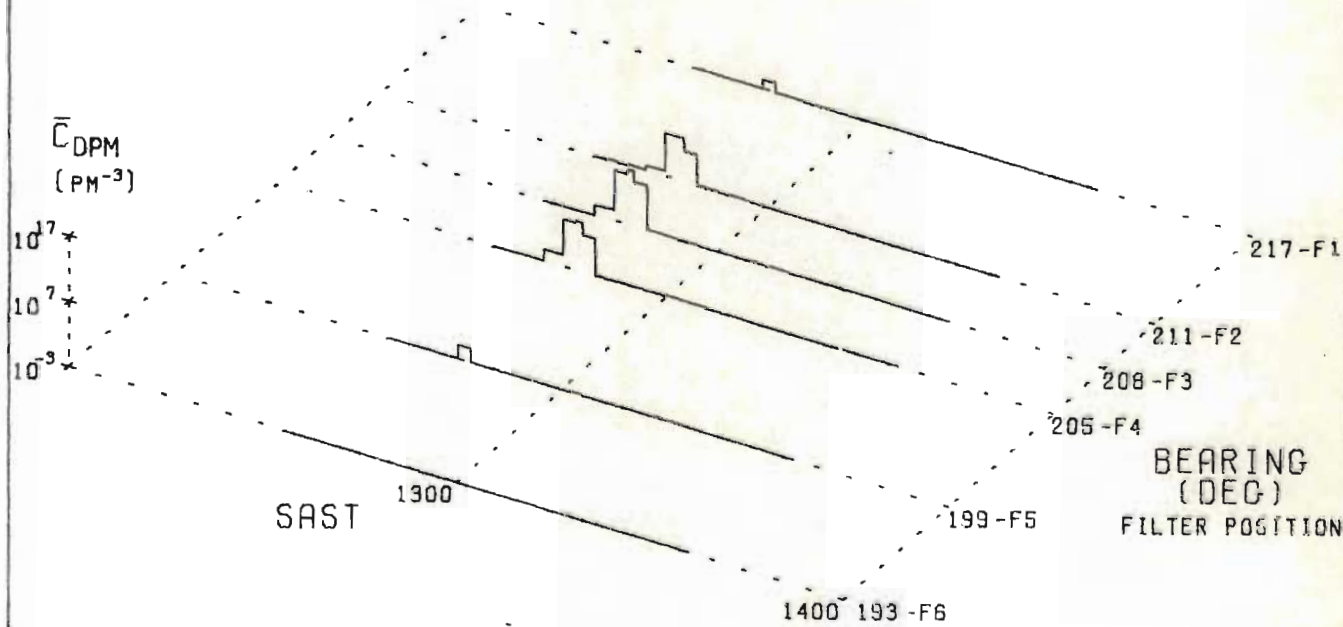


Figure (5.34) shows that a fresh N.E. wind persisted during the run, with speeds up to 9 m s^{-1} at the 10 m level. As a result, membrane filter receptors were positioned in a close array beyond the large smelting works [Alusaf] [fig. (5.33c)]. The effect of the gradual westward movement of wind-direction between 13h00 and 13h27 is evident in the measured filter concentration histograms [fig. (5.36)]. However, even the DPM proved incapable of predicting the large along-wind spreads associated with filters 10, 11 and 16.

The near-neutral conditions would lead to a relatively flat velocity profile. However, the assumption of roughness lengths $z_0 = 0,2 \text{ m}$ [grass, stands of trees, isolated bushes] and $z_0 = 1,2 \text{ m}$ over the industrial buildings [section (4.2.4), appendix (A4.4)] should make the neutral profile more gradual in the affected region [equation (1.15)]. Although DPM concentration histograms display two or three times the spread of the GPM histograms, the wind-shear apparently cannot explain the low concentrations observed after 13h00. It is possible that some form of elution mechanism was active whereby particles were held up in relatively stagnant areas within vegetation and amongst buildings. On the other hand, the DPM cannot account for a rapid increase of velocity with height in a shallow layer near ground-level, because of the layered structure of the lagrangian puff solution [section (2.4.4.2)].

Figure (5.35) shows that the DPM provides a good estimate for filter 2 and a fair estimate for filter 1,

For filter 6, with a measured mean concentration of $4,4 \times 10^3 \text{ p m}^{-3}$, the DPM predicts $21,3 \times 10^3 \text{ p m}^{-3}$ whilst the GPM predicts $42,4 \times 10^3 \text{ p m}^{-3}$. In general, DPM predictions are only slightly better than the GPM predictions.

5.2.8 Run 723 (23.7.76).

Run 723 covers a short, calm transition period between N.E. and S.W. gradient wind conditions. An initial northerly breeze gives way to a variable land-breeze between 04h30 and 06h30 [fig. (5.38)]. After 07h00 the influence of the south-westerly becomes stronger, with sharply deteriorating stability [fig. (5.37a)]. Temperature gradients at masts 3 and 6, near the bay, lag until 09h00 before becoming superadiabatic. At 09h00, conditions over the entire region are near-neutral [fig. (5.37e)].

Some major differences are apparent in the concentration histograms predicted by DPM and GPM solutions [fig. (5.40)]. Lateral wind-shear associated with the eastwards transient between 04h00 and 05h00 extends the DPM distribution sufficiently to provide an accurate estimate of the mean concentration recorded by filter 4 ($88,4 \text{ p m}^{-3}$) at site F6 [fig. (5.39)]. For the same reason, the DPM provides a better estimate than the GPM for filter 8 ($77,4 \text{ p m}^{-3}$ measured) at site F7 during the second eastwards transient beginning at 06h30. Although agreement with measurements is only fair, DPM predictions are better than GPM predictions in all cases except for filter 11.

The DPM concentration distribution at 05h00 [fig. (5.41a)] shows that the variation in shear direction has extended the cloud over a large area. The stronger breeze near masts 5 and 6 about 04h30 has operated only on the portion of the plume which crossed that area, leading to

RUN 723 (23/7/76)

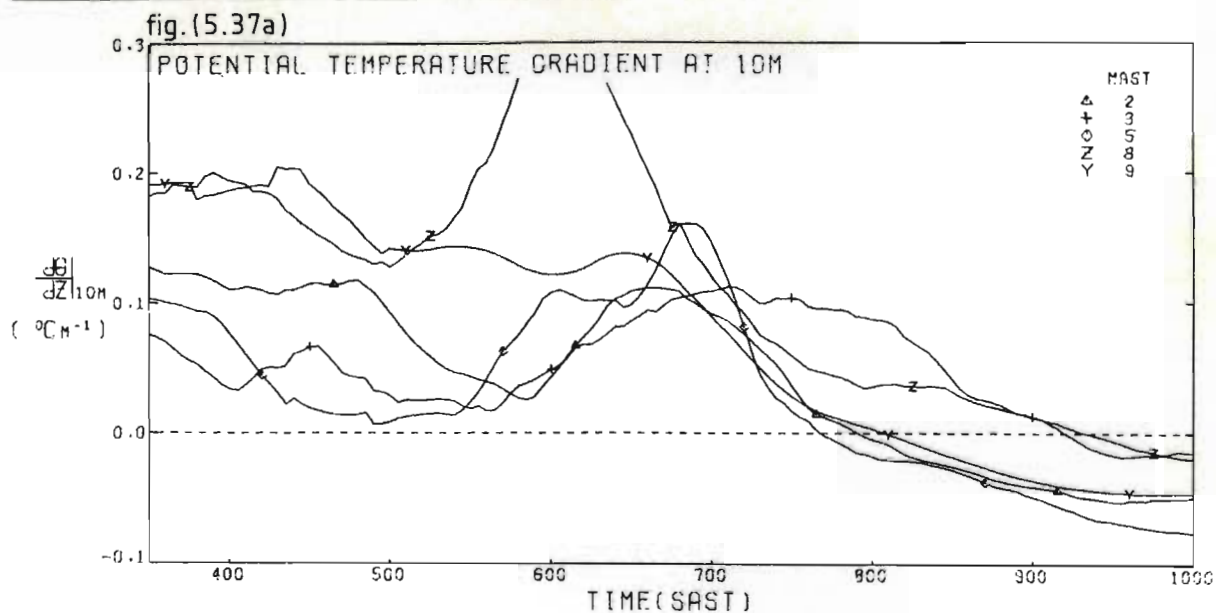


fig.(5.37b)

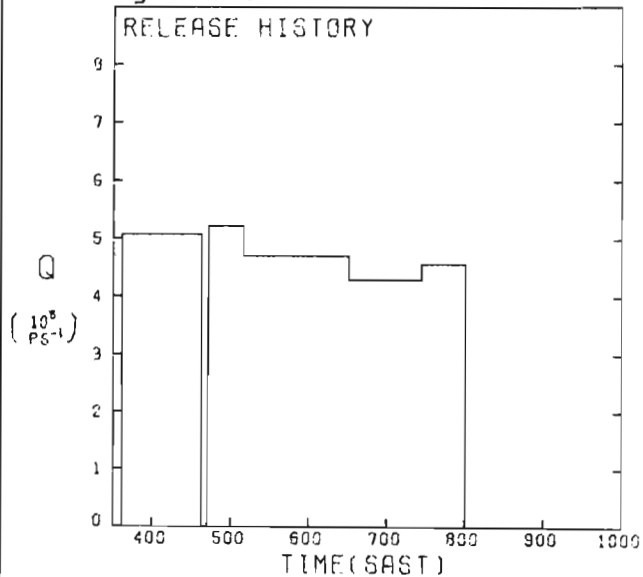


fig.(5.37c)

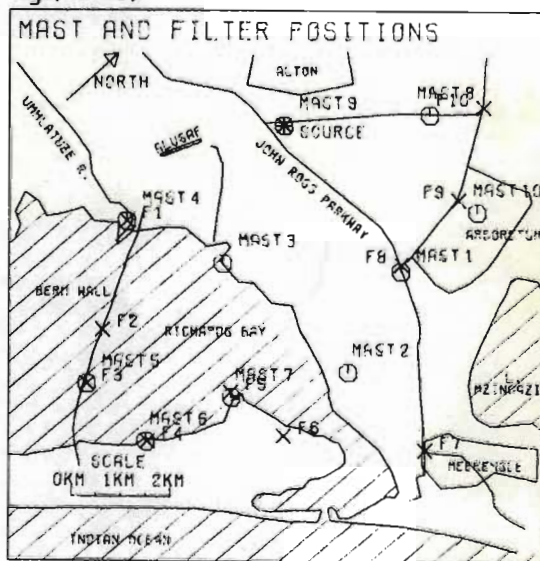


fig.(5.37d)

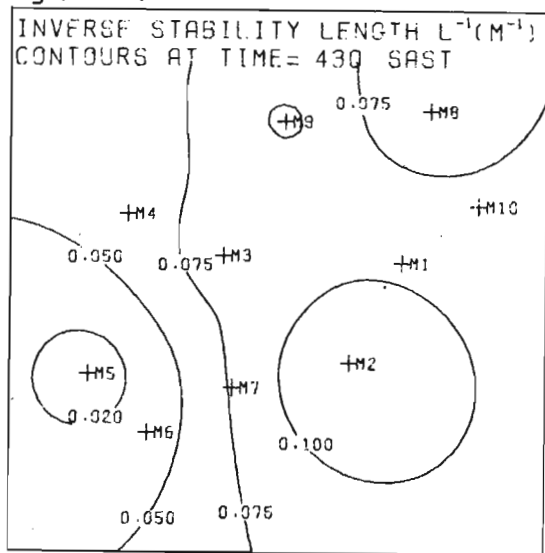


fig.(5.37e)

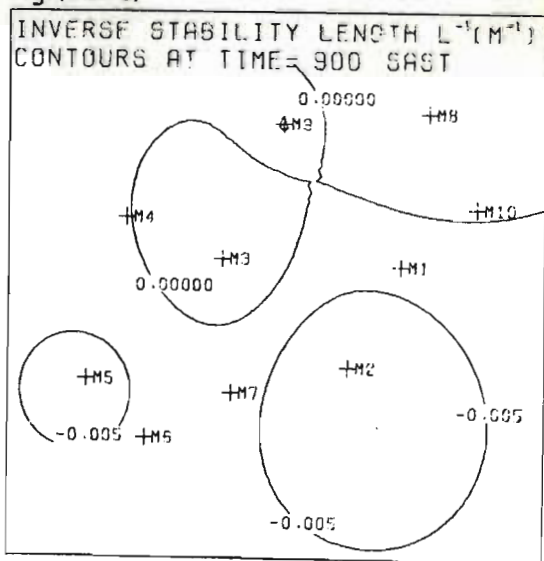


fig. (5.38)

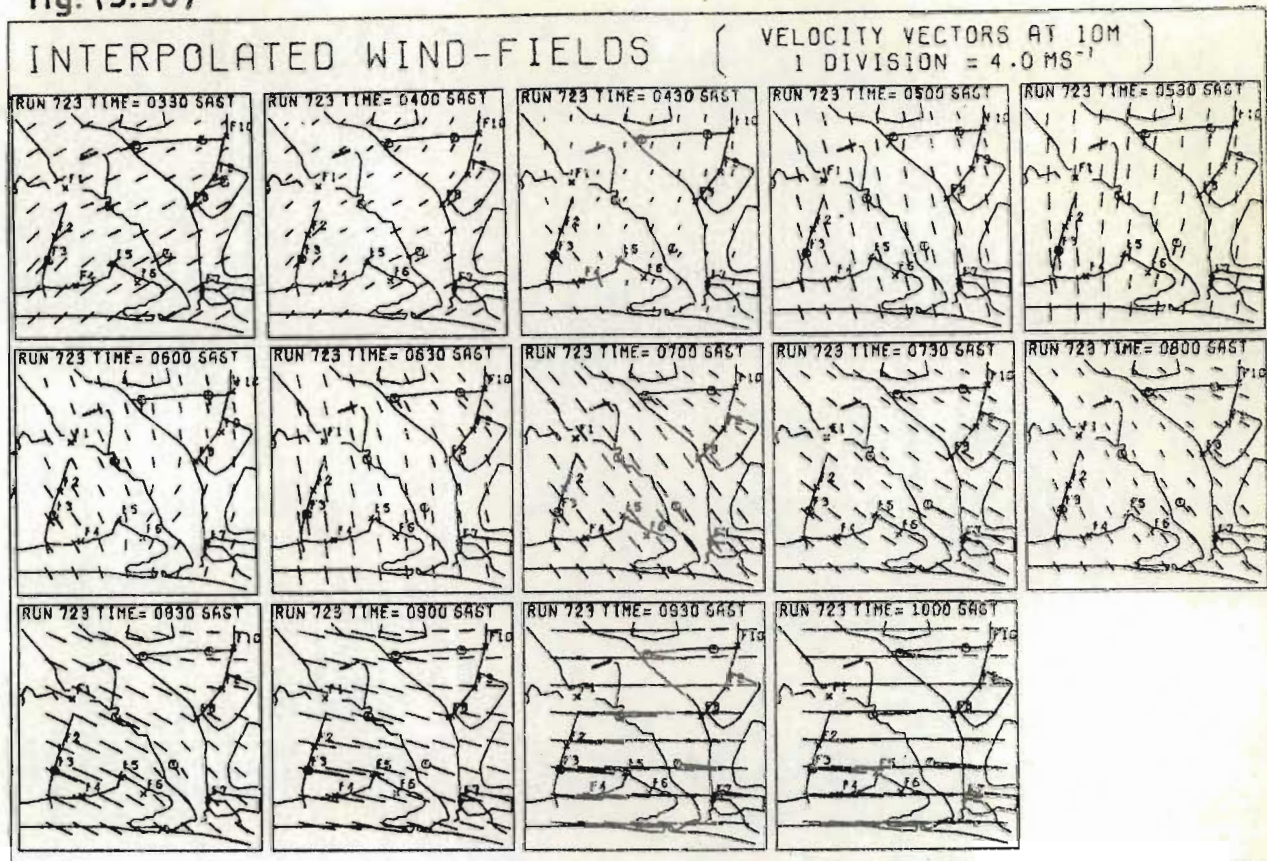
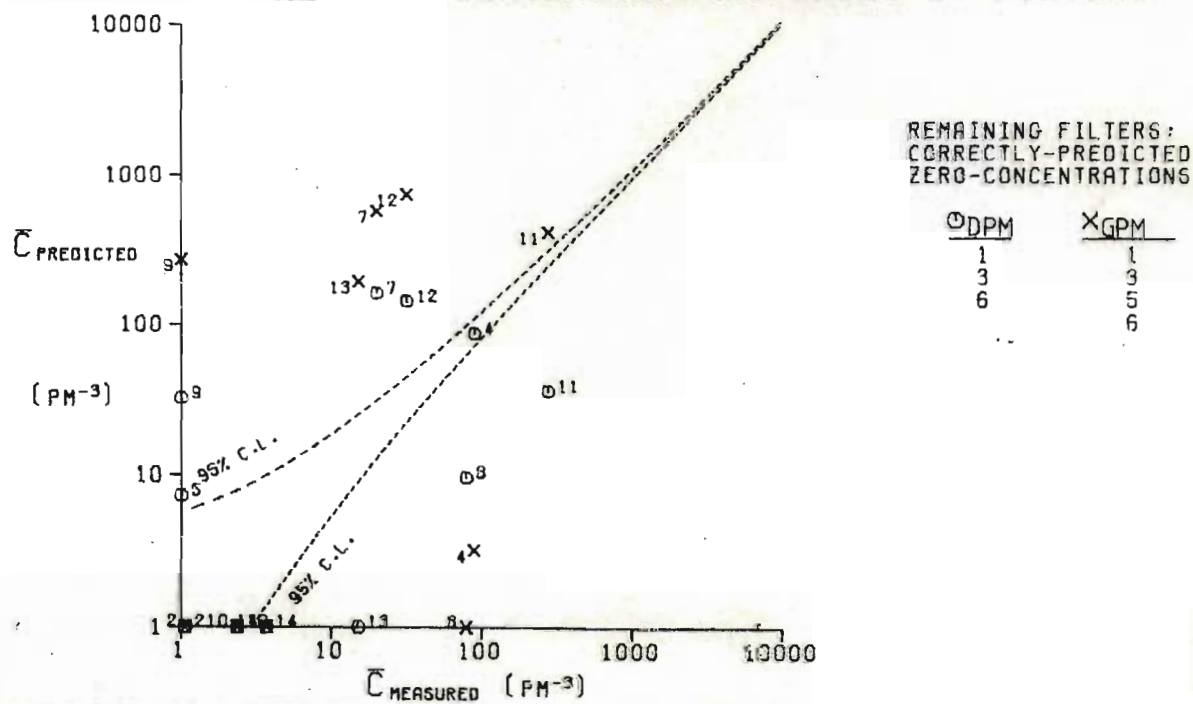
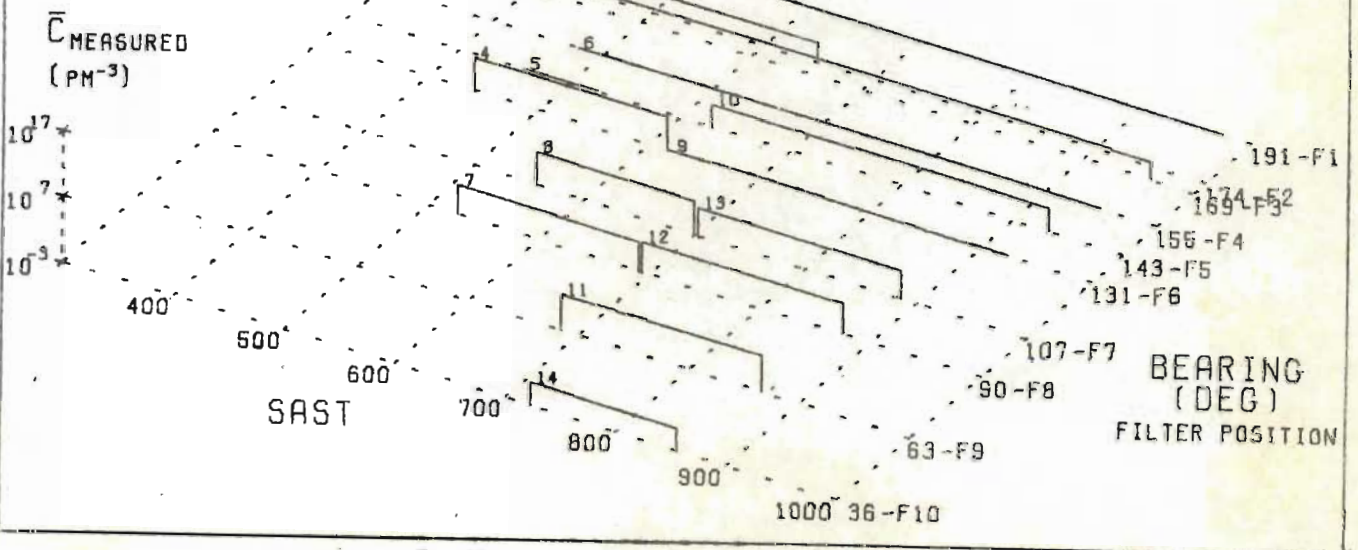
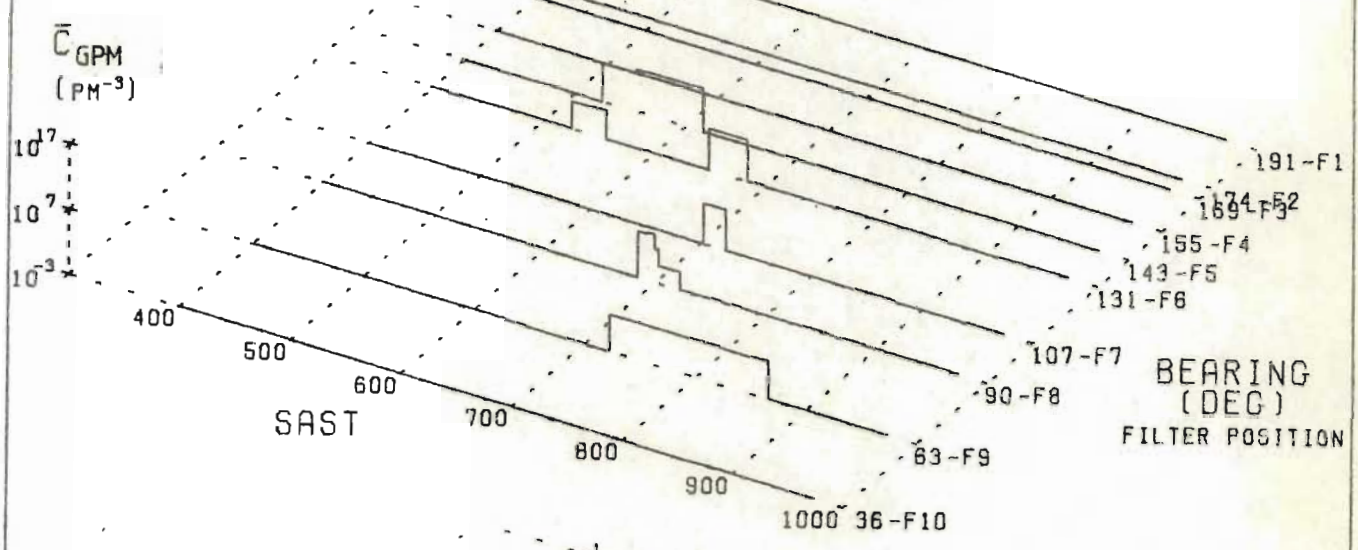
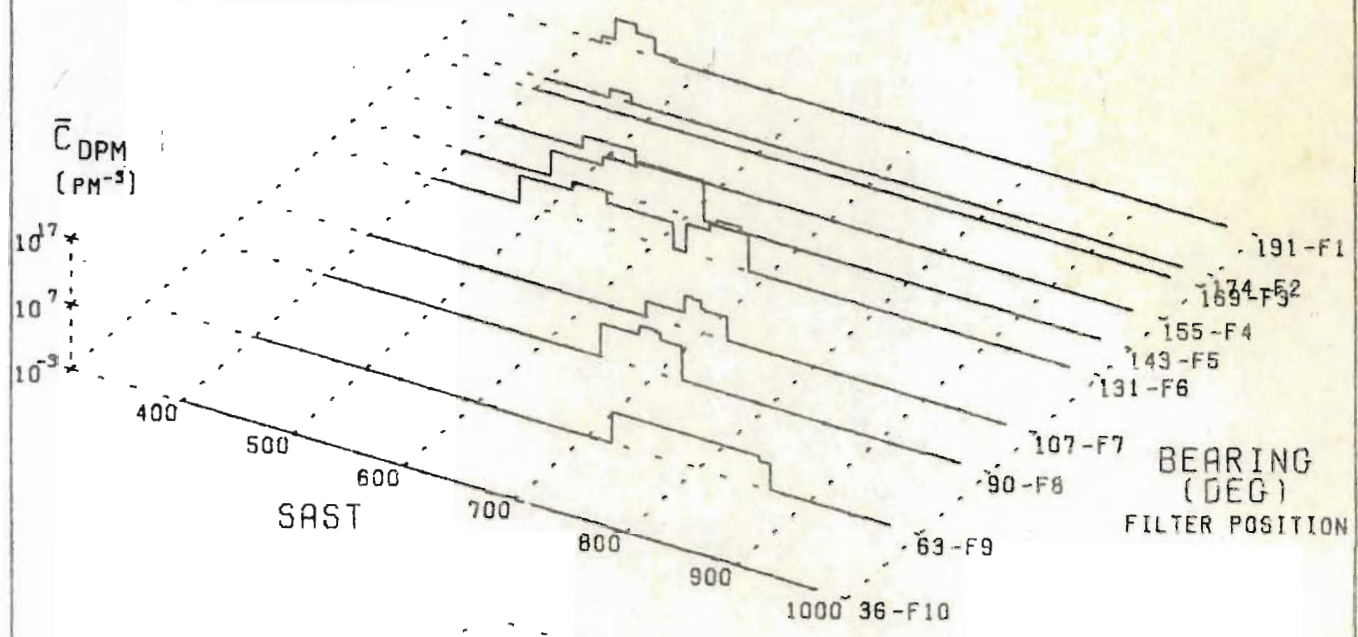


fig. (5.39)

RUN 723 : COMPARISON OF PREDICTED AND MEASURED MEAN CONCENTRATIONS RECORDED BY FILTERS



RUN 723 : PREDICTED AND MEASURED MEAN CONCENTRATION HISTOGRAMS



a slight bifurcation of the distribution, The low concentration allocated to filter 5 by this diffuse cloud does not differ significantly from the measured zero-concentration [fig. (5.39)].

The origin of the divergence in the 05h00 distribution is demonstrated by the 05h00 locus set up by trajectories with release times 03h30, 04h00 and 04h30 in fig. (5.41b). Mean concentrations suggested by the P.I.C. dosage distribution for filters 7 and 8 (sites F8 and F7) are too low and too high respectively. Whereas mean concentrations of 19,7 and 77,4 p m^{-3} were recorded by these filters, fig. (5.41c) shows that the mean concentrations predicted by the P.I.C. model at sites F8 and F7 for the period 05h30 to 07h00 were 0 p m^{-3} and about 10^3 p m^{-3} respectively. The sharp boundary between this distribution and that for the period 07h00 to 08h30 [fig. (5.41d)] indicates a monotonic eastwards variation in wind direction. As in the gaussian puff histogram [fig. (5.40)], the P.I.C. model predicts that the distribution will only affect site F7 after 07h00. In contrast, the DPM histogram for site F7 shows considerable spread about the gaussian puff arrival time, allowing the DPM to contribute significantly to filter 8 (9,5 p m^{-3} predicted, 77,4 p m^{-3} measured). The tendency for DPM traverse histograms to be centred on the GPM histogram peaks suggests that the 10 m tracking height used in the GPM and P.I.C. models must be close to optimum.

5.3 Simulation of Run 723 using predicted wind-fields.

An early motive for the development of a generalised dispersion model was its planned use in conjunction with the mesoscale wind-field model of Scholtz and Brouckaert (1976) [section (1.3.1)]. It is pointed out in appendix (A1.2) that a limited number of complete solved wind-fields may be supplied to the DPM as alternative input information. In the simulation of run 723, these wind-fields were supplied at 30 minute intervals. The lack of information concerning perturbations with shorter periods has led to a smoothing of the predicted quantities.

The series of wind-fields predicted for the N.E. to S.W. transition period of run 723 is presented in fig. (5.42). The positive sense of the vectors is generally towards the coast. The effective gradient-wind component for this period has been estimated by subtracting the predicted land-breeze and slope-wind from the measured velocity at mast 9 [fig. (4.4)]. Whereas the land-breeze potential was considered proportional to the difference between a "land" temperature measured at mast 8 and a sea temperature of $22,09^{\circ}\text{C}$ [equation (1.33)], slope wind potentials were based on an estimated temperature increase through the inversion layer [equation (1.34)].

The effectiveness of the wind-field model may be gauged by comparison with the interpolated measured wind-fields in fig. (5.38). The dependence of the predicted wind-field on the velocity measured at mast 9 is easily

fig. (5.42)

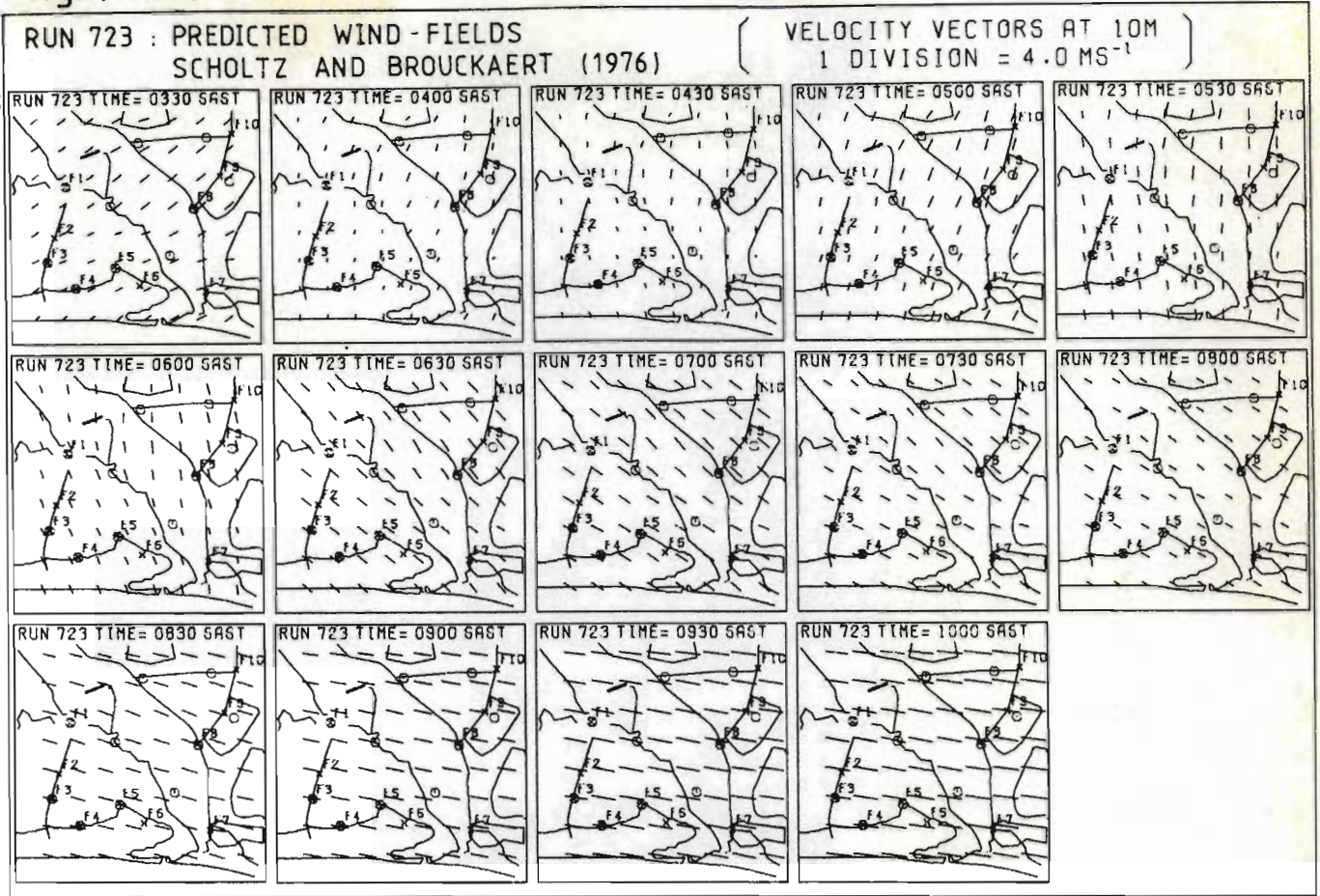


fig.(5.43) Predicted wind-fields :
Mean trajectories at z=10m

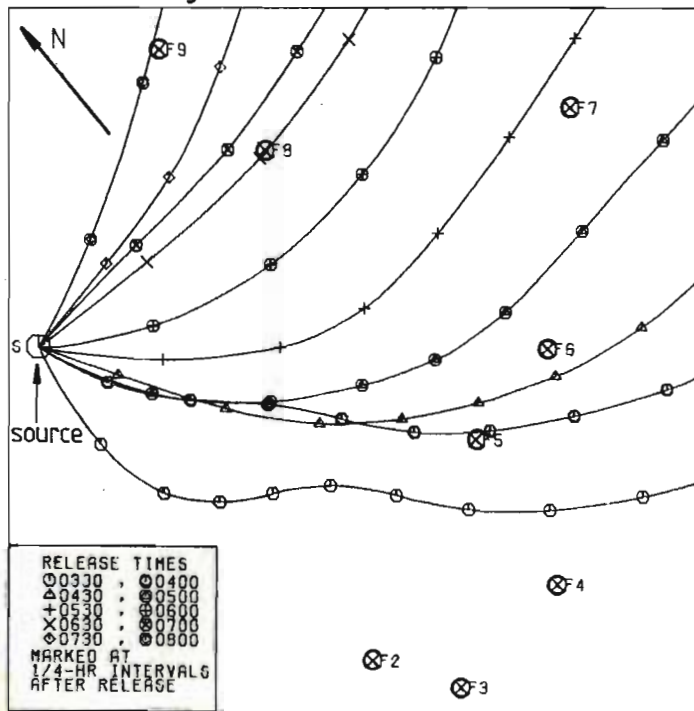


fig. (5.44)

RUN 723 : PREDICTED AND MEASURED
MEAN CONCENTRATION HISTOGRAMS
USING PREDICTED WIND-FIELDS

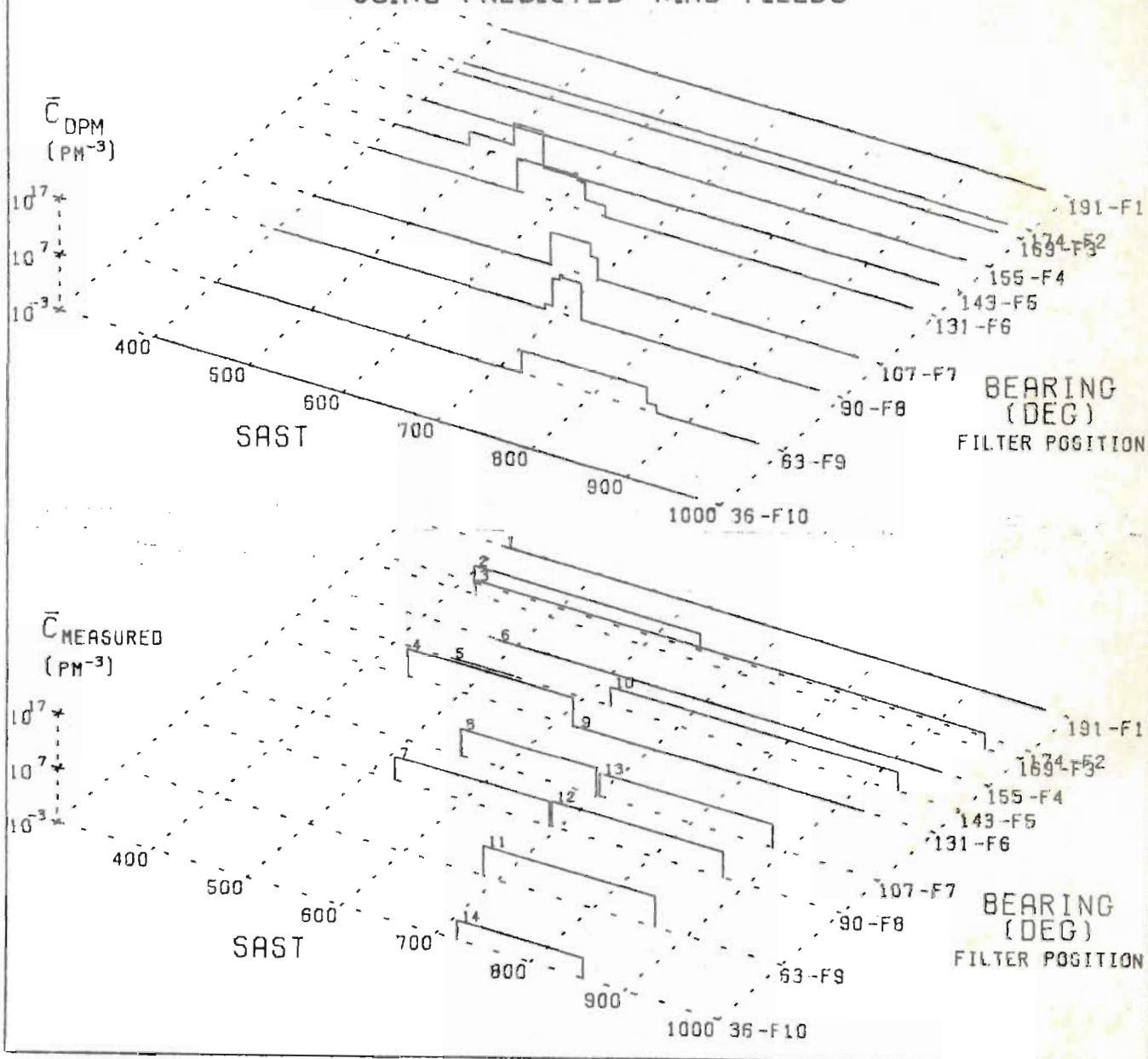
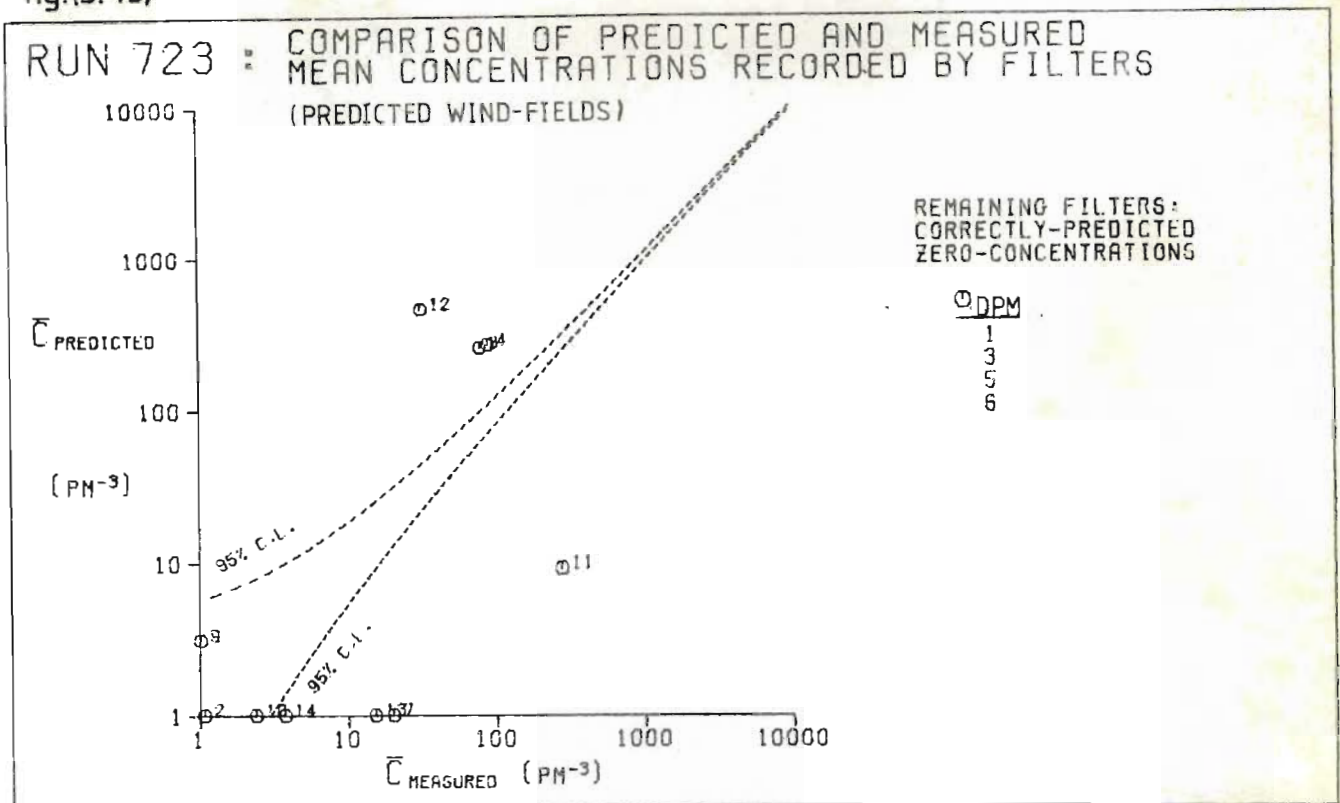


fig.(5.45)



recognised, though the model correctly predicts convergence over the bay at 04h30 and 06h00. Observed temporal transients tend to progress rapidly across the wind-field creating a temporary spatial incongruity. Since the wind-field model is based on steady-state continuity, the entire predicted wind-field responds immediately to the gradient-wind component detected at mast 9. Hence the modelled wind-field for 06h30 is based on the early response of mast 9 to a fresh westerly component, and is unrealistic through the remainder of the region. For complex synoptic weather variations, a more centrally-situated indicator mast would be desirable. The wind-field model grid-scale used in this application was relatively coarse (635 m). The detail of spatial variations will improve with smaller grid intervals.

Only masts 2, 3, 5, 8 and 9 actively supplied meteorological data during run 723, the remaining masts having been dismantled. Modelled wind-fields were supplemented with stability information using an inverse square interpolation amongst the available masts.

Comparison of the 10 m trajectories in fig. (5.43) with those calculated from the measured wind-field in fig. (5.41b) shows that the 30-minute interpolation periods between solved wind-fields have had a severe smoothing effect. The result is an almost monotonic gradual swing to the east, so that much of the complexity of the DPM solution, associated with shorter and more varied temporal transients, will be lost. Indeed, the concentration histograms in fig. (5.44) show simple traverses as the plume moves eastward, and the dual traverses at sites F5 and F6 are omitted [fig. (5.40)]. However, comparison of figs. (5.45) and (5.39) shows that the loss of the second traverse at F6 has led to a better estimate of filter 9 ($3,1 \text{ p m}^{-3}$ predicted, 0 p m^{-3} measured) whilst the slower traverse of F7 has given an improved estimate of filter 8 (256 p m^{-3} predicted, $77,4 \text{ p m}^{-3}$ measured). The only other filter concentration estimate to display a marked difference as a result of the modelled wind-field is that for filter 7, which decreased from 160 p m^{-3} to 0 p m^{-3} in comparison with $19,7 \text{ p m}^{-3}$ measured. In the measured wind-field, the final directional transient which carries the plume across site F8 is much larger, and thus induces more spread than in the predicted wind-field. This lateral spread contributes

significantly to filter 7, whereas the predicted wind-field gives no contribution.

Despite the lack of temporal detail in the predicted wind-fields, filter-concentration predictions are only slightly inferior to those for the measured wind-fields. It is likely that filter integration periods have absorbed shorter differences, though the effectiveness of the modelled wind-fields will certainly improve with better temporal resolution. The dominance of synoptic transients in run 723 has largely masked the ability of the wind-field model to predict local stable wind-currents.

CHAPTER 6

DISCUSSION

6.1 Motivation.

In the siting of new industries, or the establishment of pollution cause-effect relationships for existing industries, there is a growing demand for realistic predictive descriptions of the atmospheric transport behaviour. Variable point-source release is the fundamental emission mechanism, and is particularly relevant when individual industries are in question.

A review of existing approaches to the modelling of point-source releases in a variable environment showed serious shortcomings in temporal/spatial resolution and accuracy [section (1.6.4)]. Even for continuous sources, the assumption of steady-state behaviour during stable-weather pollution episodes will lead to unrealistic localisation of the effect. The temporal variability of both wind-fields and stability is clearly demonstrated by the observations in section (5.2). Although steady-state models such as those proposed by Hino (1968), Ito (1970), Ragland (1973), Roffman, Rao and Grimble (1975), Ragland and Dennis (1975), and Lebedeff and Hameed (1975) may provide accurate descriptions in a steady-state atmosphere, conversions of such models to temporally- and spatially-variant environments are fraught with approximations, not the least of

which is the neglect of lateral wind-shear.

More realistic attempts to simulate atmospheric transport using 3-dimensional grid models have been undertaken by Randerson (1970), Egan and Mahoney (1972b) and Shir and Shieh (1974). However, the coarseness of the solution grids in these models limits their useful application to large area-sources. Moreover, the satisfaction of stability criteria [equations (1.64), (1.65)] does not guarantee numerical accuracy.

The simple "trajectory" models presented by Leahey (1975) and Chu and Seinfeld (1975), in which vertical columns of air are advected at some mean effective velocity, suffer the disadvantage that they neglect wind-shear and horizontal diffusion. Hameed (1974b) and Liu and Goodin (1976) tackle the equivalent eulerian problem by performing mass-balances over adjacent vertical cells.

Resolution inadequacy in the grid models stems entirely from computation/storage limitations. By localising the solution in the neighbourhood of the diffusing material, lagrangian puff models offer a means of improving resolution. Such an approach was proposed by Lamb and Neiburger (1971), based on an analytical puff solution. However, the limitations of analytical puff descriptions [Quesada (1971), Saffman (1962), Chatwin (1968)] led to a decision in the present work to provide a numerical solution for the lagrangian puff.

6.2 Development of the dispersion model.

The prime difficulty encountered in the development of a generalised dynamic puff model was to retain the identity of each puff, the dimensions of which could become extended in any direction through the action of wind-shear. It became necessary to create a "proximate curve" which followed the mass-distribution, representing the position of a curvi-linear vertical solution grid. The distribution of each puff was resolved into this grid in the form of its zeroth, first and second moments. Solution for the diffusion and advection of moments parallel to the grid was performed numerically. By minimising wind-shear normal to this surface, the orthogonal distribution was adequately described as gaussian at any point in this surface. The "numerical diffusion" problems encountered by earlier models [Molenkamp (1968)] were avoided by introducing lagrangian shifts in the grid strata, or first moments, instead of solving for advection by finite differences. A stable "limiting value" method was developed in order to provide a fast, explicit solution for the diffusion step.

Peripheral procedures, such as locating the puff in eulerian space, and supplying it with representative velocity and diffusivity information, could to a large extent be controlled externally, for example, by improving the resolution of the available data. In order to establish the accuracy of the puff solution itself, it was compared with the analytical description of Quesada (1971)

and the moment description of Saffman (1962) [section (3.1)]. Comparison with the Quesada solution for linearly-sheared unbounded puffs showed a slight lag in the response of the numerical solution to wind-shear. Puffs resulting from a ground-level release in linear shear were constructed using the first three moments provided by Saffman. Agreement with the numerical solution was good, the dynamic puff model also showing pronounced positive skewness at ground-level, as predicted by Saffman.

The numerical puff solution was also used to simulate several published observations of experimental instantaneous releases, though the necessary wind and diffusivity profile information provided in the associated studies was rather poor [section (3.2)]. Although predicted concentration time-histories had the same form and spread as those observed by Nickola Ludwick and Ramsdell (1970) and Drivas and Shair (1974), the "leading edge" of predicted puffs generally arrived at measurement sites earlier than the observed puffs. Predictions near the source showed insufficient spread, probably as a result of initial inaccuracy following the "seeding" of the numerical solution with a gaussian puff [section (2.3.2)]. The continued development of a cloud as it passes an observation point tends to give positive skewness to the observed concentration-history, despite the fact that the cloud may have positive skewness with respect to downwind distance in the lagrangian frame. The contention of Drivas and Shair (1974), that positive skewness in

the observed concentration-history represents that predicted by Saffman (1962) for the lagrangian frame, is thus incorrect.

Further assessments of the validity of the puff solution were made by its application in continuous steady-state releases [section (3.3)]. Agreements with the gaussian plume formula (1.41) and a solution which included power-law variations in velocity and diffusivity [Peters and Klinzing (1971)] were good, though a slight deterioration was evident with increasing distance from the core of the plume. Since concentrations in these regions were low, the error introduced should not be significant. Reasonable agreement was also obtained with the numerical solution provided by Ito (1970).

The concentration distributions presented in section (3.4) illustrate the important redistribution effect of horizontal wind-shear. Material initially separated by a small vertical distance undergoes a large relative displacement in the horizontal. The continuous interaction of this mechanism with vertical diffusion leads to rapid horizontal expansion at heights affected even by low wind-shears. Observed mesoscale wind-fields under stable conditions show continuous temporal transients [section (5.2)]. Although these transients may be small over certain periods, the magnitude of the redistribution effect following a transition in shear direction indicates that it must be accounted for to avoid serious error in the distribution.

Numerical solution for the lagrangian puff allowed the inclusion of several removal mechanisms [section (2.3.4)].

The effect of ground-level absorption was approximated during each time-step by applying an adjustment factor profile based on an initially uniform vertical distribution. Although this assumption may appear crude, it has the advantage that the additional vertical transport induced by the mechanism occurs only as a result of the mechanism, allowing normal vertical diffusion to be dealt with separately. Illustrative solutions showed that sedimentation and ground-level absorption had a similar effect in moving the ground-level distribution forward, owing to the increasing importance of material carried forward by higher-velocity strata. On the other hand, uniform decay as in washout or chemical reaction led to a uniform "shrinking" of the cloud.

Several limitations are inherent in the formulated dynamic puff model:-

- (1) The model is based on the diffusion equation (1.39) which is only approximately valid for gradual spatial and temporal variations, and relatively short turbulence time-scales [section (1.4.1)].
- (2) The distribution normal to the proximate curve at any point is assumed to be gaussian, whereas significant skewness may develop with wind-shear in this direction [section (2.2.4)].
- (3) Variations in velocity, diffusivity and removal parameters encountered by the puff as it moves through eulerian space are assumed to apply immediately to the entire puff [section (2.2.3)].

- (4) The processes of advection and diffusion, and the various removal mechanisms, are assumed to act independently during each trajectory time-step [section (2.3.1)].
- (5) The validity of the solution in the lagrangian frame is dependent on the approximate linearity of the transformation \tilde{T}_p (2.8).
- (6) The expanded puff is located in eulerian space by fixing the proximate curve on three tracking points. This may lead to significant inconsistencies in wind-fields with strong streamline curvature [section (2.4.4.1)].
- (7) When the model is applied to continuous releases, position and distribution parameters are interpolated independently in space or time in order to locate additional puffs [section (2.4.1.2)].

Positional problems such as location, interpolation and determining the effective values of parameters stem from attempting to deal with the elongated puffs as lagrangian entities. Although measures could be taken to alleviate associated errors, they all involve much additional computation, and would detract from the viability of the approach.

Despite these limitations, it is felt that the importance of wind-shear, and the flexibility of the model in dealing with arbitrary spatial and temporal transients and removal mechanisms, justify the complexity of the solution.

The only means of gauging the benefits of such a model is by measuring it against the best possible form of some simpler model. As a result, a second lagrangian puff model was developed based on the analytical solution for a gaussian puff [appendix (A2)]. The only functional difference between this model and the dynamic puff model lay in the fact that velocities and diffusivities were fixed on the values at one specified height. Diffusivities determining the size of the puff at any point on its trajectory were based on the time-mean values experienced by it en route, whilst sedimentation could only be accounted for by allowing the eulerian vertical scale to slide upwards.

Initial tests showed vast differences in the concentration distributions predicted by the dynamic puff model (DPM) and the gaussian puff model (GPM) [section (3.4)]. For a continuous, steady release in a steady-state wind-field, this effect will be largely obscured by superposition, assuming that an optimum effective velocity is chosen for the gaussian puff. The fact that release-rates are often variable and wind-fields are always variable means that the GPM will normally under-predict the area affected.

It is frequently the case that the observer during a pollution episode is interested in short-period exposures and peak concentrations, for example, following an accidental release of some toxic or radioactive substance. Accurate knowledge of the distribution and its variation with time

will be indispensable . However, a more common requirement is for long-period dosage information during a steady release, and it might reasonably be expected that the relative performance of the GPM will improve in these applications. This is because the variability of trajectories over a long period provides an effective horizontal diffusion which absorbs much of the complexity of instantaneous distributions. The series of tracer experiments conducted in this study involved membrane filter measurements with dosage periods short enough to give some indication of the instantaneous distribution. Identical input information was supplied to the dynamic and gaussian puff models, their predictions revealing the expected limitations of the GPM despite its use in the dosage mode.

6.3 Description of the mesoscale system.

Whereas a simple dispersion model will not warrant a detailed meteorological description of the system, the development of a complex model which accounts for velocity and diffusivity variations demands suitable input information in order to be effective. Not only is the user of such a model faced with an additional computation cost, but he must provide detailed measurements or predictions of the atmospheric behaviour in order to benefit from it.

It has been pointed out that the successive improvement of dispersion models, incurring large computation and measurement costs, usually results in diminishing returns

owing to the essentially stochastic nature of atmospheric behaviour [section (1.10.2)]. However, there has been a recent trend for pollution-conscious cities and industries to undertake extensive air-monitoring programmes, so that the type of meteorological input required by sophisticated models is becoming more available. Further, Fortak (1974) points out that modern methods of stochastic dynamic prediction will eventually allow statistical forecasts, one or two days in advance, of mesoscale meteorology, whilst the deterministic prediction of mesoscale wind-fields shows promise as a source of detailed advance information [e.g. Scholtz and Brouckaert (1976) - section (1.3.1)].

During the tracer experiments conducted in the present work, detailed measurements of the wind-field and atmospheric stability were provided by a radio-telemetry system [section (4.2.2)]. Perhaps the most significant errors arising from the use of this data-base lay in the obvious limitations imposed on spatial resolution by the 9 meteorological stations. The value of a parameter required at some point in the region was estimated using a weighted interpolation scheme based on inverse-square distance from the measurement stations [Wendell (1972)]. This procedure can result in false divergence in the wind-field, and workers such as Endlich (1967), Dickerson (1973) and Liu and Goodin (1976) have proposed schemes designed to minimise divergence. Unless entire wind-fields could be stored at short time-intervals, these schemes would entail a large amount of computation during model execution, and for this reason

they were not included in the present work. Moreover, the relatively close mast spacing used during the experiments should minimise undefined wind-currents [fig. (4.4)].

In its present form, the dynamic puff model does not account for the possible variation of wind direction with height. Where this directional shear does not occur simply as a result of the Coriolis force ["Ekman Spiral"], it becomes necessary to define the vertical structure by such means as balloon sondes. Csanady (1972) conducted tracer experiments over 30 km, finding that the only significant deviations from expected gaussian distributions occurred in the presence of extreme cross-wind shear, and could not be attributed to the Coriolis effect. Since it is unlikely that the Coriolis effect will play a major part in boundary-layer diffusion over shorter ranges at mid-latitudes, and since measurements of other forms of directional shear are generally not available, the omission of directional shear is reasonable.

Another effect which complicates the true vertical structure arises from the inhomogeneity of typical terrain [section (1.2.2)]. As wind flows over a change in surface roughness, an internal boundary-layer develops which grows upwards at a rate of about 1/10 of distance downwind of the discontinuity [Panofsky and Townsend (1964), Taylor (1969)]. Peterson (1971) points out that significant errors may arise through assuming average values for the friction velocity u_* and roughness length z_0 over heterogeneous terrain. In the present simulation of tracer experiments

it was necessary to define a roughness-length distribution based on general classifications of surface-types [section (4.2.4)]. Related spatial variations in velocity and diffusivity profiles were assumed to act on the entire cloud immediately it entered a new region.

The velocity and diffusivity profiles used in the dynamic puff model were based on those suggested by Dyer (1974) [section (2.4.2)]. These profiles were extended for strong stability following the treatment of Webb (1970), and were assumed to apply throughout the surface layer. [Carl, Tarbell and Panofsky (1973)]. Horizontal diffusivity was related to vertical diffusivity using established relations for the Sutton diffusion parameters [Venter, Halliday and Prinsloo (1973)]. The defining parameters for the profiles were friction velocity u_* , Monin-Obukhov stability length L , and the roughness-length z_0 . Where measurements were provided by the radio-telemetry system, they were processed by a meteorology sub-model [appendix (A4)] to form readily-accessible point-histories of the profile parameters.

Stability measurements showed significant spatial variations, mainly resulting from the presence of a large water surface [Richards Bay] in the region of interest [section (5.2)]. The surface temperature lag caused by the convective distribution of heat in the water bulk resulted in relative instability over the water at night, and enhanced stability for up to 4 hours after sunrise. Similar observations were recorded by Munn and Richards

(1963). The interpolated stability field presented to the dynamic puff model was necessarily crude when the physical origin of the spatial variations is considered. However, the distribution of meteorological masts appears to have adequately defined the important influence of the water-surface. Under typical land-breeze conditions, tracer released at mast 9 [fig. (4.4)] would be carried across the bay at night, experiencing higher diffusivities and flatter wind-profiles than over the land surface.

In a separate report, Mulholland, Scholtz and Brouckaert (1977) present the 75-hour data-base which spans the 8 tracer experiments. This publication includes all of the emission, dosage and meteorological information used in the present work, as well as the estimated roughness-length distribution.

6.4 Simulation of tracer experiments using wind-field and stability measurements.

The aim of the tracer experiments was to define some of the complex transport behaviour which might be expected in a real spatially- and temporally-variant system. However, limitations in the number of membrane filters which could be sited, and in the frequency of filter changes, as well as the difficult task of anticipating atmospheric behaviour (despite the availability of "on-line" information), all provided obstacles to an ideal definition by measurement. Nevertheless, an attempt was made to site filters in areas particularly affected, and to renew them as often as possible

during temporal transients. The enormity of the task facing a single mobile filter-changing team can be gauged from the mean-concentration histograms presented in section (5.2).

Both the dynamic puff model (DPM) and the gaussian puff model (GPM) were employed to predict filter dosages, as well as selected concentration distributions. Although the predictions included a settling velocity of $1,64 \times 10^{-3} \text{ ms}^{-1}$, the effects of surface retention and fluorescence decay were neglected largely due to the lack of suitable information [section (5.1)]. Particle inertia and sedimentation were found to cause only negligible deviations from the diffusion behaviour of air. This was established for $3,74 \text{ }\mu\text{m}$ ZnSCdS particles under typical conditions of turbulence, using the diffusivity-ratio expressions of Peskin (1971) and Meek and Jones (1973) [section (4.1.4)].

The dynamic puff model has a fixed-parameter input in the sense that certain parameters such as release-time interval, solution grid-size and the size of the contributing margin around the region of interest, may be specified. The release-time interval spaces actually-solved puffs, solutions between these times being provided by interpolation. Depending on the speed of temporal transients, this parameter will determine the quality of the final solution. In fact, the DPM automatically defines features such as short releases, though a release-interval of 900s was commonly used in the simulations. This value was based on the availability of

averaged wind-field information at intervals of 180s [section (4.2.2)]. The filter-dosage solution for run 627 was performed using a release-time interval of 700s as well, in order to establish the sensitivity of the result to this parameter. Differences in predicted dosages were negligible, and it was concluded that the 900s interval provided an adequate description. The solution for run 630 was likewise found to be relatively insensitive to the lower weightings applied to masts 6 and 7, and the inclusion of a limited form of directional shear [section (5.2.2)].

The experiments conducted at Richards Bay, and the simulations thereof, are presented in full in chapter (5). Mulholland, Scholtz and Brouckaert (1977) present the dosage measurements and predictions in tabular form. The important differences between DPM and GPM predictions all resulted from the two-dimensional wind-shear present in a continuously varying wind-field. Temporal transients both induced new lateral wind-shear, and revealed existent longitudinal wind-shear in the diffusing material. Although the effect of shear is most striking in the concentration distributions presented in section (5.2), evidence of its contribution was also found in the filter-dosage predictions. Predicted concentration histograms at the filter sites showed that registered dosages occurred largely during relatively short plume traverses. The associated temporal transients produced significant spread in the DPM plume, whereas GPM predictions showed highly peaked concentrations over short periods.

Wind-field behaviour frequently displayed large directional oscillations in response to synoptic weather variations. One means of detecting the shear component was thus by filters positioned beyond the trajectory extremes of these oscillations. Thus filters No. 14 (run 705), 18 (705), 3 (714) and 4 (723) were so positioned and timed as to detect concentrations which the DPM accounted for, but which the GPM gave no indication of due to the absence of lateral shear.

During complete traverses, filters were occasionally timed so as to benefit from the upwind or downwind spread predicted by the DPM [7 (705), 8 (723)]. The tendency for sharp gaussian plume peaks to be centred in these concentration histories indicated that the GPM tracking height of 10 m was close to optimum for the 25,31 m release-height.

Although longitudinal shear in the original wind direction will play a part in subsequent traverses, the effect of this shear will become more important in variable releases. Hence the interruption of release between 01h54 and 03h06 during run 708 [section (5.2.4)] produced a large gap in the gaussian distribution. The ensuing temporal transient passed this gap over site F5, whereas the upwind and downwind longitudinal spread present in the DPM plume [fig. (5.21a)] contributed correctly to filter 7 (708) at this site. However, longitudinal spread was apparently underestimated in the instantaneous release of run 722 [section (5.2.7)]. At site F2, some 3700 m from the

source, significant concentrations were recorded for more than 20 minutes. As expected from the relatively flat velocity profiles accompanying instability, the bulk of the material traversed the receptor sites during the short period predicted by the DPM. The low concentrations recorded thereafter were not predicted by the DPM, and it is possible that they arose through an elution mechanism associated with stagnant regions within vegetation and amongst buildings.

The high concentration gradients present under stable conditions demand an accurate wind-field description if concentration distributions are to be predicted correctly. Where aspirated filters integrate entire traverses, positional errors will be less obvious. However, a few cases were observed where concentrations measured on the extremes of directional oscillations were incorrectly predicted by both the DPM and the GPM, and where the measured concentrations could not be accounted for by the interpolated wind-field [8 (630), 9 (630), 28 (630), 29 (630), 13 (711), 19 (711)]. These discrepancies may result from a variation of wind direction with height. Such directional shear would tend to shift the cloud centroid away from its expected trajectory based on ground-level wind directions. The associated positions would also be sensitive to slight positional errors in the estimated trajectories, due to inadequate spatial resolution in the measured wind data. Nevertheless, the infrequent significance of such errors would not justify the expensive task of providing better spatial resolution.

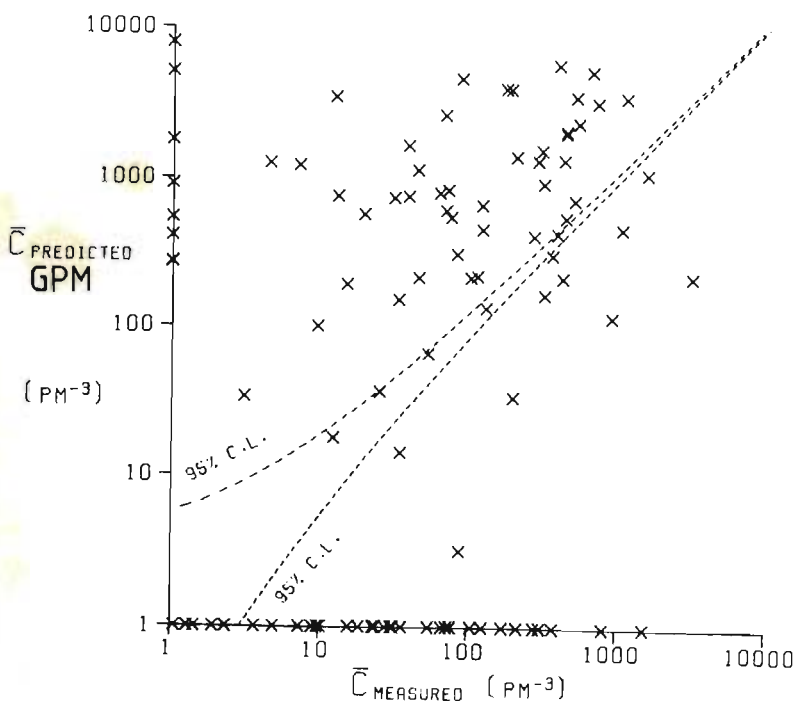
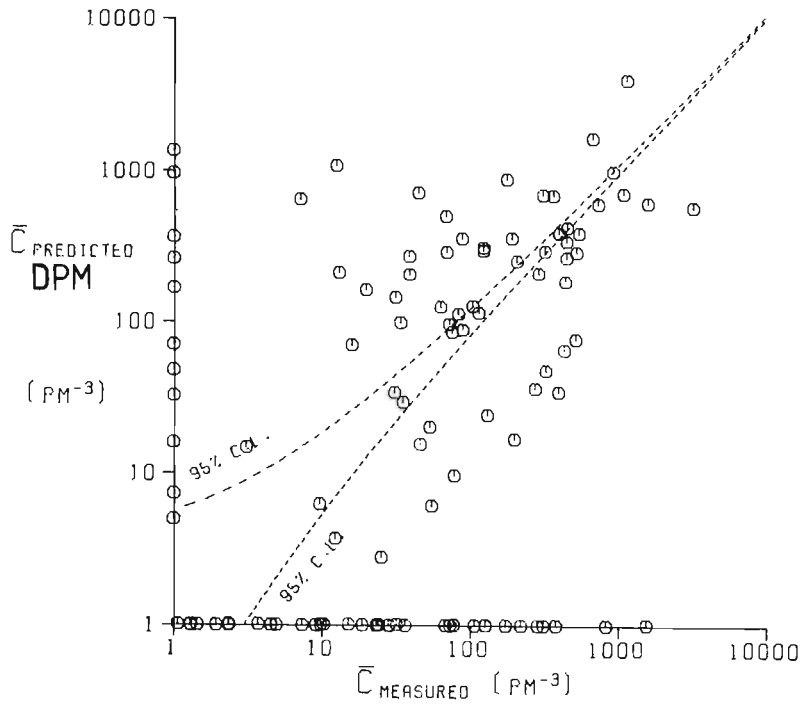
Although the effects of spatial and temporal variations in stability were easily identified in GPM distributions, they were less obvious in DPM distributions due to the masking effect of wind-shear. The ground-level distribution at 08h25 in run 630 [section (5.2.2)] shows that the gaussian plume expands as it passes over the unstable region near mast 2, whereas the more obvious effect in the DPM plume is a smaller lateral spread in the section affected by the flatter wind profiles over this area during the traverse. Concentration profile measurements at mast 3 during run 627 [section (5.2.1)] showed a significant increase of concentration with height some 3000 m from the source. The effect of instability over the bay at night, or during fumigation after sunrise, will be to mix this material down to ground-level, as well as provide additional horizontal spread.

In attempting to assess overall model performance, several reservations are in order. Seinfeld (1975) suggests that models do not as yet provide predictions which are commensurate with observation, so that comparisons to date have been based on qualitative rather than formal statistical methods. In fact, workers such as Shir and Shieh (1974), Ruff and Fox (1974), and Fabrick and Sklarew (1975) quote coefficients of correlation between predicted and observed concentrations. However, the magnitude of the correlation coefficient only indicates the degree to which comparison points lie on any straight line, and mean relative error, or standard deviation, are probably better performance indices [Hameed (1974a), Lebedeff and Hameed (1975)]. A

further obstacle to providing a common basis for comparison lies in the fact that models must work from the same database and predict the same data quantities in order to be comparable. Hence GPM predictions may be expected to improve relative to DPM predictions as dosage periods (averaging times) are increased. Moreover, applied studies such as those of Randerson (1970), and Shir and Shieh (1974) deal with multiple-source or area-source problems. In such systems, spatial concentration variations are likely to be smooth, so that observations and predictions will display none of the spatial and temporal sensitivity of the point-source problem. For example, a comparative study presented by Lebedeff and Hameed (1975), for SO_2 transport in Nashville, displays only gradual variations in predicted and observed concentration, the latter varying only seven-fold in the available data.

Observed pollutant concentrations are generally found to have log-normal frequency distributions, regardless of averaging time, though Bencala and Seinfeld (1976) could only explain this phenomenon directly in terms of the near log-normality of wind-speed distributions. The high spatial concentration gradients in the present work have revealed the full extent of this range, and predicted and measured mean concentrations are most conveniently plotted on logarithmic scales. The combined results for all simulations using measured wind-fields [section (5.2)] are presented in fig. (6.1). Once again, predicted and measured concentrations have been restricted to a threshold of 1 particle per

fig. (6.1) Combined results – Dynamic Puff Model and Gaussian Puff Model predictions for mean filter concentrations



cubic metre, whilst the numerous filters for which both predicted and measured values were below this threshold have been omitted.

It is interesting to note in both the DPM and GPM comparisons that significant concentrations were more often measured and not predicted, than predicted and not measured. It is likely that this effect arises from the lack of definition for smaller wind-currents which would have given greater variability to the true trajectories.

table (6.1) ANALYSIS OF DPM AND GPM COMBINED PREDICTIONS.

	LOGARITHMIC SCALE			LINEAR SCALE	
	Correlation Coefficient	R.M.S. Error [$\log_{10}(\bar{C} \text{ p m}^{-3})$]	R.M.S. Error [Concn. Factor]	Correlation Coefficient	R.M.S. Error [p m^{-3}]
DYNAMIC PUFF MODEL	0,364	1,233	17,1 ×	0,733	1714
GAUSSIAN PUFF MODEL	0,274	1,495	31,3 ×	0,677	14030

Table (6.1) presents a limited comparison of the DPM and GPM in terms of correlation coefficients and standard deviation of the predictive error. These parameters are based on predicted and measured values as plotted in fig. (6.1). The low positive correlation coefficients for the logarithmic scale arise from the poorly-defined positive

gradient in the scattered data. Since the measurements may have been relatively concentrated about a particular value, say 200 p m^{-3} , it is really only the mean error, or R.M.S. error, that will provide an indication of model performance.

Based on the logarithmic scale, the DPM gives a 17-fold R.M.S. error whilst the GPM gives a 31-fold R.M.S. error. Although the threshold values have contributed quite heavily to these indices, GPM predictions are seen to be too high in general, whilst DPM predictions straddle the region enclosed by the 95% confidence limits for the measured concentration. In the tracer experiments, attempts were made to define the spatial distribution of tracer by concentrating receptors in the currently-affected region. The simplified view of the wind-field presented to the GPM, together with the lack of wind-shear, probably acted to maintain high GPM predictions in this limited area, imposing a bias in the available data.

No study was found which was directly comparable with the present point-source simulation. However, Shir and Shieh (1974) used a 3-dimensional grid model to predict the transport of SO_2 from multiple point and area sources in St. Louis. Plots of predicted vs. measured 24 hr-averaged SO_2 concentrations showed similar scatter to the DPM predictions in fig. (6.1), though the log-scale correlation coefficient was somewhat higher at 0,81, dropping to 0,71 for 2 hr-averages. Linear-scale correlation coefficients for both averaging periods were lower than the corresponding

DPM value. It is likely that the 5000 ft. horizontal interval in the grid model imposed a severe limitation on spatial resolution.

Shir and Shieh (1974) performed parallel simulations using a gaussian plume model, obtaining predictions which were generally too high, in much the same way as the present GPM predictions are higher than observations. Despite this shift in the present GPM results, relative spread was only slightly greater than in the DPM predictions, and a study was undertaken to identify parameters which might contribute to the deviation of DPM predictions from observations.

Some 15 variables were prescribed in such a way that they could be quantified for each filter. The selected variables were divisible into 6 broad categories.

- (i) Probability : measured concentration;
- (ii) Weather : mean wind-speed, stability, rate of change of wind direction;
- (iii) Wind-field definition : mean R.M.S. distance from meteorological masts en route to filter;
- (iv) Sedimentation : distance to filter, time of travel to filter;
- (v) Terrain : mean surface properties en route, fraction water surface;
- (vi) Operation : number of filters previously mounted/dismounted during run (fatigue errors), battery usage (aspirator reliability).

The quality of each filter-concentration prediction was represented by the parameter $\log(\bar{C}_{\text{predicted}}/\bar{C}_{\text{measured}})$, which was plotted against each of the 15 "influencing" variables. The only clear trend to emerge from this analysis was the expected convergence of the ordinate to zero for large measured concentrations, due to reduced sample variance [section (4.1.5.3)]. $\log(\bar{C}_p/\bar{C}_m)$ possibly decreased slightly with increasing time-of-travel to the filter. Since the associated travel-times were generally less than 2 hrs., this discrepancy may arise from an under-estimation of sedimentation velocity. For the GPM predictions, a plot of $\log(\bar{C}_p/\bar{C}_m)$ against potential temperature gradient showed increased positive deviation as well as greater variability as stability increased. The inferior performance of the GPM in a stable environment follows from its neglect of wind-shear.

The absence of any obvious cause for DPM discrepancies tends to preclude any refinement of the model based on the present data. Even the measure of wind-field definition, based on the mean R.M.S. distance of trajectories from the meteorological masts, showed no relationship to deviations. Despite the detailed nature of the DPM, it seems that random atmospheric variations will always impose appreciable random deviations on deterministic predictions. Nevertheless, DPM predictions do represent an improvement on GPM predictions, and this improvement may be expected to become more significant for shorter sampling periods.

The P.I.C. column model [appendix (A3)] appeared to describe the dosage distribution adequately, provided dosage periods were long enough to include smoothing temporal variations. Spatial resolution in the estimate may be improved by decreasing cell-size and increasing trajectory frequency, though any improvement on the GPM point-dosage predictions will clearly be fortuitous. Although the P.I.C. method is restricted to spatial distributions of dosage, it requires less computation in this application, and such distributions are often of more interest to planners.

The present dynamic puff model serves a purpose in revealing the extent and origin of shortcomings in simpler models. However, its use in routine pollution surveys and assessments may not be justifiable in terms of cost and benefit at present. Even if meteorological information of commensurate quality were available, the DPM requires some five times the computation required by the GPM. In the tracer experiment dosage simulations of section (5.2), DPM computer process time on a Burroughs 5700 machine ran at approximately 2 times the real dissemination period in each experiment. Tests on an IBM 360/155 computer indicated that execution time would be reduced to about 1/8 of that on the B5700, though the cost would remain considerable at present process-time rates.

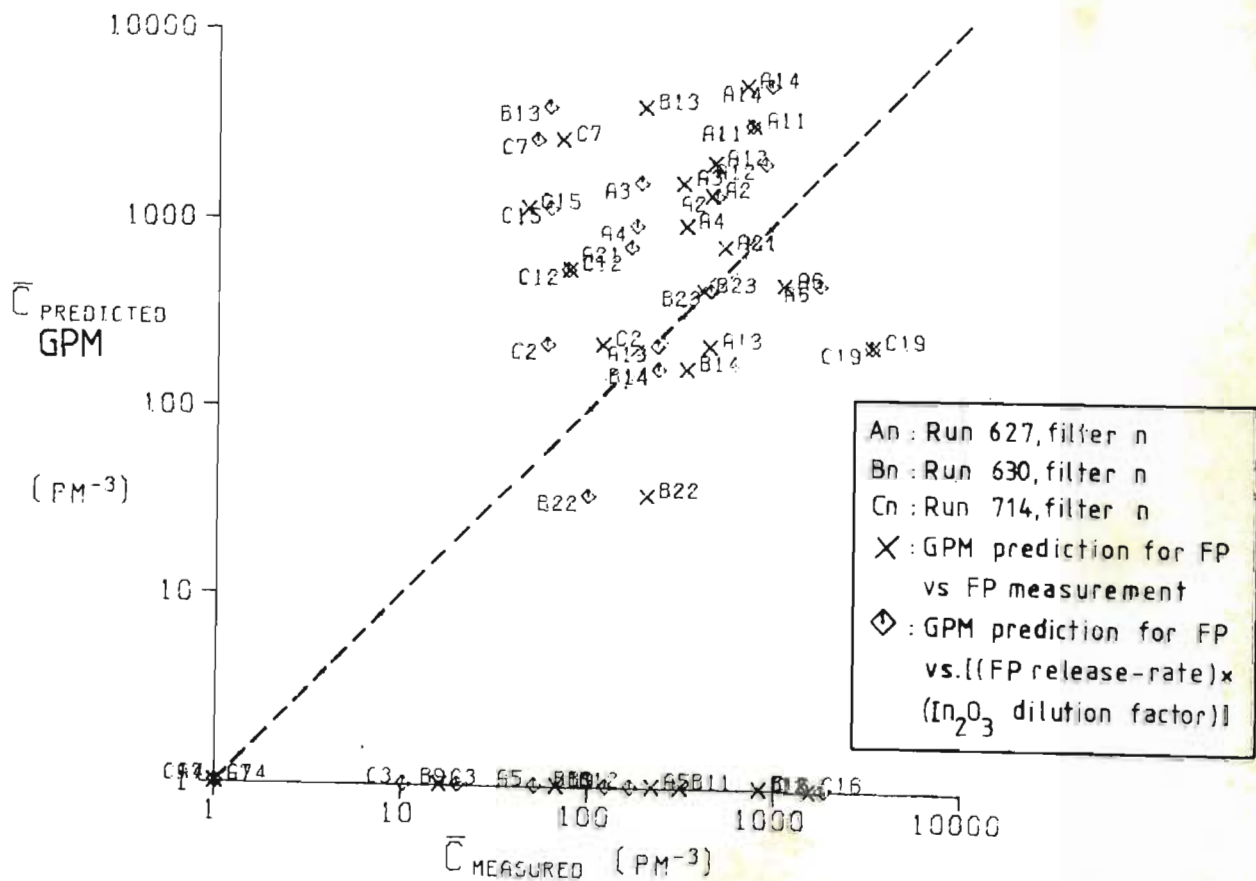
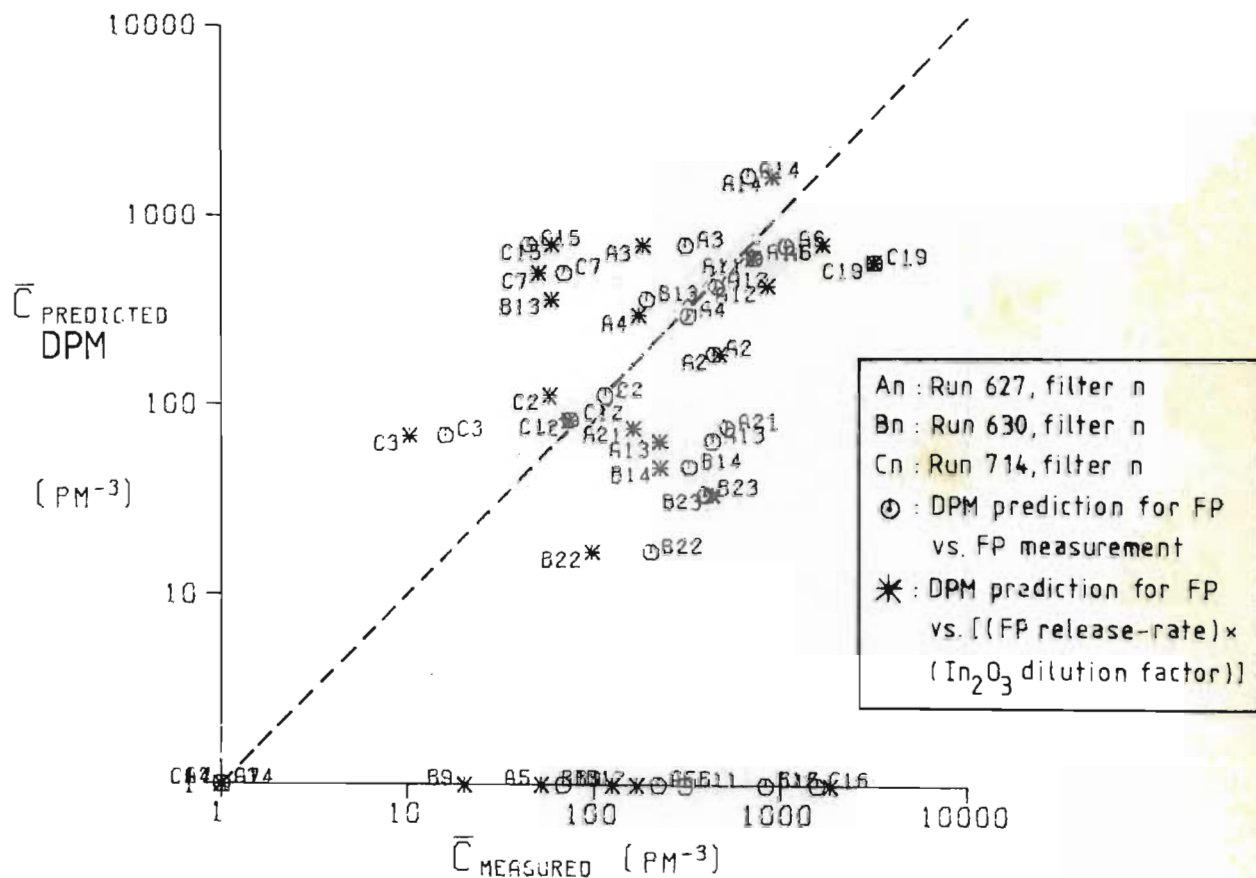
Nevertheless, the unique ability of the DPM in predicting short-period dosages and spatial concentration distributions will be important even when minimal meteorological

information is available. The recognition given to underlying physical processes should prove invaluable in the simulation of contentious pollution incidents. As pointed out by Hameed (1975), attempts to account for these processes should only be abandoned once it can be shown that a simpler model consistently provides results of equivalent quality.

6.5 Comparison with indium oxide tracer measurements.

During the experimental runs described in chapter (5), an indium oxide tracer was released simultaneously with the ZnSCdS (FP2267) tracer, at a point separated by only 1 m from the F.P. source. In the dissemination method devised by Norden and van As (1977a), an indium chloride solution in ethanol was used to fuel a high-temperature burner supported at 24 m on mast 9 [fig. (4.4)]. The resultant oxide was formed as a fine powder with mean particle size about 0,1 μm . Although release rates of $4,94 \times 10^{-3} \text{ g In s}^{-1}$ eliminated the low particle-count significance problems discussed in section (4.1.5.3), the indium displayed a threshold detection limit in the region of the same dilution factor (concentration/release-rate) represented by the 1 p m^{-3} threshold of the FP tracer. Despite the 0,65 μm pore-size of the cellulose acetate membrane filters, virtually all of the small In_2O_3 particles were retained, probably electrostatically. After the FP counts, filters were analysed for indium by neutron activation [Norden and van As (1977b)].

fig. (6.2) Indium oxide tracer : Predicted versus Measured mean filter concentrations using In_2O_3 dilution factors



Differences between recorded F.P. and In concentrations should only arise through dissimilar sedimentation/deposition behaviour, and on statistical grounds (low particle counts). Observed dilution factors [concentration/release-rate] seldom differed by as much as two-fold, F.P. dilution factors showing a tendency to be higher. For typical trajectory travel-times of 2 hrs., F.P. sedimentation velocities of about $1,64 \times 10^{-3} \text{ m s}^{-1}$ will enhance ground-level concentrations, and this is probably the origin of observed differences. In order to compare the indium tracer measurements with model predictions, they have been converted to effective F.P. concentrations by multiplying In dilution factors by the mean F.P. release-rate. Comparisons with DPM and GPM predictions for the available In analyses are presented in fig. (6.2). Both DPM and GPM predictions appear to be in slightly better agreement with In-based measurements than with the F.P. measurements [table (6.2)].

table (6.2) ANALYSIS OF DPM AND GPM PREDICTIONS
FOR INDIUM-BASED MEASUREMENTS.

	LOGARITHMIC SCALE		
	Correlation Coefficient	R.M.S. Error [$\log_{10}(C \text{ pm}^{-3})$]	R.M.S. Error [Concn. Factor]
DPM Predictions vs In-Based Concn.	0,479	1,113	12,96 ×
DPM Predictions vs FP Concn.	0,359	1,266	18,47 ×
GPM Predictions vs In-Based Concn.	0,491	1,235	17,16 ×
GPM Predictions vs FP Concn.	0,392	1,345	22,11 ×

Figure (6.2) shows that GPM predictions for In-based concentrations remain too high in general, leading to a 17-fold R.M.S. error as opposed to the 13-fold R.M.S. error of the DPM predictions. Of course, both DPM and GPM predictions include the $1,64 \times 10^{-3} \text{ m s}^{-1}$ sedimentation velocity expected of $3,6 \text{ }\mu\text{m}$ ZnSCdS particles. It was suggested in section (6.4) that this effective sedimentation velocity may have been slightly low in terms of the collected particles. It is possible that the negligible sedimentation velocities of the In_2O_3 particles have thus led to better agreement with model predictions.

6.6 Simulation of Run 723 using predicted wind-fields and stability measurements.

It has been pointed out that inverse square interpolation for the wind-field [Wendell (1972)] may lead to false divergence [section (1.3.2)]. The only means of accounting for such local effects as katabatic flows, land-sea breezes and topographically-induced currents is by direct use of a suitable wind-field model. Whereas a model such as that proposed by Scholtz and Brouckaert (1976) will provide a rational description in terms of input information, direct measurements at a number of points in the area can outweigh the advantages of wind-field integrity. Best descriptions are probably provided by compromise schemes in which, for example, divergence is minimised subject to a number of

point-measurements [Endlich (1967), Dickerson (1973), Liu and Goodin (1976)].

Nevertheless, the objective of the Scholtz and Brouckaert wind-field model was to provide the best estimate based on a minimum of meteorological information, and it was used in this mode for simulation of the wind-fields in run 723 [section (5.3)]. The chief disadvantage of the model, as used, lay in the limitation on temporal resolution imposed by storing complete wind-fields at 30-minute intervals. In fact, if a continuous indication of the synoptic gradient-wind were available, this limitation would easily be rectified: Resultant wind-fields are obtained by linear combination of standard flow-potential fields, the various factors depending on gradient wind and temperature. The velocity at any time could be evaluated quite speedily by performing the calculation as required, so that only the potential fields would need permanent storage.

However, the predicted wind-fields would still represent a series of steady-state solutions. In order to minimise the effect of the fast-moving spatial discontinuity which usually accompanies synoptic transients, the gradient wind component should preferably be detected centrally in the region of interest.

The smoothed temporal variations in the interpolated velocities supplied to the dynamic puff model reduced the wind-shear contributions usually predicted by this model. However, filter concentration predictions were only slightly

worse than those predicted using the measured wind-field [section (5.2.8)]. Differences in the predictions were probably largely absorbed by the long filter integration periods.

The ability of the wind-field model to predict local stable wind-currents was largely masked by the dominant synoptic transients in run 723. Improved temporal resolution and central gradient-wind detection will provide a realistic overall representation of the wind-field. In conjunction with the dynamic puff dispersion model, it should then be possible to provide an unparalleled description of mesoscale atmospheric transport, based on the limited meteorological information which is usually available.

CHAPTER 7.

CONCLUSIONS

A review of current approaches to the modelling of atmospheric dispersion showed serious resolution limitations, or neglect of temporal transients and wind-shear. In order to simulate transport from a variable point-source in an arbitrary environment, it became necessary to solve for serially-released lagrangian puffs on a "subgrid" scale.

Numerical solution for the zeroth, first and second moments of the puff distribution in a positioned lagrangian frame allowed the incorporation of variable diffusion, horizontal wind-shear, sedimentation, ground-absorption, washout and first-order chemical reaction. The validity of the puff solution was established by comparison with certain analytical and numerical solutions for instantaneous and continuous point sources, as well as by simulation of instantaneous release experiments presented in the literature. In particular, it was found that the combined action of wind-shear and vertical diffusion spread material over a much larger area than is suggested by the popular gaussian distribution. This effect is especially important when a temporal variation in wind direction induces shear in a second dimension.

A new dissemination technique for ZnS-CdS particulate tracer was developed, based on the spraying of an acetone suspension. In a series of field experiments, detailed wind-field and stability information was provided by a radio-

telemetry system. Recorded velocities showed continuous temporal transients in the region. Although long filter dosage periods absorbed much of the complexity of concentration distributions predicted by the dynamic puff model, predicted dosages showed evidence of extensive wind-shear. Neglect of wind-shear in an equivalent gaussian puff model gave localised concentrations which were generally much higher than observations, leading to R.M.S. predictive errors about twice those of the dynamic puff model for both zinc-cadmium sulphide and indium oxide tracers.

The high concentration gradients associated with a point source in a stable environment gave the predictive problem great spatial sensitivity. Undefined random atmospheric currents appear to have acted on these gradients to cause significant deviation from predictions. Since more detailed wind-field measurements are generally not possible, it seems that observations will always display an appreciable random deviation from deterministic predictions.

Nevertheless, it is the mean quantities predicted by deterministic models which are of interest to planners and industrialists. The only obligations left with the modeller are to represent the wind-field as accurately as possible, and simulate the transport processes as realistically as possible. It is frequently the case that only minimal meteorological information is available. As a result, a wind-field model has been developed by Scholtz and Brouckaert (1976) to account for the effects of topography and temperature anomalies in determining spatially-

variant velocities. Wind-fields predicted by this model were used in the simulation of one tracer experiment, producing filter dosage predictions only slightly inferior to those predicted using the measured wind-fields.

The performance of the simpler gaussian puff model, or even the particle-in-cell column model, may be expected to improve for longer dosage periods. However, under typical conditions the neglect of wind-shear in these models will lead to serious error in predicted short-period distributions and peak concentrations. In contentious issues such as the accidental release of radioactive material, the dynamic puff model will provide a class of information that is not presently available from any other source.

APPENDIX

CHAPTER A1

DYNAMIC PUFF MODEL

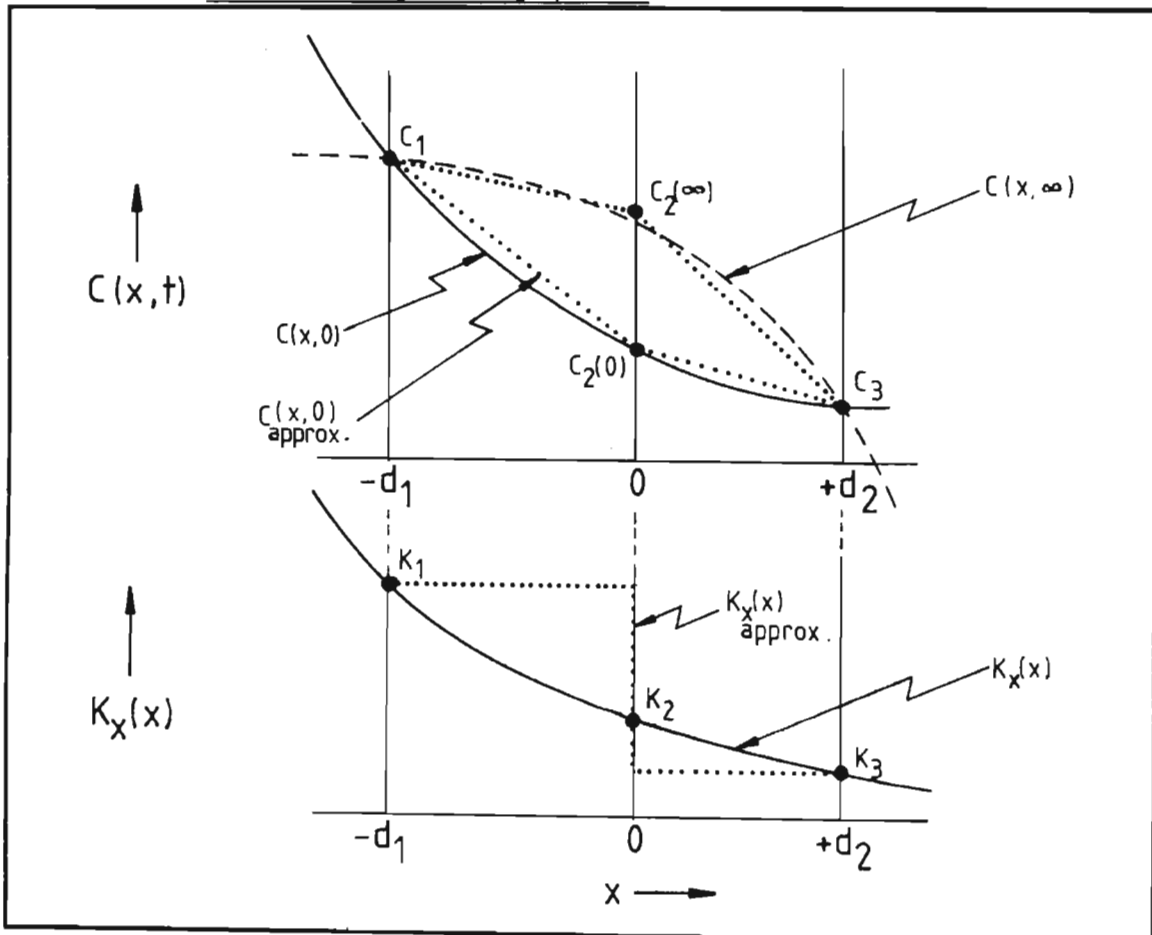
A1.1 Solution for the diffusion step: limiting value method.

Consider the case of linear diffusion defined by

$$\frac{\partial C}{\partial t} = \frac{\partial}{\partial x} \left[K_x(x) \frac{\partial C}{\partial x} \right] \quad (\text{A1.1})$$

The concentrations and diffusivities at three neighbouring points may be represented as in figure (A1.1).

fig. (A1.1) Concentrations and diffusivities at three neighbouring points



Interest lies in the adjustment of the central point $C(0,t)$ under the constraint of fixed boundary-values (but variable gradients). For example, if K_x were constant, $C(0,\infty)$ would lie on the straight line joining $C(-d_1,0)$, $C(d_2,0)$. In general, $C(x,\infty)$ must satisfy the condition of constant flux through the region. The boundary conditions are:

$$\left. \begin{array}{l} C(-d_1,t) = C_1 \\ C(d_2,t) = C_3 \end{array} \right\} 0 \leq t < \infty \quad (\text{A1.2})$$

and the initial condition is the otherwise arbitrary form of $C(x,0)$, where $C_2 = C(0,0)$. However, more information is necessary in order to solve for the distribution $C(x,t)$, and this is provided in the form of the hypothesis that the rate of change of $C(x,t)$ is proportional to its deviation from the equilibrium value $C(x,\infty)$.

$$\frac{\partial C}{\partial t} = a [C(x,\infty) - C(x,t)] \quad (\text{A1.3})$$

For the above initial condition, equation (A1.3) may be solved to obtain

$$C(x,t) = C(x,\infty) [1 - e^{-at}] + C(x,0)e^{-at} \quad (\text{A1.4})$$

so that the problem reduces to finding "a" which satisfies equation (A1.1). From equation (A1.1), $C(x,\infty)$ must observe

$$K_x(x) \frac{\partial C}{\partial x} = \text{const.} \quad (\text{A1.5})$$

The solution may be simplified by replacing $K_x(x)$ [fig. (A1.1)] with an approximate step function

$$K_x(x) \approx \begin{cases} K_x(-d_1) = K_1, & -d_1 \leq x \leq 0 \\ K_x(+d_2) = K_3, & 0 < x \leq d_2 \end{cases} \quad (\text{A1.6})$$

Then, for the boundary-conditions (A1.2), equation (A1.5) solves to give

$$C(x, \infty) = \begin{cases} B_0 \left[\frac{x}{K_1} + \frac{d_1}{K_1} \right] + C_1, & -d_1 \leq x \leq 0 \\ B_0 \left[\frac{x}{K_3} + \frac{d_1}{K_1} \right] + C_1, & 0 < x \leq d_2 \end{cases} \quad (\text{A1.7})$$

where $B_0 = (C_3 - C_1) / \left(\frac{d_1}{K_1} + \frac{d_2}{K_3} \right)$

Now integrate equation (A1.1) with respect to x to obtain

$$\int_{-d_1}^{d_2} \frac{\partial C}{\partial t} dx = K_x(d_2) \frac{\partial C}{\partial x} \Big|_{d_2} - K_x(-d_1) \frac{\partial C}{\partial x} \Big|_{-d_1}$$

Substitution using equation (A1.4) and solution for "a" yields

$$a = \frac{K_x(d_2) C'(x, 0) \Big|_{d_2} - K_x(-d_1) C'(x, 0) \Big|_{-d_1}}{\int_{-d_1}^{d_2} [C(x, \infty) - C(x, 0)] dx} \quad (\text{A1.8})$$

where the prime indicates the x -derivative. A further approximation is now made in that the initial distribution $C(x, 0)$ is represented as the linear interpolation:

$$C(x, 0) \approx \begin{cases} C_2 + (C_1 - C_2)(-x/d_1), & -d_1 \leq x \leq 0 \\ C_2 + (C_3 - C_2)(x/d_2), & 0 < x \leq d_2 \end{cases} \quad (\text{A1.9})$$

Substitution of equations (A1.7) and (A1.9) in equation (A1.8) leads to

$$a = 2 \left[\frac{K_3 d_1 + K_1 d_2}{d_1 d_2 (d_1 + d_2)} \right] \quad (\text{A1.10})$$

and at the point of interest ($x=0$), equation (A1.4) gives

$$C(0,t) = C(0,0) + \left[\frac{(C_3 - C_1)}{\left(1 + \frac{K_1}{K_3} \cdot \frac{d_2}{d_1}\right)} + C_1 - C_2 \right] (1 - e^{-at}) \quad (\text{A1.11})$$

Clearly, the accuracy of this result would improve if the boundary-values $C(-d_1,t)$, $C(d_2,t)$ were allowed to vary in time, though this is impossible without further information about the distribution surrounding the considered cell. The accuracy of $C(0,t)$ improves if the boundary-values used are those predicted at $\frac{1}{2}t$, also using equation (A1.11), and this is the procedure followed in the present solution. Notice from equation (A1.11) that this "limiting value" method will be unconditionally stable.

A1.2 Storage and interpolation of variables.

In section (2.4.2) it was concluded that the system could be adequately defined for heat, mass and momentum transfer using the following spatially- and temporally-variant parameters:

$U_{z_G}(x,y,t)$	x-velocity at height z_G
$V_{z_G}(x,y,t)$	y-velocity at height z_G
$\bar{\theta}'_{z_G}(x,y,t)$	potential temperature gradient $\partial\bar{\theta}/\partial z _{z_G}$
$L^{-1}(x,y,t)$	inverse Monin-Obukhov stability length
$z_0(x,y)$	roughness length
$d(x,y)$	zero-plane displacement
$w_d(x,y)$	deposition velocity representing ground absorption

The variables z_0 , d and w_d are always stored as discrete values in 2-dimensional (xy) arrays. This makes for easy acquisition of a value at (x,y) by two-dimensional linear interpolation.

For the time-variant quantities, two modes of storage are allowed by the meteorology sub-model [appendix (A4.2)]:

- (i) As three-dimensional discrete-value arrays A_{ijt} .
[A series of x-y grids representing values at specified times t_k].
- (ii) As discrete time-histories at a limited number of points with arbitrary positions (x_i, y_i) .

In the case of storage as A_{ijt} (i), values at (x,y,t) are easily extracted using a 3-dimensional linear interpolation. However, a more sophisticated interpolation is required to deal with the arbitrary positions of the discrete time-histories (ii). Though values are linearly interpolated with respect to time in the time-series, an inverse-square interpolation [Wendell (1972), equation (1.35)] is used in x-y space. As pointed out, this method may lead to false divergence in the wind-field. If the correcting schemes proposed by Endlich (1967), Dickerson (1973) or Liu and Goodin (1976) were employed [section (1.3.2)] computer-time would escalate. In the applications of the dispersion model to date, however, arbitrary-point time-series measurements have represented the wind-field with fair resolution, and such false divergence is not expected to be an important consideration. A provision is made in the inverse-square interpolation scheme for the weighting of contributions from individual space-points. In this way, for example, measurements made in a poor location may be weighted-down with respect to other measurements.

Because of computer-storage limitations, the three-dimensional grid storage A_{ijt} will have crude spatial or temporal resolution in most applications. In particular, if these measurements were derived from a limited number of spatial points, this means of storage would prove most inefficient in comparison with the arbitrary-point time-histories storage (ii). However, if information is to be supplied by a wind-field sub-model such as that of Scholtz

and Brouckaert (1976) [section 1.3.1], it will normally prove necessary to use the A_{ijt} input.

Current interpolated values of U_{zG} , V_{zG} , L^{-1} , $\bar{\theta}'_{zG}$, z_0 , d and w_d are supplied by dedicated sub-routines in the dispersion model. Friction velocity, and finally the values of $U(z)$, $V(z)$, $K_x(z)$, $K_y(z)$ and $K_z(z)$ are supplied by further sub-routines according to equations (2.72) to (2.75).

A1.3 Release-time sequence.

A1.3.1 Simulation of motion.

In general, the position of the centroid (for example) of a cloud will be a function of atmospheric diffusion and wind-shear. Thus Saffman (1962) showed that for a ground-level instantaneous release with linear shear, the ground-level centroid at \bar{X} could be expected to accelerate as $\bar{X} \sim t^{\frac{3}{2}}$ [equation (1.59)]. Under the arbitrary conditions to which the dispersion model is to be applied, it is in fact necessary to solve for the growth of each puff in order to be certain that it will or will not contribute to the concentrations or dosages in the region-of-interest. The idea of a region-of-interest was conceived both to enhance solution resolution and to reduce computation by limiting the release-periods which would actually have to be solved for. The approach in this model is thus to estimate the "position" of a cloud approximately, and then to allow an

additional specifiable space- or time-margin which will account for contributions from neighbouring clouds by shear or diffusion.

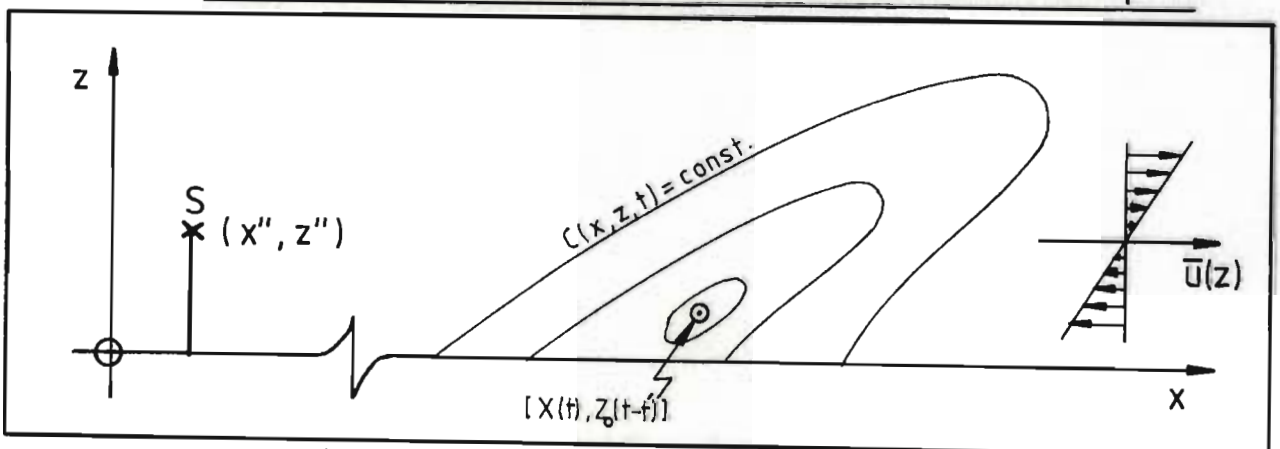
The objective is to define some optimal height $Z_0(t-t')$, such that a "particle" released with the puff at (x'', y'', t') , and moving with xy-velocity $[\bar{u}(x, y, Z_0), \bar{v}(x, y, Z_0)]$, thus having a position determined by the lagrangian integral

$$[X(t), Y(t)] = [x'', y''] + \int_{t'}^t [\bar{u}\{X(\tau), Y(\tau), Z_0(\tau-t'), \tau\}, \bar{v}\{X(\tau), Y(\tau), Z_0(\tau-t'), \tau\}] d\tau, \quad (A1.12)$$

will remain close to the region of the puff-distribution which is of "maximum interest". At the outset, note that necessarily $Z_0(0) = z''$, the release height.

Consider, at time t , the 2-dimensional (xz) distribution of a puff which was released at (x'', y'', z'', t') [fig. (A1.2)]

fig.(A1.2) Concentration distribution for a two-dimensional puff



For the case of a unit release and a vertical diffusivity K_z which is invariant with height, equation (1.53) may be used to solve for the zeroth x-moment as

$$\theta_0(z,t) = [4\pi K_z \cdot (t-t')]^{-\frac{1}{2}} \left[\exp\left\{-\frac{(z-z')^2}{4K_z(t-t')}\right\} + \exp\left\{-\frac{(z+z')^2}{4K_z(t-t')}\right\} \right] \quad (A1.13)$$

Note that this result is independent of wind-shear. By differentiation of equation (A1.13) it is found that the vertical distribution has a maximum at

$$Z_{\max} = [z' - 2K_z \cdot (t-t')]^{\frac{1}{2}}$$

Further, multiplication of equation (A1.13) by z and integration from 0 to ∞ gives the vertical centroid

$$\bar{Z} = 2 \left[\frac{K_z(t-t')}{\pi} \right]^{\frac{1}{2}} \exp\left[\frac{-z'^2}{4K_z(t-t')} \right] + z' \operatorname{erf}\left[\frac{z'}{2\sqrt{K_z(t-t')}} \right]$$

Whereas the velocity at \bar{Z} should approximate to the bulk movement of the distribution, the velocity at height Z_{\max} will represent the dominant region of the distribution - an important consideration as far as ground-level concentrations are concerned. Numerous attempts to find an optimum form of $Z_0(t)$ have centred on combinations of \bar{Z} , Z_{\max} , such as $Z_0 = (\bar{Z} + Z_{\max})/2$, but this approach has always shown eventual deviation from true puff behaviour. The method outlined below accounts for the degree of wind-shear, and has proved quite successful in practice.

Assume that the wind profile is linear, say $\bar{u}(z) = \alpha[z - z']$. In order to solve for the first x-moment,

the zeroth moment (A1.13) is substituted into equation (1.54), yielding

$$\frac{\partial \theta_1(z,t)}{\partial t} - K_z \frac{\partial^2 \theta_1(z,t)}{\partial z^2} = \frac{\alpha z}{[4\pi K_z t_1]^{\frac{1}{2}}} \left[\exp\left\{\frac{-(z-z')^2}{4K_z t_1}\right\} + \exp\left\{\frac{-(z+z')^2}{4K_z t_1}\right\} \right] \quad (\text{A1.14})$$

where $t_1 = t - t'$. Equation (A1.14) is solved subject to an impervious boundary at the ground, using Laplace transformations.

$$\theta_1(z,t) = \frac{\alpha}{4K_z} \left[z \left\{ \frac{K_z t_1}{\pi} \right\}^{\frac{1}{2}} \left\{ \exp\left(\frac{-(z-z')^2}{4K_z t_1}\right) + \exp\left(\frac{-(z+z')^2}{4K_z t_1}\right) \right\} + \left\{ K_z t_1 - z'(z-z') \right\} \operatorname{erfc}\left\{ \frac{z+z'}{(4K_z t_1)^{\frac{1}{2}}} \right\} \right] \quad (\text{A1.15})$$

[From Abramowitz and Stegun (1970), pp. 299, 300

$$i^n \operatorname{erfc}(z) = \frac{\exp[-z^2/2]}{(2^{n-1}\pi)^{\frac{1}{2}}} D_{-n-1}(z\sqrt{2})$$

where $i = \sqrt{-1}$, D_n is the parabolic cylinder function of order n [Whittaker and Watson (1950)], and

$$i^{-1} \operatorname{erfc}(z) = 2\pi^{-\frac{1}{2}} \exp[-z^2]$$

Using these relations, it can be shown that equation (A1.15) reduces to the solution of Saffman (1962) (1.57) for $z' = 0$.]

Division of equation (A1.15) by (A1.13) yields the position of the x-centroid at height z ,

$$\bar{X}(z, z'', t) = \theta_1(z, z'', t) / \theta_0(z, z'', t)$$

Further, differentiation of \bar{X} with respect to time allows evaluation of the velocity of the centroid at height z relative to the wind velocity at height z'' .

$$\frac{d\bar{X}(z, z'', t)}{dt} = \frac{\alpha(z-z'')}{2} + \frac{g}{(a+b)^2} \left[(2K_z t_1 + h)d(a+b) + (z+z'') \frac{(a+b)b \cdot h}{(\pi K_z t_1)^{\frac{1}{2}}} - \left(\frac{d \cdot h}{2K_z t_1} \right) \left\{ a(z-z'')^2 + b(z+z'')^2 \right\} \right]$$

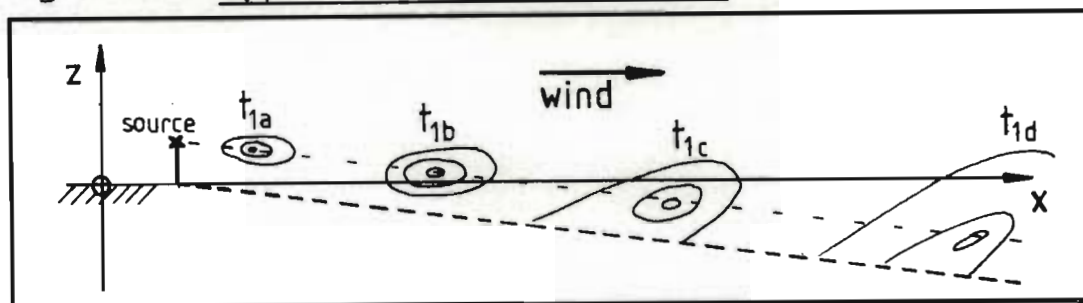
where

$$\begin{aligned} t_1 &= t - t' \\ a &= \exp[-(z-z'')^2 / 4K_z t_1] \\ b &= \exp[-(z+z'')^2 / 4K_z t_1] \\ d &= \operatorname{erfc}[(z+z'') / 2(K_z t_1)^{\frac{1}{2}}] \\ g &= \alpha(\pi / K_z t_1)^{\frac{1}{2}} / 4 \\ h &= K_z t_1 - z''(z-z'') \end{aligned}$$

An absolute velocity for the centroid at height z may then be defined as

$$U_c(z) = \bar{u}(z'') + \frac{d\bar{X}(z, z'', t)}{dt}$$

where the profile $\bar{u}(z)$ must be linear with slope α . The effect of settling at constant velocity w_s is approximated by allowing both the objective and reflective contributions to sink according to $w_s t_1$. [figure (A1.3)].

fig.(A1.3) Approximate sedimentation

This is achieved by allowing the vertical scales in equations (A1.13), (A1.15) to slide upwards as $w_s t_1$, so that finally

$$U_c(z) = \bar{u}[z'' - w_s(t-t')] + \left. \frac{d\bar{X}}{d\tau}[z + w_s(t-t'), z'', \tau] \right|_{\tau=t} \quad (\text{A1.16})$$

It remains now to define effective values for the constants α , K_z , because it is intended to apply this strategy to arbitrary velocity and diffusivity profiles. Since interest lies in the centroid velocity at height z , it is reasonable to use as α the average gradient between z and the "bulk" of the material at $(z'' - w_s(t-t'))$, i.e.

$$\alpha = [\bar{u}(z) - \bar{u}(z'' - w_s(t-t'))] / [z - z'' + w_s(t-t')]$$

However, equation (A1.16) has an obvious flaw for $w_s > z'' / (t-t')$, and in this case the effective gradient is taken as $\alpha = \bar{u}(z)/z$, and the first term on the R.H.S. of equation (A1.16) is replaced with the velocity

$$u_1 = \alpha [z'' - w_s(t-t')].$$

In this way, the correct behaviour of the centroid is preserved, based on a hypothetical velocity profile below the ground. The effective diffusivity K_z is also based on the mean of the heights $z, [z'' - w_s \cdot (t - t')]$, and in the event of $w_s > z'' / (t - t')$, it is taken as the average between z and the ground.

To extend this approach to the two-dimensional problem $[\bar{u}(z), \bar{v}(z)]$, note that the x-centroid will be independent of the y-centroid (1.54), so that $V_c(z)$ may be defined identically. By assuming linearity in the region of the vertical centroid, it has been possible to express the velocity $[U_c(z), V_c(z)]$ as a correction of the velocity near the "vertical centroid", viz. $[\bar{u}\{z'' - w_s \cdot (t - t')\}, \bar{v}\{z'' - w_s \cdot (t - t')\}]$. Hence the concept of an effective tracking height $Z_0(t - t')$ has been bypassed, and it is now possible to follow the centroid for a specific height - typically the height at which dosages or concentrations are required. If this height is Z_t , equation (A1.12) may be replaced with

$$[X(t), Y(t)] = [x'', y''] + \int_{t'}^t [U_c\{X(\tau), Y(\tau), Z_t, \tau\}, V_c\{X(\tau), Y(\tau), Z_t, \tau\}] d\tau, \quad (\text{A1.17})$$

where the additional arguments in U_c, V_c arise because of the extension of \bar{u}, \bar{v} to spatial and temporal variability.

A1.3.2 Application.

Returning to the motivation for the development of equation (A1.17) it was noted that the region-of-interest concept demanded identification beforehand of the release periods which would contribute to dosages or concentrations [section (2.4.1.2)]. The alternative would be to solve for all release-times, a costly and inefficient exercise. Though equation (A1.16) is approximate, and does not account e.g. for surface absorption, it has provided realistic estimates of the true location of clouds, and errors are easily allowed for by specifying adequate release-time margins.

A release history $Q(t')$ is provided for the point (x'', y'', z'') , say from t'_1 to t'_2 . This interval is discretised with a specified step-size $\Delta t_R = (t'_2 - t'_1) / n_R$. The centroid-trajectories for the n_R releases $Q(t'_1 + i\Delta t_R)\Delta t_R$, $i = 1, n_R$, are then solved for by discretising the lagrangian integral (A1.17), and integrating until times "t" which are greater than the maximum time of interest. For concentration-distributions, equation (A1.17) will define a locus of centroid-positions at a specified time-of-interest [fig. (2.3)]. The release-times at which this locus enters and leaves the region-of-interest are noted, and provision is made for up to 3 such locus-segments to be contributed for a single time-of-interest. Each locus-segment is then expanded out of the region-of-interest by expanding the release-time sequence using a specified factor. The corresponding release-time

sequences are then supplied to the lagrangian puff model, which discretises each sequence and solves for individual puffs until the appropriate time-of-interest. The location of these puffs in eulerian space depends entirely on their actual growth in the wind-field.

In the evaluation of point-dosages, the prediction of centroid locations is only necessary to provide an estimate of the earliest release-time which will affect the region-of-interest during the earliest dosage-interval. The application of equation (A1.17) in this case is analogous to that for the concentration distributions.

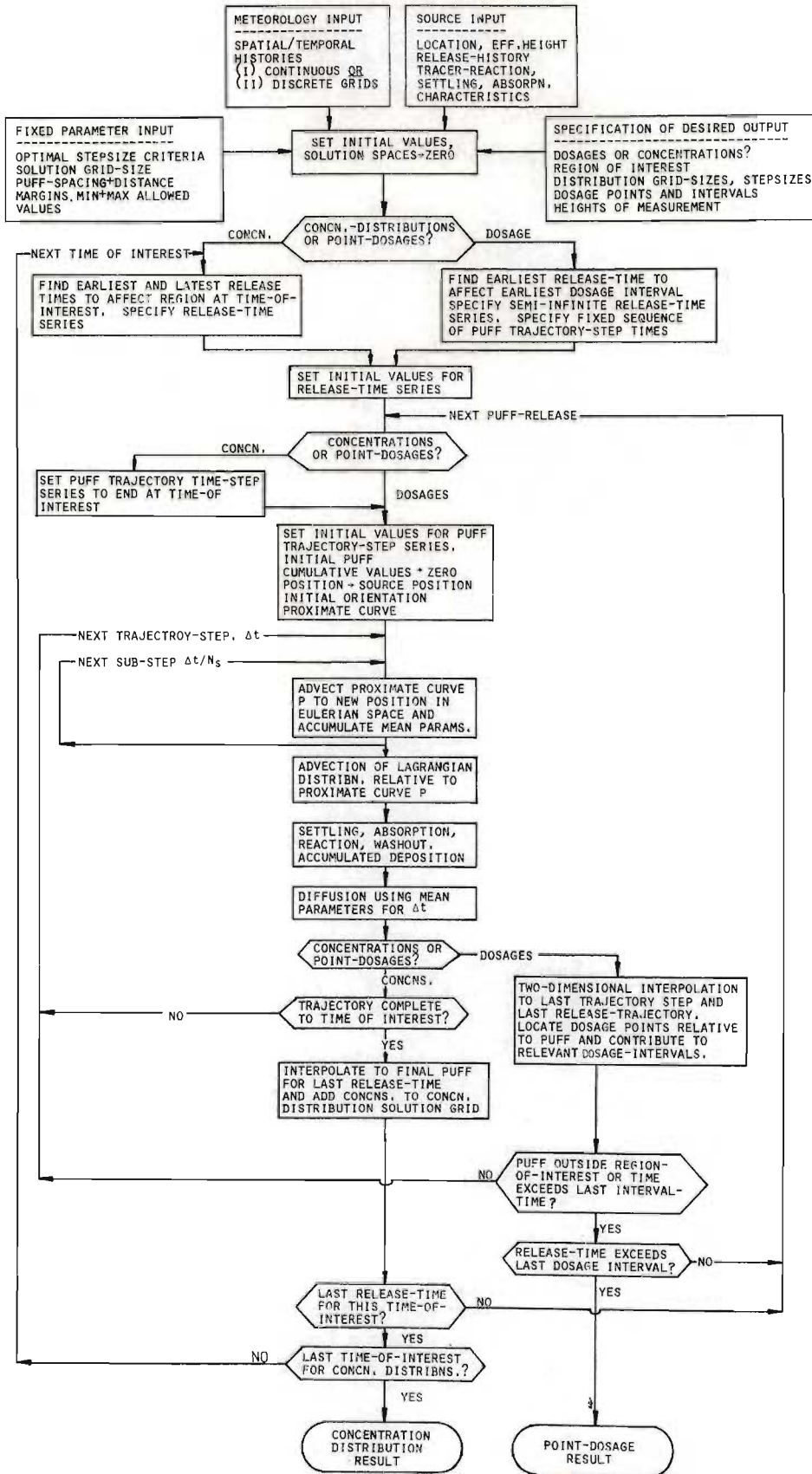
A1.4 Computer program.

The important calculation procedures used in the numerical model have all been discussed in chapter (2). Reference to figure (A1.4) shows that four distinct classes of input information are required.

- (i) Meteorological data - temporal/spatial variation of velocity, diffusivity, as dependent on surface roughness, stability.
- (ii) Release information - location and effective height of source, release history, tracer characteristics for sedimentation, reaction, absorption.
- (iii) Specification of desired output - region of interest, times of interest for concentration distributions, or points and time-intervals for dosages, grid resolution for distributions.
- (iv) Fixed parameter values - optimal step-size criteria, lagrangian puff solution grid-size, puff spacing and distance margins, minimum and maximum allowed values.

Whilst the fixed parameter values (iv) are set internally by the model (but may be altered), inputs (i), (ii) and (iii) are supplied as filed data via a meteorology sub-model [appendix (A4)], the purpose of which is to convert raw meteorological information to the standard input formats required by the dispersion model. It is convenient to input the release information (ii) and the output

FIGURE (A1.4). DYNAMIC PUFF MODEL : FLOW DIAGRAM



specification (iii) to the meteorology sub-model for filing along with the reduced meteorological data.

Though some differences arise between the concentration-distribution and dosage applications [section (2.4.1.1)], it is noted that the numerical model is dominated by two nested iterative procedures. The outlying procedure concerns the release of instantaneous puffs at a series of release-times, whilst the nested procedure concerns the solution for each of these puffs in a series of "trajectory" time-steps. During each trajectory time-step, the puff is translated in a series of small steps through eulerian space, using velocity information for the current position and time. At the same time, meteorological information is accumulated, so that time-averaged values for the trajectory-step are available for subsequent operations in the lagrangian frame section (2.3.1), equation (2.37).

At the end of each release-time step, all intermediate information is stored alternately in two files. The purpose of this procedure is to allow continuation of the solution regardless of when the model execution may be interrupted. On the completion of a concentration-distribution or dosage solution, all results are similarly filed for subsequent processing.

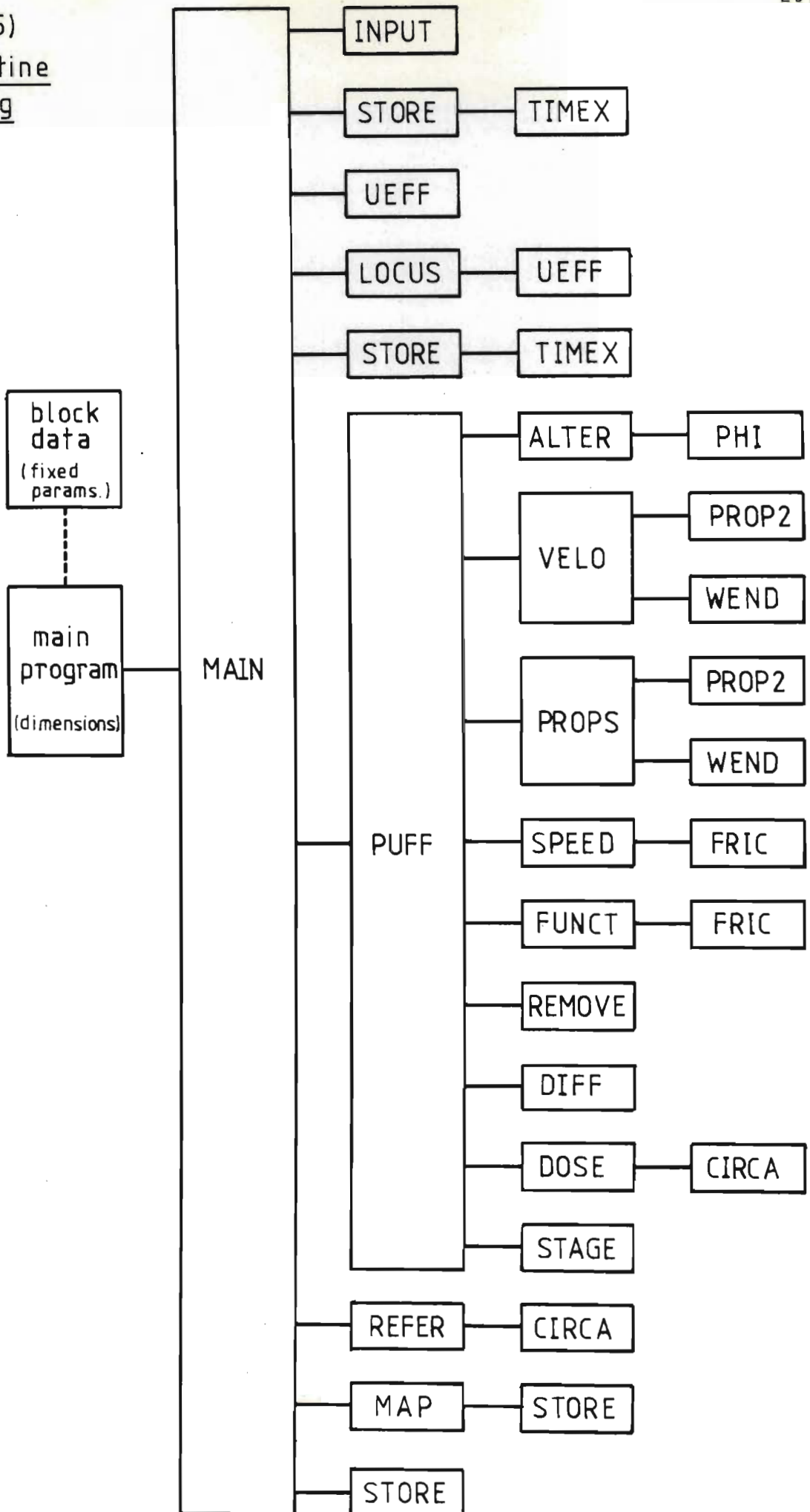
A1.4.1 Functions of subroutines.

A listing of the Dynamic Puff Model (DPM) computer program (in FORTRAN) is presented in appendix (A1.4.3). All fixed parameters are specified in the program as "block data", but these may be altered according to the application. The main program is simply a facility to allow alteration of the various array sizes in order to minimise computer storage requirements. The controlling administrative procedures are all conducted by subroutine "MAIN", the key position of which is illustrated in the stacking diagram, fig. (1.5). The functions of the 23 subroutines employed in the program are outlined below.

A1.4.1.1 MAIN

1. Reads input data (INPUT, STORE).
2. Initialises parameters.
3. Selects release sequence (LOCUS, UEFF) for either point-dosage or concentration-distribution outputs.
4. Controls release-sequence loop, requiring solution for serially-released puffs (PUFF).
5. Administers storage of intermediate data (STORE) and accumulation of data for concentration distributions (REFER, CIRCA).

fig. (A1.5)
Subroutine
stacking



6. Calculates trajectory time-step sequence for each released puff,

$$\begin{aligned}\Delta t_1 &= \Delta' / 2 \\ \Delta t_{i+5j} &= (j+1)\Delta', \quad i = 1, \dots, 5 \\ &\quad j = 0, 1, \dots, \infty \\ &\quad i+5j \neq 1\end{aligned}$$

where Δ' is a basic stepsize which is adjusted to allow concentration distribution solutions to terminate at the time of interest [section (2.4.3)].

7. Stores final point-dosage or concentration distribution solutions (STORE, MAP).

A1.4.1.2 INPUT.

1. Reads filed data covering: (a) meteorology input
(b) source input
(c) specification of output.
2. Allows for meteorology input in form of (x,y,t) grids or continuous histories at selected points (appendix (A1.2)).

A1.4.1.3 STORE.

1. Acquires intermediate data from storage file to continue an interrupted execution.
2. Writes intermediate data into storage file after each solved puff-release, provided a specified elapsed time has been exceeded (TIMEX).

3. Initialises files at the beginning of a new run-execution.
4. Stores final results (point-dosages or concentration distributions) in an output file.

A1.4.1.4 TIMEX

1. Provides program elapsed (total) time for monitoring purposes.

A1.4.1.5 LOCUS

1. Estimates release-sequences which affect the region-of-interest at a specified time-of-interest.
2. Simulates motion of puff centroid at height-of-interest using subroutine UEFF.

A1.4.1.6 UEFF

1. Estimates velocity of the puff centroid at the height-of-interest using equation (A1.17) [appendix (A1.3)].

A1.4.1.7 PUFF

1. Solves for the development of the lagrangian puff under the specified conditions [chapter (2)]. Controls the trajectory-step loop.
2. Advection step: translates proximate curve to new position in eulerian frame and performs relative

advection in the lagrangian frame (VELO, SPEED)

$$C_n(x, z, t + \Delta t) = C_n \left[\left(x - \int_t^{t+\Delta t} \bar{U}(z, \tau) d\tau \right), z, t \right].$$

3. Solves for the removal of material by sedimentation, ground-absorption, washout, first order chemical reaction, and accumulates associated ground deposition. (REMOVE).
4. Performs diffusion step (DIFF).
5. Allocates dosage contributions to dosage-points (DOSE).
6. Terminates trajectory-solution on reaching the time-of-interest, or exceeding the last dosage interval, or moving beyond contributing margin around the region-of-interest.

A1.4.1.8 ALTER

1. Alters vertical and horizontal stepsizes in the lagrangian solution grid in order to satisfy the optimality criteria (2.76):

$$\Delta x_{OPT} = (K_x \Delta t / 0.4)^{\frac{1}{2}}, \quad \Delta z_{OPT} = (K_z \Delta t / 0.4)^{\frac{1}{2}}$$

2. Adjusts stepsizes at the grid centre to meet these criteria provided their average deviation exceeds a specified tolerance.
3. Allows horizontal stepsizes to expand outwards from the grid-centre [section (2.3.3)] (PHI).

A1.4.1.9 PHI

1. Calculates the horizontal distance sequence for grid positions, using stepsizes Δx which expand linearly outwards from the grid-centre.

Grid-centre stepsizes are based on optimal values, whilst extreme stepsizes are fixed by a specified ratio.

A1.4.1.10 VELO

1. Extracts point-values for the velocity components at a specified height (present parameter format).
2. Interpolates values either from A_{ijt} grid storage (linear) or selected point "continuous" data (linear in time, weighted inverse square in space) (PROP2, WEND).

A1.4.1.11 PROP2

1. Interpolates for parameter values at a point (x,y,t) using grid-stored data (A_{ijt}) [appendix (A1.2)].
Linear interpolations in time and space.

A1.4.1.12 WEND

1. Interpolates for parameter values at a point (x,y) given the values at a series of points (X_i, Y_i) , $i = 1, n$.
2. Uses a weighted inverse square method, in which the weights may be specified.

3. Rejects interpolation unless usable data are available at a specified minimum number of points i .

A1.4.1.13 PROPS

1. Extracts point-values for the stability parameters at (x,y,t) and constant surface properties at (x,y) .
2. For stability parameters, interpolates values either from A_{ijt} grid storage (linear) or selected point "continuous" data (linear in time, weighted inverse square in space) (PROP2, WEND).
3. Interpolates constant surface parameters linearly from (x,y) storage grids.

A1.4.1.14 SPEED

1. Obtains friction velocity from fixed height velocity measurements (VELO) by inverting equation (2.72) (FRIC).
2. Calculates the x- and y-velocity components at any required height, using equation (2.72).

A1.4.1.15 FRIC

1. Inverts equation (2.72) in order to establish friction velocity u_* from supplied velocity data at a specified height.

A1.4.1.16 FUNCT

1. Calculates entire vertical and horizontal diffusivity profiles using equations (2.73), (2.74) and (2.75).

A1.4.1.17 REMOVE

1. Accounts for removal due to ground-absorption, washout and first-order chemical reaction by adjusting the lagrangian puff concentration distribution according to equation (2.63).
2. Calculates ground deposition for depositing processes (i.e. excluding chemical reaction). Deposition distributions are subsequently used in subroutine DOSE.

A1.4.1.18 DIFF

1. Performs the lagrangian puff diffusion step [section (2.3.3)].
2. Uses the "limiting value" method described in appendix (A1.1).
3. Pre-evaluates cell boundary-concentrations at $\frac{1}{2}\Delta t$ for use in final prediction.

A1.4.1.19 DOSE

1. Allocates dosage-contributions to the dosage-points for the appropriate dosage intervals [section (2.3.5)].

2. Transforms the lagrangian distribution into the eulerian grid using a circular arc representation of the proximate curve (CIRCA).
3. Allocates deposition contributions if required.

A1.14.1.20 CIRCA

1. Calculates the centre, radius and sense of a circular arc passing through the forward, centre and rear tracking points used to locate the lagrangian puff in eulerian space [section (2.4.4.1)].
2. Approximates the advected "proximate curve" discussed in section (2.2.2), thus allowing representation of the puff distribution in eulerian space.

A1.14.1.21 REFER

1. Allocates puff-concentration contributions to the result grid covering the region-of-interest, for concentration distribution solutions.
2. Assumes a gaussian distribution normal to the lagrangian puff solution surface at any point, and locates this surface using CIRCA [section (2.3.5)].

A1.14.1.22 MAP

1. Stores concentration distribution solutions in output file (STORE).
2. Prints out result grid.

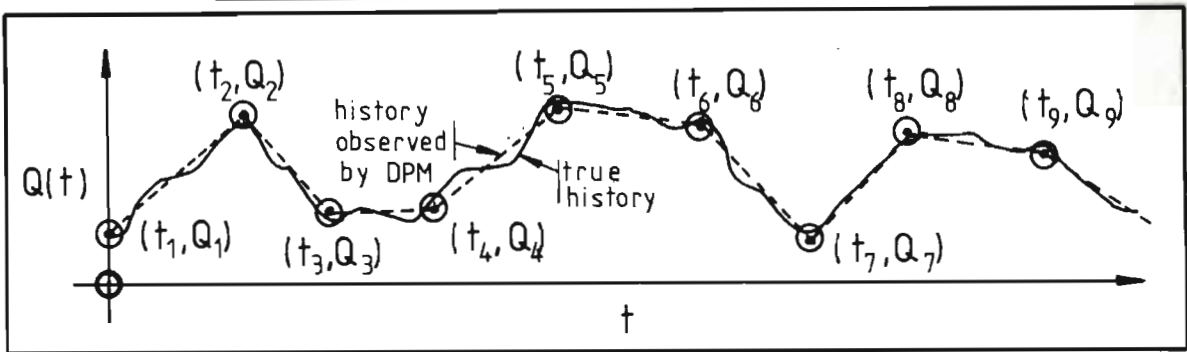
A1.14.1.23 STAGE

1. Prints out information concerning the numerical solution for the lagrangian puff, as it develops. Suitable specification of a flag will suppress this print-out, which is mainly for diagnostic purposes.

A1.4.2 INPUT-OUTPUT SPECIFICATIONS.

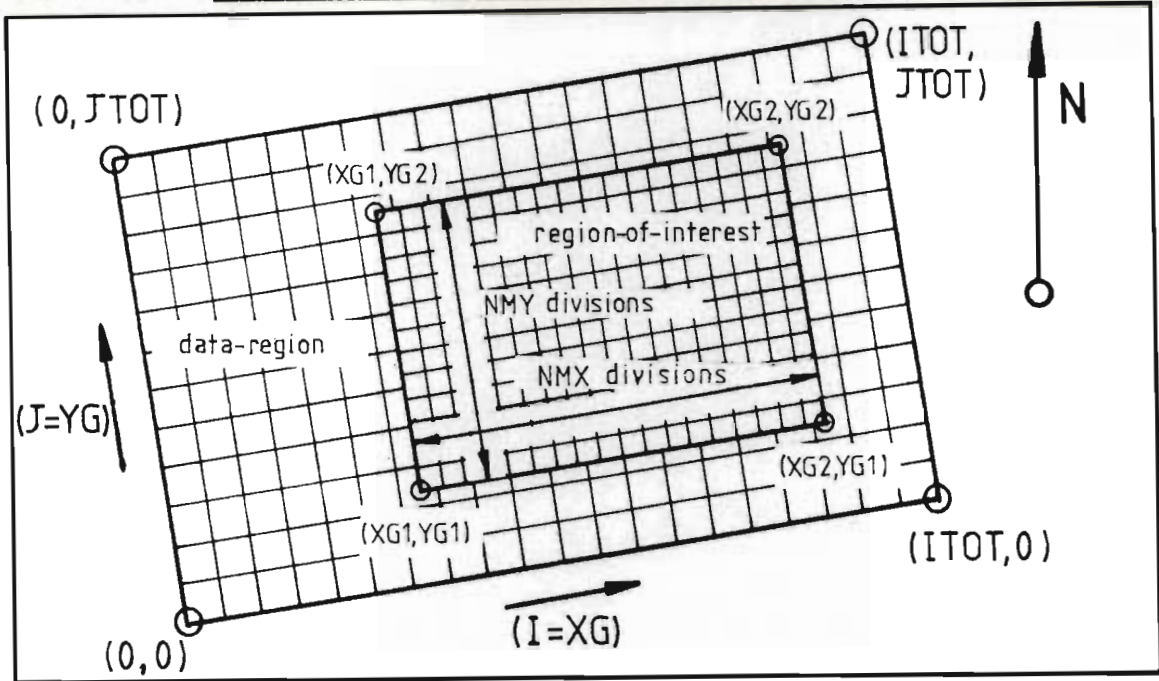
In the specification of source or meteorology input data for the Dynamic Puff Model, it should be noted that point values are extracted from all time-series by linear interpolation. (In the case of the Monin-Obukhov (1954) stability length, L^{-1} is linearly interpolated). Hence a time-series should be specified so as to define the important features in the development of a parameter [fig. (A1.6)].

fig.(A1.6) Specification of time-series



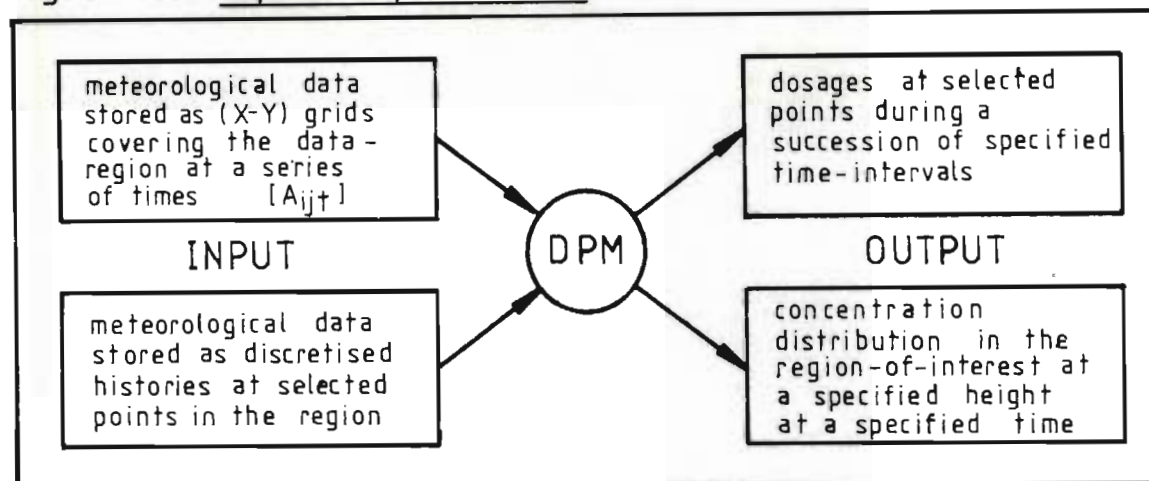
The meteorological variables are only used in subroutines SPEED, FUNCT and FRIC [appendices (1.4.1), (1.4.3)] so that they may be used to carry other properties if alternative relations are substituted in these subroutines. Note that S.I. (Systeme Internationale) units should be used in specifying input data and fixed parameters.

The relationship between the data-grid and solution-grid (region-of-interest) is clarified by figure (A1.7).

fig.(A1.7) Data-grid and solution grid (region-of-interest)

Clearly, the solution-grid must be enclosed within, or coincident with, the region in which data are available. In the case of the point-dosage solution, the region-of-interest must be specified so as to enclose all dosage points. This follows from the use of the region-of-interest to establish whether a puff is likely to contribute to any dosage point. All "grid" coordinates used in the DPM relate to the basic data-grid, which obviously represents some portion of the earth's surface.

A review of the input-output specifications contained in appendix (A1.4.3) shows that the DPM has two input modes and two output modes, giving a total of 4 modes of operation [fig. (A1.8)]. When data are based on measurements at a limited number of points (e.g. meteorological masts) it is

fig. (A1.8) Input-output modes

clearly advantageous to store them as the discretised point-histories. On the other hand, if it is desired to use some rationalised form of the wind-field (e.g. a predicted wind-field), it will be necessary to use the A_{ijt} grid-storage [appendix (A1.2)]. Array sizes need only be altered in the main program in order to accommodate particular input or output formats. Required minimum sizes are easily calculated as the product of the variable dimensions in subroutine MAIN.

In the file READ and WRITE statements, integers are occasionally mixed with reals. If the program is run on a computer which provides different storage for reals and integers (e.g. one-word integers, two-word reals), care must be taken to supply the correct "dummy" spacings given in appendix (A1.4.3). Further, record lengths should accommodate the maximum requirement of 60 reals or 60 integers.

The input and output formats employed by the DPM computer program are detailed in appendix (A1.4.3). The program included in appendix (A1.4.4) is designed to set up a test input data-set for the DPM. The corresponding printed output of the DPM is presented in appendix (A1.4.5).

The following input variable lists should further help to clarify the input requirements of the model.

A1.4.2.1 Meteorological data.

GRID INPUT AND POINT-HISTORY INPUT	}	NTDAT - number of times at which data are provided (TDAT(J),J=1,NTDAT) - sequence of times at which data are provided (point histories: NTDAT=2,TDAT(1)=0,TDAT(2)= t_{max}) ITOT - number of X-divisions in data-grid JTOT - number of Y-divisions in data-grid DXB - X-stepsize for data-grid DYB - Y-stepsize for data grid ZO(I,J) - roughness-length distribution in data-grid D(I,J) - zero-plane-displacement distribution in data-grid (not used in model at present). ZG - height of velocity measurements and potential-temperature gradient
---	---	---

GRID INPUT
ONLY

UZG(I,J,T) - X-velocity at height ZG
 VZG(I,J,T) - Y-velocity at height ZG
 STAB(I,J,T)- inverse Monin-Obukhov (1954)
 stability length (L^{-1})
 PARAM(I,J,T)- potential temperature gradient
 at height ZG ($\partial\bar{\theta}/\partial Z|_{ZG}$).

POINT-HISTORY
INPUT ONLY

NMCD - number of measurement points (masts)
 NTCD - number of time-points in histories
 TSCD - first time in history sequence (set=0)
 DTCD - interval between times in history
 sequence.
 ((XGMAST(J),YGMAST(J)),J=1,NMCD) - grid positions
 of measurement points.
 (WEIGHTINGFACTOR(J),J=1,NMCD) - weighting
 factor (0,0 to 1,0) for each measure-
 ment location.
 ((PARAM1(K,T),K=1,NMCD),T=1,NTCD) - X-velocity
 at height ZG for each location at each
 time
 ((PARAM2(K,T),K=1,NMCD),T=1,NTCD) - Y-velocity
 at height ZG for each location at
 each time
 ((PARAM3(K,T),K=1,NMCD),T=1,NTCD) - inverse
 Monin-Obukhov (1954) stability length
 (L^{-1}) for each location at each time
 ((PARAM4((K,T),K=1,NMCD),T=1,NTCD) - potential
 temperature gradient at height ZG for each
 location at each time in sequence.

A1.4.2.2 Release information

XGS,YGS - grid-coordinates of source.

ZS - height of release point.

NSTR - number of time-nodes in release history

(TSTR(J),J=1,NSTR) - time-node sequence for release history.

(QSTR(J),J=1,NSTR) - release-rates at time-nodes in sequence.

REACTION/
REMOVAL
PARAMETERS

WS - sedimentation velocity

PREM - constant first-order rate constant
(positive for decay)

TDES - time at which washout commences

TDEF - time at which washout ends

PDEP - washout rate constant ("coefficient")

((RAB(I,J),I=1,ITOT),J=1,JTOT) - distribution
of ground-absorption deposition velocity
in the data-region

A1.4.2.3 Specification of desired output

CONCENTRATION
DISTRIBUTIONS
AND
POINT-DOSAGES

ITJEK - flag for diagnostic "check-plane"
option (usually set = 0)

XG1,XG2,YG1,YG2 - grid-coordinates defining
limits of the region-of-interest (in
which the concentration-distribution
will be provided, or which must enclose
the dosage-points)

CONCENTRATION
DISTRIBUTION
OUTPUT ONLY

NTIME - number of times-of-interest
 (TIME(J),J=1,NTIME) - sequence of times-of-interest
 NHANS - number of heights at which X-Y distributions are required
 (HANS(J),J=1,NHANS) - sequence of heights at which X-Y distributions are required
 (XGA,YGA),(XGB,YGB),(XGW,YGW) - grid-coordinates of marker-points A,B and W in the concentration distribution output.
 NMX,NMY - number of X and Y sub-divisions in the region-of-interest, determining resolution of the result-grid.

POINT-DOSAGE
OUTPUT ONLY

NTDOS - number of times in dosage interval boundary-time sequence (= number of dosage intervals plus one)
 (TDOS(J),J=1,NTDOS) - dosage interval boundary-time sequence, determining the sequence of (NTDOS-1) dosage intervals
 NPDOS - number of points in region-of-interest at which dosages are required
 ((XDOS(J),YDOS(J)),J=1,NPDOS) - data-grid coordinates of points at which dosages are required during the interval sequence.
 ZDOS - height at which dosages are required.

A1.4.2.4 Procedure variables.

MUL - run number

DELTA - release-time scan stepsize for establishing which release-intervals contribute at a particular time.

DELTB - trajectory time-step for locating relevant release-intervals (used in conjunction with DELTA).

DELTC - finer release-time step for fixing release-interval boundaries (after DELTA).

DELTD - finer trajectory-time-step for fixing release-interval boundaries (used in conjunction with DELTC).

NSDT - number of sub-steps to each trajectory-step in the puff solution, for the purpose of advection in the eulerian frame.

A1.4.3 Dynamic Puff Model : FORTRAN program listing.

DPM /ECPMMUL
 =====

```

$ SET IBM026
$ SET TAPE
FILE 2 = INPUT          ,UNIT = READER
FILE 3 = OUTPUT         ,UNIT = PRINTER
FILE 40 = DAT0/ECPMMUL,UNIT=DISK,BLOCKING=1,RECORD=60
FILE 41 = DAT1/ECPMMUL,UNIT=DISK,BLOCKING=1,RECORD=60
FILE 42 = DAT2/ECPMMUL,UNIT=DISK,BLOCKING=1,RECORD=60
FILE 43 = DAT3/ECPMMUL,UNIT=DISK,BLOCKING=1,RECORD=60
FILE 44 = DAT4/ECPMMUL,UNIT=DISK,BLOCKING=1,RECORD=60
FILE 45 = DAT5/ECPMMUL,UNIT=DISK,BLOCKING=1,RECORD=60
FILE 46 = DAT6/ECPMMUL,UNIT=DISK,BLOCKING=1,RECORD=60
FILE 47 = DAT7/ECPMMUL,UNIT=DISK,BLOCKING=1,RECORD=60
FILE 48 = DAT8/ECPMMUL,UNIT=DISK,BLOCKING=1,RECORD=60
FILE 49 = DAT9/ECPMMUL,UNIT=DISK,BLOCKING=1,RECORD=60
FILE 51 = DAT11/ECPMMUL,UNIT=DISK,BLOCKING=1,RECORD=60
    
```

=====

DYNAMIC PUFF MODEL
 FOR ATMOSPHERIC POINT-SOURCES

M. MULHOLLAND
 DEPARTMENT OF CHEMICAL ENGINEERING
 UNIVERSITY OF NATAL
 DURBAN, SOUTH AFRICA.
 11TH SEPTEMBER, 1977.

=====

A. DATA INPUT
 =====

LINEAR INTERPOLATION IS USED TO EXTRACT POINT-VALUES FROM ALL DATA
 EXPRESSED AS TIME-SERIES - CHOOSE TIME-NODES TO DEFINE ALL IMPORTANT
 FEATURES (SOURCE DATA, METEOROLOGICAL DATA)
 (USE S.I. (SYSTEME INTERNATIONAL) UNITS: KG,M,S)

(1) CARDS

- (1) CONTINUATION FROM PREVIOUS EXECUTION
 - INTERMEDIATE DATA EX FILE M1(51)-SET 1ST CARD "1" IN (11)
 - INTERMEDIATE DATA EX FILE M2(48)-SET 1ST CARD "2" IN (11)
 - (2) INITIAL EXECUTION
 - SET 1ST CARD "0" IN (11)
- (1) AND (2) ABOVE...
- 2ND CARD: ELAPSED (TOTAL) TIME (MINUTES) IN (14) BEFORE FIRST
 REFILEING OF INTERMEDIATE DATA.

C 3RD CARD(LAST): INTERMEDIATE PRINTOUT FLAG-SET IN (11) AS FOLLOWS:
 C "1" NO INFORMATION RE PUFF ITERATIONS
 C "2" BASIC INFORMATION RE PUFF ITERATIONS
 C "3" BASIC INFORMATION WITH OCCASIONAL PRINTOUTS OF PUFF
 C -----

(11) FILED INFORMATION

ALL FILES USED IN SERIAL READ/WRITE MODE
 REMEMBER: MAX 60 WORDS (REALS OR INTEGERS) PER RECORD

(1)

DATA-DESCRIPTOR LABELS- EACH LABEL READ AS 80A1 AND FILED IN
 FILE(47) AS TWO CONSECUTIVE RECORDS OF 40
 INTEGERS. RECORDS 0 TO 119 OCCUPIED BY
 LABELS 1 TO 60 (LET) AS FOLLOWS:-
 (INSERT DUMMY VALUES FOR MISSING LABELS)

LABEL

- 01-RUN NUMBER,MUL
- 02-NUMBER OF DATA-TIMES,NTDAT (SET=2 FOR CONTINUOUS DATA INPUT)
- 03-DATA-TIMES,TDAT(J) (SET TDAT(1)=0)
- 05-X AND Y GRID POSITIONS IN MET. DATA GRID,ITOT,JTOT
- 06-X AND Y STEPSIZES IN MET. DATA GRID,DXB,DYB
- 07-LIST OF DATA-TIME WEIGHTING FACTORS FOR W/F MODEL INPUT,
 WF1,WF2,WF3,WF4
- 08-GRID COORDINATES OF (SUB-)REGION OF INTEREST,XG1,XG2,YG1,YG2
- 09-GRID COORDINATES OF SOURCE(XGS,YGS) AND HEIGHT ZS IN (M)
- 10-NUMBER OF TIME-POINTS IN SOURCE-STRENGTH HISTORY,NSTR
- 11-SOURCE-STRENGTHS AT TIME-NODES,QSTR(J)
- 12-TIMES FOR SOURCE STRENGTH TIME-NODES,TSTR(J)
- 13-CONCN.DISTRIBUTION,NO. OF TIMES OF INTEREST,NTIME
- 14-CONCN. DISTRIBUTION SOLUTION,TIMES-OF-INTEREST,TIME(J)
- 16-RELEASE-TIME SCAN STEPSIZE FOR RELEVANT RELEASE INTERVALS,DELTA
- 17-TRAJECTORY TIME-STEP FOR LOCATING RELEASE INTERVALS,DELTB
- 18-FINER RELEASE-TIME STEPS FOR FIXING RELEASE INTERVAL BOUNDARIES,
 DELTC
- 19-FINER TRAJECTORY TIME-STEPS FOR FIXING RELEASE INTERVAL
 BOUNDARIES,DELTD
- 23-NUMBER OF TRAJECTORY ADVECTION STEPS PER BASIC TIME-STEP,NSDT
- 26-CONCN.DISTRIBUTION SOLUTION,REGION OF INTEREST RESULT GRID
 DIVISIONS,NMX,NMY
- 27-VERTICAL STEPSIZE IN SOLN-SPACE DMZ (NOT FOR CONCN. DISTRIBS. OR
 DOSAGES)
- 29-FLAG FOR CHECK PLANE DIAGNOSTIC SOLUTION,-SET ITJEK=0 NORMALLY
- 30-NO. OF CONCN.DISTRIBUTION HEIGHTS REQUIRED,NHANS (MAX=2)
- 31-CONCN.DISTRIBUTION HEIGHTS,HANS(J)...
- 32-MARKERS A,B,W FOR FINAL MAP AT GRID POSITIONS XGA,XGB,XGW,YGA,
 YGB,YGW
- 33-SEDIMENTATION VEL.WS,WASHOUT RATE CONST.PDEP,TIME RAIN START TDES
 TIME RAIN END TDEF,CONST. 1ST ORDER RATE CONST. PREM
- 48-HEIGHT OF VELOCITY INPUT COMPONENTS (EG. MEASUREMENT HEIGHT),ZG,
 AND KARMAN CONST. VK
- 51-NUMBER OF DOSAGE INTERVAL BOUNDARY-TIMES,NTDOS, (MAX 60), (SET
 =0 FOR CONCN. DISTRIBUTION SOLUTION)
- 52-DOSAGE INTERVAL BOUNDARY-TIMES,TDOS(J) (DOSAGE SOLUTIONS)
- 53-NUMBER OF DOSAGE POSITIONS,NPODS (MAX 40)
- 54-LIST OF DOSAGE POSITIONS,XDOS(J),YDOS(J) (NEGATIVE VALUES FOR
 COORDINATES GIVES DEPOSITION INSTEAD OF DOSAGE FOR INTERVAL)

55=HEIGHT AT WHICH DOSAGE PREDICTIONS REQUIRED,ZDOS(M)

(2)

GENERAL DATA

NOTE:

"DUMMY"=DUMMY VARIABLE(REAL)

"IDUMMY"=DUMMY VARIABLE(INTEGER)

ALL VARIABLES BEGINNING WITH I,J,K,L,M,N,O ARE INTEGERS,
THE REST ARE REALS.

FILE(41) RECORD(0)

MUL(SEE LABEL 1 ABOVE),NTDAT(L2),ITOT(L5),JTOT(L5),DXB(L6),DYS(L6),
DUMMY,DUMMY,DUMMY,XG1,XG2,YG1,YG2(SEE L8),XGS,YGS,ZS(L9),NSTR(L10),
WS(L33),DELTA(L16),DELTB(L17),DELTC(L18),DELTD(L19),DUMMY,DUMMY,
PREM(L33)

FILE(41) RECORD(1)

TDOS,TOEF,PDEP(SEE LABEL 33 ABOVE),DUMMY,NMX,NMY(SEE L26),IDUMMY,
DMZ(DUMMY-SEE L27),DUMMY,IDUMMY,IDUMMY,IDUMMY,IDUMMY,
NSDT(SEE L23),ITJEK(L29),NHANS(L30),XGA,XGB,XGW,YGA,YGB,YGW(L32),
NTDOS(L51+SEE BELOW),NPDOS(L53),ZDOS(L55),ZG(L48)

NOTE:IF NTDOS=0,CONCN,DISTRIBUTION SOLUTION IS ASSUMED,
==== AND NPDOS,XDOS,YDOS,TDOS DON'T MATTER(ANY VALUES)

FILE(41) RECORD(2) = (TDAT(J),J=1,NTDAT-SEE L3), (DUMMY(J),J=1,NTDAT)
----- (SET TDAT(1)=TSCD,TDAT(2)=TSCD+(NTCD-1)*DTCO,
AND NTDAT=2, FOR CONTINUOUS DATA OPTION(1) BELOW)

FILE(41) RECORD(3) = (QSTR(J),J=1,NSTR-SEE L11)

FILE(41) RECORD(4) = (TSTR(J),J=1,NSTR-SEE L12)

FILE(41) RECORD(5) = NTIME(SEE L13), (TIME(J),J=1,NTIME-SEE L14)
----- (USE DUMMIES IF NTDOS IS NON-ZERO(L51))

FILE(41) RECORD(6) = (HANS(J),J=1,3-SEE L31 - DUMMIES IF NECESSARY)

FILE(41) RECORD(7) TO RECORD(6+ITOT)

ROUGHNESS LENGTH DISTRIBUTION IN BASIC DATA GRID,ROWS I=1 TO I=
ITOT AS (ZO(I,J),J=1,JTOT) IN EACH RECORD(SEE L5).

FILE(41) RECORD(7+ITOT) TO RECORD(6+2*ITOT)

SURFACE OBSTACLE ZERO-PLANE DISPLACEMENT(NOT USED IN PRESENT MODEL
- SET DUMMY VALUES) -DISTRIBUTION IN BASIC DATA GRID,ROWS I=1 TO
I=ITOT AS (U(I,J),J=1,JTOT) IN EACH RECORD(SEE L5)

FILE(41) RECORD(7+2*ITOT) = (DUMMY(J),J=1,2*NTDAT)

FILE(41) RECORD(8+2*ITOT) = (DUMMY(J),J=1,2*NTDAT)

FILE(41) RECORD(9+2*ITOT) = (TDOS(J),J=1,NTDOS-SEE L52)

NOTE:BY SPECIFYING NEGATIVE VALUES OF COORDINATES XDOS(J),YDOS(J) FOR
==== ANY POINT,GET DEPOSITION AT THIS POINT INSTEAD OF DOSAGE...

FILE(41) RECORD(10+2*ITOT) = (XDOS(J),J=1,NPDOS -SEE L54)

FILE(41) RECORD(11+2*ITOT) = (YDOS(J),J=1,NPDOS -SEE L54)

FILE(41) RECORD(12+2*ITOT) TO RECORD(11+3*ITOT)

EFFECTIVE DEPOSITION VELOCITY W/D DUE TO SURFACE ABSORPTION -
(DISTRIBUTION) IN BASIC DATA GRID(I.E.AS MET.DATA),ROWS I=1 TO
I=ITOT AS (RAB(I,J),J=1,JTOT) IN EACH RECORD - (SEE L5).

(3)

NOTE:THESE METEOROLOGICAL PARAMETERS ARE ONLY USED IN SUBROUTINES
==== SPEED(VELOCITY) AND FUNCT(DIFFUSIVITY) AND MAY BE USED TO CARRY
OTHER VARIABLES IF RELATIONS IN THESE SUBROUTINES ARE CHANGED.
LIKEWISE THE VARIABLES ZO AND D.

METEOROLOGY INPUT OPTION(1) : CONTINUOUS DATA AT SELECTED POINTS
----- (MASTS)

FILE(40) RECORD(0) = NMCD,NTCD,TSCD,DTCO

WHERE:NMCD=NUMBER OF MASTS- IF NMCD IS SET TO 0 THEN NO MORE DATA
ARE READ FROM FILE(40) AND THE GRID INPUT A(I,J,T)(OPTION(2))
IS ASSUMED (BELOW)
NTCD=NUMBER OF TIME POINTS IN HISTORIES FOR EACH MAST
TSCD=FIRST TIME IN THE HISTORY SERIES(EG.0)
DTCO=TIME INTERVAL IN THE SERIES.

FILE(40) RECORD(1) = MAST POSITIONS AND WEIGHTING FACTORS(0.0 TO 1.0)
----- ..AS ((XGMAST(J),YGMAST(J)),J=1,NMCD),
(WEIGHTING FACTOR(J)),J=1,NMCD)

FILE(40) RECORD(2) TO RECORD(NMCD*NTCD*4/60+0.99999)

VELOCITY AND STABILITY PARAMETERS AS MAST HISTORIES

AS FOLLOWS :-

PARAM1:VELOCITY COMPONENT AT HEIGHT ZG(SEE LABEL 48 ABOVE)
IN GRID X-DIRECTION

PARAM2:VELOCITY COMPONENT AT HEIGHT ZG IN GRID Y-DIRECTION
PARAM3:INVERSE MONIN*OBUKHUV(1954) STABILITY LENGTH(L**1)
PARAM4:POTENTIAL TEMPERATURE GRADIENT AT HEIGHT ZG,VIZ.
DTP/DZ)ZG

NOTE:IF ANY VALUE IS NOT AVAILABLE SET PARAMJ TO =31000.0 FOR
==== THAT POINT

60 VALUES PER RECORD IN ORDER (PARAM1 TO PARAM4) FOR
(MASTS 1 TO NMCD) FOR (TIMES 1 TO NTCD)..(I.E.
(((CU(VAL=MAST,TIME),VAL=PARAM1 TO PARAM4),MAST=1 TO NMCD)

METEOROLOGY INPUT OPTION(2) : X-Y GRIDS COVERING THE REGION AT A LIMITED (NTDAT) SERIES OF SELECTED TIMES(TDAT).

FILE(43) RECORD(0) TO RECORD(NTDAT*ITOT-1)(SEE LABELS2+5 ABOVE)

X=VELOCITY COMPONENT AT HEIGHT ZG(SEE L48) AS (UZG(I,J,T),J=1, JTOT), IN EACH RECORD FOR I=1, TO ITOT, AND T=1 TO TDAT AS THE OUTSIDE LOOP(T REPRESENTS TIMES TDAT(T))

FILE(44) RECORD(0) TO RECORD(NTDAT*ITOT-1)(SEE L2+L5 ABOVE)

Y=VELOCITY COMPONENT AT HEIGHT ZG(SEE L48) IN SAME ORDER AS FILE(43) ABOVE.

FILE(45) RECORD(0) TO RECORD(NTDAT*ITOT-1)(SEE L2+L5 ABOVE)

INVERSE MUNIN=OBUKHOV(1954) STABILITY LENGTH(I.E. L**=-1) AT X,Y GRID POINTS AT TIMES TDAT IN SAME ORDER AS FILE(43) ABOVE.

FILE(46) RECORD(0) TO RECORD(NTDAT*ITOT-1)(SEE L2+L5 ABOVE)

POTENTIAL TEMPERATURE GRADIENT AT HEIGHT ZG(SEE L48) IN SAME ORDER AS FILE (45) ABOVE.

B.FIXED PARAMETERS - SPECIFIED AS BLOCK DATA

(MAY BE ALTERED AS NECESSARY)
(UNITS: S.I.(SYSTEME INTERNATIONAL) - KG,M,S)

SPAR(J) (REALS)

1. PBFR=FRACTION OF VERTICAL STEPSIZE DZ TO FIRST VERTICAL GRID=PUINT(0.5)
2. OTOS=MAXIMUM RELEASE-TIME INTERVAL BETWEEN SOLVED PUFFS(DUSAGE SOLUTION)(900.0)
3. DISTANCE MARGIN (OUTSIDE REGION OF INTEREST) AT ENDS OF CONC. LUCI(CONCN. DISTRIBUTION SOLUTION)(750.0)
4. DISTANCE BETWEEN SOLVED PUFFS IN CONC. LUCUS(800.0)
5. MAXIMUM NUMBER OF SOLVED PUFFS ALLOWED IN CONCENTRATION LUCUS(20.0)
6. NZ=NO. OF VERTICAL POSITIONS IN LAGRANGIAN PUFF SOLUTION GRID(12.0)
7. NX=NO. OF HORIZONTAL POSITIONS IN LAGRANGIAN PUFF SOLUTION GRID(280.0)
8. STEPSIZE DX EXPANSION FACTOR FROM GRID CENTRE TO HORIZONTAL EXTREMES(3.0)
9. NPINT=NUMBER OF INTERPOLATED PUFFS BETWEEN SOLVED PUFFS(SEE 5.) ALONG CONCENTRATION LUCUS(20.0)
10. SPACING BETWEEN LAGRANGIAN PUFF PROXIMATE CURVE TRACKING POINTS(1500.0)
11. HEIGHT INCREMENT FOR FINDING LOCAL VELOCITY GRADIENT DU/DZ(0.25)
12. MINIMUM ALLOWED VALUE OF DU/DZ IN 11. FOR FINDING BEST TRACKING HEIGHT(0.002)
13. OPTIMAL SPATIAL STEPSIZE FACTOR:(DIFFUSIVITY)*(TIME-STEP)/

(SPATIAL STEP)**2(=0.4 AT PRESENT)

14. MINIMUM ALLOWED HEIGHT OF LAGRANGIAN SOLUTION FRAME(50.0)
15. MINIMUM ALLOWED RATIO(SOLN. FRAME HEIGHT)/(RELEASE HEIGHT)(=2.0)
16. DECREASE IN ALLOWED MINIMUM FRACTION OF MASS RETAINED IN LAGRANGIAN FRAME AFTER ADVECTION LOSSES, WITH EACH INCREASE IN TIME-STEP DT(0.2)
17. MARGIN AROUND REGION OF INTEREST FOR TERMINATION OF DOSAGE SOLUTION TRAJECTORIES(2500.0)
18. TIME INTERVAL BETWEEN INTERPOLATED PUFFS ALONG TRAJECTORY(FOR DUSAGES)(90.0)
19. TIME INTERVAL BETWEEN INTERPOLATED RELEASE-TIMES(TRAJECTORIES) (FOR DUSAGES)(90.0)
20. UVMAX(IT)=MINIMUM ALLOWED VELOCITY FOR CALCULATING SOLVED PUFF SPACING IN CONC. DISTRIBUTION SOLUTIONS(0.05)
21. MINIMUM CENTROID POSITION IN LAGR. FRAME (AS FRACTION OF NX) BEFORE ADJUSTING TRACKING HEIGHT(0.39)
22. DEVIATION FROM OPTIMUM STEPSIZE(AVERAGE OF DX AND DZ) TOLERATED BEFORE ADJUSTING STEPSIZES(0.5)
23. MINIMUM AVERAGING HEIGHT FOR FINDING EFFECTIVE DIFFUSIVITY IN GROUND=ABSORPTION SOLUTION(50.0)
24. BASIC MINIMUM TRAJECTORY REAL-TIME STEPSIZE(100.0)
25. BLANK(0.0)
26. BLANK(0.0)
27. MAXIMUM ALLOWED LAGRANGIAN SOLUTION FRAME LENGTH(10000.0)
28. MAXIMUM ALLOWED LAGRANGIAN FRAME VERTICAL STEPSIZE DZ(25.0)
29. MAX. NO. OF TIMES DZ IS GREATER THAN OPTIMUM DZ, BEFORE PREVENTION OF FURTHER RELATIVE ADVECTION(2.0)
30. MINIMUM RELEASE-HISTORY EVENT TIME WHICH IT IS REQUIRED TO DEFINE TO AN ACCURACY OF EXISTENT SPAR(19)/SOAR(2).(2.0)

ISPAR(J) (INTEGERS)

1. GENERAL INPUT FILE NO.(41)
2. BLANK=UNUSED FILE NO.(42)
3. X-VELOCITY FILE NO.(43)
4. Y-VELOCITY FILE NO.(44)
5. INVERSE STABILITY LENGTH FILE NO.(45)
6. POTENTIAL TEMPERATURE GRADIENT FILE NO.(46)
7. DATA DESCRIPTOR STORAGE FILE NO.(47)
8. INTERMEDIATE DATA STORAGE FILE(FOR CONTINUATION) NO. (48)
9. RESULT OUTPUT FILE NO.(49)
10. ALTERNATING INTERMEDIATE DATA STORAGE FILE(FOR CONTINUATION) NO.(51)
11. WORDS(=REALS OR INTEGERS)PER FILE RECORD(60)
12. CARD INPUT FILE NO.(2)
13. PRINTER OUTPUT FILE NO.(3)
14. CONTINUOUS DATA INPUT(OPTION(2)=HISTORIES AT SELECTED MASTS) INPUT FILE NO.(40)

C.COMPUTER CLOCK FACILITY

PROGRAM MAKES USE OF FUNCTION SUBPROGRAM TIME(J) WHICH GIVES TIME-OF-DAY(1/60 SECS) FOR J=1 AND PROGRAM PROCESS TIME(1/60 SECS) FOR J=2. IF SUCH FACILITY NOT AVAILABLE, INCLUDE A DUMMY SUBPROGRAM AND SET TIME(1)=TIME(2)=0.

D.ARRAY SIZES
=====

MINIMUM ARRAY SIZES SHOULD BE USED TO SAVE COMPUTER STORAGE.
EG. IF CONTINUOUS DATA INPUT OPTION(2) IS USED, SET DIMENSIONS OF
UB,VB,STAB,PARAM TO (2*ITOT*JTOT). THESE ARE SIMPLY ALTERED IN THE
MAIN PROGRAM WHICH IS REALLY A DUMMY MAIN PROGRAM. IT IS NOT
WORTHWHILE TO ALTER THE SMALLER ARRAY DIMENSIONS.

E.AVAILABILITY OF METEOROLOGICAL DATA

=====

THE INPUT DATA MUST COVER ALL RELEASE-TIMES AND DOSAGE PERIODS
(OR CONC. DISTRIBUTION "TIMES-OF-INTEREST"). DATA MUST BE
AVAILABLE IN A MARGIN(SAY 100 SECS) PRECEDING THE START OF RELEASE.

F.CONTINUATION OF EXECUTION IN THE EVENT OF ANY INTERRUPTION

=====

SET FIRST DATA CARD ACCORDING TO LAST FILE(1 OR 2) WHICH WAS
SUCCESSFULLY WRITTEN TO.
(SEE SECTION A.(I)(1) ABOVE)

G.FORMAT OF FINAL OUTPUT DATA IN FILE NO.49

=====

(1) POINT-DOSAGE SOLUTION

FILE(49) RECORD(0) - RUN NUMBER, MUL

FILE(49) RECORD(1) - DOSAGE INTERVAL BOUNDARY-TIME SEQUENCE,
----- (TDOS(J), J=1, NTDOS) WHERE NTDOS=MAX.60

FILE(49) RECORD(2) - X-GRID POSITIONS OF DOSAGE SITES(XDOS(J), J=1,
----- NPDOS)

FILE(49) RECORD(3) - Y-GRID POSITIONS OF DOSAGE SITES(YDOS(J), J=1,
----- NPDOS)

FILE(49) RECORD(4) TO RECORD(43)

DOSAGES(CONCENTRATION*TIME) 1 TO 59 BETWEEN THE 1 TO 60 BOUNDARY-
TIMES AS VALUES 1 TO 59 IN EACH RECORD, WITH ONE RECORD FOR EACH
DOSAGE POSITION(IN SEQUENCE),(1 TO 40)

(2) CONCENTRATION DISTRIBUTION SOLUTION

(1) FILE(49) RECORD(0) - NREC=NEXT RECORD TO BE WRITTEN TO IN THIS
----- FILE(FOR NEXT "TIME-OF-INTEREST" RESULT SET)
(SET TO 1 IN FIRST EXECUTION FOR A NEW RUN)

(1) FILE(49) RECORD(1) - NHANS(SEE LABEL 30 ABOVE), NOUT(PRINTER
----- OUTPUT FILE NO.), XGA, XGB, XGW, YGA, YGB, YGW(SEE

L32), XG1, YG1(SEE L8), DXB, DYB(L6), DMX, DMY(STEP
-SIZES IN SOLUTION GRID ANS), NMY, NMX(L26), MUL
(L1), (HANS(J), J=1, NHANS=L31), IT(TIME-OF-
INTEREST NO., =MAX, NTIME=SEEL13, L14), NTIME(L13)
, TIME(IT=SEE L14)

(III) FILE(49) RECORD(2) TO RECORD(1+NMX*NMY*NHANS/60+0.99999)

CONCENTRATIONS AT TIME(IT) AT SOLUTION-GRID(NMX*NMY)-POINTS(I,E,
IN REGION-OF-INTEREST). ORDER IS ((ANS(I,J,K), K=1, NHANS), J=1, NMY),
I=1, NMX) IN CONTINUOUS SEQUENCE SPLIT INTO RECORDS OF 60 VALUES.

NOTE: FOR FURTHER TIMES-OF-INTEREST(I.E. IT=2,3,4...), THE SEQUENCE
==== (II) THEN (III) ABOVE IS REPEATED, AND THE RECORD TOTAL IN (I)
IS UPDATED.

BLOCK DATA

FIXED PARAMETERS- THESE VALUES MAY BE ALTERED(SEE SECTION B.ABOVE)

COMMON /SPEC/SPAR(30)

COMMON /ISPEC/ISPAR(15)

DATA SPAR(1), SPAR(2), SPAR(3), SPAR(4)/0.5, 900.0, 750.0, 800.0/
DATA SPAR(5), SPAR(6), SPAR(7), SPAR(8)/20.0, 12.0, 280.0, 3.0/
DATA SPAR(9), SPAR(10), SPAR(11), SPAR(12)/20.0, 1500.0, 0.25, 0.002/
DATA SPAR(13), SPAR(14), SPAR(15), SPAR(16)/0.4, 50.0, 2.0, 0.2/
DATA SPAR(17), SPAR(18), SPAR(19), SPAR(20)/2500.0, 90.0, 90.0, 0.05/
DATA SPAR(21), SPAR(22), SPAR(23), SPAR(24)/0.39, 0.5, 50.0, 100.0/
DATA SPAR(25), SPAR(26), SPAR(27), SPAR(28)/0.0, 0.0, 10000.0, 25.0/
DATA SPAR(29), SPAR(30)/2.0, 2.0/
DATA ISPAR(1), ISPAR(2), ISPAR(3), ISPAR(4)/41, 42, 43, 44/
DATA ISPAR(5), ISPAR(6), ISPAR(7), ISPAR(8)/45, 46, 47, 48/
DATA ISPAR(9), ISPAR(10), ISPAR(11), ISPAR(12)/49, 51, 60, 2/
DATA ISPAR(13), ISPAR(14)/3, 40/
END

DIMENSION UB(4128), VB(4128), STAB(4128), PARAM(4128)

DIMENSION ZU(2064), U(2064), RAB(2064), GW(15), DIR(15), TC(15)

DIMENSION SLC(15), VARY(3360), AVY(3360), PR(3360)

DIMENSION P(3360), PL(3360), AVYL(3360), VARYL(3360)

DIMENSION XH(280), XF(280), NFILT(15), HIMA(15), TUAT(15)

DIMENSION HANS(3), A(1), F(2,12), ANS(3600), DEP(280)

DIMENSION PIN(3360), AVYIN(3360), VARYIN(3360), XFIN(280)

DIMENSION NFL(3), P1(3360), AVYI(3360), XFP(280), XFN(280), VARYI(3360)

THE ABOVE DIMENSIONS MAY BE ALTERED TO SAVE SPACE(SEE SECTION
D. ABOVE)

COMMON/SPEC/SPAR(30)

COMMON/ISPEC/ISPAR(15)

THIS MAIN PROGRAM IS EMPLOYED TO SET UP THE VARIABLE DIMENSIONS.

```

NX=IFIX(SPAR(7))
NZ=IFIX(SPAR(6))
LF=ISPAR(1)
C-----DIMENSIONS OBTAINED FROM INPUT FILE
  READ(LF)MUL,NTDAT,ITOT,JTOT,DXB,DYB,GWV,DIRN,TCUN,XGM1,XGM2,YGM1,
  $YGM2,XGS,YGS,ZS,NSTR,WS,DELTA,DELTB,DELTC,DELTD,FREXT,DT1,PREM
  READ(LF)TUES,TDEF,PDEP,DTMIN,NMX,NMY,NMZ,DMZ,SLCON,NDJ,NFL,JHALF,
  $NSDT,ITJEK,NHANS,XGA,XGB,XGW,YGA,YGB,YGW,NTDOS,NPDUS,ZDOS
C-----PRUCEEU TO EFFECTIVE MAIN PROGRAM...
  CALL MAIN(ITOT,JTOT,NTDAT,NX,NZ,NMX,NMY,NMZ,NHANS,UB,VB,
  $STAB,PARAM,ZO,D,RAB,GW,DIR,TC,SLC,VARY,AVY,PR,P,PL,AVYL,VARYL,
  $XFL,XF,NFILT,HIMA,TDAT,HANS,A,F,ANS,PIN,AVYIN,VARYIN,XFIN,PT,
  $AVYT,XFP,XFN,VARYT,DEP)
  STOP
  END

SUBROUTINE INPUT(NTDAT,ITOT,JTOT,DELTA,DELTB,DELTC,DELTD,FREXT,
$DT1,DTMIN,NMX,NMY,NMZ,DMZ,SLCON,NDJ,JHALF,
$NSDT,ITJEK,NHANS,XGA,XGB,XGW,YGA,YGB,YGW,NFILT,HIMA,TDAT,TIME,
$NTIME,ZO,D,GW,DIR,TC,SLC,HANS,NX,NZ,
$SRAB,UB,VB,STAB,PARAM,NIN,NOUT)
C-----THIS SUBROUTINE ACQUIRES THE ORIGINAL INPUT DATA..(SEE SECTION
C A.(II) ABOVE)
C
  DIMENSION ZC(ITOT,JTOT),D(ITOT,JTOT),GW(NTDAT),DIR(NTDAT)
  DIMENSION TC(NTDAT),SLC(NTDAT),RAB(ITOT,JTOT),LET(60,80)
  DIMENSION UB(ITOT,JTOT,NTDAT),VB(ITOT,JTOT,NTDAT)
  DIMENSION STAB(ITOT,JTOT,NTDAT),PARAM(ITOT,JTOT,NTDAT)
  DIMENSION NFILT(NTDAT),HIMA(NTDAT)
  DIMENSION TDAT(NTDAT),HANS(NHANS)
  DIMENSION TIME(15)
  COMMON/DQSA/DOS(59,40),TDOS(60),XDOS(40),YDOS(40),NTDOS,NPDUS,ZDOS
  COMMON/DQSB/QSTR(30),TSTR(30),NSTR,XPL,YPL
  COMMON/DQSD/XPLLT,YPLLT,TLT,DXB,DYB,QTRL,QTR,XVLLT,YVLLT,XRLLT,
  $YRLLT,XRL,YRL,PDEP,TDEF,TDES,WS,PREM
  COMMON/STUR2/XGS,YGS,ZS
  COMMON/STUR3/MUL,GWV,DIRN,TCUN,XGM1,XGM2,YGM1,YGM2
  COMMON/STOR6/JTSD(5),NFL(3),DT(300)
  COMMON/ISPEC/ISPAR(15)
  COMMON/CONDAT/NMCD,NTCD,TSCU,DTCD,CD(16000),PMCU(15,2)
  COMMON/ZSTAN/ZG
  COMMON/SWEND/WFMCD(15)
C-----DATA INPUT -----
C-----
  LF=ISPAR(7)
C-----INPUT DATA-DESCRIPTOR LABELS...
  DO 111 I=1,60
  READ(LF)(LET(I,J),J=1,40)
  READ(LF)(LET(I,J),J=41,80)
111 CONTINUE

```

```

CLOSE LF
112 FORMAT(1H0,80A1)
LF=ISPAR(1)
REWIND LF
C-----INPUT FILE(41) DATA (SECTION A.(II))
  READ(LF)MUL,NTDAT,ITOT,JTOT,DXB,DYB,GWV,DIRN,TCUN,XGM1,XGM2,YGM1,
  $YGM2,XGS,YGS,ZS,NSTR,WS,DELTA,DELTB,DELTC,DELTD,FREXT,DT1,PREM
  READ(LF)TUES,TDEF,PDEP,DTMIN,NMX,NMY,NMZ,DMZ,SLCON,NDJ,NFL,JHALF,
  $NSDT,ITJEK,NHANS,XGA,XGB,XGW,YGA,YGB,YGW,NTDOS,NPDUS,ZDOS,ZG
  READ(LF)(TDAT(K),K=1,NTDAT),(HIMA(K),K=1,NTDAT)
  READ(LF)QSTR
  READ(LF)TSTR
  READ(LF)NTIME,TIME
  READ(LF)HANS
  DO 201 I=1,ITOT
201 READ(LF)(ZC(I,J),J=1,JTOT)
  DO 202 I=1,ITOT
202 READ(LF)(D(I,J),J=1,JTOT)
  READ(LF)(GW(K),K=1,NTDAT),(DIR(K),K=1,NTDAT)
  READ(LF)(TC(K),K=1,NTDAT),(SLC(K),K=1,NTDAT)
  READ(LF)TUOS
  READ(LF)XDOS
  READ(LF)YDOS
  DO 204 I=1,ITOT
204 READ(LF)(RAB(I,J),J=1,JTOT)
  CLOSE LF
C-----TEST FOR CONTINUOUS DATA AVAILABILITY...
  LF=ISPAR(14)
  READ(LF)NMCD,NTCD,TSCU,DTCD
  IF(NMCD.EQ.0)GO TO 151
C-----INPUT CONTINUOUS DATA EX FILE(40)..(SECTION A.(II)OPTION(1))
  READ(LF)((PMCD(I,J),J=1,2),I=1,NMCD),(WFMCD(I),I=1,NMCD)
  LREC=ISPAR(11)
  K=NMCD*NTCD*4
C-----TOTAL RECORDS AT LREC VALUES PER RECORD
  IP2=FLOAT(K)/FLOAT(LREC)+0.9999999
  DO 152 I=1,IP2
  JP1=(I-1)*LREC+1
  JP2=I*LREC
  IF(I.EQ.IP2)JP2=K
  READ(LF)(CD(J),J=JP1,JP2)
152 CONTINUE
  CLOSE LF
C-----INPUT GRID-STORED DATA..(SECTION A.(II)OPTION(2))
C-----X-VELOCITY AT HEIGHT ZG...
  DO 251 K=1,NTDAT
  DO 251 I=1,ITOT
251 READ(ISPAR(3))(UB(I,J,K),J=1,JTOT)
  CLOSE ISPAR(3)
C-----Y-VELOCITY AT HEIGHT ZG...
  DO 252 K=1,NTDAT
  DO 252 I=1,ITOT
252 READ(ISPAR(4))(VB(I,J,K),J=1,JTOT)
  CLOSE ISPAR(4)
C-----INVERSE MONIN-OBUKHOV STABILITY LENGTH(L**=1)
  DO 253 K=1,NTDAT
  DO 253 I=1,ITOT

```

```

253 READ(ISPAR(5))(STAB(I,J,K),J=1,JTOT)
CLOSE ISPAR(5)
C-----POTENTIAL TEMPERATURE GRADIENT AT HEIGHT ZG (DTP/DZ)ZG)
DO 254 K=1,NTDAT
DU 254 I=1,ITOT
254 READ(ISPAR(6))(PARAM(I,J,K),J=1,JTOT)
CLOSE ISPAR(6)
153 CONTINUE

```

```

C- PRINT INPUT DATA -----
C-----

```

```

WRITE(NOUT,112)(LET(1,J),J=1,80)
WRITE(NOUT,102)MUL
102 FORMAT(1H0,"DATASET NO. ",I5)
101 FORMAT(1X,24I3)
103 FORMAT(1X,8F10.4)
104 FORMAT(1X,8E10.4)
WRITE(NOUT,112)(LET(2,J),J=1,80)
WRITE(NOUT,101)NTDAT
WRITE(NOUT,112)(LET(3,J),J=1,80)
WRITE(NOUT,103)(TDAT(J),J=1,NTDAT)
WRITE(NOUT,112)(LET(4,J),J=1,80)
WRITE(NOUT,103)(HIMA(J),J=1,NTDAT)
WRITE(NOUT,112)(LET(5,J),J=1,80)
WRITE(NOUT,101)ITOT,JTOT
WRITE(NOUT,112)(LET(6,J),J=1,80)

```

```

WRITE(NOUT,103)DXB,DYB
WRITE(NOUT,112)(LET(7,J),J=1,80)
DU 279 J=1,NTDAT
WRITE(NOUT,122)J,GW(J),DIR(J),TC(J),SLC(J)
122 FORMAT(1X,I3,8F10.5)
279 CONTINUE
WRITE(NOUT,112)(LET(8,J),J=1,80)
WRITE(NOUT,103)XGM1,XGM2,YGM1,YGM2
WRITE(NOUT,112)(LET(9,J),J=1,80)
WRITE(NOUT,103)XGS,YGS,ZS
WRITE(NOUT,112)(LET(10,J),J=1,80)
WRITE(NOUT,103)XGA,XGB,XGW,YGA,YGB,YGW
WRITE(NOUT,112)(LET(11,J),J=1,80)
WRITE(NOUT,104)(QSTR(J),J=1,NSTR)
WRITE(NOUT,112)(LET(12,J),J=1,80)
WRITE(NOUT,103)(TSTR(J),J=1,NSTR)
WRITE(NOUT,112)(LET(13,J),J=1,80)
WRITE(NOUT,104)WS,PDEP,TDES,TDEF,PREM
IF(NTDUS.EQ.0)GO TO 121
WRITE(NOUT,112)(LET(14,J),J=1,80)
WRITE(NOUT,101)NTDUS
WRITE(NOUT,112)(LET(15,J),J=1,80)
WRITE(NOUT,103)(TDUS(J),J=1,NTDUS)
WRITE(NOUT,112)(LET(16,J),J=1,80)
WRITE(NOUT,101)NPDUS
WRITE(NOUT,112)(LET(17,J),J=1,80)
DU 132 J=1,NPDUS
C*FOR DEPOSITION AT (XDOS,YDOS),PRECEDE XDOS,YDOS VALUES WITH MINUS....
WRITE(NOUT,103)XDOS(J),YDOS(J)
132 CONTINUE
WRITE(NOUT,112)(LET(18,J),J=1,80)

```

```

WRITE(NOUT,103)ZDOS
GO TO 123
121 WRITE(NOUT,112)(LET(13,J),J=1,80)
WRITE(NOUT,101)NTIME
WRITE(NOUT,112)(LET(14,J),J=1,80)
WRITE(NOUT,103)(TIME(J),J=1,NTIME)
123 CONTINUE
WRITE(NOUT,112)(LET(16,J),J=1,80)
WRITE(NOUT,103)DELTA
WRITE(NOUT,112)(LET(17,J),J=1,80)
WRITE(NOUT,103)DELTB
WRITE(NOUT,112)(LET(18,J),J=1,80)
WRITE(NOUT,103)DELTG
WRITE(NOUT,112)(LET(19,J),J=1,80)
WRITE(NOUT,103)DELTU
WRITE(NOUT,112)(LET(23,J),J=1,80)
WRITE(NOUT,101)NSDT
WRITE(NOUT,112)(LET(26,J),J=1,80)
WRITE(NOUT,101)NMX,NMY,NMZ
WRITE(NOUT,112)(LET(27,J),J=1,80)
WRITE(NOUT,103)DMZ
WRITE(NOUT,112)(LET(29,J),J=1,80)
WRITE(NOUT,101)ITJEK
WRITE(NOUT,112)(LET(30,J),J=1,80)
WRITE(NOUT,101)NHANS

IF(NHANS.EQ.0)GO TO 120
WRITE(NOUT,112)(LET(31,J),J=1,80)
WRITE(NOUT,103)(HANS(J),J=1,NHANS)
120 CONTINUE
IP1=XGM1+0.5
IP2=XGM2+0.5
JP1=YGM1+0.5
JP2=YGM2+0.5
WRITE(NOUT,105)
105 FORMAT(/,1H0,"SAMPLE VALUES OF CONSTANT SURFACE DATA AT CORNERS OF
$ REGION OF INTEREST",/ ,33X,"(XGM1,YGM1) (XGM2,YGM1) (XGM1,YG
SM2) (XGM2,YGM2)")
WRITE(NOUT,106)ZC(IP1,JP1),ZC(IP2,JP1),ZC(IP1,JP2),ZC(IP2,JP2)
106 FORMAT(1X,"ZC(X,Y) (CONSTANT)",10X,"=" ,4(E11.4,4X))
WRITE(NOUT,107)D(IP1,JP1),D(IP2,JP1),D(IP1,JP2),D(IP2,JP2)
107 FORMAT(1X,"D(X,Y) (CONSTANT)",10X,"=" ,4(E11.4,4X))
WRITE(NOUT,148)RAB(IP1,JP1),RAB(IP2,JP2),RAB(IP1,JP2),RAB(IP2,JP2)
148 FORMAT(1X,"RAB(X,Y) (CONSTANT)",10X,"=" ,4(E11.4,4X))
IF(NMCD.NE.0)GO TO 154
WRITE(NOUT,117)
117 FORMAT(/,1H0,"SAMPLE VALUES OF TIME-SURFACE DATA AT CORNERS OF REG
$ ION OF INTEREST",/ ,33X,"(XGM1,YGM1) (XGM2,YGM1) (XGM1,YGM2)
$ (XGM2,YGM2)")
DU 205 IT=1,NTDAT
205 WRITE(NOUT,109)TDAT(IT),UB(IP1,JP1,IT),UB(IP2,JP1,IT),UB(IP1,JP2,I
ST),UB(IP2,JP2,IT)
109 FORMAT(1X,"AT TIME=",F10.2," UB(X,Y,T)= ",4(E11.4,4X))
DU 206 IT=1,NTDAT
206 WRITE(NOUT,116)TDAT(IT),VB(IP1,JP1,IT),VB(IP2,JP1,IT),VB(IP1,JP2,I
ST),VB(IP2,JP2,IT)
116 FORMAT(1X,"AT TIME=",F10.2,3X,"VB(X,Y,T)= ",4(E11.4,4X))
DU 207 IT=1,NTDAT
207 WRITE(NOUT,113)TDAT(IT),STAB(IP1,JP1,IT),STAB(IP2,JP1,IT),STAB(IP1
S,JP2,IT),STAB(IP2,JP2,IT)
113 FORMAT(1X,"AT TIME=",F10.2,1X,"STAB(X,Y,T)= ",4(E11.4,4X))

```

```

DU 208 IT=1,NTUAT
208 WRITE(NOUT,115)TDAT(IT),PARAM(IP1,JP1,IT),PARAM(IP2,JP1,IT),PARAM(
  $IP1,JP2,IT),PARAM(IP2,JP2,IT)
115 FORMAT(1X,"AT TIME=",F10.2,"PARAM(X,Y,T)= ",4(E11.4,4X))
      RETURN
C-----CONTINUOUS DATA INPUT(OPTION(2)) ONLY
154 CONTINUE
C-----MAST POSITIONS...
      WRITE(NOUT,159)
159 FORMAT("MAST POSITIONS...(X,Y), AND WEIGHTING FACTORS")
      DU 160 K=1,NMCD
160 WRITE(NOUT,103)(PMCD(K,J),J=1,2),WFMCD(K)
C-----SOME SAMPLE VALUES FOR CONTINUOUS DATA OPTION...
      WRITE(NOUT,155)(I,I=1,6)
155 FORMAT("OTIME",4X,6(6X,"MAST",13,7X))
      WRITE(NOUT,156)
156 FORMAT(9X,6(" UB VB 1/L PTG ")
      J=60
      IF(J.GT.N!CD)J=NTCD
      DU 157 K=1,J
      IP1=(K-1)*NMCD*4+1
      IP2=IP1+23
      TIM=TSCU+(K-1)*DTCD
      WRITE(NOUT,156)TIM,(CD(1),I=IP1,IP2)
157 CONTINUE
158 FORMAT(1X,F7.1,1X,6(F5.2,F5.2,F5.1,F5.2))
      RETURN
      END

```

```

SUBROUTINE STURE(IMOD,IJOB,PR,P,PL,AVYL,VARYL,XFL,XF,NFILT,HIMA,
  $TDAT,HANS,A,F,ANS,ITOT,JTOT,NTUAT,NX,NZ,NMX,NMY,NMZ,NHANS,NELP,
  $NELAN,NELA)

```

```

C-----THIS SUBROUTINE PERFORMS ALL FILE READS+WRITES EXCEPT FOR THE
C----- UNALTERED BASIC INPUT DATA COVERED IN SUBROUTINE INPUT...
C

```

```

COMMON/STUR1/IEND,ICONTROL,NOUT,
  $NUJ,JHALF,NSDT,ITJEK,NTIME,K,IP1,IP2,JP1,JP2,
  $SIG,JG,KUR,NPRIS,IS,IFLAG,ITS,ITP,MFLAG,IT,KA,ISET,MI,NST,NITP,
  $IPRUC,JP,NPUFFS,JCH,NPUFF1,NP,NSUSED,NTSOL,NPINT,IN,JST,NTJX,
  $NTJZ,IA,IOR,NTEMP,JA,KA,DELTA,DELTA,DELTC,DELTD,FREXT,DT1,
  $
  $DTMIN,UMZ,SLCON,XGA,XGB,XGW,YGA,YGB,YGW,PBR,F,DZATSV,ZPBS,TREL,XG,
  $YG,TIM,UXY,VXY,XP,YP,STABP,PARAM,ZOP,DP,VEL,ITRAV,EZ,ZM,US,VS,
  $UVS,TDIFF, TID,D1,D2,D3,D4,TREM,TRIN,TRUT,TPERIOD,DELTE,TEND,
  $OXATSV,ZJ,PERIOD,TSTART,PNT,DTPUFF,XMAP1,XMAP2,YMAP1,YMAP2,UMX,
  $OMY,XTJIN,YTJIN,XTJUT,YTJUT, SUM,SIGMA1,XS,YS,ZPB,UXS,VXS,
  $SIGMA2,PDX,PDX,PDX,PDX,PDX,PDX,PDX,PDX,PDX,PDX,PDX,PDX,PDX,PDX,
  $S42,DZIN,ZBIN,IR,DTSTR,HANS,AV,DEFF,DIST,DTJX,DTJY,XGP,YGP,DISOR,
  $SGP,XEF,SP,FRI,ZB,THI,QUIV,FRK,PA,PB,PEFF,XB,YB,SB,SY,G1,C2,C1,
  $G2,YCUT,XCUT,DOR,DOT,TOR,ARM,VAL1,XPF,YOUT,PXL,PZL,PORL,PORL,
  $POTL,POTL,SIGL,SIGL, DSDT,SOTI,NTREU,TSOS, TRAUD,
  $NSOH,XRRL,TREPL,MF,NIN

```

```

DIMENSION PR(NELP),P(NELP),PL(NELP)
DIMENSION AVYL(NELP),VARYL(NELP),XFL(NX),XF(NX)
DIMENSION NFILT(NTUAT),HIMA(NTDAT)
DIMENSION TUAT(NTDAT),HANS(NHANS)
DIMENSION A(NELA),F(2,NZ),ANS(NELAN)
COMMON/STUR2/XGS,YGS,ZS
COMMON/STUR3/MUL,GNV,DIRN,TCUN,XGM1,XGM2,YGM1,YGM2
COMMON/STUR4/TRELIN(15,4),TRELUT(15,4)
COMMON/STUR5/TIME(15),UVMAX(15)
COMMON/STUR6/JTSOL(5),NFL(3),DT(300)
COMMON/STUR7/EMIN(2,15,4),TRED(180)
COMMON/DOISA/DUS(59,40),TDS(60),XDUS(40),YDUS(40),NTDUS,NPDS,ZDUS
COMMON/DOSB/OSTR(30),TSTR(30),NSTR,XPL,YPL,TRTEM
COMMON/DOSC/XVANL,YVANL,TACTL,DZL,ZPBL,TRAJ(7,300),NLP,DTUS
COMMON/DOSD/XPLLT,YPLLT,TLLT,DXB,DTB,OTRLT,OTR,XVLLT,YVLLT,XRLLT,
  $YRLLT,XRL,YRL,PDEP,TDEF,TDOS,WS,PREM
COMMON/DOSS/S(24000),XFIOR(40)
COMMON/ELAP/KLAPSM,KLAST,KTEXP
COMMON/ISPEC/ISPAR(15)
COMMON/PPROG/INFORM

```

```

LREC=ISPAR(11)
IF(IMOD.EQ.1)GO TO 301
IF(IMOD.EQ.2)GO TO 302
IF(IMOD.EQ.3)GO TO 303
IF(IMOD.EQ.4)GO TO 304
IF(IMOD.EQ.5)GO TO 305

```

```

C-DECIDE WHETHER REQUIRE TO CONTINUE PREVIOUS SOLUTION USING INTERMEDIAT
C--E DATA STORED IN FILE ISPAR(8) OR ISPAR(10) -----
C-----

```

```

MF=ISPAR(8)
READ(NIN,119)I
IF(I.EQ.1)MF=ISPAR(10)
IF(I.EQ.2)MF=ISPAR(8)
IF((I.LT.0).OR.(I.GT.2))ERRUR=SQRT(-1.0)
MFALT=ISPAR(10)
IF(I.EQ.1)MFALT=ISPAR(8)
CALL TIMEX(J)
KLAPSM=0
READ(MF)IEND

```

```

C-----ERROR SIGNAL FOR INCOMPLETE WRITE TO A FILE...
IF(IEND.NE.1)MF=MFALT
IF(IEND.NE.1)MF=ISPAR(10)
IF(IEND.NE.1)READ(MF)IEND
IF(IEND.NE.1)ERROR=SQRT(-1.0)
READ(MF)ICONTROL

```

```

READ(NIN,240)KTEXP
C-----INFORM=0..NO PUFF PROGRESS INFORMATION
C-----INFORM=1..PUFF PROGRESS PARAMETERS.
C-----INFORM=2..PUFF PROGRESS PARAMETERS AND DISTRIBUTIONS
READ(NIN,119)INFORM
119 FORMAT(I1)
240 FORMAT(I4)
IJOB=0
IF(I.EQ.0)IJOB=333

```

```

C-----FLAG FOR INITIALISING A NEW RUN...
IF(IJOB.EQ.333)RETURN
REWIND MF

```

```

C-----READ INTERMEDIATE DATA FOR PREVIOUS INCOMPLETE EXECUTION..
READ(MF)IEND
READ(MF) ICONTROL,NOUT,I,J,MUL,NTDAT,ITOT,JTOT,NSTR,NMX,NMY,NMZ,
  $NUJ,JHALF,NSDT,ITJEK,NHANS,NTIME,K,IP1,IP2,JP1,JP2,(G,JG,KUR,NPRIS

```

```

& IS,IFLAG,ITS,ITP,NX,MFLAG,IT,KA, ISET,MI,NST,NITP,NZ,IPROC,JP,NPUF
& FS,JCH,NPUF1,NP,NUSED,NTSUL,NPINT,IN,JST,NTJX,NTJZ,IA,IOR,NTE,P,
& JA,KK
  READ(MF)   UXB,DYB,GWV,DIRN,TCON,XGM1,XGM2,YGM1,YGM2,XGS,YGS,ZS,
& NS,DELTA,DELTB,DELTC,DELTD,FREXT,DT1,DES,DEF,PDEP,DTMIN,DMZ, S
& LCON,XGA,XGB,XGW,YGA,YGB,YGW,PBFR,DZATSV,ZPBS,TREL,XGY,TIM,UXY,
& VXY,XP,YP,STABP,PARAMP,ZCP,DP,VEL,TTRAV,EZ,ZM,US,VS,UVS,TDIFF,PREM
  READ(MF)   TID,D1,D2,D3,D4,TREM,TRIN,TROT,TPERIOD,DELTE,TEND,DXAT
& SV,ZJ,PERIOD,TSTART,PNT,UTPUFF,XMAP1,XMAP2,YMAP1,YMAP2,UMX,DMY,XTJ
& IN,YTJIN,XTJOT,YTJUT,DTMIN,UT1,SUM,SIGMA1,XS,YS,ZPB,DXSVEX,SIGMA2,
& SPDX,PDZ,PURX,PURY,PUTX,PITY,SIG1,SIG2,XUR,YOR,XUT,YUT,SG1,SG2,DZIN
& ZPBIN,TR,DTSTR,HANSAV,TRTEM
  READ(MF)   @EFF,DIST,DTJX,DTJOR,XGP,YGP,DISOR,DGP,XEF,SP,FRI,ZB,T
& SHT,ZDIV,FRK,PA,PB,PEFF,XB,YB,SB,SY,G1,C2,C1,G2,YCUT,XCUT,DOR,DOT,
& TURU,ARM,VAL1,XP,YUUT,PDXL,PUZL,PORXL,PURYL,PUTXL,POTYL,SIG1L,SIG
& 2L,ZPBL,DSOT,SUTI,NTRED,TSUUS,DTOS,TRAUU,NSUM,@TR,XNERL,YREKL
  IMA=FIX(FLOAT(NELP)/FLOAT(LREC)+0.99999999)
  JFF=NELP
  DO 233 I=1,IMA
  JRS=(I-1)*LREC+1
  JRF=I*LREC
  IF(I.EQ.IMA)JRF=JFF
  READ(MF)(PR(J),J=JRS,JRF)
  READ(MF)(PC(J),J=JRS,JRF)
  READ(MF)(PL(J),J=JRS,JRF)
  READ(MF)(AVYL(J),J=JRS,JRF)
  READ(MF)(VARYL(J),J=JRS,JRF)
233 CONTINUE
  IMA=FIX(FLOAT(NX)/FLOAT(LREC)+0.99999999)
  JFF=NX
  DO 242 I=1,IMA
  JRS=(I-1)*LREC+1
  JRF=I*LREC
  IF(I.EQ.IMA)JRF=JFF
  READ(MF)(XF(J),J=JRS,JRF)
  READ(MF)(XFL(J),J=JRS,JRF)

242 CONTINUE

  READ(MF)TRELIN
  READ(MF)TREL0T

  READ(MF)UVMAX
  READ(MF)JTSUL,NFL
  DO 234 I=1,5
  J1=(I-1)*60+1
  J2=I*60
  READ(MF)(DT(J),J=J1,J2)
234 CONTINUE
  IF(NELAN.EQ.0)GO TO 361
  IMA=FIX(FLOAT(NELA)/FLOAT(LREC)+0.99999999)
  JFF=NELA
  DO 235 I=1,IMA
  JRS=(I-1)*LREC+1
  JRF=I*LREC
  IF(I.EQ.IMA)JRF=JFF
  READ(MF)(A(J),J=JRS,JRF)
235 CONTINUE
361 CONTINUE
  READ(MF)(F(1,J),J=1,NZ)
  READ(MF)(F(2,J),J=1,NZ)
  IF(NELAN.EQ.0)GO TO 362

```

```

  IMA=FIX(FLOAT(NELAN)/FLOAT(LREC)+0.99999999)
  JFF=NELAN
  DO 237 I=1,IMA
  JRS=(I-1)*LREC+1
  JRF=I*LREC
  IF(I.EQ.IMA)JRF=JFF
  READ(MF)(ANS(J),J=JRS,JRF)
237 CONTINUE
362 CONTINUE
  READ(MF)(EMIN(1,I,J),I=1,15),J=1,4)
  READ(MF)(EMIN(2,I,J),I=1,15),J=1,4)
  DO 238 J=1,40
  READ(MF)(DDS(I,J),I=1,59)
238 CONTINUE
  READ(MF)(TRED(J),J=1,60)
  READ(MF)(TRED(J),J=61,120)
  READ(MF)(TRED(J),J=121,180)
  DO 262 I=1,7
  DO 262 J=1,5
  J1=(J-1)*60+1
  J2=J*60
  READ(MF)(TRAJ(I,K),K=J1,J2)
262 CONTINUE
  READ(MF)XFIUR
  IMA=FIX(24000.0/FLOAT(LREC)+0.99999999)
  JFF=24000
  DO 322 I=1,IMA
  JRS=(I-1)*LREC+1
  JRF=I*LREC
  IF(I.EQ.IMA)JRF=JFF
  READ(MF)(S(J),J=JRS,JRF)
322 CONTINUE

  RETURN
301 CONTINUE
C-----STORAGE OF INTERMEDIATE DATA...
  CALL TIMEX(KTIMEX)
  I=KTIMEX+40
C-----ONLY WRITE ONCE THE SPECIFIED ELAPSED(TOTAL) TIME HAS BEEN
C- - EXCEEDED(SECTION A.(1)) - THIS SAVES COMPUTER-TIME...
  IF(KTEXP.GT.I)RETURN

C*STORE INTERMEDIATE DATA IN FILES ISPAR(8) AND ISPAR(10) ALTERNATELY...
  IF(MF.EQ.ISPAR(8))GO TO 250
  MF=ISPAR(8)
  GO TO 251
250 MF=ISPAR(10)
251 CONTINUE
  IF(MF.EQ.ISPAR(10))I=1
  IF(MF.EQ.ISPAR(8))I=2
  WRITE(NUIT,923)I
C-----THE FOLLOWING MESSAGE IS BLANKED OUT IF THE FILE WRITE IS
C- - SUCCESSFULLY COMPLETED...
923 FORMAT(10X,"ERROR" TRANSFER TO FILE M",I1," INCOMPLETE")
  REWIND MF
  IEND=1094
  WRITE(MF)IEND
  WRITE(MF) @CONTROL,NOUT,I,J,MUL,NTDAT,ITOT,JTOT,NSTR,NMX,NMY,NHZ,
& NDJ,JHALF,NSDT,ITJER,NHANS,NTIME,K,IP1,IP2,JP1,JP2,IG,JG,KOH,NPHIS
& IS,IFLAG,ITS,ITP,NX,MFLAG,IT,KA, ISET,MI,NST,NITP,NZ,IPROC,JP,NPUF

```

```
SI S, JCH, NPUF1, NP, NSUSED, NTSOL, NPINT, IN, JST, NTJX, NTJZ, IA, IQK, NTEMP,
$JA, KK
WRITE(MF) DUB, DYB, GWV, DIRN, TCON, XGM1, XGM2, YGM1, YGM2, XGS, YGS, ZS,
& NS, DELTA, DELTB, DELTC, DELTD, FNEXT, UT1, TUES, TDEF, PDEF, DTMIN, DMZ, S
& LCON, XGA, XGB, XGW, YGA, YGB, YGW, PBF, DZATS, ZPBS, TREL, XG, YG, TIM, UXY,
& SVXY, XP, YP, STAP, PARAMP, ZOP, UP, VEL, TTRAV, EZ, ZH, US, VS, UVS, TDIFF, PREM
WRITE(MF) TIU, D1, D2, D3, D4, TREM, THIN, TROT, TPERIOD, DELTE, TEND, DXAT
& SV, ZJ, PERIOD, TSTART, PNT, DTPUFF, XMAP1, XMAP2, YMAP1, YMAP2, DMX, DMY, XTJ
& SIN, YTJIN, XTJOT, YTJUT, DTHIN, UT1, SUM, SIGMA1, XS, YS, ZPB, DXS, VEX, SIGMA2,
& PDX, PDZ, PURX, PURY, PUTX, PUTY, SIG1, SIG2, XUR, YUR, XUT, YUT, SG1, SG2, DZIN
```

```
$, ZPBIN, TR, DTSTR, HANS, AV, TRTEM
WRITE(MF) QEFF, DIST, DTJX, UTJUR, XGP, YGP, DISOR, DGP, XEF, SP, FRI, ZB, T
& SHT, ZDIV, FRK, PA, PB, PEF, XB, YB, SX, SY, G1, C2, C1, G2, YCUT, XCUT, DUR, DOT,
& STORU, ARM, VAL1, XPF, YUUT, PDXL, PDZL, PORXL, PORYL, PUTXL, POTYL, SIG1, SIG
& 2L, ZPBL, DSOT, SOTI, NTRED, TSOUS, DUTS, TRADD, NSUM, QTR, XRERL, YRERL
IMA=FIX(FLUAT(NELP)/FLUAT(LREC)+0.99999999)
JFF=NELP
DU 223 I=1, IMA
JRS=(I-1)*LREC+1
JRF=I*LREC
IF(1.EQ. IMA) JRF=JFF
WRITE(MF) (PK(J), J=JRS, JRF)
WRITE(MF) (P(J), J=JRS, JRF)
WRITE(MF) (PL(J), J=JRS, JRF)
WRITE(MF) (AVYL(J), J=JRS, JRF)
WRITE(MF) (VARYL(J), J=JRS, JRF)
```

```
223 CONTINUE
IMA=FIX(FLUAT(NX)/FLUAT(LREC)+0.99999999)
JFF=NX
DU 243 I=1, IMA
JRS=(I-1)*LREC+1
JRF=I*LREC
IF(1.EQ. IMA) JRF=JFF
WRITE(MF) (XF(J), J=JRS, JRF)
WRITE(MF) (XFL(J), J=JRS, JRF)
243 CONTINUE
```

```
WRITE(MF) TRELIN
WRITE(MF) TRELQT
WRITE(MF) DUMAX
WRITE(MF) JTSOL, NFL
DU 224 I=1, 5
J1=(I-1)*60+1
J2=1*60
WRITE(MF) (DT(J), J=J1, J2)
224 CONTINUE
```

```
IF(NELA.EQ.0) GO TO 363
IMA=FIX(FLUAT(NFLA)/FLUAT(LREC)+0.99999999)
JFF=NELA
DU 225 I=1, IMA
JRS=(I-1)*LREC+1
JRF=I*LREC
IF(1.EQ. IMA) JRF=JFF
WRITE(MF) (A(J), J=JRS, JRF)
225 CONTINUE
363 CONTINUE
WRITE(MF) (F(1, J), J=1, N2)
WRITE(MF) (F(2, J), J=1, N2)
IF(NELAN.EQ.0) GO TO 364
IMA=FIX(FLUAT(NELAN)/FLUAT(LREC)+0.99999999)
JFF=NELAN
```

```
DU 227 I=1, IMA
JRS=(I-1)*LREC+1
JRF=I*LREC
IF(1.EQ. IMA) JRF=JFF
WRITE(MF) (ANS(J), J=JRS, JRF)
227 CONTINUE
364 CONTINUE
WRITE(MF) ((LMIN(1, J), I=1, 15), J=1, 4)
WRITE(MF) ((LMIN(2, J), I=1, 15), J=1, 4)
DU 239 J=1, 40
WRITE(MF) (DUS(1, J), I=1, 59)
239 CONTINUE
WRITE(MF) (TRED(J), J=1, 60)
WRITE(MF) (TRED(J), J=61, 120)
WRITE(MF) (TRED(J), J=121, 180)
DU 261 I=1, 7
DU 261 J=1, 5
J1=(J-1)*60+1
J2=J*60
WRITE(MF) (TRAJ(1, K), K=J1, J2)
261 CONTINUE
WRITE(MF) XFIQR
IMA=FIX(24000.0/FLUAT(LREC)+0.999999)
JFF=24000
DU 323 I=1, IMA
JRS=(I-1)*LREC+1
JRF=I*LREC
IF(1.EQ. IMA) JRF=JFF
WRITE(MF) (S(J), J=JRS, JRF)
323 CONTINUE
REWIND MF
IEND=1
WRITE(MF) IEND
WRITE(NUOT, 924)
924 FORMAT(1H+, 9X, "XXXXXX", 22X, "XX")
RETURN
302 CONTINUE
C-----ON COMPLETION OF RUN EXECUTION SET FLAG IN INTERMEDIATE DATA FILE
ICONTROL=0
MF=1SPAR(8)
REWIND MF
IEND=1
WRITE(MF) IEND
WRITE(MF) ICONTROL
RETURN
303 CONTINUE
C-----ON INITIALISING A NEW RUN EXECUTION, SET FLAG IN OUTPUT FILE(49)
ICONTROL=1
LF=1SPAR(9)
REWIND LF
NREC=1
WRITE(LF) NREC
RETURN
304 CONTINUE
C-----STORE CONCENTRATION DISTRIBUTION SOLUTION IN OUTPUT FILE(49) (SEE
C- SECTION 4.(2))
LF=1SPAR(9)
REWIND LF
WRITE(LF) NRC
C-----THE FOLLOWING MESSAGE IS BLANKED OUT IF WRITE SUCCESSFULLY
C- - COMPLETES...
```

```

191 WRITE(NOUT,191)
   FORMAT(1H,"ERROR- TRANSFER TO FILE LF INCOMPLETE")
   NSKIP=NR-1
   IF(NSKIP.LE.0)GO TO 311
   LU 312 K=1,NSKIP
   READ(LF)FILA
312 CONTINUE
311 CONTINUE
   WRITE(LF)NHANS,NOUT,XGA,XGB,XGW,YGA,YGB,YGW,XGM1,YGM1,DXB,DYB,
   $DMX,DMY,NMY,NMX,MUL,HANS,IT,NTIME,TIME(IT)
   IMA=FIX(PLUAT(NELAN)/FLOAT(LREC)+0.99999999)
   JFF=NELAN
   DU 171 I=1,IMA
   JRS=(I-1)*LREC+1
   JRF=I*LREC
   IF(1.EQ.IMA)JRF=JFF
   NR=NR+1
   WRITE(LF)(ANS(J),J=JRS,JRF)
171 CONTINUE
   NREC=NR+1
   REWIND LF
   WRITE(LF)NREC
   WRITE(NOUT,192)
192 FORMAT(1H+,"XXXXXX",22X,"XX")
   RETURN
305 CONTINUE
C-----STURE POINT-DOSE SOLUTION IN OUTPUT FILE(49) (SEE SECTION
C-      - G.(1))
C-----THE FOLLOWING MESSAGE IS BLANKED OUT IF WRITE SUCCESSFULLY
C-      - COMPLETES...
   WRITE(NOUT,267)
267 FORMAT(1H,"ERROR- TRANSFER TO FILE LF INCOMPLETE")
   LF=1SPAR(9)
   REWIND LF
   WRITE(LF)MUL
   WRITE(LF)TDUS
   WRITE(LF)XDUS
   WRITE(LF)YDUS
   DU 268 J=1,40
   WRITE(LF)(DOS(I,J),I=1,59)
268 CONTINUE
   WRITE(NOUT,270)
270 FORMAT(1H+,"XXXXXX",22X,"XX")
   RETURN
   END

```

```

DIMENSION UB(ITUT,JTUT,NTDAT),VB(ITUT,JTUT,NTDAT)
DIMENSION STAB(ITUT,JTUT,NTDAT),PARAM(ITUT,JTUT,NTDAT)
DIMENSION ZC(ITUT,JTUT),D(ITUT,JTUT),POSUX(20),KAB(ITUT,JTUT)
DIMENSION PUSURX(20),PUTILX(20),PUSURY(20),POTILY(20)
DIMENSION ATJ(1,1),GW(NTDAT),DIR(NTDAT),TC(NTDAT),SLC(NTDAT)
DIMENSION VARY(NX,NZ),AVY(NX,NZ),PUSUZ(20),XFIN(NX)
DIMENSION PR(1,NX,NZ),PC(NX,NZ),PL(NX,NZ)
DIMENSION AVYL(NX,NZ),VARYL(NX,NZ),XFL(NX)
DIMENSION XF(NX),NFILT(NTDAT),HIMA(NTDAT)
DIMENSION TUAT(NTDAT),HANS(NHANS),AC(NMX,NMY,NMZ)
DIMENSION F(2,NZ),ANS(NHX,NMY,NHANS)
DIMENSION PT(NX,NZ),AVYT(NX,NZ),XFP(NX,NZ)
DIMENSION XFN(NX),VARYT(NX,NZ),PIN(NX,NZ)
DIMENSION AVYIN(NX,NZ),VARYIN(NX,NZ),DEP(NX)
COMMON/ELAP/KLAPSM,KLAST,KTEXP
COMMON/DOSA/DOS(59,40),TUS(60),XDUS(40),YDUS(40),NTDOS,NPDUS,ZUDS
COMMON/DOSB/DSTR(30),TSTR(30),NSTR,XPL,YPL,TRTEM
COMMON/DOSC/XVANL,YVANL,TACTL,DZL,ZPBL,TRAJ(7,300),NLP,UTOS
COMMON/DOSD/XPLLT,YPLLT,TLT,DXB,DYB,QTRLT,QTR,XVLLT,YVLLT,XRLL,
$YRLLT,XRL,YRL,PUEP,DEP,DEFS,HS,PREM
COMMON/SPEC/SPAR(30)
COMMON/STUR1/IEND,ICONTROL,NOUT,
$NDJ,JHALF,NSDT,ITJEK,NTIME,K,IP1,IP2,JP1,JP2,
$IG,JG,KUR,NPRIS,IS,IFLAG,ITS,ITP,MFLAG,IT,KA,ISET,MI,NST,NITP,
$IPRUC,JP,NPUFFS,JCH,NPUFP1,NP,NSUSED,NTSOL,NPINT,IN,JUST,NTJX,
$NTJZ,IA,IUR,NTEMP,JA,KK,DELTA,DELTB,DELTC,DELTD,FREXT,DT1,
$
$DTMIN,DMZ,SLCON,XGA,XGB,XGW,YGA,YGB,YGW,PBFR,DZATSV,ZPBS,TREL,XG,
$YG,TIN,UXY,VXY,XP,YP,STAB,PARAM,ZOP,DP,VEL,THAV,EZ,ZH,US,VS,
$UYS,TDIFF,      TID,D1,D2,D3,D4,TREM,TRIN,TRUT,TPERIOD,DELTE,TELU,
$DXATSV,ZJ,PERIOD,START,PNT,DTPUFF,XMAP1,XMAP2,YMAP1,YMAP2,DMX,
$DMY,XTJIN,YTJIN,XTJUT,YTJUT,      SUM,SIGMA1,XS,YS,ZPB,UXSVEX,
$SIGMA2,PDX,PDZ,PORX,PORY,PUTX,PUTY,SIG1,SIG2,XOR,YOR,XOT,YOT,$G1,
$SG2,DZIN,ZPIN,TR,DTSTR,HANS,AV,AEFF,DIST,DTJX,DTJOR,XGP,YGP,DISUR,
$DGP,XEF,SP,FR1,ZB,THT,ZDIV,FRK,PA,PB,PEFF,XB,YB,SB,SY,G1,C2,C1,
$G2,YCUT,XCUT,DOR,DUT,TURU,ARM,VAL1,XPF,YOUT,PUXL,PDZL,PORXL,PORYL,
$POTXL,PUTYL,SIG1L,SIG2L,      DSOT,SOTI,NTRED,TSOOS,      TRAUD,
$NSUM,XKRL,YKRL,MF,NIN
COMMON/STUR2/XGS,YGS,ZS
COMMON/STUR3/MUL,GWV,DIRH,TCGN,XGM1,XGM2,YGM1,YGM2

COMMON/STUR4/TRELIN(15,4),TRELDT(15,4)
COMMON/STUR5/TIME(15),UVMAX(15)
COMMON/STUR6/JTSOL(5),NFL(3),DT(300)
COMMON/STUR7/EMIN(2,15,4),TRED(180)
COMMON/ISPEC/ISPAR(15)

```

```

C*TIME-VARIANT DISPERSION - M,MULHOLLAND
NIN=ISPAR(12)
NOUT=ISPAR(13)
NELP=NX*NZ
NELAN=NMX*NMY*NHANS
NELA=NHX*NMY*NMZ
IMDU=0
C-----FIND WHETHER NEED TO CONTINUE WITH A PREVIOUS RUN EXECUTION..
CALL STURE(IMDU,IJOB,PR,P,PL,AVYL,VARYL,XFL,XF,NFILT,HIMA,TUAT,
$HANS,A,F,ANS,ITUT,JTUT,NTDAT,NX,NZ,NMX,NMY,NMZ,NHANS,NELP,NELAN,
$NELA)
C-----INPUT BASIC UNALTERED DATA..
CALL INPUT(NTUT,ITUT,JTUT,DELTA,DELTB,DELTC,DELTD,FREXT,

```

```

SUBROUTINE MAIN(ITUT,JTUT,NTDAT,NX,NZ,NMX,NMY,NMZ,NHANS,UB,VB,
$STAB,PARAM,ZO,D,KAB,GW,DIR,TC,SLC,VARY,AVY,PR,P,PL,AVYL,VARYL,
$XFL,XF,NFILT,HIMA,TUAT,HANS,A,F,ANS,PIN,AVYIN,VARYIN,XFIN,PT,
$SAVY,XFP,XFN,VARYT,DEP)
C-----THIS SUBROUTINE PERFORMS ALL ADMINISTRATIVE OPERATIONS EXCLMT
C-      - FOR THE LAGRANGIAN POINT SOLUTION.....

```

```

$DT1,DTMIN,NMX,NMY,NMZ,DMZ,SLCON,NDJ,JHALF,
$NSDT,ITJEK,NHANS,XGA,XGB,XGW,YGA,YGB,YGW,YGWFILF,HIMA,TDAT,TIME,
$NTIME,ZO,D,GH,DIR,TC,SLC,HANS,NX,NZ,
$RAB,UB,VB,STAB,PARAM,NIN,NDUT)
IF(IJOB.NE.333)GO TO 242
IMOD=3
C-----IN EVENT OF NEW RUN EXECUTION, INITIALISE OUTPUT FILE(49)...
CALL STORE(IMOD,IJOB,PR,P,PL,AVYL,VARYL,XFL,XF,NFILF,HIMA,TDAT,
SHANS,A,F,ANS,ITOT,JTOT,NTDAT,NX,NZ,NMX,NMY,NMZ,NHANS,NELP,NELAN,
SNELA)
C= ASSIGN PARAMETERS -----
C-----
PBFR=SPAR(1)
DZATSV=2.0
ZPBS=PBFR*DZATSV
IG=IP1
JG=JP1
KOR=IFIX((ZS-ZPBS)/DZATSV+2.5)
C*DOSAGE APPROX. RELEASE-TIME INTERVAL SIZE,DTOS
DTOS=SPAR(2)
C*AVERAGE SOLUTION HEIGHT...
C-----THIS GIVES THE HEIGHT AT WHICH THE CENTROID IS FOLLOWED..
HANSV=0.5*ZS
IF(NHANS.EQ.0)GO TO 62
SUM=0.0
DO 61 K=1,NHANS
61 SUM=SUM+HANS(K)
C-----FOR CONCENTRATION DISTRIBUTIONS..
HANSV=SUM/FLOAT(NHANS)
62 CONTINUE
IF(NTDOS.EQ.0)GO TO 124
C-----FOR POINT-DOSAGE SOLUTIONS...
HANSV=ZDOS
C-----DOSAGE OPTION-DETERMINE RELEASE-TIME RANGE-----
C-----
C*ASSUME u=0 OUTSIDE SPECIFIED TIME RANGE...
NTIME=1
TIME(1)=TDOS(1)
GO TO 124
125 CONTINUE
C-----TRELIN WILL BE THE EARLIEST RELEASE TIME TO AFFECT THE REGION OF
- INTEREST AT TIME TDOS(1)..
IF(TRELIN(1,1).EQ.-30.0)TRELIN(1,1)=TSTR(1)
IF(TRELIN(1,1).GT.500000.0)TRELIN(1,1)=TRELIN(1,1)-500000.0
IF(TRELIN(1,1).GE.TSTR(1))GO TO 126
DO 127 J=1,NSTR
IF(WSTR(J).GT.0.0)GO TO 128
127 CONTINUE
ERROR=SQRT(-1.0)
128 IF(J.LT.2)J=2
D1=TSTR(J-1)
GO TO 129
126 D1=TRELIN(1,1)
129 CONTINUE
D2=TDOS(NTDOS)
DO 351 J=1,NSTR
351 IF(TSTR(J).GT.D2)GO TO 359
J=NSTR+1

```

```

352 J=J-1
359 IF(WSTR(J).LE.0.0)GO TO 352
IF(J.EQ.NSTR)J=NSTR+1
IF(D2.GT.TSTR(J+1))D2=TSTR(J+1)
C-----NUMBER OF RELEASE INTERVALS..
NTRED=IFIX((D2-D1)/DTOS+1.0)
C-----ACTUAL INTERVAL BETWEEN SOLVED PUFF RELEASE-TIMES...
DTOS=(D2-D1)/FLOAT(NTRED)
TRED(1)=D1
C-----TOTAL NUMBER OF SOLVED PUFF RELEASE-TIMES...
NTRED=NTRED+1
DO 353 J=2,NTRED
C-----RELEASE-TIME SEQUENCE...
TRED(J)=TRED(1)+(J-1)*DTOS
353 CONTINUE
NSUSED=300
DO 356 J=1,NPDOS
DO 356 I=1,NTDOS
DOS(I,J)=0.0
356 CONTINUE
IPRUC=0
NPUFFS=NTRED-1
NPUFF1=NTRED
IT=1
JP=1
DA=3.0
TIME(1)=0.9E+20
XMAP1=XGM1*DXB
XMAP2=XGM2*DXB
YMAP1=YGM1*DYB
YMAP2=YGM2*DYB
C-----SET MARGIN AROUND REGION-OF-INTEREST FOR TERMINATION OF DOSAGE
C= - TRACKING.
D1=XMAP1-SPAR(17)
D2=XMAP2+SPAR(17)
D3=YMAP1-SPAR(17)
D4=YMAP2+SPAR(17)
C-----ESTIMATE TRAVEL-TIME FOR FIRST RELEASE...
SUM=0.0
XP=XGS*DXB
YP=YGS*DYB
C-----INITIALISE TRACKING HEIGHT...
ZEZ=ZS
DO 357 J=1,20000
TACT=TRED(1)+(J-1)*DELTD+0.5*DELTD
TRADU=J*DELTD
IF(TACT.GT.TDAT(NTDAT))GO TO 358
C-----EXTRACT VELOCITY PARAMETERS...
CALL VELOC(XP,YP,TACT,UXY,VXY,VEL,UB,VB,TDAT,NTDAT,DXB,DYB,ITOT,
$JTOT)
C-----EXTRACT STABILITY PARAMETERS..
CALL PROPS(TACT,XP,YP,STAB,PARAM,ZO,D,STABP,PARAMP,ZOP,DP,DXB,DYB,
$TDAT,NTDAT,ITOT,JTOT,RAB,RABP)
C-----FIND DIFFUSIVITY AT HEIGHT ZEZ...
CALL FUNCT(XP,YP,TACT,STABP,PARAMP,DELTD,ZOP,DP,VEL,XF,0.0,F,NX,
$Z,TRADU,ZEZ)
EZ=F(2,2)
SUM=SUM+EZ
EZ=SUM/FLOAT(J)
C-----SUBROUTINE UEFF PROVIDES EFFECTIVE VELOCITY OF CENTROID AND
C= - ALTERS THE TRACKING HEIGHT,ZEZ...
CALL UEFF(TRADU,ZS,EZ,WS,HANSV,PBFR,UXY,VXY,STABP,PARAMP,ZOP,
$DP,US,VS,UVS,DELTD,ZEZ)

```

```

XP=XP+US*DELTD
YP=YP+VS*DELTD
C-----IS THE CENTROID BEYOND THE MARGIN YET...
IF((XP.LT.D1).OR.(XP.GT.D2).OR.(YP.LT.D3).OR.(YP.GT.D4))GO TO 358
357 CONTINUE
ENRUR=SQRT(-1.0)
358 TTRAV=TRAUD
GO TO 355

```

```

C- IDENTIFY RELEVANT LOCI RELEASE BOUNDS -----
C-----
124 CONTINUE
CALL LOCUS(NTIME,NTDAT,DELTA,NSTR,XGS,YGS,IFLAG,DELTB,ITOT,
SJTOT,DXB,DYB,NX,ZS,ZM,DXATSV,DZATSV,ZPBS,XGM1,XGM2,YGM1,YGM2,MFLAG
S,DELTC,DELTD,NZ,ZJ,TDAT,TSTR,QSTR,UB,VB,STAB,PARAM,ZO,D,TIME,TRELI
SN,TRELOT,UVMAX,EMIN,NOUT,KOK,NTDOS,NS,HANSAV,PBFR,F,XF,RAB)
IF(NTDOS.NE.0)GO TO 125

```

```

C- COMPUTE REQUIRED CONCENTRATION DISTRIBUTIONS -----
C-----
C----- (IT=1 FOR USAGE SOLUTIONS,BUT LOOP IS ENTERED AT STATEMENT 355)
DO 67 IT=1,NTIME

```

```

C+ SET SOLUTION SPACES TO ZERO FOR TIME IT ++++++
C+++++
C-----TRELIN LESS THAN ZERO IMPLIES NO CONTRIBUTING LOCUS...
IF((TRELIN(IT,1).LT.0).AND.(TRELIN(IT,2).LT.0).AND.(TRELIN(IT,3).L
ST.0).AND.(TRELIN(IT,4).LT.0))GO TO 67
IF(NMX*NMZ*NMZ.EQ.0)GO TO 86
DO 85 K=1,NMZ
DO 85 J=1,NMY
DO 85 I=1,NMX
A(I,J,K)=0.0
85 CONTINUE
86 IF(NHANS.EQ.0)GO TO 169
DO 168 K=1,NHANS
DO 168 J=1,NMY
DO 168 I=1,NMX
ANS(I,J,K)=0.0
168 CONTINUE
169 CONTINUE
DO 133 K=1,20
DO 133 I=1,50
IF(ITJEK.NE.1)GO TO 133
ATJ(I,K)=0.0
133 CONTINUE
IPRUC=0

```

```

C+ EXPAND SOLUTION LOCUS TO ALLOW FOR EXTERNAL CONTRIBUTIONS,AND+++++
C+ DETERMINE NO. OF PUFFS AND SOLUTION SPACE STEP-SIZES,+++++
C+++++
DO 68 JP=1,3
IF(TRELIN(IT,JP).LT.0.0)GO TO 68
XP=XGS*DXB
YP=YGS*DYB
PERIOD=SPAR(3)/UVMAX(IT)
C-----500000 WAS ADDED TO ENTRY OR EXIT TIMES IN "LOCUS" AS SIGNAL

```

```

C- - THAT BOUNDS ARE DETERMINED BY RELEASE PERIOD...
IF(TRELIN(IT,JP).LT.500000.0)GO TO 341
TRIN=TRELIN(IT,JP)-500000.0
GO TO 342
341 CONTINUE
TRIN=TRELIN(IT,JP)-PERIOD
C*USE SOURCE STARTING TIME HERE.....
TSTART=TDAT(1)
IF(TRIN.LT.TSTART)TRIN=TSTART
IF(TRIN.LT.TSTR(1))TRIN=TSTR(1)

```

```

342 CONTINUE
IF(TRELOT(IT,JP).LT.500000.0)GO TO 343
TROT=TRELOT(IT,JP)-500000.0
GO TO 344
343 CONTINUE
TROT=TRELOT(IT,JP)+PERIOD
C*USE SOURCE END-TIME HERE.....
TEND=TDAT(NTDAT)
IF(TROT.GT.TEND)TROT=TEND
IF(TROT.GT.TIME(IT))TROT=TIME(IT)
IF(TROT.GT.TSTR(NSTR))TROT=TSTR(NSTR)

```

```

344 CONTINUE
PNT=UVMAX(IT)/SPAR(4)
NPUFFS=IFIX(PNT*(TROT-TRIN)+2.1)
C*ADJUST HERE AS NECESSARY
I=IFIX(SPAR(5))
IF(NPUFFS.GT.I)NPUFFS=I
DTPUFF=(TROT-TRIN)/FLOAT(NPUFFS)

```

```

C*STEPSIZES IN REGION OF INTEREST
C----- AND BOUNDS OF REGION OF INTEREST IN LENGTH UNITS...
XMAP1=XGM1*DXB
XMAP2=XGM2*DXB
YMAP1=YGM1*DYB
YMAP2=YGM2*DYB
DMX=(XMAP2-XMAP1)/FLOAT(NMX)
IF((NHANS.NE.0).AND.(NMY.GT.75))NMY=75
DMY=(YMAP2-YMAP1)/FLOAT(NMY)
DMZ=DMZ
IF(ITJEK.NE.1)GO TO 155

```

```

C+ DETERMINE LIMITS FOR CHECK-SYSTEM PLANE ++++++
C+++++
C-----THIS IS A DIAGNOSTIC 2-DIMENSIONAL SOLUTION WITH LAGRANGIAN
C- - SOLUTIONS RESOLVED INTO A VERTICAL PLANE (NOT INVOLVED IN
C- - CONCEN. DISTRIBUTION OR USAGE SOLUTIONS)...
JCH=-1
154 CONTINUE
TREL=TRIN
IF(JCH.GT.0)TREL=TRUT
XG=XGS
YG=YGS
TPERIOD=TIME(IT)-TREL
IF(TPERIOD.LT.DELTD)GO TO 152
NST=IFIX(TPERIOD/DELTD+1.0)
DELTE=TPERIOD/FLOAT(NST-1)
NITP=NST-1
DO 153 ITP=1,NITP
TIM=TREL+(ITP-1)*DELTE
XP=XG*DXB
YP=YG*DYB
CALL VELO(XP,YP,TIM,UXY,VXY,UVS,UB,VB,TDAT,NTDAT,DXB,DYB,ITOT,JTOT
S)

```

```

CALL PRUPS(ITM,XP,YP,STAB,PARAM,ZO,D,STABP,PARAMP,ZOP,DP,DXB,DYB,T
SDAT,NTDAT,ITOT,JTOT,RAB,RABP)
CALL SPEED(UXY,VXY,STABP,PARAMP,ZOP,DP,ZJ,DZATSV,DXATSV,US,VS,UVS,
SZPBS)
XG=XG+US*DELTE/DXB
YG=YG+VS*DELTE/DYB
153 CONTINUE
152 CONTINUE
IF(JCH.GT.0)GO TO 156
XTJIN=XG*DXB
YTJIN=YG*DYB
JCH=+1
GO TO 154
156 XTJUT=XG*DXB
YTJUT=YG*DYB
155 CONTINUE

C+ SOLVE FOR EACH PUFF ++++++
C+++++
NPUFP1=NPUFFS+1
355 CONTINUE
DO 69 NP=1,NPUFP1
C-----RELEASE-TIME FOR DOSAGE PUFFS...
IF(NTDOS.NE.0)TREL=TRED(NP)
IF(NTDOS.NE.0)TTRAV=TRADD
IF(NTDOS.NE.0)GO TO 371
C-----RELEASE-TIME FOR CONC. DISTRIBUTION PUFFS...
TREL=TRIN+(NP-1)*DTPUFF
C-----TRAVEL-TIME FOR CONC. DISTRIBUTION PUFFS...
TTRAV=TIME(IT)-TREL

C+SET TIME-STEP STRATEGY FOR EACH PUFF+++++
C+++++
C-----THESE ARE REAL-TIME STEPS ALONG THE TRAJECTORY...
IF(NP.NE.NPUFP1)GO TO 371
C-----LAST PUFF..
TTRAV=20.0
DT(1)=20.0
NSUSED=1
TREL=TIME(IT)-20.0
GO TO 372
371 CONTINUE
C-----CALCULATE STEP-SIZE SEQUENCE...
SUM=0.5*SPAR(24)
DO 71 K=1,50
SUM=SUM+5*K*SPAR(24)
IF(TTRAV.LE.SUM)GO TO 72
71 CONTINUE
ERROR=SQRT(-1.0)
72 D1=5.5
J=6
IF(K.EQ.1)GO TO 73
DO 77 I=1,5
SUM=SUM-K*SPAR(24)
IF(SUM.LE.TTRAV)GO TO 78
77 CONTINUE
ERRUR=SQRT(-1.0)
78 D1=FLOAT(IFIX((SUM-SPAR(24))/2.0+0.001)/SPAR(24))+0.5
J=K+1-I
73 CONTINUE
C-----RECALCULATED NEAREST BASIC STEPSIZE(DT(2)) FOR CONCENTRATION

```

```

C- = DISTRIBUTION SOLUTIONS...
D4=TTRAV/D1
IF(NTDOS.EQ.0)NSUSED=J
DT(1)=0.5*D4
DO 79 K=1,50
C-----ONLY INCREASE STEPSIZE ONCE EVERY FIVE STEPS...
DO 79 J=1,5
I=(K-1)*5+J+1
DT(1)=K*D4
79 CONTINUE
372 CONTINUE

C+ SET PARAMETERS, AND SPATIAL STEPS AND GRID-SIZE FOR PUFF ++++++
C+++++
NTSOL=1
JTSOL(1)=NSUSED
C-----SOURCE POSITION(X,Y) IN LENGTH UNITS...
XS=XGS*DXB
YS=YGS*DYB
C*THESE MUST APPLY FOR WHOLE PLUME .....
C*MINIMUM VALUE OF EX, EXSMIN=D2
D2=LMIN(1,IT,JP)
C*MINIMUM VALUE OF EZ, EZSMIN=D3
D3=LMIN(2,IT,JP)
C*OPTIMAL SPATIAL STEPSIZES...
DXATSV=SQRT(D2*DT(2)/SPAR(13))
DZATSV=SQRT(D3*DT(2)/SPAR(13))
C-----VERTICAL GRID-POINTS IN LAGRANGIAN FRAME...
NZ=IFIX(SPAR(6))
D3=(NZ*DZATSV+ZPB)/2.0
D1=SPAR(14)/2.0
PDZ=DZATSV
PDX=DXATSV
IF(D3.LT.D1)DZATSV=SPAR(14)/FLOAT(NZ-1)
D3=(NZ*DZATSV+ZPB)/SPAR(15)
C-----ADJUST VERTICAL STEPSIZE TO MEET MINIMUM FRAME HEIGHT CRITERIA...
IF(D3.LT.ZS)DZATSV=SPAR(15)*ZS/FLOAT(NZ-1)
ZPB=PBFR*DZATSV
IF(DXATSV.LT.DZATSV)DXATSV=DZATSV
C*****..... INSTEAD WILL ALLOW TO CONTINUE AND RESET DX,DZ IN PUFF
IPRUC=1
C-----HORIZONTAL GRID-POINTS IN LAGRANGIAN FRAME...
NX=IFIX(SPAR(7))
C-----EXTREME HORIZONTAL STEPSIZE...
DXSVEX=SPAR(8)*DXATSV
IF(DXSVEX.LT.DXATSV)DXSVEX=DXATSV
C-----BASIC INFORMATION FOR PUFF SOLUTION...
WRITE(NOUT,921)NP,NPUFFS,IT,TIME(IT),JP,TREL,TTRAV,D4,NSUSED,NX,
$NZ,PDX,PDZ,DXATSV,DZATSV
921 FORMAT("0ND,"I3," RELEASE (NF,"I3,") FOR TIME,"I2," (T="F8.1,
$"),LOCUS NO.,"I2,". RELEASE T="F8.1,". EXPECTED TRAVEL T="F8.1,
$," WITH INITIAL DT="F7.2,"/10X," EXPECTED TRAJ. STEPS="I2,"/10X,
$" SOLUTION FRAME SIZE=NX="I3,". NZ="I3,". MINIMUM POSSIBLE (DX,DZ
$)=(F5.2,"",F5.2,"") AND MINIMUM ALLOWED (DX,DZ)=(F5.2,"",
$F5.2,"")

IMOD=1
C-----STORE INTERMEDIATE DATA IF REQUIRED...
CALL STORE(IMOD,IJOB,PR,P,PL,AVYL,VARYL,XFL,XF,NFILT,HIMA,TRAT,
$HANS,A,F,ANS,ITOT,JTOT,NTDAT,NX,NZ,NMX,NMY,NMZ,NHANS,NELP,NELAN,
$NELA)

```

```

C+ CALL PUFF SOLUTION ++++++
C+-----SOLVE FOR LAGRANGIAN PUFF UNDER THE SPECIFIED CONDITIONS...
CALL PUFF(TREL,JTSOL,NTSOL,DT,DZATSV,DXATSV,NX,NZ,DXB,DYB,UB
$,VB,STAB,PAHAM,ZO,U,TDAT,PR,NSDT,XS,YS,ZS,NTDAT,POSDX,POSDZ,POSURX
$,POSORY,POTILX,POTILY,XF,DXSVEX,DEP,ZPB,NOUT,TOES,TDEF
$,PDEP,HS,ITOT,JTOT,VARY,AVY,NTDOS,XMAP1,XMAP2,YMAP1,YMAP2,TRADQ,
$,NP,NSUM,XRER,YRER,HANSAV,PREM,RAH,PT,AVYT,XFP,XFIN,VARYT,F,P)

```

```

C-----
C-----
IF(NTDOS.NE.0)GO TO 69
DU 74 K=1,NZ
DU 74 I=1,NX
74 P(I,K)=PR(1,I,K)

```

C-----FINAL PUFF POSITION AND STEPSIZE DATA...

```

PUX=POSDX(1)
PUZ=POSDZ(1)
PORX=POSORX(1)
PORY=POSORY(1)
POTX=POTILX(1)
POTY=POTILY(1)
SIG1=SIGMA1
SIG2=SIGMA2
IF(NP.EQ.1)GO TO 75

```

C+REFER PUFFS TO ANSWER GRIDS+++++

```

C-----ACCUMULATE PUFF SOLUTIONS IN RESULT GRID FOR CONCENTRATION DISTR.
C- SOLUTIONS...
CALL REFER(NX,NZ,XFL,XF,AVYL,VARYL,AVY,VARY,PL,P,PDXL,PDZL,P
$,SDX,PDZ,PORXL,PORX,PORYL,PORY,POTXL,POTYL,POTX,POTY,XRERL,XRER,YRER
$,SL,YRER,ZPBL,ZPB,TREL,DTPUFF,NSTR,TSTR,QSTR,ITJEK,NHANS,NMX,NMY,NMZ
$,XMAP1,YMAP1,DMX,DMY,HANS,ANS,NPINT,A,DTJX,NTJX,ATJ,XTJIN,XTJOT,
$,YTJIN,YTJOT,OSDT,NOUT,PIN,AVYIN,VARYIN,XFIN)

```

75 CONTINUE

C+ RESET PARAMETERS FOR NEXT INTERPOLATED SEQUENCE ++++++

```

C+-----
DO 76 I=1,NX
XFL(I)=XF(I)
DO 76 K=1,NZ
AVYL(I,K)=AVY(I,K)
VARYL(I,K)=VARY(I,K)
76 PL(I,K)=P(I,K)
PUXL=PODX
POZL=PODZ

```

C-----STORE LAST POSITIONS AND STEPSIZES...

```

PORXL=PORX
PORYL=PORY
POTXL=PUTX
POTYL=PUTY
SIG1L=SIG1
SIG2L=SIG2

```

```

XRERL=XRER
YRERL=YRER
ZPBL=ZPB
69 CONTINUE
IF(NTDOS.NE.0)GO TO 263
68 CONTINUE
IF(IPROC.EQ.0)GO TO 67
IF(ITJEK.EQ.1)GO TO 141

```

C+ PRINT OUT LEVELS OR VOLUMES OPTIONS ++++++

```

C+-----
WRITE(NOUT,110)TIME(IT),XMAP1,XMAP2,YMAP1,YMAP2,DMX,DMY,DMZ
110 FORMAT(//////,1H0,5HTIME=,F7.0,3X,23HY-Z SECTIONS IN (XMAP1=,F7.0,
$,6HXMAP2=,F7.0,6HYMAP1=,F7.0,6HYMAP2=,F7.0,11H) WITH DMX=,F6.1,6H
$,DMY=,F6.1,6H DMZ=,F6.1)
IF(NHANS.EQ.0)GO TO 166

```

C-----SUBROUTINE MAP WILL STORE (AS OUTPUT) AND PRINT OUT CONCEN-

C- DISTRIBUTION SOLUTIONS...

```

CALL MAP(NHANS,NOUT,HANS,XGA,XGB,XGW,YGA,YGB,YGW,XGM1,YGM1,D
$,XGB,DYB,DMX,DMY,NMY,NMX,ANS,MUL,IT,NTIME,TIME(IT),PR,P,PL,AVYL,
$,VARYL,XFL,XF,NFILT,HIMA,TDAT,A,F,ITOT,JTOT,NTDAT,NX,NZ,NMZ)
GO TO 67
166 CONTINUE
DU 91 I=1,NMX
WRITE(NOUT,108)I
108 FORMAT(//,1X,2HI=,I3,/)
DU 91 KK=1,NMZ
K=NMZ-KK+1
WRITE(NOUT,114)(A(I,J,K),J=1,NMY)
114 FORMAT(1X,20F6.2)
91 CONTINUE
GO TO 67

```

C+PRINT OUT DOSAGE OPTION ++++++

```

C+-----
263 CONTINUE
WRITE(NOUT,264)MUL
264 FORMAT(1H1,"DOSAGES AT SELECTED POINTS- DATA SET NO.",I5/)
KK=NTDOS-1
DU 265 J=1,NPDOS
DU 265 I=1,KK
WRITE(NOUT,266)J,XDUS(J),YDUS(J),I,TDOS(I),TDOS(I+1),DOS(I,J)
265 CONTINUE
266 FORMAT(1X,"POSITION",I3," ("F7.3," ",F7.3,") FOR TIME-INTERVAL",
$,I3," ("F8.2," TO ",F8.2,") DOSAGE="E11.4)
IMOD=5

```

C-----STORE DOSAGE RESULTS IN OUTPUT FILE(49)...

```

CALL STORE(IMOD,IJOB,PR,P,PL,AVYL,VARYL,XFL,XF,NFILT,HIMA,TDAT,
$,HANS,A,F,ANS,ITOT,JTOT,NTDAT,NX,NZ,NMX,NMY,NMZ,NHANS,NELP,NELAN,
$,NELA)
GO TO 269

```

C+ PRINT OUT CHECK-PLANE OPTIONS ++++++

```

C+-----
C-----THIS IS ONLY USED IN THE CASE OF THE CHECK-PLANE DIAGNOSTIC
C- SOLUTION...
141 CONTINUE
WRITE(NOUT,142)TIME(IT),DTJX,DMZ,HIMA(1),UB(IG,JG,1),VB(IG,JG,1)
142 FORMAT(//////,1H0,5HTIME=,F7.0,3X,8F10.4,///)

```

```

DU 143 I=1,NTJX
DU 7667 K=1,NMZ
IF(ATJ(I,K).LE.0.0)GO TO 7667
ATJ(I,K)=ALOG(ATJ(I,K))/2.302585093
7667 CONTINUE
143 WRITE(NOUT,114)(ATJ(I,K),K=1,NMZ)
DSOT=SQRT((XTJOT-XS)**2+(YTJOT-YS)**2)
IF((YS.LT.YTJOT).AND.(YS.GT.YTJIN)).OR.((YS.GT.YTJOT).AND.(YS.LT.
$YTJIN))DSOT=-DSOT
SOTI=DSOT/DTJX
WRITE(NOUT,162)DSOT,SOTI
162 FORMAT(1X,"DISTANCE FROM I=NTJX TO SOURCE=",F10.2,3X,"WHICH IS EQU
$IVALENT TO ",F8.4,2X,"DIVISIONS")
VEL=SQRT(UB(IG,JG,1)**2+VB(IG,JG,1)**2)
67 CONTINUE
C-----
C-----
269 CONTINUE
IMOD=2
C-----RESET FLAGS TO INDICATE TERMINATION OF THE RUN...
CALL STORE(IMOD,IJOB,PR,P,PL,AVYL,VARYL,XFL,XF,NFILT,HIMA,TOAT,
$HANS,A,F,ANS,ITOT,JTOT,NTDAT,NX,NZ,NMX,NMY,NMZ,NHANS,NELP,NELAN,
$NELA)

RETURN
END

```

```

SUBROUTINE REFER(NX,NZ,XFL,XF,AVYL,VARYL,AVY,VARY,PL,P,PDXL,PDZL,P
$DX,PDZ,PORXL,PORX,PORYL,PORY,POTXL,POTYL,POTX,POTY,XRERL,XRER,YRER
$LYRER,ZPBL,ZPB,TREL,DTPUFF,NSTR,TSTR,QSTR,ITJEK,NHANS,NMX,NMY,NMZ
,$XMAP1,YMAP1,DMX,DMY,HANS,ANS,NPINT,A,DTJX,NTJX,ATJ,XTJIN,XTJOT,
$YTJIN,YTJOT,DSOT,NOUT,PIN,AVYIN,VARYIN,XFIN)

```

```

C-----THIS SUBROUTINE ALLOCATES LAGRANGIAN PUFF CONTRIBUTIONS TO THE
C- " EULERIAN CONC. DISTRIBUTION SOLUTION GRID COVERING THE REGION-
C- " -OF INTEREST...

```

```

DIMENSION PIN(NX,NZ),AVYIN(NX,NZ),VARYIN(NX,NZ),XFIN(NX)
DIMENSION XFL(NX),XF(NX),AVYL(NX,NZ),VARYL(NX,NZ),AVY(NX,NZ)
DIMENSION VARY(NX,NZ),PL(NX,NZ),P(NX,NZ),TSTR(30),QSTR(30)
DIMENSION HANS(NHANS),ANS(NMX,NMY,NHANS),A(NMX,NMY,NMZ),ATJ(50,20)
COMMON/SPEC/SPAR(30)

```

```

C+ COMPUTE CHARACTERISTIC PARAMETERS FOR INTERPOLATION OF PUFFS ++++++
C+-----
C*IN VIEW OF PUFF SEPARATION = 800M, SPACE INTPUFFS AT 40M ...
NPINT=IFIX(SPAR(9))
DU 81 IN=1,NPINT
C-----INTERPOLATE POSITIONS...
XOR=(NPINT-IN)*PORXL/FLOAT(NPINT)+IN*PORX/FLOAT(NPINT)
YOR=(NPINT-IN)*PORYL/FLOAT(NPINT)+IN*PORY/FLOAT(NPINT)

```

```

XOT=(NPINT-IN)*POTXL/FLOAT(NPINT)+IN*POTX/FLOAT(NPINT)
YOT=(NPINT-IN)*POTYL/FLOAT(NPINT)+IN*POTY/FLOAT(NPINT)
SG1=(NPINT-IN)*SIG1L/FLOAT(NPINT)+IN*SIG1/FLOAT(NPINT)
SG2=(NPINT-IN)*SIG2L/FLOAT(NPINT)+IN*SIG2/FLOAT(NPINT)
XRR=(NPINT-IN)*XRERL/FLOAT(NPINT)+IN*XRER/FLOAT(NPINT)
YRR=(NPINT-IN)*YRERL/FLOAT(NPINT)+IN*YRER/FLOAT(NPINT)
DU 98 I=1,NX
XFIN(I)=(NPINT-IN)*XFL(I)/FLOAT(NPINT)+IN*XF(I)/FLOAT(NPINT)
CONTINUE
DU 82 K=1,NZ
DO 82 I=1,NX
D1=-115.0
D2=-115.0
IF(PL(I,K).GT.0.0)D1=ALOG(PL(I,K))
IF(P(I,K).GT.0.0)D2=ALOG(P(I,K))
C-----INTERPOLATE ZEROth, FIRST AND SECOND MOMENTS...
PIN(I,K)=EXP((NPINT-IN)*D1/FLOAT(NPINT)+IN*D2/FLOAT(NPINT))
AVYIN(I,K)=(NPINT-IN)*AVYL(I,K)/FLOAT(NPINT)+IN*AVY(I,K)/FLUAT(NPI
$NT)
VARYIN(I,K)=(NPINT-IN)*VARYL(I,K)/FLOAT(NPINT)+IN*VARY(I,K)/FLOAT
$NPINT)
82 CONTINUE
DZIN=(NPINT-IN)*PDZL/FLOAT(NPINT)+IN*PDZ/FLOAT(NPINT)
ZPBIN=(NPINT-IN)*ZPBL/FLOAT(NPINT)+IN*ZPB/FLOAT(NPINT)
C*EFFECTIVE RELEASE TIME OF INTERPOLATED PUFF
TR=TREL-DTPUFF+IN*DTPUFF/FLOAT(NPINT)
C*SOURCE STRENGTH AT THAT TIME
DU 83 JST=1,NSTR
IF(TR.LT.TSTR(JST))GO TO 84
83 CONTINUE
84 IF((JST.EQ.1).OR.(JST.GT.NSTR))GO TO 81
DTSTR=TSTR(JST)-TSTR(JST-1)
QEFF=((TR-TSTR(JST-1))/DTSTR)*QSTR(JST)+((TSTR(JST)-TR)/DTSTR)*Q
$STR(JST-1)*DTPUFF/FLOAT(NPINT)
C*USE BROUCCAERT GRID AS BASIS
IF(ITJEK.NE.1)GO TO 131

```

```

C+ INTERPOLATION OF PUFFS FOR CHECK-PLANE OPTION ++++++
C+-----
C*-----THIS SECTION IS ONLY FOR DIAGNOSTIC PURPOSES...

```

```

DIST=SQRT((YTJOT-YTJIN)**2+(XTJOT-XTJIN)**2)
NTJX=IFIX(2.0*DIST/(DMX+DMY)+0.5)
DTJX=DIST/FLOAT(NTJX)
NTJZ=NMZ
DTJUR=SQRT((XOR-XTJIN)**2+(YOR-YTJIN)**2)
DU 134 IA=1,NTJX
XGP=XTJIN+IA*(XTJOT-XTJIN)/FLOAT(NTJX)
YGP=(XGP-XTJIN)/(XTJOT-XTJIN)*(YTJOT-YTJIN)+YTJIN
DISOR=SQRT((XGP-YOR)**2+(YGP-YOR)**2)
DGP=SQRT((XGP-XTJIN)**2+(YGP-YTJIN)**2)
IF(DGP.GT.DTJUR)DISOR=DISOR
IOR=IFIX(FLOAT(NX)/2.0+0.51)
XEF=XFIN(IOR)+DISOR

```

```

IF((XEF.LE.XFIN(1)).OR.(XEF.GE.XFIN(NX)))GO TO 134
DU 137 I=1,NX
IF(XEF.LT.XFIN(I))GO TO 138
137 CONTINUE
138 SP=XFIN(I)-XFIN(I-1)
FRI=(XEF-XFIN(I-1))/SP
DU 139 KA=1,NTJZ
ZB=(KA-1)*DMZ

```

```

THT=(NZ-2)*DZIN+ZPBIN
ZDIV=(ZB-ZPBIN)/DZIN
IF(ZB.GT.THT)GO TO 139
K=FIX(ZDIV+3.0)
FRK=ZDIV+3.0-FLUAT(K)
U1=-115.0
U2=-115.0
U3=-115.0
U4=-115.0
IF(PIN(I,K).GT.0.0)D1=ALOG(PIN(I,K))
IF(PIN(I-1,K).GT.0.0)U2=ALOG(PIN(I-1,K))
IF(PIN(I,K-1).GT.0.0)D3=ALOG(PIN(I,K-1))
IF(PIN(I-1,K-1).GT.0.0)U4=ALOG(PIN(I-1,K-1))
PA=FRI*U1+(1.0-FRI)*D2
PB=FRI*U3+(1.0-FRI)*D4
PEFF=EXP(FRK*PA+(1.0-FRK)*PB)
IF(IA.GT.50).OR.(IA.LT.1).OR.(KA.GT.20).OR.(KA.LT.1))WRITE(3,6522
6522  $)IA,KA,NTJX,NTJZ,NMX,NMY,NMZ,DMX,DMY,DMZ,DXB,DYB,XGM1,XGM2,YGM1,YG
$M2,XTJOT,XTJIN,YTJOT,YTJIN,DIST
FORMAT(1H0,"IA,KA,NTJX,NTJZ,NMX,NMY,NMZ,DMX,DMY,DMZ,DXB,DYB,XGM1,X
$GM2,YGM1,YGM2,XTJOT,XTJIN,YTJOT,YTJIN,DIST",/ ,1H ,7I3,5F6.1,4F6.2,
$5F7.0,/)
ATJ(IA,KA)=ATJ(IA,KA)+QEFF*PEFF
139 CONTINUE
134 CONTINUE
GO TO 81

C+ INTERPOLATION OF PUFFS FOR LEVELS OR VOLUME OPTIONS ++++++
C+++++
C-----HERE ALLOCATIONS ARE MADE TO THE SOLUTION GRIDS...
131 CONTINUE
IDR=FIX(FLUAT(NX)/2.0+0.51)
NTEMP=NMZ
IF(NHANS.NE.0)NMZ=NHANS
C-----FIND THE CENTRE,RADIUS AND SENSE OF THE ARC FITTED TO THE
C- TRACKING POINTS...
CALL CIRCA(XOT,YOT,XOR,YOR,XRR,YRR,XC,YC,RADC,THET1,THET2)
DO 86 IA=1,NMX
DO 86 JA=1,NMY
DO 86 KA=1,NMZ
XB=XMAP1+IA*DMX
YB=YMAP1+JA*DMY
ZB=(KA-1)*DMZ
IF(NHANS.NE.0)ZB=NHANS(KA)
C*FIND POSITION RELATIVE TO MOVING FRAME.....
C*DISTANCE ALONG ARC FROM CORE .....
D1=XB-XC
IF(D1.EQ.0.0)D1=0.00000001
THETB=ATAN((YB-YC)/D1)
IF(D1.LT.0.0)THETB=THETB+3.141592654
IF(THETB.LT.0.0)THETB=THETB+2.0*3.141592654
IF(THETB-THETB.GT.3.141592654)THETB=THETB-2.0*3.141592654
IF(THETB-THETB.LT.-3.141592654)THETB=THETB+2.0*3.141592654
IF(THETB-THETB.LT.-3.141592654)THETB=THETB-2.0*3.141592654
D1=THETB-THETB1
D4=THETB-THETB
D3=U1+D4
IF(D3.EQ.0.0)D3=0.00000001
D1=D3/ABS(D3)
XPF=XFIN(IDR)+D1*RADC*ABS(THETB-THETB2)
C*DISTANCE FROM ARC.(USF LEFT-HAND COORD=SET)
D2=SQRT((XB-XC)**2+(YB-YC)**2)

```

```

D4=U2-RADC
IF(THET2.LT.THET1)U4=-D4
YOUT=U4
IF((XPF.LE.XFIN(1)).OR.(XPF.GT.XFIN(NX)))GO TO 86
DO 87 I=1,NX
IF(XPF.LE.XFIN(I))GO TO 88
87 CONTINUE
88 SP=XFIN(I)-XFIN(I-1)
FRI=(XPF-XFIN(I-1))/SP
THT=(NZ-2)*DZIN+ZPBIN
ZDIV=(ZB-ZPBIN)/DZIN
IF(ZB.GT.THT)GO TO 86
K=FIX(ZDIV+3.0)
FRK=ZDIV+3.0-FLUAT(K)
D1=-115.0
D2=-115.0
D3=-115.0
D4=-115.0
IF(PIN(I,K).GT.0.0)D1=ALOG(PIN(I,K))
IF(PIN(I-1,K).GT.0.0)D2=ALOG(PIN(I-1,K))
IF(PIN(I,K-1).GT.0.0)D3=ALOG(PIN(I,K-1))
IF(PIN(I-1,K-1).GT.0.0)D4=ALOG(PIN(I-1,K-1))
C-----LOGARITHMIC INTERPOLATION FOR VALUE IN LAGRANGIAN FRAME...
PA=FRI*U1+(1.0-FRI)*D2
PB=FRI*U3+(1.0-FRI)*D4
PEFF=EXP(FRK*PA+(1.0-FRK)*PB)
C*INTERPOLATE FIRST AND SECOND MOMENTS.....
VARA=FRI*VARYIN(I,K)+(1.0-FRI)*VARYIN(I-1,K)
VARB=FRI*VARYIN(I,K-1)+(1.0-FRI)*VARYIN(I-1,K-1)
AVA=FRI*AVYIN(I,K)+(1.0-FRI)*AVYIN(I-1,K)
AVB=FRI*AVYIN(I,K-1)+(1.0-FRI)*AVYIN(I-1,K-1)
AVA=FRK*AVA+(1.0-FRK)*AVB
VARA=FRK*VARA+(1.0-FRK)*VARB
IP1=I+1
IM2=I-2
IP2=I+2
KP1=K+1
IF(IP1.GT.NX)IP1=NX
IF(IM2.LT.1)IM2=1
IF(IP2.GT.NX)IP2=NX
IF(KP1.GT.NZ)KP1=NZ
C-----ERROR OUTPUT...(NEGATIVE VARIANCE)
IF((VARA.LE.0.0).AND.(PEFF.GT.0.0))WRITE(NOUT,27)I,K,FRI,FRK,XPF,V
$ARA,AVA,PEFF,VARYIN(IM2,K),VARYIN(I-1,K),VARYIN(I,K),VARYIN(IP1,K)
$,VARYIN(IP2,K),VARYIN(I,K-1),VARYIN(I,KP1)
27 FORMAT(2I4,13E9.2)
IF(VARA.LE.0.0)GO TO 86
C*RELATIVE DEVIATION FROM AVA.....
SY=YOUT-AVA
C-----ASSUME GAUSSIAN DISTRIBUTION...
G1=(QEFF*PEFF/VARA/2.50663)*FXP(-SY**2/2.0/VARA/VARA)
IF(NHANS.EQ.0)GO TO 170
C-----INCREMENT DISTRIBUTION GRID...
ANS(IA,JA,KA)=ANS(IA,JA,KA)+G1
GO TO 86
170 CONTINUE
A(IA,JA,KA)=A(IA,JA,KA)+G1
86 CONTINUE
NMZ=NTEMP
51 CONTINUE
RETURN
END

```

```

-----
SUBROUTINE TIMEX(KTIMEX)
C
C-----THIS SUBROUTINE FINDS PROGRAM ELAPSED (TOTAL) TIME FROM TIME-
C-      = -OF-DAY.
C
COMMON/ELAP/KLAPSM,KLAST
C-----FUNCTION TIME IS A COMPUTER UTILITY ROUTINE(SEE SECTION C• ABOVE)
JT1=TIME(1)
KVAL=FIX(FLOAT(JT1)/3600.0)
K=KVAL-KLAST
IF(K.LT.0)K=K+1440
KLAST=KVAL
KLAPSM=KLAPSM+K
KTIMEX=KLAPSM
RETURN
END

```

```

-----
SUBROUTINE MAP(NHANS,NUUT,HANS,XGA,XGB,XGW,YGA,YGB,YGW,XGM1,YGM1,
SDXB,DYB,DMX,DMY,NMY,NMX,ANS,MUL,IT,NTIME,TIME,PR,P,PL,AVYL,VARYL,
SXFL,XF,NFILT,HIMA,TDAT,A,F,ITOT,JTOT,NTDAT,NX,NZ,NMZ)
C-----THIS SUBROUTINE STURES(AS OUTPUT IN FILE(49)) AND MAPS THE CONC.
C-      = DISTRIBUTION RESULTS(GRID PRINT-OUT)
DIMENSION ANS(NMX,NMY,NHANS),HANS(NHANS),LAT(400)
DIMENSION PR(1,NX,NZ),P(NX,NZ),PL(NX,NZ)
DIMENSION AVYL(NX,NZ),VARYL(NX,NZ),XFL(NX)
DIMENSION XF(NX),NFILT(NTDAT),HIMA(NTDAT)
DIMENSION TDAT(NTDAT),A(NMX,NMY,NMZ),F(2,NZ)
DATA LAA,LAB,LAW,LAM,LAS/1HA,1HB,1HW,1H=,1H /
NELP=NX*NZ
NELAN=NMX*NMY*NHANS
NELA=NMX*NMY*NMZ
IMOD=4
C-----WRITE RESULTS INTO OUTPUT FILE...
CALL STURE(IMOD,IJOB,PR,P,PL,AVYL,VARYL,XFL,XF,NFILT,HIMA,TDAT,
SHANS,A,F,ANS,ITOT,JTOT,NTDAT,NX,NZ,NMX,NMY,NMZ,NHANS,NELP,NELAN,
$NELA)
C-----PRINT OUT RESULTS...
DO 167 KH=1,NHANS
WRITE(NUUT,178)HANS(KH)
178 FORMAT(1H0,"CONCENTRATIONS ON SURFACE AT HEIGHT=",F10.3,2X,"ABOVE
$GROUND LEVEL")

```

```

IGA=FIX((XGA-XGM1)*DXB/DMX+0.5)
IGB=FIX((XGB-XGM1)*DXB/DMX+0.5)
IGW=FIX((XGW-XGM1)*DXB/DMX+0.5)
JGA=FIX((YGA-YGM1)*DYB/DMY+0.5)
IF((JGA.LT.1).OR.(JGA.GT.NMY))IGA=-555
JGB=FIX((YGB-YGM1)*DYB/DMY+0.5)
IF((JGB.LT.1).OR.(JGB.GT.NMY))IGB=-555
JGW=FIX((YGW-YGM1)*DYB/DMY+0.5)
IF((JGW.LT.1).OR.(JGW.GT.NMY))IGW=-555
IPAG=FIX(FLOAT(NMY)/12.0+0.9999999)
DO 181 IP=1,IPAG
WRITE(NUUT,180)IP
180 FORMAT(1H1,"PAGE",I3)
JS=(IP-1)*12+1
JF=IP*12
IF(JF.GT.NMY)JF=NMY
DO 182 I=1,NMX
DO 183 J=1,NMY
183 LAT(J)=LAS
C-----FILL IN MARKER POINTS...
IF(I.EQ.IGA)LAT(JGA)=LAA
IF(I.EQ.IGB)LAT(JGB)=LAB
IF(I.EQ.IGW)LAT(JGW)=LAW
WRITE(NUUT,175)I,(ANS(I,J,KH),J=JS,JF)
WRITE(NUUT,176)(LAT(J),J=JS,JF)
175 FORMAT(1X,I4,1X,12E10.3)
176 FORMAT(1H+,4X,12(2X,A1,7X))
182 CONTINUE
WRITE(NUUT,177)(J,J=JS,JF)
177 FORMAT(/,5X,12(I3,7X))
181 CONTINUE
167 CONTINUE
RETURN
END

```

```

-----
START OF
SUBROUTINE PUFF(TREL,JTSOL,NTSOL,DT,DZATSV,DXATSV,NX,NZ,DXB,DYB,UB
$,VB,STAB,PARAM,ZO,D,TDAT,PR,NSDT,XS,YS,ZS,NTDAT,POSUX,POSUZ,POSURX
$,POSORY,POTILX,POTILY,XF,DXSVEX,DEP,ZPB,NUUT,TDES,TDEF
$,PDEL,WS,ITOT,JTOT,VARY,AVY,NTDUS,XMAP1,XMAP2,YMAP1,YMAP2,TRADD,
$NTRA,NSUM,XREF,YREF,HANSAV,PREM,RAB,PT,AVYT,XFP,XFN,VARYT,F,P)
C
C-----THIS SUBROUTINE SOLVES FOR THE DEVELOPMENT OF THE LAGRANGIAN PUFF
C-      = UNDER THE SPECIFIED CONDITIONS....
C
DIMENSION F(2,NZ),POSORX(20),POTILX(20),POTILY(20),POSORY(20)
DIMENSION JTSOL(5),DT(300),UB(ITOT,JTOT,NTDAT),VB(ITOT,JTOT,NTDAT)
DIMENSION STAB(ITOT,JTOT,NTDAT),PARAM(ITOT,JTOT,NTDAT)
DIMENSION ZO(ITOT,JTOT),D(ITOT,JTOT),DEPCNX)
DIMENSION POSUX(20),POSUZ(20),TDAT(NTDAT),PR(1,NX,NZ),XF(NX)
DIMENSION PT(NX,NZ),PCNX(NZ),AVYT(NX,NZ),RAB(ITOT,JTOT)
DIMENSION XFP(NX),XFN(NX),VARY(NX,NZ),VARYT(NX,NZ),AVY(NX,NZ)
DIMENSION SEE(82)

```

```

EQUIVALENCE (SEE(4),RZVAN),(SEE(5),RZRER),(SEE(12),ALPHA)
EQUIVALENCE (SEE(13),ZM),(SEE(14),XP),(SEE(15),YP),(SEE(16),XVAN)
EQUIVALENCE (SEE(17),YVAN),(SEE(18),XSTRK),(SEE(19),YSTRK)
EQUIVALENCE (SEE(20),FACTOR),(SEE(21),SDT)
EQUIVALENCE (SEE(24),GAMT),(SEE(25),ANGT)
EQUIVALENCE (SEE(26),STABAV),(SEE(27),RAMAV),(SEE(28),ZOAV)
EQUIVALENCE (SEE(29),DAV),(SEE(30),RABAV),(SEE(31),UVAV)
EQUIVALENCE (SEE(32),UBAV),(SEE(33),VBAV),(SEE(34),UVBAV)
EQUIVALENCE (SEE(67),STABAM),(SEE(68),RAMAM),(SEE(69),ZOAM)
EQUIVALENCE (SEE(70),DAM),(SEE(71),UVAM),(SEE(72),UVBAM)
EQUIVALENCE (SEE(81),XHAV),(SEE(82),YHAV)
COMMON/SPEC/SPAR(30)
COMMON/PPROG/INFORM
SEE(2)=TIME(1)/60.0
SEE(1)=TIME(2)/60.0

```

```

NXM=NX-1
NZM=NZ-1
ZPBS=ZPB

```

```

IUR=FIX(FLOAT(NX)/2.0+0.51)
KUR=FIX((ZS-ZPBS)/DZATSV+2.5)

```

```

C-----FIND INITIAL VELOCITY AND DIFFUSIVITY PARAMETERS...

```

```

CALL VELO(XS,YS,TREL,U,V,UV,UB,VB,TDAT,NTDAT,DXB,DYB,ITOT,JTOT)
CALL PROPS(TREL,XS,YS,STAB,PARAM,ZO,D,STABP,PARAMP,ZOP,DP,DXB,DYB,
SDAT,NTDAT,ITOT,JTOT,RAB,RABP)
CALL SPEED(U,V,STABP,PARAMP,ZOP,DP,ZS,DZATSV,DXATSV,US,VS,UVS,ZPBS)

```

```

VATS=UV
TACT=TREL
XP=XS
YP=YS
DZ=DZATSV
DX=DXATSV
DXE=SPAR(8)*DX

```

```

C-----SET UP INITIAL HORIZONTAL DISTANCE SEQUENCE FOR GRID-POINTS...

```

```

CALL PHI(NX,DX,DXE,XF)
INSOL=JTSOL(NTSOL)
STABAM=0.0
RAMAM=0.0
ZOAM=0.0
DAM=0.0
UVAM=0.0
UVBAM=0.0
TTRAV=0.0
NSUSED=JTSOL(1)

```

```

C-----FIND TOTAL TRAVEL-TIME(CONCN. DISTRIBUTION SOLUTIONS)

```

```

DO 14 K=1,NSUSED
TTRAV=TTRAV+DT(K)
14 CONTINUE
IF(NTDGS.NE.0)TTRAV=TRADD
IF(NTDGS.NE.0)NLP=NSUM

```

```

C-----SET UP INITIAL POSITIONS OF FRAME-ORIENTATION TRACKING POINTS...

```

```

C-----WISH TO "STREAK" TO SEPARATIONS OF SPAR(10) DURING 1ST TIME-STEP.
C-----THIS REQUIRES EXPANSION OF TIME=STEP...

```

```

TIM=SPAR(10)/UVS

```

```

C-----USE ACTUAL STEPSIZE DT(1)/NSDT,BUT CONTRACT INTO INTERVAL DT(1),

```

```

C- " USING FACTOR DT(1)/TIM...

```

```

NTIT=NSDT*TIM/DT(1)+1.0
D1=TIM/FLOAT(NTIT)
XVAN=XS
YVAN=YS
XRER=XS

```

```

YRER=YS
RZVAN=1.0
RZRER=1.0

```

```

C-----"STREAK" UPWIND AND DOWNWIND FROM SOURCE.....

```

```

C-----I.E. ALONG STREAMLINE...
DO 271 K=1,NTIT

```

```

DTOT=TREL+(DT(1)/TIM)*(K*D1-0.5*D1)

```

```

C-----DOWNWIND.....

```

```

CALL VELO(XVAN,YVAN,DTOT,U,V,UV,UB,VB,TDAT,NTDAT,DXB,DYB,ITOT,JTOT)
CALL PRUPS(DTUT,XVAN,YVAN,STAB,PARAM,ZO,D,STABP,PARAMP,ZOP,DP,DXB,
SDYB,TDAT,NTDAT,ITOT,JTOT,RAB,RABP)
CALL SPEED(U,V,STABP,PARAMP,ZOP,DP,ZS,DZATSV,DXATSV,US,VS,UVS,
ZPBS)
XVAN=XVAN+US*D1
YVAN=YVAN+VS*D1

```

```

C-----UPWIND.....

```

```

CALL VELO(XRER,YRER,DTOT,U,V,UV,UB,VB,TDAT,NTDAT,DXB,DYB,ITOT,JTOT)
CALL PRUPS(DTUT,XRER,YRER,STAB,PARAM,ZO,D,STABP,PARAMP,ZOP,DP,DXB,
SDYB,TDAT,NTDAT,ITOT,JTOT,RAB,RABP)
CALL SPEED(U,V,STABP,PARAMP,ZOP,DP,ZS,DZATSV,DXATSV,US,VS,UVS,
ZPBS)
XRER=XRER+US*D1
YRER=YRER+VS*D1

```

```

C-----NOTE:"VAN" REPRESENTS THE FORWARD TRACKING POINT AND "RER"

```

```

C- " REPRESENTS THE REAR TRACKING POINT...

```

```

271 CONTINUE

```

```

C-----INITIALISE VARIABLES...

```

```

TIM=0.0
PICUNS=1.0
ITERM=0
DZOPT=0.0

```

```

TFRAC=1.0

```

```

TADV=0.0
DTLAS=DT(1)
VAFRAC=1.0
LFLAG=0
NCALD=0
SIGUEL=0.0

```

```

C-----MAIN LOOP FOR TIME-STEPS ALONG TRAJECTORY FOLLOWS...

```

```

DO 102 JT=1,INSOL
TIM=TIM+DT(JT)

```

```

IF(JT.EQ.1)TACT=TREL

```

```

C-----SET PREVIOUS POSITION...

```

```

XPREV=XP
YPREV=YP
XVPREV=XVAN
YVPREV=YVAN
SDT=DT(JT)/FLOAT(NSDT)

```

```

C-----RESET ACCUMULATING REGISTERS FOR AVERAGING PROPERTIES...

```

```

STABT=0.0
PARAMT=0.0
ZUT=0.0
DTOT=0.0
RABT=0.0
UVT=0.0
UVBT=0.0
UBT=0.0
VBT=0.0
DZOPTL=DZOPT

```

```

C*SET ZM=ZS FOR FIRST PUFF OR ZERO RELATIVE ADVECTION.....
IF((JT.EQ.1).OR.(ITERM.EQ.1))ZM=ZS
IF((JT.EQ.1).OR.(ITERM.EQ.1))GO TO 145
C-----ZERO RELATIVE ADVECTION IF (OPT,DZ/ACT,DZ) TOO SMALL IN LAST DT.
IF(UZOPTL.EQ.-1.0)ZM=ZS
IF(UZOPTL.EQ.-1.0)GO TO 145
C*FEEDBACK ALTERATION OF TRACKING HEIGHT...
C*.....TU POSITION X-CENTROID OF LEVEL OF INTEREST...
C*FIND VELOCITY GRADIENT AT HEIGHT ZM...
CALL VELO(XP,YP,TACT,U,V,UV,UB,VB,TDAT,NTDAT,DXB,DYB,ITOT,JTOT)
CALL PRUPS(TACT,XP,YP,STAB,PARAM,ZO,D,STABP,PARAMP,ZOP,DP,DXB,DYB,
STUAT,NTUAT,ITOT,JTOT,RAB,RABP)
CALL SPEED(U,V,STABP,PARAMP,ZOP,DP,ZM,DZ,DX,US,VS,UVS,ZPB)
ZQ=ZM+SPAR(11)
CALL SPEED(U,V,STABP,PARAMP,ZOP,DP,ZQ,DZ,DX,US,VS,ALPHA,ZPB)
C-----VELOCITY GRADIENT AT HEIGHT ZM...
ALPHA=(ALPHA-UVS)/SPAR(11)
D1=ABS(ALPHA)
IF(D1.LT.SPAR(12))ALPHA=+SPAR(12)
C-----CHECK SENSE OF WIND-COMPONENT IN FRAME (APPROX.)....
D1=XVAN-XP
IF(D1.EQ.0.0)D1=0.1E-08
D2=ATAN(CYVAN-YP)/D1
IF(D1.LT.0.0)D2=D2+3.141592654
D3=U
IF(D3.EQ.0.0)D3=0.1E-08
D4=ATAN(V/D3)
IF(D3.LT.0.0)D4=D4+3.141592654
D1=COS(D4-D2)
IF(D1.EQ.0.0)D1=0.1E-08
ISENS=D1/ABS(D1)
C-----ALTER POINT-SLOPE ALPHA ACCORDING TO SENSE...
ALPHA=ISENS*ALPHA
C-----DO NOT RESOLVE FOR COMPONENT IN PLANE AS THIS MAY EXAGGERATE -
C- - LATERAL MOVEMENT UNDULY....
C*FIND X-CENTROID AT HEIGHT OF INTEREST..POINT=(NOT DISTANCE),WEIGHTED
Z=(HANSAV-ZPB)/DZ+2.0
K=FIX(Z)
KP=K+1
FRA=Z-FLOAT(K)
SUM1=0.0
SUM2=0.0
D1=0.0
D2=0.0
C-----ACCUMULATE FOR FIRST AND ZEROth X-MOMENT...
DO 141 I=2,NXM
SUM1=SUM1+I*P(I,K)
SUM2=SUM2+I*P(I,KP)
D1=D1+P(I,K)
D2=D2+P(I,KP)
141 CONTINUE
C-----NOTE THAT IOR IS THE VALUE OF "I" AT THE (HORIZONTAL) CENTRE OF
C- - THE GRID.
D3=FLOAT(IOR)
D4=FLOAT(IOR)
IF(D1.NE.0.0)D3=SUM1/D1
IF(D2.NE.0.0)D4=SUM2/D2
D3=FRA*D4+(1.0-FRA)*D3
I=FIX(D3)
IP=I+1
FRA=D3-FLOAT(I)
XD=FRA*XF(IP)+(1.0-FRA)*XF(I)
C-----DEVIATION OF X-CENTROID FROM X-GRID-CENTRE...

```

```

XD=XD-XF(IOR)
SEE(9)=XD
C*CALCULATE DESIRED MINIMUM ULTIMATE POSITION FOR CENTROID...
I=FIX(X(SPAR(21)*FLOAT(NX)+0.5))
D3=XF(I)-XF(IOR)
IF(XD.LT.D3)D3=LFLAG=1
D4=-D3/2.0
SEE(10)=D3
SEE(11)=D4
IF(XD.GT.D4)D4=LFLAG=1
IF(LFLAG.EQ.0)GO TO 145
C*AIM TO BRING CENTROID UP TO THIS POINT DURING THIS TIME-STEP...
C*ADDITIONAL RELATIVE VELOCITY REQUIRED AT THIS HEIGHT...
D1=(D3-XD)/DT(JT)
C*HENCE ALTER TRACKING HEIGHT AS FOLLOWS...
C-----FEEDBACK CONTROL- ADJUST TRACKING HEIGHT TO BRING CENTROID BACK
C- - TO GRID CENTRE...
ZM=ZM-D1/ALPHA
IF(ZM.LT.ZPB)ZM=ZPB
145 CONTINUE
ZQ=ZM
C
C-----SOLVE FOR ADVECTION OF LAGRANGIAN FRAME (PROXIMATE CURVE) IN
C- - NSDT SMALLER STEPS, AND ACCUMULATE VELOCITY AND STABILITY
C- - PARAMETERS EN ROUTE FOR AVERAGING...
DU 101 JSDT=1,NSDT
TACT=TACT+SDT
C-----VELOCITY AT CENTRAL POINT...
CALL VELO(XP,YP,TACT,U,V,UV,UB,VB,TDAT,NTDAT,DXB,DYB,ITOT,JTOT)
CALL PRUPS(TACT,XP,YP,STAB,PARAM,ZO,D,STABP,PARAMP,ZOP,DP,DXB,DYB,
STUAT,NTUAT,ITOT,JTOT,RAB,RABP)
C*PREVIOUS DX AND DZ APPLY HERE...
CALL SPEED(U,V,STABP,PARAMP,ZOP,DP,ZQ,DZ,DX,US,VS,UVS,ZPB)
XP=XP+US*SDT
YP=YP+VS*SDT
C-----VELOCITY AT FORWARD POINT...
CALL VELO(XVAN,YVAN,TACT,UVAN,VVAN,UVVAN,UB,VB,TDAT,NTDAT,DXB,DYB,
SITOT,JTOT)
CALL PRUPS(TACT,XVAN,YVAN,STAB,PARAM,ZO,D,STABV,PARAMV,ZOV,UV,DXB,
SDYB,TDAT,NTDAT,ITOT,JTOT,RAB,RABV)
ZVAN=RZVAN*ZQ
CALL SPEED(UVAN,VVAN,STABV,PARAMV,ZOV,OV,ZVAN,OZ,DX,USV,VSU,UVSV,
ZPB)
XVAN=XVAN+USV*SDT
YVAN=YVAN+VSU*SDT
C-----VELOCITY AT REAR POINT...
C*TRACKING AT LEVEL OF REAR CURVATURE POINT.....
CALL VELO(XRER,YRER,TACT,UVAN,VVAN,UVVAN,UB,VB,TDAT,NTDAT,DXB,DYB,
SITOT,JTOT)
CALL PRUPS(TACT,XRER,YRER,STAB,PARAM,ZO,D,STABV,PARAMV,ZOV,UV,DXB,
SDYB,TDAT,NTDAT,ITOT,JTOT,RAB,RABV)
ZRER=RZRER*ZQ
CALL SPEED(UVAN,VVAN,STABV,PARAMV,ZOV,OV,ZRER,OZ,DX,USV,VSU,UVSV,Z
SPB)
XRER=XRER+USV*SDT
YRER=YRER+VSU*SDT
D1=0.9E+15
IF(STABP.EQ.0.0)GO TO 761
D1=1.0/STABP
761 CONTINUE
C-----ACCUMULATE PARAMETERS...
STABT=STABT+D1

```

```

PARAM=PARAMT+PARAMP
ZOT=ZOT+ZOP
DTOT=DTOT+OP
RABT=RABT+RABP
UVT=UVT+UVS
UBT=UBT+UB
VBT=VBT+V
UVBT=UVBT+SQR(U**2+V**2)
101 CONTINUE
SEE(6)=JT
SEE(7)=DT(JT)
SEE(8)=TACT
SEE(22)=XKER
SEE(23)=YKER

C-----FIND EFFECTIVE INCIDENT VELOCITY ON LAGRANGIAN FRAME...
C-----"STREAK" TO THE DISTANCE OF (XVPREV,YVPREV) USING MEAN VELOCITIES
C-----DURING DT.....
DIST=SQR((YVPREV-YPREV)**2+(XVPREV-XPREV)**2)
D1=SQR((XP-XPREV)**2+(YP-YPREV)**2)
D2=SQR((XVAN-XVPREV)**2+(YVAN-YVPREV)**2)
FACTOR=2.0*DIST/(D1+D2)
NTIT=FACTOR*DT(JT)/SDT+1.0
SDT=FACTOR*DT(JT)/FLOAT(NTIT)
C-----CONTRACT TIME INTO INTERVAL DT(JT) USING 1.0/FACTOR....
C-----"STREAK" FROM (XPREV,YPREV)...
C-----I.E. ALONG STREAMLINE...
J=0
274 XSTRK=XPREV
YSTRK=YPREV
DO 272 K=1,NTIT
TSTRK=TACT-DT(JT)+(K*SDT-0.5*SDT)/FACTOR
CALL VELO(XSTRK,YSTRK,TSTRK,U,V,UV,UB,VB,TDAT,NTDAT,DXB,DYB,ITOT,
$JTOT)
CALL PRUPS(TSTRK,XSTRK,YSTRK,STAB,PARAM,ZO,D,STABP,PARAMP,ZOP,DP,
$DXB,DYB,TDAT,NTDAT,ITOT,JTOT,RAB,RABP)
CALL SPEED(U,V,STABP,PARAMP,ZOP,DP,ZQ,DZ,DX,US,VS,UVS,ZPB)
C-----ADJUST POSITION IN NTIT SMALLER STEPS...
XSTRK=XSTRK+US*SDT
YSTRK=YSTRK+VS*SDT
272 CONTINUE
C-----ALLOW A 3 PERCENT ERROR....
J=J+1
D3=SQR((XSTRK-XPREV)**2+(YSTRK-YPREV)**2)
IF(ABS(D3-DIST)/DIST.LT.0.03)GO TO 273
SDT=(DIST/D3)*SDT
FACTOR=SDT*NTIT/DT(JT)
IF(J.GT.20)WRITE(NOUT,275)D3,DIST
C-----THIS IS NOT A SERIOUS ERROR...
275 FORMAT('NON-CONVERGENCE - STREAK D3="F10.2," INSTEAD OF" F10.2)
IF(J.GT.20)GO TO 273
GO TO 274
273 CONTINUE
SDT=J
C-----EFFECTIVE ANGLE OF INCIDENCE OF WIND ON CURVE FROM (XPREV,YPREV)
C-----TO (XVPREV,YVPREV)...
C-----ANGLE OF (XVPREV,YVPREV).....
D1=XVPREV-XPREV
IF(D1.EQ.0.0)D1=0.1E-08
D2=ATAN((YVPREV-YPREV)/D1)
IF(D1.LT.0.0)D2=D2+3.141592654
C-----ANGLE OF (XSTRK,YSTRK).....

```

```

D3=XSTRK-XPREV
IF(D3.EQ.0.0)D3=0.1E-08
D4=ATAN((YSTRK-YPREV)/D3)
IF(D3.LT.0.0)D4=D4+3.141592654
C-----ANGLE BETWEEN "CURVES"...
THET=D4-D2
C-----
C
C*EVALUATE THE EFFECTIVE ANGLE OF THE CURVED PLANE AT (XP,YP)... GAMT..
D1=XP-XPREV
IF(D1.EQ.0.0)D1=0.000001
ANGT=ATAN((YP-YPREV)/D1)
IF(D1.LT.0.0)ANGT=ANGT+3.141592654
C-----EFFECTIVE ANGLE OF PLANE .....
GAMT=ANGT-THET
C
C-----
C-----AVERAGE VALUES OF PARAMETERS EN ROUTE...
STABAV=0.9E+15
IF(STABT.EQ.0.0)GO TO 762
STABAV=1.0/(STABT/FLOAT(NSDT))
762 CONTINUE
RAMAV=PARAM/FLOAT(NSDT)
ZUAV=ZOT/FLOAT(NSDT)
DAV=DTOT/FLOAT(NSDT)
RABAV=RABT/FLOAT(NSDT)
UVAV=UVT/FLOAT(NSDT)
UBAV=UBT/FLOAT(NSDT)
VBAV=VBT/FLOAT(NSDT)
UVBAV=UVBT/FLOAT(NSDT)
STABAM=STABAM+DT(JT)/STABAV
RAMAM=RAMAM+RAMAV*DT(JT)
ZOAM=ZOAM+ZOAV*DT(JT)
DAM=DAM+DAV*DT(JT)
UVAM=UVAM+UVAV*DT(JT)
UVBAM=UVBAM+UVBAV*DT(JT)

C*SCHEME TO ADJUST TO OPTIMUM SPATIAL STEPS FOR DIFFUSIVITY AT ZS ...
DZA=ZS-ZPB
CALL FUNCT(XP,YP,TACT,STABAV,RAMAV,DTAV,ZOAV,DAV,UVBAV,XF,DZA,F,NX
$3,TIM,ZPB)
EXS=F(1,3)
Ezs=F(2,3)
C-----STORE DATA FOR "PUFF=PROGRESS" PRINT-OUT...
SEE(35)=EXS
SEE(36)=Ezs
SEE(37)=DXATSV
SEE(38)=DXSVEX
SEE(39)=DZATSV
SEE(40)=ZPBS
SEE(41)=XF(NX)
C-----ALTER SPATIAL STEPSIZES(DX,DZ) TO OPTIMUM VALUES,IF NECESSARY.
CALL ALTER(UVBAV,DT,JT,EXS,Ezs,ZS,NZ,NX,DTNOW,DTLAS,ITERM,
$UXATSV,DZATSV,ZPBS,DXSVEX,PT,IGR,XF,XFP,XFN,P,AVY,VARY,AVYT,VARYT,
$NOUT)
C-----OPTIMAL VERTICAL STEP SIZE...
D1=DT(JT)
IF(JT.EQ.1)D1=2.0*DT(JT)
DZOPT=SQR(Ezs*D1/SPAR(13))
D2=SPAR(29)*DZOPT

```

```

IF(UZATSV,LE,D2)GO TO 132
DZOPT=-1.0
C*EFFECTIVE CORE POSITION .....
132 KOR=IFIX((ZS-ZPBS)/UZATSV+2.5)

DZ=UZATSV
ZPB=ZPBS
DX=UXATSV
DXE=DXSVEX
C-----"PHI" SETS UP DISTANCE SEQUENCE OF HORIZONTAL GRID POSITIONS
C= - IN XF(I)....
CALL PHI(NX,DX,DXE,XF)
C-----STORE DATA FOR "PUFF-PROGRESS" PRINTOUT...
SEE(42)=DX
SEE(43)=DXE
SEE(44)=DZ
SEE(45)=ZPB
SEE(46)=XF(NX)
SEE(47)=ITERM
SEE(50)=PICONS
SEE(80)=DZOPTL
C-----CHECK FOR TERMINATION OF RELATIVE ADVECTION WITHIN THE FRAME..
IF(DZOPTL.EQ.-1.0)GO TO 143
IF(ITERM.EQ.1)GO TO 143
IF(JT.EQ.1)GO TO 148
C-----
C-----
C-----
SUM1=0.0
C-----EVALUATE TOTAL MASS OF MATERIAL IN THE FRAME BEFORE RELATIVE
C= - ADVECTION...
DO 158 K=2,NZM
DO 159 I=2,NXM
SUM1=SUM1+0.5*(XF(I+1)-XF(I-1))*P(I,K)
159 CONTINUE
158 CONTINUE
SEE(49)=TIME(1)/60.0
SEE(48)=TIME(2)/60.0

SEE(51)=TFRAC
ITES1=TIME(1)/60.0
ITES2=TIME(2)/60.0

C-----RELATIVE ADVECTION OF MOMENTS WITHIN LAGRANGIAN FRAME...
C*ADVECTION OF PROPERTIES.....
C-----ASSUMING LINEAR STEPSIZE INCREASES FROM CORE,FIND RATIOS...

ADXA=XF(IOR+2)-2.0*XF(IOR+1)+XF(IOR)
BDXA=XF(IOR+1)-XF(IOR)-ADXA
IF(ADXA.NE.0)VBAAB=BDXA/ADXA+0.5
ADXB=2.0*XF(IOR-1)-XF(IOR-2)-XF(IOR)
BDXB=XF(IOR)-XF(IOR-1)-ADXB
IF(ADXB.NE.0)VBAB=BDXB/ADXB+0.5
C-----DISTANCE TRAVELLED BY CORE...
DIST=SQRT((XP-XPREV)**2+(YP-YPREV)**2)
COSI=COS(THET)
SINTH=SIN(THET)
DO 103 K=2,NZ

```

```

Z=(K-2)*DZ+ZPB
CALL SPEED(UBAV,VBAV,STABAV,RAVAV,ZOAV,DAV,Z,DZ,DX,US,VS,UVS,ZPB)
C-----RELATIVE DISTANCE SHIFT AT HEIGHT Z...
DELU=UVS*DT(JT)-DIST
DELF=-DELD*COSTH
DELYF=-DELD*SINTH
DO 401 I=1,NX
XFD=XF(I)-XF(IOR)
C-----X=POINT=UF-ORIGIN OF MATERIAL...
ARR=XFD+DELF
IF(ARR.LT.0)GO TO 152
IF(ADXA.EQ.0)RI=ARR/BDXA
IF(ADXB.EQ.0)GO TO 153
RI=-VBAA+SQRT(VBAA*VBAA+2.0*ARR/ADXA)
153 RIF=FLOAT(IOR)+RI
GO TO 402
152 IF(ADXB.EQ.0)RI=-ARR/BDXB
IF(ADXB.EQ.0)GO TO 323
RI=-VBAB+SQRT(VBAB*VBAB+2.0*ARR/ADXB)
323 RIF=FLOAT(IOR)-RI
402 IF(RIF.LT.1)GO TO 112
IF(RIF.GE.NX)GO TO 114
C-----GRID POSITION BEFORE AND GRID POSITION AFTER THIS POINT...
IB=IFIX(RIF)
IA=IB+1
FRA=RIF-FLOAT(IB)
FRB=1.0-FRA
C-----INTERPOLATE CONCENTRATION...
IF(JT.GT.5)GO TO 328
PT(I,K)=FRA*P(IA,K)+FRB*P(IB,K)
GO TO 325
328 D1=-115.0
D2=-115.0
D3=P(IA,K)
D4=P(IB,K)

C-----USE LOGARITHMIC INTERPOLATION NORMALLY...
IF(D3.GT.0.0)D1=ALOG(D3)
IF(D4.GT.0.0)D2=ALOG(D4)
PT(I,K)=EXP(FRA*D1+FRB*D2)
325 CONTINUE
C-----INTERPOLATE AND INCREMENT MEAN...
AVYT(I,K)=FRA*AVY(IA,K)+FRB*AVY(IB,K)-DELYF
C-----INTERPOLATE VARIANCE...
VARYT(I,K)=FRA*VARY(IA,K)+FRB*VARY(IB,K)
GO TO 401
C-----ORIGINATING OUTSIDE FRAME...
C-----SET TO BOUNDARY-VALUES...
112 PT(I,K)=P(1,K)
AVYT(I,K)=AVY(1,K)-DELYF
VARYT(I,K)=VARY(1,K)
GO TO 401
114 PT(I,K)=P(NX,K)
AVYT(I,K)=AVY(NX,K)-DELYF
VARYT(I,K)=VARY(NX,K)
401 CONTINUE
103 CONTINUE
SEE(53)=TIME(1)/60.0
SEE(52)=TIME(2)/60.0

SUM=0.0

```

```

C-----FIND MASS OF MATERIAL LEFT IN LAGRANGIAN FRAME...
  DU 160 K=2,NZM
  DU 161 I=2,NXM
  SUM=SUM+0.5*(XF(I+1)-XF(I-1))*PT(I,K)
161 CONTINUE
160 CONTINUE
  IF(JT.GT.4)PICONS=PICONS*(SUM/SUM1)
  IF(JT.GT.15)GO TO 421
  IF(DTNOW.GT.DTLAS)VAFRAC=VAFRAC-SPAR(16)
421 DTLAS=DTNOW
C-----IF FRACTION OF MATERIAL LOST THROUGH ADVECTION EXCEEDS ALLOWANCE,
C- - TERMINATE RELATIVE ADVECTION UNTIL GRID EXPANDS AGAIN WITH NEXT
C- - INCREASE IN TIME-STEP...
  IF(PICONS.LT.VAFRAC)ITERM=1
  TADV=TADV+DT(JT)
  TFRAC=TADV/TTRAV
  GO TO 146
143 DO 147 K=1,NZ
  DO 147 I=1,NX
C-----SWOP ARRAYS...
  AVY(I,K)=AVY(I,K)
  VARY(I,K)=VARY(I,K)
147 PT(I,K)=P(I,K)
146 CONTINUE
  SEE(54)=PICONS
  SEE(55)=TFRAC
C
-----
C*REMOVAL PROCESSES=SETTLING,GROUND ABSORPTION, AND UNIFORM DECAY...
C*SETTLING SPEED = WS,GROUND ABSORPTION PARAMETER=RABAV,
C- DECAY PARAMETER = PREM+PDEP,WHERE PDEP IS NON-ZERO FOR TOES)TDEF
  CALL REMOVE(WS,PREM,TOES,TDEF,PDEP,RABAV,DT(JT),DZ,ZPB,NZ,NX,JT,
  SPT,P,AVY,VARY,TACT,AVYT,VARYT,XP,YP,STABAV,RAMAV,DTAV,ZOAV,DAV,
  $UVBAV,ZS,TIM,F,XF,DEP,XFP,XFN)
-----
C
148 CALL FUNCT(XP,YP,TACT,STABAV,RAMAV,DTAV,ZOAV,DAV,UVBAV,XF,DZ,F,NX,
  $NZ,TIM,ZPB)
  IF(JT.NE.1)GO TO 7777
  DO 150 I=1,NX
  DEP(I)=0.0
  XFP(I)=0.0
  XFN(I)=0.0
150 CONTINUE
  Q=1.0
  EX=F(1,KOK)
  EZ=F(2,KOR)
  D3=Q/(4.0*3.14159*DT(1))*(EX*EZ)**0.5)
C-----INITIALISE PUFF USING A GAUSSIAN DISTRIBUTION AFTER THE FIRST
C- - TIME-STEP...
  DO 149 K=1,NZ
  DO 149 I=1,NX
  D1=XF(I)-XF(IOR)
  D2=(K-KOR)*DZ
  P(I,K)=D3*EXP(-D1*D1/(4.0*DT(1)*EX)-D2*D2/(4.0*DT(1)*EZ))
  VARY(I,K)=SQRT(2.0*EX*DT(1))
  AVY(I,K)=0.0
149 CONTINUE
  GO TO 96
7777 CONTINUE
  SEE(57)=TIME(1)/60.0
  SEE(56)=TIME(2)/60.0
C-----SUBROUTINE "DIFF" PERFORMS THE DIFFUSION STEP...

```

```

CALL DIFF(P,AVY,VARY,F,NX,NZ,XF,DT(JT),DZ,NSOR,KOR,NOUT,PT,AVYT,
  $VARYT)
SEE(59)=TIME(1)/60.0
SEE(58)=TIME(2)/60.0
96 CONTINUE
C-----STORE POSITION DATA FOR SUBSEQUENT USE IN CONCENTRATION DISTR.
C- - SOLUTION.
  DO 108 JSOL=1,NTSOL
  IF(JT.NE.JTSOL(JSOL))GO TO 108
  DO 110 K=1,NZ
  DO 110 I=1,NX
  PK(JSOL,I,K)=P(I,K)
110 CONTINUE
  POSURX(JSOL)=XP
  POSURY(JSOL)=YP
  POTILX(JSOL)=XVAN
  PUTILY(JSOL)=YVAN
  POSUX(JSOL)=DX
  POSUZ(JSOL)=DZ
108 CONTINUE
-----
C*INTERMEDIATE PRINT-OUT.....
C-----THIS PRINT-OUT IS SIMPLY FOR DIAGNOSTIC PURPOSES AND MAY BE
C- - SUPPRESSED BY SETTING "INFORM" TO "0" OR "1" (SEE SECTION A.(1)
C- - ABOVE.
  IF(INFORM.NE.2)GO TO 57
  I=6*IFIX(FLOAT(NTRA+4)/6.0)-4
  IF(1.NE.NTRA)GO TO 57
  IF(JT.LT.17)GO TO 57
  J=JT+2
  I=5*IFIX(FLOAT(J)/5.0)
  JSKIP=+1
  IF(1.NE.J)JSKIP=-1
  WRITE(NOUT,9973)JT,DT(JT),DX,DZ,XF(NX),WS,ZSET,ZM,ZMAX,ZPB,ITERM
9973 FORMAT(1X,"JT=",I3," DT(JT)="F6.1, " DX="F6.2," DZ="F6.2," XF(N
  $X)="F8.2," WS="E10.3," ZSET="E10.3," ZM="F6.2," ZMAX="F6.2,
  $" ZPB="F5.2," ITERM=",I2)
  WRITE(NOUT,9974)
9974 FORMAT(" P(I,K)")
  IE=4*IFIX(FLOAT(NX)/4.0)
  KE=2*IFIX(FLOAT(NZ)/2.0)
  DO 9976 I=4,IE,4
9976 WRITE(NOUT,9979)(P(I,K),K=2,NZ)
  IF(JSKIP.EQ.-1)GO TO 57
  WRITE(NOUT,9975)
9975 FORMAT(" AVY(I,K)")

  DO 9977 I=4,IE,4
9977 WRITE(NOUT,9979)(AVY(I,K),K=2,NZ)
  WRITE(NOUT,9972)
9972 FORMAT(" VARY(I,K)")
  DO 9978 I=4,IE,4
9978 WRITE(NOUT,9979)(VARY(I,K),K=2,NZ)
9979 FORMAT(1X,16E8.2)
57 CONTINUE
-----
  SEE(61)=WS*DT(JT)
  SEE(60)=WS
  IF(NTDUS.EQ.0)GO TO 100

```

```

263 CONTINUE
C*EFFECTIVE REPLACEMENT DIFFUSIVITY FOR GROUND IMPACTION/ABSORPTION...
  D1=ZS
  IF(D1.LT.SPAR(23))D1=SPAR(23)
  D2=D1/FL0AT(NZ)
  D3=D2*ZPB/DZ
  CALL FUNCT(XP,YP,TACT,STABAV,RAMAV,DTAV,ZOAV,DAV,UVBVAV,XF,D2,F,NX,
  $NZ,TIM,D3)
  SUM=0.0
  DO 21 K=2,NZ
  SUM=SUM+F(2,K)
21 CONTINUE
  EZ=SUM/FLUAT(NZ-1)
  SEE(62)=EZ
  SEE(64)=TIME(1)/60.0
  SEE(63)=TIME(2)/60.0
C
C-----"DUSE ALLOCATES THE DOSAGE CONTRIBUTIONS TO DOSAGE POINTS
C- - FOR THE APPROPRIATE DOSAGE INTERVAL...
  CALL DOSE(P,AVY,VARY,JT,XP,YP,XVAN,YVAN,TACT,XF,IOR,NX,NZ,DZ,ZPB,
  $TREL,NTRA,NSUM,XRER,YRER,DEP,XFP,XFN,NOUT,FLAST)

  SEE(66)=TIME(1)/60.0
  SEE(65)=TIME(2)/60.0

  TRADD=TIM
C-----FIND EFFECTIVE POSITION OF CENTRE-POINT AT LEVEL OF INTEREST...
  D1=(HANSVAV-ZPB)/DZ+2.0
  IB=IFIX(D1)
  IA=IB+1
  FRA=D1-FLUAT(IB)
C-----LATERAL POSITION OF MEAN...
  DELYF=FRA*AVY(IOR,IA)+(1.0-FRA)*AVY(IOR,IB)
  CALL CIRCA(XVAN,YVAN,XP,YP,XRER,YRER,D1,D2,RADC,D3,D4)
  IF(D3.GT.D4)DELYF=-DELYF
  RADC=RADC+DELYF
  XHAV=D1+RADC*COS(D4)
  YHAV=D2+RADC*SIN(D4)
C-----TEST WHETHER THIS POINT IS STILL WITHIN THE REGION-OF-INTEREST..
  D1=XMAP1-SPAR(17)
  D2=XMAP2+SPAR(17)
  D3=YMAP1-SPAR(17)
  D4=YMAP2+SPAR(17)
  IF((XHAV.LT.D1).OR.(XHAV.GT.D2).OR.(YHAV.LT.D3).OR.(YHAV.GT.D4))GO
  $ TO 261
C-----ALSO TERMINATE AFTER LAST DOSAGE INTERVAL....
  IF(TACT.GT.FLAST)GO TO 261
100 CONTINUE
  SEE(77)=SEE(75)
  SEE(78)=SEE(76)
  SEE(75)=TIME(2)/60.0
  SEE(76)=TIME(1)/60.0
C-----"STAGE" PRINTS OUT INTERMEDIATE INFORMATION RE PUFF DEVELOPMENT..
102 CONTINUE
  CALL STAGE(INFORM,0,NX,P,SEE,NOUT,DXB,DYB,NZ,NTDOS)
C-----END OF TRAJECTORY...
261 CONTINUE
  IF(NTDOS.NE.0)CALL STAGE(INFORM,0,NX,P,SEE,NOUT,DXB,DYB,NZ,NTDOS)
  IF(JT.GE.300)WRITE(NOUT,262)
262 FORMAT(1X,"ERROR = PUFF TERMINATED BEFORE REACHING FINAL POSITION"
  $)
  TRADD=TIM

```

```

C-----FRACTION OF TIME DURING WHICH RELATIVE ADVECTION WAS ALLOWED...
  IF(NTDOS.NE.0)TFRAC=TTRAV*TFRAC/TIM
C-----AVERAGE VALUES OF PARAMETERS FOR PUFF TRAJECTORY...
  IF(STABAM.EQ.0.0)GO TO 763
  STABAM=1.0/(STABAM/TIM)
  GO TO 764
763 STABAM=0.9E+15
764 CONTINUE
  RAMAM=RAMAM/TIM
  ZOAM=ZOAM/TIM
  DAM=DAM/TIM
  UVAM=UVAM/TIM
  UVBAM=UVBAM/TIM
  SEE(79)=TFRAC
  SEE(74)=TIME(1)/60.0
  SEE(73)=TIME(2)/60.0
C-----PRINT OUT PUFF TERMINATION INFORMATION...
  CALL STAGE(INFORM,1,NX,P,SEE,NOUT,DXB,DYB,NZ,NTDOS)
  RETURN
  END

-----
SUBROUTINE ALTER(UVBVAV,DT,JT,EXS,EZS,ZS,NZ,NX,DTNOW,DTLAS,ITERM,
  $DXATSV,DZATSV,ZPBS,DXSVEX,PT,IOR,XF,XFP,XFN,P,AVY,VARY,AVYT,VARYT,
  $NOUT)
C
C-----THIS SUBROUTINE ALTERS LAGRANGIAN FRAME SPATIAL STEPSIZES
C- - TO THEIR OPTIMUM VALUES (IF NECESSARY) AND PERFORMS THE
C- - NECESSARY INTERPOLATIONS OF GRID DATA...
C
  DIMENSION XF(NX),XFP(NX),XFN(NX),PT(NX,NZ),P(NX,NZ),DT(300)
  DIMENSION AVYT(NX,NZ),AVY(NX,NZ),VARYT(NX,NZ),VARY(NX,NZ)
  COMMON/SPEC/SPAR(30)
  DTSUB=DT(JT)
  IF(JT.EQ.1)DTSUB=DT(2)
C-----OPTIMUM GRID-CENTRE STEPSIZES...
  DXATS2=SQRT(EXS*DTSUB/SPAR(13))
  DZATS2=SQRT(EZS*DTSUB/SPAR(13))
  D1=SPAR(15)*ZS
C-----CONSTRAINTS...
  IF(D1.LT.SPAR(14))D1=SPAR(14)
  D1=D1/FL0AT(NZ-1)
  IF(DZATS2.LT.D1)DZATS2=D1
  IF(DZATS2.GT.SPAR(28))DZATS2=SPAR(28)
  IF(DXATS2.LT.DZATS2)DXATS2=DZATS2
  D1=(SPAR(8)+1.0)*DXATS2*NX/2.0
  IF(D1.GT.SPAR(27))DXATS2=2.0*SPAR(27)/((SPAR(8)+1.0)*NX)
C*TIME-SAVER...
  IF(JT.GT.15)GO TO 422
  DTNOW=DT(JT)
  IF(DTNOW.GT.DTLAS)ITERM=0
  422 CONTINUE
C*ONLY ALTER X-STEP SIZE WHEN AN INCREASE IS REQUIRED....
  DN=0.5*(DXATS2-UXATSV)+0.5*(DZATS2-DZATSV)

```

```

C-----"DN" IS THE AVERAGE STEPSIZE DEVIATION...
  IF((-SPAR(22).LT.DN).AND.(DN.LT.SPAR(22)))RETURN
  IF(DN.LE.=SPAR(22))DXATS2=DXATSV
  IF((JT.EQ.2).OR.(JT.EQ.3))RETURN
  ZPBS2=ZPBS*(DZATS2/DZATSV)
  DXSEX2=SPAR(8)*DXATS2
C-----FIND OLD AND NEW HORIZONTAL DISTANCE SEQUENCES...
  IF(DXSEX2.LT.DXATS2)DXSEX2=DXATS2
  CALL PHI(NX,DXATSV,UXSVEX,XFP)
  CALL PHI(NX,DXATS2,UXSEX2,XFN)
  IF(JT.EQ.1)GO TO 135
  DO 120 K=1,NZ
  DO 120 I=1,NX
  PT(I,K)=0.0
  AVYT(I,K)=0.0
  VARYT(I,K)=0.0
120 CONTINUE
  DO 121 I=1,NX
  IF(1.GT.IUR)GO TO 122
  DN=XFN(IOR)-XFN(I)
  DPMAX=XFP(IOR)-XFP(1)
C-----ALLOW EXTERNAL POINTS TO REMAIN ZERO...
  IF(DN.GT.DPMAX)GO TO 121
C-----LOCATE X-POSITION IN OLD GRID...
  DO 123 IN=1,IOR
  DP=XFP(IOR)-XFP(IN)
  IF(DP.LT.DN)GO TO 124
123 CONTINUE
  IN=IOR
124 FRIL=(DN-DP)/(XFP(IN)-XFP(IN-1))
  GO TO 125
122 DN=XFN(I)-XFN(IOR)
  DPMAX=XFP(NX)-XFP(IOR)
  IF(DN.GT.DPMAX)GO TO 121
  DO 126 IN=IOR,NX
  DP=XFP(IN)-XFP(IOR)
  IF(DP.GE.DN)GO TO 127
126 CONTINUE
127 FRIL=(DP-DN)/(XFP(IN)-XFP(IN-1))
125 CONTINUE
  DO 128 K=1,NZ
C-----LOCATE Z-POSITION IN OLD GRID...
  ZN=ZPBS2+(K-2)*DZATS2
  ZPMIN=ZPBS-DZATSV
  ZPMAX=ZPBS+(NZ-2)*DZATSV
  IF((ZN.LT.ZPMIN).OR.(ZN.GE.ZPMAX))GO TO 128
  DO 129 KN=1,NZ
  ZP=ZPBS+(KN-2)*DZATSV
  IF(ZN.LT.ZP)GO TO 130
129 CONTINUE
130 FRKL=(ZP-ZN)/DZATSV
  IF(JT.LE.5)GO TO 321
  D1=-115.0
  D2=-115.0
  D3=-115.0
  D4=-115.0
  IF(P(IN-1,KN).GT.0.0)D1=ALOG(P(IN-1,KN))
  IF(P(IN,KN).GT.0.0)D2=ALOG(P(IN,KN))
  IF(P(IN-1,KN-1).GT.0.0)D3=ALOG(P(IN-1,KN-1))
  IF(P(IN,KN-1).GT.0.0)D4=ALOG(P(IN,KN-1))
  PA=FRIL*D1+(1.0-FRIL)*D2
  PB=FRIL*D3+(1.0-FRIL)*D4
C-----USUALLY USE LOGARITHMIC INTERPOLATION FOR ZEROETH MOMENT...

```

```

PT(I,K)=EXP(FRKL*PB+(1.0-FRKL)*PA)
GO TO 322
321 CONTINUE
PA=FRIL*P(IN-1,KN)+(1.0-FRIL)*P(IN,KN)
PB=FRIL*P(IN-1,KN-1)+(1.0-FRIL)*P(IN,KN-1)
PT(I,K)=FRKL*PB+(1.0-FRKL)*PA
322 CONTINUE
C-----LINEAR INTERPOLATION FOR FIRST AND SECOND MOMENTS...
AVA=FRIL*AVY(IN-1,KN)+(1.0-FRIL)*AVY(IN,KN)
AVB=FRIL*AVY(IN-1,KN-1)+(1.0-FRIL)*AVY(IN,KN-1)
AVY(I,K)=FRKL*AVB+(1.0-FRKL)*AVA
VARA=FRIL*VARY(IN-1,KN)+(1.0-FRIL)*VARY(IN,KN)
VARB=FRIL*VARY(IN-1,KN-1)+(1.0-FRIL)*VARY(IN,KN-1)
VARYT(I,K)=FRKL*VARB+(1.0-FRKL)*VARA
128 CONTINUE
121 CONTINUE
C-----REVERT TO ORIGINAL ARRAYS...
DO 131 K=1,NZ
DO 131 I=1,NX
P(I,K)=PT(I,K)
PT(I,K)=0.0
VARY(I,K)=VARYT(I,K)
VARYT(I,K)=0.0
AVY(I,K)=AVYT(I,K)
AVYT(I,K)=0.0
131 CONTINUE
135 CONTINUE
C-----NEW STEPSIZES...
DXATSV=DXATS2
DXSVEX=UXSEX2
DZATSV=DZATS2
ZPBS=ZPBS2
RETURN
END
-----
SUBROUTINE DIFF(P,AVY,VARY,F,NX,NZ,XF,DT,DZ,NSUR,KOR,NOUT,PT,AVYT,
&VARYT)
  DIMENSION P(NX,NZ),F(2,NZ),PT(NX,NZ),XF(NX)
  DIMENSION AVY(NX,NZ),AVYT(NX,NZ),VARY(NX,NZ),VARYT(NX,NZ)
C
C-----SUBROUTINE TO PERFORM DIFFUSION STEP FOR ZEROETH,FIRST AND SECOND
C- MOMENTS ...
C-----A "LIMITING-VALUE" METHOD IS USED (MULHOLLAND(1977))..
C
  NXM=NX-1
  NZM=NZ-1
C-----CONVERT MEAN AND S.D. TO FIRST AND SECOND MOMENTS...
  DO 20 K=2,NZM
  DO 20 I=2,NXM
  VARYT(I,K)=(VARY(I,K)**2+AVY(I,K)**2)*P(I,K)
  AVYT(I,K)=AVY(I,K)*P(I,K)
  PT(I,K)=P(I,K)

```

```

20 CONTINUE
C-----THE METHOD PREDICTS BOUNDARY VALUES AT THE 1/2 TIME-STEP FOR
C-   - USE IN THE FINAL PREDICTION...
DO 22 K=2,NZM
  KM=K-1
  KMM=KM-1
  KP=K+1
  KPP=KP+1
C-----RESET EXTERNAL POINTS(NON-DIFFUSIVE BOUNDARY)
  IF(KM.LT.2)KM=2
  IF(KMM.LT.2)KMM=2
  IF(KP.GT.NZM)KP=NZM
  IF(KPP.GT.NZM)KPP=NZM
  EX=F(1,K)
  EZMM=F(2,KMM)
  EZM=F(2,KM)
  EZ=F(2,K)
  EZP=F(2,KP)
  EZPP=F(2,KPP)
  VAL=DT/(2.0+DZ*DZ)
  BZB=EXP(-(EZMM+EZ)*VAL)
  BZ=EXP(-(EZM+EZ)*VAL)
  BZA=EXP(-(EZ+EZPP)*VAL)
  RZB=EZ/(EZMM+EZ)
  RZ=EZP/(EZM+EZ)
  RZA=EZPP/(EZ+EZPP)
C-----THE Z-FACTORS ARE EVALUATED EXACTLY...
  FZMM=(1.0-RZ)*(1.0-RZB)*(1.0-BZB)
  FZM=(1.0-RZ)*BZB
  FZ=RZ*(1.0-BZA)*(1.0-RZA)-1.0+RZB*(1.0-RZ)*(1.0-BZB)
  FZP=RZ*BZA
  FZPP=RZ*RZA*(1.0-BZA)
  RELZ=1.0-BZ*BZ
  DO 22 I=2,NXM
    IM=I-1
    IMM=IM-1
    IP=I+1
    IPP=IP+1
C-----RESET EXTERNAL POINTS ( NON-DIFFUSIVE BOUNDARY )...
  IF(IM.LT.2)IM=2
  IF(IMM.LT.2)IMM=2
  IF(IP.GT.NXM)IP=NXM
  IF(IPP.GT.NXM)IPP=NXM
  DX1=XF(I)-XF(I-1)
  DX2=XF(I+1)-XF(I)
  AX=2.0*EX/(DX1+DX2)
  BX=EXP(-AX*DT*0.5)
  BXM=1.0-BX
  RX=DX1/(DX1+DX2)
  RXM=1.0-RX
C-----THE BOUNDARY X-FACTORS MAY BE BASED ON THE CENTRAL VALUES WITH
C-   - LITTLE ERROR DUE TO THE SLOW VARIATION OF DX.....
  FXMM=RXM*RXM*BXM
  FXM=RXM*BX
  FX=2.0*RX*RXM*BXM-1.0
  FXP=RX*BX
  FXPP=RX*RX*BXM
  RELX=1.0-BX*BX
C-----ZEROETH MOMENT...
  PP=PT(I,K)
  DELX=FXMM*PT(IMM,K)+FXM*PT(IM,K)+FX*PP+FXP*PT(IP,K)+FXPP*PT(IPP,K)
  DELZ=FZMM*PT(I,KMM)+FZM*PT(I,KM)+FZ*PP+FZP*PT(I,KP)+FZPP*PT(I,KPP)
  TP=PP+DELX*RELX+DELZ*RELZ

```

```

P(I,K)=TP
C-----FIRST MOMENT...
  TAVY=0.0
  IF(TP.LE.0.0)GO TO 33
  AP=AVYT(I,K)
  DELX=FXMM*AVYT(IMM,K)+FXM*AVYT(IM,K)+FX*AP+FXP*AVYT(IP,K)+
  SFXPP*AVYT(IPP,K)
  DELZ=FZMM*AVYT(I,KMM)+FZM*AVYT(I,KM)+FZ*AP+FZP*AVYT(I,KP)+
  SFZPP*AVYT(I,KPP)
  TAVY=(AP+DELX*RELX+DELZ*RELZ)/TP
33  AVY(I,K)=TAVY
C-----SECOND MOMENT.....
  TVARY=0.0
  IF(TP.LE.0.0)GO TO 34
  VP=VARYT(I,K)
  DELX=FXMM*VARYT(IMM,K)+FXM*VARYT(IM,K)+FX*VP+FXP*VARYT(IP,K)+
  SFXPP*VARYT(IPP,K)
  DELZ=FZMM*VARYT(I,KMM)+FZM*VARYT(I,KM)+FZ*VP+FZP*VARYT(I,KP)+
  SFZPP*VARYT(I,KPP)
  VAL=(VP+DELX*RELX+DELZ*RELZ)/TP-TAVY*TAVY+2.0*EX*DT
  IF(VAL.LE.0.0)GO TO 34
  TVARY=SQRT(VAL)
34  VARY(I,K)=TVARY
C-----SET BOUNDARY VALUES...
  IE=I
  KE=K
  IF(I.EQ.2)IE=1
  IF(I.EQ.NXM)IE=NX
  IF(K.EQ.2)KE=1
  IF(K.EQ.NZM)KE=NZ
  IF((IE.EQ.I).AND.(KE.EQ.K))GO TO 22
  P(IE,KE)=TP
  AVY(IE,KE)=TAVY
  VARY(IE,KE)=TVARY
22  CONTINUE
  RETURN
  END

```

```

SUBROUTINE DDOSE(P,AVY,VARY,JT,XP,YP,XVAN,YVAN,TACT,XF,IOR,NX,NZ,
SDZ,ZPB,TREL,NTRA,NSUM,XR,YR,DEP,DAVY,DARY,NOUT,FLAST)
C
C-----THIS SUBROUTINE ALLOCATES DOSAGES TO THE DOSAGE POINTS FOR THE
C-   - APPROPRIATE DOSAGE INTERVAL...
C
  DIMENSION P(NX,NZ),AVY(NX,NZ),VARY(NX,NZ),XF(NX)
  DIMENSION DEP(NX),DAVY(NX),DARY(NX),CM(40),FR(4)
  COMMON/DOSA/DOS(59,40),TDDS(60),XDOS(40),YDOS(40),NTDOS,NPDDS,ZDD
  COMMON/DOSB/QSTR(30),TSTR(30),NSTR,XPL,YPL,TRTEM
  COMMON/DOSC/XVANL,YVANL,TACTL,DZL,ZPBL,TRAJ(7,300),NLP,DTOS
  COMMON/DOSD/XPLLT,YPLLT,TLLT,DXB,DYB,QTRLT,QTR,XVLLT,YVLLT,XRLLT,
  SYRLLT,XRL,YRL,PDEP,TDEF,TDES,WS,PREM

```

```

COMMON/DOSF/DAB(4,700),XFOR(4),TRELLT
COMMON/DOSG/S(24000),XFIDR(40)
COMMON/SPEC/SPAR(30)
NSX=100
FLAST=TDOS(NTDOS)
IF(NX.LT.NSX)NSX=NX
ISP=FLOAT(NX)/FLOAT(NSX)+0.999999
NSX=FLOAT(NX)/FLOAT(ISP)
THT=(NZ-2)*DZ*ZPB
ZDIV=(ZDOS-ZPB)/DZ
IF(ZDOS.GT.THT)ERROR=SQRT(-1.0)
KP=IFIX(ZDIV+3.0)
FRK=ZDIV+3.0-FLOAT(KP)
FRKM=1.0-FRK
NSX7=7*NSX
C-----ARRAY "DAB" CONTAINS PREVIOUS TIME AND PREVIOUS TRAJECTORY
C- - INFORMATION AT DOSAGE HEIGHT...
DO 71 I=1,NSX7
DAB(2,I)=DAB(1,I)
DAB(4,I)=DAB(3,I)
71 CONTINUE
XFOR(2)=XFOR(1)
XFOR(4)=XFOR(3)
XFOR(1)=XFIDR
XFOR(3)=XFIDR(JT)
C-----UPDATE ARRAY DAB...
DO 72 I=1,NSX
DAB(1,I)=XF(ISP*I)
D1=-115.0
D2=-115.0
D3=P(ISP*I,KP)
D4=P(ISP*I,KP-1)
IF(D3.GT.0.0)D1=ALOG(D3)
IF(D4.GT.0.0)D2=ALOG(D4)
DAB(1,I+NSX)=EXP(FRK*D1+FRKM*D2)
DAB(1,I+2*NSX)=FRK*AVY(ISP*I,KP)+FRKM*AVY(ISP*I,KP-1)
DAB(1,I+3*NSX)=FRK*VARY(ISP*I,KP)+FRKM*VARY(ISP*I,KP-1)
DAB(1,I+4*NSX)=DEP(ISP*I)
DAB(1,I+5*NSX)=DAVY(ISP*I)
DAB(1,I+6*NSX)=DARY(ISP*I)
72 CONTINUE
C-----CANNOT INTERPOLATE IF HAVE RUN OUT OF SOLUTIONS (NLP) IN PREVIOUS
C- - TRAJECTORY.
IF(JT.GT.NLP)GO TO 74
IF(NTRA.EQ.1)GO TO 74
JSM=(JT-1)*NSX7
DO 75 I=1,NSX7
DAB(3,I)=S(JSM+I)
75 CONTINUE
74 CONTINUE
IF(JT.EQ.1)GO TO 25
IF(NTRA.EQ.1)GO TO 28
IF(JT.GT.NLP)GO TO 28
GO TO 29
C*STORE LAST TRAJECTORY RELEASE-TIME...
25 TRELLT=TRTEM
TRTEM=TREL
NLP=NSUM
NSUM=0
29 CONTINUE
C*SET NUMBER OF INTERPOLATED PUFFS PER UNIT TIME .....
PPUT=1.0/SPAR(18)
C-----FIND MINIMUM INTERPOLATION TIME TO DEFINE ANY RELEASE EVENT

```

```

C- - GREATER THAN SPAR(30) TO AN ACCURACY OF SPAR(19)/SPAR(2)....
IRELS=1
IRELE=NSTR
DO 61 I=1,NSTR
IF(TSTR(I).LE.TRELLT)IRELS=I
IF(TSTR(I).LT.TREL)IRELE=I
61 CONTINUE
TINMIN=TREL-TRELLT
IRELP=IRELS+1
IRELE=IRELE+1
DO 62 I=IRELP,IRELE
D1=TSTR(I)-TSTR(I-1)
IF(D1.LT.SP(30))D1=0.1E+10
IF(D1.LT.TINMIN)TINMIN=D1
62 CONTINUE
D1=(SPAR(19)/SPAR(2))*TINMIN
IF(D1.GT.SP(19))D1=SP(19)
C*SET NUMBER OF INTERPOLATED TRAJECTORIES....
NTRIN=IFIX(DTOS/D1+0.5)
DTR=DTOS/FLOAT(NTRIN)
DELT=TACT-TACTL
NP=IFIX(PPUT*DELT+1.0)
DTP=DELT/FLOAT(NP)
C-----PARAMETERS FOR 2-DIMENSIONAL INTERPOLATION...
XPLT=TRAJ(1,JT)
YPLT=TRAJ(2,JT)
TLT=TRAJ(3,JT)
XVLT=TRAJ(4,JT)
YVLT=TRAJ(5,JT)
XRLT=TRAJ(6,JT)
YRLT=TRAJ(7,JT)
IF(JT.EQ.1)GO TO 28
DO 51 I=1,NTRIN
FRA=FLOAT(I)/FLOAT(NTRIN)
FRB=(1.0-FRA)
XPTR=FRA*XP+FRB*XPLT
YPTR=FRA*YP+FRB*YPLT
XPLTR=FRA*XPL+FRB*XPLLT
YPLTR=FRA*YPL+FRB*YPLLT
TTR=FRA*TACT+FRB*TLT
TLTR=FRA*TACTL+FRB*TLT
XVTR=FRA*XVAN+FRB*XVLT
YVTR=FRA*YVAN+FRB*YVLT
XRTR=FRA*XR+FRB*XRLT
YRTR=FRA*YR+FRB*YRLT
XVLTR=FRA*XVANL+FRB*XVLLT
YVLTR=FRA*YVANL+FRB*YVLLT
XRLTR=FRA*XR+FRB*XRLLT
YRLTR=FRA*YR+FRB*YRLLT
C*RELEASE-RATE.....
TREFF=FRA*TREL+FRB*TRELLT
QA=0.0
IF((TREFF.LT.TSTR(1)).OR.(TREFF.GT.TSTR(NSTR)))GO TO 16
DO 15 J=2,NSTR
IF(TSTR(J).GE.TREFF)GO TO 17
15 SP=TSTR(J)-TSTR(J-1)
FRA=(TREFF-TSTR(J-1))/SP
QA=FRA*QSTR(J)+(1.0-FRA)*QSTR(J-1)
16 IF(QA.EQ.0.0)GO TO 51
DU 52 J=1,NP
FRA=FLOAT(J)/FLD(NT)
FRB=(1.0-FRA)
C*ESTIMATED POSITION AT TIME=TA.....

```

```

XA=FRA*XPTR+FRB*XPLTR
YA=FRA*YPTR+FRB*YPLTR
TA=FRA*TTR+FRB*TLTR
IF((TA.LT.TDOS(1)).OR.(TA.GE.TDOS(NTDOS)))GO TO 52
XVA=FRA*XVTR+FRB*XVLTR
YVA=FRA*YVTR+FRB*YVLTR
XRA=FRA*XRTR+FRB*XRLTR
YRA=FRA*YRTR+FRB*YRLTR
C*FIND ARC PARAMETERS.....
CALL CIRCA(XVA,YVA,XA,YA,XRA,YRA,XCA,YCA,RADA,THA1,THA2)
DO 53 K=1,NTDOS
53 IF(TA.LT.TDOS(K))GO TO 54
   ERROR=SQRT(-1.0)
54 INT=K-1
   DO 41 L=1,NPDOS
   CM(L)=1.0
41 CONTINUE
FR(1)=(FLOAT(I)/FLOAT(NTRIN))*(FLOAT(J)/FLOAT(NP))
FR(2)=(FLOAT(I)/FLOAT(NTRIN))*(FLOAT(NP-J)/FLOAT(NP))
FR(3)=(FLOAT(NTRIN-I)/FLOAT(NTRIN))*(FLOAT(J)/FLOAT(NP))
FR(4)=(FLOAT(NTRIN-I)/FLOAT(NTRIN))*(FLOAT(NP-J)/FLOAT(NP))
DO 55 LM=1,4
DO 55 L=1,NPDOS
DU=0.0
IDEP=0
X=ABS(XDOS(L))*DXB
Y=ABS(YDOS(L))*DYB
IF((XDOS(L).LT.0).AND.(YDOS(L).LT.0))IDEP=1
C*DISTANCE ALONG ARC FROM CORE.....
D1=X-XCA
IF(D1.EQ.0.0)D1=0.00000001
C-----SORT OUT ARC SENSE...
THA=ATAN((Y-YCA)/D1)
IF(D1.LT.0.0)THA=THA+3.141592654
IF(THA.LT.0.0)THA=THA+2.0*3.141592654
IF(THA2-THA.GT.3.141592654)THA=THA+2.0*3.141592654
IF(THA2-THA.LT.-3.141592654)THA1=THA1+2.0*3.141592654
IF(THA2-THA.LT.-3.141592654)THA2=THA2+2.0*3.141592654
D1=THA2-THA1
D4=THA2-THA
D3=D1*D4
IF(D3.EQ.0.0)D3=0.00000001
D1=D3/ABS(D3)
XPF=XFOR(LM)+D1*RADA+ABS(THA-THA2)
C*DISTANCE FROM ARC (USE LEFT-HAND COORDINATE SET)....
D2=SQRT((X-XCA)**2+(Y-YCA)**2)
D4=U2-RADA
IF(THA2.LT.THA1)D4=-D4
YOUT=D4
IF((XPF.LE.DAB(LM,1)).OR.(XPF.GT.DAB(LM,NSX)))GO TO 57
DO 87 IP=2,NSX
IF(XPF.LE.DAB(LM,IP))GO TO 88
87 CONTINUE
88 SP=DAB(LM,IP)-DAB(LM,IP-1)
   FRIA=(XPF-DAB(LM,IP-1))/SP
   FRIB=1.0-FRIA
C*INTERPOLATE ZEROETH, FIRST AND SECOND MOMENTS...
LAP=(1+IDEP*3)*NSX
LAA=(2+IDEP*3)*NSX
LAV=(3+IDEP*3)*NSX
D1=-115.0
D2=-115.0
D3=DAB(LM,LAP+IP)

```

```

D4=DAB(LM,LAP+IP-1)
C-----USUALLY USE A LOGARITHMIC INTERPOLATION FOR ZEROETH MOMENT...
IF(D3.GT.0.0)D1=ALOG(D3)
IF(D4.GT.0.0)D2=ALOG(D4)
PA=EXP(FRIA*D1+FRIB*D2)
D3=EXP(-115.0)
IF(PA.LE.D3)GO TO 57
AVA=FRIA*DAB(LM,LAA+IP)+FRIB*DAB(LM,LAA+IP-1)
VARA=FRIA*DAB(LM,LAV+IP)+FRIB*DAB(LM,LAV+IP-1)
C*RELATIVE DEVIATION FROM AVA .....
SY=YOUT-AVA
C*DOUSAGE CONTRIBUTION .....
IF(VARA.GT.0.0000001)GO TO 9991
WRITE(3,9992)JT,IP,KP,VARA,VARB,XP,YP
9992 FORMAT(1X,3I3,10E10.3)
GO TO 57
9991 CONTINUE
C-----ASSUME GAUSSIAN DISTRIBUTION "ACROSS-FRAME"...
DD=(DTP+QA*DTR+PA/(VARA*2.50663))*EXP(-SY*SY/(2.0*VARA*VARA))
57 IF(DD.LE.0.0)DD=0.1E-44
   CM(L)=CM(L)*DD**FR(LM)
55 CONTINUE
DO 58 L=1,NPDUS
DDS(INT,L)=DDS(INT,L)+CM(L)
58 CONTINUE
52 CONTINUE
51 CONTINUE
C*STORAGE OF PREVIOUS PROPERTIES.....
28 CONTINUE
C*STORE MOMENTS.....
I=JT*NSX7
IF(I.GT.24000)WRITE(NOUT,78)
78 FORMAT("OERROR- TOO MANY TIME-STEPS TO BE ACCOMMODATED BY ARRAY S(
$24000),",/, " INCREASE DIMENSION, INTERMEDIATE FILING IN *STORE*, A
$ND ABOVE TOLERANCE, TO CONTINUE....")
JSM=(JT-1)*NSX7
DO 77 I=1,NSX7
S(JSM+I)=DAB(1,I)
77 CONTINUE
XFIUR(JT)=XFUR(1)
XPLLT=XPLT
YPLLT=YPLT
TLT=TLT
XVLLT=XVLT
YVLLT=YVLT
XRLLT=XRLT
YRLLT=YRLT
TRAJ(1,JT)=XP
TRAJ(2,JT)=YP
TRAJ(3,JT)=TACT
TRAJ(4,JT)=XVAN
TRAJ(5,JT)=YVAN
TRAJ(6,JT)=XR
TRAJ(7,JT)=YR
NSUM=NSUM+1
XPL=XP
YPL=YP
TACTL=TACT
XVANL=XVAN
YVANL=YVAN
XRL=XR
YRL=YR

```

DZL=DZ
ZPBL=ZPB
RETURN
END

IF(D1.LT.0.0)THET2=THET2+3.141592654
D1=(X1-XC)
IF(D1.EQ.0.0)D1=0.00000001
THET1=ATAN((Y1-YC)/D1)
IF(D1.LT.0.0)THET1=THET1+3.141592654
CONTINUE

28

C-----GET ANGLES INTO 0 TO 2*PI RANGE...
IF(THET1.LT.0.0)THET1=THET1+2.0*3.141592654
IF(THET2.LT.0.0)THET2=THET2+2.0*3.141592654
IF(THET1-THET2.GT.3.141592654)THET2=THET2+2.0*3.141592654
IF(THET1-THET2.LT.-3.141592654)THET1=THET1+2.0*3.141592654
RETURN
END

SUBROUTINE CIRCA(X1,Y1,X2,Y2,X3,Y3,XC,YC,R,THET1,THET2)

C
C*SUBROUTINE TO FIND CIRCLE-FIT PARAMETERS....
C

C*TEST FOR STRAIGHT LINE.....
D1=(Y2-Y1)*(X3-X2)-(Y3-Y2)*(X2-X1)
D4=ABS(D1)

C*WILL HAVE TO CHANGE TOLERANCES (D4,R) FOR OTHER UNITS OR LARGER SYSTM
IF(D4.GT.0.1E+01)GO TO 25
D1=Y2-Y1
D2=X2-X1
IF(D1.EQ.0.0)D1=0.1E-07
IF(D2.EQ.0.0)D2=0.1E-07
SLP=-D2/D1

C*WILL HAVE TO CHANGE TOLERANCES(D4,R)FOR OTHER UNITS OR LARGER SYSTEM.
R=0.3E+06
DELX=R/SQRT(1.0+SLP**2)

C-----X- AND Y-COORDINATES OF CENTRE...
XC=X2+DELX
YC=Y2+SLP*DELX

C-----RECALCULATE R TO ACCOUNT FOR NUMERICAL ERROR...
R=SQRT((XC-X2)**2+(YC-Y2)**2)
THET2=ATAN((Y2-YC)/(X2-XC))
IF(X2.LT.XC)THET2=THET2+3.141592654
D1=X1-XC
IF(D1.EQ.0.0)D1=0.00000001
THET1=ATAN((Y1-YC)/D1)
IF(D1.LT.0.0)THET1=THET1+3.141592654
GO TO 28

C*CIRCLE.....
25 CONTINUE

A1=2.0*(X2-X1)
A2=2.0*(Y2-Y1)
A3=X2*X2+Y2*Y2-X1*X1-Y1*Y1
B1=2.0*(X3-X2)
B2=2.0*(Y3-Y2)
B3=X3*X3+Y3*Y3-X2*X2-Y2*Y2
D1=B1*A2-A1*B2
D2=B1*A3-A1*B3

C-----Y-COORDINATE OF CENTRE...
YC=D2/D1

IF(B1.NE.0.0)XC=(B3-YC*B2)/B1
IF(A1.NE.0.0)XC=(A3-YC*A2)/A1

C-----CIRCAL RADIUS...

R=SQRT((X2-XC)**2+(Y2-YC)**2)
D1=(X2-XC)
IF(D1.EQ.0.0)D1=0.00000001
THET2=ATAN((Y2-YC)/D1)

SUBROUTINE LOCUS(NTIME,NTDAT,DELTA,NSTR,XGS,YGS,IFLAG,DELTB,ITOT,
SJTOT,DXB,DYB,NX,ZS,ZM,DXATSV,DZATSV,ZPBS,XGM1,XGM2,YGM1,YGM2,MFLAG
S,DELTC,DELTD,NZ,ZJ,TDAT,TSTR,QSTR,UB,VB,STAB,PARAM,ZO,D,TIME,TRELI
SN,TRELOT,UVMAX,EMIN,NOUT,KOR,NTDOS,WS,HANSAV,PBFR,F,XF,RAB)

C

C-----THIS SUBROUTINE ESTIMATES THE START AND END RELEASE-TIMES FOR
C- = EACH CENTROID-LOCUS TO AFFECT THE REGION-OF-INTEREST AT A
C- = PARTICULAR TIME...
C

DIMENSION TRELST(15,4),TDAT(NTDAT),TSTR(30),QSTR(30)
DIMENSION UB(ITOT,JTOT,NTDAT),VB(ITOT,JTOT,NTDAT)
DIMENSION STAB(ITOT,JTOT,NTDAT),PARAM(ITOT,JTOT,NTDAT)
DIMENSION ZO(ITOT,JTOT),DC(ITOT,JTOT)
DIMENSION XF(NX),F(2,NZ),TIME(15),TRELIN(15,4)
DIMENSION TRELOT(15,4),UVMAX(15),EMIN(2,15,4),RAB(ITOT,JTOT)
COMMON/SPEC/SPAR(30)

C* TAG RELEVANT LOCI WITH RELEASE TIMES ++++++
C+++++
C-----ADD MARGIN TO THE REGION-OF-INTEREST...

XGB1=XGM1-SPAR(17)/DXB
XGB2=XGM2+SPAR(17)/DXB
YGB1=YGM1-SPAR(17)/DYB
YGB2=YGM2+SPAR(17)/DYB

DO 38 I=1,NTIME
DO 38 J=1,4
TRELST(I,J)=-20.0

38

CONTINUE
NPRIS=IFIX((TDAT(NTDAT)-TDAT(1))/DELTA)
DO 15 IT=1,NPRIS

C*ECONOMISE HERE BY ONLY CONSIDERING RELEASE TIMES DURING WHICH SOURCE
C*OPERATES.....

TREL=(IT-1)*DELTA+TDAT(1)
IF(TREL.LT.TSTR(1))GO TO 15
IF(TREL.GE.TSTR(NSTR))GO TO 15
DO 16 IS=1,NSTR
IF(TREL.LT.TSTR(IS))GO TO 17

16

CONTINUE

```

17 CONTINUE
IF(NTDOS.NE.0)GO TO 321
IF((QSTR(IS).LT.0.1E-35).AND.(QSTR(IS-1).LT.0.1E-35))GO TO 15
321 XG=XGS
YG=YGS
IFLAG=0
ITS=FIX((TDAT(NTDAT)-TREL)/DELTB)
IF(ITS.LT.1)GO TO 15
SUM=0.0
ZEZ=ZS
DO 35 ITP=1,ITS
TIM=TREL+(ITP-1)*DELTB
XP=XG+DXB
YP=YG+DYB
C-----VELOCITY PARAMETERS AT HEIGHT ZEZ...
CALL VELO(XP,YP,TIM,UXY,VXY,VEL,UB,VB,TDAT,NTDAT,DXB,DYB,ITDT,JTOT
S)
CALL PROPS(TIM,XP,YP,STAB,PARAM,ZO,D,STABP,PARAMP,ZOP,DP,DXB,DYB,T
SDAT,NTDAT,ITOT,JTOT,RAB,RABP)
VEL=SQRT(UXY**2+VXY**2)
TTRAV=TIM-TREL+0.5*DELTB
CALL FUNCT(XP,YP,TIM,STABP,PARAMP,DELTB,ZOP,DP,VEL,XF,0,F,NX,2,TT
SRAV,ZEZ)
EZ=F(2,2)
SUM=SUM+EZ
EZ=SUM/FLQAT(ITP)
C-----FIND VELOCITY AT ESTIMATED HEIGHT OF CENTROID...
CALL UEFF(TTRAV,ZS,EZ,WS,HANSAV,PBFR,UXY,VXY,STABP,PARAMP,ZOP,DP,
SUS,VS,UVS,DELTB,ZEZ)
XG=XG+US*DELTB/DXB
YG=YG+VS*DELTB/DYB
IF((XG.LT.XGB1).OR.(XG.GT.XGB2).OR.(YG.LT.YGB1).OR.(YG.GT.YGB2))GO
S TO 36
DO 37 I=1,NTIME
TDIFF=ABS(TIME(I)-TIM)
C*MAY VARY THIS ALLOWED VARIATION*****
TID=0.5*DELTA
IF(TDIFF.GT.TID)GO TO 37
D1=ABS(TREL-TRELST(I,1))
D2=ABS(TREL-TRELST(I,2))
D3=ABS(TREL-TRELST(I,3))
D4=ABS(TREL-TRELST(I,4))
IF(((D1.LT.0.001).OR.(D2.LT.0.001)).OR.((D3.LT.0.001).OR.(D4.LT.0.
S001)))GO TO 37
TREM=TREL-DELTA
D1=ABS(TREM-TRELST(I,1))
D2=ABS(TREM-TRELST(I,2))
D3=ABS(TREM-TRELST(I,3))
D4=ABS(TREM-TRELST(I,4))
MFLAG=0
IF(((D1.LT.0.001).OR.(D2.LT.0.001)).OR.((D3.LT.0.001).OR.(D4.LT.0.
S001)))MFLAG=1
C*USE TRELST(I,4) AS A CHECK AGAINST SEQUENCING..
IF(MFLAG.EQ.1)TRELST(I,4)=TREL
IF(MFLAG.EQ.1)GO TO 37
DO 39 J=1,3
IF(TRELST(I,J).GE.0.0)GO TO 39
TRELST(I,J)=TREL
GO TO 37
39 CONTINUE
C-----THIS TIME-OF-INTEREST REQUIRES TOO MANY RELEASE-TIME LOCI...
WRITE(NOUT,41)
41 FORMAT(1H0,21HERROR=TOO MANY PASSES)

```

```

37 CONTINUE
36 CONTINUE
35 CONTINUE
15 CONTINUE
C*SINCE TRELST IS EARLIEST TIME, ENSURE IN REGION BY INCREASING...
DO 235 I=1,NTIME
DO 235 J=1,3
IF(TRELST(I,J).GE.0.0)TRELST(I,J)=TRELST(I,J)+0.51*DELTA
235 CONTINUE
WRITE(NOUT,42)
42 FORMAT("ORELEASE TIMES TO AFFECT REGION OF INTEREST AT GIVEN TIME.
SAMBIGUITY LATER REMOVED",//,1H,10X,10HGIVEN TIME,15X,31HSEQUENCE
SEARLIEST RELEASE TIMES/)
DO 44 I=1,NTIME
WRITE(NOUT,43)TIME(I),(TRELST(I,J),J=1,3)
44 CONTINUE
43 FORMAT(12X,F10.1,5X,4F10.1)
C+ ESTABLISH RELEASE BOUNDS OF TAGGED LOCI *****
C*****
DO 47 I=1,15
DO 47 J=1,3
C-----PRESET FLAGS IN ENTRY AND EXIT RELEASE = TIMES...
TRELIN(I,J)=-30.0
TRELDT(I,J)=-30.0
47 CONTINUE
DO 48 IT=1,NTIME
UVMAX(IT)=SPAR(20)
IF(TRELST(IT,1).LT.0.0)GO TO 48
DO 49 J=1,3
C-----SOLVE FOR ENTRY AND EXIT RELEASE=TIMES FOR EACH LOCUS(MAX.3) FOR
C- EACH TIME-OF-INTEREST...
EMIN(1,IT,J)=200.0
EMIN(2,IT,J)=200.0
IF(TRELST(IT,J).LT.0.0)GO TO 49
IF(J.EQ.1)GO TO 33
KA=J-1
DO 34 K=1,KA
TROTAD=TRELDT(IT,K)
IF(TROTAD.GE.500000.0)TROTAD=TROTAD-500000.0
TRINAD=TRELIN(IT,K)
IF(TRINAD.GE.500000.0)TRINAD=TRINAD-500000.0
IF((TRELST(IT,J).LE.TROTAD).AND.(TRELST(IT,J).GE.TRINAD))GO TO 49
34 CONTINUE
33 CONTINUE
ISET=+1
C*ENTRY TIME AND EXIT TIME
57 CONTINUE
XG=XGS
YG=YGS
DO 50 MI=1,400
C-----TRY RELEASE TIMES BEFORE AND AFTER TAGGED VALUE(ISET=+1 DR -1).
TREL=TRELST(IT,J)-(MI-1)*DELTC*ISET
C*ECONOMISE HERE BY ONLY CONSIDERING TREL DURING WHICH SOURCE OPERATED
IF((TREL.LE.TDAT(1)).AND.(ISET.GT.0))TRIN=TDAT(1)
IF((TREL.LE.TDAT(1)).AND.(ISET.GT.0))GO TO 55
IF((TREL.GE.TDAT(NTDAT)).AND.(ISET.LT.0))TROT=TDAT(NTDAT)
IF((TREL.GE.TDAT(NTDAT)).AND.(ISET.LT.0))GO TO 58
IF((TREL.GT.TIME(IT)).AND.(ISET.LT.0))TROT=TIME(IT)
IF((TREL.GT.TIME(IT)).AND.(ISET.LT.0))GO TO 58
IF((TREL.LE.TSTR(1)).OR.(TREL.GT.TSTR(NSTR)))GO TO 83
DO 81 KTR=1,NSTR

```

```

IF(TREL.LT.TSTR(KTR))GO TO 82
81 CONTINUE
82 IF((QSTR(KTR).LT.0.1E-35).AND.(QSTR(KTR-1).LT.0.1E-35))GO TO 83
GO TO 84
83 IF(ISET.GT.0)GO TO 85
C-----BOUNDS DETERMINED BY AVAILABLE RELEASE SEQUENCE...
TROT=TREL+500000.0
GO TO 58
85 TRIN=TREL+500000.0
GO TO 55
84 CONTINUE
XG=XGS
YG=YGS
TPERIOD=TIME(IT)-TREL
IF(TPERIOD.LT.DELTD)GO TO 52
NST=IFIX(TPERIOD/DELTD+1.0)
DELTE=TPERIOD/FLOAT(NST-1)
NITP=NST-1
SUM=0.0
ZEZ=ZS
C-----ESTIMATE TRAJECTORY OF CENTROID AT THIS RELEASE-TIME...
DO 53 ITP=1,NITP
TIM=TREL+(ITP-1)*DELTE
XP=XG+DXB
YP=YG+DYB
CALL VELO(XP,YP,TIM,UXY,VXY,VEL,UB,VB,TDAT,NTDAT,DXB,DYB,ITOT,JTOT
S)
CALL PROPS(TIM,XP,YP,STAB,PARAM,ZO,D,STABP,PARAMP,ZOP,DP,DXB,DYB,T
SDAT,NTDAT,ITOT,JTOT,RAB,RABP)
TEND=TIM-TREL
VEL=SQRT(UXY**2+VXY**2)
CALL FUNCT(XP,YP,TIM,STAB,PARAM,DELTE,ZOP,DP,VEL,XF,0.0,F,NX,2,T
SEND,ZEZ)
IF(ITP.EQ.1)GO TO 231
IF(F(1,2).LT.EMIN(1,IT,J))EMIN(1,IT,J)=F(1,2)
IF(F(2,2).LT.EMIN(2,IT,J))EMIN(2,IT,J)=F(2,2)
231 CONTINUE
EZ=F(2,2)
SUM=SUM+EZ
EZ=SUM/FLOAT(ITP)
C-----"UEFF" GIVES EFFECTIVE VELOCITY OF CENTROID...
CALL UEFF(TEND,ZS,EZ,NS,HANSAV,PBFR,UXY,VXY,STAB,PARAMP,ZOP,DP,
SUS,VS,UVS,DELTE,ZEZ)
IF(UVS.GT.UVMAX(IT))UVMAX(IT)=UVS
XG=XG+US*DELTE/DXB
YG=YG+VS*DELTE/DYB
53 CONTINUE
52 CONTINUE
C-----IS THE CENTROID BEYOND THE MARGIN YET...
IF((XG.LT.XGB1).OR.(XG.GT.XGB2).OR.(YG.LT.YGB1).OR.(YG.GT.YGB2))GO
S TO 54
50 IF((TREL.LT.TSTR(1)).OR.(TREL.GT.TSTR(NSTR)))GO TO 65
CONTINUE
WRITE(NOUT,71)
71 FORMAT("OERROR = DELTC NOT LARGE ENOUGH TO INCLUDE RELEASE-TIME LI
SMIT")
STOP
54 IF(MI.EQ.1)GO TO 49
65 IF(ISET.LT.0)GO TO 56
TRIN=TREL
ZJ=ZS
55 CONTINUE
ISET=-1

```

```

GO TO 57
56 TROT=TREL
58 CONTINUE
TRELIN(IT,J)=TRIN
TRELIT(IT,J)=TROT
49 CONTINUE
48 CONTINUE
C-----PRINT OUT ENTRY AND EXIT RELEASE-TIMES FOR EACH LOCUS- NEGATIVE
C- - VALUES INDICATE THAT LOCUS DID NOT CONTRIBUTE...
WRITE(NOUT,61)
61 FORMAT(////,1X,5X,16HTIME OF INTEREST,10X,19HENTRY RELEASE TIMES,/,
S/)
DO 62 I=1,NTIME
DO 236 J=1,3
IF(TRELIN(I,J).LT.0.0)TRELIT(I,J)=-30.0
IF(TRELIT(I,J).LT.0.0)TRELIN(I,J)=-30.0
236 CONTINUE
62 WRITE(NOUT,43)TIME(I),(TRELIN(I,J),J=1,3)
WRITE(NOUT,63)
63 FORMAT(////,1X,5X,16HTIME OF INTEREST,10X,18HEXIT RELEASE TIMES,/,
S)
DO 64 I=1,NTIME
64 WRITE(NOUT,43)TIME(I),(TRELIT(I,J),J=1,3)
RETURN
END

```

```

-----
SUBROUTINE VELO(X,Y,T,U,V,UV,UB,VB,TDAT,NTDAT,DXB,DYB,ITOT,JTOT)
C
C-----THIS SUBROUTINE EXTRACTS THE BASIC VELOCITY DATA FROM OPTIONS(1)
C- - OR (2) INPUT (SECTION B. ABOVE) - X + Y-VELOCITY AT HEIGHT ZG.
C
DIMENSION UB(ITOT,JTOT,NTDAT),VB(ITOT,JTOT,NTDAT),TDAT(NTDAT)
DIMENSION VA(15)
COMMON/CONDAT/NMCD,NTCD,TSCD,DTCD,CD(16000),PMCD(15,2)
XIB=X/DXB
YJB=Y/DYB
IF(NMCD.NE.0)GO TO 14
C-----LINEAR INTERPOLATIONS...
CALL PROP2(XIB,YJB,T,UB,UXY,TDAT,NTDAT,ITOT,JTOT)
CALL PROP2(XIB,YJB,T,VB,VXY,TDAT,NTDAT,ITOT,JTOT)
U=UXY
V=VXY
UV=SQRT(UXY**2+VXY**2)
RETURN
14 CONTINUE
C-----CONTINUOUS DATA WENDELL INTERPOLATION...X,Y VELOCITIES...
IF((T.LT.TDAT(1)).OR.(T.GE.TDAT(NTDAT)))ERROR=SQRT("1.0)
C-----POSITION IN SEQUENCE...
R=(T-TSCD)/DTCD+1.0
NB=R
FR=R-FLUAT(NB)

```

```

C-----X=VELOCITY,Y=VELOCITY...
DD 16 L=1,2
DD 15 I=1,NMCD
IPA=NB*NMCD*4+(I-1)*4+L
IPB=IPA-NMCD*4
VA(I)=-31000.0
C-----"-31000.0" IS THE SIGNAL FOR DATA=VALUE NOT AVAILABLE...
IF((CD(IPA),LT.=30000.0).AND.(CD(IPB),LT.=30000.0))GO TO 15
IF(CD(IPA),LT.=30000.0)IPA=IPB
IF(CD(IPB),LT.=30000.0)IPB=IPA
VA(I)=FR*CD(IPA)+(1.0-FR)*CD(IPB)
15 CONTINUE
C-----"WEND" PERFORMS THE WEIGHTED INVERSE SQUARE INTERPOLATION...
CALL WEND(XIB,YJB,VA,NMCD,PMCD,VEL)
IF(VEL,LT.=30000.0)ERROR=SQRT(-1.0)
IF(L,EQ.1)U=VEL
IF(L,EQ.2)V=VEL
16 CONTINUE
UV=SQRT(U**2+V**2)
RETURN
END

```

SUBROUTINE PROPS(T,X,Y,STAB,PARAM,ZO,D,STABP,PARAMP,ZOP,DP,DXB,DY,
SB,TDAT,NTDAT,ITOT,JTOT,RAB,RABP)

```

C
C-----THIS SUBROUTINE EXTRACTS THE STABILITY AND SURFACE DATA FROM
C-   - STORAGE FOR POINT (X,Y,T) ...
C
DIMENSION STAB(ITOT,JTOT,NTDAT),PARAM(ITOT,JTOT,NTDAT),V(15)
DIMENSION ZO(ITOT,JTOT),D(ITOT,JTOT),TDAT(NTDAT),RAB(ITOT,JTOT)
COMMON/CONDAT/NMCD,NTCD,TSCD,DTCD,CD(16000),PMCD(15,2)
XIB=X/DXB
YJB=Y/DYB
IF(NMCD.NE.0)GO TO 90
C-----LINEAR INTERPOLATIONS...
CALL PROP2(XIB,YJB,T,STAB,STINV,TDAT,NTDAT,ITOT,JTOT)
IF(STINV,EQ.0.0)STINV=1.0/0.9E+15
STABP=1.0/STINV
CALL PROP2(XIB,YJB,T,PARAM,PARAMP,TDAT,NTDAT,ITOT,JTOT)
GO TO 91
90 CONTINUE
C-----CONTINUOUS DATA WENDELL INTERPOLATION.... STAB AND PARAM...
IF((T.LT.TDAT(1)).OR.(T.GE.TDAT(NTDAT)))ERROR=SQRT(-1.0)
C-----POSITION IN SEQUENCE.....
R=(T-TSCD)/DTCD+1.0
NB=R
FR=R-FLOAT(NB)
C-----STAB,PARAM.....
DD 16 L=3,4
DD 15 I=1,NMCD
IPA=NB*NMCD*4+(I-1)*4+L
IPB=IPA-NMCD*4

```

```

C-----"-31000.0" IS THE SIGNAL FOR DATA NOT AVAILABLE...
V(I)=-31000.0
IF((CD(IPA),LT.=30000.0).AND.(CD(IPB),LT.=30000.0))GO TO 15
IF(CD(IPA),LT.=30000.0)IPA=IPB
IF(CD(IPB),LT.=30000.0)IPB=IPA
V(I)=FR*CD(IPA)+(1.0-FR)*CD(IPB)
15 CONTINUE
C-----"WEND" PERFORMS THE WEIGHTED INVERSE SQUARE INTERPOLATION...
CALL WEND(XIB,YJB,V,NMCD,PMCD,R)
IF(R,LT.=30000.0)ERROR=SQRT(-1.0)
IF((L,EQ.3).AND.(R,EQ.0.0))R=0.00000001
IF((L,EQ.3)STABP=1.0/R
IF((L,EQ.3).AND.(R,EQ.-31000.0))STABP=-31000.0
IF(L,EQ.4)PARAMP=R
16 CONTINUE
IF((STABP,EQ.-31000.0).OR.(PARAMP,LT.=30000.0))ERROR=SQRT(-1.0)
C-----CONSTANT SURFACE DATA.....
C-----USE A TWO-DIMENSIONAL LINEAR INTERPOLATION...
91 CONTINUE
ISET=0
JSET=0
I1=XIB
J1=YJB
FRI=XIB-FLOAT(I1)
FRJ=YJB-FLOAT(J1)
I2=I1+1
J2=J1+1
IF(I2.GT.ITOT)ISET=ITOT
IF(I1.LT.1)ISET=1
IF(J2.GT.JTOT)JSET=JTOT
IF(J1.LT.1)JSET=1
IF((ISET,EQ.0).AND.(JSET,EQ.0))GO TO 93
IF(ISET,EQ.0)ZOP=EXP((1.0-FRI)*ALOG(ZO(I1,JSET))+FRI*ALOG(ZO(I2,JSET)))
IF(ISET,EQ.0)RABP=(1.0-FRI)*RAB(I1,JSET)+FRI*RAB(I2,JSET)
IF(JSET,EQ.0)ZOP=EXP((1.0-FRJ)*ALOG(ZO(ISET,J1))+FRJ*ALOG(ZO(ISET,J2)))
IF(JSET,EQ.0)RABP=(1.0-FRJ)*RAB(ISET,J1)+FRJ*RAB(ISET,J2)
IF((ISET,EQ.0).OR.(JSET,EQ.0))RETURN
ZOP=ZO(ISET,JSET)
DP=D(ISET,JSET)
RABP=RAB(ISET,JSET)
RETURN
93 CONTINUE
C-----SURFACE=ROUGHNESS ZO IS BETTER INTERPOLATED AS ITS LOGARITHM..
ZJ1=(1.0-FRI)*ALOG(ZO(I1,J1))+FRI*ALOG(ZO(I2,J1))
ZJ2=(1.0-FRI)*ALOG(ZO(I1,J2))+FRI*ALOG(ZO(I2,J2))
ZOP=EXP((1.0-FRJ)*ZJ1+FRJ*ZJ2)
DJ1=(1.0-FRI)*D(I1,J1)+FRI*D(I2,J1)
DJ2=(1.0-FRI)*D(I1,J2)+FRI*D(I2,J2)
DP=(1.0-FRJ)*DJ1+FRJ*DJ2
RJ1=(1.0-FRI)*RAB(I1,J1)+FRI*RAB(I2,J1)
RJ2=(1.0-FRI)*RAB(I1,J2)+FRI*RAB(I2,J2)
RABP=(1.0-FRJ)*RJ1+FRJ*RJ2
RETURN
END

```

```

SUBROUTINE WEND(X,Y,VP,NP,PP,V)
C-----SUBROUTINE TO PERFORM WENDELL INTERPOLATION...
C-----A WEIGHTED INVERSE-SQUARE INTERPOLATION...
C
DIMENSION VP(15),PP(15,2),D2(15)
COMMON/SWEND/WFMC(15)
DATA LPMIN/2/
C-----FIND DISTANCES SQUARED
LP=0
DO 21 K=1,NP
C-----TEST WHETHER DATA=VALUE IS AVAILABLE...
IF(VP(K).LT.=30000.0)GO TO 21
LP=LP+1
D2(K)=(PP(K,1)-X)**2+(PP(K,2)-Y)**2
IF(D2(K).EQ.0.0)GO TO 25
D2(K)=1.0/D2(K)
21 CONTINUE
C-----TEST FOR MINIMUM NUMBER OF POINTS,LPMIN
IF(LP.GE.LPMIN)GO TO 23
V=-31000.0
RETURN
23 CONTINUE
SUMN=0.0
SUMD=0.0
DO 22 K=1,NP
IF(VP(K).LT.=30000.0)GO TO 22
SUMN=SUMN+D2(K)*VP(K)*WFMC(K)
SUMD=SUMD+D2(K)*WFMC(K)
22 CONTINUE
V=SUMN/SUMD
RETURN
25 CONTINUE
C-----VALUE AT A MAST...
V=VP(K)
RETURN
END

```

```

SUBROUTINE PHI(NX,DX,DXE,XF)
C-----SUBROUTINE TO SET UP SPACING OF HORIZONTAL POINTS IN LAGRANGIAN
C-----GRID AS A DISTANCE SEQUENCE XF(1) ...
DIMENSION XF(NX)
IOR=IFIX(FLOAT(NX)/2.0+0.51)
XF(1)=DXE
C-----POINTS BEFORE CENTRE...
DO 4 I=2,IOR
FRA=FLOAT(I)/FLOAT(IOR)
XF(I)=XF(I-1)+FRA*DX+(1.0-FRA)*DXE
4 CONTINUE

```

```

IORP1=IOR+1
C-----POINTS AFTER CENTRE...
DO 5 I=IORP1,NX
FRA=FLOAT(NX-I)/FLOAT(NX-IORP1)
XF(I)=XF(I-1)+FRA*DX+(1.0-FRA)*DXE
5 CONTINUE
RETURN
END

```

```

SUBROUTINE PROP2(X,Y,TIM,A,AXY,TDAT,NTDAT,ITOT,JTOT)
C-----SUBROUTINE TO PERFORM 3-DIMENSIONAL (X,Y AND TIME) LINEAR
C-----INTERPOLATION FOR GRID-STORED VARIABLES...
C
DIMENSION A(ITOT,JTOT,NTDAT),TOAT(NTDAT)
DO 31 IT=1,NTDAT
IF(TIM.LT.TDAT(IT))GO TO 32
31 CONTINUE
ERRDR=SQRT(-1.0)
C=ERROR=-OUTSIDE AVAILABLE TIME=DATA
32 FR=(TIM-TDAT(IT-1))/(TDAT(IT)-TDAT(IT-1))
ISET=0
JSET=0
XTOT=FLOAT(ITOT)
YTOT=FLOAT(JTOT)
C-----SET TO BOUNDARY=VALUES IF OUTSIDE DATA=REGION...
IF(X-XTOT)2,8,8
8 ISET=ITOT
2 IF(Y-YTOT)3,9,9
9 JSET=JTOT
3 IF(1.0-X)4,4,10
10 ISET=1
4 IF(1.0-Y)5,5,11
11 JSET=1
5 IF(ISET+JSET)21,21,17
17 IF(ISET)7,7,6
6 IS=ISET
JS=IFIX(Y+0.5)
7 IF(JSET)19,19,16
16 JS=JSET
IF(ISET)19,18,19
18 IS=IFIX(X+0.5)
19 NEX=NEX+1
AXY=FR*A(IS,JS,IT)+(1.0-FR)*A(IS,JS,IT-1)
RETURN
21 CONTINUE
I2=IFIX(X)
I3=I2+1
J2=IFIX(Y)
J3=J2+1
BF=A(I2,J3,IT)*(1.0-X+I2)+(X-I2)*A(I3,J3,IT)
BG=A(I2,J2,IT)*(1.0-X+I2)+(X-I2)*A(I3,J2,IT)
AIT=BG*(1.0-Y+J2)+(Y-J2)*BF

```

```

BF=A(I2,J3,IT-1)*(1.0-X+I2)+(X=I2)*A(I3,J3,IT-1)
BG=A(I2,J2,IT-1)*(1.0-X+I2)+(X=I2)*A(I3,J2,IT-1)
AITM1=BG*(1.0-Y+J2)+(Y=J2)*BF
AXY=FR*AIT+(1.0-FR)*AITM1
RETURN
END

```

```

SUBROUTINE UEFF(TRAT,ZS,EZ,WS,HAV,PBFR,UXY,VXY,STABP,PARAMP,ZOP,DP
S,US,VS,UVS,DELT,ZEZ)

```

```

C
C-----SUBROUTINE TO SIMULATE MOTION OF PUFF CENTROID - ESTIMATES
C= - EFFECTIVE VELOCITY...
C
COMMON/SPEC/SPAR(30)
C*NOTE--- THIS SUBROUTINE ASSUMES UNITS OF METRES,SECONDS...
C*PROTECT AGAINST SINGULARITY AT TRAV=0
TRAV=TRAT
C*FIND THE EXPECTED VERTICAL STEPSIZE AT THIS POINT...
D1=0.5*SQRT(1.0+40.0*TRAV/SPAR(24))-0.5
DT=SPAR(24)*(0.2*D1+0.1)
DZ=SQRT(EZ*DT/SPAR(13))
ZPB=PBFR*DZ
C*SET UP TRACKING LEVEL TO MATCH NUMERICAL PUFF...
ZTR=HAV
IF(ZTR.LT.ZPB)ZTR=ZPB
C*OBTAIN SLOPE ALPHA BETWEEN ZTR AND (ZS=WS*TRAV)...
ZC=ZS-WS*TRAV
IF(ZC.LT.0.0)ZC=0.0
ZEZ=0.5*(ZTR+ZC)
IF(ZTR.EQ.ZC)ZTR=ZTR+0.01
CALL SPEED(UXY,VXY,STABP,PARAMP,ZOP,DP,ZC,DZ,DX,US,VS,UC,ZPB)
CALL SPEED(UXY,VXY,STABP,PARAMP,ZOP,DP,ZTR,DZ,DX,US,VS,UTR,ZPB)
ALPHA=(UC-UTR)/(ZC-ZTR)
ZC=ZS-WS*TRAV
IF(ZC.LT.0.0)UC=ALPHA*ZC
Z=ZTR-ZS+WS*TRAV
T=TRAV
C*CALCULATE THE MEAN RELATIVE VELOCITY OF THE X-CENTROID AT HEIGHT ZTR..
C*CALCULATE ERFC...
D1=1.0
A1=0.3480242
A2=-0.0958798
A3=0.7478556
P1=0.47047
DU 6 M=1.2
T=TRAV+(M-1)*DELT
VALT=EZ*T
IF(VALT.LT.0.1E-06)D=0.0
IF(VALT.LT.0.1E-06)GO TO 5
ARG=(Z+2.0*ZS)/(2.0*SQRT(EZ*T))
IF(ARG.LT.0.0)D1=-1.0
ARG=ABS(ARG)

```

```

R=1.0/(1.0+P1*ARG)
ERF=1.0-(A1*R+A2*R+R+A3*R**3)*EXP(-ARG*ARG)
D=1.0-D1*ERF
C*RELATIVE VELOCITY OF CENTROID...
G=ALPHA*SQRT(3.14159*T/EZ)+0.5*(EZ*T-Z*ZS)
A=EXP(-Z*Z/(4.0*EZ*T))
B=EXP(-(Z+2.0*ZS)**2/(4.0*EZ*T))
R=A+B
IF(R.EQ.0.0)R=0.1
D=0.5*ALPHA*Z*T+G*D/R
5 CONTINUE
IF(M.EQ.1)VS=D
6 CONTINUE
DXDT=(D-VS)/DELT
C*HENCE TOTAL SPEED OF CENTRID IS...
UVS=UC+DXDT
UVB=SQRT(UXY+UXY+VXY+VXY)
US=UXY+UVS/UVB
VS=VXY+UVS/UVB
RETURN
END

```

```

SUBROUTINE SPEED(UZG,VZG,STABP,PARAMP,ZOP,DP,Z,DZ,DX,US,VS,UVS,ZPB
S)

```

```

C
C-----SUBROUTINE TO CALCULATE VELOCITY AT HEIGHT Z ACCORDING TO ANY
C= - GIVEN RELATIONS - MAY BE ALTERED...
C
COMMON/ZSTAN/ZG
VK=0.38
C-----FIND FRICTION VELOCITIES FROM VELOCITIES AT HEIGHT ZG...
CALL FRIC(1.0,STABP,PARAMP,ZG,ZOP,DP,RATIO,VK,2)
U=RATIO*UZG
V=RATIO*VZG
C*USE FLUX RELATIONS REC. BY DYER,
C*BOUNDARY-LAYER METEOROLOGY,(1974),7,363-372.
C----- WITH EXTENSION AFTER WEBB(1970)
C----- QUART,J.R.MET.SOC.(1970),96,PP.67-90.
US=0.0
VS=0.0
UVS=0.0
IF(Z.LE.ZOP)RETURN
ZO=ZOP
EL=STABP
UFRIC=U
VFRIC=V
IF(EL.LT.0)GO TO 403
VAL=ALOG(Z/ZO)+5.0*(Z-ZO)/EL
IF(Z.GT.EL)VAL=6.0*ALOG(Z/EL)-ALOG(ZO/EL)+5.0-5.0*ZO/EL
GO TO 402
403 AT=(1.0-16.0*ZO/EL)**0.25
RT=(1.0-16.0*Z/EL)**0.25
D1=2.0*(0.5*ALOG((AT+1.0)/(AT-1.0)))-ATAN(AT))

```

```

D2=2.0*ATAN(RT)
D3=ALOG(RT+1.0)/(RT-1.0)
VAL=D1+D2-D3
402 CONTINUE
C-----X- AND Y-COMPONENTS...
US=UFRIC*VAL/VK
VS=VFRIC*VAL/VK
UVS=SQR(UV*US+VS*VS)
RETURN
END

```

```

-----
SUBROUTINE FUNCT(X,Y,TACT,ATABAV,RAHAV,DTAV,ZOAV,DAV,UVZG,XF,DZ,F,
SNX,NZ,TIM,ZPB)
C-----SUBROUTINE TO CALCULATE VERTICAL AND HORIZONTAL DIFFUSIVITY
C-   " PROFILES ACCORDING TO ANY GIVEN RELATIONS - MAY BE ALTERED..
C.
DIMENSION XF(NX),F(2,NZ)
COMMON/ZSTAN/ZG
C*USE FLUX RELATIONS RECOMMENDED BY DYER,
C*BOUNDARY-LAYER METEOROLOGY,(1974),7,363-372.
C----- WITH EXTENSION DUE TO WEBB(1970).
C----- QUART.J.R.MET.SOC.(1970),96,67-90.
VK=0.38
EL=ATABAV
C-----FIND FRICTION VELOCITY FROM VELOCITY AT HEIGHT ZG...
CALL FRIC(UVZG,EL,RAHAV,ZG,ZOAV,DAV,UV,VK,2)
UVFRIC=UV
C*COMPUTE EX USING SUTTON RESULT..FY/EZ=(CY/CZ)**2,USING VENTERS DATA..
C-----VENTER,HALLIDAY AND PRINSLON,
C-----ATMOS.ENV.(1973),7,P.593.
EN=4.0*RAHAV+0.37
CX=0.57*EN+0.106
CZ=0.38*EN+0.112
EXEZ=(CX/CZ)**2
DO 33 K=2,NZ
C-----CALCULATE ENTIRE PROFILE...
Z=(K-2)*DZ+ZPB
IF(EL.GE.0)EZ=UVFRIC*VK*Z/(1.0+5.0*Z/EL)
IF(EL.LT.0)EZ=UVFRIC*VK*Z*SQR(1.0-16.0*Z/EL)
IF((EL.GE.0).AND.(Z.GT.EL))EZ=UVFRIC*VK*Z/6.0
EX=EXEZ
F(1,K)=EX
F(2,K)=EZ
33 CONTINUE
RETURN
END

```

```

SUBROUTINE REMOVE(HS,PREM,TDES,TDEF,PDEP,RABAV,DT,DZ,ZPB,NZ,NX,JT,
SPT,P,AVY,VARY,TACT,AVYT,VARYT,XP,YP,STABAV,RAHAV,DTAV,ZOAV,DAV,
SUVBAV,ZS,TIM,F,XF,DEP,DAVY,DARY)
C
C*REMOVAL PROCESSES=SETTLING,GROUND=ABSORPTION,AND UNIFORM DECAY...
C*SETTLING SPEED = WS, GROUND ABSORPTION PARAMETER=RABAV,
C- DECAY PARAMETER=PREM+PDEP, WHERE PDEP IS NON-ZERO FOR TDES)T)TDEF..
C
DIMENSION P(NX,NZ),AVY(NX,NZ),VARY(NX,NZ),PT(NX,NZ)
DIMENSION AVYT(NX,NZ),VARYT(NX,NZ),XF(NX),F(2,NZ),DEP(NX),DAVY(NX)
DIMENSION DARY(NX)
COMMON/SPEC/SPAR(30)
C*EFFECTIVE REPLACEMENT DIFFUSIVITY FOR GROUND IMPACTION/ABSORPTION...
D1=ZS
IF(D1.LT.SPAR(23))D1=SPAR(23)
D2=D1/FLOAT(NZ)
D3=D2*ZPB/DZ
CALL FUNCT(XP,YP,TACT,STABAV,RAHAV,DTAV,ZOAV,DAV,UVBAV,XF,D2,F,NX,
SNZ,TIM,D3)
SUM=0.0
DO 21 K=2,NZ
SUM=SUM+F(2,K)
21 CONTINUE
EZ=SUM/FLOAT(NZ-1)
A1=0.3480242
A2=-0.0958798
A3=0.7478556
P1=0.47047
C*CALCULATE DECAY EXPONENT...
EDEP=0.0
IF((TACT.GE.TDES).AND.(TACT.LE.TDEF))EDEP=PDEP
EXPT=PREM+EDEP
DECFR=EXP(-EXPT*DT)
ZSET=WS*DT
FRK=ZSET/DZ
NZM1=NZ-1
DO 25 I=1,NX
DEP(I)=WS*DT*PT(I,2)
DAVY(I)=DEP(I)*AVYT(I,2)
DARY(I)=DEP(I)*(VARYT(I,2)**2+AVYT(I,2)**2)
25 CONTINUE
C*EXECUTE COMBINED REDISTRIBUTION PROCESSES...
DO 22 K=2,NZM1
Z=(K-2)*DZ+ZPB
DH=DZ
IF(K.EQ.2)DH=ZPB+0.5*DZ
D1=0.5*Z/SQR(EZ*DT)
D2=(0.5*Z+RABAV*DT)/SQR(EZ*DT)
T1=1.0/(1.0+P1*D1)
C-----CALCULATE ERROR FUNCTIONS...
ERFCD1=(A1*T1+A2*T1*T1+A3*T1*T1*T1)*EXP(-D1*D1)
T1=1.0/(1.0+P1*D2)
ERFCD2=(A1*T1+A2*T1*T1+A3*T1*T1*T1)*EXP(-D2*D2)
RAB=1.0-ERFCD1+EXP(RABAV*(Z+RABAV*DT)/EZ)*ERFCD2
KB=FIX(FLOAT(K)+FRK)
KA=KB+1
FRA=FLOAT(K-KB)+FRK
IF(KB.LT.2)KB=2

```

```

IF(KA.LT.2)KA=2
IF(KB.GT.NZ)KB=NZ
IF(KA.GT.NZ)KA=NZ
DO 22 I=1,NX
IF(JT.LE.5)GO TO 23
D1=-115.0
D2=-115.0
D3=PT(I,KB)
D4=PT(I,KA)
IF(D3.GT.0.0)D1=ALOG(D3)
IF(D4.GT.0.0)D2=ALOG(D4)
C-----USUALLY USE A LOGARITHMIC INTERPOLATION FOR ZEROth MOMENT...
CTRAN=EXP((1.0-FRA)*D1+FRA*D2)
GO TO 24
23 CONTINUE
CTRAN=(1.0-FRA)*PT(I,KB)+FRA*PT(I,KA)
24 CONTINUE
C-----INTERPOLATE 1ST AND 2ND MOMENTS...
AVY(I,K)=(1.0-FRA)*AVYT(I,KB)+FRA*AVYT(I,KA)
VARY(I,K)=(1.0-FRA)*VARYT(I,KB)+FRA*VARYT(I,KA)
C-----ADJUST ZEROth MOMENT FOR LOSSES...
P(I,K)=CTRAN*RAB*DECFR
C*FIND FRACTION OF REMOVAL DUE TO NON-SETTLING DEPOSITION PROCESSES ONLY
EPTT=ALOG(RAB)/DT-EXPT
IF(EPTT.EQ.0.0)GO TO 22
FD=((EPTT+PREM)/(EPTT))*(1.0-RAB*DECFR)
CDEP=FD*CTRAN*DH
C-----THESE ARRAYS (DEP,DAVY,DARY) REPRESENT THE DEPOSITION DISTRIB-
C= -UTION AND ARE USED IN SUBROUTINE "DOSE" TO ALLOCATE DEPOSITION
C= - INSTEAD OF DOSAGE AS REQUIRED (BY SPECIFYING NEGATIVE VALUES
C= - OF DOSAGE=POINT GRID COORDINATES) ...
DEP(I)=DEP(I)+CDEP
DAVY(I)=DAVY(I)+CDEP*AVY(I,K)
DARY(I)=DARY(I)+CDEP*(VARY(I,K)**2+AVY(I,K)**2)
22 CONTINUE
C----- DEPOSITION ARRAYS INTO REQUIRED FORM...
DO 26 I=1,NX
D1=DEP(I)
IF(D1.LE.0.0)GO TO 27
DAVY(I)=DAVY(I)/D1
D2=DARY(I)/D1-DAVY(I)**2
IF(D2.LE.0.0)GO TO 27
DARY(I)=SQRT(D2)
DEP(I)=DEP(I)/DT
GO TO 26
27 CONTINUE
DEP(I)=0.0
DAVY(I)=0.0
DARY(I)=0.0
26 CONTINUE
RETURN
END

```

SUBROUTINE FRIC(VEL,EL,GTPZG,HA,ZO,D,US,VK,IOPT)

```

C
C-----SUBROUTINE TO EVALUATE FRICTION VELOCITY FROM GIVEN VELOCITY AT
C= - HEIGHT ZG...
C-----THE SAME THEORY IS USED AS IN SUBROUTINE "SPEED" ...
C
      IF(IOPT.EQ.2)GO TO 81
C-----FROM MEAN VELOCITY...
      ERROR=SQRT(-1.0)
      STOP
      81 CONTINUE
C-----FROM MEASUREMENT AT HEIGHT HA...
      ZM=HA
      RZ=ZM/EL
      RO=ZO/EL
      IF(RZ)82,83,84
C-----UNSTABLE
      82 CONTINUE
      A=(1.0-16.0*RO)**0.25
      B=(1.0-16.0*RZ)**0.25
      V1=2.0*ATAN(B)-2.0*ATAN(A)
      V2=ALOG(((B+1.0)*(A-1.0))/((B-1.0)*(A+1.0)))
      US=VK*VEL/(V1-V2)
      RETURN
C-----NEUTRAL
      83 CONTINUE
      US=VK*VEL/ALOG(ZM/ZO)
      RETURN
C-----STABLE...
      84 CONTINUE
      IF(RZ.GT.1.0)GO TO 85
      US=VK*VEL/(ALOG(ZM/ZO)+5.0*(RZ-RO))
      RETURN
      85 CONTINUE
      US=VK*VEL/(6.0*ALOG(RZ)-ALOG(RO)+5.0*5.0*RO)
      RETURN
      END

```

```

-----
SUBROUTINE STAGE(INFORM,ICOMPL,NX,P,TEE,NOUT,DXB,DYB,NZ,NTDOS)
C
C-----SUBROUTINE TO PRINT PUFF DEVELOPMENT INFORMATION...
C
      DIMENSION SEE(82),LIN(120),P(NX,NZ),TEE(82)
      COMMON/SPEC/SPAR(30)
      DATA NLEV,NCH/3,120/
      DO 40 J=1,82
      40 SEE(J)=TEE(J)
      IF(ICOMPL.EQ.1)GO TO 55
      IF(INFORM.EQ.0)RETURN
      JT=SEE(6)
      SEE(81)=SEE(81)/DXB
      SEE(82)=SEE(82)/DYB
      WRITE(NOUT,41)JT,(SEE(J),J=7,13),SEE(81),SEE(82)
      41 FORMAT(4X,"JT=",I2," DT(JT)=",F7.2," TACT=",F9.2," X-CENTROID=",
      SF7.1," (BOUNDS..",F7.1,"",F7.1,"") DU/DZ(ZMPREV)=",F5.3," ZM=",

```

```

$F6.2," XH=","F5.2," YH=","F5.2)
DO 31 J=14,22,2
IF(J.EQ.20)GO TO 31
SEE(J)=SEE(J)/DXB
SEE(J+1)=SEE(J+1)/DYB
31 CONTINUE
WRITE(NOUT,42)(SEE(J),J=14,23)
42 FORMAT(10X,"GRID POSNS=XP=","F5.2," YP=","F5.2," XVAN=","F5.2," YVAN="
$,"F5.2," XSTRK=","F5.2," YSTRK=","F5.2," FACTOR=","F5.2," JSTRK=","
$F3.0," XRER=","F5.2," YRER=","F5.2)
SEE(24)=180.0*SEE(24)/3.14159
SEE(25)=180.0*SEE(25)/3.14159
WRITE(NOUT,43)(SEE(J),J=24,30)
43 FORMAT(10X,"GAMT(DEG)=","F7.2," ANGT(DEG)=","F7.2," STABAV=","E10.3,
$," RAMAV=","E10.3," ZOAV=","E10.3," DAV=","F6.3," RABAV=","E10.3)
WRITE(NOUT,44)(SEE(J),J=31,36)
44 FORMAT(10X,"UVAV=","F5.2," UBAV=","F6.3," VBAV=","F6.3," UVBAV=","F6.3
$," EXAV(ZS)=","E10.3," EZAV(ZS)=","E10.3)
WRITE(NOUT,45)(SEE(J),J=37,41)
45 FORMAT(10X,"BEFORE ALTER-DX=","F6.2," DXE=","F6.2," DZ=","F6.2," ZPB="
$,"F5.2," FRAME LENGTH=","F8.2)
WRITE(NOUT,46)(SEE(J),J=42,46)
46 FORMAT(10X,"AFTER ALTER-DX=","F6.2," DXE=","F6.2," DZ=","F6.2," ZPB="
$,"F5.2," FRAME LENGTH=","F8.2)
C-----OPTIMAL STEPSIZES...

DTSUB=SEE(7)
IF(JT.EQ.1)DTSUB=2.0*DTSUB
EXS=SEE(35)
Ezs=SEE(36)
DXOPT=SQR(XS=DTSUB/SPAR(13))
DZOPT=SQR(EZS*DTSUB/SPAR(13))
ITERM=SEE(47)
WRITE(NOUT,47)DXOPT,DZOPT,(SEE(J),J=60,62)
DZOPTL=SEE(80)
IF((ITERM.EQ.1).OR.(JT.EQ.1).OR.(DZOPTL.EQ.-1.0))WRITE(NOUT,48)
47. FORMAT(10X,"OPTIMAL STEPSIZES = DX=","F6.3," DZ=","F6.3," WS=","E10.3
$," ZSETTLE=","E10.3," IMPACT/ABS EZ=","E10.3)
48. FORMAT(1H+,"107X,"***NO ADVECTION***")

C-----PROCESS AND ELAPSED TIMES...
PAD=SEE(52)-SEE(48)
EAD=SEE(53)-SEE(49)
IF(EAD.LT.0)EAD=EAD+86400.0
IF((ITERM.EQ.1).OR.(JT.EQ.1))PAD=0.0
IF((ITERM.EQ.1).OR.(JT.EQ.1))EAD=0.0
PDF=SEE(58)-SEE(56)
EDF=SEE(59)-SEE(57)
IF(EDF.LT.0)EDF=EDF+86400.0
IF(JT.EQ.1)PDF=0.0
IF(JT.EQ.1)EDF=0.0
PDS=SEE(65)-SEE(63)
EDS=SEE(66)-SEE(64)
IF(EDS.LT.0)EDS=EDS+86400.0
IF(NTDOS.EQ.0)PDS=0.0
IF(NTDOS.EQ.0)EDS=0.0
C-----PR. AND ELAP. TIMES FOR WHOLE TRAJECTORY-STEP...
PTRS=SEE(75)-SEE(77)
ETRS=SEE(76)-SEE(78)
IF(JT.EQ.1)PTRS=SEE(75)-SEE(1)
IF(JT.EQ.1)ETRS=SEE(76)-SEE(2)

```

```

IF(ETRS.LT.0)ETRS=ETRS+86400.0
WRITE(NOUT,49)PAD,PDF,PDS,PTRS,SEE(50)
WRITE(NOUT,50)EAD,EDF,EDS,ETRS,SEE(54)
49. FORMAT(10X,"PROCESS TIMES = PAD=","F9.2," PDF=","F9.2," PDS=","F9.2,"
$ PTRS=","F9.2," BEFORE ADVECTION PICONS=","F7.5)
50. FORMAT(10X,"ELAPSED TIMES = EAD=","F9.2," EDF=","F9.2," EDS=","F9.2,"
$ ETRS=","F9.2," AFTER ADVECTION PICONS=","F7.5)
C-----PLOT LOWER STRATA OF CONCENTRATION DISTRIBUTION...
C-----9=10*(-3)
C-----1=10*(-11)
C-----0=LT.10*(-11)
C-----*GT.10*(-3)
DO 71 KK=1,NLEV
L=NLEV+2-KK
DO 72 M=1,NCH
RP=(FLOAT(M)/FLOAT(NCH))*FLOAT(NX-1)+0.999999
IPB=RP
IPA=IPB+1
FRA=RP-IPB
VPA=P(IPA,L)
VPB=P(IPB,L)
IF(VPA.LE.0.0)VPA=0.1E-44
IF(VPB.LE.0.0)VPB=0.1E-44
V=FRA*ALOG10(VPA)+(1.0-FRA)*ALOG10(VPB)
IV=V+0.5
ICH=IV+12
IF(ICH.LT.0)ICH=0
LIN(M)=ICH
72. CONTINUE
C-----PRINT OUT LOWEST THREE LEVELS OF LAGRANGIAN PUFF ZEROth MOMENT AS
C = LOG EQUIVALENTS...
WRITE(NOUT,73)(LIN(J),J=1,NCH)
73. FORMAT(12X,120I1)
71. CONTINUE
RETURN
C-----ENDOFF TRAJECTORY...
55. CONTINUE
WRITE(NOUT,51)(SEE(J),J=67,72)
51. FORMAT(10X,"TRAJECTORY MEANS= STAB=","E10.3," PARAM=","E10.3," ZO=","
$E10.3," D=","F5.2," UV=","F5.3," UVB=","F5.3)
PTR=SEE(73)-SEE(1)
ETR=SEE(74)-SEE(2)
IF(ETR.LT.0)ETR=ETR+86400.0
WRITE(NOUT,52)PTR,ETR,SEE(79)
52. FORMAT(10X,"TRAJECTORY PROCESS TIME=","F9.2," ELAPSED TIME=","F9.2,
$ ADVECTION FRACTION OF TRAVEL TIME=","F6.4)
RETURN
END
-----

```

A1.4.4 Generation of a test data-set for the Dynamic Puff Model.

The following program constructs and files test input conditions for the DPM, in accordance with the instructions contained in section (A1.4.3). Meteorological data are presented as time-histories at specified points. The DPM is required to provide dosage predictions for selected locations.

A1.4.5 Dynamic Puff Model program execution for the test data-set.

The following printed output for the DPM program allows a limited testing for normal operation of the model. The program is employed in its dosage mode, using the test data generated in section (A1.4.4).

```

RUN NUMBER*HUL
DATASET NO. 9261
NUMBER OF DATA-TIMES*NTDAT(SET=2 FOR CONTINUOUS DATA INPUT)
2
DATA-TIMES*TDAT(J)(SET TDAT(1)=0)
0.0000 0.0000
.....
X AND Y GRID POSITIONS IN NET. DATA GRID*ITOT*JTOT
40 40
X AND Y STEPSIZES IN NET. DATA GRID*DXB*DYB
500.0000 500.0000
LIST OF 4 W/F MODEL PARAMETERS *FOR EACH DATA-TIME* WF1*WF2*WF3*WF4
1 0.00000 0.00000 0.00000 0.00000
2 0.00000 0.00000 0.00000 0.00000
GRID COORDINATES OF (SUB)REGION OF INTEREST*XG1*XG2*YG1*YG2
4.0000 14.0000 12.0000 22.0000
GRID COORDINATES OF SOURCE(XGS*YGS) AND HEIGHT ZS IN (M)
5.0000 20.0000 25.0000
MARKERS A*B*H FOR FINAL MAP AT GRID POSITIONS XGA*XGB*XGM*YGA*YGB*YGM
0.0000 0.0000 0.0000 0.0000 0.0000 0.0000
NUMBER OF TIME-POINTS IN SOURCE-STRENGTH HISTORY*NSTH
3
SOURCE-STRENGTHS AT TIME NODES* QSTR(J)
.5000E 04 .1000E 10 .4000E 09
TIMES FOR SOURCE-STRENGTH TIME-NODES* TSTR(J)
2000.0000 2400.0000 3000.0000
SQUARED-SLOPE*W*SHOUT H*CONST DEP*TRAIN START TDES*T*END TDEF*IST URDER R*C* PREM
.2000E*02 .1000E*02 .2600E 04 .3100E 04 .1000E*03
NUMBER OF DUSAGE INTERVAL BOUNDARY-TIMES*NTDOS(MAX 60,SET=0 FOR CONCEN-DISTRIBN.)
5
DUSAGE INTERVAL BOUNDARY-TIMES*TDUS(J)(DUSAGE SOLUTIONS)
2600.0000 3000.0000 3300.0000 3600.0000 4000.0000
NUMBER OF DUSAGE POSITIONS*NPONS(MAX 40)
4
LIST OF DUSAGE POSNS*XDOS(J)*YDOS(J)(*VE VALUES FOR COORDS-GIVES DEPOSITION)
8.0000 17.0000
12.0000 15.1300
13.0000 20.0000
10.0000 21.8197
HEIGHT AT WHICH DUSAGE PREDICTIONS ARE REQUIRED*ZDOS(M)
1.0000
RELEASE-TIME SCAN STEPSIZE FOR RELEVANT RELEASE INTERVALS*DELTA
100.0000
TRAJECTORY TIME-STEP FOR LOCATING RELEASE INTERVALS*DELTA
50.0000
FINER RELEASE-TIME STEPS FOR FIXING RELEASE INTERVAL BOUNDARIES*DELTA
20.0000
FINER TRAJECTORY TIME-STEPS FOR FIXING RELEASE INTERVAL BOUNDARIES*DELTA
20.0000
NUMBER OF TRAJECTORY ADVECTION STEPS PER BASIC TIME-STEP*NSDT
4
CONCN-DISTRIBUTION SOLN*REGION OF INTEREST RESULT GRID DIVISIONS*MX*MY
2 2 0
VERTICAL STEPSIZE IN SOLN-SPACE DMZ(NOT FOR CONCEN-DISTRIBS OR DUSAGES)
0.0000
FLAG FOR CHECK PLANE DIAGNOSTIC SOLUTION*SET ITJEM=0 NORMALLY
0
NO. OF CONCEN-DISTRIBUTION HEIGHTS REQUIRED*NHANS(MAX=2)
1
CONCN-DISTRIBUTION HEIGHTS*HANS(J)...
0.0000
SAMPLE VALUES OF CONSTANT SURFACE-DATA AT CORNERS OF REGION OF INTEREST
(XGM1*YGM1) (XGM2*YGM1) (XGM1*YGM2) (XGM2*YGM2)
Z0(X*Y) (CONSTANT) = .1840E*01 .2340E*01 .1540E*01 .2040E*01
D(X*Y) (CONSTANT) = .0 .0 .0 .0
RAB(X*Y) (CONSTANT) = .1124E*02 .1294E*02 .1194E*02 .1294E*02
MAST POSITIONS*..(X*Y) AND WEIGHTING FACTORS
5.0000 20.0000 1.0000
10.0000 15.0000 0.8000
TIME MAST 1 MAST 2 MAST 3 MAST 4 MAST 5 MAST 6
UH VB I/L PTG UB VB I/L PTG
0.0 2.00*2.00 0.0 0.02 4.00 0.00 *0.0*0.00
100.0 2.00*2.00 0.0 0.02 4.00 0.00 *0.0*0.00
200.0 2.00*2.00 0.0 0.02 4.00 0.00 *0.0*0.00
300.0 2.00*2.00 0.0 0.02 4.00 0.00 *0.0*0.00
400.0 2.00*2.00 0.0 0.02 4.00 0.00 *0.0*0.00
500.0 2.00*2.00 0.0 0.02 4.00 0.00 *0.0*0.00
600.0 2.00*2.00 0.0 0.02 4.00 0.00 *0.0*0.00
700.0 2.00*2.00 0.0 0.02 4.00 0.00 *0.0*0.00
800.0 2.00*2.00 0.0 0.02 4.00 0.00 *0.0*0.00
900.0 2.00*2.00 0.0 0.02 4.00 0.00 *0.0*0.00
1000.0 2.00*2.00 0.0 0.02 4.00 0.00 *0.0*0.00
1100.0 2.00*2.00 0.0 0.02 4.00 0.00 *0.0*0.00
1200.0 2.00*2.00 0.0 0.02 4.00 0.00 *0.0*0.00
1300.0 2.00*2.00 0.0 0.02 4.00 0.00 *0.0*0.00
1400.0 2.00*2.00 0.0 0.02 4.00 0.00 *0.0*0.00
1500.0 2.00*2.00 0.0 0.02 4.00 0.00 *0.0*0.00
1600.0 2.00*2.00 0.0 0.02 4.00 0.00 *0.0*0.00
1700.0 2.00*2.00 0.0 0.02 4.00 0.00 *0.0*0.00
1800.0 2.00*2.00 0.0 0.02 4.00 0.00 *0.0*0.00
1900.0 2.00*2.00 0.0 0.02 4.00 0.00 *0.0*0.00

```

2000.0 2.00*2.00 0.0 0.02 4.00 0.00 *0.0*0.00
2100.0 2.00*2.00 0.0 0.02 4.00 0.00 *0.0*0.00
2200.0 2.00*2.00 0.0 0.02 4.00 0.00 *0.0*0.00
2300.0 2.00*2.00 0.0 0.02 4.00 0.00 *0.0*0.00
2400.0 2.00*2.00 0.0 0.02 4.00 0.00 *0.0*0.00
2500.0 2.00*2.00 0.0 0.02 4.00 0.00 *0.0*0.00
2600.0 2.00*2.00 0.0 0.02 4.00 0.00 *0.0*0.00
2700.0 2.00*2.00 0.0 0.02 4.00 0.00 *0.0*0.00
2800.0 2.00*2.00 0.0 0.02 4.00 0.00 *0.0*0.00
2900.0 2.00*2.00 0.0 0.02 4.00 0.00 *0.0*0.00
3000.0 2.00*2.00 0.0 0.02 4.00 0.00 *0.0*0.00
3100.0 2.00*2.00 0.0 0.02 4.00 0.00 *0.0*0.00
3200.0 2.00*2.00 0.0 0.02 4.00 0.00 *0.0*0.00
3300.0 2.00*2.00 0.0 0.02 4.00 0.00 *0.0*0.00
3400.0 2.00*2.00 0.0 0.02 4.00 0.00 *0.0*0.00
3500.0 2.00*2.00 0.0 0.02 4.00 0.00 *0.0*0.00
3600.0 2.00*2.00 0.0 0.02 4.00 0.00 *0.0*0.00
3700.0 2.00*2.00 0.0 0.02 4.00 0.00 *0.0*0.00
3800.0 2.00*2.00 0.0 0.02 4.00 0.00 *0.0*0.00
3900.0 2.00*2.00 0.0 0.02 4.00 0.00 *0.0*0.00
4000.0 2.00*2.00 0.0 0.02 4.00 0.00 *0.0*0.00
4100.0 2.00*2.00 0.0 0.02 4.00 0.00 *0.0*0.00
4200.0 2.00*2.00 0.0 0.02 4.00 0.00 *0.0*0.00
4300.0 2.00*2.00 0.0 0.02 4.00 0.00 *0.0*0.00
4400.0 2.00*2.00 0.0 0.02 4.00 0.00 *0.0*0.00
4500.0 2.00*2.00 0.0 0.02 4.00 0.00 *0.0*0.00
4600.0 2.00*2.00 0.0 0.02 4.00 0.00 *0.0*0.00
4700.0 2.00*2.00 0.0 0.02 4.00 0.00 *0.0*0.00
4800.0 2.00*2.00 0.0 0.02 4.00 0.00 *0.0*0.00
4900.0 2.00*2.00 0.0 0.02 4.00 0.00 *0.0*0.00
5000.0 2.00*2.00 0.0 0.02 4.00 0.00 *0.0*0.00
5100.0 2.00*2.00 0.0 0.02 4.00 0.00 *0.0*0.00
5200.0 2.00*2.00 0.0 0.02 4.00 0.00 *0.0*0.00
5300.0 2.00*2.00 0.0 0.02 4.00 0.00 *0.0*0.00
5400.0 2.00*2.00 0.0 0.02 4.00 0.00 *0.0*0.00
5500.0 2.00*2.00 0.0 0.02 4.00 0.00 *0.0*0.00
5600.0 2.00*2.00 0.0 0.02 4.00 0.00 *0.0*0.00
5700.0 2.00*2.00 0.0 0.02 4.00 0.00 *0.0*0.00
5800.0 2.00*2.00 0.0 0.02 4.00 0.00 *0.0*0.00
5900.0 2.00*2.00 0.0 0.02 4.00 0.00 *0.0*0.00

RELEASE TIMES TO AFFECT REGION OF INTEREST AT GIVEN TIME+AMBIGUITY LATER REMOVED

GIVEN TIME SEQUENCE EARLIEST RELEASE TIMES

2600.0 2051.0 *20.0 *20.0

TIME OF INTEREST ENTRY RELEASE TIMES

2600.0 501991.0 *30.0 *30.0

TIME OF INTEREST EXIT RELEASE TIMES

2600.0 2600.0 *30.0 *30.0

NU 1 RELEASE (OF 2) FOR TIME 1 (T=*****). LOCUS NO. 1. RELEASE T= 2000.0 EXPECTED TRAVEL T= 2120.0 WITH INITIAL DT= 114.59

EXPECTED TRAJ. STEPS***

SOLUTION FRAME SIZE N*W*H=280, WZ= 12. MINIMUM POSSIBLE (DX*DY)=(10.81, 8.86) AND MINIMUM ALLOWED (UX*UZ)=(10.81, 8.86)
***** TRANSFER TO FILE #1 NMCMPLETE
JT= 1 DT(JT)= 57.30 TACT= 2057.30 X*CENTROID= 0.0 (BOUNDS... 0.0, 0.0) DU/DZ(ZMPREV)=0.000 ZH= 25.00 XH= 5.32 YH=19.00
GRID POSNS*XP= 5.32 YP=19.68 XVAN= 7.66 YVAN=17.82 XSTRK= 7.24 YSTRK=18.08 FACTOR= 6.66 JSTRK= 1. XER= 3.17 YER=2.176
GAMT(OG)= *44.80 ANGT(OEG)= *44.96 STABAV= *37.0E 02 RAMAV= *17.9E*01 Z0AV= *10.6E*01 DAV= 0.000 HABAV= *11.9E*02
UVAV= 3.90 UBAV= 2.002 VBAV= *1.998 UVHAV= 2.828 EXAV(ZS)= *49.2E 00 EZAV(ZS)= *30.1E 00
BEFORE ALTER*DX= 10.81 DYE= 32.43 DZ= 8.46 ZPB= 4.23 FRAME LENGTH= 6636.47
AFTER ALTER*DX= 11.87 DYE= 35.62 DZ= 9.29 ZPB= 4.64 FRAME LENGTH= 6636.47
OPTIMAL STEPSIZES = DX=11.872 DZ= 9.287 NS = *200E*02 ZSETTLE= *11.5E 00 IMPACT/ABS EZ= *27.3E 00 **AND ADVECTION**
PROCESS TIMES = PAD= 0.00 PDF= 0.00 PDS= 0.75 PTRS= 19.13 BEFORE ADVECTION PICUN=1.00000
ELAPSED TIMES = EAD= 0.00 EDF= 0.00 EDS= 5.32 ETRS= 37.23 AFTER ADVECTION PICUN=0.00000

JT= 2 DT(JT)= 114.59 TACT= 2171.89 X*CENTROID= 0.0 (BOUNDS... *44.6, 223.4) DU/DZ(ZMPREV)=0.054 ZH= 25.00 XH= 5.94 YH=19.00
GRID POSNS*XP= 5.94 YP=19.06 XVAN= 8.52 YVAN=17.58 XSTRK= 7.60 YSTRK=17.60 FACTOR= 3.29 JSTRK= 1. XER= 3.82 YER=21.16
GAMT(OG)= *43.58 ANGT(OEG)= *44.20 STABAV= *37.0E 02 RAMAV= *17.5E*01 Z0AV= *10.6E*01 DAV= 0.000 HABAV= *11.9E*02
UVAV= 3.89 UBAV= 2.028 VBAV= *1.972 UVHAV= 2.829 EXAV(ZS)= *50.2E 00 EZAV(ZS)= *30.0E 00
BEFORE ALTER*DX= 11.87 DYE= 35.62 DZ= 9.29 ZPB= 4.64 FRAME LENGTH= 6636.47
AFTER ALTER*DX= 11.87 DYE= 35.62 DZ= 9.29 ZPB= 4.64 FRAME LENGTH= 6636.47
OPTIMAL STEPSIZES = DX=11.998 DZ= 9.369 NS = *200E*02 ZSETTLE= *22.9E 00 IMPACT/ABS EZ= *27.0E 00
PROCESS TIMES = PAD= 10.47 PDF= 22.72 PDS= 0.75 PTRS= 54.13 BEFORE ADVECTION PICUN=1.00000
ELAPSED TIMES = EAD= 22.82 EDF= 35.93 EDS= 8.40 ETRS= 100.52 AFTER ADVECTION PICUN=1.00000

JT= 3 DT(JT)= 114.59 TACT= 2286.49 X*CENTROID= *55.3 (BOUNDS... *44.6, 223.4) DU/DZ(ZMPREV)=0.092 ZH= 25.00 XH= 6.63 YH=18.00
GRID POSNS*XP= 6.63 YP=18.48 XVAN= 9.45 YVAN=17.40 XSTRK= 8.51 YSTRK=17.56 FACTOR= 3.36 JSTRK= 2. XER= 4.46 YER=20.55
GAMT(OG)= *40.37 ANGT(OEG)= *40.76 STABAV= *40.9E 02 RAMAV= *10.8E*01 Z0AV= *17.9E*01 DAV= 0.000 HABAV= *11.9E*02
UVAV= 3.87 UBAV= 2.140 VBAV= *1.852 UVHAV= 2.837 EXAV(ZS)= *54.0E 00 EZAV(ZS)= *33.3E 00
BEFORE ALTER*DX= 11.87 DYE= 35.62 DZ= 9.29 ZPB= 4.64 FRAME LENGTH= 6636.47
AFTER ALTER*DX= 11.87 DYE= 35.62 DZ= 9.29 ZPB= 4.64 FRAME LENGTH= 6636.47
OPTIMAL STEPSIZES = DX=12.871 DZ= 9.470 NS = *200E*02 ZSETTLE= *28.9E 00 IMPACT/ABS EZ= *29.6E 00
PROCESS TIMES = PAD= 10.38 PDF= 23.70 PDS= 0.73 PTRS= 56.52 BEFORE ADVECTION PICUN=1.00000
ELAPSED TIMES = EAD= 24.12 EDF= 36.85 EDS= 5.30 ETRS= 100.78 AFTER ADVECTION PICUN=1.00000

JT= 4 DT(JT)= 114.59 TACT= 2401.08 X*CENTROID= *141.6 (BOUNDS... *44.6, 223.4) DU/DZ(ZMPREV)=0.056 ZH= 25.00 XH= 7.36 YH=18.00
GRID POSNS*XP= 7.36 YP=18.00 XVAN= 10.42 YVAN=17.30 XSTRK= 9.45 YSTRK=17.39 FACTOR= 3.37 JSTRK= 2. XER= 5.10 YER=19.92
GAMT(OG)= *33.11 ANGT(OEG)= *33.37 STABAV= *49.2E 02 RAMAV= *13.0E*01 Z0AV= *10.0E*01 DAV= 0.000 HABAV= *12.0E*02
UVAV= 3.85 UBAV= 2.483 VBAV= *1.587 UVHAV= 2.891 EXAV(ZS)= *65.2E 00 EZAV(ZS)= *40.2E 00
BEFORE ALTER*DX= 11.87 DYE= 35.62 DZ= 9.29 ZPB= 4.64 FRAME LENGTH= 6636.47
AFTER ALTER*DX= 13.67 DYE= 41.00 DZ= 10.73 ZPB= 5.37 FRAME LENGTH= 7639.28
OPTIMAL STEPSIZES = DX=13.666 DZ=10.732 NS = *200E*02 ZSETTLE= *22.9E 00 IMPACT/ABS EZ= *35.3E 00
PROCESS TIMES = PAD= 10.42 PDF= 24.53 PDS= 0.77 PTRS= 81.77 BEFORE ADVECTION PICUN=1.00000
ELAPSED TIMES = EAD= 17.38 EDF= 35.75 EDS= 5.28 ETRS= 140.83 AFTER ADVECTION PICUN=1.00000

JT= 5 DT(JT)= 114.59 TACT= 2515.68 X*CENTROID= *203.8 (BOUNDS... *51.4, 257.2) DU/DZ(ZMPREV)=0.051 ZH= 25.00 XH= 8.19 YH=17.00
GRID POSNS*XP= 8.19 YP=17.65 XVAN= 11.40 YVAN=17.22 XSTRK= 10.39 YSTRK=17.29 FACTOR= 3.34 JSTRK= 1. XER= 5.73 YER=19.29
GAMT(OG)= *22.84 ANGT(OEG)= *22.80 STABAV= *7.11E 02 RAMAV= *10.0E*01 Z0AV= *10.5E*01 DAV= 0.000 HABAV= *12.0E*02
UVAV= 3.92 UBAV= 2.818 VBAV= *1.182 UVHAV= 3.060 EXAV(ZS)= *92.1E 00 EZAV(ZS)= *57.2E 00
BEFORE ALTER*DX= 13.67 DYE= 41.00 DZ= 10.73 ZPB= 5.37 FRAME LENGTH= 7639.28
AFTER ALTER*DX= 16.24 DYE= 48.73 DZ= 12.81 ZPB= 6.40 FRAME LENGTH= 9080.82
OPTIMAL STEPSIZES = DX=16.244 DZ=12.804 NS = *200E*02 ZSETTLE= *22.9E 00 IMPACT/ABS EZ= *49.0E 00
PROCESS TIMES = PAD= 10.47 PDF= 25.33 PDS= 0.77 PTRS= 81.40 BEFORE ADVECTION PICUN=1.00000
ELAPSED TIMES = EAD= 15.73 EDF= 38.88 EDS= 5.30 ETRS= 140.48 AFTER ADVECTION PICUN=1.00000

CHAPTER A2

GAUSSIAN PUFF MODEL.

A2.1 Introduction.

Consider an atmosphere in which velocity and diffusivity are constant with height. An instantaneous release under such conditions should result in a gaussian distribution provided horizontal scales for variations in velocity and diffusivity are much larger than the puff dimensions. Though these assumptions are usually unrealistic, the attractive simplicity of the gaussian solutions (1.40), (1.41) has led to their use in numerous dispersion models. In the case of the dynamic puff model proposed in chapter (2), the use of an analytically-derived formula instead of the numerically-solved distribution would greatly reduce computation. If such a model, using the same database, consistently provides solutions of equivalent accuracy, then it must be preferred to the complex numerical solution. An important part of the present work thus concerns the comparative effectiveness of a gaussian puff model.

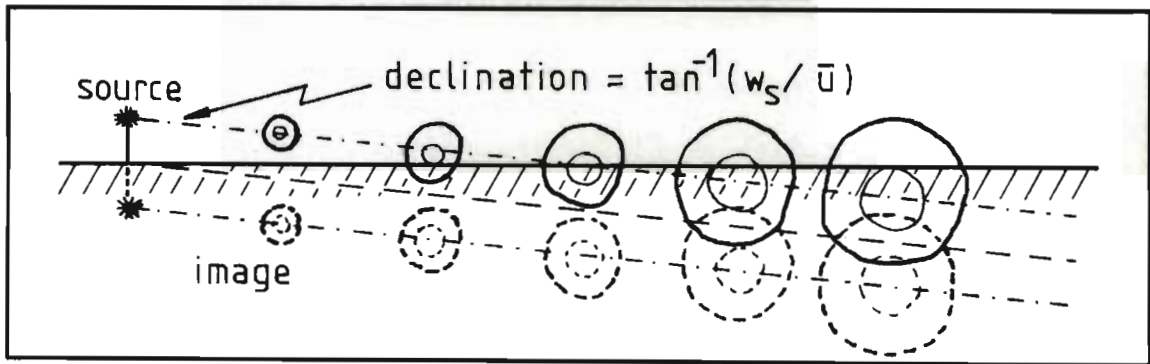
A2.2 Theory.

The gaussian puff model (GPM) has been formulated by replacing the numerically-solved puff in the dynamic puff model (DPM) with a gaussian distribution. In its present

form the GPM excludes surface-absorption, washout and decay, and certain assumptions have been made with regard to surface reflection, sedimentation and the variation of diffusivity along the puff trajectory.

In order to deal with the ground boundary, the usual assumption of surface reflection is invoked. The effect of sedimentation is then superimposed by allowing the vertical scale to slide upwards according to the settling velocity [figure (A2.1)].

fig.(A2.1) Approximation of sedimentation



At time t , the centroid of the objective puff will be found at $[X(t), Y(t), Z(t)]$, where

$$X(t) = x'' + \int_{t'}^t \bar{u}[X(\tau), Y(\tau), z_1, \tau] d\tau \quad (\text{A2.1})$$

$$Y(t) = y'' + \int_{t'}^t \bar{v}[X(\tau), Y(\tau), z_1, \tau] d\tau \quad (\text{A2.2})$$

$$Z(t) = z'' - w_s \cdot (t - t') \quad (\text{A2.3})$$

It is understood here that release occurred at (x'', y'', z'', t') , and that it has been chosen to follow the velocity-field at some fixed "representative" height z_1 . The centroid of the

image puff will be located at $[X(t), Y(t), Z(t) - 2z']$. Then for unit instantaneous release, equation (1.40) yields

$$C(x,y,z,t) = \frac{1}{8[\pi(t-t')]^{\frac{3}{2}} [\bar{K}_x(t)\bar{K}_y(t)\bar{K}_z(t)]^{\frac{1}{2}}} \exp\left[\frac{-1}{4(t-t')} \left\{ \frac{(x-X(t))^2}{\bar{K}_x(t)} + \frac{(y-Y(t))^2}{\bar{K}_y(t)} \right\} \right] \cdot \left[\exp\left\{ \frac{-(z-Z(t))^2}{4(t-t')\bar{K}_z(t)} \right\} + \exp\left\{ \frac{-(z-Z(t)+2z')^2}{4(t-t')\bar{K}_z(t)} \right\} \right] \quad (\text{A2.4})$$

It is necessary to make some assumption about the diffusivities $\bar{K}_i(t)$ which best represent the puff at time t . The procedure adopted is to use trajectory-mean values at the specified height z_1 , for example

$$\bar{K}_z(t) = \frac{1}{(t-t')} \int_{t'}^t K_z(X(\tau), Y(\tau), z_1, \tau) d\tau \quad (\text{A2.5})$$

The values of $\bar{u}(x,y,z_1,t)$, $\bar{v}(x,y,z_1,t)$ and $K_i(x,y,z_1,t)$ are provided by the same algorithms used in the dynamic puff model [section (2.4.2)], using the same input information [appendix (A1.4.2)]. Depending on the extent of wind-shear, the choice of z_1 may have a critical effect on the result. A typical value might be $z_1=10\text{m}$, a height frequently used for meteorological measurements.

The output modes included in the gaussian puff model are the same dosage-history and concentration distribution, though an additional option provides dosage-distributions using a particle-in-cell (P.I.C.) "column" model [appendix (A3)]. The concept of a region-of-interest follows that in section (2.4.1.2), and interpolation of additional release-times and trajectory-steps is again employed to reduce

computation. Nevertheless, the GPM requires as much as 25% of the computer time used by the DPM, in the same application.

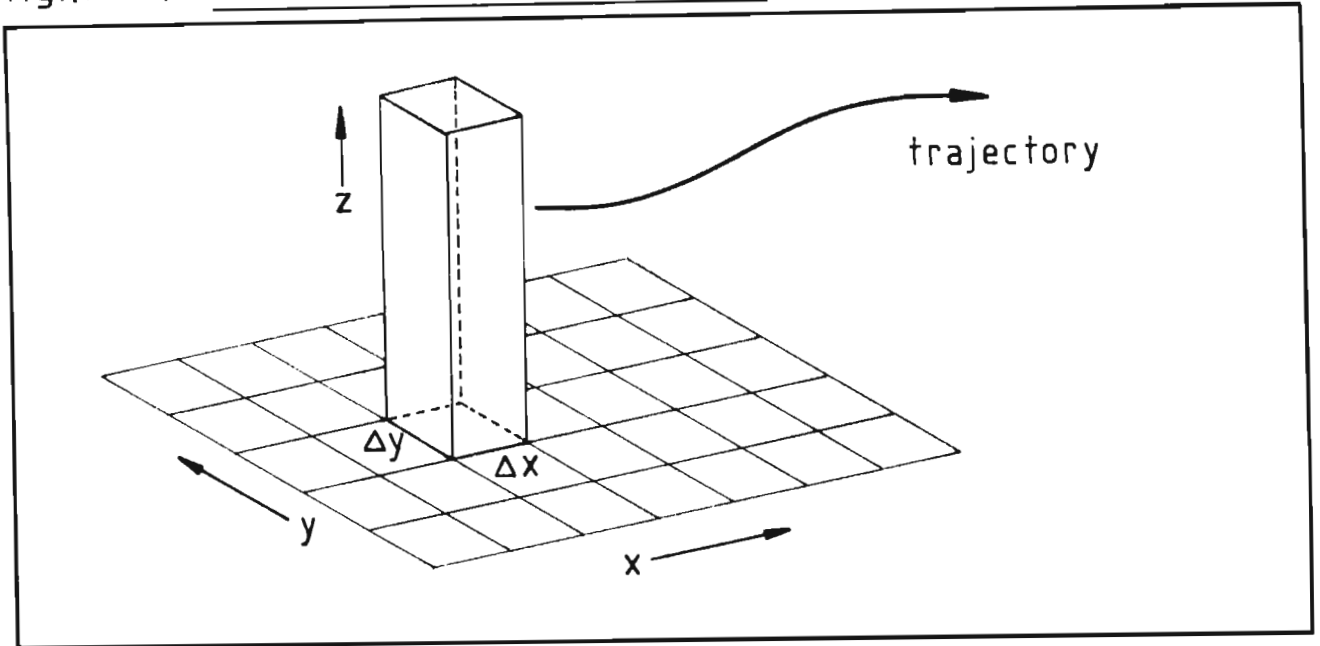
CHAPTER A3VERTICAL COLUMN PARTICLE-IN-CELL MODEL
FOR DOSAGE DISTRIBUTIONS

In order to provide a series of dosage patterns for specified dosage intervals it is necessary to accumulate dosages in some eulerian grid—for example, a two-dimensional xy grid representing dosages at a specified height. Even for the gaussian puff model, the task of computing dosage contributions at each point in a grid of reasonable resolution would require an impractical amount of computation.

A typical dosage interval will include significant time-variation in the wind-field, and the dosage may be expected to represent contributions from a variety of puff-trajectories. This "smoothing" effect suggests that the inherent irregularities of a particle-in-cell method will not manifest themselves in the final dosage-distribution. In effect, horizontal diffusion is replaced with a "trajectory-diffusion".

Consider that the instantaneous release is confined to a semi-infinite vertical column with ground-level base $\Delta x \cdot \Delta y$ [fig.(A3.1)]. If Δx and Δy are reasonably small, the horizontal distribution within the column should soon be uniform, so that only the vertical distribution need be solved for. Integration of equation (A2.4) throughout x-y space, and then averaging over $\Delta x \Delta y$ yields the concentration at height z,

fig.(A3.1) Vertical column PIC model



$$C(z,t) = \frac{1}{2 [\pi(t-t')]^{\frac{1}{2}} [\bar{k}_z(t)]^{\frac{1}{2}} \Delta x \Delta y} \left[\exp \left\{ \frac{-(z-Z(t))^2}{4(t-t')\bar{k}_z(t)} \right\} + \exp \left\{ \frac{-(z-Z(t)+2z')^2}{4(t-t')\bar{k}_z(t)} \right\} \right]$$

where $Z(t)$ and $\bar{k}_z(t)$ are again described by equations (A2.3), (A2.5).

The column distribution is considered to be advected in eulerian space as a lagrangian entity, so that at time t it will be centred at $(x,y)=[X(t),Y(t)]$, these coordinates being described by equations (A2.1), (A2.2), using a

specified representative height z_1 . If the nearest grid-point to $[X(t), Y(t)]$ is $[i\Delta x, j\Delta y]$, then the dosage for the height of interest, z , viz. $D_{ij}(z, t_1, t_2)$, is incremented by the amount $C(z, t) \cdot Q(t') \Delta t_R \Delta t$, provided $t_1 < t \leq t_2$. In this expression, $Q(t)$ is the release rate at time t , Δt_R is the release discretisation time-interval, and Δt is the real-time trajectory step-size. As in the dynamic puff model [chapter (2)], consideration is given to all release times which affect the region of interest during the specified dosage intervals.

CHAPTER A4METEOROLOGY SUB-MODELA4.1 Objectives.

The meteorology sub-model (MSM) serves a broad purpose in the general preparation of input information for the dispersion model [section (2.4.2)]. However, its basic function is to convert raw measurement data into discretised forms of the variables:

$U_{Z_G}(x,y,t)$	x velocity component at height z_G
$V_{Z_G}(x,y,t)$	y velocity component at height z_G
$L^{-1}(x,y,t)$	inverse Monin-Obukhov stability length
$\bar{\theta}'_{Z_G}(x,y,t)$	potential temperature gradient $\partial\bar{\theta}/\partial z _{Z_G}$
$z_0(x,y)$	roughness length
$d(x,y)$	zero-plane displacement
$w_d(x,y)$	deposition velocity representing ground absorption

The procedures which are available for preparation of this information are outlined below.

A4.2 Input-output modes.

The constant parameters z_0 , d and w_d are presented as a series of point-measurements at (x_i, y_i) , $i=1, n$. Values are then interpolated to fill three x-y storage grids which cover the entire region of interest. Interpolation is based on the inverse square method [equation (1.35)]. The variation of z_0 over non-homogeneous terrain tends to be log-linear with respect to distance, so that it is interpolated as its logarithm.

It should be clear that storage of the time-variant information U_{ZG} , V_{ZG} , L^{-1} and $\bar{\theta}'_{ZG}$ as a series of xy grids representing different times would reduce access time. However, this imposes serious resolution limitations, so that two options have been made available.

- (i) A_{ijt} grid storage: MSM input information is specified either by the Mesoscale Wind-field Model [Scholtz and Brouckaert (1976)], or at discrete points for interpolation onto the grid, or by combinations of both these methods.
- (ii) Discrete point time-histories: MSM input information is necessarily presented as discrete point time-histories of the raw meteorological data.

Whereas output information is fixed as either representation of U_{ZG} , V_{ZG} , L^{-1} and $\bar{\theta}'_{ZG}$, the input information may have several forms. If velocity data are provided by the wind-field model; it is necessary to supplement this

fig.(A4.1) Origin of meteorological measurements

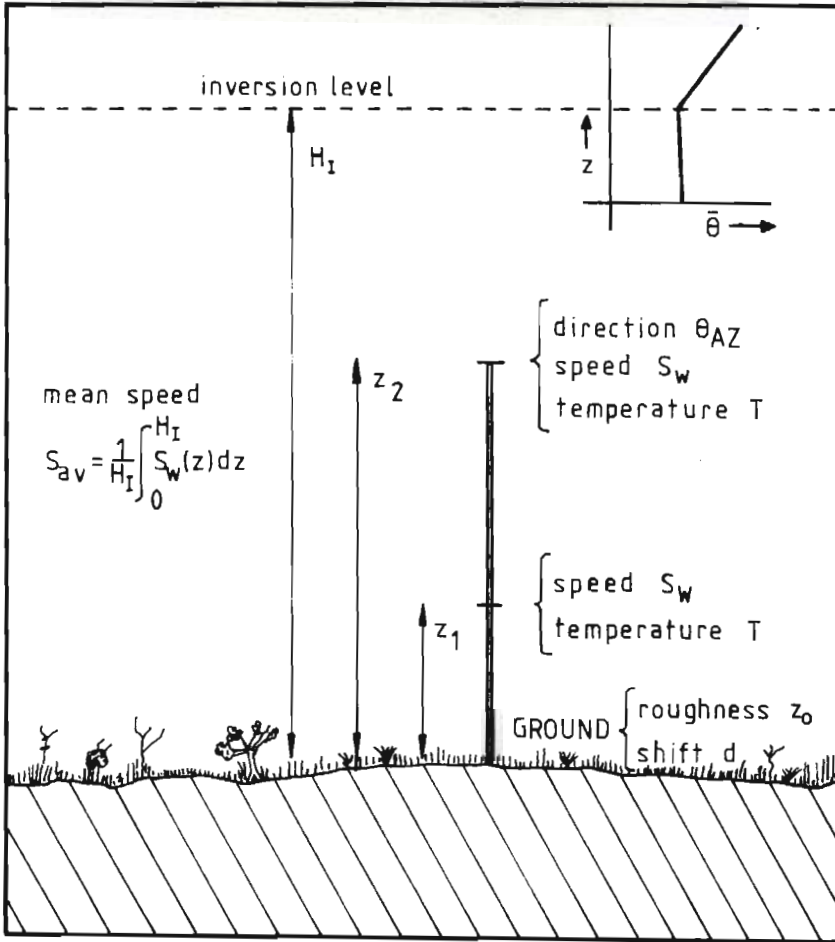


table (A4.1) Parameter conversions.

PROCEDURE	AVAILABLE	PREDICTED
1	$S_w(z_2), T(z_2), \theta_{AZ}, T(z_1), z_0, d$	$u_*, \theta_{AZ}, L, z_0, d \Rightarrow \bar{u}(z), \bar{\theta}(z)$
2	$S_w(z_2), T(z_2), \theta_{AZ}, S_w(z_1), T(z_1), d$	$u_*, \theta_{AZ}, L, z_0, d \Rightarrow \bar{u}(z), \bar{\theta}(z)$
3	$U_{av}, V_{av}, H_I, T(z_2), T(z_1), z_0, d$	$u_*, \theta_{AZ}, L, z_0, d \Rightarrow \bar{u}(z), \bar{\theta}(z)$
4	$u_*, \theta_{AZ}, L, z_0, d, z_G$	$U_{ZG}, V_{ZG}, L^{-1}, z_0, d, \bar{\theta}'_{ZG}, z_G$

information with specified stability data (L^{-1} , $\bar{\theta}'_{zG}$).

However, the general problem involves determination of the profile parameters at specific points (meteorological masts) based on measurement, followed by interpolation for the form (i), or direct representation as (ii).

Figure (A4.1) is a schematic representation of the allowed sources of measurement, whilst table (A4.1) details the procedures which are incorporated in the MSM, based on equations (1.29), (1.30), (2.70). Where velocity measurements are available at two heights, procedure (2) may be used to evaluate z_0 . In conjunction with available roughness-length information [section (1.2.2)] these values are used to estimate z_0 elsewhere, so that procedure (1) may be applied where necessary. Procedure (3) is used when data are supplied in this form by the mesoscale wind-field model. Procedure (4) converts the output of (1), (2) or (3) to the standard input format for the dispersion model, and the reverse procedure is used in that model to establish the basic profile parameters.

A4.3 Estimation of friction velocity and stability length.

A4.3.1 Available measurements include $S_w(z_m), T(z_2), T(z_1), z_0$.

Using equations (1.21), (1.22) define the integrals

$$F_m(\zeta_m, \zeta_a) = \int_{\zeta_a}^{\zeta_m} \frac{\phi_m(\zeta)}{\zeta} d\zeta, \quad F_T(\zeta_2, \zeta_1) = \int_{\zeta_1}^{\zeta_2} \frac{\phi_T(\zeta)}{\zeta} d\zeta$$

such that

$$S_w(z_m) = \frac{u_*}{k} F_m\left(\frac{z_m}{L}, \frac{z_0}{L}\right), \quad \bar{\theta}(z_2) - \bar{\theta}(z_1) = \theta_* F_m\left(\frac{z_2}{L}, \frac{z_1}{L}\right) \quad (\text{A4.1})$$

Equations (1.20) and (1.22) give

$$L = \frac{T_a u_*^2}{k^2 g \theta_*} = \frac{T_a S_w^2(z_m)}{g [\bar{\theta}(z_2) - \bar{\theta}(z_1)]} \cdot \left[\frac{F_T\left(\frac{z_2}{L}, \frac{z_1}{L}\right)}{F_m^2\left(\frac{z_m}{L}, \frac{z_0}{L}\right)} \right] \quad (\text{A4.2})$$

The value of L is determined by solution of equation (A4.2) using a Newton iteration. The friction velocity u_* then follows from equation (A4.1). The potential temperatures $\bar{\theta}(z_2), \bar{\theta}(z_1)$ are evaluated from $T(z_2), T(z_1)$ by assuming a dry adiabatic lapse rate, $\Gamma = 0,00986^\circ \text{K m}^{-1}$, in equation (1.8).

The forms of ϕ_m, ϕ_T used are those proposed by Dyer (1974) [(1.29), (1.30)], with extensions to strong stability after Webb (1969) (2.70). These flux relations lead to the profiles (2.72) and (2.73).

A4.3.2 Available measurements include $S_{av}, H_I, T(z_2), T(z_1), z_0$

Following from equation (1.21) define the integral

$$G_m(\zeta_H, \zeta_0) = \frac{1}{(\zeta_H - \zeta_0)} \int_{\zeta_0}^{\zeta_H} \int_{\zeta_0}^{\zeta'} \frac{\phi_m(\zeta)}{\zeta} d\zeta d\zeta'$$

so that $S_{av} = (u_* / k) G_m(\frac{H_I}{L}, \frac{z_0}{L})$. Replacing F_m with G_m in section (A4.3.1), an identical development leads to solutions for L, u_* .

A4.3.3 Some typical results.

The dependence of predicted velocity and diffusivity profiles (2.72) and (2.73) on temperature measurements at two heights, and a single velocity measurement, is best illustrated by an example. Assume that it has been possible to estimate z_0 , and that the measurements $T(z_1), T(z_2), S_w(z_m)$ are available, with $d=0$. Consider $z_1 = 2$ m, $z_2 = 12$ m, $z_m = 10$ m, and the lower temperature fixed at $T(2m) = 10^\circ\text{C}$. Then table (A4.2) presents the estimated values of u_*, L which would be required to give a common velocity $S_w(10m) = 4,0$ m s⁻¹.

The plot number in table (A4.2) refers to the corresponding velocity or mass-diffusivity profile in fig. (A4.2). Note that $T(12m) - T(2m) = -0,1^\circ\text{C}$ will be close to the neutral (adiabatic) temperature profile. The region of the atmosphere which is affected by appreciable shear

fig.(A4.2) Velocity and mass-diffusivity profiles after Dyer (1974) [equations (2.72),(2.73)]

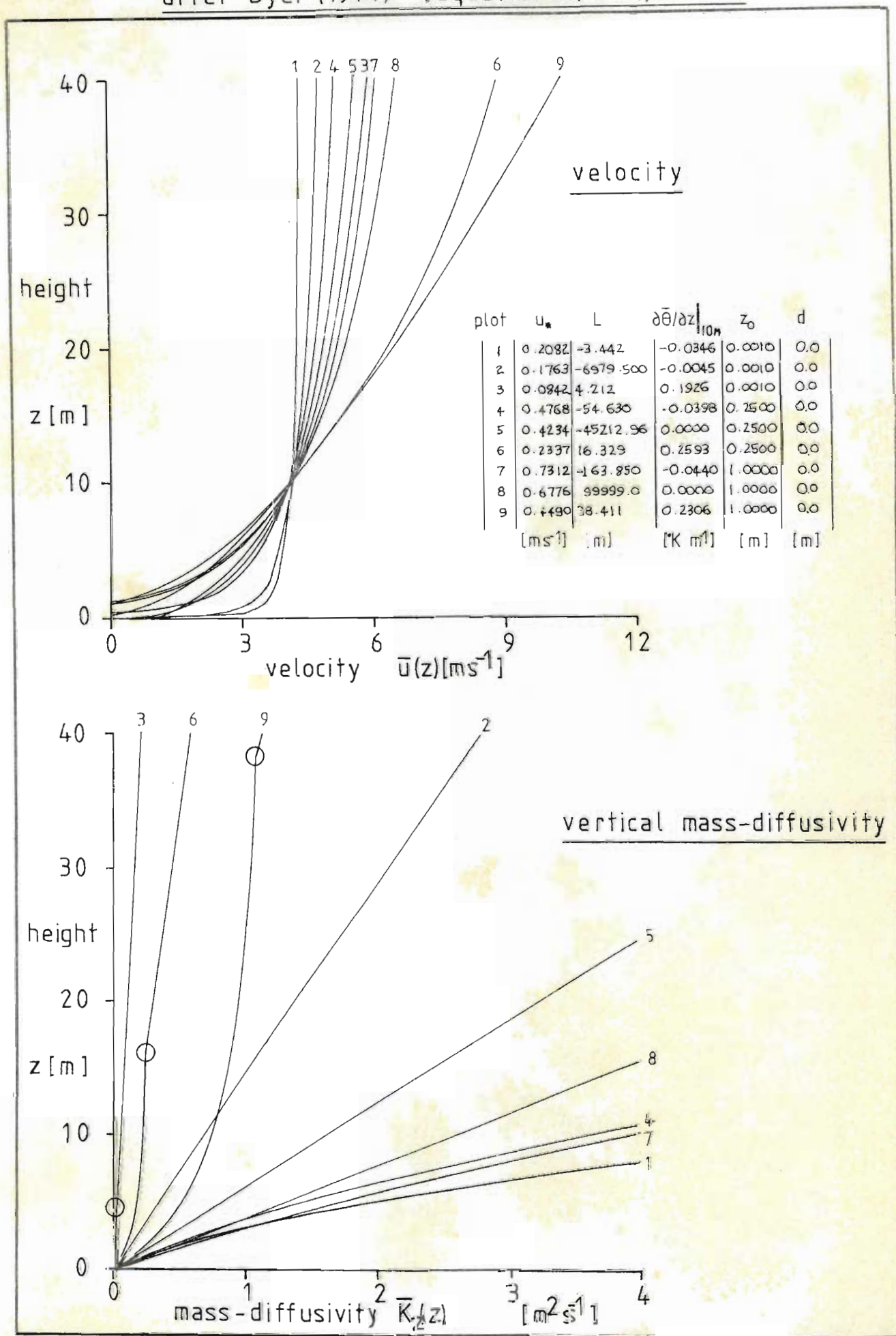


table (A4.2) Estimated u_* , L as a function of temperature gradient and roughness length.

	$T(z_2)-T(z_1) = -1,0^{\circ}\text{C}$			$T(z_2)-T(z_1) = -0,1^{\circ}\text{C}$			$T(z_2)-T(z_1) = +3,0^{\circ}\text{C}$		
	$u_* [\text{ms}^{-1}]$	$L [\text{m}]$	Plot	$u_* [\text{ms}^{-1}]$	$L [\text{m}]$	Plot	$u_* [\text{ms}^{-1}]$	$L [\text{m}]$	Plot
$z_0 = 0,001\text{m}$	0,2082	-3,442	1	0,1763	-6979,5	2	0,0842	4,212	3
$z_0 = 0,25\text{m}$	0,4768	-54,63	4	0,4234	-45213,	5	0,2337	16,33	6
$z_0 = 1,0\text{m}$	0,7312	-163,8	7	0,6776	∞	8	0,4490	38,41	9

is seen to increase both with z_0 and with increasing stability (higher temperature gradients). The slope discontinuities in stable diffusivity profiles 3, 6 and 9 are due to the extension for strong stability ($z > L, L > 0$) following Webb (1970).

A4.4 Surface roughness categories for the Richards Bay area.

In order to define the surface-roughness distribution for the Richards Bay area during June and July, 1976, roughness lengths z_0 were specified at 152 locations in the region in such a way as to define the major surface features. Values of z_0 were drawn from 17 categories based on equation (1.17) due to Lettau (1969), the tabulated results of Priestley (1959), Sutton (1953) and Sheppard (1947) [table (1.1)], and on values calculated from velocity and temperature profile measurements [table (4.1)]. Estimates of z_0 for cultivated forests, coastal bush, and industrial and

suburban buildings were based on measurements made by Leonard and Federer (1973) [section (1.2.2)] and on data presented by Davenport (1965). No recognition was given to the boundary-layer effect at a roughness change [Panofsky and Townsend (1964)]. Instead it was assumed that the inverse-square interpolated variations of z_0 were smooth enough for the effect not to be significant. Moreover, non-homogeneous terrain has already been approximated using equation (1.17) due to Lettau (1969). The 17 selected roughness categories are presented in table (A4.3).

table (A4.3) Estimated roughness length categories for Richards Bay.

CAT.	DESCRIPTION	z_0 [m]
1	dense forest plantation	0,7
2	suburban houses and trees	0,5
3	coastal bush (dense)	1,0
4	industrial buildings	1,2
5	sparser forest	0,4
6	stands of trees with ~50% open grass	0,2
7	scattered trees/bushes, vlei	0,2
8	grass and scrub (scattered)	0,15
9	sugar cane (cultivated)	0,15
10	coastal bush with ~50% open grass	0,2
11	vlei	0,12
12	sparse grass ~0,3 m on flat sand	0,02
13	open grassland (~0,35 m)	0,05
14	sparse sugar-cane (~1,5 m) on flat sand	0,20
15	open sea	0,001
16	bay, lakes	0,00001
17	flat sand and water	0,0001

NOMENCLATURE.

(* : concentrations may also be expressed in terms of numbers of particles).

	<u>UNITS (S.I.)</u>
A - area of ground occupied by each roughness element	m^2
A_i - projected area of a single roughness element on which the wind is incident	m^2
A_{ijt} - array containing properties stored as a 3-dimensional grid (x-y-t)	
A_p - projected plan area of a single roughness element	m^2
A_T - temperature anomaly coefficient for induced vertical velocity	$m\ s^{-1}\ K^{-1}$
c_p - heat capacity at constant pressure	$J\ kg^{-1}\ K^{-1}$
c_v - heat capacity at constant volume	$J\ kg^{-1}\ K^{-1}$
C - concentration of emitted material in the air	$kg\ m^{-3}\ *$
C_A - proportionality constant for area-source cell concentration estimates	
C_E - gas-phase equilibrium concentration	$kg\ m^{-3}\ *$
\bar{C}_m - measured concentration of material in the air expressed as a time-average	$kg\ m^{-3}\ *$
C_n - nth moment of the concentration distribution in the y-direction	$kg\ m^{n-2}\ *$
\bar{C}_p - predicted concentration of material in the air expressed as a time-average	$kg\ m^{-3}\ *$

C_{sh}	- Sutton diffusion parameter for the horizontal spread in a plume	$m^{n/2}$
C_{sz}	- Sutton diffusion parameter for the vertical spread in a plume	$m^{n/2}$
d	- profile zero-plane displacement due to surface features	m
d_p	- effective Stokes diameter of airborne particle	m
D	- dosage $\int_{t_1}^{t_2} C dt$	$kg\ s\ m^{-3}\ *$
D_m	- molecular diffusivity	$m^2\ s^{-1}$
D_n	- parabolic cylinder function of order n	
E	- expectation (average)	
f	- primitive $\int [\phi_m(z/L)/z] dz$	
f_c	- Coriolis parameter, $2\Omega \sin(\lambda)$, λ latitude, Ω angular velocity of rotation of the earth	s^{-1}
F_c	- conversion factor to published concentration units	various
F_r	- concentration adjustment factor for losses due to reaction and ground absorption	
\tilde{g}	- $(g_1, g_2, g_3), (0,0,g)$ gravitational acceleration vector	$m\ s^{-2}$
G	- Green's function for the concentration distribution in the eulerian frame	
G'	- Green's function for the concentration distribution in the lagrangian frame, as transformed by \tilde{T}_p	

h	- height of ground surface above a horizontal datum	m
h_*	- average height of roughness elements	m
H	- height of an impervious boundary	m
H_I	- height of an impervious inversion layer	m
ΔH_p	- asymptotic plume rise due to buoyancy	m
k	- Kármán constant	
k_1	- first-order rate constant	s^{-1}
k_f	- katabatic flow constant	$m K^{-1} s^{-1}$
\bar{k}_r	- combined mean first-order rate-constant $\bar{k}_1 + \bar{\Lambda}$	s^{-1}
k_T	- thermal conductivity	$W_m^{-1} K^{-1}$
K_F	- fluid eddy diffusivity for mass	$m^2 s^{-1}$
K_G	- overall mass-transfer coefficient based on the gas phase	$kg m^{-2} s^{-1} *$
K_h	- horizontal eddy diffusivity for mass	$m^2 s^{-1}$
K_i^*	- virtual (long-period) mass eddy diffusivity in direction x_i	$m^2 s^{-1}$
K_M	- vertical eddy diffusivity for horizontal momentum	$m^2 s^{-1}$
K_p	- mass eddy diffusivity for particulate material	$m^2 s^{-1}$
K_T	- vertical eddy diffusivity for heat	$m^2 s^{-1}$
K_W	- vertical eddy diffusivity for water-vapour	$m^2 s^{-1}$
K_x	- mass eddy diffusivity in direction x	$m^2 s^{-1}$
K_y	- mass eddy diffusivity in direction y	$m^2 s^{-1}$
K_z	- mass eddy diffusivity in direction z	$m^2 s^{-1}$

L	- Monin-Obukhov stability length [equation (1.20)]	m
L_L	- lagrangian length-scale for atmospheric turbulence	m
L_E	- eulerian length-scale for atmospheric turbulence	m
m_p	- particle mass	kg
m_y	- y-centroid of distribution	m
n	- Sutton turbulence parameter	
n_s	- number of advection sub-steps for each solution time-step Δt	
p	- number of particles	
P	- pressure	Pa
\hat{P}	- pressure deviation from equilibrium value	Pa
P_0	- pressure at ground-level	Pa
\bar{P}_j	- mean value of property P_j (e.g. $P_j=L^{-1}$) during solution time-step Δt .	various
q_3	- vertical heat flux [equation (1.19)]	$W m^{-2}$
Q	- source emission rate	$kg s^{-1}^*$
r_k	- distance to point k	m
R	- rate of change of concentration due to reaction, absorption	$kg m^{-3} s^{-1}^*$
\bar{R}'	- overall first-order rate constant for lagrangian frame	s^{-1}
R_E	- eulerian velocity auto-correlation	
$R_{i\Delta}$	- gradient Richardson Number based on finite differences	

R_L	- lagrangian velocity auto-correlation	
R_W	- rate of change of concentration due to washout	$\text{kg m}^{-3} \text{ s}^{-1*}$
S	- rate of change of concentration due to source distribution	$\text{kg m}^{-3} \text{ s}^{-1*}$
S_w	- horizontal wind-speed $\sqrt{U^2+V^2}$	m s^{-1}
t	- time (real-time)	s
Δt	- real-time step length (finite difference in numerical solution)	s
t'	- emission-time	s
\bar{t}	- centroid-time in observed eulerian concentration history	s
t_a	- length of time-averaging period	s
Δt_R	- discretisation interval for emission time	s
T	- absolute temperature	K
\hat{T}	- temperature deviation from equilibrium value	K
T_0	- absolute temperature at ground-level	K
\tilde{T}_p	- coordinate transformation to lagrangian frame, defined in section (2.2.2)	
T_s	- ground surface-temperature	K
u	- $\bar{u} + u'$ velocity component in x-direction, sum of mean and turbulent components	m s^{-1}
\tilde{u}	- $(u_1, u_2, u_3), (u, v, w)$ velocity vector	m s^{-1}
u_*	- friction velocity $\sqrt{\tau_0/\rho_0}$	m s^{-1}
u_p	- velocity of an airborne particle	m s^{-1}
\tilde{U}	- (\bar{U}, \bar{V}) mean horizontal velocity vector	m s^{-1}
U_c	- x-direction velocity component for centroid at prescribed height	m s^{-1}

U_e	- internal energy per unit mass	$J\ kg^{-1}$
\bar{U}_G	- geostrophic wind component in x-direction	$m\ s^{-1}$
U_{zG}	- x-direction velocity component at height z_G	$m\ s^{-1}$
v	- $\bar{v} + v'$ velocity component in y-direction, sum of mean and turbulent components	$m\ s^{-1}$
V_c	- y-direction velocity component for centroid at prescribed height	$m\ s^{-1}$
V_{zG}	- y-direction velocity component at height z_G	$m\ s^{-1}$
w	- $\bar{w} + w'$ velocity component in z-direction, sum of mean and turbulent components	$m\ s^{-1}$
w_d	- effective deposition velocity due to ground-absorption based on ground-level concentration	$m\ s^{-1}$
w_s	- sedimentation velocity (terminal velocity of heavy particles)	$m\ s^{-1}$
x	- Cartesian spatial coordinate (horizontal)	m
Δx	- finite spatial stepsize in x-direction	m
x''	- value of x-coordinate at point-source position	m
\tilde{x}	- (x_1, x_2, x_3) , (x, y, z) position vector	m
x_ℓ	- x-coordinate of an ambient particle which is transported in the mean wind-field	m
X	- x-coordinate of a particle (or centroid) which is transported in the mean wind-field	m
\tilde{X}	- (X_1, X_2, X_3) , (X, Y, Z) position vector for a particle transported in the mean wind-field	m

y	- Cartesian spatial coordinate (horizontal)	m
Δy	- finite spatial stepsize in y-direction	m
y''	- value of y-coordinate at point-source position	m
y_ℓ	- y-coordinate of an ambient particle which is transported in the mean wind-field	m
Y	- y-coordinate of a particle (or centroid) which is transported in the mean wind-field	m
z	- Cartesian spatial coordinate (vertical)	m
z''	- value of z-coordinate at point-source position	m
z_0	- surface roughness-length [sections (1.2.1), (1.2.2)]	m
z_s	- height of point-source above ground-level	m
Z_0	- optimum tracking height for simulating the advection of the puff centroid	m
Z_t	- fixed height at which it is desired to follow puff centroid	m

GREEK LETTERS:

α'	- dimensionless velocity gradient for linear velocity profile [section (3.1)]	
γ	- c_p/c_v	
γ_1	- skewness [section (3.2)]	
Γ	- adiabatic lapse rate	$K m^{-1}$
δ	- Dirac delta: $\delta(t)=0, t \neq 0; \int_{-\infty}^{\infty} \delta(t) dt = 1$	

δ_{ik}	- Kronecker delta: $\delta_{ik} = 0, i \neq k, \delta_{ii} = 1$	
δ_w	- wind-field divergence, $\tilde{\nabla} \cdot \tilde{u}$	s^{-1}
Δ	- distance between fluid particle and solid particle	m
Δ'	- basic finite time stepsize for DPM numerical solution [section (2.4.3)]	s
ζ	- z/L dimensionless height	
ζ_0	- z_0/L dimensionless roughness-length	
η	- Cartesian spatial coordinate (horizontal) in lagrangian frame	m
θ	- $\bar{\theta} + \theta'$ potential temperature, sum of mean and turbulent components [section (1.2.1)]	K
θ_*	- $-\bar{q}_3 / (\rho c_p k u_*)$ scaling temperature	K
θ_{AZ}	- azimuthal wind direction (heading)	radians
θ_{mn}	- $\int_{-\infty}^{\infty} \int_{-\infty}^{\infty} x^m y^n C dx dy$ horizontal moments of puff distribution	$kg m^{m+n-1}$ *
$\bar{\theta}'_{zG}$	- $\partial \bar{\theta} / \partial z \Big _{zG}$ potential temperature gradient at height z_G	$K m^{-1}$
Λ	- washout coefficient	s^{-1}
Λ_r	- washout coefficient for reversible absorption	s^{-1}
μ	- viscosity	$kg m^{-1} s^{-1}$
μ_a	- viscosity of air	$kg m^{-1} s^{-1}$
ξ	- Cartesian spatial coordinate (horizontal) in lagrangian frame	m
ρ	- density of air	$kg m^{-3}$
$\hat{\rho}$	- air density deviation from equilibrium value	$kg m^{-3}$

ρ_0	- density of air at ground-level	kg m^{-3}
ρ_p	- particle density	kg m^{-3}
σ_{AZ}	- standard deviation of azimuthal wind direction	radians
σ_x	- standard deviation of distribution in x-direction	m
σ_y	- standard deviation of distribution in y-direction	m
σ_z	- standard deviation of distribution in z-direction	m
τ	- time	s
τ_0	- shear stress at ground-level	Nm^{-2}
τ_E	- eulerian time-scale	s
τ_L	- lagrangian time-scale	s
ϕ	- flow potential	$\text{m}^2 \text{s}^{-1}$
ϕ_m	- $\frac{kz}{u_*} \left(\frac{\partial \bar{u}}{\partial z} \right)$ dimensionless wind shear	
ϕ_T	- $\frac{z}{\theta_*} \left(\frac{\partial \bar{\theta}}{\partial z} \right)$ dimensionless temperature gradient	
ϕ_W	- $\frac{kz}{u_*} \left(\frac{\partial C_W}{\partial z} \right)$ dimensionless water-vapour concentration gradient	
Φ	- rate of generation of heat by sources in the fluid	W m^{-3}
Ψ	- rate of generation of heat by viscous dissipation	W m^{-3}

ABBREVIATIONS:

ADI	- Alternating Direction Implicit
B5700	- Burroughs B5700 DCMCP mark XVI.0.08 and intrinsics mark XVI.0.05 Computer

CDC1700 - Control Data Corporation CDC1700 process
control Computer

DPM - Dynamic Puff Model [chapter (2)]

FP - Fluorescent Particle

GPM - Gaussian Puff Model [appendix (A2)]

IBM360/155 - International Business Machines series
IBM360/155 Computer

ID - Internal Diameter

MSM - Meteorology Sub-Model [appendix (A4)]

PIC - Particle-In-Cell [PIC Model: appendix (A3)]

RHS - Right-Hand-Side

RMS - Root Mean Square

SAST - South African Standard Time (30°E)

TLV - Threshold Limit Value

USRC - United States Radium Corporation
(P.O. Box 409, Hackettstown, N.J. 07840, U.S.A.)

UV - Ultra-Violet

VHF - Very High Frequency

W/F - Wind-Field

BIBLIOGRAPHY

(* : not studied in original form)

- Abramowitz, M. and Stegun, I.A., "Handbook of Mathematical Functions", Dover Publications Inc., New York, 1970.
- Anderson, G.E., J. Appl. Met., 10, 377 (1971).
- Angell, J.K., Pack, D.H., Hoecker, W.H. and Delper, N., Quart. J. R. Met. Soc., 97, 87 (1971).
- * Aris, R., Proc. Roy. Soc. A, 235, 67 (1956).
- * Baron, T., Gerhard, E.R. and Johnstone, H.F., Ind. and Eng. Chem., 41, 2403 (1949).
- * Batchelor, G.K., Arch. Mech. Stosowanej 3, 16, 661 (1964).
- Benarie, M., Atmospheric Environment, 9, 552 (1975).
- Bencala, K.E. and Seinfeld, J.H., Atmospheric Environment, 10, 941 (1976).
- Bierly, E.W. and Hewson, E.W., J. Appl. Met., 2, 390 (1963).
- * Blackadar, A.K., J. Geophys. Res., 67, 3095 (1962).
- * Braham, R.R., Seely, B.K., and Crozier, W.D., Trans. Amer. Geophys. Union, 33, 825 (1952).
- * Briggs, G.A., "A Smoke Plume Rise Theory (Preliminary)", Atmospheric Turbulence and Diffusion Laboratory, Oak Ridge, Tennessee, 1964.
- * Briggs, G.A., "Plume Rise", USAEC Critical Review Series TID-25075, Clearinghouse for Federal Scientific and Technical Information, Springfield, Va., 1969.
- Briggs, G.A., Atmospheric Environment, 6, 507 (1972).
- Businger, J.A., Wyngaard, J.C., Izumi, Y. and Bradley, E.F., J. Atmos. Sci., 28, 181 (1971).
- * Calder, K.L., Q.J. Mech. Appl. Math., 2, 153 (1949).
- Calder, K.L., Quart. J.R. Met. Soc., 91, 514 (1965).

- Calder, K.L., Quart. J.R. Met. Soc., 94, 88 (1968).
- Caput, C., Belot, Y., Guyot, G., Samie, C. and Seguin, B.,
Atmospheric Environment, 7, 75 (1973).
- Carl, D.M., Tarbell, T.C. and Panofsky, H.A., J. Atmos. Sci.,
30, 788 (1973).
- * Chamberlain, A.C., "Aspects of Travel and Deposition of
Aerosol and Vapour Clouds", A.E.R.E., HP/R 1261,
H.M.S.O., 1953.
- * Chamberlain, A.C., "Aspects of the Deposition of Radioactive
and other Gases and Particles", Int. J. Air Poll.,
3, 1961.
- Chatwin, P.C., Quart. J.R. Met. Soc., 94, 350 (1968).
- Chu, K.J. and Seinfeld, J.H., Atmospheric Environment,
9, 375 (1975).
- Clough, W.S., Atmospheric Environment, 9, 1113 (1975).
- Counihan, J., Atmospheric Environment, 5, 637 (1971).
- * Cramer, H.E., et al, "The study of diffusion of gases or
aerosols in the lower atmosphere", AFRC-TR-59-207,
AF19-(604)-3460, (Defence Documentation Centre,
AD 210482), 1959.
- * Crowley, W.P., Mon. Wea. Rev., 96, 1 (1968).
- Csanady, G.T., Atmospheric Environment, 3, 25 (1969a).
- * Csanady, G.T., J. Atmos. Sci., 26, 414 (1969b).
- Csanady, G.T., Atmospheric Environment, 6, 221 (1972).
- * Davenport, A.G., "The Relationship of Wind Structure to
Wind Loading, in Wind Effects on Buildings and
Structures", National Physical Laboratory,
Symposium 16, Her Majesty's Stationary Office,
London, 1965.
- Davey, W.L.E., "Development and application of a fluorescent-
particle analyser", Ph.D. thesis in preparation,
Dept. of Chemical Engineering, University of Natal,
Durban, 1977.

- * Dickerson, M.H., "A mass-consistent wind field model for the San Francisco Bay Area", Lawrence Livermore Laboratory, Livermore, California, UCRL-74265, 1973.
- Dilley, J.F. and Yen, K.T., Atmospheric Environment, 5, 843 (1971).
- Drivas, P.J. and Shair, F.H., Atmospheric Environment, 8, 475, (1974).
- * Dumbauld, R.K., J. Appl. Met., 1, 437 (1962).
- Dyer, A.J., Boundary-Layer Meteorol., 7, 363 (1974).
- * Dyer, A.J. and Hicks, B.B., Quart. J. R. Met. Soc., 96, 715 (1970).
- Egan, B.A. and Mahoney, J.R., J. Appl. Met., 11, 312 (1972a).
- Egan, B.A. and Mahoney, J.R., J. Appl. Met., 11, 1023 (1972b).
- Echols, W.T. and Wagner, N.K., J. Appl. Met., 11, 658 (1972).
- Eggleton, A.E.J. and Thompson, N., Nature, 192, 935 (1961).
- Eimutis, E.C. and Konicek, M.G., Atmospheric Environment, 6, 859 (1972).
- Endlich, R.M., J. Appl. Met., 6, 837 (1967).
- Fabrick, A.J. and Sklarew, R.C., "Cross Evaluation of Regional Air Pollution Models", Paper No. 75-04.6, 68th. Annual Meeting of the APCA, June, 1975.
- * Fay, J.A., Escudier, M. and Hoult, D.P., Atmospheric Environment, 3, 311 (1969).
- Fiedler, F. and Panofsky, H.A., Quart. J.R. Met. Soc., 98, 213 (1972).
- Fortak, H.G., "Mathematical modelling of urban pollution", Institut für Theoretische Meteorologie, Freie Universität Berlin, Federal Republic of Germany, 1974.
- Fosberg, M.A., Fox, D.G., Howard, E.A. and Cohen, J.D., Atmospheric Environment, 10, 1053 (1976).
- * Gartrell, F.E., Thomas, F.W. and Carpenter, S.B., J. Am. Ind. Hyg. Ass., 24, 113 (1963).

- * Gartrell, F.E., et al, "Full-scale study of dispersion of stack gases. A Summary Report", U.S. Public Health Service - TVA, 1964.
- Gee, J.H. and Davies, D.R., Quart. J. R. Met. Soc., 89, 542 (1963).
- Gee, J.H. and Davies, D.R., Quart. J. R. Met. Soc., 90, 478 (1964).
- Gifford, F.A. and Hanna, S.R., Atmospheric Environment, 7, 131 (1973).
- Gifford, F.A. and Pack, D.H., Nuclear Safety, 3, 76 (1962).
- Hale, W.E., Atmospheric Environment, 6, 419 (1972).
- Hales, J.M., Atmospheric Environment, 6, 635 (1972).
- * Halliday, E.C. and Venter, G.P.N., Atmospheric Environment, 5, 815 (1971).
- Hameed, S., Atmospheric Environment, 8, 555 (1974a).
- Hameed, S., Atmospheric Environment, 8, 1003 (1974b)
- Hameed, S., Atmospheric Environment, 9, 270 (1975).
- * Hay, J.S. and Pasquill, F., J. Fluid Mech., 2, 299 (1957).
- * Hay, J.S. and Pasquill, F., Advances in Geophysics, 6, 345 (1959).
- Heines, T.S. and Peters, L.K., Atmospheric Environment, 7, 39 (1973).
- Heines, T.S. and Peters, L.K., Atmospheric Environment, 8, 1143 (1974).
- Hino, M., Atmospheric Environment, 2, 541 (1968).
- * Högström, U., Tellus, 16, 205 (1964).
- Hsi, G. and Nath, J.H., J. Appl. Met., 9, 592 (1970).
- Hsu, S.A., J. Geophys. Res., 76, 2880 (1971).
- Ito, S., "A mechanism of turbulent diffusion in the atmospheric surface layer", Papers in Meteorology and Geophysics, 21, 141 (1970).

- Joynt, R.C. and Blackman, D.R., *Atmospheric Environment*, 10, 433 (1976).
- Kao, S.K., *J. Atmos. Sci.*, 33, 157 (1976).
- Knox, J.B., *J. APCA*, 24, 660 (1974).
- * Kung, E., "Climatology of aerodynamic roughness parameter and energy dissipation", Annual Rept., Dept. of Meteorology, University of Wisconsin, Madison, 1963.
- * Kutzback, J., "Investigations of the modification of wind profiles by artificially controlled surface roughness", Annual Rept., Dept. of Meteorology, University of Wisconsin, Madison, 1961.
- * Lamb, R.G., *Atmospheric Environment*, 7, 235 (1973).
- Lamb, R.G. and Neiburger, M., *Atmospheric Environment*, 5, 239 (1971).
- Leahey, D.M., *Atmospheric Environment*, 9, 817 (1975).
- Leahey, D.M. and Halitsky, J., *Atmospheric Environment*, 7, 49 (1973).
- Lebedeff, S.A. and Hameed, S., *Atmospheric Environment*, 9, 333 (1975).
- Lebedeff, S.A. and Hameed, S., *J. Appl. Met.*, 15, 326 (1976).
- Leighton, P.A., Perkins, W.A., Grinnell, S.W. and Webster, F.X., *J. Appl. Met.*, 4, 334 (1965).
- Leonard, R.E. and Federer, C.A., *J. Appl. Met.*, 12, 302 (1973).
- Lettau, H., *J. Appl. Met.*, 8, 828 (1969).
- Liu, C.Y. and Goodin, W.R., *Atmospheric Environment*, 10, 513 (1976).
- Liu, M.K. and Seinfeld, J.H., *Atmospheric Environment*, 9, 555 (1975).
- * Matsuoka, H., *J. Met. Soc. Japan*, 39, 324 (1961).

- McMahon, T.A., Denison, P.J. and Fleming, R., Atmospheric Environment, 10, 751 (1976).
- McVehil, G.E., Quart. J. R. Met. Soc., 90, 136 (1964).
- Meek, C.C. and Jones, B.G., J. Atmos. Sci., 30, 239 (1973).
- * Meetham, A.R., Quart. J.R. Met. Soc., 70, 359 (1950).
- Molenkamp, C.R., J. Appl. Met., 7, 160 (1968).
- * Monin, A.S. and Obukhov, A.M. "Basic regularity in turbulent mixing in the surface layer of the atmosphere", Trud. Geofiz. Inst. Akad. Nauk, S.S.S.R., 24:151, 163 (1954).
- * Monin, A.S. and Yaglom, A.M., "Statistical Fluid Mechanics", M.I.T., Cambridge, Mass., 1971.
- Mulholland, M., Scholtz, M.T. and Brouckaert, C.J.
"Emission, Dosage and Meteorological Measurements taken in the Atmospheric Tracer Experiments conducted at Richards Bay during June and July, 1976", - submitted to the Council for Scientific and Industrial Research, Pretoria, for publication as a South African National Scientific Programmes Report.
- Munn, R.E. and Richards, T.L., Quart. J.R. Met. Soc., 89, 411 (1963).
- * Neiburger, M., Private communication with Liu and Goodin, 1974.
- Nickola, P.W., J. Appl. Met., 10, 962 (1971).
- Nickola, P.W., Ludwick, J.D. and Ramsdell, J.V., J. Appl. Met., 9, 621 (1970).
- Niemeyer, L.E. and McCormick, R.A., J. APCA, 18, 403 (1968).
- Norden, C.E. and van As, D., "A technique for generating indium aerosols for use in atmospheric dispersion measurements", - in preparation, Atomic Energy Board, Pretoria, South Africa, 1977a.

- Norden, C.E. and van As, D., "Rapid analysis of trace amounts of indium by neutron activation and solvent extraction", - in preparation, Atomic Energy Board, Pretoria, South Africa, 1977b.
- Ootaki, A., "A diffusion model for air quality simulation", Paper No. 75-04.4, 68th. Annual Meeting of the APCA, June, 1975.
- Owers, M.J. and Powell, A.W., Atmospheric Environment, 8, 63 (1974).
- Panofsky, H.A. and Townsend, A.A., Quart. J. R. Met. Soc., 90, 147 (1964).
- * Pasquill, F., Met. Mag., 90, 33 (1961).
- * Pasquill, F., Quart. J. R. Met. Soc., 88, 70 (1962).
- Pasquill, F., "Atmospheric Diffusion", van Nostrand, London, 239 (1968).
- Pasquill, F. and Butler, H.E., Quart. J. R. Met. Soc., 90, 79 (1964).
- Peaceman, D.W. and Rachford, H.H., J. Soc. Appl. Math., 3, 28 (1955).
- * Perkins, W.A., Leighton, P.A., Grinnell, S.W. and Webster, F.X., Proc. Second Natl. Air Poll. Symposium, Pasadena, Calif., 42 (1952).
- Peskin, R.L., "Stochastic estimation applications to turbulent diffusion", International Symposium on Stochastic Hydraulics, Pittsburgh, May, 1971.
- Peters, L.K. and Klinzing, G.E., Atmospheric Environment, 5, 497 (1971).
- Peterson, E.W., J. Appl. Met., 10, 958 (1971).
- Peterson, J.T., Atmospheric Environment, 6, 433 (1972).
- Preston-Whyte, R.A., S.A. Geog. Journal, 57, 17 (1975).
- * Priestley, C.H.B., "Turbulent transfer in the lower atmosphere", University of Chicago Press, 1959.

- * Prodan, L., J. Ind. Hyg. Toxicol., 14, 174 (1932).
- Pruitt, W.O., Morgan, D.L. and Lourence, F.J., Quart. J. R. Met. Soc., 99, 370 (1973).
- Quesada, A.F., "Some solutions of the diffusion equation for an expanding gas cloud in a constant shear flow", Air Force Cambridge Research Laboratories 71-0111, Physical Sciences Research Papers No. 446, February, 1971.
- Ragland, K.W., Atmospheric Environment, 7, 1017 (1973).
- Ragland, K.W. and Dennis, R.L., Atmospheric Environment, 9, 175 (1975).
- Randerson, D., Atmospheric Environment, 4, 615 (1970).
- Roffman, A., Rao, R.K. and Grimble, R., "Application of a three-dimensional diffusion model for predicting air pollution under thermal inversion breakup fumigation conditions", Paper No. 75-04.1, 68th. Annual Meeting of the APCA, June, 1975.
- Rao, K.S., Lague, J.S., Egan, B.A. and Chu, Y.H., "A dynamic plume model for the prediction of atmospheric effects associated with cooling tower operation", Paper No. 75-04.5, 68th. Annual Meeting of the APCA, June, 1975.
- * Ritchmeyer, R.D. and Morton, K.W., "Difference methods for initial value problems", Interscience, New York, 1967.
- * Roberts, O.F.T., Proc. R. Soc. A104, 640 (1923).
- Rosinski, J., Glaess, H.E. and McCully, C.R., Analytical Chemistry, 28, 486 (1956).
- * Rounds, W., Trans. Am. Geophys. Union, 36, 395 (1955).
- Ruff, R.E. and Fox, D.G., "Evolution of air quality models through the use of the RAPS data base", Paper No. 74-124, National Environmental Research Centre, EPA, Research Triangle Park, N.C. 27711, 1974.

- Runca, E. and Sardei, F., *Atmospheric Environment*, 9, 69 (1975).
- Saffman, P.G., *Quart. J. R. Met. Soc.*, 88, 382 (1962).
- Sasaki, Y., *Monthly Weather Rev.*, 98, 875 (1970).
- Scholtz, M.T. and Brouckaert, C.J., "Modelling of the flow of stable air over a complex region", South African National Scientific Programmes Report No. 9, C.S.I.R., Pretoria, 1976.
- * Schwartz, J. and Tulin, M.P., *Atmospheric Environment*, 6, 19 (1971).
- * Scorer, R.S., "Natural Aerodynamics", Pergamon, New York, 1958.
- Scriven, R.A. and Fisher, B.E.A., *Atmospheric Environment*, 9, 49 (1975).
- Seinfeld, J.H., "Air Pollution-Physical and Chemical Fundamentals", McGraw-Hill, New York, 1975.
- * Sellers, W., "Physical Climatology", University of Chicago Press, 1965.
- Sharma, V., *Atmospheric Environment*, 10, 1027 (1976).
- Shepherd, J.G. *Atmospheric Environment*, 8, 69 (1974).
- * Sheppard, P.A., *Proc. Roy. Soc., A*, 188, 208 (1947).
- Shir, C.C. and Shieh, L.J., *J. Appl. Met.*, 13, 185 (1974).
- * Singer, I.A. and Smith, M.E., *Int. J. Air Wat. Pollut.*, 10, 125 (1966).
- * Sklarew, R.C., "Preliminary report on the S³ urban air pollution model simulation of carbon monoxide in Los Angeles", Systems, Science and Software, Inc., La Jolla, Calif., 1970.
- * Slawson, P.R. and Csanady, G.T., *J. Fluid Mech.*, 28, 311 (1967).
- Slinn, W.G.N., *Atmospheric Environment*, 8, 233 (1974).
- Slinn, W.G.N., *Atmospheric Environment*, 10, 763 (1976).
- * Smith, F.B., *J. Fluid Mech.*, 2, 49 (1957).

- Smith, F.B., Quart. J. R. Met. Soc., 91, 318 (1965).
- Soo, S.L., "Fluid dynamics of multiphase systems",
Blaisdell, Waltham, Mass., 1967.
- * Spiegel, E.A. and Veronis, G., Astrophys. J., 131, 442 (1960).
- Spomer, L.A., Atmospheric Environment, 7, 353 (1973).
- Starkey, J.R., Instrumentation Handbooks I/TN/6/75 : EL427,
I/TN/7/75 : EL427 and I/TN/25/75 : EL431, Atomic
Energy Board, Pretoria, South Africa, 1976.
- * Sutton, O.G., Proc. Roy. Soc. A, 135, 143 (1932).
- Sutton, O.G., "Micrometeorology", McGraw-Hill, New York, 1953.
- Swinbank, W.C., Quart. J. R. Met. Soc., 90, 119 (1964).
- Swinbank, W.C., Quart. J. R. Met. Soc., 94, 460 (1968).
- * Takeuchi, K., J. Met. Soc. Japan, Ser.II, 39, 346 (1961).
- Tang, C.M., Atmospheric Environment, 3, 583 (1969).
- * Taylor, G.I., Proc. London Math. Soc., Ser. 2, 20, 196 (1921).
- * Taylor, G.I., Proc. Roy. Soc. A, 219, 186 (1953).
- * Taylor, G.I., Ibid., 225, 473 (1954).
- Taylor, P.A., Quart. J. R. Met. Soc., 95, 77 (1969).
- * Taylor, R.J., Quart. J.R. Met. Soc., 86, 67 (1960).
- Thompson, R., Quart. J. R. Met. Soc., 97, 93 (1971).
- Tyldesley, J.B. and Wallington, C.E., Quart. J. R. Met. Soc.,
91, 158 (1965).
- Venter, G.P.N., Halliday, E.C. and Prinsloo, L.A., Atmospheric
Environment, 7, 593, (1973).
- * Walters, T.S., Atmospheric Environment, 3, 461 (1969).
- Webb, E.K., Quart. J. R. Met. Soc., 96, 67 (1970).
- Wedin, B., Frössling, N. and Aurivillius, B., Advances in
Geophysics, Academic Press, N.Y., 6, 425 (1959).
- Wendell, L.L., Mon. Wea. Rev., 100, 565 (1972).
- * Whittaker, E.T. and Watson, G.N., "Modern Analysis", Cambridge
University Press, 1950.